Vol. 19. No 1, 2017

ISSN 1507-2711
Cena: 25 zł (w tym 5% VAT)

EKSPLOATACJA I NIEZAWODNOŚĆ
MAINTENANCE AND RELIABILITY

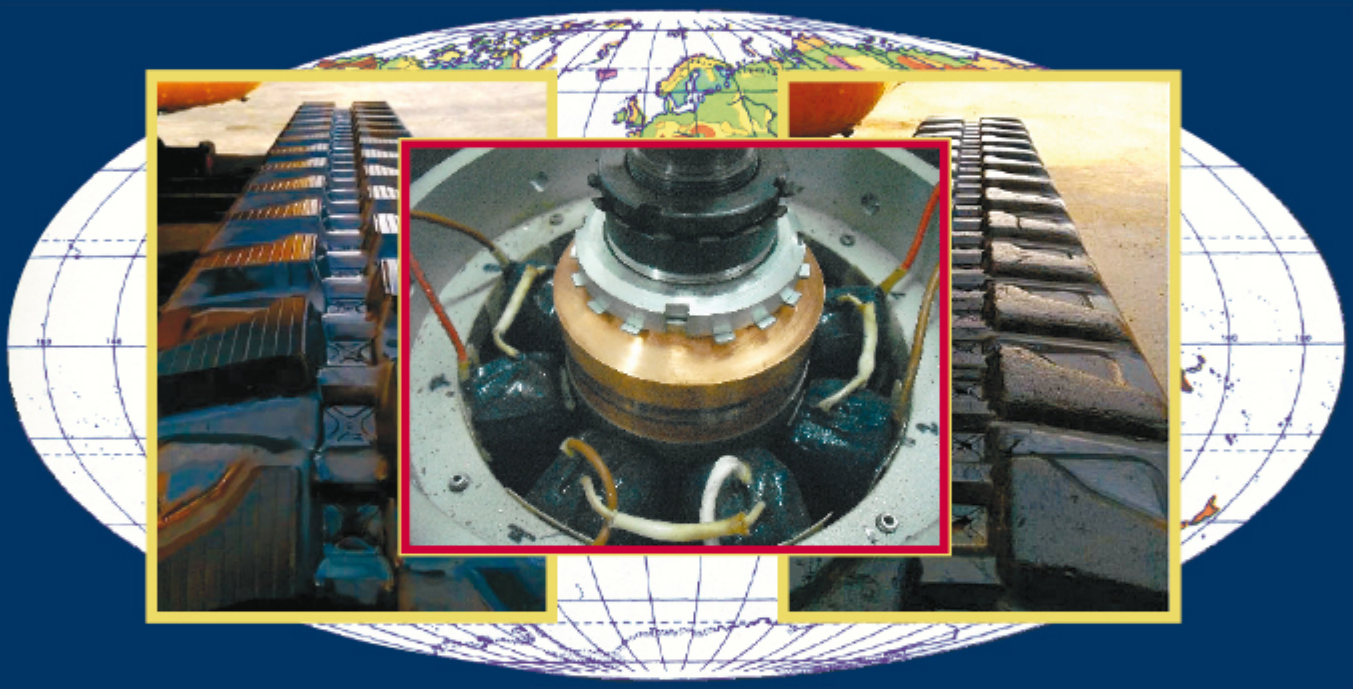

Polskie Naukowo Techniczne Towarzystwo Eksploatacyjne
Warszawa

Polish Maintenance Society
Warsaw

Co-financed by the Minister of Science and Higher Education

The Journal is indexed and abstracted in the Journal Citation Reports (JCR Science Edition), Scopus, Science Citation Index Expanded (SciSearch®) and Index Copernicus International.

The Quarterly appears on the list of journals credited with a high impact factor by the Polish Ministry of Science and Higher Education and is indexed in the Polish Technical Journal Contents database – BAZTECH and the database of the Digital Library Federation.

All the scientific articles have received two positive reviews from independent reviewers.

Our 2015 Impact Factor is 1.248

Editorial staff:	Dariusz Mazurkiewicz, PhD, DSc (Eng), Associate Professor (Editor-in-Chief, Secretary of the Scientific Board) Tomasz Klepka, PhD, DSc (Eng), Associate Professor (Deputy Editor-in-Chief) Teresa Błachnio-Krolopp, MSc (Eng) (Editorial secretary) Andrzej Koma (Typesetting and text makeup) Krzysztof Olszewski, PhD (Eng) (Webmaster)
Publisher:	Polish Maintenance Society, Warsaw
Scientific patronage:	Polish Academy of Sciences Branch in Lublin
Address for correspondence:	"Eksploatacja i Niezawodność" – Editorial Office ul. Nadbystrzycka 36, 20-618 Lublin, Poland e-mail: office@ein.org.pl http://www.ein.org.pl/
Circulation:	550 copies

Science and Technology

SZYMICZEK M. **Ultrasonic and thermal testing as a diagnostic tool for the evaluation of cumulative discontinuities of the polyester – glass pipes structure**. Eksploatacja i Niezawodnosc – Maintenance and Reliability 2017; 19 (1): 1–7, http://dx.doi.org/10.17531/ein.2017.1.1.

The aim of the work was to develop a methodology for evaluating the accumulation of discontinuities with the application of non-destructive methods. Commercial polyester-glass pipes produced by a method of helical filament winding were tested. The observed discontinuities were the result of post-production flaws, but first of all, the aging-fatigue degradation process. Evaluation of the degradation degree directly related to the process of discontinuities propagation was performed with the use of active thermography and ultrasonic inspection. Diagnostic characteristics were the heating and cooling rate estimated from the temperature distribution on the heat-activated surface. In the case of ultrasonic inspection, as the value of the diagnostics was assumed, transition time of ultrasonic wave was determined by the application of the echo method. Structural changes were indirectly determined on the basis of water absorption. It has been found that there is a correlation between the properties set out in the non-destructive testing and water absorption. The higher absorption, which indicates a greater number of defects, the lower the heating and cooling rate and transition time of ultrasonic wave.

SZYMICZEK M. **Badania ultradźwiękowe i termowizyjne jako narzędzie diagnostycznej oceny kumulacji nieciągłości struktury rur poliestrowo-szklanych**. Eksploatacja i Niezawodnosc – Maintenance and Reliability 2017; 19 (1): 1–7, http://dx.doi.org/10.17531/ein.2017.1.1.

Celem pracy jest opracowanie metodyki oceny kumulacji nieciągłości metodami nieniszczącymi. Badaniom poddano handlowe rury poliestrowo-szklane wytwarzana metodą nawijania śrubowego. Obserwowane nieciągłości były efektem zarówno wad poprodukcyjnych, ale przede wszystkim procesu degradacji starzeniowo-zmęczeniowej. Oceny stopnia degradacji bezpośrednio związanej z procesem propagacji nieciągłości dokonano przy użyciu termowizji aktywnej oraz defektoskopii ultradźwiękowej. Charakterystyką diagnostyczną w przypadku termografii była prędkość nagrzewania i chłodzenia określona na podstawie rozkładu temperatury na powierzchni aktywowanej cieplnie. W przypadku defektoskopii ultradźwiękowej jako wielkość diagnostyczną przyjęto czas przejścia fali ultradźwiękowej wyznaczony metodą echa. Zmiany struktury pośrednio określono na podstawie chłonności wody. Stwierdzono, że istnieje korelacja pomiędzy własnościami określonymi w badaniach nieniszczących a chłonnością wody. Im wyższa chłonność, co świadczy o większej liczbie wad, tym niższe prędkości nagrzewania i chłodzenia oraz czas przejścia fali ultradźwiękowej.

RODRÍGUEZ-PICÓN LA. **Reliability assessment for systems with two performance characteristics based on gamma processes with marginal heterogeneous random effects**. Eksploatacja i Niezawodnosc – Maintenance and Reliability 2017; 19 (1): 8–18, http://dx.doi.org/10.17531/ein.2017.1.2.

In this paper, a reliability modeling approach for products with two performance characteristics related to two degradation processes is developed. The joint modeling of such processes is performed by using a copula function in order to consider the dependence structure between degradation processes. The proposed approach considers that different random effects affect the stochastic behavior of each performance characteristic. For such approach, different bivariate models with marginal gamma processes with heterogeneous random effects as marginal distributions are considered. As the random effects may differ between performance characteristics, different modifications of the structure of the parameters of the gamma process are proposed. Such that the random effects affect both the drift and diffusion, just the drift, and just the diffusion of the marginal gamma processes. The statistical inference of the joint bivariate models is performed via Bayesian approach. The obtained results show that a bivariate model with heterogeneous random effects has a slight better performance among the proposed models. Which implies that the bivariate heterogeneous random effects gamma process models may provide a better approach to model multivariate degradation data, and thus a better reliability assessment of the product under study.

RODRÍGUEZ-PICÓN LA. **Ocena niezawodności systemów o dwóch parametrach użytkowych oparta na procesach gamma z brzegowymi niejednorodnymi efektami losowymi**. Eksploatacja i Niezawodnosc – Maintenance and Reliability 2017; 19 (1): 8–18, http://dx.doi.org/10.17531/ein.2017.1.2.

W niniejszym artykule opracowano sposób modelowania niezawodności produktów posiadających dwa parametry użytkowe związane z dwoma procesami degradacji. Procesy takie można modelować łącznie wykorzystując funkcję kopuły, która pozwala na analizę struktury zależności między procesami degradacji. Proponowane podejście zakłada, że na stochastyczne zachowanie każdego z parametrów użytkowych wpływają różne efekty losowe. Przy takim założeniu, należy wziąć pod uwagę różne modele dwuwymiarowe, w których rozkłady brzegowe są brzegowymi procesami gamma z niejednorodnymi efektami losowymi. Jako że efekty losowe mogą być odmienne dla różnych parametrów użytkowych, zaproponowano różne modyfikacje struktury parametrów procesu gamma, takie, że efekty losowe wpływają zarówno na dryf jak i dyfuzję, tylko na dryf, lub tylko na dyfuzję procesów brzegowych gamma. Wnioskowanie statystyczne dla wspólnych modeli dwuwymiarowych przeprowadzono metodą Bayesa. Uzyskane wyniki pokazują, że dwuwymiarowy model z niejednorodnymi efektami losowymi ma nieznaczną przewagę nad pozostałymi zaproponowanymi modelami. Oznacza to, że dwuwymiarowe modele procesu gamma z niejednorodnymi efektami losowymi mogą stanowić lepszy sposób modelowania wielowymiarowych danych degradacyjnych, tym samym umożliwiając lepszą ocenę niezawodności badanego produktu.

PILCH R. **Reliability evaluation of networks with imperfect and repairable links and nodes**. Eksploatacja i Niezawodnosc – Maintenance and Reliability 2017; 19 (1): 19–25, http://dx.doi.org/10.17531/ein.2017.1.3.

The paper presents the method for determining the reliability of a network whose elements (links and nodes) are imperfect (can fail) and repairable. The presented method uses the factoring algorithm, proposed π method and computer simulation. The factoring algorithm is used to obtain a formula for accurate computation of network reliability as a probability of connectedness among the specified set of nodes K ($R_{N(K)}$). The reliability calculated in this way relates to cases when only links can fail and are unrepairable. In order to calculate the reliability of a network with repairable links and nodes, we introduced quasi-failures of links which occur as a result of failures of adjacent nodes – the π method. The developed method allows accounting for the repair of all the network elements after failure, as well as choosing the set of nodes (N_f) which can fail independently. In addition, the probability distributions of failure time of freely specified sets of nodes and links can be different. A simulation computational model was developed for the method which allows for determining the reliability ($R_{N(K)}(t)$) of a network with repairable links and nodes. Examples of numerical calculations were performed according to the developed model and the results are presented.

PILCH R. **Niezawodność sieci z uszkadzającymi się i odnawianymi połączeniami oraz węzłami**. Eksploatacja i Niezawodnosc – Maintenance and Reliability 2017; 19 (1): 19–25, http://dx.doi.org/10.17531/ein.2017.1.3.

W opracowaniu przedstawiono metodę wyznaczania niezawodności sieci, w których elementy (połączenia i węzły) mogą się uszkadzać i są odnawiane. Przedstawiona metoda wykorzystuje algorytm faktoryzacji, zaproponowaną metodę π oraz symulację komputerową. Na podstawie algorytmu faktoryzacji wyznaczany jest wzór do dokładnego obliczania niezawodności sieci jako prawdopodobieństwa połączenia między wybranym zbiorem K węzłów ($R_{N(K)}$). Obliczana w ten sposób niezawodność dotyczy przypadków gdy tylko połączenia mogą się uszkadzać i nie są odnawiane. W celu obliczania niezawodności sieci z odnawianymi połączeniami i węzłami wprowadzono quasi uszkodzenia połączeń, które występują na skutek uszkodzeń węzłów do nich przyległych – metoda π. Opracowana metoda pozwala uwzględnić odnawianie wszystkich elementów sieci po uszkodzeniu jak również możliwość wyboru zbioru węzłów (N_f), które mogą się niezależnie uszkadzać. Ponadto rozkłady prawdopodobieństwa czasu pracy do uszkodzenia dowolnie określonych zbiorów węzłów i połączeń mogą być różne. Do zaproponowanej metody opracowano symulacyjny model obliczeniowy, który umożliwia wyznaczenie niezawodności sieci ($R_{N(K)}(t)$) z odnawianymi połączeniami i węzłami. Zgodnie z opracowanym modelem wykonano przykładowe obliczenia numeryczne i przedstawiono ich wyniki.

BALLESTEROS A, SANDA R, MAQUA M, STEPHAN J-L. **Maintenance related events in nuclear power stations**. Eksploatacja i Niezawodnosc – Maintenance and Reliability 2017; 19 (1): 26–30, http://dx.doi.org/10.17531/ein.2017.1.4.

This paper presents the essential results of a study performed by the European Clearinghouse on Operational Experience Feedback, in cooperation with IRSN and GRS, aiming to analyse events where their direct or root cause was an inappropriate maintenance at nuclear power stations. The databases of IRSN, GRS, U.S. NRC and IAEA IRS were screened to select relevant events related to maintenance that took place in the period 2002-2013. The examination of the selected events resulted in their classification into nine categories or groups with sub-division in families and, if necessary, sub-families. In total 921 events were analysed. One of the event classifications performed was according to the type of maintenance (periodic, predictive, planned and corrective). The operational experience data analysis indicated

BALLESTEROS A, SANDA R, MAQUA M, STEPHAN J-L. **Zdarzenia eksploatacyjne w elektrowniach jądrowych**. Eksploatacja i Niezawodnosc – Maintenance and Reliability 2017; 19 (1): 26–30, http://dx.doi.org/10.17531/ein.2017.1.4.

W niniejszej pracy przedstawiono najważniejsze wyniki badania dotyczącego informacji zwrotnych na temat doświadczeń z eksploatacji urządzeń przeprowadzonego przez European Clearinghouse we współpracy z IRSN oraz GRS. Badanie miało na celu analizę zdarzeń, których bezpośrednią lub zasadniczą przyczyną była nieodpowiednia eksploatacja urządzeń w elektrowni jądrowej. W badaniu, przeszukiwano bazy danych których operatorami są IRSN, GRS, U.S. NRC oraz IAEA IRS w celu wyłonienia istotnych zdarzeń eksploatacyjnych z lat 2002-2013. Analiza wybranych zdarzeń pozwoliła na sklasyfikowanie ich według dziewięciu kategorii lub grup, które z kolei podzielono na rodziny i, jeśli zachodziła taka potrzeba, także na pod-rodziny. W sumie przeanalizowano 921 zdarzeń. Jedna z klasyfikacji zdarzeń została oparta na kryterium rodzaju utrzymania ruchu (okresowe, predykcyjne, planowe oraz korekcyjne). Analiza danych dotyczących

that 47% of the events reported were related to periodic maintenance. The main affected components were „valves", followed by „electric power components". The main root causes observed are „maintenance performed incorrectly" (e.g., improper use of tools, breach of authorization, lapse, etc.), „deficiencies in written procedures or documents" and „deficiencies in management or organization". Regarding the impact on safety, the dominant family is „potential effects on safety function" (57%), followed by „significant effect on operation" (20%). Based on a detailed analysis of selected events, recommendations were developed and some of them are presented in this paper. This study highlights that the continuous analysis of maintenance related events and the efficient utilization of operational experience provide important insights for improving the quality of maintenance and for preventing the occurrence of unusual events and thus helps to enhance nuclear safety.

doświadczeń operacyjnych wykazała, że 47% zgłaszanych zdarzeń było związanych z konserwacją okresową. Głównymi elementami, których dotyczyły badane zdarzenia były "zawory", a w drugiej kolejności "części elektryczne" Najważniejszymi zasadniczymi przyczynami zdarzeń były "nieprawidłowo wykonana konserwacja" (np. nieprawidłowe użycie narzędzi, naruszenie autoryzacji, pomyłka, itd), "niedoskonałe procedury pisemne lub niedoskonała dokumentacja" oraz "niedociągnięcia w zarządzaniu lub organizacji". W odniesieniu do wpływu na bezpieczeństwo, dominującą rodzinę zdarzeń stanowiło "potencjalne oddziaływanie na funkcję bezpieczeństwa" (57%), a w drugiej kolejności "znaczący wpływ na pracę" (20%) W oparciu o szczegółową analizę wybranych zdarzeń, opracowano rekomendacje, z których część przedstawiono w niniejszym artykule. Omawiane badanie zwraca uwagę na fakt, iż ciągła analiza zdarzeń eksploatacyjnych oraz skuteczne wykorzystanie doświadczeń z eksploatacji dostarczają istotnej wiedzy na temat możliwości doskonalenia jakości utrzymania ruchu oraz zapobiegania występowaniu zdarzeń, pomagając w ten sposób zwiększyć bezpieczeństwo produkcji energii jądrowej.

GERDES M, GALAR D, SCHOLZ D. **Decision trees and the effects of feature extraction parameters for robust sensor network design**. Eksploatacja i Niezawodnosc – Maintenance and Reliability 2017; 19 (1): 31–42, http://dx.doi.org/10.17531/ein.2017.1.5.

Reliable sensors and information are required for reliable condition monitoring. Complex systems are commonly monitored by many sensors for health assessment and operation purposes. When one of the sensors fails, the current state of the system cannot be calculated in same reliable way or the information about the current state will not be complete. Condition monitoring can still be used with an incomplete state, but the results may not represent the true condition of the system. This is especially true if the failed sensor monitors an important system parameter. There are two possibilities to handle sensor failure. One is to make the monitoring more complex by enabling it to work better with incomplete data; the other is to introduce hard or software redundancy. Sensor reliability is a critical part of a system. Not all sensors can be made redundant because of space, cost or environmental constraints. Sensors delivering significant information about the system state need to be redundant, but an error of less important sensors is acceptable. This paper shows how to calculate the significance of the information that a sensor gives about a system by using signal processing and decision trees. It also shows how signal processing parameters influence the classification rate of a decision tree and, thus, the information. Decision trees are used to calculate and order the features based on the information gain of each feature. During the method validation, they are used for failure classification to show the influence of different features on the classification performance. The paper concludes by analysing the results of experiments showing how the method can classify different errors with a 75% probability and how different feature extraction options influence the information gain.

GERDES M, GALAR D, SCHOLZ D. **Wykorzystanie drzew decyzyjnych oraz wpływu parametrów ekstrakcji cech do projektowania odpornych sieci czujników**. Eksploatacja i Niezawodnosc – Maintenance and Reliability 2017; 19 (1): 31–42, http://dx.doi.org/10.17531/ein.2017.1.5.

Niezawodne monitorowanie stanu wymaga niezawodności czujników i pochodzących z nich informacji. Systemy złożone są zazwyczaj monitorowane przez wiele czujników, co pozwala na ocenę stanu technicznego oraz aspektów eksploatacyjnych. Gdy jeden z czujników ulega uszkodzeniu, uniemożliwia to obliczenie bieżącego stanu systemu z dotychczasową niezawodnością lub uzyskanie kompletnych informacji o bieżącym stanie. Stan można co prawda monitorować nawet przy niekompletnych danych, ale wyniki takiego monitorowania mogą nie odpowiadać rzeczywistemu stanowi systemu. Sytuacja taka ma miejsce w szczególności, gdy uszkodzony czujnik jest odpowiedzialny za monitorowanie istotnego parametru systemu. Problem uszkodzenia czujnika można rozwiązywać na dwa sposoby. Pierwszy polega na zwiększeniu złożoności systemu, co umożliwia jego sprawniejsze działanie w sytuacji, gdy dane są niekompletne. Drugim sposobem jest wprowadzenie nadmiarowego sprzętu (hardware'u) lub oprogramowania. Niezawodność czujników stanowi krytyczny aspekt systemu. Oczywiście, ze względu na ograniczenia przestrzenne, ekonomiczne i środowiskowe nie wszystkie czujniki w systemie mogą być nadmiarowe. Redundancja powinna dotyczyć wszystkich czujników, które dostarczają istotnych informacji na temat stanu systemu, natomiast dopuszczalne są błędy mniej ważnych czujników. W niniejszej pracy pokazano jak obliczać istotność informacji o systemie dostarczanych przez poszczególne czujniki z wykorzystaniem metod przetwarzania sygnałów oraz drzew decyzyjnych. Zademonstrowano również w jaki sposób parametry przetwarzania sygnałów wpływają na poprawność klasyfikacji metodą drzewa decyzyjnego, a tym samym na poprawność dostarczanych informacji. Drzew decyzyjnych używa się do obliczania i porządkowania cech w oparciu o przyrost informacji charakteryzujący poszczególne cechy. Podczas weryfikacji zastosowanej metody, drzewa decyzyjne wykorzystano do klasyfikacji uszkodzeń celem przedstawienia wpływu różnych cech na dokładność klasyfikacji. Pracę kończy analiza wyników eksperymentów pokazujących w jaki sposób zastosowana metoda pozwala na klasyfikację różnych błędów z 75-procentowym prawdopodobieństwem oraz jak różne opcje ekstrakcji cech wpływają na przyrost informacji.

KONIUSZY A, KOSTENCKI P, BERGER A, GOLIMOWSKI W. **Power performance of farm tractor in field operations**. Eksploatacja i Niezawodnosc – Maintenance and Reliability 2017; 19 (1): 43–47, http://dx.doi.org/10.17531/ein.2017.1.6.

Many studies have examined the effects of agriculture tractor engine energy performance. This paper presents an evaluation method of such engine actual power use during plowing operations. It includes results of a comparative study of power performance of a 230 kW tractor model John Deere 8330 subject to soil plowing operations as a function of field size: A (26 ha), B (12.74 ha), C (3.22 ha). Statistical data clustering, a relatively novel approach in studies on actual utilization of engine power, was used. A positive correlation was observed between field size and the active state of the engine: 75.2% field A; 68.8% field B; 46.8% field C. The actual power utilization of agriculture tractor engine as a function of field size was 0.62, 0.58 and 0.39 respectively for the three fields used in this study. With this evaluation approach, performance indexes of operational power performance in various conditions were obtained for possible use in optimization of plowing operations.

KONIUSZY A, KOSTENCKI P, BERGER A, GOLIMOWSKI W. **Wykorzystanie mocy ciągnika rolniczego w pracach polowych**. Eksploatacja i Niezawodnosc – Maintenance and Reliability 2017; 19 (1): 43–47, http://dx.doi.org/10.17531/ein.2017.1.6.

Ocena stanu obciążenia silnika spalinowego w pojeździe podczas eksploatacji jest przedmiotem wielu prac badawczych. W artykule przedstawiono nową metodę oceny wykorzystania mocy silnika ciągnika rolniczego eksploatowanego podczas orki. Zaprezentowano wyniki badań porównawczych nad wykorzystaniem mocy ciągnika John Deere 8330 (230 kW) w odniesieniu do powierzchni uprawianych pól: A (26 ha), B (12,74 ha) i C (3,22 ha). Do analizy danych pomiarowych zastosowano po raz pierwszy statystyczną metodę grupowania punktów pomiarowych. Na podstawie wyników badań stwierdzono silną korelację dodatnią pomiędzy powierzchnią pól a stanem obciążenia silnika: 75,2% pole A; 68,8% pole B; 46,8% pole C. Opracowany wskaźnik efektywnego wykorzystania mocy silnika ciągnika rolniczego wyniósł odpowiednio: 0,62, 0,58 i 0,39. Stwierdzono, że uzyskane wartości wskaźnika efektywności wykorzystania mocy silnika mogą być przydatne do optymalizacji pracy ciągnika w pracach polowych.

BŁACHNIO J, BOGDAN M, ZASADA D. **Increased temperature impact on durability of gas turbine blades**. Eksploatacja i Niezawodnosc – Maintenance and Reliability 2017; 19 (1): 48–53, http://dx.doi.org/10.17531/ein.2017.1.7.

The paper presents the research results of a microstructure of the turbine rotor blades made of nickel-based super alloys. The purpose of the research was to determine the high temperature impact on the microstructure stability of the material of the blades. The degree of advancement of the super alloy microstructure changes after the exposure to high temperature was compared to the mictrostructure condition of new blades. The research material includes blades made of EI 867 and ŻS 32 types of alloys. The microstructure research of blades subject to the high temperature impact, and the blades after operation showed the occurrence of adverse changes in

BŁACHNIO J, BOGDAN M, ZASADA D. **Wpływ podwyższonej temperatury na trwałość łopatek turbiny gazowej**. Eksploatacja i Niezawodnosc – Maintenance and Reliability 2017; 19 (1): 48–53, http://dx.doi.org/10.17531/ein.2017.1.7.

W artykule przedstawiono wyniki badań mikrostruktury łopatek wirnika turbiny wykonanych z nadstopów na bazie niklu. Celem badań było określenie skutków oddziaływania wysokiej temperatury na stabilność mikrostruktury materiału łopatek. Stopień zaawansowania zmian mikrostruktury nadstopu po oddziaływaniu wysokiej temperatury porównywano ze stanem mikrostruktury łopatek nowych. Materiałem do badań były łopatki ze stopów typu EI 867 oraz ŻS 32. Badania mikrostruktury łopatek poddawanych oddziaływaniu wysokiej temperatury oraz łopatek po eksploatacji wykazały występowanie niekorzystnych zmian w stosunku do mikrostruktury łopatek nowych. Stwierdzono, że przyczyną niekorzystnych zmian w mikrostrukturze było przegrzanie nadstopu. Łopatka w takim

relation to the microstructure of new blades. It was found that the cause of adverse changes in the microstructure was the super alloy overheating. The blade in such a condition has low heat and creep resistance. The element, in which the overheating will occur, is exposed to damage, which usually entails faulty turbine operation. This type of damage is removed during the engine major repair, which is associated with huge costs.

stanie wykazuje niską żaroodporność oraz żarowytrzymałość. Element, w którym wystąpi przegrzanie jest narażony na uszkodzenie, co przeważnie pociąga za sobą wadliwą pracę turbiny. Tego typu uszkodzenia usuwa się w trakcie naprawy głównej silnika co wiąże się z ogromnymi kosztami.

RUSEK J. **Application of Support Vector Machine in the analysis of the technical state of development in the LGOM mining area**. Eksploatacja i Niezawodnosc – Maintenance and Reliability 2017; 19 (1): 54–61, http://dx.doi.org/10.17531/ein.2017.1.8.

The paper presents the results of the analysis of technical wear of buildings located within impact of mining plant in the Legnica - Głogów Copper District (LGOM). The study used method related to neural networks, support vector (Support Vector Machine) in regression approach ε-SVR (Support Vector Regression). The aim of the study was to assess the impact of variables describing the structural protection and renovations on the course modeled phenomenon. The basis for the analysis was created model of technical wear of buildings in the form of a network ε-SVR. In addition to the variables determining the level of structural protection and renovations in the model included variables describing: terrain deformation, mining intensity tremors and the age of the buildings. The choice of model parameters were performed using, as gradientlessness optimization method, genetic algorithm. Based on the established model ε-SVR two types of sensitivity analysis were applied. Assessing the impact of the structural protections have been studying by the analysis of variability of the gradient vector for the modeled hypersurface. The analysis of the impact of renovations on the course modeled process was carried out based on the comparator simulation results of ε-SVR model. The results confirmed the usefulness of the methodology of research and allowed to draw important conclusions on the impact of analyzed factors on the technical wear traditional buildings LGOM.

RUSEK J. **Zastosowanie metody Support Vector Machine w analizie stanu technicznego zabudowy terenu górniczego LGOM**. Eksploatacja i Niezawodnosc – Maintenance and Reliability 2017; 19 (1): 54–61, http://dx.doi.org/10.17531/ein.2017.1.8.

W pracy przedstawiono wyniki analizy zużycia technicznego budynków zlokalizowanych w zasięgu wpływów eksploatacji górniczej na terenie Legnicko-Głogowskiego Okręgu Miedziowego (LGOM). W badaniach zastosowano pokrewną sieciom neuronowym metodę wektorów podpierających (Support Vector Machine) w podejściu regresyjnym ε-SVR (Support Vector Regression). Celem badań było uzyskanie oceny wpływu zmiennych opisujących zabezpieczenia konstrukcyjne i remonty na przebieg modelowanego zjawiska. Podstawą do analiz był utworzony model zużycia technicznego budynków w postaci sieci ε-SVR. Oprócz zmiennych określających poziom zabezpieczeń konstrukcyjnych i remontów, w modelu uwzględniono zmienne opisujące: deformacje terenu pochodzenia górniczego, intensywność wstrząsów oraz wiek budynków. Dobór parametrów modelu przeprowadzono z wykorzystaniem, jako bezgradientowej metody optymalizacyjnej, algorytmu genetycznego. Bazując na utworzonym modelu ε-SVR przeprowadzono dwurodzajową analizę wrażliwości. Oceny wpływu zabezpieczeń konstrukcyjnych dokonano badając zmienność wektora gradientu modelowanej hiperpowierzchni. Natomiast analiza wpływu remontów na przebieg modelowanego procesu została przeprowadzona na bazie komparacji wyników symulacji modeluε-SVR. Wyniki badań potwierdziły przydatność przyjętej metodyki badań oraz pozwoliły na sformułowanie istotnych wniosków dotyczących wpływu analizowanych czynników na zużycie techniczne tradycyjnej zabudowy LGOM.

DOMBEK G, NADOLNY Z. **Thermal properties of a mixture of synthetic and natural esters in terms of their application in high voltage power transformers**. Eksploatacja i Niezawodnosc – Maintenance and Reliability 2017; 19 (1): 62–67, http://dx.doi.org/10.17531/ein.2017.1.9.

The article presents research results of thermal properties of mixtures of synthetic and natural esters in terms of their application in the cooling system of a high-voltage power transformer during its operation. The investigated properties of an analysed mixture were: thermal conductivity coefficient λ, kinematic viscosity υ, density ρ, specific heat c_p, and thermal expansion β. On the basis of presented research results, the authors determined the heat transfer factor α of a mixture of synthetic and natural esters. This factor defines the ability of an insulating liquid to transport heat in the transformer, thus determining its reliability. For the research the authors used the following percentage proportions of the mixture of both the esters: 100/0, 95/5, 80/20, 50/50, 20/80, 5/95, 0/100. The measurements were taken for the temperatures: 25ºC, 40ºC, 60ºC, and 80ºC.

DOMBEK G, NADOLNY Z. **Właściwości cieplne mieszaniny estrów syntetycznych i estrów naturalnych w aspekcie zastosowania w transformatorach dużej mocy**. Eksploatacja i Niezawodnosc – Maintenance and Reliability 2017; 19 (1): 62–67, http://dx.doi.org/10.17531/ein.2017.1.9.

W artykule przedstawiono wyniki badań właściwości cieplnych mieszaniny estrów syntetycznych i estrów naturalnych, w aspekcie ich zastosowania w układzie chłodzenia transformatora wysokiego napięcia w trakcie jego eksploatacji. Badanymi właściwościami analizowanej mieszaniny były przewodność cieplna właściwa λ, lepkość kinematyczna υ, gęstość ρ, ciepło właściwe c_p oraz rozszerzalność cieplna β. W oparciu o przedstawione wyniki badań określono współczynnik przejmowania ciepła α mieszaniny estrów syntetycznych i estrów naturalnych. Współczynnik ten określa zdolność cieczy elektroizolacyjnej do transportu ciepła w transformatorze, warunkując tym samym jego niezawodność. Do badań wykorzystano następujące procentowe proporcje mieszaniny obu estrów: 100/0, 95/5, 80/20, 50/50. 20/80, 5/95, 0/100. Pomiary przeprowadzono dla temperatury: 25ºC, 40ºC, 60ºC i 80ºC.

NOWAKOWSKA M. **Spatial and temporal aspects of prior and likelihood data choices for Bayesian models in road traffic safety analyses**. Eksploatacja i Niezawodnosc – Maintenance and Reliability 2017; 19 (1): 68–75, http://dx.doi.org/10.17531/ein.2017.1.10.

In a Bayesian regression model, parameters are not constants, but random variables described by some posterior distributions. In order to define such a distribution, two pieces of information are combined: (1) a prior distribution that represents previous knowledge about a model parameter and (2) a likelihood function that updates prior knowledge. Both elements are analysed in terms of implementing the Bayesian approach in road safety analyses. A Bayesian multiple logistic regression model that classifies road accident severity is investigated. Three groups of input variables have been considered in the model: accident location characteristics, at fault driver's features and accident attributes. Since road accidents are scattered in space and time, two aspects of information source choices in the Bayesian modelling procedure are proposed and discussed: spatial and temporal ones. In both aspects, priors are based on selected data that generate background knowledge about model parameters – thus, prior knowledge has an informative property. Bayesian likelihoods which modify priors are data that deliver: (1) information specific to a road – in the spatial aspect or (2) the latest information – in the temporal aspect. The research experiments were conducted to illustrate the approach and some conclusions have been drawn.

NOWAKOWSKA M. **Przestrzenny i czasowy aspekt wyboru rozkładów apriorycznych i danych dla funkcji wiarygodności dla modeli bayesowskich w analizach bezpieczeństwa ruchu drogowego**. Eksploatacja i Niezawodnosc – Maintenance and Reliability 2017; 19 (1): 68–75, http://dx.doi.org/10.17531/ein.2017.1.10.

Parametry bayesowskiego modelu regresji nie są wartościami stałymi tylko zmiennymi losowymi opisanymi przez pewne rozkłady aposterioryczne. W celu zdefiniowania takiego rozkładu łączy się dwa źródła informacji: (1) rozkład aprioryczny, który reprezentuje wcześniejszą wiedzę o parametrze modelu oraz (2) funkcję wiarygodności (wiarygodność bayesowską), która uaktualnia wiedzę a'priori. Oba te elementy są przedmiotem badań w kontekście wykorzystania podejścia bayesowskiego w analizach bezpieczeństwa ruchu drogowego. Badaniom podlega model wielokrotnej regresji logistycznej, który klasyfikuje status zdarzenia drogowego. W modelu uwzględniono trzy grupy zmiennych objaśniających: charakterystyki miejsca lokalizacji wypadku, cechy kierującego sprawcy oraz atrybuty wypadku. Ponieważ wypadki drogowe są rozproszone w czasie i przestrzeni, zaproponowano i poddano dyskusji dwa aspekty wyboru źródeł informacji w procedurze modelowania bayesowskiego: czasowy i przestrzenny. W obu podejściach rozkłady aprioryczne są definiowane na podstawie danych wybranych jako te, które generują uogólnioną wiedzę o parametrach modelu, tworząc tło podlegające modyfikacji – w ten sposób wiedza aprioryczna ma cechę informatywności. Wiarygodność bayesowska, modyfikująca rozkłady a'priori, jest definiowana za pomocą danych wprowadzających: (1) informację specyficzną dla wybranej drogi – w przypadku aspektu przestrzennego lub (2) informację najnowszą – w przypadku aspektu czasowego. Zaproponowane podejście zilustrowano w eksperymentach badawczych i przedstawiono wynikające z nich wnioski.

CHEN X, XU D, XIAO L. **Joint optimization of replacement and spare ordering for critical rotary component based on condition signal to date**. Eksploatacja i Niezawodnosc – Maintenance and Reliability 2017; 19 (1): 76–85, http://dx.doi.org/10.17531/ein.2017.1.11.

CHEN X, XU D, XIAO L. **Wspólna optymalizacja wymiany i zamawiania części zamiennych dla krytycznego komponentu obrotowego na podstawie dotychczasowego sygnału stanu**. Eksploatacja i Niezawodnosc – Maintenance and Reliability 2017; 19 (1): 76–85, http://dx.doi.org/10.17531/ein.2017.1.11.

It is widely accepted that condition-based replacement can not only make full use of components, but also decline inventory cost if the procurement of spare parts can be triggered upon accurate failure prediction. Most of the existing degradation or failure prediction models and approaches are population-based failures or suspensions, namely, to predict the failure time of a component, there are some failure or suspension histories of same type or similar components which can be used as reference. However, in practice, there exists the phenomenon in which no failure or suspension histories for some components can be used, what can be utilized is just the collected condition monitoring signals to date. In that case, failure time and probability are difficult to be estimated accurately. In this paper, a novel degradation prediction approach is introduced. Meantime, a new failure probability estimation function is developed based on component "service time" and "degradation extent" simultaneously. Then replacement and spare part ordering are jointly optimized according to the estimated failure probability. The optimization objective is to minimize long-run cost rate. Two bearing datasets are used to validate the proposed approach.

Powszechnie przyjmuje się, że wymiana w oparciu o stan techniczny pozwala nie tylko na pełne wykorzystanie elementów składowych, ale także na zmniejszenie kosztów magazynowych (związanych z przechowywaniem zapasów) jeśli zamawianie części zamiennych da się powiązać z trafnym prognozowaniem uszkodzeń. Większość istniejących modeli i teorii predykcji degradacji lub uszkodzeń opiera się na danych populacyjnych o uszkodzeniach lub zawieszeniu pracy co oznacza, że czas uszkodzenia komponentu przewiduje się w odniesieniu do historii uszkodzeń lub zawieszeń pracy tego samego typu lub podobnego typu elementów składowych. Jednak w praktyce zdarza się, że dla niektórych komponentów nie istnieją historie uszkodzeń lub zawieszenia pracy, do których można by się odnieść; jedyne co można wykorzystać to zgromadzone dotychczas sygnały z monitorowania stanu. W takim przypadku, trudno jest ocenić dokładnie czas i prawdopodobieństwo wystąpienia uszkodzenia. W niniejszej pracy, przedstawiono nowatorskie podejście do przewidywania degradacji. Opracowano nową funkcję szacowania prawdopodobieństwa uszkodzenia opartą na jednoczesnym wykorzystaniu "czasu pracy" oraz "stopnia degradacji" komponentu. Następnie wspólnie zoptymalizowano procesy wymiany i zamawiania części zamiennych zgodnie z szacowanym prawdopodobieństwem wystąpienia uszkodzenia. Celem optymalizacji była minimalizacja długoterminowego wskaźnika kosztów . Poprawność proponowanego podejścia zweryfikowano z wykorzystaniem dwóch zbiorów danych dotyczących łożysk.

SMOLINSKI M, PERKOWSKI T, MYSTKOWSKI A, DRAGAŠIUS E, EIDUKYNAS D, JASTRZEBSKI RP. **AMB flywheel integration with photovoltaic system for household purpose – modelling and analysis**. Eksploatacja i Niezawodnosc – Maintenance and Reliability 2017; 19 (1): 86–94, http://dx.doi.org/10.17531/ein.2017.1.12.

Abstract—This paper presents the design and investigation of a photovoltaic–flywheel system for household purposes. The main goal of this work is the electrical and mechanical integration of the electromechanical high speed kinetic energy storage as UPS (Uninterruptible Power Supply) with photovoltaic solar system. The paper contains calculation and division of photovoltaic panels system according to its integration with active magnetic bearing (AMB) flywheel and external electric grid. The photovoltaic solar installation costs as well as its size were considered. The composite shell AMB flywheel prototype configuration design (using CAD-software) and two different material variants are investigated and presented. In particularly, the structural composite shell stress calculations of two different materials vs rotational speed are performed using a direct coupling of SolidWorks and Matlab® software. The analytical calculations of PV–flywheel system are provided in order to choose optimal type of photovoltaic panels according to motor/generator flywheel and household energy system requirements. All elements of PV–flywheel system as transducers, bridges, wiring diagrams, etc., are optimized using Simscape tools. Finally, short- and long-time simulations results of PV–AMB–flywheel system and initial experimental results are presented and discussed.

SMOLINSKI M, PERKOWSKI T, MYSTKOWSKI A, DRAGAŠIUS E, EIDUKYNAS D, JASTRZEBSKI RP. **Integracja łożyskowanego magnetycznie zasobnika energii kinetycznej z układem paneli fotowoltaicznych dla zastosowań w gospodarstwach domowych – modelowanie i analiza**. Eksploatacja i Niezawodnosc – Maintenance and Reliability 2017; 19 (1): 86–94, http://dx.doi.org/10.17531/ein.2017.1.12.

W artykule przedstawiono wstępne badania zintegrowanego układu paneli fotowoltaicznych z łożyskowanym magnetycznie zasobnikiem energii kinetycznej. Głównym celem pracy jest próba integracji elementów elektrycznych i mechanicznych wysokoobrotowego elektromechanicznego magazynu energii kinetycznej jako urządzenia UPS z układem paneli fotowoltaicznych. W szczególności przeprowadzono obliczenia najważniejszych parametrów elektrycznych łożyskowanego magnetycznie zasobnika energii połączonego z układem paneli fotowoltaicznych celem jego integracji z trakcją sieci elektrycznej niskiego napięcia. Wykorzystując pakiety oprogramowania: CAD, SolidWorks i Matlab, wykonano badania symulacyjne wskaźników wytrzymałości koła zamachowego zasobnika energii kinetycznej w szerokim zakresie prędkości obrotowej dla dwóch różnych typów materiałów kompozytowych. Następnie, wykorzystując między innymi narzędzia Simscape, przeprowadzono optymalizację elementów systemu celem dopasowania jego głównych parametrów do wymagań stawianym domowym instalacjom fotowoltaicznym z akumulatorami energii elektrycznej. Wyniki badań symulacyjnych, przeprowadzone w cyklach krótko– i długo– czasowych, układu paneli fotowoltaicznych zintegrowanych z elektromechanicznym akumulatorem energii potwierdziły wstępne obliczenia i założenia.

GRYGIER D. **The impact of operation of elastomeric track chains on the selected properties of the steel cord wires**. Eksploatacja i Niezawodnosc – Maintenance and Reliability 2017; 19 (1): 95–101, http://dx.doi.org/10.17531/ein.2017.1.13.

The track running systems enable movement of heavy vehicles on unpaved and rough terrain, snow-covered, marshy or swampy surfaces, as well as overcoming natural or artificial barriers. The important structural component of the elastomeric tracks is a steel cord sunk in the elastomer creating the tread with the purpose of stiffening the structure, maintaining its proper deflection and giving the adequate resistance to tensile forces. The results of the studies presented in the work have shown that operation of the elastomeric track chains in conditions where they are continuously exposed to contact with foundation, frequent braking and bumping against roughness lead to damage of the steel cord material and a change in its mechanical properties.

GRYGIER D. **Wpływ eksploatacji gąsienic elastomerowych na wybrane własności drutów stalowego kordu**. Eksploatacja i Niezawodnosc – Maintenance and Reliability 2017; 19 (1): 95–101, http://dx.doi.org/10.17531/ein.2017.1.13.

Gąsienicowe układy bieżne umożliwiają poruszanie się ciężkich pojazdów po powierzchniach nieutwardzonych oraz w trudnym terenie, zaśnieżonym, bagnistym lub grząskim, a także pokonywanie przeszkód naturalnych i sztucznych. Ważnym elementem konstrukcyjnym gąsienic elastomerowych jest stalowy kord, zatopiony w elastomerze tworzącym rzeźbę bieżnika, ma on na celu usztywnienie konstrukcji, zachowanie jej właściwego ugięcia oraz nadanie odpowiedniej odporności na siły rozciągające. Wyniki badań prezentowanych w pracy wykazały, że eksploatacja gąsienic elastometrowych w warunkach, w których narażone są na ciągłą styczność z podłożem, częste hamowanie oraz uderzenia w nierówności prowadzi do uszkadzania materiału stalowego kordu i zmiany jego własności mechanicznych.

ZALESKI K. **The effect of vibratory and rotational shot peening and wear on fatigue life of steel**. Eksploatacja i Niezawodnosc – Maintenance and Reliability 2017; 19 (1): 102–107, http://dx.doi.org/10.17531/ein.2017.1.14.

The paper reports the experimental results of investigation of the effect of tribological wear of C45 steel specimens subjected to grinding and vibratory and rotational shot peening on their fatigue life. The study also investigated the effect of wear on surface roughness and the distribution of residual stresses in the surface layer of the tested specimens. Counterspecimen pressure on the specimen was variable during the wear process. Fatigue life was investigated on a specially constructed test stand enabling cyclic bending of the tested specimen. It was found that increasing the counterspecimen pressure leads to an increase in surface roughness and fatigue life as well as generates undesired residual stresses. The negative effects of tribological wear were more visible for the specimens subjected to grinding than for those which were exposed to vibratory and rotational shot peening.

ZALESKI K. **Wpływ kulkowania wibracyjno – rotacyjnego i zużywania stali na trwałość zmęczeniową**. Eksploatacja i Niezawodnosc – Maintenance and Reliability 2017; 19 (1): 102–107, http://dx.doi.org/10.17531/ein.2017.1.14.

W pracy przedstawiono wyniki badań doświadczalnych wpływu zużywania tribologicznego próbek ze stali C45, szlifowanych oraz kulkowanych wibracyjno – rotacyjnie, na trwałość zmęczeniową. Badano też wpływ zużywania na chropowatość powierzchni oraz rozkład naprężeń własnych w warstwie wierzchniej badanych próbek. Parametrem zmiennym w procesie zużywania był nacisk przeciwpróbki na próbkę. Trwałość zmęczeniową badano na specjalnym stanowisku, umożliwiającym cykliczne zginanie badanej próbki. Stwierdzono, że ze wzrostem nacisku przeciwpróbki następuje pogorszenie chropowatości powierzchni, ukształtowanie mniej korzystnych naprężeń własnych oraz zmniejszenie trwałości zmęczeniowej. Negatywne skutki zużycia tribologicznego bardziej widoczne są dla próbek szlifowanych niż dla kulkowanych wibracyjno – rotacyjnie.

GNIŁKA J, MĘŻYK A. **Experimental identification and selection of dynamic properties of a high-speed tracked vehicle suspension system**. Eksploatacja i Niezawodnosc – Maintenance and Reliability 2017; 19 (1): 108–113, http://dx.doi.org/10.17531/ein.2017.1.15.

GNIŁKA J, MĘŻYK A. **Identyfikacja doświadczalna oraz dobór cech dynamicznych układu jezdnego szybkobieżnego pojazdu gąsienicowego**. Eksploatacja i Niezawodnosc – Maintenance and Reliability 2017; 19 (1): 108–113, http://dx.doi.org/10.17531/ein.2017.1.15. Zróżnicowanie materiałowe podzespołów wchodzących w skład gąsienicowego układu jezdnego oraz stopień jego zużycia wpływają na trudność określenia

The material diversity of subassemblies making up the tracked vehicle suspension system and the system wear level make it difficult to determine the value of forces acting in it. This paper presents a manner in which parameters of the model of a high-speed tracked vehicle suspension system can be adjusted using the genetic algorithm optimization method. The vehicle motion is tested experimentally to find reference characteristics of kinematic quantities of the system selected points. The simulation results obtained from numerical analyses are presented in charts and compared to the results of experimental testing. Finally, damping values in the vehicle shock-absorbers are determined based on an adopted criterion.

wartości sił działających w tym układzie. W artykule poprzez zastosowanie metody optymalizacji algorytmami genetycznymi, przedstawiono sposób dostosowania parametrów modelu układu zawieszenia szybkobieżnego pojazdu gąsienicowego. Przeprowadzono badania doświadczalne ruchu pojazdu, w celu wyznaczenia charakterystyk wielkości kinematycznych wybranych punktów układu, które zostały przyjęte jako referencyjne. W rezultacie przeprowadzonych analiz otrzymano wyniki symulacji numerycznych, które zestawiono na wykresach i porównano z wynikami badań doświadczalnych. W końcowym etapie na podstawie przyjętego kryterium określono wartości tłumienia w amortyzatorach pojazdu.

OZ MA, KAYMAKCI OT, KOYUN A. **A safety related perspective for the power supply systems in railway industry**. Eksploatacja i Niezawodnosc – Maintenance and Reliability 2017; 19 (1): 114–120, http://dx.doi.org/10.17531/ein.2017.1.16.

Within its structure railway transportation systems contain very critical subsystems that can seriously harm the system itself, people or the environment if not properly controlled. Therefore, these critical subsystems are analysed according to the related standards and necessary safety functions are implemented, verified and operated. On the other hand, railway power supply system, which is a critical subsystems, is generally properly analysed from a reliability perspective whereas the corresponding safety related functions are roughly examined. This paper proposes that the railway power supply systems should be considered as safety critical systems and justifies this proposal using risk analysis as presented in the standard IEC 61508. The safety related functions of the system are examined and each function is modelled in detail using Markov modelling method. These models are implemented over a power supply system of Istanbul Transportation Co. and SIL values of the safety functions are calculated using these modular and easily adaptable Markov models. Furthermore the obtained results are compared with simplistic Fault Tree analysis (FTA) and the significance of accurate calculation is demonstrated.

OZ MA, KAYMAKCI OT, KOYUN A. **Bezpieczeństwo systemów zasilania w przemyśle kolejowym**. Eksploatacja i Niezawodnosc – Maintenance and Reliability 2017; 19 (1): 114–120, http://dx.doi.org/10.17531/ein.2017.1.16.

W skład struktury kolejowych systemów transportowych wchodzą krytyczne podsystemy, które, nieodpowiednio monitorowane, mogą narażać sam system, a także ludzi oraz środowisko na poważne szkody. Dlatego też, podsystemy krytyczne analizuje się zgodnie z odpowiednimi normami oraz wdraża w nich, weryfikuje i realizuje niezbędne funkcje bezpieczeństwa. W przypadku systemów zasilania kolei, które należą do grupy podsystemów krytycznych, system na ogół analizuje się dokładnie z punktu widzenia niezawodności, natomiast funkcje bezpieczeństwa bada się jedynie pobieżnie. W prezentowanej pracy postuluje się że systemy zasilania kolei powinny być traktowane jako krytyczne dla bezpieczeństwa, co autorzy uzasadniają z wykorzystaniem analizy ryzyka przedstawionej w normie IEC 61508. W proponowanym rozwiązaniu, bada się funkcje bezpieczeństwa systemu, przy czym każda funkcja zostaje szczegółowo zamodelowana za pomocą metody modelowania Markowa. Modele tego typu wdrożono w systemie zasilania firmy Istanbul Transportation Co. Wartości poziomu nienaruszalności bezpieczeństwa (SIL) badanych funkcji bezpieczeństwa obliczano za pomocą wspomnianych modularnych modeli Markowa charakteryzujących się łatwością adaptacji. Ponadto, uzyskane wyniki porównano z symplistyczną analizą drzewa błędów (FTA), a także wykazano znaczenie prowadzenia dokładnych obliczeń.

MARCZUK A, CABAN J, SAVINYKH P, TURUBANOV N, ZYRYANOV D. **Maintenance research of a horizontal ribbon mixer**. Eksploatacja i Niezawodnosc – Maintenance and Reliability 2017; 19 (1): 121–125, http://dx.doi.org/10.17531/ein.2017.1.17.

During operation of the mixing device there are many technical problems affecting technological processes implemented with their involvement. In order to improve the efficiency of feeding with mixed feed, mixed feed should be prepared from quality mixes. Despite the widespread use of various types of mixers, their operation is not sufficiently understood, therefore the study of the effects of the design and technological parameters on mix quality is an urgent task. Experimental studies were carried out in the livestock farming mechanisation laboratory of the North-East Scientific Research Institute of Agriculture of the Federal State Budgetary Scientific Institution. The article presents the research of the feed mix composed of barley and rice as a base mix, and feed mix of peas used as a reference component.

MARCZUK A, CABAN J, SAVINYKH P, TURUBANOV N, ZYRYANOV D. **Badania eksploatacyjne mieszalnika wstęgowego poziomego**. Eksploatacja i Niezawodnosc – Maintenance and Reliability 2017; 19 (1): 121–125, http://dx.doi.org/10.17531/ein.2017.1.17.

Podczas eksploatacji urządzenia mieszającego występuje wiele czynników technicznych wpływających na procesy technologiczne. W celu poprawienia przyswajalności mieszanek paszowych, powinny one być wytworzone na mieszalnikach zapewniających jednorodność i wysoką jakość mieszanek. Pomimo powszechnego stosowania różnych rodzajów mieszalników, procesy w nich zachodzące nie są do końca rozpoznane, a zatem badanie wpływu konstrukcji i parametrów technicznych na jakość mieszanki jest zagadnieniem stale aktualnym. Badania doświadczalne zostały przeprowadzone w Laboratorium Mechanizacji Produkcji Zwierzęcej w Strefowym Instytucie Naukowo-Badawczym Rolnictwa Północno-Wschodniego Rosyjskiej Akademii Nauk. W artykule przedstawiono badania mieszanki paszy złożonej z jęczmienia i ryżu jako mieszanki bazowej oraz mieszanki paszowej grochu wykorzystywanej jako komponent odniesienia.

SKAČKAUSKAS P, ŽURAULIS V, VADLUGA V, NAGURNAS S. **Development and verification of a shock absorber and its shim valve model based on the force method principles**. Eksploatacja i Niezawodnosc – Maintenance and Reliability 2017; 19 (1): 126–133, http://dx.doi.org/10.17531/ein.2017.1.18.

In this paper, a mathematical model of a monotube shock absorber's shim valve, which is developed by applying the force (flexibility) method, is described. This method expresses the relationship between displacements and the forces existing in the shock absorber structure. An application of the force method in the field of practical modification of vehicle shock absorbers enables to effectively analyse the influence of a wide range of parameters, including the number of shims in the valve, their disposition and the properties of the material on the level of the damping force. The damping of the shock absorber considerably impacts comfort and road holding characteristics of the vehicle. In addition, a whole model of a monotube shock absorber is designed in this paper. The validation and practical application of the mathematical model were evaluated by carrying out experimental measuring of the characteristics of the shock absorber using a special stand.

SKAČKAUSKAS P, ŽURAULIS V, VADLUGA V, NAGURNAS S. **Modelowanie i ocena amortyzatora i jego zaworu talerzowego oparte na zasadach metody sił**. Eksploatacja i Niezawodnosc – Maintenance and Reliability 2017; 19 (1): 126–133, http://dx.doi.org/10.17531/ein.2017.1.18.

W danej publikacji został opisany model matematyczny zaworu talerzowego jednorurowego amortyzatora, wyprowadzenia którego zastosowano metodę sił. Metoda ta wyraża związki pomiędzy przemieszczeniami i siłami działającymi na elementy amortyzatora. Stosowanie metody sił w praktycznej sferze modyfikacji amortyzatorów samochodowych pozwala efektywnie analizować wpływ różnych parametrów, w tym ilość, wzajemne położenie i właściwości materiałów talerzy zaworu, na generowaną amortyzatorem wielkość siły tłumienia. Tłumienie, które generuje amortyzator, wywiera znaczący wpływ na komfort jazdy samochodem oraz jego dynamikę. W publikacji również został stworzony kompletny model jednorurowego amortyzatora. Walidacja modelu matematycznego oraz możliwość zastosowania jego w praktyce zostały ocenione na podstawie eksperymentalnych pomiarów charakterystyk amortyzatorów na specjalnym stanowisku.

LEGÁT V, MOŠNA F, ALEŠ Z, JURČA V. **Preventive maintenance models – higher operational reliability**. Eksploatacja i Niezawodnosc – Maintenance and Reliability 2017; 19 (1): 134–141, http://dx.doi.org/10.17531/ein.2017.1.19.

The authors present a method for determining the optimal interval for preventive periodical maintenance and an optimal diagnostic parameter for predictive maintenance/replacement. Additionally, the authors raise the question: how does preventive maintenance influence the probability of failure and the operational reliability of system elements that have undergone preventive periodical maintenance? They answer the question using analytical and simulation computing approaches. The results are in quantitative form, giving relationships between preventive maintenance intervals

LEGÁT V, MOŠNA F, ALEŠ Z, JURČA V. **Modele konserwacji zapobiegawczej a wyższa niezawodność eksploatacyjna**. Eksploatacja i Niezawodnosc – Maintenance and Reliability 2017; 19 (1): 134–141, http://dx.doi.org/10.17531/ein.2017.1.19.

Autorzy przedstawiają metodę określania optymalnego czasu przerwy na okresową konserwację zapobiegawczą oraz optymalnego parametru diagnostycznego dla konserwacji predykcyjnej/wymiany Dodatkowo, autorzy zadają pytanie, jaki jest wpływ konserwacji zapobiegawczej na prawdopodobieństwo wystąpienia uszkodzenia oraz na niezawodność eksploatacyjną elementów systemu, w stosunku do których zastosowano okresową konserwację zapobiegawczą. Odpowiedzi na te pytania, autorzy poszukują posługując się metodami analizy i symulacji komputerowej. Wyniki podane w formie ilościowej,

and reliability functions. Examples demonstrate suitability of the method for typical engineering objects using a three parameters Weibull distribution. Application of the method is of substantial benefit to both the manufacturer and the user of technical equipment.

informują o związkach między przerwami na konserwację predykcyjną a funkcjami niezawodnościowymi. Podane przykłady pokazują, z wykorzystaniem trójparametrowego rozkładu Weibulla, że proponowana metoda może być stosowana w przypadku typowych obiektów inżynieryjnych. Zastosowanie omawianej metody przynosi znaczące korzyści zarówno wytwórcom jak i użytkownikom sprzętu technicznego.

KORNACKI A, WAWRZOSEK J, BOCHNIAK A, SZYMANEK A, PAWLAK H. **Critical values of driver response time and its impact on reducing reliability and safety in road traffic**. Eksploatacja i Niezawodnosc – Maintenance and Reliability 2017; 19 (1): 142–148, http://dx.doi.org/10.17531/ein.2017.1.20.

Road traffic is among the most dangerous types of human activity. The main causes of road accidents are driver fatigue, poor physical and mental condition of drivers and overestimating one's skills while driving. This study focuses on the estimation of driver response time, as the basis of a hypothetical system that uses short and long-range radars, which determines the physical and mental condition of a driver, based on the analysis of „acceleration noise" of the vehicle following its predecessor. This work highlights serious consequences of the fact that driver response time is described by means of a distribution with heavy tails, and thus may be a source of hazard in the driver-vehicle system. Extremes of driver response time were treated as outliers in this study. Their detection was attained by using the Akaike information criterion [1, 2], which is an alternative to conventional methods of testing hypotheses. Untypical, on account of their outlying nature, values are interpreted as critical driver response time values which potentially endanger the reliability of driving.

KORNACKI A, WAWRZOSEK J, BOCHNIAK A, SZYMANEK A, PAWLAK H. **Krytyczne wartości czasu reakcji kierowcy i ich wpływ na obniżenie niezawodności i bezpieczeństwa ruchu drogowego**. Eksploatacja i Niezawodnosc – Maintenance and Reliability 2017; 19 (1): 142–148, http://dx.doi.org/10.17531/ein.2017.1.20.

Ruch drogowy należy do najbardziej niebezpiecznych rodzajów działalności człowieka. Główne przyczyny wypadków drogowych to zmęczenie kierowców, zły stan psychofizyczny kierujących oraz przecenianie swoich umiejętności podczas prowadzenia pojazdu. W niniejszej pracy skupiono uwagę na estymacji czasu reakcji kierowców, jako podstawie hipotetycznego systemu wykorzystującego radary dalekiego i krótkiego zasięgu a określającego stan psychofizyczny kierowcy w oparciu o analizę „szumu przyspieszeń" pojazdu podążającego za poprzednikiem. Wskazuje się na groźne konsekwencje faktu, że czas reakcji kierowcy jest opisywany rozkładem z ciężkimi ogonami, gdyż z tego powodu może być źródłem zagrożenia w układzie kierowca-pojazd. Skrajne wartości czasu reakcji kierowców potraktowano w pracy, jako wartości odstające. Do ich wykrycia zastosowano kryterium informacyjne Akaike [1, 2] co stanowi alternatywę w stosunku do klasycznych metod testowania hipotez. Nietypowe, bo odstające wartości interpretuje się, jako krytyczne czasy reakcji kierowców potencjalnie zagrażające niezawodności jazdy.

Article citation info:
SZYMICZEK M. Ultrasonic and thermal testing as a diagnostic tool for the evaluation of cumulative discontinuities of the polyester – glass pipes structure. Eksploatacja i Niezawodnosc – Maintenance and Reliability 2017; 19 (1): 1–7, http://dx.doi.org/10.17531/ein.2017.1.1.

Małgorzata SZYMICZEK

ULTRASONIC AND THERMAL TESTING AS A DIAGNOSTIC TOOL FOR THE EVALUATION OF CUMULATIVE DISCONTINUITIES OF THE POLYESTER-GLASS PIPES STRUCTURE

BADANIA ULTRADŹWIĘKOWE I TERMOWIZYJNE JAKO NARZĘDZIE DIAGNOSTYCZNEJ OCENY KUMULACJI NIECIĄGŁOŚCI STRUKTURY RUR POLIESTROWO-SZKLANYCH*

The aim of the work was to develop a methodology for evaluating the accumulation of discontinuities with the application of non-destructive methods. Commercial polyester-glass pipes produced by a method of helical filament winding were tested. The observed discontinuities were the result of post-production flaws, but first of all, the aging-fatigue degradation process. Evaluation of the degradation degree directly related to the process of discontinuities propagation was performed with the use of active thermography and ultrasonic inspection. Diagnostic characteristics were the heating and cooling rate estimated from the temperature distribution on the heat-activated surface. In the case of ultrasonic inspection, as the value of the diagnostics was assumed, transition time of ultrasonic wave was determined by the application of the echo method. Structural changes were indirectly determined on the basis of water absorption. It has been found that there is a correlation between the properties set out in the non-destructive testing and water absorption. The higher absorption, which indicates a greater number of defects, the lower the heating and cooling rate and transition time of ultrasonic wave.

***Keywords**: ultrasound, thermovision, ageing-fatigue tests, polyester –glass composites, pipes.*

Celem pracy jest opracowanie metodyki oceny kumulacji nieciągłości metodami nieniszczącymi. Badaniom poddano handlowe rury poliestrowo-szklane wytwarzana metodą nawijania śrubowego. Obserwowane nieciągłości były efektem zarówno wad poprodukcyjnych, ale przede wszystkim procesu degradacji starzeniowo-zmęczeniowej. Oceny stopnia degradacji bezpośrednio związanej z procesem propagacji nieciągłości dokonano przy użyciu termowizji aktywnej oraz defektoskopii ultradźwiękowej. Charakterystyką diagnostyczną w przypadku termografii była prędkość nagrzewania i chłodzenia określona na podstawie rozkładu temperatury na powierzchni aktywowanej cieplnie. W przypadku defektoskopii ultradźwiękowej jako wielkość diagnostyczną przyjęto czas przejścia fali ultradźwiękowej wyznaczony metodą echa. Zmiany struktury pośrednio określono na podstawie chłonności wody. Stwierdzono, że istnieje korelacja pomiędzy własnościami określonymi w badaniach nieniszczących a chłonnością wody. Im wyższa chłonność, co świadczy o większej liczbie wad, tym niższe prędkości nagrzewania i chłodzenia oraz czas przejścia fali ultradźwiękowej.

***Słowa kluczowe**: ultradźwięki, termowizja, badania starzeniowo – zmęczeniowe, kompozyty poliestrowo – szklane, rury.*

1. Introduction

The wide spectrum of applications with reference to polymer composites causes that they are exposed to many degradation factors which have significant impact on their functional properties. These are both environmental factors (e.g temperature, microorganisms or UV radiation) [1, 2, 5, 6, 8, 10, 12] and fatigue ones (e.g. the value of tensions, frequency) [4, 18, 19]. Synergism of the phenomena triggered by these factors leads to gradual material degradation, which is particularly important in the case of polymer material [18, 22].

Properties of the polymer constructional composites, including glass-polyester ones depend, among others, on characteristics of input materials (reinforcements, matrixes), their mutual, adhesive connection and the technology of production. If wrongly matched, even one of the factors, causes the decrease in composite properties. Relatively large impact on the quality of obtained composites has the technology of their production [9, 11, 13]. It has been proved that in the winding technology [11] wrongly matched tension force causes bad fiber supersaturation, which in turn leads to appearance of flaws like voids or discontinuities.

(*) Tekst artykułu w polskiej wersji językowej dostępny w elektronicznym wydaniu kwartalnika na stronie ***www.ein.org.pl***

Identification of changes appearing in composites has been widely researched. Studies of epoxy-carbon composite structure conducted by Tarlej [18] allowed to define subsequent stages, from cracks individual fibres, through micro-cracks matrix, breaking the adhesive bonds up to delamination. These are, first of all, the effects of composite fatigue degradation. Particularly importance for the observed degradation processes is the heat, which, according to the Arrhenius law [10], accelerates to large extent the rate of reaction. Combination of thermal effect with e.g. UV radiation or water, results in, among others, the release of free radicals or hydrolysis reaction. Water absorption, which indirectly allows the evaluation of degradation level, is determined by material, exploitation temperature and the working environment [5, 6, 15].

The evaluation of the degradation level with reference to composite materials makes the basis to assess the usefulness of given construction for exploitation. The methods described in scientific works [2, 12, 18, 19] cause the failure of the construction which is costly and may prove unjustified. Constant monitoring of the impact of degradation processes on every stage of their use, up to its failures, makes it possible to predict the time of construction safe usefulness. Such observation is possible thanks to non-destructive research methods e.g. ultrasonic, thermovision and radiographic, which allow non-invasive diagnosing of the composite construction condition. [3, 8, 17, 20, 23, 24].

Within the presented work, the evaluation of progress in composite degradation was conducted in accordance with the established methodology, which makes use of measurement of transition time of the ultrasonic wave as well as the rate of the heating and cooling (thermovision). The changes in structure were indirectly established on the basis of water absorption.

2. Experimental research

2.1. Research program

The experimental part of the work include the following research:

- ageing-fatigue,
- thermovision,
- ultrasonic,
- water absorption.

Ageing-fatigue research, the aim of which was to obtain the proper of composite pipes degradation level, were conducted in the thermostatic water bath at the temperature of 30°C, with the cycle of stress amplitude of 3 MPa with rectangular extortion and the time of 7 s (1,5s time of pressure increase, 2s time of maintaining the maximum pressure). The way of pipes assembly and sealing, described in [22] assured the elimination of longitudinal stress which is in compliance with the theory of exerting pipes without bottoms, on the basis of the Huber's hypothesis of reduced stress [7]. The designed system of mounting caused that a pipe was only subjected to hoop and longitudinal deformation, which is shown in Fig.1, with radial stress negligible. On the inside surface they amount to 7 MPa, while on the outside surface they equal zero. Hoop stresses at the maximum load of 7 MPa are 96.95 MPa and 89.95 MPa respectively. Under given load, the increase of a pipe diameter occurs as well a decrease of length of a tested pipe.

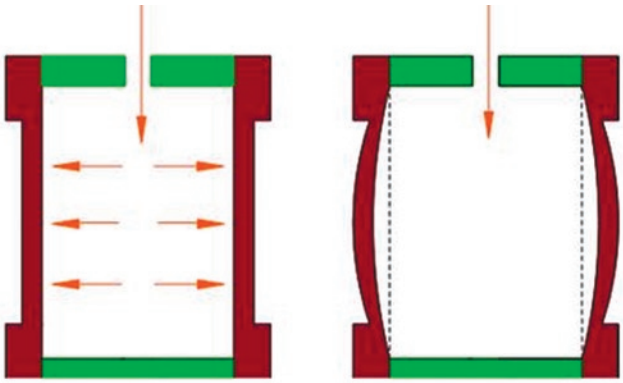

Fig.1. Scheme of the pipes deformation

Thermovision tests were conducted at the working station described in the work [17]. The changes of temperature during the heating and cooling were determined on the basis of thermovision tests by activating thermally the outside surface of a pipe for 60 s. The change in temperature in time, recorded by means of thermovision camera Flir A615, which was used to establish the rate of heating and cooling.

The transition time of the ultrasonic wave was determined in the aquatic environment with the use of heads Parametrics with the frequency of 2.25 MHz co-operating with the defectoscope UMT 17.

The research on water absorption, which indirectly allowed the evaluation of the structure condition, was conducted in accordance with the procedure described in the norm PN-ISO 8361-1:1994 [14]. The thermovision, ultrasonic and water absorption research were conducted successively, initially (up to 10×103 cycles) at 2.5×103 fatigue cycles, and the every 10×10^3 cycles.

2.2. Research material

The research was carried out glass-polyester pipes produced by winding method. The winding angle was 54°, with glass weight participation of 52%. For the matrix the composition of polyester resins Polimal 104 TS and Estromal 14.CNP -03/P was used. These are the resins containing flame retardant substances which make it possibile to obtain the flammability class V0 according to the norm PN-EN 60695. As the reinforcement glass roving ER 3003 was used with vinyl-silane aperture; as far as interlayers are concerned, the glass mat EMC 300 with silane preparation was applied. The endings of pipe samples were strengthened by hoop wound collars. The aim of the collars was to ensure the proper ring stiffness in the sealing places. Figure 2 presents the view of the sample with 16 measurement points marked 4 on each of forming, designated by its axial rotation of 90°.

Before the beginning of the ageing-fatigue research, all the samples were subjected to hardening process at the temperature of 60°C for 24 h. The result was to stabilize properties pipes.

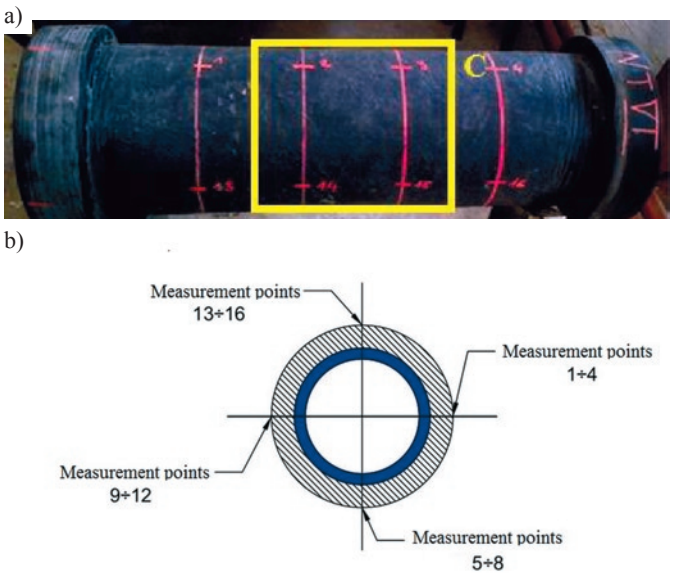

Fig. 2. View of the tested sample (a) schema of indicated measurement points (b)

The tests of water absorption were conducted on the samples in the shape of beams measuring 95×20×6 mm, cut out of the central part of pipes marked as C in the Fig. 2a.

2.3. The results and the analysis.

2.3.1. Ultrasonic tests

On the basis of the conducted ultrasonic tests, the transition time of the ultrasonic wave was determined in the marked measurement points (Fig. 2b) depending on the number of fatigue cycles. The changes in the transition time of the ultrasonic wave allow the evaluation of structural changes which occur during the process of ageing-fatigue degradation. It is much shorter in the areas in which discontinuities occur. Figure 3 presents the distribution of the transition time on the surface of the pipe (in accordance with Fig. 2b) On the circuit, the given measurement points were marked, with the transition time of the ultrasonic wave on the axis **y**. This is the standard diagram for the pipe subjected to fatigue load according to given parameters and $50x10^3$ fatigue cycles. The observed discrepancies for the sample not subjected to the process of ageing-fatigue degradation result from variable wall thickness of the pipe, which is connected with the production technology.

Figure 4 shows the change in transition time of the ultrasonic wave for two points 14 and 10, chosen on the basis of observed changes for the investigation characteristics. In point 14 a rapid decrease in the transition time occurs which confirm macrocracks. Point 10 shows slow, continuous shortening of transition time. The changes in transition time of the ultrasonic wave illustrate the progressive process of ageing -fatigue degradation which manifests itself in microdefects in the first stage (minimal shortening of the transition time) being the potential area of cracks nucleation leading to delamination.

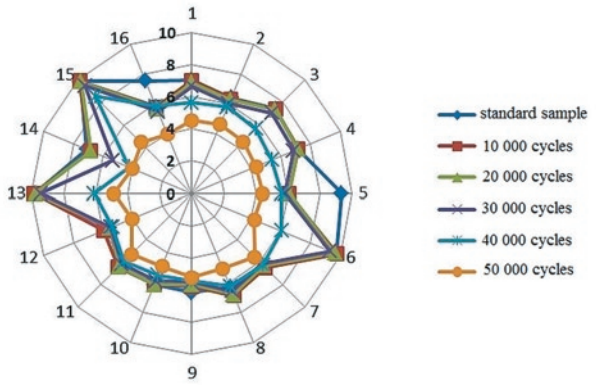

Fig. 3. Change of the transition time of the ultrasonic wave in the function of fatigue cycles

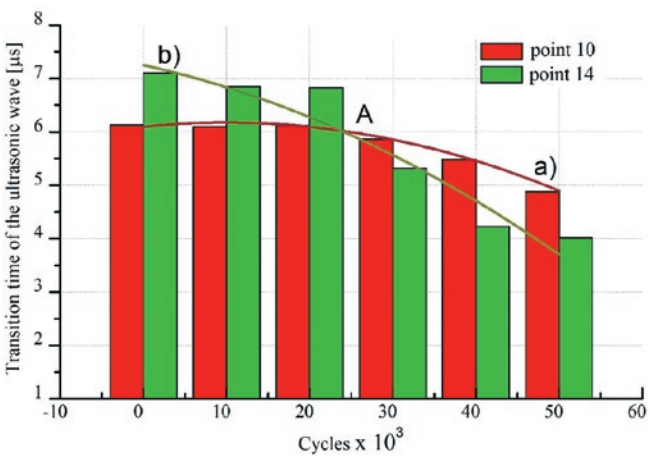

Fig. 4. Change of the transition time of the ultrasonic wave in the function of fatigue cycles in point a) 10 and b) 14 for a chosen pipe

The changes in transition time of the ultrasonic wave are described by a second degree polynomial:

• curve a):

$$\mathbf{y} = 7.25 - 0.03\mathbf{N} - 7.34\mathbf{e}^{-4}\,\mathbf{N}^2 \tag{1}$$

with a correlation coefficient **R = 0,92**,

• curve b):

$$\mathbf{y} = 6.09 + 0.02\mathbf{N} - 7.99\mathbf{e}^{-4}\,\mathbf{N}^2 \tag{2}$$

with a correlation coefficient **R = 0,989**.

Relations 1 and 2 allow to obtain the best fit of approximation function for the research results. These are however, the significant relations for the tested glass-polyester wound pipes subjected to the ageing -fatigue degradation process within the established range.

As it can be observed in Fig. 3 and 4, in the first phase of the research, the transition time of ultrasonic wave does not change or it changes slightly. Developed curves a and b (Fig. 4) cross in point A i.e. about 30×10^3 fatigue cycles. The clear shortening of wave transition time correspond to structural changes observed, first of all as a result of fatigue degradation.

Due to the differences in the measured transition time, resulting from the thickness of samples (7±1 mm) and progressive destruction process, the analysis of the frequency in which the given value of transition time in the subsequent phases of degradation process appeared. Assuming the frequency function of occurrence of examined value to be in accordance with Gauss' distribution, the most common value was established. Such established value was taken as the basis to determine the relation between the transition time of the ultrasonic wave and the number of cycles. Figure 5 shows the function of given value occurrence frequency for the exemplary samples, not subjected to the ageing-fatigue process. It is described by the following equation:

$$y = y_0 + \frac{A}{w\sqrt{\pi/2}}\,e^{-2\frac{(x-X_e)^2}{w^2}} \tag{3}$$

where: $\mathbf{y_0 = 17.18;\ X_c = 3.51\ [\mu s];\ w = 1.61\ [\mu s];\ A = 1378.75[\mu s]}$.

correlation coefficient of the function described by relation 3 equals **R = 0.99**.

Together with the progression in the ageing-fatigue degradation process, the decrease in the correlation coefficient with reference to occurrence frequency function for given transition time of the ultrasonic wave value was observed (it complied with the Gauss' distribution as much as up R = 0.68 at the number of cycles 150×10^3) as well as its flattening, which confirms the increase in the results dispersion. The obtained values are still within the 30% dispersion range, which is acceptable in case of composites.

Figure 6 shows the relation of the transition time of the ultrasonic wave in the function of the number of fatigue cycles, determined in accordance with the above described procedure.

The results were approximated by exponential function, which, like in relations 1 and 2 is the best way to describe the transition time by the function of the number of cycles (correlation coefficient **R=0.95)**, in the following form:

$$\mathbf{t_u} = -0.41\mathbf{e}^{(-\mathbf{N}/-82,81)} + 3.92 \tag{4}$$

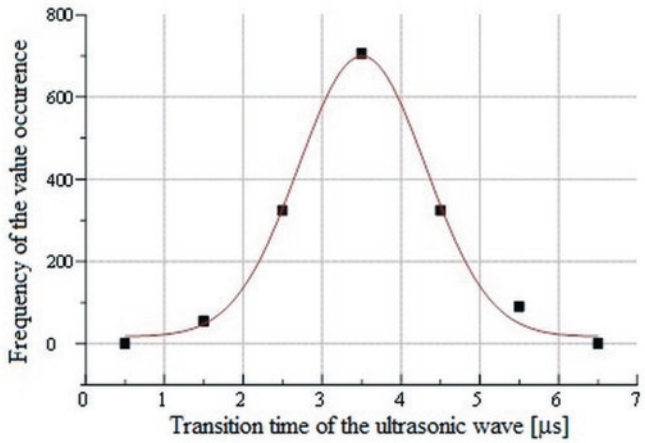

Fig. 5. Functions of occurence frequency with reference to the value of the transition time of the ultrasonic wave for the standard sample

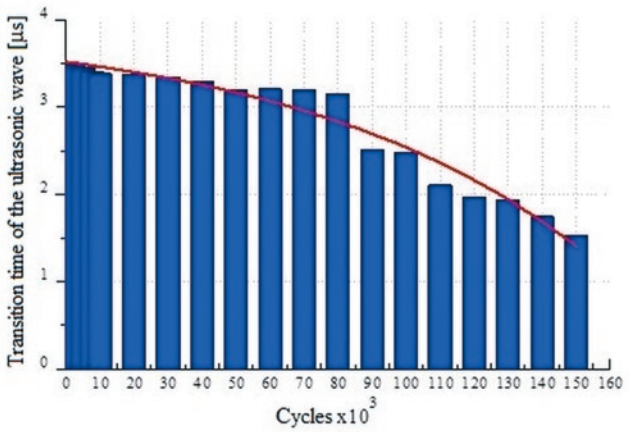

Fig. 6. Relation between the transition time of the ultrasonic wave and the number of fatigue cycles

where: t_u – transition time of the ultrasonic wave [µs], N – number of fatigue cycles.

As it can be observed in Fig. 6, in the first phase of degradation process, i.e. about 5×10^3 fatigue cycles, the transition time of the ultrasonic wave changes to a very limited extent. Micro-cracks that accompany the degradation process manifest moderate and even decrease in the transition time. More rapid change, in an individual case may be caused by the accumulation of discontinuities or delamination. In the diagram (Fig. 6) this effect is observed in the rapid form after about 80×10^3 number of cycles. The decrease is explained by the advancement level of the fatigue defects accumulation. Quantitative identification of established correlation may be assumed as diagnostic basis for the degree of exhaustion for the loading capacity of the examined materials.

2.3.2. Thermovision test

On the basis of thermovision temperature distribution on the external surface of the pipe obtained during the thermovision research (Fig. 7) the analysis was conducted which referred to the changes in the material condition, depending on the number of fatigue cycles. The analysis was conducted on the basis of designated changes in rate of heating and cooling. In figure 8, the pie charts of changes in the heating (Fig. 8a) and cooling rate (Fig. 8b) are shown for a chosen pipe subjected to the process of ageing-fatigue degradation after 30×10^3 of cycles. Area A, in which structural changes occur, was marked.

Figures 8 and 9 show the diagrams of changes in rate of heating and cooling observed in points 10 and 14 (clear cracks) of the same pipe. The results of its ultrasonic tests were presented in Fig. 3 and 4.

Obtained results were approximated by second degree polynomial. The changes in heating rate may be described:

- curve (a) in the area without delamination:

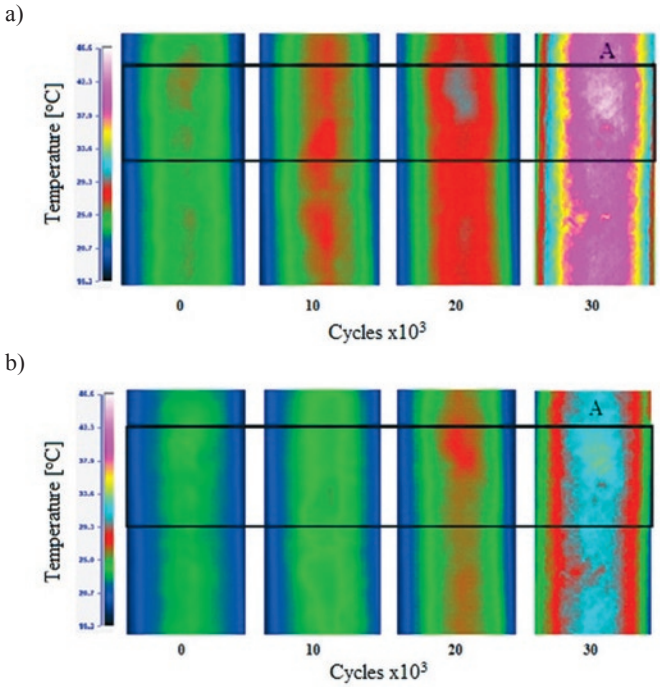

Fig. 7. Thermogram with the area of damage marked (A) in the course of (a) heating and (b) cooling process

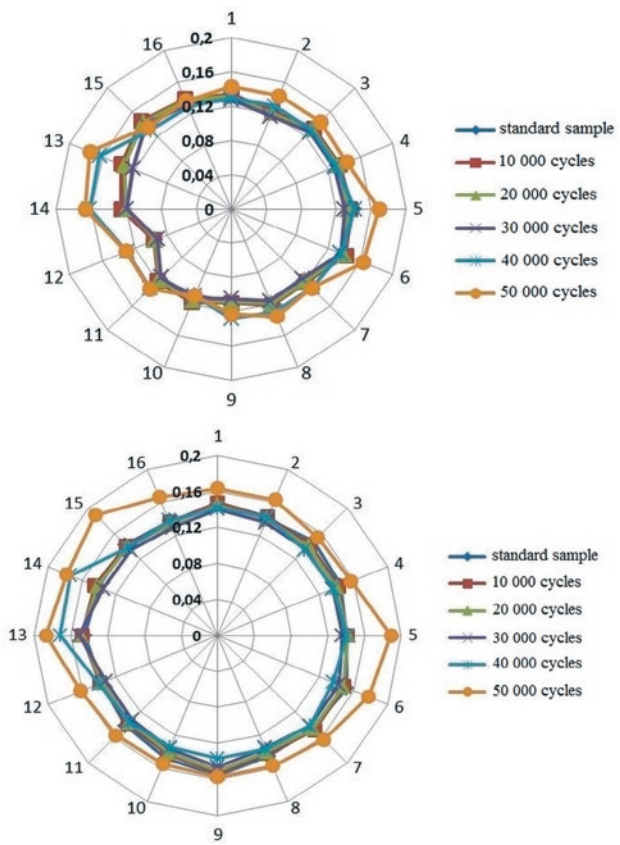

Fig. 8. Change of the heating a) and cooling b) rate, in the function of the number of fatigue cycles

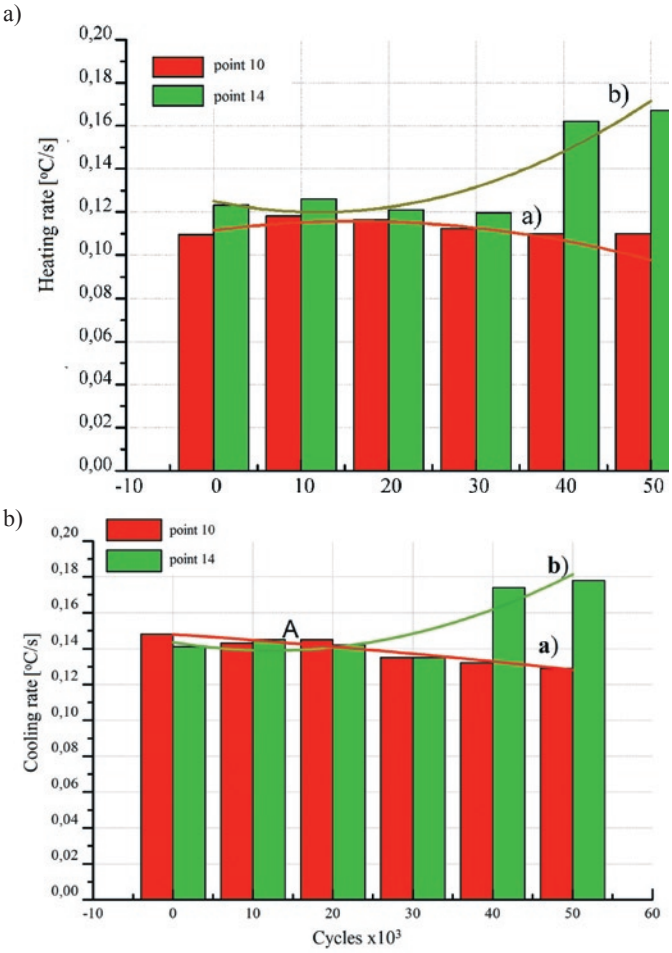

Fig. 9. Change of the heating a) and cooling b) rate, in the function of the number of fatigue cycles in points 10 (curve a) and 14 (curve b)

$$\mathbf{y} = 0.125 - 8.52\mathbf{e}^{-4}\mathbf{N} + 3\mathbf{e} - 5\mathbf{N}^2 \tag{5}$$

with the correlation coefficient R = 0.91.

- curve (b) in the area with clear macrocracks:

$$\mathbf{y} = 0.11 + 5.03\mathbf{e}^{-4}\mathbf{N} - 1.55\mathbf{e} - 5\mathbf{N}^2 \tag{6}$$

with the correlation coefficient R = 0.93,

The changes in the cooling rate are described as follows:

- curve (b) in the area without delamination:

$$\mathbf{y} = 0.15 - 2.77\mathbf{e}^{-4}\mathbf{N} - 3.17\mathbf{e} - 6\mathbf{N}^2 \tag{7}$$

with the correlation coefficient R = 0.99,

- curve (a) in the area with clear macrocracks:

$$\mathbf{y} = 0.14 - 7.43\mathbf{e}^{-4}\mathbf{N} + 3\mathbf{e} - 5\mathbf{N}^2 \tag{8}$$

with the correlation coefficient R = 0.88.

It was observed that the flaws in the shape of microcracks do not essentially influence the changes of examined thermal characteristics. As far as delamination and cracks are concerned, they result in rapid changes in both heating and cooling temperatures. It is mainly caused by the changes in thermal conductivity and specific heat, which in turn is indispensably connected with the appearance of structural flaws. In the quoted example, the areas (points 13-16, and 5-6) with clear cracks in composite layer could have been easily observed.

Due to discrepancies in the designated heating and cooling rate in the whole population of examined samples, in order to determine the value of given rate in the next phase of degradation, the analysis was conducted, concerning the frequency of occurrence with the described function, in compliance with Gauss' distribution. Figure 10 shows designated functions of occurrence frequency with reference to heating (Fig. 10a) and cooling (Fig.10b) rate for a pipe which was not subjected to degradation with coefficients respectively for a process:

- thermal activation: $\mathbf{y_0 = 6.80986}$, $\mathbf{x_c = 0.1179}$ **[°C/s], w = 0.01534 [°C/s], A = 4.58613 [°C/s].** Correlation coefficient equals R = 0.99,
- flow of heat after turning off the source of activation: $\mathbf{y_0 = 9.04342}$, $\mathbf{x_c = 0.17883}$ **[°C/s], w = 0.01706 [°C/s], A = 4.3785 [°C/s]**. Correlation coefficient equals R = 0.99.

The correlation coefficients presented in Fig. 10 were decreasing together with the progress of degradation process. It is a process similar to the one observed in case of the transition time of ultrasonic wave.

An important advantage of non-destructive thermovisual diagnostics is the posssibility of observing lad localize the flaws on the depth as early as at the stage conducting registration of temperature distribution. It is possible, among others, thanks to the temperature contrast principle [23]. The higher under the surface the flaw is located, the higher is the heating temperature. On the basis of the non-destructive thermovisual research conducted, the characteristics concerning the

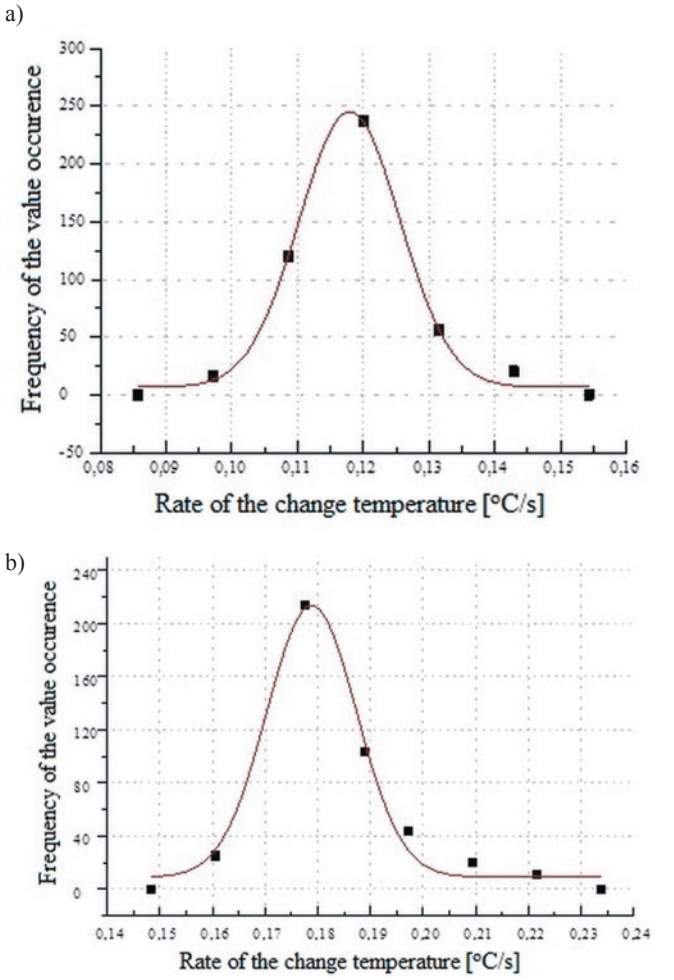

Fig. 10. Functions of occurence frequency with reference to the value of temperature changes in the process of (a) thermal activation and (b) cooling for the standard sample

changes in heating and cooling temperatures in the function of the number of cycles were created (Fig. 11). The dependence were approximated by the second degree polynomial, which has the following shape:

- for the heating phase:

$$\mathbf{v_n} = -1.36\mathbf{e}^{-6}\mathbf{N}^2 - 1.83\mathbf{e}^{-4}\mathbf{N} + 0{,}17 \tag{9}$$

with correlation coefficient **R = 0,97,**

- for the cooling phase:

$$\mathbf{v_{ch}} = -1.11\mathbf{e}^{-6}\mathbf{N}^2 - 1.43\mathbf{e}^{-7}\mathbf{N} + 0{,}12 \tag{10}$$

with correlation coefficient **R = 0,93.**

Higher rates were observed for the cooling process.

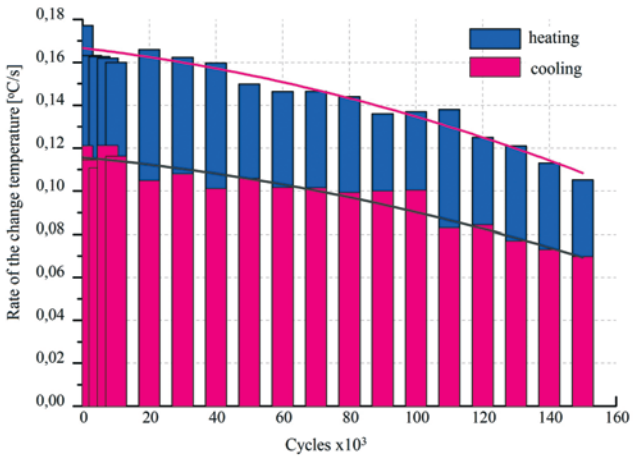

Fig. 11. Changes in heating and cooling rate in the function of the number of cycles

2.3.3. Water absorption research

The results of water absorption in the function of the cycles number is shown in Fig. 12. Water absorption in a given point is the average out of 15 values after rejecting the extreme ones. As it can be observed water absorption increases with the progress in the propagation of damage, which results from fatigue degradation.

The results were approximated by the exponential function in the following form:

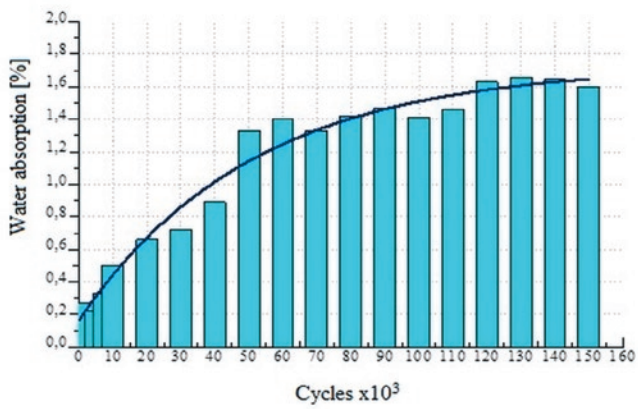

Fig. 12. Dependence of water absorption on the number of cycles

$$\mathbf{W} = 1.67 - 1.51\mathbf{e}^{-\mathbf{N}/46{,}66}, \tag{11}$$

with correlation coefficient R = 0.98.

The observed changes in water absorption may indirectly characterize the condition of the composite layer structure. The more defects within the volume of material, the higher is the water absorption, which was published, among others in work [21]. Microcracks appearing as a result of gradual joining, lead to creating bigger discontinuities which fulfill deformation criterion FPF (First Ply Failure) [1]. The accumulation of dissipated microcracks may lead to the cracks propagation which violate composite continuity. It is important from the point of view of strength properties of the tested material.

The differences observed in the course of researched characteristics result from the adopted methodology of research. In case of water absorption, clear increase in absorption value was notified for 50×10^3 of fatigue cycles (Fig. 12). It is caused by the deformation condition of pipes during ageing-fatigue research in accordance with Fig. 1. The samples were taken from the area with the largest deformation (Fig. 2a), and in connection with that, the biggest structural changes were notified, which are the effect of microcracks creating capillaries absorbing water.

In case of ultrasonic research, conducted with the use of the echo method, the ultrasonic wave deflects from the first discontinuity encountered. Taking into account the fact that the largest hoop stresses appear on the internal surface of the pipe, in compliance with the Huber's hypothesis, the destruction of layers occurs at that side. The clear shortening of transition time of the ultrasonic wave at 80×10^3 fatigue cycles is the effect of the flaws appearing from the side of internal surface (Fig. 6). This method however, requires the access to the examined object. The results of the thermovision research confirm the structural changes in the material, however, the point of clear decrease in the heating or cooling rate cannot be decidedly determined (Fig. 11). Macro-defects cause significant increase in the rate of heating or cooling (Fig. 9).

4. Conclusions

On the basis of the conducted research we can conclude that:

1. The transition time of the ultrasonic wave was in decrease together with the number of fatigue cycles. The applied echo method, taking advantage of longitudinal wave, allows identification of discontinuities appearing in plane which is perpendicular in relation to the direction of ultrasonic wave propagation.
2. Changes in the heating and cooling rate, thermovisually registered (by the reflection method) in the adopted measurement conditions were in decrease together with the increase in the number of cycles. The main cause of such a phenomenon is the process of discontinuities accumulation which leads to delamination. The structural changes cause lowering of composite thermal properties (e.g. thermal conductivity coefficient).
3. In the area of macro defects the rapid shortening of ultrasonic wave trasition time occurs, which is not observed in case of micro discontinuities appearing gradually. Both the heating and cooling rate in the area of microdefects are in decrease. The process of microcracks accumulation leading to delamination in the final stage, results in the rapid increase of measured thermovision values.
4. Distribution of measured thermovisual and ultrasonic values on the pipe circuit (Fig. 3 and 8) are comparable and allow identification of the areas exposed to destruction.
5. For the appropriate evaluation of the polymer composites degradation level, non-destructive tests should be conducted by means of at least two methods, and the results should refer

to standard sample, not subjected to the process of ageing-fatigue degradation.

6. The effect of progressing ageing-fatigue process of composite pipe shells were discontinuities in the structure, which resulted, first of all, fatigue load. Those defects influenced the increased water absorption in the examined composite. Water absorption in the final stage amounted to about 1.6%.

References

1. Bamford C.H. Degradation of polymers. Serie: Comprehensive chemical kinetic, Vol. 14 New York: Elsevier, 1975.
2. Brondsted P., Andersen S.I., Lilholt H. Fatigue performance of glass/polyester laminates and the monitoring of material degradation. Mechanics of Composites Materials 1996; 32 (1): 21-29, http://dx.doi.org/10.1007/BF02254644.
3. Gholizadeh S. A review of non-destructive testing methods of composites materials. Procedia Structural Integrity, 2016; 1:50-57, http://dx.doi.org/10.1016/j.prostr.2016.02.008.
4. Hasin Z., Rotem A. A cumulative - damage theory of fatigue failure. Materials Science and Engineering 1978; 34(2): 147-160, http://dx.doi.org/10.1016/0025-5416(78)90045-9.
5. Huang G., Sun A. Effect of water absorption on the mechanical properties of glass/polyester composites. Materials and Design 2007; 28(5):1647-1650, http://dx.doi.org/10.1016/j.matdes.2006.03.014.
6. Imielińska K., Wojtyra R.: Wpływ absorpcji wody na własności laminatów winyloestrowych wzmocnionych włóknem aramidowym i szklanym. Kompozyty - Composites 2003; 3(7): 192-197.
7. Jakubowicz A., Orłoś Z. Wytrzymałość materiałów. Warszawa: Wydawnictwo Naukowo Techniczne, 1981.
8. Katunin A. Degradacja cieplna laminatów polimerowych. Radom: Wydawnictwo Instytutu Technologii Eksploatacji Państwowego Instytutu Badawczego, Seria Biblioteka Problemów Eksploatacji nr 2326, 2012.
9. Kokan D. Development of an Improved Filament-Winding Process Model. Georgia Institute of Technology: Doctors Thesis, 1997.
10. Martin R. Ageing of composites. Cambridge: Woodhead Publishing Limited, 2008.
11. Mertiny P., Ellyin F. Influence of the filament winding tension on physical and mechanical properties of reinforced composites. Composites: Part A 2002; 33: 1615 - 1622, http://dx.doi.org/10.1016/S1359-835X(02)00209-9.
12. Mouzakis D.E., Zoga H., Galiotis C. Accelerated environmental ageing study of polyester/glass fiber reinforced composites (GFRPCs). Composites Part B 2008; 39 (3): 467-475, http://dx.doi.org/10.1016/j.compositesb.2006.10.004.
13. Peters S.T. Composite Filament Winding. Ohio: ASM International, 2011.
14. PN-ISO: Rury i kształtki z termoplastycznych tworzyw sztucznych – Chłonność wody – Ogólna metoda badania.
15. Stabik J. Ageing of laminates in boiling NaCl water solution. Polymer Testing 2005; 24 (1): 101-103, http://dx.doi.org/10.1016/j.polymertesting.2004.06.004.
16. Staszewski W., Boller Ch., Tomlinson G.: Health monitoring of aerospace structures, John Willey & Sons, Chichester, 2004, ISBN 9780470092866.
17. Szymiczek M., Wróbel G., Rojek M., Czapla T. Simulation diagnostics of the polyester-glass pipes degradation process; experimental basis. Journal of Achievements in Materials and Manufacturing Engineering 2013; 59 (1): 37-47.
18. Talreja R. Fatigue-induced damage mechanisms in carbon fibre-reinforced plastic composites, Proceedings of the Royal Society of London. Series A, Mathematical and Physical Sciences 1981; 378 (1775): 461-475, http://dx.doi.org/10.1098/rspa.1981.0163.
19. Walczak K., Mamos J. Wytrzymałość zmęczeniowa rur laminowanych GRP stosowanych w górnictwie. Kompozyty - Composites 2004; 4 (10): 194-199.
20. Więcek B., De Mey G. Termowizja w podczerwieni. Podstawy i zastosowania. Warszawa: Wydawnictwo PAK, 2011.
21. Wróbel G., Szymiczek M.: Wykorzystanie własności łańcucha Markowa w analizie procesu degradacji nośnych rur poliestrowych wzmocnionych włóknem szklanym. Zeszyty Naukowe Wyższej Szkoły Oficerskiej Sił Powietrznych w Dęblinie, 2015, 4(27): 155-168.
22. Wróbel G., Szymiczek M., Rojek M. Charakterystyki cieplne w diagnostyce zmian starzeniowo - zmęczeniowych powłok kompozytowych. Przetwórstwo Tworzyw, 2014, 1: 110-115.
23. Wysocka-Fotek O. Szacownie wielkości i położenia defektów podpowierzchniowych za pomocą impulsowej termografii podczerwieni. Instytut Podstawowych Problemów Techniki Polskiej Akademii Nauk: Rozprawa doktorska, 2012.
24. Zhu Y.K., Tian G.Y., Lu R.S., Zhang H. A review of optical NDT technologies. Sensors 2011; 11:7773-7798, http://dx.doi.org/10.3390/s110807773.

Małgorzata SZYMICZEK
Department of Theoretical and Applied Mechanics
Silesian University of Technology
ul. Konarskiego 18A, 44-100 Gliwice, Poland
E-mail: malgorzata.szymiczek@polsl.pl

Article citation info:
RODRÍGUEZ-PICÓN LA. Reliability assessment for systems with two performance characteristics based on gamma processes with marginal heterogeneous random effects. Eksploatacja i Niezawodnosc – Maintenance and Reliability 2017; 19 (1): 8–18, http://dx.doi.org/10.17531/ein.2017.1.2.

Luis Alberto RODRÍGUEZ-PICÓN

RELIABILITY ASSESSMENT FOR SYSTEMS WITH TWO PERFORMANCE CHARACTERISTICS BASED ON GAMMA PROCESSES WITH MARGINAL HETEROGENEOUS RANDOM EFFECTS

OCENA NIEZAWODNOŚCI SYSTEMÓW O DWÓCH PARAMETRACH UŻYTKOWYCH OPARTA NA PROCESACH GAMMA Z BRZEGOWYMI NIEJEDNORODNYMI EFEKTAMI LOSOWYMI

In this paper, a reliability modeling approach for products with two performance characteristics related to two degradation processes is developed. The joint modeling of such processes is performed by using a copula function in order to consider the dependence structure between degradation processes. The proposed approach considers that different random effects affect the stochastic behavior of each performance characteristic. For such approach, different bivariate models with marginal gamma processes with heterogeneous random effects as marginal distributions are considered. As the random effects may differ between performance characteristics, different modifications of the structure of the parameters of the gamma process are proposed. Such that the random effects affect both the drift and diffusion, just the drift, and just the diffusion of the marginal gamma processes. The statistical inference of the joint bivariate models is performed via Bayesian approach. The obtained results show that a bivariate model with heterogeneous random effects has a slight better performance among the proposed models. Which implies that the bivariate heterogeneous random effects gamma process models may provide a better approach to model multivariate degradation data, and thus a better reliability assessment of the product under study.

***Keywords**: degradation, gamma process, random effect, heterogeneous effect, copula function.*

W niniejszym artykule opracowano sposób modelowania niezawodności produktów posiadających dwa parametry użytkowe związane z dwoma procesami degradacji. Procesy takie można modelować łącznie wykorzystując funkcję kopuły, która pozwala na analizę struktury zależności między procesami degradacji. Proponowane podejście zakłada, że na stochastyczne zachowanie każdego z parametrów użytkowych wpływają różne efekty losowe. Przy takim założeniu, należy wziąć pod uwagę różne modele dwuwymiarowe, w których rozkłady brzegowe są brzegowymi procesami gamma z niejednorodnymi efektami losowymi. Jako że efekty losowe mogą być odmienne dla różnych parametrów użytkowych, zaproponowano różne modyfikacje struktury parametrów procesu gamma, takie, że efekty losowe wpływają zarówno na dryf jak i dyfuzję, tylko na dryf, lub tylko na dyfuzję procesów brzegowych gamma. Wnioskowanie statystyczne dla wspólnych modeli dwuwymiarowych przeprowadzono metodą Bayesa. Uzyskane wyniki pokazują, że dwuwymiarowy model z niejednorodnymi efektami losowymi ma nieznaczną przewagę nad pozostałymi zaproponowanymi modelami. Oznacza to, że dwuwymiarowe modele procesu gamma z niejednorodnymi efektami losowymi mogą stanowić lepszy sposób modelowania wielowymiarowych danych degradacyjnych, tym samym umożliwiając lepszą ocenę niezawodności badanego produktu.

***Słowa kluczowe**: degradacja, proces gamma, efekt losowy, efekt niejednorodny, funkcja kopuły.*

1. Introduction

In recent years, important developments have been presented in the area of reliability inference of products and systems based on degradation models. Such models are important tools to obtain reliability information when few failure data is available [11], and consists in analyzing the gradual deterioration in performance of a performance characteristic (PC), also known as degradation process, in terms of the accumulated damage over time [27]. For some products, a failure would be defined at a specified critical level of degradation, which means that the product may not stop working completely as in the case of hard failures, but be defined when the cumulative degradation path crosses the critical level of degradation; such failures are known as soft failures. In general, if a failure can be defined in terms of a specified critical level of degradation it is possible to obtain a reliability assessment based on degradation process models [12]. Based on this, a modeling approach for degradation processes may consist in relating the degradation over time with a continuous stochastic process such that it is possible to describe the failure generating mechanisms.

For certain PC, the desirable properties that a model must have to describe its degradation process are that the degradation process should always be positive and strictly increasing. In this paper, the gamma process is considered as a model to govern the degradation process of certain PC, given the characteristics that its increments are independent and non-negative having a gamma distribution that results in an always positive, strictly increasing stochastic process. As performance can only decrease over time, this is why it is considered to be suitable to model wear, crack growth, corrosion, consumption, fatigue, erosion, or any PC [16]. Some important applications of the gamma process in the reliability assessment of products can be found in Bagdonavicius and Nikulin [2], Park and Padgett [22], and Bagdonavicius and Nikulin [3].

However, in most of the degradation processes, it can be found that the degradation of a product's characteristic is affected by different sources of variation. Which implies that the degradation in a product population has a large variation due to some unobservable effects. These effects are described by the variation in the degradation increments over time for every specific product's degradation path and the different behaviors of the degradation paths for every product, i.e., the degradation rate. The simple gamma process is unable to capture such variations. However, these variations have been well modeled by incorporating random effects into the gamma process. Lawless and Crowder [10] considered that the scale parameter of the gamma process have different realizations among products, and let the parameter to be random following a gamma distribution. Different applications of this model can be found in Tsai et al. [29], Wang et al. [30], Wang [32], and Pulcini [25]. In the classical random effects gamma process model it can be noted that both the mean and variance of the process are affected by the random effect parameter, which results in a degradation process with random drift and random diffusion. Nevertheless, for some products it may be the case that the degradation paths are just characterized by a random drift or just a random diffusion.

Another important aspect to consider is that the functionality of a product may be related to multiple PC. In such cases, it is important to consider multivariate models to obtain robust reliability estimates. Some important applications of multivariate gamma processes in reliability analysis have been presented by Hao et al. [9], Pan and Balakrishnan [18], Pan and Balakrishnan [19], Pan et al. [20], Pan et al. [21], Park and Padgett [23], Sari et al. [26], Wang et al. [31], and Zhou et al. [36]. In most of the multivariate degradation models, it is considered that each of the multiple PC are governed by a univariate stochastic gamma process and then the joint model is obtained via copula functions. By modeling with copula functions, the independence assumption is not assumed. Indeed it can be tested by considering the association parameter of the copula function [8], which makes the copula modeling approach quite attractive. In addition, most of the developed works do not consider random effects in the modeling [18-21, 26, 36]. Random effects are an important aspect to consider in the degradation modeling of almost any product under study, given that most of the time there is a substantial subject-to-subject variability among the degradation processes of different individuals [33]. Which, accounts to describe the individual variability that determines the heterogeneity among the degradation paths of different product units, also known as individual variability [35].

Considering that a product may consist in multiple PC and that random effects affect in different ways the multiple PC. It result important to develop multivariate models with heterogeneous random effects. Furthermore, each PC may experience different sources of variation, which means that the random effects may be characterized in different ways in the degradation paths. For example, the degradation paths of a PC 1 may be characterized by a large variation of the degradation rate and a low variation of the within degradation increments, and the degradation paths of a second PC may be characterized by both a large variation of the degradation rate and the within degradation increments. It is important to consider such scenarios when dealing with the degradation modeling. The importance relies on describing the heterogeneous behavior of the multiple PC degradation in terms of their best fitting stochastic gamma process with random effects to obtain robust reliability assessments. Hao et al. [9] and Wang et al. [31] developed bivariate gamma processes with random effects, however they only considered the classical gamma process with random effects as marginal distributions. The classical gamma process with random effects consider that the scale parameter is random, which means that the mean and variance of the gamma process are affected by the random effects parameter. This results in processes with random drift and random diffusion. In this paper, we model the degradation processes of two PC considering an Archimedean copula function and different gamma processes with heterogeneous random effects as marginal distributions. This, by proposing different modifications of the structure of the parameters of the marginal gamma processes, such that a random drift and a random diffusion gamma process models are obtained. A time-scale monotone transformation is considered to assure that degradation is a linear function of time [34]. As the joint distributions are complex, the estimation of the parameters is performed via Gibbs sampling and Markov chain Monte Carlo (MCMC) implemented in OpenBUGS. The models are illustrated with the reliability assessment of a case study that consists of crack propagation data of two terminals of an electronic device.

The rest of the paper is organized as follows. Section 2 presents the simple gamma process and the bivariate modeling based on two PC. In Section 3, the different gamma processes with random effects for two PC are introduced. Section 4 presents the bivariate modeling based on the Frank copula function, and the heterogeneous random effects models are defined. Section 5 deals with inference method for the bivariate degradation model with random effects. Section 6 addresses the implementation of the proposed models in a fatigue-crack growth dataset. Finally, in Section 7 some concluding remarks are provided.

2. Gamma process for two performance characteristics

Considering a non-negative-valued process $\{Z(t),t>0\}$, where $Z(t)$ represents the measured degradation for an individual unit at time t, then the gamma process has the following properties: (a) $Z(t+\Delta t)-Z(t)=\Delta Z(t)$ follows a gamma distribution $Ga(v[\tau(t+\Delta t)-\tau(t)],u)$, and (b) $Z(t)$ has independent increments, $Z(t_4)-Z(t_3)$ and $Z(t_2)-Z(t_1)$ are independent $\forall t_1<t_2<t_3<t_4$.

Now, let $v(\tau(t))$ be a non-negative shape parameter with a time scale transformation in the form of $\tau(t,\gamma)=t^{\gamma}$, thus $\Delta\tau(t)=\tau(t+\Delta t)-\tau(t)$, $t\geq 0$, $v(0)\equiv 0$, and $u>0$ be a scale parameter. Then, $Z(t),t>0$ is governed by a gamma process with the parameters described above. Thus, the gamma process $Ga(v(\Delta\tau(t)),u)$ describes the degradation level of some characteristic at time t, and has a mean $v(\Delta\tau(t))/u$ and variance $v(\Delta\tau(t))/u^2$, the probability density function (PDF) of $\Delta Z(t)$ is given by:

$$f_{\mathcal{G}a}\left(\Delta Z(t)v,\gamma,u\right)=\frac{u^{v(\Delta\tau(t))}\Delta Z(t)^{v(\Delta\tau(t))-1}}{\Gamma\left(v\left(\Delta\tau(t)\right)\right)}\exp\left\{-u\Delta Z(t)\right\} \quad (1)$$

where $\Gamma(a)=\int_0^{\infty}t^{a-1}e^{-t}dt,\quad a>0$ is the gamma function.

Considering that the degradation process of a certain product is governed by a gamma process, a failure of the product is said to have occurred the moment when the degradation path $Z(t)$ crosses a critical level of degradation ω. Known also as the first-passage time. Thus, the first-passage time is defined as $T_{\omega}=\inf\{t_{\omega}:Z(t)\geq\omega\}$. The cumulative distribution function (CDF) of t_{ω} con be obtained as $P\left(Z(t)\geq\omega\right)=1-F_{\mathcal{G}a}\left(\omega,v(\Delta\tau(t)),u\right)$ or as:

$$P\left(Z(t)\geq\omega\right)=\int_{\omega}^{\infty}f_{Z(t)}(z)dz=\frac{\Gamma\left(v(\tau(t_{\omega})),\omega u\right)}{\Gamma\left(v(\tau(t_{\omega}))\right)} \quad (2)$$

where $\Gamma(v(\tau(t\omega)),\omega u)$ is the upper incomplete gamma function defined by $\Gamma\left(v(\tau(t_{\omega})),\omega u\right)=\int_{\omega u}^{\infty}\vartheta^{v(\tau(t_{\omega}))-1}e^{-\vartheta}d\vartheta$.

Now consider that a product has two PC and that are marginally governed by a gamma process with a time-scale transformation.

Also considering a degradation test (DT) with the next characteristics: N units are tested and M measurements for all the units are observed up to the termination time T, which results in degradation measurements $Z_{ik}(t_j)$ of the ith unit at the corresponding time t_j, i=1,2,…,N,j=1,2,…,M, and k=1,2 PC. Then, the degradation data can be presented as follows:

$$X_{2N\times M}=\begin{pmatrix} Z_1 \\ Z_2 \end{pmatrix}=\begin{pmatrix} Z_{11}(t_1) & \cdots & Z_{11}(t_M) \\ \vdots & \ddots & \vdots \\ Z_{N1}(t_1) & \cdots & Z_{N1}(t_M) \\ Z_{12}(t_1) & \cdots & Z_{12}(t_M) \\ \vdots & \ddots & \vdots \\ Z_{N2}(t_1) & \cdots & Z_{N2}(t_M) \end{pmatrix} \tag{3}$$

According to the independent increment property of the gamma process, and $\Delta Z_{ik}(t_j)=Z_{ik}(t_j)-Z_{ik}(t_{j-1}), t_0=0, \Delta\tau(t_j,\gamma_k)=-\tau(t_{j-1},\gamma_k)=t_j^{\gamma_k}-t_{j-1}^{\gamma_k}$, , for i=1,2,…,N,j=1,2,…,M, and k=1,2 PC. Thus, it is possible to obtain independent random variables $\Delta Z_{ik}(t_j) \sim Ga(v_k(\Delta\tau(t_j,\gamma_k)),u_k)$, with the next PDF and CDF:

$$f_{Ga}\left(\Delta Z_{ik}(t_j)v_k,\gamma_k,u_k\right)=\frac{u_k^{v_k(\Delta\tau(t_j,\gamma_k))}\Delta Z_{ik}(t_j)^{v_k(\Delta\tau(t_j,\gamma_k))-1}}{\Gamma\left(v_k(\Delta\tau(t_j,\gamma_k))\right)}\exp\left\{-u_k\Delta Z_{ik}(t_j)\right\} \tag{4}$$

$$F_{Ga}\left(\Delta Z_{ik}(t_j)v_k,\gamma_k,u_k\right)=\frac{\zeta\left(v_k(\Delta\tau(t_j,\gamma_k)),u_k\Delta Z_{ik}(t_j)\right)}{\Gamma\left(v_k(\Delta\tau(t_j,\gamma_k))\right)} \tag{5}$$

where $\zeta\left(v_k(\Delta\tau(t_j,\gamma_k)),u_k\Delta Z_{ik}(t_j)\right)=\int_0^{u_k\Delta Z_{ik}(t_j)} t^{v_k(\Delta\tau(t_j,\gamma_k))-1}e^{-t}dt$ is the lower incomplete gamma function, i=1,2,…,N,j=1,2,…,M, and k=1,2 PC. If ω_k is the critical degradation level of each PC for k=1,2. Then the CDF of t_{ω_k} can be obtained from (2) as $P(Z_{ik}(t_j)\geq\omega_k)$.

3. Gamma processes with random effects

Considering that the sampled product under study may experience different sources of variation during its operation, it results appropriate to incorporate product-to-product variability in the modeling of the degradation processes. In this case, it is assumed that γ_k and v_k are fixed parameters that are common to all products. The random effects are introduced by letting that u_k be a random parameter that follows a gamma distribution representing the heterogeneity among different products. Considering that, a product has two performance characteristics whose degradation have been observed during a DT with degradation measurements $Z_{ik}(t_j)$ of the ith unit at the corresponding time t_j, i=1,2,…,N,j=1,2,…,M, and k=1,2 PC. Then, the gamma process with random effects (RE) for k=1,2 can be written as $\Delta Z_{ik}(t_j)\sim Ga(v_k(\Delta\tau(t_j,\gamma_k)),u_k)$,$u_k\sim Ga(\delta_k,\varphi_k)$,$u_k>0$. Thus, u_k is a random parameter with mean δ_k/φ_k and variance δ_k/φ_k^2 with PDF defined as follows:

$$f_{Ga}(u_k\mid\delta_k,\varphi_k)=\frac{\varphi_k^{\delta_k}u_k^{\delta_k-1}}{\Gamma(\delta_k)}\exp\{-u_k\varphi_k\} \tag{6}$$

Thus, the PDF of the degradation increments $\Delta Z_{ik}(t_j)$ of the ith unit at the corresponding time t_j, i=1,2,…,N,j=1,2,…,M,k=1,2 is given by:

$$f_{RE}\left(\Delta Z_{ik}(t_j)\right)=\int_0^\infty f_{Ga}\left(\Delta Z_{ik}(t_j)v_k\Delta\tau(t_j,\gamma_k),u_k\right)f_{Ga}(u_k\delta_k,\varphi_k)du_k$$

$$=\frac{\Gamma\left(v_k(\Delta\tau(t_j,\gamma_k))+\delta_k\right)}{\Gamma\left(v_k(\Delta\tau(t_j,\gamma_k))\right)\Gamma(\delta_k)}\frac{\varphi_k^{\delta_k}\Delta Z_{ik}(t_j)^{v_k(\Delta\tau(t_j,\gamma_k))-1}}{\left(\varphi_k+\Delta Z_{ik}(t_j)\right)^{v_k(\Delta\tau(t_j,\gamma_k))+\delta_k}} \tag{7}$$

According to Lawless and Crowder [10], for any fixed t, the random variable $Y_{ik}(t_j)=(\delta_k\Delta Z_{ik}(t_j))/(\varphi_k v_k(\Delta\tau(t_j,\gamma_k)))$ follows an F-distribution with $2v_k\Delta\tau(t_j,\gamma_k)$ and $2\delta_k$ degrees of freedom, thus, the CDF of $\Delta Z_{ik}(t_j)$ is defined as:

$$F_{RE}\left(\Delta Z_{ik}(t_j)\right)=P\left(Y_{ik}(t_j)\leq\frac{\delta_k\Delta Z_{ik}(t_j)}{\varphi_k v_k(\Delta\tau(t_j,\gamma_k))}\right)$$

$$=F_{2v_k(\Delta\tau(t_j,\gamma_k)),2\delta_k}\left(\frac{\delta_k\Delta Z_{ik}(t_j)}{\varphi_k v_k(\Delta\tau(t_j,\gamma_k))}\right) \tag{8}$$

Taking into account (8), then the CDF of the lifetime when any of the degradation paths of the k=1,2 PC reach the respective critical level ω_k is defined as $t_{\omega_k}=\inf\left\{T_{\omega_k}:Z_k(t)\geq\omega_k\right\}$. The CDF of t_{ω_k} con be obtained as:

$$F(t_{\omega_k})=1-F_{2v_k(\tau(t_{\omega_k},\gamma_k)),2\delta_k}\left(\frac{\delta_k\omega_k}{\varphi_k v_k(\tau(t_{\omega_k},\gamma_k))}\right) \tag{9}$$

Given that the means $(v_k(\Delta\tau(t_j,\gamma_k)))/u_k$ and variances $(v_k(\Delta\tau(t_j,\gamma_k)))/(u_k^2)$ of the respective k=1,2 gamma processes are affected by the random effects parameters u_k. It is expected that, the degradation rates of the degradation paths tend to have a larger dispersion in both processes. In addition, it is also expected that the variances of the degradation observations within each unit of both processes tend to be large. Figure 1 provides pseudo-random paths of the gamma degradation process under the RE model. However, it may be the case that for some products, both PC present only large dispersions of the degradation rates or that only present large variances of the degradation observations within each unit.

A modification of the parameters' structure of the gamma processes is proposed as $Z_{ik}(t_j)\sim Ga(\eta_k(\Delta\tau(t_j,\gamma_k))u_k,u_k)$ with u_k following a gamma distribution. The degradation means and variances of this model can be obtained as $\eta_k(\Delta\tau(t_j,\gamma_k))$ and $(\eta_k(\Delta\tau(t_j,\gamma_k)))/u_k$, respectively. It can be noted that only the variances are affected by the random parameter u_k. Thus, the gamma process with random diffusion (RV) results in $\Delta Z_{ik}(t_j)\sim Ga(\eta_k(\Delta\tau(t_j,\gamma_k))u_k,u_k)$,$u_k\sim Ga(\delta_k,\varphi_k)$,$u_k>0$, with PDF described as:

$$f_{RV}\left(\Delta Z_{ik}(t_j)\mid\eta_k,\gamma_k,\delta_k,\varphi_k\right)=\int_{u_k>0}f_{Ga}\left(\Delta Z_{ik}(t_j)\mid\eta_k(\Delta\tau(t_j,\gamma_k))u_k,u_k\right)f_{Ga}(u_k\mid\delta_k,\varphi_k)du_k$$

$$=\int_{u_k>0}\frac{u_k^{\eta_k(\Delta\tau(t_j,\gamma_k))u_k+\delta_k-1}\Delta Z_{ik}(t_j)^{\eta_k(\Delta\tau(t_j,\gamma_k))u_k-1}\varphi_k^{\delta_k}}{\Gamma\left(\eta_k(\Delta\tau(t_j,\gamma_k))u_k\right)\Gamma(\delta_k)}\exp\left\{-u_k\left(\Delta Z_{ik}(t_j)+\varphi_k\right)\right\}du_k \tag{10}$$

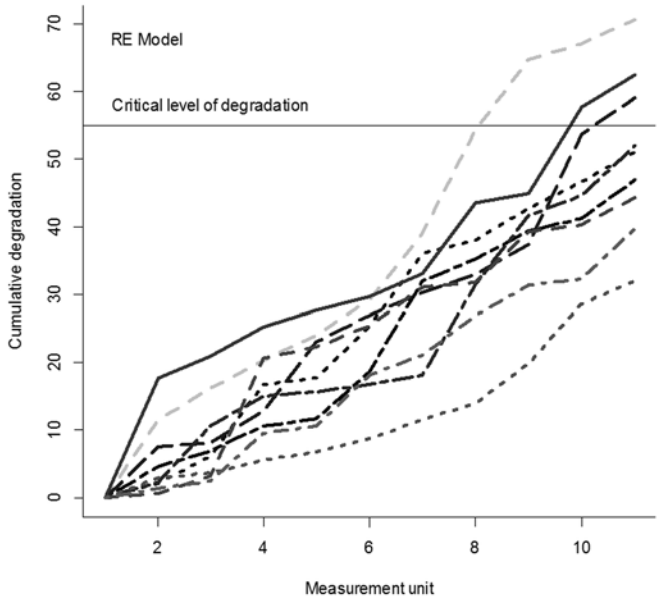

Fig. 1. Pseudo-random paths of the gamma degradation process under the RE model

The CDF of the lifetime when the degradation paths of any of the PC for k=1,2 reach a critical level ω_k is defined as $t_{\omega_k} = \inf\left\{T_{\omega_k} : Z_k(t) \geq \omega_k\right\}$ and it is obtained in the same way as:

$$\int_{u_k>0} \left\{ \frac{\Gamma\left(\eta_k\left(\tau\left(t_j,\gamma_k\right)\right)u_k, \omega_k u_k\right)}{\Gamma\left(\eta_k\left(\tau\left(t_j,\gamma_k\right)\right)u_k\right)} \right\} \frac{\varphi_k^{\delta_k} u_k^{\delta_k - 1}}{\text{“}\left(\delta_k\right)} \times \exp\left\{-u_k\varphi_k\right\} du_k \quad (11)$$

As random effects are involved in the scale parameter u_k of the RV model, it is expected that the variance of the degradation observations within each unit to be significant. However, a low level of variation in the degradation rates may be observed. Thus, the RV model is suitable for the degradation modeling of products for which overall degradation rate is low and a large unit-specific degradation variation exists. Figure 2 provides pseudo-random paths of the gamma degradation process under the RV model.

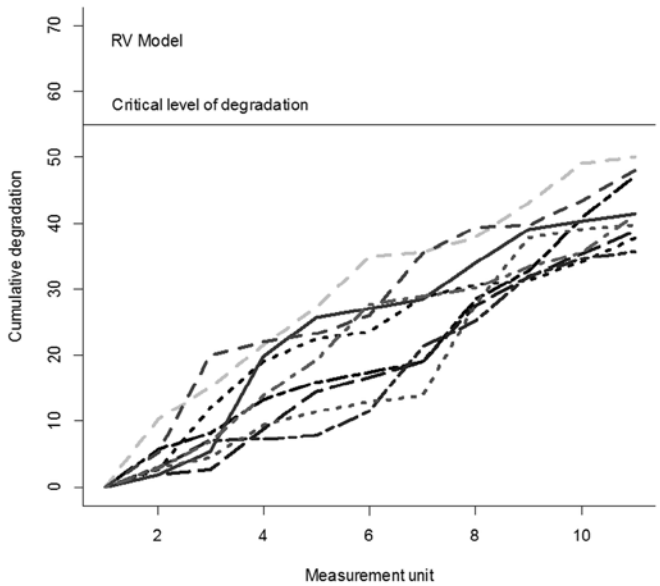

Fig. 2. Pseudo-random paths of the gamma degradation process under the RV model

A second modification of the structure of the parameters of the gamma process is proposed as $Z_{ik}\left(t_j\right) \sim Ga\left(\zeta_k\left(\Delta\tau\left(t_j,\gamma_k\right)\right)u_k^2, u_k\right)$, the degradation means and variances of this model are defined as $\zeta_k(\Delta\tau(t_j,\gamma_k))u_k$ and $\zeta_k\Delta(\tau(t_j,\gamma_k))$, respectively. Again, if u_k follows a gamma distribution, only the means are affected by the random effects parameters. Thus, the random drift gamma process (RD) for k=1,2 PC results in $\Delta Z_{ik}\left(t_j\right) \sim Ga\left(\zeta_k\left(\Delta\tau\left(t_j,\gamma_k\right)\right)u_k, u_k\right), u_k \sim Ga\left(\delta_k,\varphi_k\right), u_k > 0$, with PDF described as:

$$f_{RD}\left(\Delta Z_{ik}\left(t_j\right)_k \mid \zeta_k,\gamma_k,\delta_k,\varphi_k\right) = \int_{u_k>0} f_{Ga}\left(\Delta Z_{ik}\left(t_j\right) \mid \zeta_k\left(\Delta\tau\left(t_j,\gamma_k\right)\right)u_k^2, u_k\right) f_{Ga}\left(u_k \mid \delta_k,\varphi_k\right) du_k$$
$$= \int_{u_k>0} \frac{u_k^{\zeta_k\left(\Delta\tau\left(t_j,\gamma_k\right)\right)u_k^2+\delta_k-1} \Delta Z_{ik}\left(t_j\right)^{\zeta_k\left(\Delta\tau\left(t_j,\gamma_k\right)\right)u_k^2-1} \varphi_k^{\delta_k}}{\Gamma\left(\zeta_k\left(\Delta\tau\left(t_j,\gamma_k\right)\right)u_k^2, u_k\right)\Gamma\left(\delta_k\right)} \times \exp\left\{-u_k\left(\Delta Z_i\left(t_j\right)+\varphi_k\right)\right\} du_k \quad (12)$$

The CDF of the lifetime when the degradation paths of any of the degradation paths for k=1,2 reach a critical level ω_k is defined as $t_{\omega_k} = \inf\left\{T_{\omega_k} : Z_k(t) \geq \omega_k\right\}$ and it is obtained in the same way as:

$$P\left(Z_{ik}\left(t_j\right) \geq \omega_k\right) = \int_{u>0} \left\{ \frac{\Gamma\left(\zeta_k\left(\tau\left(t_j,\gamma_k\right)\right)u_k^2, \omega_k u_k\right)}{\Gamma\left(\zeta_k\left(\tau\left(t_j,\gamma_k\right)\right)u_k^2\right)} \right\} \frac{\varphi_k^{\delta_k} u_k^{\delta_k-1}}{\Gamma\left(\delta_k\right)} \times \exp\left\{-u_k\varphi_k\right\} du_k \quad (13)$$

Because random effects are considered in the parameters u_k, the means of the RD gamma process varies to a certain level. It leads to a larger dispersion of the degradation rates, which is reflected in larger variations of the first-time passage distributions. Thus, this model is appropriate for the modeling of the degradation of products in which significant variation of the degradation rate within the products' samples is observed. In Figure 3, a set of pseudo-random paths of the gamma degradation process under RD model are illustrated.

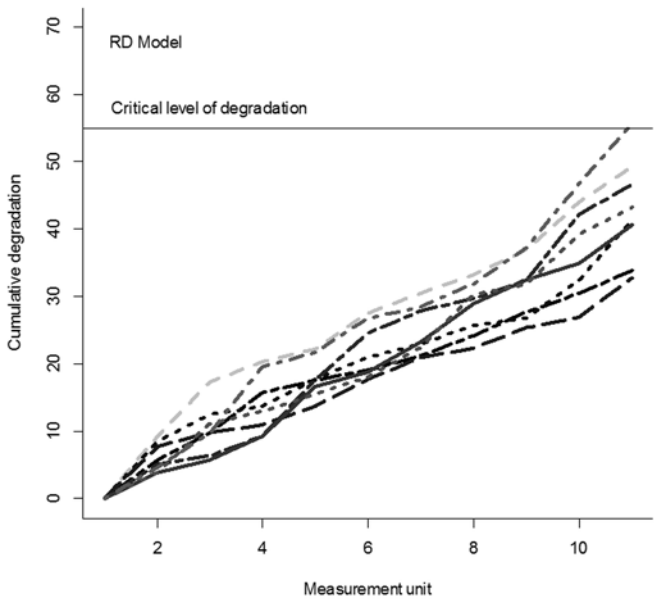

Fig. 3. Pseudo-random paths of the gamma degradation process under the RD model

4. Bivariate modeling with copula functions

Supposing that the degradation process of k=1,2 PC are observed for i=1,2,…,N units and j=1,2,…,M observations are recorded at specified times t_j for each degradation process. Now consider that, stochastic gamma processes govern the degradation process of each PC as $f_{\mathcal{G}a}\left(\Delta Z_{ik}\left(t_j\right)\right)$. In this paper, it is considered that the dependence structure between degradation processes k=1,2 is described by a copula function in the form $H(x,y)=C\{F(x),G(y)\}$. Where, $F(x)$,$G(y)$ are two marginal CDF and x,y are two random variables. If $H(x,y)$ is a joint distribution with marginal distributions $F(x)$ and $G(y)$, then there exists a unique copula C for x,y [15]. Thus, a bivariate copula is a CDF defined in $[0,1]^2$ with uniform marginal distributions [0,1]. In this case, an Archimedean Frank copula is considered to model two degradation measurements $Z_{ik}(t_j)$ with k=1,2 PC, i=1,2,…,N,j=1,2,…,M as $H(\Delta Z_{i1}(t_j), Z_{i2}(t_j))=C(F(\Delta Z_{i1}(t_j)), F(\Delta Z_{i2}(t_j))\,|\,\theta)$, where $F(\Delta Z_{ik}(t_j))$ is the CDF of the respective marginal stochastic process for k=1,2 and θ is the association parameter of the copula function. It should be noted that the distributions described in (7 – 13) refer to the case where the degradation levels before t_j are unknown. Instead, when it is assumed that the degradation levels measured before t_j are known, the conditional CDF are considered as $F(\Delta Z_{ik}(t_j))\,|\,Z_{i1}(t_1),\ldots,Z_{i1}(t_{(j-1)}))$ for k=1,2, i=1,2,…,N, and j=1,2,…,M. Such that the bivariate copula results in $H(\Delta Z_{i1}(t_j), Z_{i2}(t_j))=C(F(\Delta Z_{i1}(t_j)\,|\,Z_{i1}(t_1),\ldots,Z_{i1}(t_{(j-1)})),$ $F(\Delta Z_{i2}(t_j)), Z_{i2}(t_1)),\ldots,Z_{i2}(t_{j-1}))\,|\,\theta$. With the marginal CDF defined as:

$$F\left(\Delta Z_{ik}\left(t_j\right)\,|\,Z_{ik}\left(t_1\right),\ldots,Z_{ik}\left(t_{j-1}\right)\right)= \int_0^{\infty} F\left(\Delta Z_{ik}\left(t_j\right)\,|\,u_k\right) f\left(u_k\,|\,Z_{ik}\left(t_1\right),\ldots,Z_{ik}\left(t_{j-1}\right)\right) du_k \tag{14}$$

where the conditional PDF of the random parameter is given by:

$$f\left(u_k\,|\,Z_{ik}\left(t_1\right),\ldots,Z_{ik}\left(t_{j-1}\right)\right)= \frac{f\left(\Delta Z_{ik}\left(t_1\right)|\,u_k\right)\cdot\ldots\cdot f\left(\Delta Z_{ik}\left(t_{j-1}\right)|\,u_k\right) f\left(u_k\right)}{\int_0^{\infty} f\left(\Delta Z_{ik}\left(t_1\right)|\,u_k\right)\cdot\ldots\cdot f\left(\Delta Z_{ik}\left(t_{j-1}\right)|\,u_k\right) f\left(u_k\right) du_k}$$

The bivariate model is denoted as $H(\Delta Z_{i1}(t_j), \Delta Z_{i2}(t_j))=C(U_{ij1}, V_{ij2})$, where $U_{ij1}=F(\Delta Z_{i1}(t_j)\,|\,Z_{i2}(t_1),\ldots,Z_{i1}(t_{(j-1)}))$ and $V_{ij2}=F(\Delta Z_{i2}(t_j)\,|\,Z_{i2}(t_1),\ldots,Z_{i2}(t_{(j-1)}))$ are the CDF of the marginal gamma process. If a simple gamma process is considered then the CDF is represented by (5). If random effects models are considered in the marginal processes and the degradation levels measured before t_j are known, then the respective CDF can be obtained from (14). If the degradation levels measured before t_j are unknown then the CDF can be obtained from (10) and (12) for the RV and RD models, respectively. Parametric copula functions impose strong assumptions or restrictions on the correlation structure among CDF. This denotes the need to determine how a specific copula function is selected, and how the chosen copula function can be validated by data. Such a topic has been widely studied in the literature, for example, by comparing the sample empirical copula and theoretical copula. Practitioners may be referred to Durrleman et al. [5] and Melchiori [14]. In this paper, the Frank copula function is considered as $C(U_{ij1},V_{ij2}\,|\,\theta)$, to illustrate the joint modeling of the proposed models with random effects for the two degradation processes. In the literature, it has been found that the Frank copula works well when dealing with systems with two PC and when dealing with crack propagation data as can be seen in the works of [9, 31, 36], as the case study presented in this paper. The Frank copula function is presented in (15). Then, the log-likelihood function of the set of parameters $\vartheta_i=\left(\nu_k,\eta_k,\zeta_k,\gamma_k,\delta_k,\varphi_k,\theta\right)$ for k=1,2, and i=1,2,…, is described in (16).

$$C\left(U_{ij1},V_{ij2}\;\theta\right)=-\frac{1}{\theta}\ln\left[1+\frac{\left(e^{-\theta U_{ij1}}-1\right)\left(e^{-\theta V_{ij2}}-1\right)}{e^{-\theta}-1}\right] \tag{15}$$

$$l\left(\vartheta_i\right)= \sum_{i=1}^{N}\sum_{j=1}^{M}\left[\ln\left(c\left(U_{ij1},V_{ij2}\,|\,\theta\right)\right)+\sum_{k=1}^{2}\ln\left(f_k\left(\Delta Z_{ik}\left(t_j\right)|\,Z_{ik}\left(t_1\right),\ldots,\Delta Z_{ik}\left(t_{j-1}\right)\right)\right)\right] \tag{16}$$

where $c(U_{ij1},V_{ij2}\,|\,\theta)=\partial(C(U_{ij1},V_{ij2}\,|\,\theta))/(\partial U_{ij1}\partial V_{ij2})$.

The product is considered to have failed if any of the PC reach the critical degradation level ω_k, k=1,2. Thus, the reliability function can be described as $R(t)=P\left\{Z_{i1}\left(t_j\right)<\omega_1, Z_{i2}\left(t_j\right)<\omega_2\right\}=C\left(R_1\left(\omega_1\right),R_2\left(\omega_2\right)\right)$.

Different combinations of the marginal processes for the bivariate modeling are proposed, these combinations are presented in Table 1. The bivariate modeling implies that the dependence structure between the degradation processes of the two characteristics can be tested by using the association parameter (θ), which justifies the use of the copula function. The models B_1,B_2, and B_2 consider bivariate gamma models with homogeneous random effects for the RE, RV, and RD models, respectively. However, another important aspect to consider is that the degradation of each characteristic may be different in terms of the random effects that affect the behavior of the degradation paths. This means that, e.g., the degradation paths of the characteristic 1 may exhibit a large variation of the degradation rate, and a low level of variation of the within degradation increments in the paths, while the characteristic 2 may exhibit a large variation in the within degradation increments in the paths and a low variation of the degradation rates. For such cases, it may be important to consider heterogeneous marginal models with random effects in the bivariate modeling. In this paper, two heterogeneous models are considered and denoted as B_4 and B_5 in Table 1, where in the model B_4 it is considered that the degradation of the characteristic 1 is governed by a gamma process with RD, while the degradation of the characteristic 2 is governed by a gamma process with RV. In the model B_5, it is considered that $U_{ij1}=F_{RE}(\Delta Z_{i1}(t_j))$ and $V_{ij2}=F_{RV}(\Delta Z_{i2}(t_j))$. Further bivariate combinations of gamma processes with heterogeneous random effects can be considered depending on the observed behavior of the degradation paths of the degradation processes under study.

5. Parameters estimation

Table 1. Bivariate models and bivariate heterogeneous Models

Model	U_{ij1}	V_{ij2}
B_1	$F_{RE}(\Delta Z_{i1}(t_j))$	$F_{RE}(\Delta Z_{i2}(t_j))$
B_2	$F_{RV}(\Delta Z_{i1}(t_j))$	$F_{RV}(\Delta Z_{i2}(t_j))$
B_3	$F_{RD}(\Delta Z_{i1}(t_j))$	$F_{RD}(\Delta Z_{i2}(t_j))$
B_4	$F_{RD}(\Delta Z_{i1}(t_j))$	$F_{RV}(\Delta Z_{i2}(t_j))$
B_5	$F_{RE}(\Delta Z_{i1}(t_j))$	$F_{RV}(\Delta Z_{i2}(t_j))$

As the bivariate functions consider different combinations of gamma processes with random effects in terms of the scale parameter of the gamma process, it is easy to note that the joint bivariate distribution function for any of the models B_i,i=1,2,3,4,5 may result in a non-standard complex form.

However, the MCMC can be utilized to estimate the parameters ϑ_i of interest from B_i, ,i=1,2,3,4,5. The MCMC procedure consists in generating samples from the joint posterior distribution. In this case, Gibbs sampling algorithm is utilized to obtain such samples from the joint distribution. Generally, the algorithm consists in dividing the parameter vector into d subvectors, $\vartheta=(\vartheta_1,\ldots,\vartheta_d)$, such that each iteration of the algorithm cycles through the subvectors of δ, drawing each subset conditional on the value of all vectors. This process can be seen as generating a realization of a Markov chain that is built from a set of base transition probabilities. When the base transition probabilities are applied in sequence the algorithm can be described as simulating a homogeneous Markov Chain $\vartheta^{(1)},\vartheta^{(2)},\vartheta^{(3)},\ldots$,. It is assumed that the prior distributions for all the parameters of interest are non-informative and there is prior independence among the parameters of interest. The implementation of the Gibbs sampling algorithm for the estimation of the parameters is implemented using the OpenBUGS package software [13]. Zeros trick is used in OpenBUGS given that the log-likelihood is not a standard distribution [17]. Important information about this algorithm can be found in Gelfand and Smith [6], Casella and George [4], Smith and Roberts [28].

Considering that degradation measurements $Z_{ik}(t_j)$ have been observed of the ith unit at the corresponding time t_j, i=1,2,…,N,j=1,2,… ,M for k=1,2 PC. Thus, $\Delta Z_{ik}(t_j)=Z_{ik}(t_j)-Z_{ik}(t_{j-1})$) is the degradation increment at the interval time t_j-t_{j-1}. Then, the degradation increments $\Delta Z_{ik}(t_j)$ are independent random variables that follow a gamma distribution as $Ga(v_k(\Delta\tau(t_j,\gamma_k)),u_k)$ for the RE model, $Ga(\eta_k(\Delta\tau(t_j,\gamma_k)),u_k)$ for the RV model, and $Ga(\zeta_k(\Delta\tau(t_j,\gamma_k)),u_k)$ for the RD model, in all cases with u_k following a gamma distribution. It should be noted that, under a gamma process with random effects, the degradation increments $\Delta Z_{ik}(t_j)$ are independent random variables only conditional to the value of (v_k,η_k,ζ_k) for any of the described random effects models. Different combinations of the bivariate models with different random effects as marginal distributions are considered as described in Section 4. Given that random effects are generated by in all the models, it is considered that $u_{k,i}$ follows the same prior distributions with hyper-parameters (δ_k,φ_k), which accounts for pooling the information of the random effects among the different degradation trajectories for k=1,2. The non-informative prior distributions for these hyper-parameters are considered as $\delta_k \sim Gamma\left(a_{\delta_k},b_{\delta_k}\right)$ and $\varphi_k \sim Gamma\left(a_{\varphi_k},b_{\varphi_k}\right)$. A non-informative normal prior distribution is considered for the Frank copula parameter as $\theta \sim Normal\left(a_\theta,b_\theta\right)$. In addition, a non-informative gamma prior distribution is considered for the shape parameters of the gamma processes (v_k,η_k,ζ_k). Lastly, a gamma distribution is considered for γ_k as $\gamma_k \sim Gamma\left(a_{\gamma_k},b_{\gamma_k}\right)$, in order to avoid negative values of the time-scale transformation. The bivariate joint Frank copula function specified in (15) is implemented in OpenBUGS with the marginal CDF described in Table 1 as B_i by considering the proposed prior distributions for every parameter of interest.

6. Case study

In the following, a case study is presented, which consisted in the fatigue-crack propagation of two cracks in two terminals of an electronic device. Each device has two terminals, whose function is to transfer a signal to a receptor. Some cracks may be present in both terminals. The propagation of the cracks to a certain critical length can lead to failure of the device given the inability of transferring the signal to the receptor. A DT based on vibration was carried out in order to study the propagation of cracks in the terminals of ten devices. As every device has two terminals, two sets of fatigue-crack growth data were obtained. The length increments of the cracks for both terminals were measured every 0.1 hundred thousand cycles until 0.9 hundred thousand cycles. The measurements for every crack were performed at the same measurement times, and by considering equally distanced inspection times. The increments of the degradation were measure by considering a vision system with special software applications to measure crack propagations. The obtained data are presented in Table 2, the units are in millimeters. In Figure 4, the crack degradation paths for the two terminals of every device are illustrated.

The propagation of the cracks can be seen as a degradation process and therefore a stochastic process. As the device counts with two terminals, the crack propagation of every terminal can be seen as degradation processes. Considering that the cracks are from different positions, it is important to assess the dependence in the cracks propagation of the terminals for every device. It is considered that the device has failed if the length of any of the two terminal' cracks cross the critical limit of 0.663 mm. Such critical level of degradation was obtained by considering the total width of the terminal defined by the customer of the product. In this case, if a crack length exceeds the total width of the terminal, a failure of the system can be obtained given that the inability of the product to transfer a signal the receptor.

Table2. Fatigue-crack growth increments dataset for terminals (in milimeters)

Terminal	Device	Hundred thousands of cycles									
		0	0.1	0.2	0.3	0.4	0.5	0.6	0.7	0.8	0.9
1	1	0	0.014	0.018	0.016	0.021	0.089	0.09	0.02	0.06	0.014
	2	0	0.031	0.017	0.075	0.011	0.024	0.025	0.08	0.01	0.043
	3	0	0.011	0.069	0.07	0.03	0.01	0.01	0.01	0.012	0.073
	4	0	0.03	0.02	0.08	0.03	0.05	0.06	0.09	0.02	0.055
	5	0	0.01	0.012	0.08	0.031	0.05	0.05	0.01	0.035	0.015
	6	0	0.011	0.05	0.09	0.026	0.084	0.085	0.022	0.036	0.016
	7	0	0.017	0.012	0.07	0.01	0.015	0.016	0.01	0.099	0.03
	8	0	0.026	0.016	0.01	0.01	0.012	0.01	0.01	0.021	0.016
	9	0	0.03	0.08	0.051	0.072	0.09	0.09	0.03	0.08	0.033
	10	0	0.08	0.012	0.016	0.032	0.01	0.01	0.02	0.013	0.034
2	1	0	0.01	0.02	0.025	0.052	0.058	0.018	0.017	0.06	0.042
	2	0	0.09	0.071	0.011	0.075	0.012	0.022	0.09	0.03	0.028
	3	0	0.01	0.05	0.021	0.037	0.024	0.016	0.011	0.063	0.03
	4	0	0.016	0.06	0.011	0.017	0.023	0.071	0.01	0.01	0.04
	5	0	0.036	0.06	0.08	0.028	0.038	0.039	0.044	0.09	0.08
	6	0	0.014	0.088	0.01	0.082	0.083	0.012	0.016	0.03	0.056
	7	0	0.037	0.027	0.014	0.018	0.028	0.04	0.07	0.02	0.072
	8	0	0.035	0.051	0.019	0.069	0.093	0.01	0.07	0.014	0.023
	9	0	0.067	0.081	0.013	0.012	0.011	0.034	0.011	0.01	0.046
	10	0	0.025	0.027	0.012	0.012	0.075	0.036	0.018	0.017	0.04

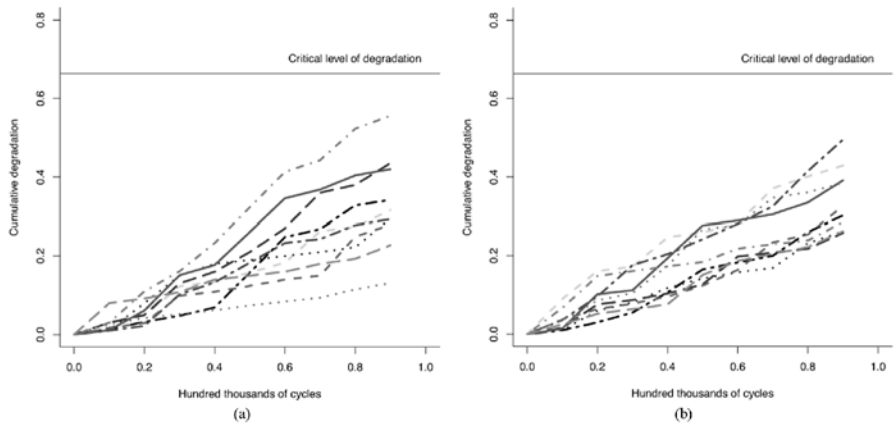

Fig. 4. Cumulative degradation paths based on the fatigue-crack growth dataset. (a) Terminal 1, (b) Terminal 2.

As can be seen from the cumulative degradation paths in Figure 4, there are several differences among the degradation paths of a single terminal and between terminals. In the degradation paths of terminal 1, a large variation of the degradation rate can be observed which may indicates that the random effects affect the degradation rate, and the opposite can be seen in the degradation paths of terminal 2, where the variation is rather small. From both terminals, it can be noted that a large variation of the within increments is observed, which may indicates that the random effects affect the diffusion of the degradation process of both terminals. From these behaviors, it can be noted that the random effects have different influences on the degradation processes as described above. The different bivariate models presented in Table 1 are considered, these models were estimated via Gibbs sampling by using OpenBUGS.

6.1. Estimation of Proposed Models

Considering the dataset described in Table 2, N=10 and M=10 and the five bivariate models B_i,i=1,2,3,4,5 described in Table 1, with parameters:

- $\vartheta_1=(v_1,\gamma_1,\delta_1,\varphi_1,v_2,\gamma_2,\delta_2,\varphi_2,\theta)$, for the bivariate RE model, with means $v_k(\Delta\tau(t_j,\gamma_k))/$ and variances $v_k(\Delta\tau(t_j,\gamma_k))/u_k^2$, for k=1,2.
- $\vartheta_2=(\eta_1,\gamma_1,\delta_1,\varphi_1,\eta_2,\gamma_2,\delta_2,\varphi_2,\theta)$ for the bivariate RV model, with means $\eta_k(\Delta\tau(t_j,\gamma_k))$ and variances $\eta_k(\Delta\tau(t_j,\gamma_k))/$, for k=1,2.
- $\vartheta_3=(\eta_1,\gamma_1,\delta_1,\varphi_1,\zeta_2,\gamma_2,\delta_2,\varphi_2,\theta)$ for the bivariate RD model, with means $\zeta_k(\Delta\tau(t_j,\gamma_k))$ and variances $\zeta_k(\Delta\tau(t_j,\gamma_k))$, for k=1,2.
- $\vartheta_4=(\zeta_k,\gamma_1,\delta_1,\varphi_2,\eta_2,\gamma_2,\delta_2,\varphi_2,\theta)$ for the bivariate heterogeneous RD-RV model, with means $\zeta_1(\Delta\tau(t_j,\gamma_k))u_1$, $\eta_2(\Delta\tau(t_j,\gamma_k))$ and variances $\zeta_1(\Delta\tau(t_j,\gamma_k))$, $\eta_2(\Delta\tau(t_j,\gamma_k))/u_2$.
- $\vartheta_5=(v_1,\gamma_1,\delta_1,\varphi_1,\eta_2,\gamma_2,\delta_2,\varphi_2,\theta)$, for the bivariate heterogeneous RE-RV model, with means $v_1(\Delta\tau(t_j,\gamma_k))/u_1$, $\eta_2(\Delta\tau(t_j,\gamma_k))$ and variances $v_1(\Delta\tau(t_j,\gamma_k))/u_1^2$, $\eta_2(\Delta\tau(t_j,\gamma_k))/u_2$.

Based on the Frank copula function (15) and the log-likelihood function in (16) with ϑ_i,i=1,2,3,4,5, the estimated parameters were obtained by using OpenBUGS. It is assumed that there are prior independence among the parameters of interest. Estimation of the parameters was performed by using the zeros trick in the developed algorithm to specify the bivariate log-likelihood function. Two sets of initial values are considered in the algorithm to assess the convergence of the parameters of interest with the Brooks-Gelman-Rubin (BGR) statistic [7]. A total of 50,000 iterations were considered for burn-in and 100,000 were considered for estimation purposes. As two sets of initial values were determined for every parameter, the BGR statistic was calculated for the parameters of interest. In general, it was found that convergence is achieved in every parameter in accordance with the BGR graphs obtained from OpenBUGS. The estimations obtained for the parameters of every model B_i, along with the standard deviation, Monte Carlo error and some percentiles are presented in Table 3.

Information criteria was used to select the best fitting random effects bivariate model. The Akaike Information Criterion (AIC) is used for such purpose, which is an appealing tool for model selection based on information. The model with the lowest value of AIC is considered as the best fitting model [1]. This criterion is defined as AIC=$-2\times l(\vartheta_1)+2R$; where, $l(\vartheta_1)$ is the evaluated log-likelihood function from (16) for any of the models i=1,2,3,4,5, for the Frank copula and R is the number of parameters. In addition, the Kendall coefficient was estimated from the copula parameter (θ), this coefficient provides a good alternative to measure the level of dependence between the marginal distributions from the copula. The Kendall coefficient can be obtained from the Frank copula as $1-4/\theta[D_1(-\theta)-1]$, where $D_s(x)=s/x^s\int_0^x t^s/e^t-1dt$ is the Debye function. The AIC and Kendall values are presented in Table 4.

Table 4. Estimation of information criteria and dependence structure for bivariate models

Model	AIC	Kendall	Ranking
B_1	−8415	0.0405	2
B_2	−8412	0.0415	3
B_3	−8410	0.0402	5
B_4	−8411	0.0411	4
B_5	−8426	0.0411	1

As can be noted from Table 4, the best fitting model is the heterogeneous model B_5, given that it has the lowest value of AIC. This model considers a RE gamma process model for the terminal 1 and a RV gamma process model for the terminal 2. The result makes sense, given that as can be seen from the cumulative degradation paths in Figure 4, the paths of terminal 1 have large variations of the degradation rate and the within degradation increments. Such characteristics are described when the RE model is considered given that both the mean and variance of the gamma process are affected by the random effects parameter. On the other hand, the degradation paths of terminal 2 have a lower level of variation of the degradation rates, and a large variation of the within degradation increments, such characteristics are described when the RV model is considered given that only the variance of the gamma process is affected by the random effects parameter, as described in Section 3. However, it must be noted that the differences among the AIC values for the proposed models is slight. Furthermore, the B_3 model, which considers that both terminals 1 and 2 are governed by a gamma process with RD, is the model with the poorest performance. The level of dependence described by the Kendall coefficient from the bivariate RE-RV model is 0.0411, which may indicates a low level of dependence, however, it must be considered when dealing with the reliability assessment of the product as a whole. In addition, from the estimates in Table 3 it can be noted that in the model B_5 the credible interval of θ include the value 0. Hence, the degradation processes seem to be independent, because for $\theta\to 0$ the marginal CDF are independent, which explains why the obtained Kendall coefficients are small. In Figure 5, the contour and density plots are presented for the best fitting heterogeneous model via Frank copula.

Table 3. Parameters estimates for the considered bivariate models

Model	Parameter	Mean	Sd	MC error			
B_1	ν_1	18.77	2.595	0.1067	14.09	18.63	24.28
	ν_2	21.79	2.916	0.1186	16.31	21.71	27.72
	γ_1	1.058	0.07221	0.0002371	0.9226	1.056	1.206
	γ_2	1.021	0.06957	0.0002173	0.8912	1.018	1.164
	φ_1	31.04	20.62	1.152	4.48	30.51	77.01
	φ_2	25.3	15.67	0.8731	7.097	20.57	64.25
	δ_1	1562	1025	57.26	232.3	1550	3780
	δ_2	1427	834.9	46.49	384.1	1197	3606
	θ	-0.3624	0.5759	0.003893	-1.5	-0.3622	0.7729
B_2	η_1	0.3747	0.03042	0.000828	0.3199	0.3729	0.439
	η_2	0.3866	0.02989	0.000836	0.3331	0.3847	0.4509
	γ_1	1.058	0.07411	0.000246	0.9188	1.055	1.209
	γ_2	1.021	0.0706	0.000225	0.8889	1.018	1.167
	φ_1	59.82	32.64	1.825	16.23	52.46	138.3
	φ_2	47.9	35.76	2.004	10.65	38.92	150.1
	δ_1	2877	1659	92.82	763.8	2450	6520
	δ_2	2496	1701	95.3	584.5	2159	7119
	θ	-0.3775	0.5809	0.004144	-1.531	-0.3794	0.7457
B_3	ζ_1	0.008603	0.002217	0.000110	0.005479	0.008195	0.01426
	ζ_2	0.00719	0.001492	0.0000723	0.004775	0.007017	0.0106
	γ_1	1.058	0.07482	0.000259	0.9176	1.055	1.212
	γ_2	1.02	0.07006	0.000218	0.8899	1.018	1.164
	φ_1	56.68	41.34	2.317	11.53	41.8	154.7
	φ_2	44.97	25.2	1.408	11.17	38.38	102.5
	δ_1	2523	1787	100.2	558.3	1904	6689
	δ_2	2399	1238	69.06	655.5	2074	5118
	θ	-0.368	0.5892	0.003918	-1.521	-0.366	0.785
B_4	ζ_1	0.007357	0.002776	0.000132	0.003668	0.006824	0.01447
	η_2	0.388	0.02938	0.000710	0.335	0.3864	0.4499
	γ_1	1.059	0.07225	0.000235	0.9242	1.057	1.208
	γ_2	1.02	0.07114	0.000230	0.8889	1.017	1.168
	φ_1	28.33	23.98	1.343	1.698	19.96	83.55
	φ_2	33.42	17.42	0.9705	4.984	32.73	66.56
	δ_1	1430	1228	68.76	89.53	1028	4625
	δ_2	1765	965.9	53.86	250.2	1683	3714
	θ	-0.3593	0.5912	0.003846	-1.518	-0.3588	0.7949
B_5	ν_1	18.72	2.501	0.09876	14.08	18.65	23.78
	η_2	0.3871	0.02964	0.0008099	0.3332	0.3857	0.4492
	γ_1	1.058	0.07298	0.0002367	0.9218	1.055	1.207
	γ_2	1.021	0.07101	0.0002234	0.8886	1.018	1.168
	φ_1	25.68	14.62	0.8119	2.076	24.05	55.83
	φ_2	75.7	56.48	3.173	15.52	54.38	221.6
	δ_1	1294	737.9	41	107.8	1215	2832
	δ_2	3811	2418	135.8	821	2948	9287
	θ	-0.3596	0.5794	0.00403	-1.506	-0.3546	0.7774

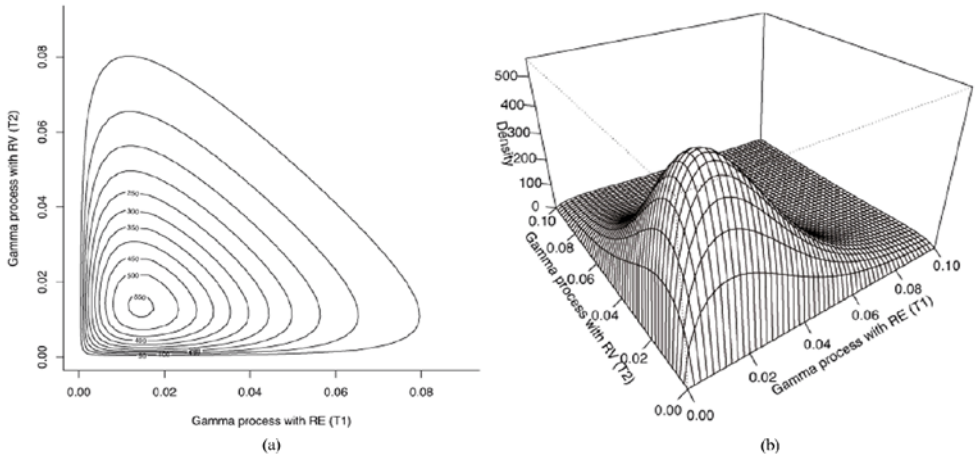

Fig. 5. Contour plot (a) and density plot (b) for the bivariate Frank copula with RE and RV marginal gamma random effects models.

6.2. Reliability Assessment

Based on the estimates obtained in Table 3, it is possible to estimate the reliability of the product. The marginal reliability functions can be obtained by considering the critical level of degradation ω_k=0.663, for k=1,2. In the case of the RE model, the marginal reliability function is obtained with (17) by simply substituting the corresponding parameter estimations form Table 3 in the function. As the parameters for the degradation process of each terminal are estimated marginally, the reliability functions can be easily obtained. In the case of the RV and RD models, the reliability functions do not have a closed form. However, the kernel density distributions of the reliability functions can be obtained via simulation-based integration [24]. Thus, by considering the reliability functions described in (18) and (19), and the posterior distributions of the parameters of interest ($\nu_k,\eta_k,{}_k,\gamma_k,\delta_k,\varphi_k$), the reliability functions can be obtained as:

$$R_{RE}\left(t_{\omega_k} \mid \nu_k,\delta_k,\varphi_k,\gamma_k\right) = F_{2\nu_k\left(\tau\left(t_{\omega_k},\gamma_k\right)\right),2\delta_k}\left(\frac{\delta_k\omega_k}{\varphi_k\nu_k\left(\tau\left(t_{\omega_k},\gamma_k\right)\right)}\right) \quad (17)$$

$$R_{RV}\left(t \mid {}_k,\delta_k,\varphi_k,\gamma_k\right) = \int_{u_k>0}\left\{\frac{\zeta\left(\eta_k\left(\tau\left(t_j,\gamma_k\right)\right)u_k,\omega_k u_k\right)}{\Gamma\left(\eta_k\left(\tau\left(t_j,\gamma_k\right)\right)u_k\right)}\right\}\frac{\varphi_k^{\delta_k}u_k^{\delta_k-1}}{\Gamma\left(\delta_k\right)}\exp\left\{-u_k\varphi_k\right\}du_k \quad (18)$$

$$R_{RD}\left(t \mid \zeta_k,\delta_k,\varphi_k,\gamma_k\right) = \int_{u_k>0}\left\{\frac{\zeta\left(\zeta_k\left(\tau\left(t_j,\gamma_k\right)\right)u_k^2,\omega_k u_k\right)}{\Gamma\left(\zeta_k\left(\tau\left(t_j,\gamma_k\right)\right)u_k^2\right)}\right\}\frac{\varphi_k^{\delta_k}u_k^{\delta_k-1}}{\Gamma\left(\delta_k\right)}\exp\left\{-u_k\varphi_k\right\}du_k \quad (19)$$

Considering the joint posterior distributions $p(\vartheta_i|Z_k)$, where $Z_k=(Z_{1k}(t_1),\ldots,Z_{1k}(t_M),\ldots,Z_{Nk}(t_1),\ldots,Z_{Nk}(t_M))$ for any bivariate model B_i with parameters ϑ_i for i=1,2,3,4,5, the reliability functions can be obtained as:

$$R_m\left(t Z_k\right) = \int_{\vartheta_i} R_m\left(t\ \vartheta_i\right)p_m\left(\vartheta_i Z_k\right)d\vartheta_i \quad (20)$$

where m=RV or RD, and p_m ($\vartheta_i|Z_k$) is the joint posterior distribution obtained from the implemented Bayesian estimation approach described in Section 4. The simulation-based integration is implemented by calculating the relevant values of R_{RV} ($t|\hat{\vartheta}_i$) and $R_{RD}(t|\hat{\vartheta}_i)$ at each generated sample $\hat{\vartheta}_i=(\hat{\nu}_k,\hat{\eta}_k,\hat{\zeta}_k,\hat{\gamma}_k,\hat{\delta}_k,\hat{\varphi}_k)$ from $p_m(\hat{\vartheta}_i|Z_k)$ for any of the k=1,2 random effects models.

Considering the bivariate models, the bivariate reliability function can be written as:

$$R(t|Z_k)=P(Z_{i1}(t_j)<\omega_1,Z_{i2}(t_j)<\omega_2)=C(R(t|Z_{i1}(t_j)),R(t|Z_{i2}(t_j))) \quad (21)$$

where $\omega_1=\omega_2$=0.663. Considering all the bivariate models B_i, i=1,2,3,4,5, and the reliability functions described in (20-21), the reliability plots for terminal 1 and 2 were obtained and are compared in Figure 6. The best fitting model is B_5, which implies a RE model for terminal 1 and a RV model for terminal 2. Considering these two marginal models, the reliability functions were also obtained and are compared in Figure 7.

From Figure 6a, it can be noted that the behavior of the reliability functions for RD and RD (with RV) is not the same. The difference between these two models is that the RD function comes from a bivariate RD model, while the RD (with RV) comes from a heteroge-

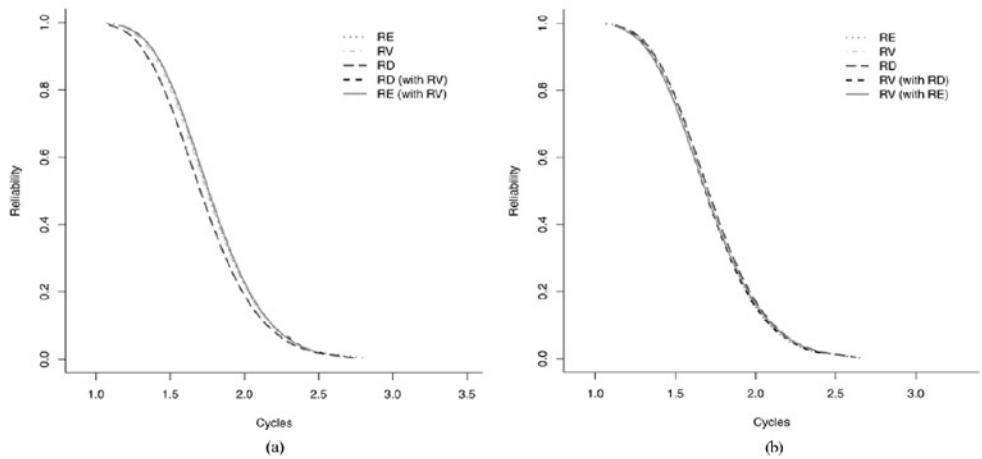

Fig. 6. Comparison of reliability functions considering dependence. (a) Terminal 1, (b) Terminal 2.

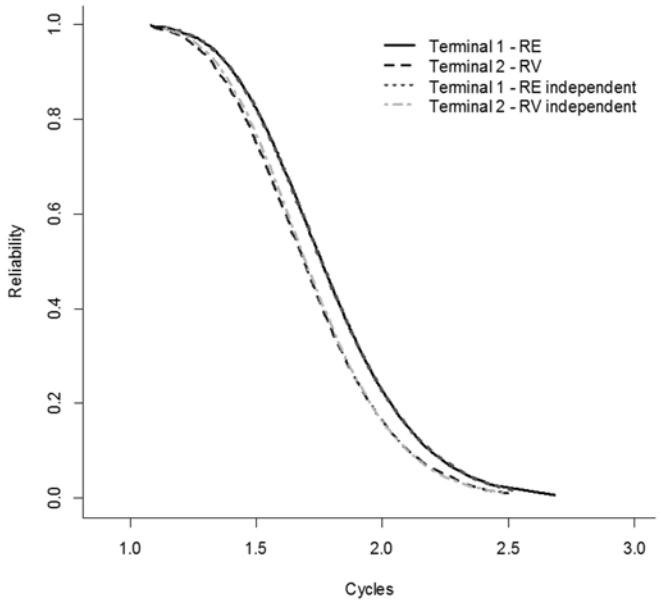

Fig. 7. Comparison of reliability functions for terminal 1 and 2 with RE and RV models.

neous RD-RV model. This denotes that there may be some differences in the reliability assessment if homogeneous or heterogeneous random effects are considered in the modeling. Although not so obvious, the same differences can be noted in the reliability functions in Figure 6b for the RV, RV (with RD), and RV (with RE) models. The device is considered to have failed if any of the two terminal's cracks exceeds the critical degradation level ω_k=0.663. As can be noted from Figure 7 the reliability of terminal 1 is higher than the reliability of terminal 2. Which can be explained by considering that the degradation mean for terminal 1 under the RE model in B_5 is 0.3715, and the degradation mean for terminal 2 under the RV model in B_5 is 0.3855. As can be noted the degradation mean for terminal 2 is greater than the degradation mean for terminal 2, which means that the first-passage times of terminal 2 will occur earlier than the ones from terminal 1. In addition, the variance of terminal 1 under RE in B_5 results in 0.007379, and the variance for terminal 2 under RV in B_5 is 0.007221. This means that, as the terminal 1 has a larger variance, some of the degradation paths will have large first-passage times, and for terminal 2 the first-time passage times may occur earlier with more probability. In addition, the reliability functions for the dependent and independent scenarios constantly overlap, which can be explained by the fact the considered level of dependence in terms of the Kendall coefficient is quite small 0.0411.

7. Concluding remarks

This paper introduces a bivariate degradation modeling approach for two PC based on marginal gamma processes with heterogeneous random effects. As the random effects may affect in different ways the degradation of each PC, different modifications of the structure of the parameters of the marginal gamma processes were performed. Such modifications are considered in the bivariate modeling, which allows to describe the heterogeneous behaviors of the degradation processes due to random effects. Different combinations of marginal gamma processes with random effects joined by a Frank copula were considered, and it was found that a bivariate model with marginal RE and RV models for the two degradation processes is slightly the best fitting model according to information criteria. The selection of the best fitting bivariate model can be explained by the behaviors of the degradation paths of each PC. The terminal 1 has a large variation of the degradation rate and the within degradation increments, such characteristics are described by the gamma process with RE. While the terminal 2, has only a large variation of the within degradation increments, which is a characteristic of the gamma process with RV. Under the selected model, it is expected that the estimations of the reliability and the remaining useful life of the product under study to be more accurate, as noted in the comparison of reliability functions in Figure 6. The comparison of the reliability functions in Figure 7 shows that terminal 2 should decide the reliability of the product. The proposed models can be extended to consider more than two marginal degradation processes. Future research can be conducted by considering different distributions for the random effects scale parameter of the gamma process, and by letting the shape parameter to be a random effects parameter.

References

1. Akaike H. A new look at the statistical model identification. IEEE Transactions on Automatic Control 1974; 19(6): 716-723, http://dx.doi.org/10.1109/TAC.1974.1100705.
2. Bagdonavicius V, Nikulin MS. Accelerated life models: modeling and statistical analysis. Boca Raton: Chapman & Hall/CRC, 2002.
3. Bagdonavicius V, Nikulin MS. Estimation in degradation models with explanatory variables. Lifetime Data Analysis 2000; 7(1): 85-103, http://dx.doi.org/10.1023/A:1009629311100.
4. Casella G, George EI. Explaining the Gibbs sampler. The American statistician 1992; 46(3): 167-174.
5. Durrleman, Valdo, Ashkan Nikeghbali, and Thierry Roncalli. "Which Copula Is the Right One?" SSRN Journal 2000, http://dx.doi.org/10.2139/ssrn.1032545.
6. Gelfand E, Smith AFM. Sampling-based approaches to calculating marginal densities. Journal of the American Statistical Association 1990; 85(410): 398-409, http://dx.doi.org/10.1080/01621459.1990.10476213.
7. Gelman A, Rubin DB. Inference from iterative simulation using multiple sequences. Statistical Sciences 1992; 7(4), 457-511, http://dx.doi.org/10.1214/ss/1177011136.
8. Genest C, Favre AC. Everything you always wanted to know about copula modeling but were afraid to ask. Journal of Hydrologic Engineering 2007; 12(4): 347-368, http://dx.doi.org/10.1061/(ASCE)1084-0699(2007)12:4(347).
9. Hao H, Su C, Li C. LED lighting system reliability modeling and inference via random effects gamma process and copula function. Mathematical Problems in Engineering 2015; 8 pages.
10. Lawless J, Crowder M. Covariates and random effects in a gamma process model with application to degradation and failure. Lifetime Data Analysis 2004; 10(3): 213-227, http://dx.doi.org/10.1023/B:LIDA.0000036389.14073.dd.
11. Lu CJ, Meeker WQ, Escobar LA. A comparison of degradation and failure-time analysis methods for estimating a time-to-failure distribution. Statistica Sinica 1996; 6: 531-546.
12. Lu CJ, Meeker WQ. Using degradation measures to estimate a time-to-failure distribution. Technometrics 1993; 35(2): 161-174, http://dx.doi.org/10.1080/00401706.1993.10485038.

13. Lunn D, Spiegelhalter D, Thomas A, Best N. The BUGS project: Evolution, critique and future directions (with discussion). Statistics in Medicine 2009; 28: 3049-3082, http://dx.doi.org/10.1002/sim.3680.
14. Melchiori, Mario R. "Which Archimedean Copula Is the Right One?" SSRN Journal 2003. doi:10.2139/ssrn.1123135, http://dx.doi.org/10.2139/ssrn.1123135.
15. Nelsen RB. An Introduction to Copulas (2nd edn). Springer, New York, 2006.
16. Noortwijk van JM. A survey of the application of gamma processes in maintenance. Reliability Engineering & System Safety 2009; 94(1): 2-21, http://dx.doi.org/10.1016/j.ress.2007.03.019.
17. Ntzoufras I. Bayesian modeling using WinBUGS. John Wiley & Sons, New Jersey, EUA, 2009, http://dx.doi.org/10.1002/9780470434567.
18. Pan Z, Balakrishnan N. Multiple-steps step-stress accelerated degradation modeling based on Wiener and gamma processes. Communications in Statistics - Simulation and Computation 2010; 39(7): 1384-1402, http://dx.doi.org/10.1080/03610918.2010.496060.
19. Pan Z, Balakrishnan N. Reliability modeling of degradation of products with multiple performance characteristics based on gamma processes. Reliability Engineering & System Safety 2011; 96(8): 949-957, http://dx.doi.org/10.1016/j.ress.2011.03.014.
20. Pan Z, Feng J, Sun Q. Lifetime Distribution and Associated Inference of Systems with Multiple Degradation Measurements Based on Gamma Processes. Eksploatacja i Niezawodnosc - Maintenance and Reliability 2016; 18(2): 307-313, http://dx.doi.org/10.17531/ein.2016.2.20.
21. Pan Z, Sun Q, Feng J. Reliability modeling of systems with two dependent degrading components based on gamma processes. Communications in Statistics - Theory and Methods 2016; 45(7): 1923-1938, http://dx.doi.org/10.1080/03610926.2013.870201.
22. Park C, Padgett WJ. Accelerated degradation models for failure based on geometric Brownian motion and gamma processes. Lifetime Data Analysis 2005; 11(4): 511-27, http://dx.doi.org/10.1007/s10985-005-5237-8.
23. Park C, Padgett WJ. Stochastic degradation models with several accelerating variables. IEEE Transactions on Reliability 2006; 55(2): 379-390, http://dx.doi.org/10.1109/TR.2006.874937.
24. Peng W, Li YF, Yang YJ, Huang HZ, Zuo MJ. Inverse Gaussian process models for degradation analysis: A Bayesian perspective. Reliability Engineering & System Safety 2014; 130: 175-189, http://dx.doi.org/10.1016/j.ress.2014.06.005.
25. Pulcini G. Modeling the mileage accumulation process with random effects. Communications in Statistics - Theory and Methods 2013; 42: 2661-2683, http://dx.doi.org/10.1080/03610926.2011.608478.
26. Sari JK, Newby MJ, Brombacher AC, Tang LC. Bivariate constant stress degradation model: led lighting system reliability estimation with two-stage modelling. Quality and Reliability Engineering International 2009; 25(8): 1067-1084, http://dx.doi.org/10.1002/qre.1022.
27. Singpurwalla ND. Survival in dynamic environments. Statistical Science 1995; 10(1): 86-103, http://dx.doi.org/10.1214/ss/1177010132.
28. Smith AFM, Roberts GO. Bayesian computation via the Gibbs sampler and related Markov Chain Monte Carlo Methods. Journal of the Royal Statistical Society. Series B 1993; 55(1): 3-24.
29. Tsai CC, Tseng ST, Balakrishnan N. Optimal design for degradation tests based on gamma processes with random effects. IEEE Transactions on Reliability 2012; 61: 604-613, http://dx.doi.org/10.1109/TR.2012.2194351.
30. Wang H, Tingxue X, Qiaoli M. Lifetime prediction based on gamma processes from accelerated degradation data. Chinese Journal of Aeronautics 2015; 28: 173-179, http://dx.doi.org/10.1016/j.cja.2014.12.015.
31. Wang X, Balakrishnan N, Guo B, Jiang P. Residual life estimation based on bivariate non-stationary gamma degradation process. Journal of Statistical Computation and Simulation 2015; 85(2): 405-421, http://dx.doi.org/10.1080/00949655.2013.824448.
32. Wang X. A pseudo-likelihood estimation method for nonhomogeneous gamma process model with random effects. Statistica Sinica 2008; 18: 1153-1163.
33. Wang X. Wiener processes with random effects for degradation data. Journal of Multivariate Analysis 2010; 101: 340-351, http://dx.doi.org/10.1016/j.jmva.2008.12.007.
34. Whitmore GA, Schenkelberg F. Modeling accelerated degradation data using Wiener diffusion with a time scale transformation. Lifetime Data Analysis 1997; 3(1): 27-45, http://dx.doi.org/10.1023/A:1009664101413.
35. Ye ZS, Chen N, Shen Y. A new class of Wiener process models for degradation analysis. Reliability Engineering & System Safety 2015; 139: 58-67, http://dx.doi.org/10.1016/j.ress.2015.02.005.
36. Zhou J, Pan Z, Sun Q. Bivariate degradation modeling based on gamma process. Proceedings of the World Congress on Engineering 2010; London, UK, 1783-1788.

Luis Alberto RODRÍGUEZ-PICÓN
Department of Industrial Engineering and Manufacturing
Institute of Engineering and Technology
Autonomous University of Ciudad Juárez
Ciudad Juárez, Chihuahua, México
E-mail: luis.picon@uacj.mx

Article citation info:
PILCH R. Reliability evaluation of networks with imperfect and repairable links and nodes. Eksploatacja i Niezawodnosc – Maintenance and Reliability 2017; 19 (1): 19–25, http://dx.doi.org/10.17531/ein.2017.1.3.

Robert PILCH

RELIABILITY EVALUATION OF NETWORKS WITH IMPERFECT AND REPAIRABLE LINKS AND NODES

NIEZAWODNOŚĆ SIECI Z USZKADZAJĄCYMI SIĘ I ODNAWIANYMI POŁĄCZENIAMI ORAZ WĘZŁAMI*

The paper presents the method for determining the reliability of a network whose elements (links and nodes) are imperfect (can fail) and repairable. The presented method uses the factoring algorithm, proposed π method and computer simulation. The factoring algorithm is used to obtain a formula for accurate computation of network reliability as a probability of connectedness among the specified set of nodes K ($R_{N(K)}$). The reliability calculated in this way relates to cases when only links can fail and are unrepairable. In order to calculate the reliability of a network with repairable links and nodes, we introduced quasi-failures of links which occur as a result of failures of adjacent nodes – the π method. The developed method allows accounting for the repair of all the network elements after failure, as well as choosing the set of nodes (N_f) which can fail independently. In addition, the probability distributions of failure time of freely specified sets of nodes and links can be different. A simulation computational model was developed for the method which allows for determining the reliability ($R_{N(K)}(t)$) of a network with repairable links and nodes. Examples of numerical calculations were performed according to the developed model and the results are presented.

***Keywords**: network reliability, factoring algorithm, imperfect nodes, imperfect links, repairable elements, π method, simulation.*

W opracowaniu przedstawiono metodę wyznaczania niezawodności sieci, w których elementy (połączenia i węzły) mogą się uszkadzać i są odnawiane. Przedstawiona metoda wykorzystuje algorytm faktoryzacji, zaproponowaną metodę π oraz symulację komputerową. Na podstawie algorytmu faktoryzacji wyznaczany jest wzór do dokładnego obliczania niezawodności sieci jako prawdopodobieństwa połączenia między wybranym zbiorem K węzłów ($R_{N(K)}$). Obliczana w ten sposób niezawodność dotyczy przypadków gdy tylko połączenia mogą się uszkadzać i nie są odnawiane. W celu obliczania niezawodności sieci z odnawianymi połączeniami i węzłami wprowadzono quasi uszkodzenia połączeń, które występują na skutek uszkodzeń węzłów do nich przyległych – metoda π. Opracowana metoda pozwala uwzględnić odnawianie wszystkich elementów sieci po uszkodzeniu jak również możliwość wyboru zbioru węzłów (N_f), które mogą się niezależnie uszkadzać. Ponadto rozkłady prawdopodobieństwa czasu pracy do uszkodzenia dowolnie określonych zbiorów węzłów i połączeń mogą być różne. Do zaproponowanej metody opracowano symulacyjny model obliczeniowy, który umożliwia wyznaczenie niezawodności sieci ($R_{N(K)}(t)$) z odnawianymi połączeniami i węzłami. Zgodnie z opracowanym modelem wykonano przykładowe obliczenia numeryczne i przedstawiono ich wyniki.

***Słowa kluczowe**: niezawodność sieci, algorytm faktoryzacji, uszkadzające się połączenia, uszkadzające się węzły, naprawialne elementy, metoda π, symulacja.*

1. Introduction

Attempts to solve the network reliability issue have been made for years. The problem is important due to growing requirements in terms of reliable operation of various networks whose reliability is considered already at the design stage [8, 23]. Computer, communication, gas, water supply, power and other networks are still expanding and becoming increasingly complex. Determination of the reliability of such networks is complicated and in many cases is a NP–hard problem [1, 2, 20]. The solutions suggested in the literature most often relate to a determination of the reliability of undirected networks due to their coherence and structure of links [22] or due to their effective distribution [6,28]. There are also attempts to account for both aspects in the reliability evaluation [18].

Three kinds of accurate computations exist for the network reliability: exact [13], approximate and boundary values [5,10]. Since Moskovitz [14] used it as an accurate method of network reliability determination due to its coherence, the factoring algorithm has very often been used, investigated and modified [17, 21]. The network model in the factoring algorithm is an undirected graph, and the reliability measure is the probability of connectedness among the specified set of nodes – *K*-terminal network reliability [7, 27]. The reliability is determined by a reduction of the graph representing the network with the assumption that the network nodes are perfectly reliable [3, 4]. The reliability determination of networks with failing links and nodes was also considered and the proposed computation methods were presented in [11, 24, 25]. As network reduction is significantly time-consuming, there was a search for quicker and more effective methods [12]. The following can be used for these purposes: series-parallel, polygon-to-chain, delta-to-star, degree-1 and degree-2 reductions, and also other methods [9, 2 6]. The formula obtained as a result of reduction allows computing a specified measure of network reliability for the chosen time. Practical applications of the factoring algorithm mainly regard real gas and water supply networks [15, 18] as well as computer networks [23].

(*) Tekst artykułu w polskiej wersji językowej dostępny w elektronicznym wydaniu kwartalnika na stronie ***www.ein.org.pl***

However, the reliability computed in this manner does not take into account the repair of failing network elements. The elements of real networks such as pipelines, telecommunication lines etc. are always repaired after failure. For the network reliability determination model to better reflect the reality, the repair of elements should be taken into account.

This paper presents the method of network reliability determination as the probability of connectedness among the specified set of nodes (K-terminal network reliability) taking into account the repair of failing links and nodes. The failures and repairs of nodes were implemented according to the proposed π method. The proposed model of reliability computation uses the classic factoring algorithm, the π method and the simulation method suitably adapted to them. The reliability computation for networks with repairable elements comprises two stages. In stage I, which is based on classic factoring algorithm, the formula is obtained for accurate computation of reliability of a network without repair of the elements. In stage II, the formula and the π method are used in the simulation procedure wherein the network reliability is determined when the nodes are repaired after failure.

2. Notation and assumptions

$G=(V,E)$ –undirected graph which represents an undirected network,
$V=(v_1,v_2,\ldots,v_n)$ – set of vertices in a graph representing nodes in a network,
$E=(e_1,e_2,\ldots,e_m)$ – set of edges in a graph representing links in a network,
v_j – vertex in a graph and node in a network, $v_j \in V$,
e_i – edge in a graph and link in a network, $e_i \in E$,
n – number of nodes in a network, $n=|V|$,
N_f – set of nodes which can fail, $n_f \subseteq V$,
m – number of links in a network, $m=|E|$,
K – specified set of vertices in a graph (nodes in a network) which should be connected in order to guarantee the network's operating state,
G_K – graph with specified set $K \subseteq V$,
$x_i(t)$ – state of link e_i at time t expressed in a binary manner, $x_i \in \{0,1\}$,
$se_i(t)$ – state of link e_i at time t expressed in a numerical manner, $se_i \in \{1,0,-1,-2\}$,
$p_i = Pr(x_i=1)$ – probability that link e_i is in an operating state,
$q_i=1-p_i=Pr(x_i=0)$ – probability that link e_i is in a failure state,
$R_{N(K)}=R(G_K)$ – network reliability – probability of connectedness among the specified set K of nodes (K-terminal network reliability),
AM – adjacency matrix of a network,
$X(t)=(x_1(t),x_2(t),\ldots,x_m(t))$ – set of all links' states at time t,
$Se(t)=(se_1(t), se_2(t),\ldots,se_m(t))$ – set of all links' states at time t expressed in a numerical manner,
$\Phi(t)=R_{N(K)}(X(t))$ – function determining in a binary manner the network state at time t, $\Phi(t)\in\{0,1\}$,
T_h – simulation time horizon,
t_e – time of event,
t_{fij} – time when the jth failure of link e_i occurs,
t_{rij} – time when the jth repair of link e_i ends,
t_{sf} – time when in sth simulation a network's failure state occurs,
s_{max} – number of simulation repetitions,
$s_f(t)$ – number of simulations which until time t ended with occurrence of the network's failure state,
$R_{N(K)}(t)$ – reliability of a network with links and nodes repairable after failure.

The following assumptions were made in order to determine the network reliability using the proposed method:

i Model of network is an undirected stochastic graph.

ii The measure of network reliability is the probability that all nodes from specified set K are connected – K-terminal network reliability.

iii All links e_i in the network can fail statistically independently of each other with known probability $q_i=1-p_i$, and the distribution of failure time of each is known.

iv To obtain the formula for computation of network reliability $R_{N(K)}$, it is assumed that the nodes are perfectly reliable: $p_{vi}=1$, and the links are unrepairable.

v When determining the reliability $R_{N(K)}(t)$ of a network with failing and repairable elements, all the links and nodes can fail statistically independently of each other with known probabilities, and the distribution of failure time of each is known.

vi A failure of a node in the network causes a quasi-failure of all links adjacent to the failed node.

vii Each network link e_i and node v_j can be in only one of two states: operating or failure.

viii Repair of each element results in restoration of its original reliability.

3. Determination of reliability of a network with perfect nodes and unrepairable links

The goal of stage I of the analysis is to obtain the formula for computation of reliability of a network with perfect nodes and unrepairable links. The factoring algorithm was used for this purpose. The formula $R_{N(K)}$ is obtained by reduction of the graph representing the network [16, 27]. The reduction process is based on a well-known principle of contracting and deleting of links which is recursively applied for all edges e_i in graph G.
Examples of reduction for specified sets K are shown in Figure 1 (a: $|K|=|V|$, b: $|K|=2:\{v_1,v_2\}$).

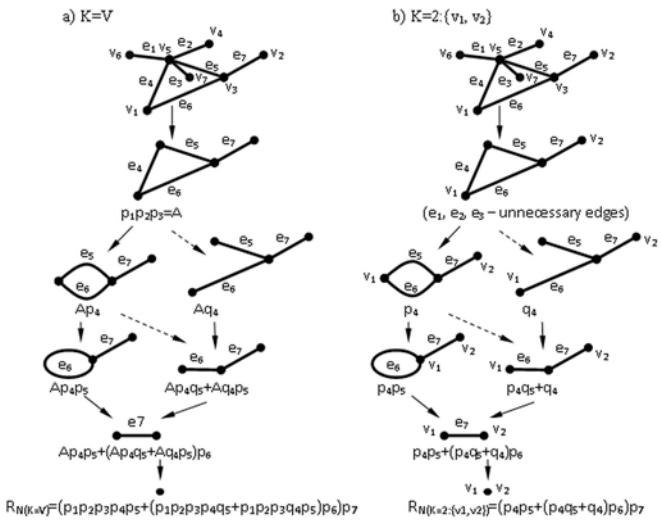

Fig. 1. Examples of reduction according to the factoring algorithm

4. Reliability of a network with imperfect and repairable links and nodes – π method

In stage II of the analysis we present the π method which takes into account the failures and repairs of links and nodes in the network.

Because, according to assumption vii, each link e_i can be only in one of two states, it was assumed that this state will be expressed in a

binary manner and denoted $x_i(t)$. As a result of failures and repairs, the values $x_i(t)$ can change in time as follows:

$$x_i(t)=\begin{cases}1-link\ e_i\ \ is\ in\ an\ operating\ state\ at\ time\ t\\ 0-link\ e_i\ is\ in\ a\ failure\ state\ at\ time\ t\end{cases} \tag{1}$$

and the set of states of all links in the network at any time t is written as:

$$X(t)=\left(x_1(t),\ x_2(t),\ldots,x_m(t)\right) \tag{2}$$

The following substitution for probability values p_i and q_i are made in formulas for network reliability ($R_{N(K)}$) obtained according to the factoring algorithm:

$$\begin{cases}p_i=x_i(t)\\ q_i=1-x_i(t)\end{cases} \tag{3}$$

Now, it can be noticed that after using formulas (1) – (3), the value of function $\Phi(t) = R_{N(K)}(X(t))$ in each case determines the network state in a binary manner due to the fact that the connectedness of nodes from set K: 1 – K nodes are connected, 0 – K nodes are not connected, which will be written as:

$$\Phi(t)=R_{N(K)}\left(X(t)\right)=\begin{cases}1-operating\ state\ of\ network\ at\ time\ t\\ 0-failure\ state\ of\ network\ at\ time\ t\end{cases}$$

(4)

It is an easy method for determining the network state at any time t for each possible case $X(t)$ resulting from combination of states $x_i(t)$ of network links.

As each link e_i connects two nodes located on its ends (these nodes are adjacent to link e_i), the adjacency matrix (AM) for any network can be written in the following form:

$$AM=\begin{bmatrix}a_{i,j} & \cdots & a_{i,n}\\ \vdots & \ddots & \vdots\\ a_{m,j} & \cdots & a_{m,n}\end{bmatrix};\qquad \begin{matrix}i=1,2,\ldots,m\\ j=1,2,\ldots,n\end{matrix} \tag{5}$$

$$a_{i,j}=\begin{cases}1-if\ node\ v_j\ is\ one\ of\ two\ nodes\ adjacent\ to\ link\ e_i\\ 0-if\ node\ v_j\ isn't\ one\ of\ two\ nodes\ adjacent\ to\ link\ e_i\end{cases} \tag{6}$$

Matrix AM will be used during calculation process to fastest finding the numbers of links which are in a failure state as a result of failure of nodes.

Analysing the structures of links in various networks, it is easy to notice that each link e_i which is adjacent to the failed node cannot be used to connect the specified set K of nodes. According to assumption vi, such a state is called a quasi-failure of the link.

If nodes v_k and v_l are adjacent to link e_i, possible cases of failure and quasi-failures of link e_i are presented in Figure 2.

The cases presented in Figure 2 cause:

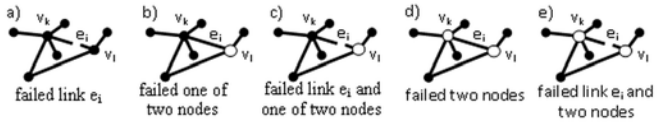

Fig. 2. Possible cases that caused a failure state and quasi-failures of link e_i

– 2a: failure of link e_i,
– 2b: quasi-failure of link e_i,
– 2c: failure and simultaneously quasi-failure of link e_i,
– 2d: double quasi-failure of link e_i,
– 2e: failure and simultaneously double quasi-failure of link e_i.

Each kind of link's failure is assumed in calculations as a failure state of that link.

The numerical value $se_i(t)$ which describes the link's state was introduced in order to allow for determining the number of failures at time t which cause the failure state of the link. If at time t the link e_i is in operating state, $se_i(t)$=1. Now, it was assumed that as a result of events, failures and repairs of link e_i and nodes v_k and v_l occurring at time t_e, values $se_i(t)$ of link e_i and other links adjacent to nodes v_k and v_l will change as follows:

– if link e_i at time t_e changes into failure state:

$$se_i(t>t_e)=se_i(t_e)-1 \tag{7}$$

– if node v_k at time t_e changes into failure state:

$$\forall i\left(i\in(1,\ldots,m)\wedge\left(AM\left(a_{i,j=k}\right)=1\right)\Rightarrow se_i(t>t_e)=se_i(t_e)-1\right) \tag{8}$$

– if node v_l at time t_e changes into failure state:

$$\forall i\left(i\in(1,\ldots,m)\wedge\left(AM\left(a_{i,j=l}\right)=1\right)\Rightarrow se_i(t>t_e)=se_i(t_e)-1\right) \tag{9}$$

– if link e_i at time t_e changes into operating state:

$$se_i(t>t_e)=se_i(t_e)+1 \tag{10}$$

– if node v_k at time t_e changes into operating state:

$$\forall i\left(i\in(1,\ldots,m)\wedge\left(AM\left(a_{i,j=k}\right)=1\right)\Rightarrow se_i(t>t_e)=se_i(t_e)+1\right) \tag{11}$$

– if node v_l at time t_e changes into operating state:

$$\forall i\left(i\in(1,\ldots,m)\wedge\left(AM\left(a_{i,j=l}\right)=1\right)\Rightarrow se_i(t>t_e)=se_i(t_e)+1\right) \tag{12}$$

hence, from formulas (7) – (12) we obtain the set of possible values $se_i(t)$ for each link:

$$se_i(t)=\left\{\begin{matrix}1-operating\ state\ of\ link\ e_i\ and\ both\ nodes\ v_k,v_l\\ 0-failure\ state\ of\ link\ e_i\ or\ node\ v_k\ or\ node\ v_l\\ -1-failure\ state\ of\ link\ e_i\ and\ one\ of\ two\ nodes\ v_k,\ v_l\ or\\ \quad operating\ state\ of\ link\ e_i\ and\ failure\ state\ of\ both\ nodes\ v_k,v_l\\ -2-failure\ state\ of\ link\ e_i\ and\ both\ nodes\ v_k,v_l\end{matrix}\right\} \tag{13}$$

The set of values $se_i(t)$ for all links in the network will be written as:

$$Se(t)=\left(se_1(t),\ se_2(t),\ldots,se_m(t)\right) \tag{14}$$

Because each type of link failure is assumed in calculations as its failure state, the state of link $x_i(t)$ can be expressed in a binary manner, rewriting the formula (1) in the following form:

$$x_i(t)=\begin{cases}1-if\ se_i(t)=1;\ operating\ state\ of\ link\ e_i\\ 0-if\ se_i(t)<1;\ failure\ state\ of\ link\ e_i\end{cases} \tag{15}$$

This proposed method of accounting for failures and repairs of links and nodes in the network (7) – (15) is called the **π method** (3.14) because:

- the state of each link depends on **3** elements: the link and two nodes adjacent to this link,
- there is only **1** possibility when the link is in an operating state: the link and both nodes adjacent to this link are in an operating state,
- the state of each link is quantified by a maximum **4** values: $se_i(t)\in\{1,0,-1,-2\}$.

In this way, using the π method we determine the state of link e_i taking into account failures of the link itself and failures of adjacent nodes.

Using formula (15) we now also obtain the set of states $X(t)$, and from formula (4) we can calculate function $\Phi(t)$. Hence, it is possible to determine the state of the whole network due to connections of nodes from set K, at imperfect and repairable links and nodes.

5. Implementation of the π method – simulation model for estimation network reliability

The simulation method is implemented according to the diagram which for the network from Figure 1a is exemplary presented in Figure 3. Successive values of failure times and repair times are sampled independently for each link e_i and node v_j (we used the method of inverse cumulative distribution function) [19]. These values are summed, thus making successive values of times t_{fij} and t_{rij}. The process continues until the simulation time horizon (T_h) is reached, or until the network is in a failure state ($\Phi(t)$=0). The nodes failures are accounted for by means of quasi-failures of links according to the π method.

The method of results analysis by using: $R_{N(K)}$ formula, matrix AM and π method is presented in Table 1.

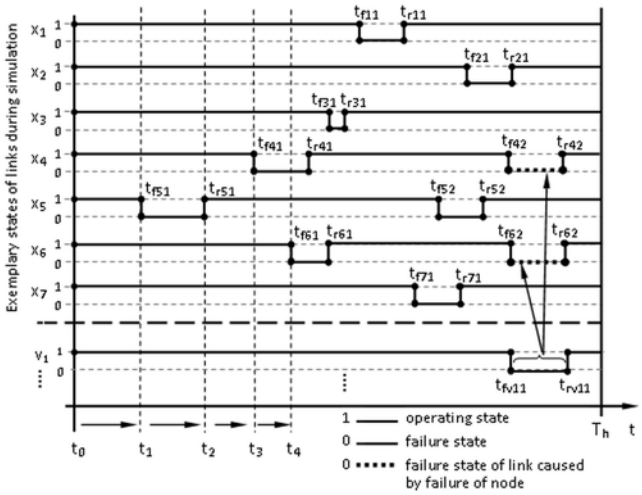

Fig. 3. Exemplary states of $x_i(t)$ of network links from Fig. 1a) during simulation

The presented method of sampling the time of events (failure and repair completion of the links and nodes) and of their analysis is applied in each simulation, which is repeated a specified number of times (s_{max}). The obtained values of times t_{sf} from all the simulations are then used to compute the reliability of a network with repairable links and nodes according to the formula:

$$R_{N(K)}(t)=1-\frac{s_f(t)}{s_{max}} \tag{16}$$

Table 1. Method of result analysis during simulation for link states from Figure 3

No.	t	$X(t)$	$R_{N(K=V)}$	$\Phi(t) = R_{N(K=V)}(X(t))$
1	t_0	$X(t_0)$ = (1,1,1,1,1,1,1)	$(p_1p_2p_3p_4p_5+[p_1p_2p_3p_4q_5+p_1p_2p_3q_4p_5]p_6)p_7$ after applying (3): $(x_1(t)x_2(t)x_3(t)x_4(t)x_5(t)+[x_1(t)x_2(t)x_3(t)x_4(t)(1-x_5(t))+x_1(t)x_2(t)x_3(t)(1-x_4(t))x_5(t)]x_6(t))x_7(t)$	1 – operating state
2	t_1	$X(t_1)$ = (1,1,1,1,0,1,1)		1 – operating state
3	t_2	$X(t_2)$ = (1,1,1,1,1,1,1)		1 – operating state
4	t_3	$X(t_3)$ = (1,1,1,0,1,1,1)		1 – operating state
5	t_4	$X(t_4)$ = (1,1,1,0,1,0,1)		0 – failure state of network: $t_4=t_{sf}$

The simulation procedure was written as a computer program using the Matlab package. The program makes it possible to compute various measures of network reliability for the following cases:

- perfectly reliable nodes ($N_f=\varnothing$),
- failures and repairs of all network nodes ($N_f= V$),
- failures and repairs of a chosen set of nodes ($|N_f|<|V|$).

In addition, any subsets of failing links and nodes can have different probability distributions of failure time and different values of repair rate.

6. Example and results of application of the method

The developed method was applied to compute the reliability of network presented in Figure 4. The model of this network in the form of an undirected graph consists of 36 links and 34 nodes.

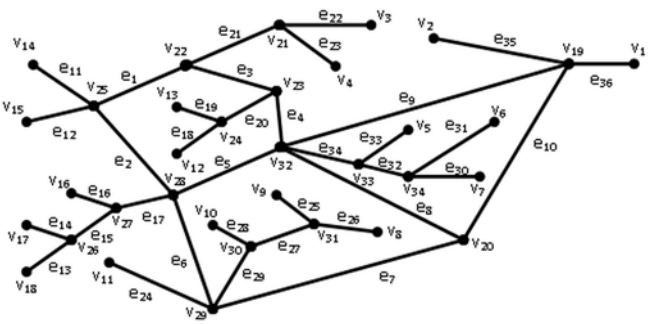

Fig. 4. Structure of the analysed network

Reductions were made for the analysed network according to the method presented in stage I, and the formulas were obtained to compute three different reliability measures: $R_{N(K=V)}$, $R_{N(K=2:\{v1,v14\})}$, $R_{N(K=18:\{v1-v18\})}$. Formulas are extensive and are not presented.

Obtained formulas were used in the simulation computations. The probability distributions of failure time and of repair of nodes and links, along with the parameters used in simulations, are presented in Table 2. In all cases, the exponential distribution of repair probability and μ=10 [1/t.u.] (t.u. – time unit) was assumed for nodes $v_j\in N_f$ and links e_i. The results of the computations for all cases from Table 3 are presented in Figures 5 and 6.

Table 2. Probability distributions and parameters used in the simulations

Network reliability measure	Set of nodes which can fail N_f	Probability distribution of failure time for nodes $v_j \in N_f$	Probability distribution of failure time for links $e_i \in E$
I: $R_{N(K=18):\{v1\text{-}v18\}}$	**1)** $N_f = \varnothing$: all nodes perfectly reliable	–	Exponential: $\lambda = 3 \cdot 10^{-4}$ [1/t.u.]
II: $R_{N(K=18):\{v1\text{-}v18\}}$	**1)** $N_f = \varnothing$	–	Normal: m=80 [t.u.]; σ=25 [t.u.]
	2) $N_f = 16$: $\{v_{19},\ldots,v_{34}\}$	Weibull: α=1.9; β=150 [t.u.]	
	3) $N_f = 16$: $\{v_{19},\ldots,v_{34}\}$	Weibull: α=1.9; β=100 [t.u.]	
III: $R_{N(K=V)}$	**1)** $N_f = \varnothing$	–	Weibull: α=1.9; β=150 [t.u.]
	2) $N_f = 16$: $\{v_{19},\ldots,v_{34}\}$	Weibull: α=1.9; β=150 [t.u.]	
	3) $N_f = V$: $\{v_1,\ldots,v_{34}\}$		
	4) $N_f = V$: $\{v_1,\ldots,v_{34}\}$	Weibull: α=1.9; β=100 [t.u.]	
IV: $R_{N(K=2):\{v1,\,v14\}}$	**1)** $N_f = \varnothing$	–	Normal: m=80 [t.u.]; σ=25 [t.u.]
	2) $N_f = 8$: $\{v_{19},v_{20},v_{22},v_{23},v_{25},v_{28},v_{29},v_{32}\}$	Weibull: α=1.9; β=150 [t.u.]	
	3) $N_f = \varnothing$	–	Weibull: α=1.9; β=150 [t.u.]
	4) $N_f = 8$: $\{v_{19},v_{20},v_{22},v_{23},v_{25},v_{28},v_{29},v_{32}\}$	Weibull: α=1.9; β=150 [t.u.]	
	5) $N_f = 8$: $\{v_{19},v_{20},v_{22},v_{23},v_{25},v_{28},v_{29},v_{32}\}$	Weibull: α=1.9; β=100 [t.u.]	links e_{11}, e_{36} – Weibull: α=1.9; β=100 [t.u.], other links – Normal: m=80 [t.u.]; σ=25 [t.u.]

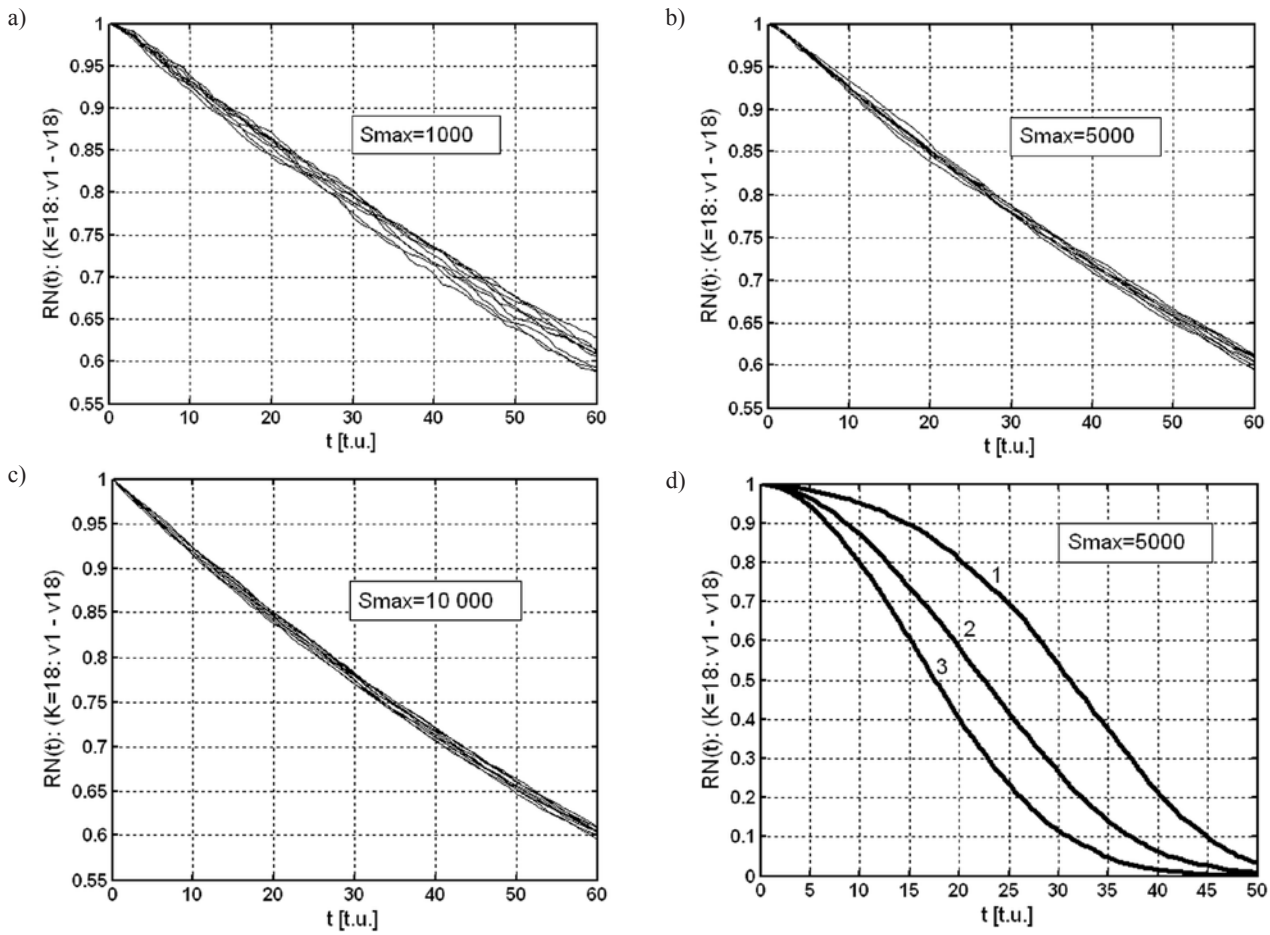

Fig. 5. Dispersion of results depending on the number of repetitions: a), b), c) – case I according to Table 2, and network reliability: d) – case II according to Table 2

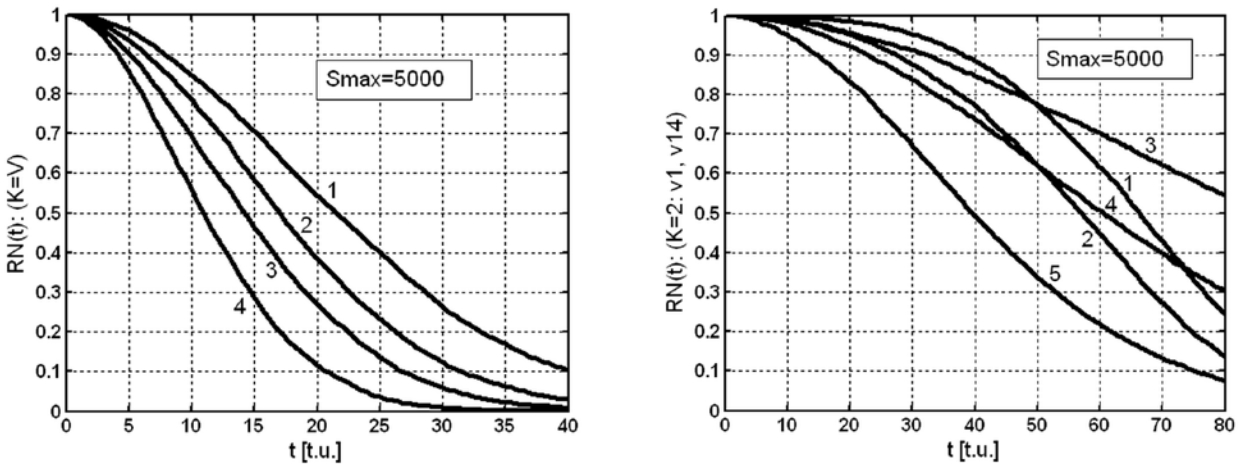

Fig. 6. Network reliability: a) – case III, b) – case IV according to Table 2

Figures 5a, 5b and 5c present the dispersion of results from 10 simulations depending on the number of repetitions (s_{max}) of a single simulation. One can notice that the increase of the number of repetitions s_{max} from 1000 to 5000 significantly improves the convergence of results, but increasing s_{max} to 10000 does not result in a significant improvement. The average computation time increased from 0.9 [s] to 2.6 [s], and for s_{max}=10000 to 4.9 [s]. The computations were performed on a standard PC with a 1.5 [GHz] processor and 2 [GB] RAM. Figure 5d presents the reliability of the analysed network $R_{N(K=18:\{v1-v18\})}(t)$ when the network nodes do not fail, and when the specified set of nodes N_f fails – case II in Table 2.

Figure 6a presents network reliability $R_{N(K=V)}(t)$ obtained for case III according to Table 2. Figure 6b presents another measure of network reliability $R_{N(K=2:\{v1,v14\})}(t)$, also obtained for various sets of failing nodes in the network and various probability distributions of failure time. In all cases, accounting for possible failures of a specified set of nodes or all nodes results in a reduced network reliability when compared to the situation with perfectly reliable nodes. For cases II, III and IV in Table 2, when the links and nodes failed, the calculation time at s_{max}=5000 was in the 5 – 20 [s] range.

7. Summary and critical discussion

The developed computation method allows determination of the various reliability measures for networks with repairable elements. This method cab be used mainly for calculating structural reliability of real water and gas supply networks as well as logistics and different kind of telecommunications networks. Especially it can be useful for computer networks where links and nodes are completely different elements but both have strong influence on network reliability. The developed model can also be applied to compute the reliability of other complex technical systems with specified (known) reliability structures which contain repairable elements.

The proposed π method allows for accounting for the failures of both links and nodes in the network by the introduction of quasi-failures of links. After applying the π method, the formulas obtained according to the factoring algorithm which account only for the failure of links allow for an easy determination of the state of the whole network when both links and nodes fail. In the developed simulation model it is possible to use various probability distributions of failure time for any subsets of links and subsets of nodes which can fail (imperfect nodes). The failing elements can also have different values of repair rate.

The results indicate that using the models with perfectly reliable nodes (N_f=∅) leads to overestimating the network reliability. Taking failures and repairs of nodes and links into account makes the model better reflect failures occurring in real networks. Hence, the presented model can be more useful in the analysis of practical cases, giving a more credible assessment of network reliability.

The inconvenience of the above method is the need to use the formulas obtained according to the factoring algorithm which, in the case of very complex network, are rather time-consuming to obtain. Further research can aim at searching for more effective network reduction methods and methods of obtaining formulas for sought network reliability measures $R_{N(K)}$, e.g. by development of computer algorithms or modification of the method and determination of the network reliability without the need to use them. Another interesting direction for future research can be a modification of the method for use in directed networks.

References

1. Ball M O. Complexity of network reliability computations. Networks 1980;10: 153-165, http://dx.doi.org/10.1002/net.3230100206.
2. Ball M O. Computational complexity of network reliability analysis: An overview. IEEE Transactions on Reliability 1986; 35 (3): 230-39, http://dx.doi.org/10.1109/TR.1986.4335422.
3. Beichelt F, Tittmann P. A generalized reduction method for the connectedness probability of stochastic networks. IEEE Transactions on Reliability 1991; 40 (2): 198-204, http://dx.doi.org/10.1109/24.87128.
4. Carlier J, Lucet C. A decomposition algorithm for network reliability evaluation. Discrete Applied Mathematics 1996; 65: 141-156, http://dx.doi.org/10.1016/0166-218X(95)00032-M.
5. Gnedenko B, Ushakov I. Probabilistic reliability engineering, Falk J Ed., Wiley, New York, Chichester, Brisbane, Toronto, Singapore 1995: 340-377, http://dx.doi.org/10.1002/9780470172421.ch9.
6. Gu C, Wu J, Li F. Reliability-based distribution network pricing. IEEE Transactions on Power Systems 2012; 27 (3): 1646-1655, http://dx.doi.org/10.1109/TPWRS.2012.2187686.
7. Hardy G, Lucet C, Limnios N. K-Terminal network reliability measures with binary decision diagrams. IEEE Transactions on Reliability 2007; 56 (3): 506-515, http://dx.doi.org/10.1109/TR.2007.898572.

8. Jan R-H. Design of reliable networks. Computers & Operations Research 1993; 20: 25-34, http://dx.doi.org/10.1016/0305-0548(93)90093-X.
9. Koide T, Shinmori S, Ishii H. Topological optimization with a network reliability constraint. Discrete Applied Mathematics 2001; 115: 135-149, http://dx.doi.org/10.1016/S0166-218X(01)00221-9.
10. Krivoulets V G, Polesskii V P. Quasipacking bounds for network reliability. Information Processes 2001; 1 (2): 126-146.
11. Lin M S, Chen D J, Horng M S. The reliability analysis of distributed computing systems with imperfect nodes. The Computer Journal 1999; 42 (2): 129-141, http://dx.doi.org/10.1093/comjnl/42.2.129.
12. Liu W Li J. An improved recursive decomposition algorithm for reliability evaluation of lifeline networks. Earthquake Engineering & Engineering Vibration 2009; 8: 409-419, http://dx.doi.org/10.1007/s11803-009-8152-2.
13. Lucet C, Manouvrier J-F. Exact methods to compute network reliability, in Statistical and Probabilistic Models in Reliability, Ionescu D C and Limnios N, Eds. Birkhauser, Boston 1999: 279-294, http://dx.doi.org/10.1007/978-1-4612-1782-4_20.
14. Moskowitz F. The analysis of redundancy networks. AIEE Trans. (Commun. Electron.) 1958; 39: 627-632.
15. Natvig B, Morch H. An application of multistate reliability theory to an offshore gas pipeline network. International Journal of Reliability, Quality and Safety Engineering 2003; 10 (4): 361-381, http://dx.doi.org/10.1142/S0218539303001214.
16. Page L B, Perry J E. A practical implementation of the factoring theorem for network reliability. IEEE Transactions on Reliability 1988; 37: 259-267, http://dx.doi.org/10.1109/24.3752.
17. Pilch R, Szybka J, Broniec Z. Determining of hot water-pipe exploitation time on the basis of limiting states. Eksploatacja i Niezawodnosc - Maintenance and Reliability 2012; 14 (3): 203-207.
18. Pilch R, Szybka J, Tuszynska A. Application of factoring and time-space simulation methods for assessment of the reliability of water-pipe networks. Eksploatacja i Niezawodnosc - Maintenance and Reliability 2014; 16 (2): 253-258.
19. Pilch R. A method for obtaining the required system reliability level by applying preventive maintenance. Simulation: Transactions of the Society for Modeling and Simulation International 2015; 91 (7): 615-624, http://dx.doi.org/10.1177/0037549715592274.
20. Provan J S. The complexity of reliability computations on planar and acyclic graphs. SIAM Journal on Computing 1986; 15 (3): 694-702, http://dx.doi.org/10.1137/0215050.
21. Ramirez-Marquez J E, Rocco C M. All-terminal network reliability optimization via probabilistic solution discovery. Reliability Engineering and System Safety 2008; 93: 1689-1697, http://dx.doi.org/10.1016/j.ress.2008.01.001.
22. Resende L. Implementation of a factoring algorithm for reliability evaluation of undirected networks. IEEE Transactions on Reliability 1988; 37 (5): 462-468, http://dx.doi.org/10.1109/24.9862.
23. Soi I M, Aggarwal K K. Reliability indices for topological design of computer communication networks, IEEE Transactions on Reliability 1981; 30: 438-443, http://dx.doi.org/10.1109/TR.1981.5221158.
24. Theologou O R, Carlier J G. Factoring and reductions for networks with imperfect vertices. IEEE Transactions on Reliability 1991; 40: 210-217, http://dx.doi.org/10.1109/24.87131.
25. Torrieri D. Calculation of node-pair reliability in large networks with unreliable nodes, IEEE Transactions on Reliability 1994; 43: 375-82, http://dx.doi.org/10.1109/24.326428.
26. Wood R K. A factoring algorithm using polygon-to-chain reductions for computing K-terminal network reliability. Networks 1985; 15: 173-190, http://dx.doi.org/10.1002/net.3230150204.
27. Wood R K. Factoring algorithms for computing K-terminal network reliability. IEEE Transactions on Reliability 1986; 35 (3): 269-278, http://dx.doi.org/10.1109/TR.1986.4335431.
28. Yannopoulos S, Spiliotis M. Water distribution system reliability based on minimum cut - set approach and the hydraulic availability. Water Resources Management 2013; 27: 1821-1836, http://dx.doi.org/10.1007/s11269-012-0163-5.

Robert PILCH
AGH University of Science and Technology
Faculty of Mechanical Engineering and Robotics
Department of Machine Design and Technology
Al. A. Mickiewicza 30, 30-059 Cracow, Poland
E-mail: pilch@agh.edu.pl

Article citation info:
BALLESTEROS A, SANDA R, MAQUA M, STEPHAN J-L. Maintenance related events in nuclear power stations. Eksploatacja i Niezawodnosc – Maintenance and Reliability 2017; 19 (1): 26–30, http://dx.doi.org/10.17531/ein.2017.1.4.

Antonio BALLESTEROS
Radian SANDA
Michael MAQUA
Jean-Luc STEPHAN

MAINTENANCE RELATED EVENTS IN NUCLEAR POWER STATIONS

ZDARZENIA EKSPLOATACYJNE W ELEKTROWNIACH JĄDROWYCH

This paper presents the essential results of a study performed by the European Clearinghouse on Operational Experience Feedback, in cooperation with IRSN and GRS, aiming to analyse events where their direct or root cause was an inappropriate maintenance at nuclear power stations. The databases of IRSN, GRS, U.S. NRC and IAEA IRS were screened to select relevant events related to maintenance that took place in the period 2002-2013. The examination of the selected events resulted in their classification into nine categories or groups with sub-division in families and, if necessary, sub-families. In total 921 events were analysed. One of the event classifications performed was according to the type of maintenance (periodic, predictive, planned and corrective). The operational experience data analysis indicated that 47% of the events reported were related to periodic maintenance. The main affected components were „valves", followed by „electric power components". The main root causes observed are „maintenance performed incorrectly" (e.g., improper use of tools, breach of authorization, lapse, etc.), „deficiencies in written procedures or documents" and „deficiencies in management or organization". Regarding the impact on safety, the dominant family is „potential effects on safety function" (57%), followed by „significant effect on operation" (20%). Based on a detailed analysis of selected events, recommendations were developed and some of them are presented in this paper. This study highlights that the continuous analysis of maintenance related events and the efficient utilization of operational experience provide important insights for improving the quality of maintenance and for preventing the occurrence of unusual events and thus helps to enhance nuclear safety.

***Keyword**: operating experience, databases, nuclear power plants, maintenance events.*

W niniejszej pracy przedstawiono najważniejsze wyniki badania dotyczącego informacji zwrotnych na temat doświadczeń z eksploatacji urządzeń przeprowadzonego przez European Clearinghouse we współpracy z IRSN oraz GRS. Badanie miało na celu analizę zdarzeń, których bezpośrednią lub zasadniczą przyczyną była nieodpowiednia eksploatacja urządzeń w elektrowni jądrowej. W badaniu, przeszukiwano bazy danych których operatorami są IRSN, GRS, U.S. NRC oraz IAEA IRS w celu wyłonienia istotnych zdarzeń eksploatacyjnych z lat 2002-2013. Analiza wybranych zdarzeń pozwoliła na sklasyfikowanie ich według dziewięciu kategorii lub grup, które z kolei podzielono na rodziny i, jeśli zachodziła taka potrzeba, także na pod-rodziny. W sumie przeanalizowano 921 zdarzeń. Jedna z klasyfikacji zdarzeń została oparta na kryterium rodzaju utrzymania ruchu (okresowe, predykcyjne, planowe oraz korekcyjne). Analiza danych dotyczących doświadczeń operacyjnych wykazała, że 47% zgłaszanych zdarzeń było związanych z konserwacją okresową. Głównymi elementami, których dotyczyły badane zdarzenia były "zawory", a w drugiej kolejności "części elektryczne" Najważniejszymi zasadniczymi przyczynami zdarzeń były "nieprawidłowo wykonana konserwacja" (np. nieprawidłowe użycie narzędzi, naruszenie autoryzacji, pomyłka, itd), "niedoskonałe procedury pisemne lub niedoskonała dokumentacja" oraz "niedociągnięcia w zarządzaniu lub organizacji". W odniesieniu do wpływu na bezpieczeństwo, dominującą rodzinę zdarzeń stanowiło "potencjalne oddziaływanie na funkcję bezpieczeństwa" (57%), a w drugiej kolejności "znaczący wpływ na pracę" (20%) W oparciu o szczegółową analizę wybranych zdarzeń, opracowano rekomendacje, z których część przedstawiono w niniejszym artykule. Omawiane badanie zwraca uwagę na fakt, iż ciągła analiza zdarzeń eksploatacyjnych oraz skuteczne wykorzystanie doświadczeń z eksploatacji dostarczają istotnej wiedzy na temat możliwości doskonalenia jakości utrzymania ruchu oraz zapobiegania występowaniu zdarzeń, pomagając w ten sposób zwiększyć bezpieczeństwo produkcji energii jądrowej.

***Słowa kluczowe**: doświadczenia operacyjne, bazy danych, elektrownie jądrowe, zdarzenia eksploatacyjne.*

1. Introduction

An in-depth analysis of Maintenance related Events has been carried out in the frame of the activities of the European Clearinghouse on Operational Experience Feedback (OEF) for Nuclear Power Plants (NPP) [7]. This analysis updates and completes a previous study on Maintenance related Events published by the European Clearinghouse in 2009 [10-11]. The updated analysis performed in 2015 covers events registered in 4 different databases for a much longer period of time. The events are reported in the IAEA-IRS database [3-4], the US NRC LER database [8], the French national database SAPIDE [12] operated by IRSN and the German database VERA operated by GRS [6], and are related to the period 2002 - 2013. Since the maintenance related events represent around 30% of the total number of events reported in a typical database it was necessary to establish appropriate criteria with the aim to select the most relevant events. The number of selected events should be significant for a statistical analysis and, at the same time, a manageable number for an in-depth evaluation by the experts. With this in mind, the study was limited to NPP operational incidents which resulted directly (direct cause) from maintenance ac-

tivities or where maintenance was a root cause of such incidents. The scope of the work was to analyse in depth the causes, root causes, contributing factors and consequences as well as to deduce lessons learned and recommendations. This paper summarizes the results of the topical study "Events related to Maintenance at Nuclear Power Plants", issued by the European Clearinghouse in February 2016 [1].

2. Methodology

For gathering the experience from events related to maintenance at nuclear power plants, four databases were screened. IRSN and GRS analysed information from their respective databases, i.e. France and Germany, while JRC processed information from the IAEA IRS database and US NRC LER database. At the latest stage, JRC integrated all results. No event was counted twice for events reported to the IRS from US, France or Germany.

The databases were firstly searched using specific searching tools (keywords and/or guidewords combined with logical operators) suitable for each database, yielding the first list of potentially relevant events. The event reports contained in this first list were reviewed individually to determine their pertinence for the study, thus obtaining a screened list of relevant events. In total 921 events were selected for analysis.

The events relevant to the topic were classified according to the following categories or groups:

- plant status (on power, hot shutdown, cold shutdown, etc.),
- type of maintenance (periodic, predictive, etc.),
- method for detection of event (in-service inspection, surveillance, etc.),
- affected system in the plant,
- affected component,
- direct cause,
- root causes,
- corrective actions,
- effect on safety (significant effect on operation, effect on safety function, etc.).

For further analyses, the categories were divided into families and, if necessary, into sub-families. The final step includes an in-depth analysis of the causes, root causes, contributing factors, consequences and lessons learned of selected events, in order to identify recommendations to avoid recurrence of similar events. Figure 1 shows the methodology followed in this topical study. This methodology has been applied also in other studies with different topics undertaken by the European Clearinghouse [2, 5, 9, 13].

3. Data analysis

The events are classified according to the type of maintenance as showed in Figure 2. Most of the periodic maintenance consists of servicing while the plant is under normal operation. The difference observed with the German database is just a reflection of a different maintenance philosophy. In fact, in Germany, all events with a replacement of components are assigned to "Planned maintenance". It has to be noted that in the German event description included in the database there is no information whether the component was replaced preventively with or without abnormal behaviour.

The data analysis shows that the essential reactor auxiliary systems and the electrical systems are the systems prone to be affected by maintenance failures. This could be explained by the fact that these systems are essential for the smooth operation of the plant, and their rate of allowed unavailability per year is among the lower rates of the

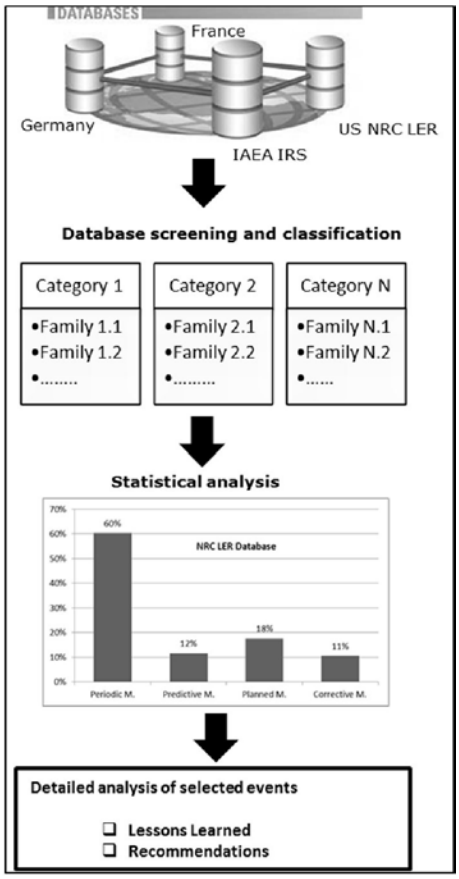

Fig. 1. Methodology

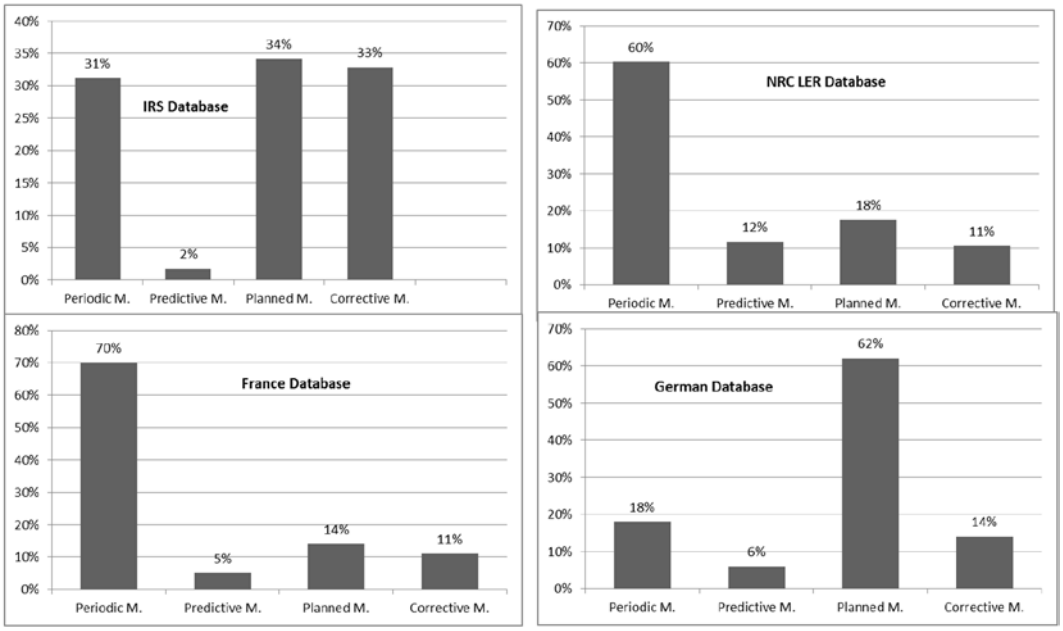

Fig. 2. Distribution of events according to maintenance type

Table 1. Root cause distribution of the events analysed in the IRS database

Root cause	Percentage
Wrong material has been used	5.84%
Corrective maintenance did not correct the problem	4.62%
Preventive maintenance inadequate	13.14%
Maintenance performed incorrectly	16.30%
Deficiencies in post maintenance testing	4.38%
Failure to exclude foreign material	2.92%
Deficiencies in written procedures or documents	19.46%
Deficiencies in management or organization	15.57%
Deficiencies in training or lack of knowledge	17.27%
Others	0.49%

plant systems. Reactor auxiliary systems and electrical systems are a priority for the maintenance activities, and they are often subjected to operational tests and in-service inspections – thus much more exposed to maintenance related failures.

Regarding the category „affected component", the valves and the electrical power components are the components most affected by week maintenance. This is in accordance with the results obtained in the analysis of most affected system. Taking into account that pumps is in the third place in the ranking of most affected component, it may be raised the idea that, apart from the electrical power components, the other most affected components are just those components more frequently subject to manoeuvring during operations and testing.

The results of the type of direct cause of the events show that in around 80% of the cases the most immediate cause triggering the event was of a technical nature (mechanical, electrical, I&C, structural or others) against a ~20% of events caused by human factors. Besides that, these results corroborate with the previous results regarding the most affected components and systems: The overwhelming part the technical failures were mechanical failures (and this is extremely plausible when thinking that the most affected components were those subjected often to manoeuvring, or put into special test or inspection configuration), followed by electrical failures (and the rate of electrical failures with respect to the total number of technical failures of any type is quite proportional to the corresponding rate of electrical components affected by maintenance-related events).

There are differences within the identified root causes of the events. While in France and in Germany the written procedures and documents appear to be quite consistent (15% in France and 11% in Germany), the situation is quite opposite in the US, where the main root cause registered was the imperfection of the written procedures and documents guiding the maintenance activities (29%). Besides that, while in the US the category „maintenance performed incorrectly" (e.g., improper use of tools, breach of authorization, lapse, etc.) is about 16%, in France and in Germany the incorrect way of performing maintenance occurred between 2 and 3 times more often.

The IRS event distribution, Table 1, shows that most of the events reported have as the most frequent root cause a deficiency in the written procedures and documents (19%), but nearly similar rates were also registered as root causes maintenance performed incorrectly (16%), deficiencies in management or organization (16%), and deficiencies in training or lack of knowledge (17%). There is one feature common to the four databases: the maintenance technicians managed to improve and maintain a better Foreign Material Exclusion Zone, since failing to exclude foreign material has quite a low contribution; the same situation is encountered for the post-maintenance testing.

The data analysis shows that there are two main corrective actions: changes in operating mode documents or procedures followed closely by repair or replacement. The corrective action „repair or replacement" was applied in a little less than half of the events. When linking the corrective actions with the root causes, the analysis shows that changes in maintenance documentation, program and personal training is a common response in the four database to correct any maintenance failure; at least two thirds of the corrective actions focused on three large administrative areas (changes in operating mode documents and procedures, changes in maintenance program and personal training). This is very consistent for the US database since the statistics revealed that in US the largest contributors (with a total of approx. 40%) were deficiencies in written procedures and documents and deficiencies in management or organization.

4. Observations from the analysed events

Lessons learned and specific recommendations from 40 selected events from the 921 events are given in [1]. Some general observations are listed below, resulting also from the events analysed. These insights should help avoiding deficiencies of the NPP´s during maintenance and reducing the number of events, especially with impact on safety.

4.1. Corrosion management

It should be checked, that existing corrosion protection measures have not been weakened by maintenance activities, especially in case of repairs or exchanges of parts. If an impact on the corrosion protection occurred, it has to be renewed. If a cathodic corrosion protection is used, the post-maintenance testing has to ensure, that the electric connection is still working after the maintenance activity.

After decontamination measures, the corresponding components have to be checked for intrusion of decontamination medium to avoid corrosion effects. Written procedures should include information on how to avoid the intrusion of corrosive medium during the decontamination of components. Additionally, the written procedures should give information about the measures to detect fluid intrusions in decontaminated components and how to clean these components, if necessary.

4.2. Ageing management

Occasionally, the ageing process of components is not in accordance with maintenance programs. Thus, components can lose their ability to ensure their function in accidental conditions. In order to ensure the availability and qualification of equipment, it is advised to:

- Specify a lifetime for the components and equipment selected within the ageing management programme;
- Maintain knowledge on the characteristics and limits of qualification which must be exhaustive;
- Prevent maintenance activities or maintenance program modifications that could prejudice the components qualification.

4.3. Housekeeping project

The housekeeping project concerns operating actors and aims at bringing good practices to plant staff for keeping their installation in a visually good state as if it was their own property. The project also involves the identification and correction of slow deviation phenomena that could impact the reliability of equipment important to safety due to their degradation or bad state of premises where they are located. For this purpose, user-friendly illustrated guides and many displays can help to implement these good practices.

4.4. Temporary device management

Whenever possible, the measurement circuits should be de-energized on relay protection and automatic control system measurement devices prior to performing technical maintenance. Whenever this condition cannot be realized, and for each equipment identified as not being possible to be de-energized before performing work on it, the manufacturer should be contacted with precise intentions to resolve shortcomings in the design of equipment not providing the necessary conditions for the safe conduct of work to remove (or install) devices.

4.5. Steam Generator maintenance

More than several hundreds of SG tube mechanical plugs are installed in each reactor. The loss of a plug can have heavy potential consequences on the safety (breach of a SG tube, migrating foreign material…), leading to a primary circuit breach. This has raised the issue of steam generator plug loss, and emphasises the high attention that must be paid to the installation and periodic check of the plugs. A periodic televisual inspection is advised to check the presence and correct position of the plugs inside the tubes.

4.6. Foreign Material Exclusion

Temporary filters should be thoroughly provided at the time work is being performed within the drywell of a BWR during periodic inspections and for construction work with the generation of a large amount of dust containing iron. In general more attention should be given to reduce the inflow of a large amount of dust containing iron into the system, by e.g. the use of blowers, which can reduce the potential of occurrence of an event. All preventive measures should be specified in the maintenance-related written procedure.

4.7. Risk of internal flooding

From the analysis of OEF, internal flooding is not sufficiently taken into account despite the fact that it could lead to the loss of equipment important to safety with a risk of common mode failures. The risk of internal floods can be induced by maintenance activities. For this purpose, the different scenarios that could damage the water circuit during maintenance activities have to be identified during risk analysis (pre-job briefing) or safety study.

4.8. Preservation of qualification

The operating organisation should ensure that the testing tools and techniques are appropriate to their scope, and whenever possible to benchmark the test results interpretation with a third party, especially when it comes to safety related components. When new developments are implemented related to material research or within the scope of inspection techniques and tools, the maintenance program should incorporate those as fast as reasonably possible.

4.9. Greasing non-compliance

Equipment is lubricated with specific grease for each kind of equipment. However, a human error from maintenance actors could lead to a mixture of these greases and thus to an unknown reaction (e.g. loss of qualification). In order to avoid this, the recommendations are as following:

- To implement in-depth measures such as to ensure proper preparation, execution and monitoring of operations and facilitate the prevention and detection of this type of non-compliance.
- Insufficient lubrication or hardened grease can lead to a stiffness of valves, which can result in the actuation of reactor protection signals. It is therefore necessary to sufficiently lubricate valves and to exchange old grease in an adequate time interval.

4.10. Post maintenance testing

The impact of any modification process should be checked against the most restrictive safety requirements that the equipment must fulfil. An independent review of any parameter modification is most welcomed and it should be performed each time when such modification is made to equipment important for safety. Post-maintenance testing should be exhaustive enough to guarantee optimal safety and operation of safety equipment. To avoid cases when equipment important to safety is installed without being properly tested by the manufacturer, especially in the cases when such equipment was repaired, the utility should by default test the equipment against the most limiting performance requirements.

4.11. Subcontractor management

Nowadays, the use of subcontractors for achieving maintenance activities is more and more frequent and is highlighted by a large number of events. Indeed, these events point out essential lacks in communication or surveillance by the operator staff.
Thus, to prevent issues during subcontracted activities, it is essential to facilitate the access to the necessary information and good working conditions. The operator should keep in mind that the subcontractor has generally a lower global knowledge about the state of the plant.

4.12. Calibration management

Many producers and vendors offer equipment with design features that ensure a long maintenance-free life expectancy. When performing ISI or any other kind of maintenance activities for this kind of equipment, the tools used by the licensee should be in accordance with the manufacturer recommendations in order to preserve a long maintenance-free life expectancy. Use of excessive force should be avoided at all times when manually stroking valves.

4.13. Maintenance procedures

All the existing procedures for replacing live relay protection and automatic control system measurement devices should be analysed, and all necessary changes to ensure instrument replacement programmes with respect to an event-free conduct of work should be implemented. This action could be performed as part of a special review of relay protection and automatic control system measurement devices used at NPPs, as a development of measures to ensure the safe removal and installation of measurement devices at live equipment.

4.14. Safety culture

The absence of a safety culture was identified as an accompanying root cause in some events. Disciplinary action, among other corrective actions, was also taken in one particular event. The presence of a strong safety culture in maintenance adds a significant value to the safe operation of the plant. With respect to plant maintenance, safety culture means keeping the maintenance process on track and in control at every stage of plant performance. When there is a strong safety culture, maintenance staff excels in the preparation and execution of the tasks in compliance with the safety, quality and technical specifications.

5. Conclusions

For this study the databases of IRSN, GRS, U.S. NRC and IAEA IRS were screened to select relevant events related to Maintenance that took place in the period 2002-2013. The examination of the selected events resulted in their classification into nine categories with families and, if necessary, sub-families. The definitions of the catego-

ries, families and sub-families are based on the preliminary results obtained for the four databases. In total 921 events were analysed.

One of the event classifications performed was according to the type of maintenance (periodic, predictive, planned and corrective). The data analysis indicated that 47% of the events reported were related to periodic maintenance. The main affected components were "valves" (with 33% of the events), followed by "electric power components" (23%). The main root causes observed are "maintenance performed incorrectly" (27%), "deficiencies in written procedures or documents"(19%) and "deficiencies in management or organization" (17%). Regarding the impact on safety, the dominant family is "potential effects on safety function" (57%), followed by "significant effect on operation" (20%).

Some general conclusions based on the analysed events are given below:

- The availability of an advanced plant data collection and storage system of maintenance events is important for trend analysis by NPP staff, which facilitates adequate classification of the types of human errors and components failures.
- The maintenance programme should be defined on the basis of real operating conditions.
- The programme effectiveness should be checked periodically.
- If probabilistic risk assessments are performed, the results can be used to help define and prioritize important systems and components.
- Adequate safety planning and risk assessment should be carried out especially when the conditions of testing or maintenance activity are changed.
- The use of OEF and timely implementation of preventive actions would have prevented the occurrence or recurrence of an event in several cases.
- Learning from plant's own maintenance history and a comprehensive human reliability analysis provide useful tools for identifying weaknesses in plant maintenance practices and procedures.

This study highlights that the continuous analysis of maintenance related events and the efficient utilization of operational experience provides important insights for improving the quality of maintenance and for preventing the occurrence of unusual events and thus helps to enhance nuclear safety.

References

1. Ballesteros A. and Sanda R., Events related to Maintenance at Nuclear Power Plants, Topical Study, NRSA/CLEAR/15-07-004 Rev. 0, February 2016.
2. Ballesteros A., Sanda R., Peinador M., Zerger B., Negri P., Wenke R., Analysis of events related to cracks and leaks in the reactor coolant pressure boundary, Nuclear Engineering and Design 2014; 275: 163-167, http://dx.doi.org/10.1016/j.nucengdes.2014.05.014.
3. IAEA International Reporting System (IRS) database (irs.iaea.org).
4. IRS Topical Study on Maintenance Events involving Quality Assurance, Human Factors and Procedural Issues, IAEA Working Material, 2007.
5. Kancev D., Duchac A., Zerger B., Maqua M., Wattrelos D., Events related to emergency diesel generators in the nuclear industry: Analysis of lessons learned from the operating experience, Progress in Nuclear Energy 2014; 75: 192-197, http://dx.doi.org/10.1016/j.pnucene.2014.05.002.
6. Michel F., Evaluation of Operating Experience with Regard to Passive Mechanical Components - Approach and New Insights. Proceedings of EUROSAFE Workshop, 2012.
7. Peinador M., Heitsch M., Ballesteros A., The European Clearinghouse For NPP Operating Experience Feedback: A Network of Regulators and TSOs Operated by the EC/JRC. Proceedings of the IAEA International Conference on Operational Safety. Vienna, Austria, 23-26 June 2015.
8. US Licensee Events Reports (LER) database (lersearch.inl.gov).
9. Volkanovski A., Ballesteros A., Peinador M., Kancev D., Maqua M., Stephan J-L., Analysis of loss of offsite power events reported in nuclear power plants, Nuclear Engineering and Design 2016; 307: 234-248, http://dx.doi.org/10.1016/j.nucengdes.2016.07.005.
10. Vuorio U., Summary Report: Analysis of Maintenance Related Events, European Clearinghouse on Operational Experience Feedback, EUR 24897 EN - 2011.
11. Vuorio U., European Clearinghouse: Analysis of Maintenance Related Events, Technical Report, number SPNR/CLEAR/09 12 001 Rev.00, 2009.
12. Wattrelos D. and Bertrand R., Operating Experience Feedback System in France. Proceedings of EUROSAFE Workshop, 2007.
13. Zerger B., Noël M., Nuclear power plant construction: What can be learned from past and on-going projects?, Nuclear Engineering and Design 2011; 241: 2916- 2926, http://dx.doi.org/10.1016/j.nucengdes.2011.05.037.

Antonio BALLESTEROS
Radian SANDA
Joint Research Centre of European Commission
IET, P.O.B. 2, NL-1755 ZG Petten, The Netherlands
Michael MAQUA
Gesellschaft für Anlagen-und-Reaktorsicherheit (GRS) gGmbH
Schwertnergasse 1, 50667 Köln, Germany
Jean-Luc STEPHAN
Institut de Radioprotection et de Sûreté Nucléaire (IRSN)
BP 17 - 92262 Fontenay-aux-Roses Cedex, France

E-mails: Antonio.Ballesteros-Avila@ec.europa.eu, Radian.SANDA@ec.europa.eu, Michael.Maqua@grs.de, jean-luc.stephan@irsn.fr

Article citation info:
GERDES M, GALAR D, SCHOLZ D. Decision trees and the effects of feature extraction parameters for robust sensor network design. Eksploatacja i Niezawodnosc – Maintenance and Reliability 2017; 19 (1): 31–42, http://dx.doi.org/10.17531/ein.2017.1.5.

Mike GERDES
Diego GALAR
Dieter SCHOLZ

DECISION TREES AND THE EFFECTS OF FEATURE EXTRACTION PARAMETERS FOR ROBUST SENSOR NETWORK DESIGN

WYKORZYSTANIE DRZEW DECYZYJNYCH ORAZ WPŁYWU PARAMETRÓW EKSTRAKCJI CECH DO PROJEKTOWANIA ODPORNYCH SIECI CZUJNIKÓW

Reliable sensors and information are required for reliable condition monitoring. Complex systems are commonly monitored by many sensors for health assessment and operation purposes. When one of the sensors fails, the current state of the system cannot be calculated in same reliable way or the information about the current state will not be complete. Condition monitoring can still be used with an incomplete state, but the results may not represent the true condition of the system. This is especially true if the failed sensor monitors an important system parameter. There are two possibilities to handle sensor failure. One is to make the monitoring more complex by enabling it to work better with incomplete data; the other is to introduce hard or software redundancy. Sensor reliability is a critical part of a system. Not all sensors can be made redundant because of space, cost or environmental constraints. Sensors delivering significant information about the system state need to be redundant, but an error of less important sensors is acceptable. This paper shows how to calculate the significance of the information that a sensor gives about a system by using signal processing and decision trees. It also shows how signal processing parameters influence the classification rate of a decision tree and, thus, the information. Decision trees are used to calculate and order the features based on the information gain of each feature. During the method validation, they are used for failure classification to show the influence of different features on the classification performance. The paper concludes by analysing the results of experiments showing how the method can classify different errors with a 75% probability and how different feature extraction options influence the information gain.

***Keywords**: decision trees, feature extraction, sensor optimization, sensor fusion, sensor selection.*

Niezawodne monitorowanie stanu wymaga niezawodności czujników i pochodzących z nich informacji. Systemy złożone są zazwyczaj monitorowane przez wiele czujników, co pozwala na ocenę stanu technicznego oraz aspektów eksploatacyjnych. Gdy jeden z czujników ulega uszkodzeniu, uniemożliwia to obliczenie bieżącego stanu systemu z dotychczasową niezawodnością lub uzyskanie kompletnych informacji o bieżącym stanie. Stan można co prawda monitorować nawet przy niekompletnych danych, ale wyniki takiego monitorowania mogą nie odpowiadać rzeczywistemu stanowi systemu. Sytuacja taka ma miejsce w szczególności, gdy uszkodzony czujnik jest odpowiedzialny za monitorowanie istotnego parametru systemu. Problem uszkodzenia czujnika można rozwiązywać na dwa sposoby. Pierwszy polega na zwiększeniu złożoności systemu, co umożliwia jego sprawniejsze działanie w sytuacji, gdy dane są niekompletne. Drugim sposobem jest wprowadzenie nadmiarowego sprzętu (hardware'u) lub oprogramowania. Niezawodność czujników stanowi krytyczny aspekt systemu. Oczywiście, ze względu na ograniczenia przestrzenne, ekonomiczne i środowiskowe nie wszystkie czujniki w systemie mogą być nadmiarowe. Redundancja powinna dotyczyć wszystkich czujników, które dostarczają istotnych informacji na temat stanu systemu, natomiast dopuszczalne są błędy mniej ważnych czujników. W niniejszej pracy pokazano jak obliczać istotność informacji o systemie dostarczanych przez poszczególne czujniki z wykorzystaniem metod przetwarzania sygnałów oraz drzew decyzyjnych. Zademonstrowano również w jaki sposób parametry przetwarzania sygnałów wpływają na poprawność klasyfikacji metodą drzewa decyzyjnego, a tym samym na poprawność dostarczanych informacji. Drzew decyzyjnych używa się do obliczania i porządkowania cech w oparciu o przyrost informacji charakteryzujący poszczególne cechy. Podczas weryfikacji zastosowanej metody, drzewa decyzyjne wykorzystano do klasyfikacji uszkodzeń celem przedstawienia wpływu różnych cech na dokładność klasyfikacji. Pracę kończy analiza wyników eksperymentów pokazujących w jaki sposób zastosowana metoda pozwala na klasyfikację różnych błędów z 75-procentowym prawdopodobieństwem oraz jak różne opcje ekstrakcji cech wpływają na przyrost informacji.

***Słowa kluczowe**: drzewa decyzyjne, ekstrakcja cech, optymalizacja czujników, fuzja czujników, dobór czujników.*

1. Introduction

This paper presents a condition monitoring system with sensor optimization capabilities to prevent unscheduled delays in the aircraft industry. Unscheduled delays cost airlines a great deal of money but can be prevented by condition monitoring [11]. The aim was to develop a simple condition monitoring system that can be understood by humans and modified by experts to incorporate knowledge that is not in the learning data set, using decision trees as the main tool. Decision trees satisfy the requirements and provide a ranking of data sources for condition monitoring.

The first section of the paper gives the motivation for developing a condition monitoring system with sensor optimization capabilities and explains the basic concepts of the proposed method. The second section explains the method in detail. Section three discusses the experiments validating it. The results of the validation experiments are given in section four. The paper concludes with a discussion of the results.

New and better monitoring approaches are required for condition monitoring, because systems are becoming more complex and more difficult to monitor [32]. Condition monitoring requires reliable sensors. To obtain enough sensing data, special attention should be given to optimizing sensor allocation to ensure system diagnosability, lower sensing cost and reduce time to diagnosis [37]. Sensors can be used to determine the system health of control systems; a failed sensor can lead to a loss of process control [18]. The information about a system is incomplete, if a sensor fails. Complex systems are often monitored by multiple sensors. An advantage of a multi sensor system is that a single failed sensor shows its effects in multiple sensors [18].This means the system condition is defined by all information from the sensors. However, the system's health status becomes uncertain when a sensor fails or sends wrong data. This could trigger incorrect maintenance, including maintenance on a part with no failure, as well as long maintenance times to find the correct fault or not noticing the fault at all.

The Safety Integrity Level (SIL) defines the probability that the system safety function for a Safety Instrumented System (SIS) can be executed. There are four SILs; level four is the level with the highest probability that an SIS can be performed. Sensor failure detection (sensor validation) is a critical part of the safety function of a system. When a failure is detected SIS is put into a safe state to avoid risk and damage to humans and machines [14, 13].

Redundancy is used to reduce the risk of model uncertainty [5]. One way to create sensor redundancy is hardware redundancy; another is analytical redundancy [5]. Analytical redundancy assumes multiple sensors deliver the same information, and, thus, a sensor fault can be compensated for. Hardware redundancy is not always possible, as it can be difficult to install multiple sensors because of physical or cost constraints [41, 22].

The proposed condition monitoring method uses a data driven model and uses machine learning methods to learn the model. Data driven modelling is a popular approach, especially as data harvesting is often cheaper than creating a physical model, offering cheap electronics, high computation power and advanced algorithms. Decision trees are used for machine learning because they create a comprehensive model, which can easily be modified and adapted. Decision trees are numerically stable, the learning is deterministic, and they are easy to test. The decision tree algorithm also sorts inputs of the model based on information gained. This latter feature is used for sensor optimization.

The novelty of this approach is that it presents a method for condition monitoring suitable for the very restricted aircraft environment. It combines decision trees with very stable and simple feature extraction methods. The method offers fast, testable and low footprint online condition monitoring for aircraft. The added sensor optimization allows the aircraft manufacturer to install redundant sensor hardware for the significant sensors, if software redundancy is not possible.

The inputs for the classifier are feature vectors (representing healthy and unhealthy states) and classifications of the vectors. The vectors for the supervised learning phase need to contain the classification of the data, because decision tree learning is supervised learning. These vectors represent the knowledge on which the classifier is based and used to classify new unknown samples.

Fig. 1. Basic Condition Monitoring Process [15]

The basic condition monitoring process is shown in Figure 1. It consists of three steps:

1. Data Acquisition: All data required for the monitoring are gathered, including data from multiple sources.
2. Data Processing: The collected data are processed and analysed. The goal is to create a meaningful collection of features for the decision making step. Operations include **signal processing** and **feature extraction**. The focus of the present research is on this step.
3. Maintenance Decision Making: The features are evaluated, and a decision is made based on this evaluation. The result can be a failure classification, a maintenance action or other relevant actions. Results are obtained by using a decision maker based on logic rules, pattern recognition, probability or some other method.

1.1. Civil Aerospace Software Development

Software development, documentation, testing, and certification in the civil aerospace industry are regulated by the DO-178B/C standard [27]. DO-187B/C defines how the software development process can be regulated to ensure safe software is written. More specifically, it defines a requirements-based development process with high and low level requirements. High level requirements concentrate on functionality, while low level requirements are often written in pseudo code or source code.

The most important step in the software development process is to define to which DAL (Design Assurance Level) the software belongs. There are five DALs; each is associated with a hazard/failure condition class defining how dangerous a software failure can be. The DALs are the following:

- **DAL A**: Catastrophic; normally with hull loss and multiple fatalities.
- **DAL B**: Hazardous; large reduction in functional capabilities and serious or fatal injury to a small number of passengers or crew.
- **DAL C**: Major; significant reduction of functional capabilities and physical distress or injuries for passengers or crew.
- **DAL D**: Minor; slight reduction in functional capabilities and physical discomfort for passengers.
- **DAL E**: No effect; no effect on operational capabilities and no inconvenience for passengers.

The software development objectives of a software developing agency are based on the DAL. DAL A requires 66 objectives, DAL B 65 objectives, DAL C 57 objectives, DAL D 28 objectives, and DAL E 0 objectives. The objectives are achieved by completing ten processes in the development of the software:

1. Software Planning Process.
2. Software Development Process.
3. Verification of Outputs of Software Requirements Process.
4. Verification of Outputs of Software Design Process.
5. Verification of Outputs of Software Coding & Integration Process.
6. Testing of Outputs of Integration Process.
7. Verification of Verification Process Results.
8. Software Configuration Management Process.
9. Software Quality Assurance Process.
10. Certification Liaison Process.

The most complex step besides coding for a software developer is testing the coded software. Based on the DAL, the testing needs to satisfy certain code coverages. For DAL D and E, for example, no code coverage is required; only the requirements need to be tested. DAL C adds statement coverage to the testing requirements. This means the tests need to address each line of code. No dead code is allowed. In addition to this, DAL B requires decision coverage; each possible path in the code must be taken. For DAL A, developers must

show that each variable for a decision in the code can influence the result (modified condition/decision coverage), as well as satisfying all other code coverages. All software testing needs to be done as black box testing. The tester cannot know the code but must work only with the compiled code, requirements and testing tools.

Robustness tests require border values of numerical values and of decisions to be tested and invalid or missing data to be identified. There can obviously be problems if algorithms use the wrong data type.

1.2. Feature Extraction

Feature extraction is the process of reducing the dimension of the initial input data to a feature set of a lower dimension containing most of the significant information of the original data [8]. Extraction is done to extract important features from noisy sensor data [19, 10] and to avoid having too many input features (especially for vibration data) in the classifier learning phase [19]. For these reasons, feature extraction is often a first and essential step for any classification [19]. Accordingly, it is part of the data processing step in the basic condition monitoring process (Figure 1).

Features are extracted from the time domain and the frequency domain (Fourier Transformation, Wavelet Transformation [10]). Basic features to extract are maximum, mean, minimum, peak, peak-too-peak interval etc. [15]. Complex feature extraction methods include principal component analysis (PCA), independent component analysis (ICA) and kernel principal component analysis (KPCA) [39].

1.2.1. Time domain features

Time domain features can be direct features like the number of peaks, zero-crossings, mean amplitude, maximum amplitude, minimum amplitude or peak-too-peak interval [15, 23]. In addition, it is possible to analyse a signal using probabilistic methods like root mean square, variance, skewness or kurtosis to get features that represent the signal [17]. Other methods include using correlation, autocorrelation, Entropy, principal component analysis (PCA), independent component analysis (ICA) and kernel principal component analysis (KPCA)[39].

1.2.2. Frequency and Time-Frequency domain

The Fast Fourier Transformation (FFT) transforms a signal from the time domain into the frequency domain. FFT takes a time series and transforms it into a complex vector that represents the frequency power in frequency domain. The basis of the FFT algorithm is the discrete Fourier transformation (DFT), defined as shown in equation 1 with $xn \ldots x_{n-1}$ as complex numbers:

$$X_k = \sum_{n=0}^{N-1} x_n e^{-i2\pi k \frac{n}{N}} \quad k = 0, \ldots, N-1 \tag{1}$$

A FFT is performed in $O(N \log N)$ operations and can be calculated in real time due to the fact that it can be executed in parallel. It is a widely used and well established method [24, 5]. Recent researches use the discrete wavelet transformation (DWT) to represent time series in the frequency domain. The DWT represents the time series in a time-scale form [15] and is especially suited to represent non-stationary signals [19].

1.2. Decision Trees

Decision trees are a method from the area of artificial intelligence and are used for machine learning. They are often binary trees, where each node has an if-then-else function on an attribute of the sample data. The ID3 algorithm (Iterative Dichotomiser 3, published by J. Ross Quinlan in 1986, used to generate decision trees [25]) was the first algorithm to construct decision trees. ID3 had some problems and was improved. The improved version of ID3 is C4.5 [26]. It enhances the ID3 algorithm with the ability to handle both discrete and continues attributes, it can handle samples with missing attributes and supports pruning of the tree at the end of the algorithm (removing branches from the tree).

Decision trees are in the proposed method used to calculate and order the features based on the information gain of each feature. During the method validation they are used for failure classification to show the influence of different features on the classification performance.

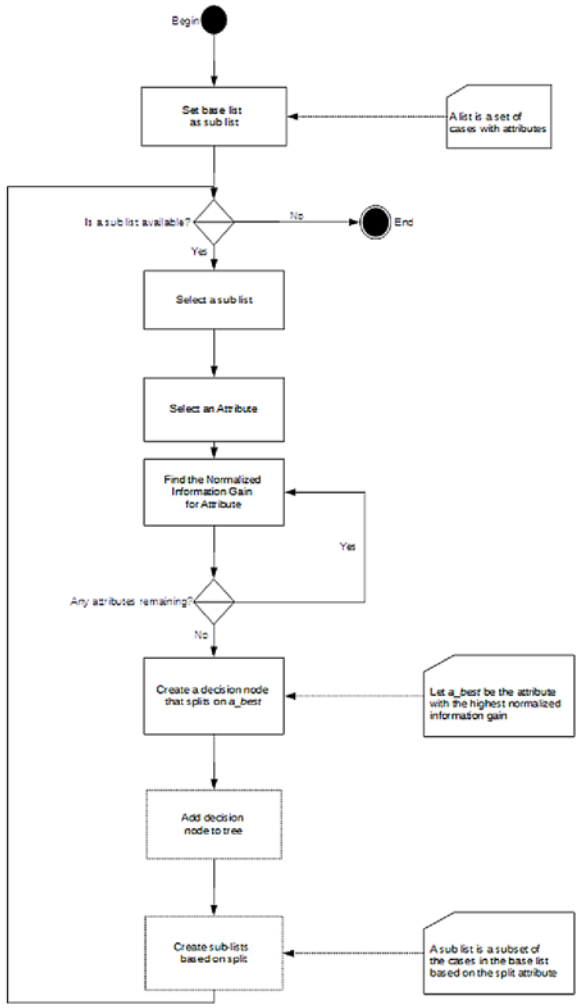

Fig. 2. Decision Tree Algorithm Flow Chart

The result of the algorithm is a binary decision tree, where the root of the tree is the attribute with the highest normalized information gain. Nodes in the following levels of the tree represent attributes with lower normalized information gain. If pure information gain is used for splitting, then classes with the most cases are favoured [26].

Information entropy is the knowledge that is contained in an answer depending on one's prior knowledge. The less is known, the more information is provided. In information theory information entropy is measured in bits. One bit of information entropy is enough to answer a yes/no question about which one has no data [29]. The information entropy is also called information and is calculated as shown below. $P(v_i)$ is the probability of the answer v_i:

$$I\left(P(v_i), \ldots, P(v_n)\right) = \sum_{i=1}^{n} - P(v_i) log_2 P(v_i) \quad (2)$$

The information gain from an attribute test is the difference between the total information entropy requirement (the amount of information entropy that was needed before the test) and the new information entropy requirement. *p* is the number of positive answers and *n* is the number of negative answers [29]:

$$Gain(X) = I\left(\frac{p}{p+n}, \frac{n}{p+n}\right) - \sum_{i=1}^{n} \frac{p_i + n_i}{p+n} \times I\left(\frac{p_i}{p_i + n_i}, \frac{n_i}{p_i + n_i}\right) \quad (3)$$

C4.5 uses the normalized information gain or the gain ratio. Split info is the information that is gained from choosing the attribute to split the samples:

$$Split\ Info\ (X) = -\sum_{i=1}^{n} \frac{p_i + n_i}{p+n} log_2 \left(\frac{p_i + n_i}{p+n}\right) \quad (4)$$

Gain ratio is the normalized information gain and is defined as shown in equation *5* [26]:

$$Gain\ Ratio\ (X) = \frac{Gain\ (X)}{Split\ Info\ (X)} \quad (5)$$

Pruning is the reduction of the depth of a decision tree. The tree gets better at classifying unknown samples, but might get worse at classifying the test samples. Normally pruning increases the overall classification accuracy, but too much pruning can increase the number of false classifications.

Decision trees are good for diagnostics in the context of condition monitoring. They classify data with low computation needs and the generated decision trees are highly comprehensible by humans. Another advantage of decision trees for condition monitoring is that they can be transformed into simple logical equations for each class that can be checked and modified by a human expert.

Decision trees are used to solve a large variety of problem e.g. tag speech parts [33], land cover mapping [9], text mining [1] or condition monitoring [36, 30, 31].

1.4. Basic Condition Monitoring Process Enhancements

Sensor optimization and sensor data fusion can be seen an enhancement of the basic condition monitoring process (Figure 1). Figure 3 shows how sensor optimization and sensor fusion can be embedded in the basic CM process.

Fig. 3. Enhanced condition monitoring process

Sensor optimization is the basis for the condition monitoring and is either performed before the monitoring process (sensor locations) or later to add new sensors [7] or to analyse the available sensor influences. Sensor fusion is done before the actual data processing to improve the performance of the data processing by improving the input from the sensors (removing redundant and low influence features).

1.5. Sensor Optimization

Often multiple sensors (sensor network) are used to give a more complete overview about the environment than a single sensor can give [40, 15]. This increases the diagnosis ability (failure detection and localization [5]) of a system and makes sensor optimization critical for failure diagnosis. The problem of designing a sensor network is to find a set of sensors so that costs, observability, reliability, estimation accuracy and flexibility are satisfied [16].

Sensor optimization shall help to design a sensor network that satisfies the requirements. It is a very wide topic and includes a number of different definitions. A few different meanings for sensor optimization are:

- Optimizing the position of sensors [35, 7].
- Optimizing the processing of sensor data [6].
- Optimizing the information gain of sensors.

Sensor optimization has the meaning of hardware redundancy optimization. Optimization is done by identifying significant sensors from a number of available sensors that give the most information about a system and thus increasing the information gain.

Goal of sensor optimization is to prevent unnecessary hardware redundancy and to improve the reliability of the condition monitoring system. This optimization can be supported by identifying redundant information in sensor data [5]. Traditional sensor optimization methods don't take into account the requirements for prognostic and health monitoring [34].

1.6. Multi-sensor Data Fusion

Having a network of different sensors that monitor a system leads to the problem of sensor data fusion. Multi-sensor data fusion covers the problem of combining sensor data from different sources into one consistent model. The main questions of sensor fusion are [2]:

- How to get accurate and reliable information from multiple and possible redundant sensors?
- How to fuse multi-sensor data with imprecise and conflicting data?

Techniques for sensor fusion can be grouped into these levels [15, 28, 3]:

- Data-level fusion (e.g. combining sensor data from same sensors directly [20]).
- Feature-level fusion (e.g. combining vectors and feature reduction techniques [28]).
- Decision-level fusion (e.g. vote schemes [28]).

Sensor data fusion is an important step for condition monitoring tasks. Most systems have more than one sensor and the sensor have different influences on the condition monitoring accuracy. Data for condition monitoring that needs to be fused is not only from sensors but can also be event and process data, which can deliver important information for the condition monitoring [15].

At the data-level fusion means the direct combination of sensor data; the data from sensors of the same kind is merged and fed into the condition monitoring system. The difficulty here is how to merge multiple sensors into one. Sensor fusion on the feature-level includes cleaning of sensor data and combining the sensor data after the features have been extracted and the dimensions reduced. Decision-level fusion can mean implementing a condition monitoring for each sensor separately and then use voting to decide on the system condition.

A condition monitoring system can use only one or multiple data fusion methods to detect the system conditions. This shows that the sensor fusion is a difficult problem that highly depends on the target system, and sensors. One solution would be to implement sensor fusion on all levels and then use a heuristic optimization like genetic algorithms, simulated annealing or hill climbing to get the bet sensor fusion methods for the given problem (data and system conditions).

2. Proposed methodology

Sensor selection and sensor fusion and consists of two steps. First a decision tree is build using feature extraction to increase the classification accuracy. The resulting decision tree may be analysed to generate a ranking of the involved sensors and features as the second step. The ranking then can be used to decide which sensors add significant information/features and which not. A sensor fusion may be performed at the feature-level. The calculated decision tree represents the feature fusion sorted by information gain. Sensor fusion on the feature-level does have the advantage that event data can also be added to the feature vector. Conventional methods use a fixed set of features to create feature vectors for the decision tree training and neglect the sensor fusion. Decision trees are used because they are good to use and implement in the aircraft environment. The task of the decision trees is merging of features from different sensor into one system health model and to use this model to classify the condition.

The focus is on hardware redundancy of sensors based on information gain to avoid having to install all sensors redundant and only focus on the sensors that give significant information for the failure detection and identification.

Goal of the method is to use information gain for ranking sensor importance and thus to have a measurement for sensor optimization. Feature extraction can increase the information gain and significance of different sensors.

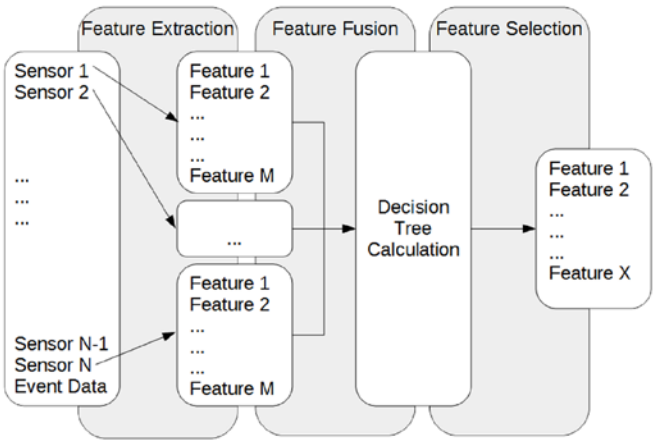

Fig. 4. Feature Selection Process

2.1. Feature Extraction and Sensor Fusion

The features extraction includes features from the time and the frequency domain. Time-frequency domain features were specifically not used. The reason was that the method shall only use basic methods thus Fast Fourier Transformation has been used. Elementary feature extraction operations can be executed in any order and allow the creation of a set of feature extraction operations the can be different for each problem [21]. This makes elementary extraction operations also good for machine learning. The used operators are also fast to compute and can be used for online monitoring.

The data from the different sensors is not merged at the sensor level; instead it is merged on the feature extraction level. A feature set is calculated for each input from each sensor. These features are then merged into one feature input vector for the decision tree learning phase. No frequency features are calculated for signals that are nearly constant (Boolean switches, discrete system settings, and certain process parameter). The features extraction includes features from the time and the frequency domain. Time-frequency domain features were specifically not used. The reason was that the method shall only use basic methods thus Fast Fourier Transformation has been used. Elementary feature extraction operations can be executed in any order and allow the creation of a set of feature extraction operations the can be different for each problem [21]. This makes elementary extraction operations also good for machine learning. The used operators are also fast to compute and can be used for online monitoring.

The data from the different sensors is not merged at the sensor level; instead it is merged on the feature extraction level. A feature set is calculated for each input from each sensor. These features are then merged into one feature input vector for the decision tree learning phase Figure 4. No frequency features are calculated for signals that are nearly constant (Boolean switches, discrete system settings, and certain process parameter).

2.2. Decision Tree Generation

This subsection describes the decision tree generation and signal processing. The decision tree is generated using algorithm C4.5. Algorithm C4.5 was used, because it is more advanced than the basic ID3 algorithm (accepts both continuous and discrete features, solves over-fitting problem by pruning handles, incomplete data points) and is available as an open source implementation J48. Input for the decision tree generation is a set of features that was extracted from sensor data. The feature extraction was controlled by different parameters. Table 1 shows the parameter list.

Table 1. Feature Extraction Parameter

Parameter	Possible Values	Default Value
Block Width	5/50/100/200	100
Noise Reduction Factor	0/1/2/5	1
Maximum Amplitude	Yes/No	Yes
Mean Amplitude	Yes/No	Yes
Maximum Power	Yes/No	Yes
Maximum Frequency	Yes/No	Yes
Mean Power	Yes/No	Yes
Number of Peaks	Yes/No	Yes
Peak Border	1/2/5	2
Global Maximum Amplitude	Yes/No	Yes
Global Mean Amplitude	Yes/No	Yes
Global Maximum Power	Yes/No	Yes
Global Mean Power	Yes/No	Yes
Global Number of Peaks	Yes/No	Yes
Confidence Factor	0.0001/0.001/0.01/0.1/1	0.001

The data types can range from Boolean data generated by switches or system conditions (event data) to high frequency data generated by sound and vibration data. Four more specific parameters will be explained in more detail below in this section.

2.2.1. Block Width

The block with defines how the frequency domain is partitioned to get features for each partition. A full transformation with the sampling frequency is done. After the fast Fourier transformation is done, the frequencies are partitioned up into blocks. The number of the frequencies that are grouped in one block is determined by the calculation parameter *Block Width*. If less then *Block Width* frequencies are available, then all frequencies are treated as one block. After partitioning all blocks are transformed back into the time domain, to get information about the behaviour of the block-signal over the time.

2.2.2. Noise Reduction Factor

Noise reduction is applied to the signal to remove random data from the samples in order to improve the feature detection of the undisturbed signal. The maximum frequency power is calculated and then every frequency signal that is below a defined fraction of the maximum frequency power is reduced to zero to remove noise from the sample. The exact fraction of the maximum frequency power for noise reduction is a parameter of the experiments *(Noise Reduction Factor)*. Noise reduction is done as shown in the Matlin Listing 1.

```
Y = fft(y);
x = mean(abs(Y)) *  NoiseReductionFactor ;
Y = Y. * ( abs (Y)>x );
```

Listing 1: Noise Reduction

2.2.3. Peak Border

The peak border is used for counting the number of frequencies that have a power above multitude of the mean power. The Matlab Listing 2 shows how the peaks are calculated. *peakBorder* is the parameter that can be varied and it defines, when a spike counts as a peak.

```
currPeakNum = 0;
for X = 1: blockWidth
  if ( Y_block (X) >= meanPower * peakBorder )
    peaks_block = peaks_block +1;
  end
end
```

Listing 2: Peak Calculation

The additional information is also calculated for the complete signal sample. Sensor Optimization

2.2.4. Confidence Factor

The confidence factor is a parameter of the software (WEKA [38]) that was used to create the decision trees and it defined how much tree pruning is done. A confidence factor of greater than 0.5 means that no pruning is done. The lower the confidence factor is the more pruning is done.

2.3. Sensor Optimization

The calculation of the *information gain* and learning of the decision tree is done by the *C4.5* algorithm that is used to construct decision trees for classification problems. Features are first extracted for each sensor signal then merged into one feature vector that is then the input for the C4.5 algorithm. The features are then sorted by the learning algorithm by the information gain. The feature with the highest information gain is placed at the root of the tree. Nodes with less information gain are placed at lower levels. For a binary decision tree this means that two nodes are in the second level of the tree, four nodes in the third level and so on. Each feature corresponds to a sensor.

The features in the decision tree are replaced with the sensor names for sensor ranking. If a sensor name appears on a level it is removed from all lower levels, so that for each sensor matches to one level in the decision tree. The sensors are now ranked by the decision tree level to which they are linked. It may happen that two sensors are at the same level.

3. VALIDATION

Two experiments were done to validate the concepts and ideas. The first experiment was done to show the effects of feature optimization and the second experiment was done to show how feature and sensor selection is done.

3.1. Feature Extraction Parameter Influence

To show the performance and concepts of the algorithm, a sensitivity analysis was performed by using different process parameters. Figure 5 shows the experiment process and how the results were generated. First samples are created and then sequentially are feature extraction parameters (see Table 1) modified. The influence of the modified parameter is measured by comparing the classification accuracy.

3.1.1. Data Sampling

The data for the experiments and the feature extraction was sampled with an autonomous box (Figure 6) that contained sensors and logic to save the data on a SD card. As a basis for the data collection a test rig was used. Vibration data with a sampling rate of 44 kHz of a simple PC fan (Figure 8) was collected. A PC fan was used to show the principals of the method. Data is saved in a raw wave format onto a SD card and then transferred onto a PC. In addition to the raw sensor data the condition of the component was saved. The fan is operated with standard speed, but three different conditions were sampled.

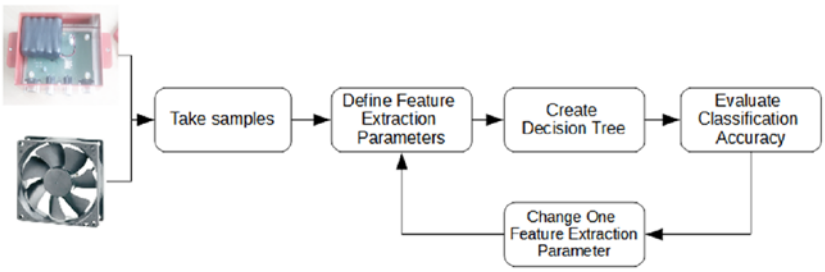

Fig. 5. Experiment Process Diagram

Data from the following conditions was collected:

- No additional weight.
- A very small weight (less than one gram) is added to one blade.
- A small coin (one Eurocent) is added to one blade.

Fig. 6. Data Recording Box

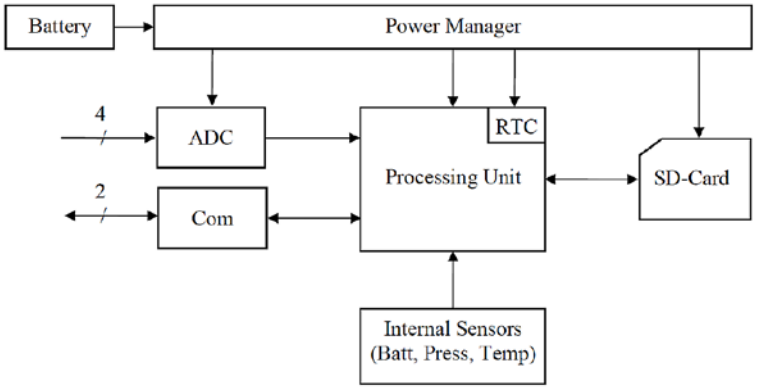

Fig. 7. Data Recording Box Architecture

Fig. 8. Used PC Fan

For each case 900 samples were collected. Every sample contains the vibration data of one second. Ten minutes passed between the individual samples. Samples were collected during office work hours and so a variety of noise is contained in the samples. In the experiment 900 "No weight" (no additional weight), 450 "Small weight" (a very small weight) and 450 "Big weight" (a small coin) samples were used. The decision tree of the J48 algorithm (an implementation of C4.5) in WEKA was validated with a 3-fold-crossvalidation (all samples are used for testing and training and the cross-validation process is repeated 3 times).

3.1.2. Calculating the Decision Tree

The decision tree is calculated with the open source Java software WEKA [38]. WEKA allows the user to test different algorithms and shows the classification errors that occurred. The correct data format is generated by using a Java program that transforms the output files from Matlab into input files for WEKA. For classification J48 is chosen, which is an implementation of the C4.5 decision tree algorithm, and a confidence factor of 0.0001. The confidence factor defines how much pruning is done to the resulting decision tree. The complete processed data is used as training data. After the generation of the decision tree the same data is used for testing the decision tree. In general the training and the testing data should not be the same, but in this case it is exactly what is wanted. The goal is not to classify new objects correctly, but to check how good the available data is classified and what part of the data gives us the most information about the system.

3.1.3. Experiment Parameters

Calculations with the same input data, but different parameter values, were performed to show the influence of the parameters on the results; Table 1 shows the available parameters with their possible values. All "Yes/No"-parameters are Boolean parameters, that toggle the calculation of that parameter during the processing. Default parameters are the values that are used, when the effect of a parameter onto the algorithm is tested. Only one value per test varies, while all other parameters keep their default value. The data processing with Matlab generates a number of different input sets for the J48 algorithm. For every input set a decision tree is generated and the influence of the modified parameter is then evaluated.

3.2. Sensor Optimization

The method was evaluated by using aircraft sensor data from the air conditioning system of an A320 aircraft. The aircraft was operated by ETIHAD Airways and was operating in the Middle East. The sensor data from the aircraft includes 589 flights over the duration of two years. Each sensor reading includes over 80 values consisting of continuous (numerical) and discrete data (Boolean). The data was sampled with a frequency of 1 Hz. Source of the data are different bus systems from the air conditioning system. Most data are temperature data and valve states. The sensor data includes:

Table 2. A320 sensor data description

Description	Bus	Type
Cabin Compartment Temperature Group 1	Zone Control	Numerical
Cabin Compartment Temperature Group 2	Zone Control	Numerical
Cabin Compartment Temperature Group 3	Zone Control	Numerical
Cabin Temperature Regulation Valve Position Group 1	Zone Control	Numerical
Cabin Temperature Regulation Valve Position Group 2	Zone Control	Numerical
Cabin Temperature Regulation Valve Position Group 3	Zone Control	Numerical
Duct Overheat Warning Group 1	Zone Control	Boolean
Duct Overheat Warning Group 2	Zone Control	Boolean
Duct Overheat Warning Group 3	Zone Control	Boolean
Duct Temperature 4 Times Limit Exceedance Group 1	Zone Control	Boolean
Duct Temperature 4 Times Limit Exceedance Group 2	Zone Control	Boolean
Duct Temperature 4 Times Limit Exceedance Group 3	Zone Control	Boolean
Duct Temperature Group 1	Zone Control	Numerical
Duct Temperature Group 2	Zone Control	Numerical
Duct Temperature Group 3	Zone Control	Numerical
G + T Fan OFF	Zone Control	Boolean
Hot Air Switch Position ON	Zone Control	Boolean
Minimum Bleed Air Pressure Demand	Zone Control	Numerical

4. Result analysis

This section analyses the results of the data processing of the previous section. It begins by evaluating the experiments and their parameters and goes on to discuss the results of the best parameter configuration.

Figure 9 summarises the validation process. Results were created using the default parameter set; then, each parameter was varied based on its type. Boolean values were simply inverted but continuous val-

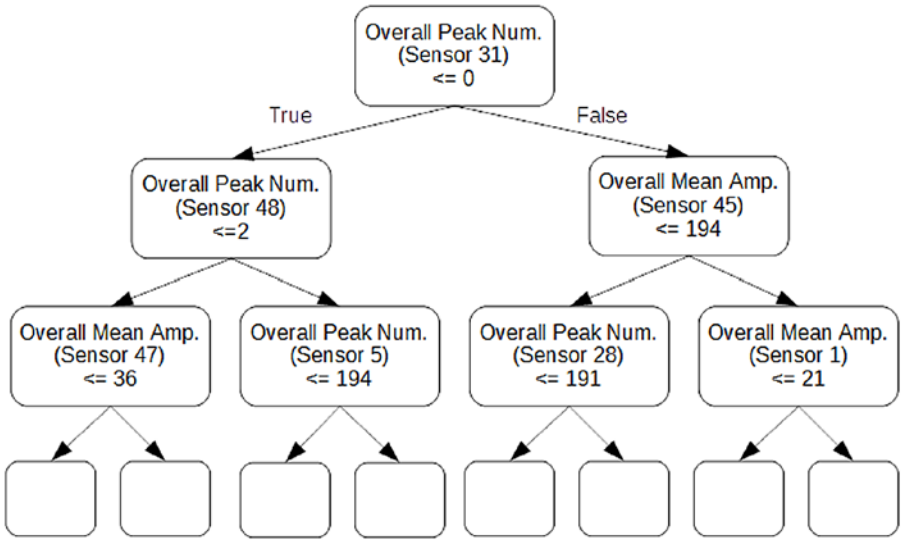

Fig. 10. Validation Process

ues were changed. A sensitivity analysis was performed after each parameter variation. After the parameter variation, a new decision tree with the same sensor data was created, and the change in the number of correctly classified samples was noted.

4.1. Parameter Evaluation

This section examines the results of the different input sets, based on the parameter variation. The influence of a parameter is judged by the number of correctly classified samples for every input set. Finding an optimal set of all parameters for the given samples, i.e., those giving the lowest overall false classification rate, is a complex problem. The complexity of the problem is so high that it is not possible to solve it in a fixed time; rather, heuristic methods have to be used. The results below are not the optimal parameter values; they only show the influence of the different parameter values on the classification accuracy and suggest the importance of optimizing the feature extraction parameters.

The first calculation was performed using the default parameters (see Table 1). The results are shown in Table 3. The numbers imply that about three quarters of the test cases are correctly classified. The error rate is quite high, but that is to be expected, because a non-optimal parameter set was selected as the default parameter set.

Table 3. Results for the Default Parameter Set

Correct Classified	False Classified
73.4 %	26.6 %

Table 4 splits the classification error into different classes. As the table shows, the majority of the samples are correctly classified. For samples with no additional weight and a big additional weight, the classification is very good, but samples with a small additional weight are often classified as samples with no additional weight. The results are still good, however, because the small attached weight is quite light, and sensing accuracy is not very high.

Table 4. Distribution of Wrongly Classified Samples

Sample Class	Classified as No	Classified as Small	Classified as Big
No	755	103	76
Small	175	218	57
Big	41	61	348

When only no additional weight and big additional weight samples are used, the number of wrongly classified samples dropps to 5 %. This is to be expected, because the features of both these classes have bigger differences than those found between the "Small" and "No" classes.

Table 6 shows the results achieved when the block width varies. The decreasing numbers imply that, at some point, an optimal block width can be reached and a minimum of false classified samples can be obtained. The error rate increases after the optimal point if the block width is too wide. The block width significantly affects how many features are calculated in total. Some features are calculated for each block. More features are calculated if the block width is low and, thus, the number of blocks is high.

Table 7 shows the experimental results for a varying noise reduction. The results indicate the accuracy of the classification can be improved by removing all frequencies with a power below the mean level. However, removing more frequencies with a high power can reduce the classification accuracy significantly because significant information about the signal is removed. This result also shows the noise frequency features have a significant influence on the accuracy of the classification.

Table 5. Results for the Default Parameter Set with no Small Weight Samples

Sample Class	Classified as No	Classified as Big
No	862	38
Big	60	390

Table 6. Results for Block Width

Block Width	False Classified
5	43.3%
50	27.4%
100	26.6%
200	24.3%

Table 7. Noise Reduction

Noise Reduction	False Classified
0	26.6%
1	24.2%
2	27.6%
5	42.6%

The calculation of the maximum amplitude can be turned on or off. Table 8 and Table 9 show the results. Results show the maximum amplitude does not have a big influence on the classification in this problem. This indicates a high resilience of the input data to noise, something relevant to entropy, or the information content in a message or information. The finding suggests the data samples contain a lot of information, and there is not much uncertainty in them [23]. This is even more interesting, because amplitude is the value recorded by the vibration sensors; it can be taken as an input without additional processing.

Table 8. Results for Maximum Amplitude per Block

Maximum Amplitude	False Classified
Yes	26.6%
No	26.5%

Table 9. Results for Global Maximum Amplitude

Global Maximum Amplitude	False Classified
Yes	26.6%
No	26.6%

Table 10 and Table 11 show the influence of the mean amplitude values. Again, the influence is quite small, similar to the influence of the maximum amplitude features. This is to be expected when the previous results are taken into account. The amplitudes are the only features based on the time domain data. This can indicate that the time domain features are not very significant for the classification as is often the case for rotary movements. More time domain features should be added to the feature extraction operations (like probabilistic moments) to give more information about the significance of the time domain signal.

Table 10. Results for Mean Amplitude per Block

Mean Amplitude	False Classified
Yes	26.6%
No	27.7%

Table 11. Results for Global Mean Amplitude

Global Mean Amplitude	False Classified
Yes	26.6%
No	26.6%

Table 12 and Table 13 show the results of the parameter variations for the maximum frequency power. Again, these features do not influence the result of the classification very much. It is interesting to note that the classification error is reduced if the block based maximum frequency power feature is turned off. This example clearly shows that having many features and features with little information gain can decrease the classification performance. It also highlights the importance of good feature selection.

Table 12. Results for Maximum Frequency Power per Block

Maximum Frequency Power	False Classified
Yes	26.5%
No	25.0%

Table 13. Results for Global Maximum Frequency

Maximum Frequency Power	False Classified
Yes	26.6%
No	26.6%

Table 14 and Table 15 show the results of the parameter variations for the frequency with the maximum power. The Hertz of the frequency with the highest power (local for each block or for the complete signal) does not influence the result in a significant way. This is to be expected because the maximum power also has little influence.

Table 14. Results for Frequency with Highest Power per Block

Frequency with Highest Power	False Classified
Yes	26.6%
No	26.3%

Table 15. Results for Global Frequency with Highest Power

Frequency with Highest Power	False Classified
Yes	26.6%
No	26.6%

Table 16 and Table 17 show the influence of the parameter variations for the mean frequency power. Mean frequency power is a big factor and can improve the classification by nearly 4 %. The global mean values give no information about the condition of the fan. This result is especially interesting, because the other frequency based features have little influence on the classification error. However similar to the maximum frequency power feature, the error rate decreases if this feature is not used.

Table 16. Results for Mean Frequency Power per Block

Mean Frequency Power	False Classified
Yes	26.6%
No	22.8%

Table 17. Results for Global Mean Frequency Power

Mean Frequency Power	False Classified
Yes	26.6%
No	26.6%

Table 18 and Table 19 show the influence of the number of peaks on the calculation. The number of peaks has an even bigger influence on the classification than the mean frequency power, and the false classification rate can be improved by nearly 5 %. To this point, this is the largest performance increase.

Table 18. Results for Number of Peaks per Block

Number of Peaks	False Classified
Yes	26.6%
No	21.8%

Table 19. Results for Global Number of Peaks

Number of Peaks	False Classified
Yes	26.6%
No	26.6%

The peak border (the value defining what a peak is) also influences the calculation, as shown in Table 20. Results for the peak border show no clear trend, but the numbers suggest an optimum exists. These results are interesting if we take into account how much the error rate improves when peaks per block are not calculated. Very few peaks are generated if the peak border is set to 5. This is quite similar to having no peaks at all.

The confidence factor determines how much the decision tree is pruned and has an influence on the classification accuracy. With less pruning, more samples are wrongly classified. Over-fitting is reduced

Table 20. Results for Peak Border

Peak Border	False Classified
1	24.3%
2	26.6%
5	22.3%

Table 21. Results for Confidence Factor

Confidence Factor	False Classified	Tree Size
1 (no pruning)	27.4%	275 Nodes
0.1	26.7%	225 Nodes
0.01	26.2%	185 Nodes
0.001	26.0%	163 Nodes
0.0001	26.6%	109 Nodes

when pruning is used. More pruning increases the generalisation ability of the decision tree, generally a good feature, but tree that is too small is not good. As in all other features, it is important to find the best value for the given classification problem.

It is interesting to note that the most significant feature seems to be the block based mean amplitude feature. The error rate increases for all other features if they are used. More experiments with different settings could ascertain how the different parameters are correlated, but finding the optimal parameter set can be really difficult. The best result (for the default parameter set and if only one parameter is modified) can be reached if the peak number is turned off. These results emphasise the importance of good feature selection and remind us of the difficulty of performing feature selection by hand. An automated feature selection is needed to find an optimal parameter set which improves the classification accuracy.

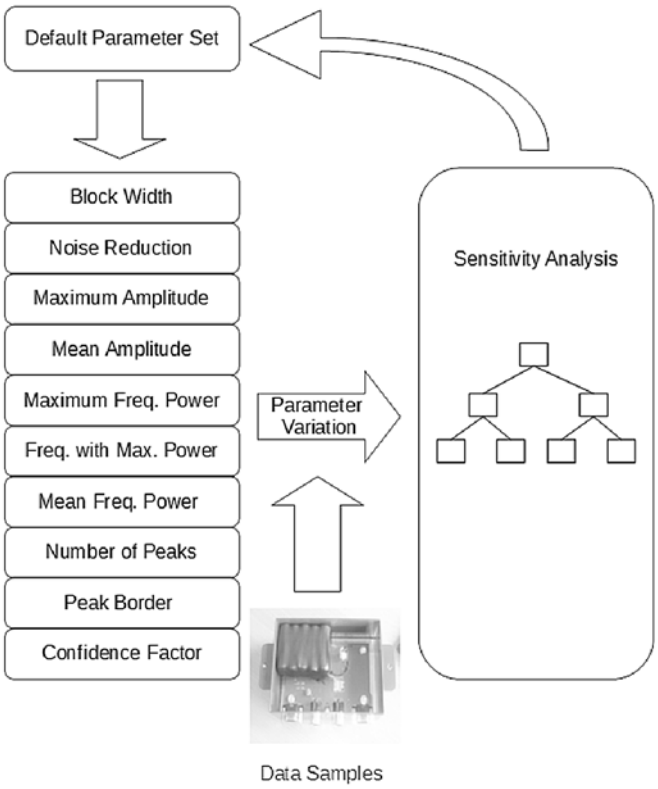

Fig. 9. Example Decision Tree

4.2. Sensor Optimization

This section shows the sensor optimization using the aircraft data with 80 sensors. Figure 10 contains a sample decision tree. The most important feature is the overall (global) number of peaks for the data source 31, followed by the overall (global) mean amplitude for sensor 45. Based on the decision tree, the sensors can be ranked as:

1. Sensor 31,
2. Sensor 48/Sensor 45,
3. Sensor 47/Sensor 5/Sensor 28/Sensor 1.

Sensor 31 is the most relevant sensor for the classification; sensors 48 and 45 are the second most significant ones. Redundancy, thus, applies to sensors 31, 48 and 45.

The decision tree also shows that the overall peak number and mean amplitude are the most relevant features. The significance of the amplitude is easily explained because the data contain switch and valve values which change slowly. The mean amplitude gives the classifier an indication of how often the switch is true and how often false. It is interesting to see that the peak number has more influence here than in the previous experiment.

5. Conclusions and Discussions

The method discussed here has been developed to handle a specific problem (classification of a small number of classes with simple features) in a specific domain (civil aircraft operation with online monitoring). Decision trees are a good solution, given these constraints. However, decision trees have limitations, and more powerful algorithms are available, if a similar problem needs to be solved outside the given constraints. More complex problems may need a different tool set. The methods used here are already well known and well researched, but their usage in this particular environment is novel. A previous paper [12] addressed the topic but evaluated the classification; it did not address sensor optimization and used an artificial experiment setup. This paper shows the result of sensor optimization by using real world data; it also explains the results and classification process in more detail than the earlier paper.

The architecture shown in Figure 4 is a good way to rank sensors by their significance for condition monitoring. The basic idea is to use a decision tree for feature ranking and feature fusion. Not all available features are used in the final decision tree thanks to tree pruning. As a result, fewer data are needed, and some sensors may not be used for the condition monitoring at all. It also improves the classification error rate and generalisation ability.

The validation experiment shows good failure classification can be performed with the proposed algorithms and methods. The feature extraction offers a modular system of elementary operations that can be used to extract features for a given problem.

The sensor optimization is best used for existing systems where reliability can be improved by additional hardware. The design is suitable when no online computation is available or data are logged but not evaluated but must be available in case of a failure for offline fault identification. The method can also be used for all systems with multiple sensors.

While the features improve the accuracy of the decision tree, it would be even better if more advanced feature extraction methods were used. Wavelet Package Transformation and KPAC are two suggestions. The method in this paper does not address how the best feature extraction parameter set is generated, but as the paper shows, this task is extremely important. Optimization algorithms are required. Future work could include using a genetic algorithm to search for the best parameter combination to classify a given dataset. The condition monitoring results can be used for trending and remaining useful life prediction.

References

1. Apte C, Damerau F, Weiss S.M. Text mining with decision trees and decision rules. In Proceedings of the Conference on Automated Learning and Discorery, Workshop 6: Learning from Text and the Web, 1998.
2. Basir O, Yuan X. Engine fault diagnosis based on multi-sensor information fusion using Dempster-Shafer evidence theory. Information Fusion 2007; 8 (4): 379-386, http://dx.doi.org/10.1016/j.inffus.2005.07.003.
3. Castanedo F. A review of data fusion techniques. The Scientific World Journal 2013, http://dx.doi.org/10.1155/2013/704504.
4. DIN EN 13306. Maintenance terminology. European Committee for Standardization, 2008.
5. Emami-Naeini A, Akhter M.M, Rock S. M. Effect of model uncertainty on failure detection: the threshold selector," IEEE Transactions on Automatic Control 1988; 33 (12): 1106-1115, http://dx.doi.org/10.1109/9.14432.
6. Farrar C.R, Park G, Puckett A.D, Flynn E.B, Mascarenas D.L, Todd M. D. Sensing and Sensor Optimization Issues for Structural Health Monitoring. 23rd Aerospace Testing Seminar, Manhatten Beach, 2006.
7. Fijany A, Vatan F. A unified and efficient algorithmic approach to model-based diagnosis and optimal sensor placement. Proceedings of 8th International Symposium on Artificial Intelligence, Robotics and Automation in Space (i-SAIRAS), 2005.
8. Fonollosa J, Vergara A, Huerta R. Algorithmic mitigation of sensor failure: Is sensor replacement really necessary?. Sensors and Actuators B: Chemical 2013; 183: 211-221, http://dx.doi.org/10.1016/j.snb.2013.03.034.
9. Friedl M.A, Brodley C.E. Decision tree classification of land cover from remotely sensed data. Remote sensing of environment 1997; 61 (3): 399-409, http://dx.doi.org/10.1016/S0034-4257(97)00049-7.
10. Fu T.-C. A review on time series data mining. Engineering Applications of Artificial Intelligence 2011; 24 (1): 164-181, http://dx.doi.org/10.1016/j.engappai.2010.09.007.
11. Gerdes, M., Scholz, D. & Randerath, B. Reducing Delays Caused by Unscheduled Maintenance and Cabin Reconfiguration. 2nd International Workshop on Aircraft System Technologies, 2009.
12. Gerdes, M., Scholz, D. Feature Extraction and Sensor Optimization for Condition Monitoring of Recirculation Fans and Filters. Deutscher Luft- und Raumfahrtkongress 2009.
13. International Electrotechnical Commission. IEC 61511: Functional Safety - Safety instrumented systems for the process industry sector. International Electrotechnical Commission, 2003.
14. International Electrotechnical Commission. IEC 61508: Functional safety of electrical/electronic/programmable electronic safety-related systems. International Electrotechnical Commission, 2010.
15. Jardine A.K, Lin D, Banjevic D. A review on machinery diagnostics and prognostics implementing condition-based maintenance. Mechanical systems and signal processing 2006; 20 (7): 1483-1510, http://dx.doi.org/10.1016/j.ymssp.2005.09.012.
16. Kotecha P. R, Bhushan M, Gudi R. D. Design of robust, reliable sensor networks using constraint programming. Computers & Chemical Engineering 2008; 32 (9): 2030-2049, http://dx.doi.org/10.1016/j.compchemeng.2008.03.005.
17. Lambrou T, Kudumakis P, Speller R, Sandler M, Linney A. Classification of audio signals using statistical features on time and wavelet transform domains. Proceedings of the 1998 IEEE International Conference on Acoustics, Speech and Signal Processing, 1998, http://dx.doi.org/10.1109/icassp.1998.679665.
18. Li, F Li F. Dynamic modeling, sensor placement design, and fault diagnosis of nuclear desalination systems. University of Tennessee 2011.
19. Lin J, Qu L. Feature extraction based on Morlet wavelet and its application for mechanical fault diagnosis. Journal of sound and vibration 2000; 234 (1): 135-148, http://dx.doi.org/10.1006/jsvi.2000.2864.
20. Lu Y, Michaels J.E. Feature extraction and sensor fusion for ultrasonic structural health monitoring under changing environmental conditions. IEEE Sensors Journal 2009; 9 (11): 1462-1471, http://dx.doi.org/10.1109/JSEN.2009.2019339.
21. Mierswa I, Morik K. Automatic feature extraction for classifying audio data. Machine Learning 2005; 58 (2-3): 127-149, http://dx.doi.org/10.1007/s10994-005-5824-7.
22. Novis A, Powrie H. PHM sensor implementation in the real world-a status report. 2006 IEEE Aerospace Conference, 2006, http://dx.doi.org/10.1109/AERO.2006.1656113.
23. Pascual D. G. Artificial Intelligence Tools: Decision Support Systems in Condition Monitoring and Diagnosis, CRC Press, 2015, http://dx.doi.org/10.1201/b18384.
24. Peng Z, Chu F, He Y. Vibration signal analysis and feature extraction based on reassigned wavelet scalogram. Journal of Sound and Vibration 2002; 253 (5): 1087-1100, http://dx.doi.org/10.1006/jsvi.2001.4085.
25. Quinlan J. R. Induction of Decision Trees. Machine Learning 1986; 81-106, http://dx.doi.org/10.1007/BF00116251.
26. Quinlan J. R. C4.5: Programs for Machine Learning. San Francisco, CA, USA: Morgan Kaufmann Publishers Inc, 1993.
27. Radio Technical Commission for Aeronautics. DO 178C: Software considerations in airbone systems and equipment certification. Radio Technical Commission for Aeronautics, 2011.
28. Ross A, Jain A. Information fusion in biometrics. Pattern recognition letters 2003; 24 (13): 2115-2125, http://dx.doi.org/10.1016/S0167-8655(03)00079-5.
29. Russell S.J, Norvig P. Artificial Intelligence: A Modern Approach. Pearson Education, 2003.
30. Saimurugan M, Ramachandran K, Sugumaran V, Sakthivel N. Multi component fault diagnosis of rotational mechanical system based on decision tree and support vector machine. Expert Systems with Applications 2011; 38 (4): 3819-3826, http://dx.doi.org/10.1016/j.eswa.2010.09.042.
31. Sakthivel N, Sugumaran V, Nair B.B. Comparison of decision tree-fuzzy and rough set-fuzzy methods for fault categorization of mono-block centrifugal pump. Mechanical systems and signal processing 2010; 24 (6): 1887-1906, http://dx.doi.org/10.1016/j.ymssp.2010.01.008.
32. Scerbo M.W, Bailey N. R. Automation-induced complacency for monitoring highly reliable systems: the role of task complexity, system experience, and operator trust. Theoretical Issues in Ergonomics Science 2007; 321-348.
33. Schmid H. Probabilistic part-of-speech tagging using decision trees. Proceedings of the international conference on new methods in language processing, 1994.
34. Shuming Y, Jing Q, Guanjun L. Sensor optimization selection model based on testability constraint. Chinese Journal of Aeronautics 2012;

25 (2): 262-268, http://dx.doi.org/10.1016/S1000-9361(11)60386-5.
35. Smith M. J. Sensor Location & Optimization Tool Set. Chemical Biological Information Systems Conference, Albuquerque, 2005.
36. Sugumaran V, Ramachandran K. Automatic rule learning using decision tree for fuzzy classifier in fault diagnosis of roller bearing. Mechanical Systems and Signal Processing 2007; 21 (5): 2237-2247, http://dx.doi.org/10.1016/j.ymssp.2006.09.007.
37. Sun J.-W, Xi L.-F, Pan E.-S, Du S.-C, Xia T.-B. Design for diagnosability of multistation manufacturing systems based on sensor allocation optimization Computers in Industry 2009; 60 (7): 501-509, http://dx.doi.org/10.1016/j.compind.2009.02.001.
38. University of Waikato, WEKA, 2009.
39. Widodo A, Yang B.-S. Application of nonlinear feature extraction and support vector machines for fault diagnosis of induction motors. Expert Systems with Applications 2007; 33 (1): 241-250, http://dx.doi.org/10.1016/j.eswa.2006.04.020.
40. Xiong N, Svensson P. Multi-sensor management for information fusion: issues and approaches. Information fusion 2002; 3 (2): 163-186, http://dx.doi.org/10.1016/S1566-2535(02)00055-6.
41. an W, Goebel K. F. Sensor validation and fusion for gas turbine vibration monitoring. AeroSense 2003.

Mike GERDES
Hamburg University of Applied Sciences
Aero - Aircraft Design and Systems Group
Berliner Tor 9, 20099 Hamburg, Germany

Luleå University of Technology
Division of Operation and Maintenance Engineering
SE-971 87 Luleå, Sweden

Diego GALAR
Luleå University of Technology
Division of Operation and Maintenance Engineering
SE-971 87 Luleå, Sweden

University of Skövde
Reliability and Maintenance Engineering
SE-54128, Skövde, Sweden

Dieter SCHOLZ
Hamburg University of Applied Sciences
Aero - Aircraft Design and Systems Group
Berliner Tor 9, 20099 Hamburg, Germany

Emails: mike.gerdes@philotech.de, diego.galar@ltu.se, info@profscholz.de

Article citation info:
KONIUSZY A, KOSTENCKI P, BERGER A, GOLIMOWSKI W. Power performance of farm tractor in field operations. Eksploatacja i Niezawodnosc – Maintenance and Reliability 2017; 19 (1): 43–47, http://dx.doi.org/10.17531/ein.2017.1.6.

Adam KONIUSZY
Piotr KOSTENCKI
Andrew BERGER
Wojciech GOLIMOWSKI

POWER PERFORMANCE OF FARM TRACTOR IN FIELD OPERATIONS

WYKORZYSTANIE MOCY CIĄGNIKA ROLNICZEGO W PRACACH POLOWYCH

Many studies have examined the effects of agriculture tractor engine energy performance. This paper presents an evaluation method of such engine actual power use during plowing operations. It includes results of a comparative study of power performance of a 230 kW tractor model John Deere 8330 subject to soil plowing operations as a function of field size: A (26 ha), B (12.74 ha), C (3.22 ha). Statistical data clustering, a relatively novel approach in studies on actual utilization of engine power, was used. A positive correlation was observed between field size and the active state of the engine: 75.2% field A; 68.8% field B; 46.8% field C. The actual power utilization of agriculture tractor engine as a function of field size was 0.62, 0.58 and 0.39 respectively for the three fields used in this study. With this evaluation approach, performance indexes of operational power performance in various conditions were obtained for possible use in optimization of plowing operations.

***Keywords**: agriculture tractor, plowing, power performance, engine operation clusters.*

Ocena stanu obciążenia silnika spalinowego w pojeździe podczas eksploatacji jest przedmiotem wielu prac badawczych. W artykule przedstawiono nową metodę oceny wykorzystania mocy silnika ciągnika rolniczego eksploatowanego podczas orki. Zaprezentowano wyniki badań porównawczych nad wykorzystaniem mocy ciągnika John Deere 8330 (230 kW) w odniesieniu do powierzchni uprawianych pól: A (26 ha), B (12,74 ha) i C (3,22 ha). Do analizy danych pomiarowych zastosowano po raz pierwszy statystyczną metodę grupowania punktów pomiarowych. Na podstawie wyników badań stwierdzono silną korelację dodatnią pomiędzy powierzchnią pól a stanem obciążenia silnika: 75,2% pole A; 68,8% pole B; 46,8% pole C. Opracowany wskaźnik efektywnego wykorzystania mocy silnika ciągnika rolniczego wyniósł odpowiednio: 0,62, 0,58 i 0,39. Stwierdzono, że uzyskane wartości wskaźnika efektywności wykorzystania mocy silnika mogą być przydatne do optymalizacji pracy ciągnika w pracach polowych.

***Słowa kluczowe**: ciągnik rolniczy, orka, wykorzystanie mocy, czas pracy silnika.*

1. Introduction

Tractors play a fundamental role in agriculture as the main power resource for operation with various add-on agriculture machinery. The most energy and labor intensive among agro-technological operations is soil plowing. The trend in a plow design favors tractors with substantial power [24, 26], but ultimately it is determined by the size and construction of the machinery satisfying the needs of smaller farms [19].

Optimal tractor and machinery parameter selection, as a function of various field operations, not only improves the economics of such activities, but also reduces exhaust pollution and other negative environmental effects. The power requirements and energy consumption may be reduced through optimizing power characteristics and engine parameters [2, 3, 11, 31].

The CO_2 emissions may be reduced by minimizing idling states of the engine and maximizing the engine work load. The operational engine parameters are engine speed, transmission gear ratios and engine torque [1, 14]. The experience and reaction time of the tractor operator also play an important role in maintaining these parameters in optimal range [4, 18, 23, 28, 29] and optimal engine utilization [4, 12, 21].

Monitoring the performance indexes of operational power in various conditions provides data of engine modes of operation and fuel consumption. Not many methods and mathematical power performance models as a function of field parameters exist.

In this paper we present our evaluation method and introduce the performance indexes of operational power performance obtained in various conditions. It includes the evaluation of power use of an agriculture tractor engine in various plowing operations and the results of a comparative study of power performance as a function of field size. Other studies [9, 10, 20] focus more on fuel and energy consumption efficiency and toxic exhaust emission characteristics.

2. Methodology

The study took place during the 2012 plowing season on the Agrofirma agricultural farm (Witkowo, Poland) for rapeseed sowing. The experimental setup included three fields (Fig. 1). The physical parameters of the three fields' soils were measured at the time of the plowing operations and are included in Table 1 [17].

This paper presents a comparative study of power performance of a 230 kW tractor model John Deere 8330 subject to soil plowing operations on the three fields. The tractor was pulling a Lemken semi-mounted reversible, full moldboard 7-furrows EuroDiamant plow unit combined with a Campbell soil compaction roller tiller. All operations involved the same one tractor operator reducing any comparative discrepancy in experiment results.

Table 1. Soil Parameters

Soil		Soil Layer	Field A		Field B		Field C	
Soil Granulation, %	2 ≥ d >1	Tillage Layer	2.7	LFS	1.5	FSL	1.7	FSL
	1 ≥ d > 0.5		7.9		6.2		6.4	
	0.5 ≥ d > 0.25		15.1		11.0		12.5	
	0.25 ≥ d > 0.1		33.2		31.6		31.1	
	0.1≥ d > 0.05		17.1		17.7		19.3	
	0.05 ≥ d > 0.02		8		14		10	
	0.02 ≥ d > 0.002		11		13		14	
	d ≤ 0.002		5		5		5	
Soil Organic Matter Content, %			2.1		1.9		2.0	
Soil Moisture (by weight), %		0 - 10 cm 10 - 20 cm 20 - 30 cm	15.0 s=2.0 15.0 s=2.3 14.3 s=2.0		13.7 s=1.0 13.5 s=0.5 13.1 s=0.3		13.3 s=1.3 13.9 s=1.2 13.9 s=1.9	
Soil Volume Density, g/cm^3		0 - 10 cm 10 - 20 cm 20 - 30 cm	1.35 s=0.10 1.57 s=0.14 1.57 s=0.10		1.31 s=0.15 1.57 s=0.04 1.52 s=0.03		1.44 s=0.15 1.62 s=0.06 1.65 s=0.07	
Soil Compactness, kPa		0 - 10 cm 10 - 20 cm 20 - 30 cm	538 s=258 1183 s=463 2212 s=588		535 s=192 1539 s=348 2423 s=533		758 s=439 2459 s=683 3257 s=373	
Soil Shear Stress, kPa		0 - 10 cm 10 - 20 cm 20 - 30 cm	24 s=10 50 s=16 56 s=11		18 s=6 35 s=6 53 s=10		18 s=4 49 s=19 67 s=15	
Plow Operation Velocity, m/s			2.53 s=0.23		2.58 s=0.46		2.61 s=0.48	
Operating Plow Depth, cm			25 s=2		22 s=2		25 s=3	
Operating Plow Width, m			3.34 s=0.05		3.36 s=0.04		3.27 s=0.03	

LFS - loamy fine sand, FSL - fine sandy loam, s-standard deviation, d - particle size

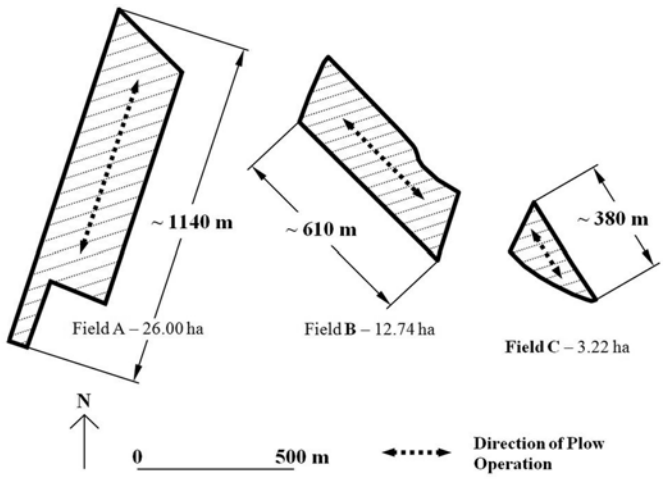

Fig. 1. Experimental Setup of three fields (based on Agrofirma geographical map)

2. Analysis method

The operational parameters (the engine speed, torque and power, fuel consumption and GPS position) were monitored with digital sensors with 1 Hz frequency using Siemens VDO -EDM 1404.01 measuring system [7]. The readings were used to calculate nominal and operational power of the engine. There are many methods of finding engine torque M_o indirectly [5, 8, 16, 22, 27, 32-34]. In our study, a method patented by the West Pomeranian University of Technology in Szczecin was utilized. In our view this method is unique and quite suitable for practical use in field operations [15, 16]. Other known methods focus more on theoretical analysis or represent laboratory experimental findings. In this study, the engine torque M_o parameter was evaluated indirectly based on the measurement of fuel consumption and engine crankshaft rotations:

$$M_o = a \cdot g_{1000}^3 + b \cdot g_{1000}^2 + c \cdot g_{1000} + d, \quad (1)$$

where:

$$g_{1000} = \frac{V_{fuel}}{n_s} \cdot 1000, \quad (2)$$

M_o – engine torque in Nm,
g_{1000} – fuel consumption in dm^3 per 1000 crankshaft revolutions,
a, b, c, d – coefficients subject to the engine type and rpm (Table 2),
V_{fuel} – fuel consumption, dm^3/min,
n_s – engine speed, rpm.

The values of torque were obtained indirectly with appropriate coefficient units to satisfy equation (2).

Engine utilization was evaluated with:

$$E_N = \frac{N_u}{N_{nom}} \cdot \frac{U_t}{100\%}, \quad (3)$$

where:
E_N – engine utilization,
N_u – plowing operation engine power, kW,
N_{nom} – nominal engine power, kW,
U_t – engine plowing operation time in relation to total engine operation time, %.

Table 2. Engine coefficients *a, b, c, d* – dyno test bench verified [16]

Engine speed range n_s, rpm	Coefficient values			
	a, Nm/dm^9	*b*, Nm/dm^6	*c*, Nm/dm^3	*d*, Nm
< 950	$-7 \cdot 10^{-6}$	0.0042	1.3992	−1.1506
950–1250	$-6 \cdot 10^{-6}$	0.0040	1.3193	14.087
1250–1550	$-8 \cdot 10^{-6}$	0.0063	0.8354	37.374
1550–1850	$-1 \cdot 10^{-5}$	0.0070	0.9304	20.479
1850–2150	$-1 \cdot 10^{-5}$	0.0094	0.3923	50.361
> 2150	$-7 \cdot 10^{-6}$	0.0068	0.5357	59.126

The engine actual torque values were obtained from (1) and (2).

The measurements of relative time of engine operation are presented in Fig. 2, 3, 4 relative to total time of engine operation [6] and based on (4):

$$TD_{(i,j)} = \frac{t_{(i,j)}}{t_c} \cdot 100\% \,, \tag{4}$$

where:

$TD_{(i,j)}$ – Relative time of engine operation (Time Density), %,
i – Index of the engine speed coordinate with $\Delta n_s = 100$ rpm,
j – Index of the engine torque with $\Delta M_o = 50$ Nm,
$t_{(i,j)}$ – time of operation at (i, j),
t_c – total time of engine operation.

Since the comparison and interpretation of the *TD* distribution plots (Fig. 2, 3, 4) may not be straightforward, a statistical data clustering (*k-means full binding*) method was used to obtain parameters for better quantitative comparison of effective utilization of the engine power at selected points (n_s, M_o). A program *Statistica* [30] with 67450 measurement points was used to generate the results.

3. Results

The measurements of relative time of engine operation as a function of engine torque and engine speed are presented in Fig. 2, 3 and 4. For better visualization of the relative time of engine operation, the plots for fields A, B and C are normalized to show the measurements within 1% range of *TD*.

Two engine operative states were considered: idle and field operation. A quantitative comparison of the time duration of the engine states was obtained also using the statistical data clustering approach, with results shown in Fig. 5. Four clusters were obtained as a function of engine speed n_s and torque M_o, as well as field size and the corresponding engine state of operation.

For fields A and B, the resulting clusters were comparatively close to each other, as opposed to the cluster locations of field C (Fig. 5). The A and B cluster location coordinates (associated with engine speed and torque) correspond to the engine plowing operation. For clusters variance analysis was performed. It showed strong difference between clusters (Table 3).

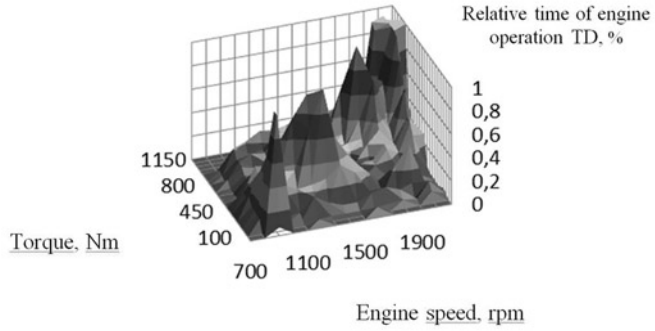

Fig. 4. Relative time of engine operation on field C

Table 3. Variance analysis for the clusters

Effect	Field A		Field B		Field C	
	F	p-Value	F	p-Value	F	p-Value
n_s	143565,8	0,00	41483,20	0,00	14324,31	0,00
M_o	140147,9	0,00	77110,79	0,00	14324,31	0,00
Number of cases	39833		20535		7082	

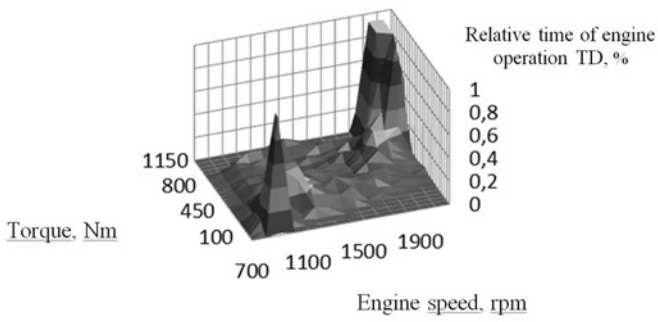

Fig. 2. Relative time of engine operation on field A

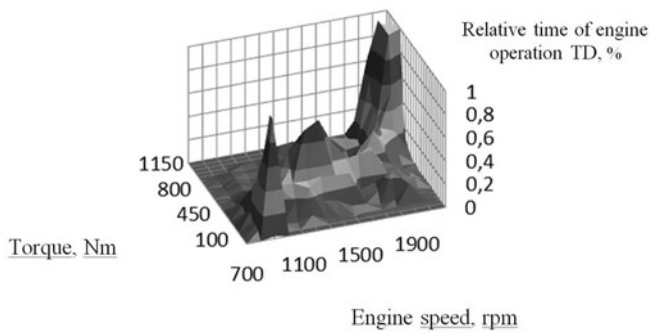

Fig. 3. Relative time of engine operation on field B

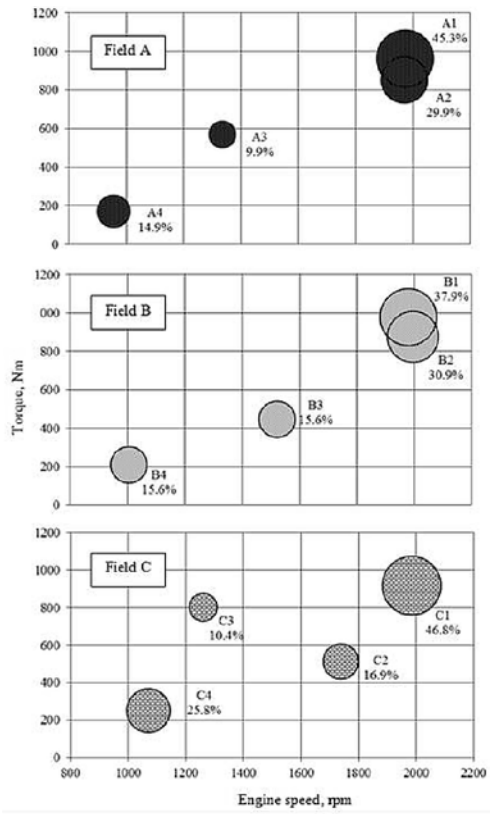

Fig. 5. Engine operation clusters for fields A, B and C; A1, … C4 – cluster name, % – relative time of engine operation in a cluster

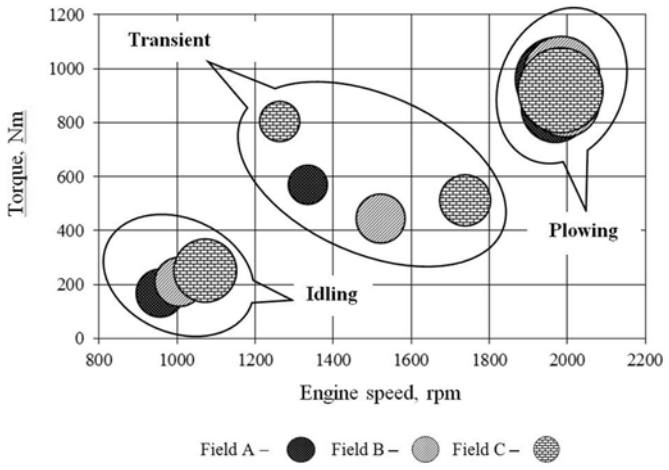

Fig. 6. Engine operationnal state clusters

During the plowing state interval, the engine was generating 190-195 kW, i.e. about 85% of nominal engine power. For fields A, B and C, the engine was generating 190-195 kW of power 75.2%, 68.8% and 46.8% of total time of engine operation respectively. In the case of engine idling state interval, the corresponding values were 14.9%, 15.6% and 25.8% (Fig. 5). The effective engine utilization E_N obtained from (3) were accordingly for field A = 0.62, for B = 0.58 and for C = 0.39.

The coordinates of engine for both plowing and idling state intervals for each field clustered within 200 rpm and 100 Nm ranges of engine speed and torque (Fig. 6). The interoperation or transient states spread over 600 rpm and 350 Nm ranges.

A Pearson correlation coefficient was obtained to evaluate the functional relation of plowing vs. idling state share to the field size. Positive correlation (0.92) at R^2 = 0,85 was attained for plowing state and strongly negative (−0.85) at R^2 = 0,72 for idling.

4. Discussion

The plowing operations comprise 30% of tractor engine operation while its power is not fully utilized [13, 18]. Continuous monitoring and analysis of economy of agriculture activities contributes to the minimization of energy usage [25]. Engine torque monitoring represents one of the key parameters in such analysis. Since its measurement requires specialized instrumentation setup, various indirect approaches have been explored [5]. Many such studies have presented their results in a general matrix form and fuel consumption profiles. In the evaluation approach here, performance indexes of operational power performance in various conditions have been presented. Implemented, they can contribute to optimal gear selection through visual display of actual engine power and to "gear up and throttle down" driving approach in transient engine states, possibly resulting in up to 20% fuel savings [4]. The actual engine utilization parameter may also be helpful in optimal tractor selection in terms of cost, as well as match of its engine power to target farm.

Our study, based on a theoretical model of engine optimal points of operation [4], implements a novel statistical data clustering and modern measurement technology approach. The time distributions of engine operation presented here confirm other studies [9, 10] validating our methodological approach. They may also help in modelling agriculture tractor engine load cycles [6], which in turn are used in evaluation of engine emissions.

Conclusions:

- The statistical data clustering approach to quantitative comparison of the effective time duration of the various engine modes of operation and fields used in this study enabled more precise evaluation of the actual power utilization of agriculture tractor engine, as a function of field size, than theoretical and simulation approaches.
- The presented statistical approach may have practical applications as an optimization tool in a more effective utilization of various add-on agriculture machinery through a visualization driver support system for optimal gear selection.
- A strong positive correlation was observed between the field size and engine plowing state, while a negative correlation was observed in the case of idling engine state of operation.
- The actual power utilization of agriculture tractor engine as a function of field size was 0.62, 0.58 and 0.39 respectively for the three fields used in this study.

References

1. Chłopek Z. Process modeling of exhaust gas emissions of combustion engine working in traction conditions. Oficyna Wydawnicza Politechniki Warszawskiej 1999;173:3-198
2. Dyer J. A., Desjardins R. L. Simulated Farm Fieldwork. Energy Consumption and Related Greenhouse Gas Emissions in Canada. Biosystems Engineering 2003;85:503-513, http://dx.doi.org/10.1016/S1537-5110(03)00072-2.
3. Dyer J. A., Desjardins R. L. Carbon Dioxide Emissions Associated with the Manufacturing of Tractors and Farm Machinery in Canada. Biosystems Engineering 2006;93:107-118, http://dx.doi.org/10.1016/j.biosystemseng.2005.09.011.
4. Grisso R., Pitman R. Gear Up and Throttle Down - Saving Fuel. Virginia Cooperative Extension. Virginia Polytechnic Institute and University. Publication 2001;6:442-450.
5. Harris H. D. Prediction of the Torque and Optimum Operating Point of Diesel Engines using Engine Speed and Fuel Consumption. Journal Agricultural Engineering Research 1992;53:93-101, http://dx.doi.org/10.1016/0021-8634(92)80076-5.
6. Hung W. T., Tong H. Y., Lee C. P., Ha K., Pao L. Y. Development of a practical driving cycle construction methodology: A case study in Hong Kong. Transportation Research Part 2007;D12:115-128, http://dx.doi.org/10.1016/j.trd.2007.01.002.
7. Intex. Fleet Management Systems. www.intex.net.pl.
8. Jahns G., Forster K.J., Hellickson M. Computer Simulation of Diesel Engine Performance. Transactions of the ASAE 1990;33:764-770, http://dx.doi.org/10.13031/2013.31398.
9. Janulevičius A., Juostas A., Pupinis G. Engine performance during tractor operational period. Energy Conversion and Management 2013;68:11-19, http://dx.doi.org/10.1016/j.enconman.2013.01.001.
10. Janulevičius A., Juostas A., Pupinis G. Tractor's engine performance and emission characteristics in the process of ploughing. Energy Conversion and Management 2013;75:498-508, http://dx.doi.org/10.1016/j.enconman.2013.06.052.
11. Kheiralla A. F., Azmi Y., Zohadie M., Ishak W. Modelling of power and energy requirements for tillage implements operating in Serdang sandy clay loam. Malaysia. Soil and Tillage Research 2004;78:21-34, http://dx.doi.org/10.1016/j.still.2003.12.011.
12. Kichler C.M., Fulton J.P., Raper R.L., Mcdonald T.P., Zech W.C. Effects of transmission gear selection on performance and fuel costs during

deep tillage operations. Soil and Tillage Research 2011;113:105-111.
13. Kim J.H., Kim K.U., Wu Y.G. Analysis of transmission load of agricultural tractors. Journal of Terramechanics 2000;37:113-125, http://dx.doi.org/10.1016/S0022-4898(99)00022-1.
14. Kim Y. J., Chung S. O., Choi C. H. Efects of gear selection of an agricultural tractor on transmission and PTO load during rotary tillage. Soil and Tillage Research 2013;134:90-96.
15. Koniuszy A. The method of making time density characteristic of agricultural tractor engine by using TRS system. Annual Review of Agriculture Engineering 2008;6:13-22.
16. Koniuszy A., Nadolny R., A method and a device of monitoring operation of the tractor. Nr PL 381892;2014.
17. Kostencki P., Łętkowska B., Nowowiejski R. Field tests of resistance to abrasive wear of ploughshares made of boron steel. Tribologia 2013;249:49-79.
18. Lindgren M. A Transient Fuel Consumption Model for Non-road Mobile Machinery. Biosystems Engineering 2005;91:139-147, http://dx.doi.org/10.1016/j.biosystemseng.2005.03.011.
19. Mehta, C. R., Singh K., Selvan M. M. A decision support system for selection of tractor-implement system used on Indian farms. Journal of Terramechanics 2011;48:65-73, http://dx.doi.org/10.1016/j.jterra.2010.05.002.
20. Mileusnić Z.I., Petrović D.V., Dević M.S. Comparison of tillage systems according to fuel consumption. Energy 2010;35:221-228, http://dx.doi.org/10.1016/j.energy.2009.09.012.
21. Moitzi G., Haas M., Wagentristl H., Boxberger J., Gronauer A. Energy consumption in cultivating and ploughing with traction improvement system and consideration of the rear furrow wheel-load in ploughing. Soil and Tillage Research 2013;134:56-60.
22. Pang S.N., Zoerb G.C., Wang G. Tractor Monitor Based on Indirect Fuel Measurement. Transactions of the ASAE 1985;28:994-998, http://dx.doi.org/10.13031/2013.32375 .
23. Peca J.O., Serrano J.M., Pinheiro A., Carvalho M., Nunes M., Ribeiro L., Santos F. Speed advice for power efficient drawbar work. Journal of Terramechanics 2010;47:55-61, http://dx.doi.org/10.1016/j.jterra.2009.07.003.
24. Renius K.T. Trends in Tractor Design with Particular Reference to Europe. Journal Agricultural Engineering Research 1994;57:3-22, http://dx.doi.org/10.1006/jaer.1994.1002.
25. Riveiro J. A., Marey-Pérez M. F., Díaz-Varela E. R., Álvarez C. J. A methodology for the analysis of the relationships between farms and their physical environment. Journal of Agricultural Science 2010;148:101-116, http://dx.doi.org/10.1017/S0021859609990347.
26. Saglam C., Akdemir B. Annual Usage of Tractors in North-West Turkey. Biosystems Engineering 2002;82:39-44, http://dx.doi.org/10.1006/bioe.2002.0046.
27. Sahay C. S., Tewari V. K. Computer Simulation of Tractor Single-point Drawbar Performance. Biosystems Engineering 2004;88:419-428, http://dx.doi.org/10.1016/j.biosystemseng.2004.05.005.
28. Serrano J. M., Peca J. O., Pinheiro A., Carvalho M., Nunes M., Ribeiro L., Santos F. The Effect of Gang Angle of Offset Disc Harrows on Soil Tilth. Work Rate and Fuel Consumption. Biosystems Engineering 2003;84:171-176, http://dx.doi.org/10.1016/S1537-5110(02)00261-1.
29. Serrano J. M., Peca J. O., Silva M., Pinheiro A., Carvalho M. Tractor energy requirements in disc harrow systems. Biosystems Engineering 2007;98:286-296, http://dx.doi.org/10.1016/j.biosystemseng.2007.08.002.
30. Statsoft, Cluster analysis. Electronic Textbook, (2015).
31. Sogaard H. T., Sorensen C. G. A Model for Optimal Selection of Machinery Sizes within the Farm Machinery System. Biosystems Engineering 2004;89:13-28, http://dx.doi.org/10.1016/j.biosystemseng.2004.05.004.
32. Souza E.G., Milanez L.F. (1988). Indirect Evaluation of the Torque of Diesel Engines. Transactions of the ASAE 1988;31:1350-1354, http://dx.doi.org/10.13031/2013.30869.
33. Souza E.G., Santa Catarina A. Optimum Working Curve for Diesel Engines. Transactions of the ASAE 1999;42:559-563, http://dx.doi.org/10.13031/2013.13216.
34. Wang G., Zoerb G.C. Determination of Optimum Working Points for Diesel Engines. Transactions of the ASAE 1989;32:1519-1522, http://dx.doi.org/10.13031/2013.31182.

Adam KONIUSZY
Piotr KOSTENCKI
Department of Systems Engineering Agronomic
West Pomeranian University of Technology
al. Piastów 17, 70-310 Szczecin, Poland

Andrew BERGER
Physics and Electrical Engineering Department
University of Scranton
PA 18510, USA

Wojciech GOLIMOWSKI
Department of Biomass Processing Technique
Institute of Technology and Life Sciences
ul. Biskupińska 76, 60-463 Poznań, Poland

E-mails: adam.koniuszy@zut.edu.pl, Berger@Scranton.edu, w.golimowski@itp.edu.pl

Article citation info:
BŁACHNIO J, BOGDAN M, ZASADA D. Increased temperature impact on durability of gas turbine blades. Eksploatacja i Niezawodnosc – Maintenance and Reliability 2017; 19 (1): 48–53, http://dx.doi.org/10.17531/ein.2017.1.7.

Józef BŁACHNIO
Mariusz BOGDAN
Dariusz ZASADA

INCREASED TEMPERATURE IMPACT ON DURABILITY OF GAS TURBINE BLADES

WPŁYW PODWYŻSZONEJ TEMPERATURY NA TRWAŁOŚĆ ŁOPATEK TURBINY GAZOWEJ*

The paper presents the research results of a microstructure of the turbine rotor blades made of nickel-based super alloys. The purpose of the research was to determine the high temperature impact on the microstructure stability of the material of the blades. The degree of advancement of the super alloy microstructure changes after the exposure to high temperature was compared to the mictrostructure condition of new blades. The research material includes blades made of EI 867 and ŻS 32 types of alloys. The microstructure research of blades subject to the high temperature impact, and the blades after operation showed the occurrence of adverse changes in relation to the microstructure of new blades. It was found that the cause of adverse changes in the microstructure was the super alloy overheating. The blade in such a condition has low heat and creep resistance. The element, in which the overheating will occur, is exposed to damage, which usually entails faulty turbine operation. This type of damage is removed during the engine major repair, which is associated with huge costs.

Keywords: *gas turbine, blade, microstructure, durability.*

W artykule przedstawiono wyniki badań mikrostruktury łopatek wirnika turbiny wykonanych z nadstopów na bazie niklu. Celem badań było określenie skutków oddziaływania wysokiej temperatury na stabilność mikrostruktury materiału łopatek. Stopień zaawansowania zmian mikrostruktury nadstopu po oddziaływaniu wysokiej temperatury porównywano ze stanem mikrostruktury łopatek nowych. Materiałem do badań były łopatki ze stopów typu EI 867 oraz ŻS 32. Badania mikrostruktury łopatek poddawanych oddziaływaniu wysokiej temperatury oraz łopatek po eksploatacji wykazały występowanie niekorzystnych zmian w stosunku do mikrostruktury łopatek nowych. Stwierdzono, że przyczyną niekorzystnych zmian w mikrostrukturze było przegrzanie nadstopu. Łopatka w takim stanie wykazuje niską żaroodporność oraz żarowytrzymałość. Element, w którym wystąpi przegrzanie jest narażony na uszkodzenie, co przeważnie pociąga za sobą wadliwą pracę turbiny. Tego typu uszkodzenia usuwa się w trakcie naprawy głównej silnika co wiąże się z ogromnymi kosztami.

Słowa kluczowe*: turbina gazowa, łopatka, mikrostruktura, trwałość.*

1. Introduction

Gas turbines are used in the energy sector in traction, marine, and aircraft engines as well as in aerospace. During operation, they are subject to variable mechanical and heat loads. The essence of low-cycle loads is a cumulative and simultaneous destructive effect of variable mechanical and heat loads of high amplitudes. These kinds of loads are especially subject to rotating blades. Along with the increasing temperature, the material strength of blades decreases. As a result of the impact of high temperature and exhaust gases with an aggressive chemical effect, the technical condition is subject to adverse changes. It results in the material overheating, its creeping and thermal fatigue [4, 17, 18, 22]. Consequently, it leads to the loss of heat and creep resistance of the material of blades.

The turbine efficiency, which is at the level of 30-45%, decreasing during the operation process, substantially depends on the exhaust gas temperature. However, the increase in exhaust gas temperature is limited by the used material properties: their resistance to creeping, microstructure change (overheating), thermal fatigue, high temperature corrosion, etc. [5, 20].

The most unreliable elements of the gas turbine include rotor blades [4, 17]. During operation, they are subject to the variable loads: mechanical ones as a result of rotation, as well as aerodynamic and heat ones from the work factor flow. In addition, the chemically aggressive exhaust gases of high temperature affect them. The reliability and durability of blades is a sum of many factors, the predominant importance of which plays the material, which they are made of. The high and stable strength properties of super alloys in structural terms constitute the proper microstructure that is not subject to weakening operational changes [2, 6, 16].

Particularly high requirements are imposed to materials used for the turbines' blades. Advances in the development of super alloys and manufacturing technology of blades resulted in a increase of operating temperature of blades almost to 1350K [8]. The improved super alloys on the turbine blades were obtained thanks to the development of alloys on the basis of nickel and cobalt. In addition, in order to increase the mechanical properties, chrome, titanium, molybdenum, vanadium, tungsten, niobium, tantalum, and other elements [1, 7, 10, 11] are added. The main component of the super alloy is the γ phase, that is Ni solid solution of a wall-centred regular structure. The composition of this phase may mainly include the elements such as Co, Cr, Mo, W and Re, which strengthen them with solution.

Due to the manufacturing methods of blades, super alloys are divided into wrought and cast ones. In the super alloys of the wrought blades, a friction of volume reinforcing with the γ' phase ranges from 20 to 45%. The blades made of these super alloys can operate to the temperature of 1173K. The further increase of the operating tempera-

(*) Tekst artykułu w polskiej wersji językowej dostępny w elektronicznym wydaniu kwartalnika na stronie ***www.ein.org.pl***

ture of blades to about 1273 K requires an increase in the volume friction of the γ' phase in the alloy. It can be achieved by modifying the chemical composition, as well as by changing the manufacturing technology, e.g. as a result of introduction of cast super alloys. In the cast super alloys, the γ' phase volume friction is approximately 60%. In order to increase the operating temperature of blades of more than 1373K, the directional crystallization is applied [16, 18, 19]. It allows an increase in the super alloy creep resistance. The further development of super alloys was associated with the elimination of grain boundaries – monocrystalline super alloys, i.e. these are made of a single crystal with a uniform internal structure of the entire volume. Using these manufacturing technologies of the turbines' blades allowed the achievement of a fivefold increase of fatigue strength and a tenfold increase of durability at a high temperature, in comparison with the blades produced from polycrystalline super alloys [8].

Moreover, heat-resistant coatings with good thermal conductivity and high structure stability are applied on the gas turbines' blades operating in extreme temperature conditions. Thermal properties of the coatings mainly depend on the chemical composition of the material and microstructure [3, 4]. Different types of protective coatings, obtained by many methods, are used. The diffusion coatings on aluminium matrix and their variations known as modified coatings are most commonly used [9, 14, 21]. These coatings consist of a priming layer and an insulation layer. They should be characterised by very low thermal conductivity.

A further step aimed at increasing the exhaust gas temperature and decreasing the blades' temperature includes their internal cooling with air from behind the engine compressor. This allows to lower the temperature of the blade material in relation to the temperature of the circumfluent exhaust stream by over 600K [21, 22]. Furthermore, better distribution of temperature onto the blades in the turbine operation transients is obtained.

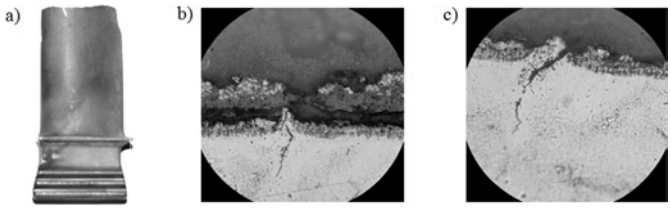

Fig. 1. The example forms of operational failures of an uncooled turbine blade made of the EI 867 type forged super alloy: a) a tip broken due to the super alloy overheating; b) stratification of heat-resistant coatings, and the super alloy crack initiation, x500; c) erosion of the heat-resistant coating and the crack penetrating into the super alloy, x500

Moreover, in order to increase durability, the complex geometric shapes of blades are designed. They are shaped in such a way, as not to create a vibration resonance during interruption of the engine operation [6]. Tip shelves at the ends or near the blade ends, which act as dampers eliminating a dangerous form and frequency of vibrations, and increasing tightness in the turbine rotor tip clearance are also applied. The minimum clearance prevents the work factor losses.

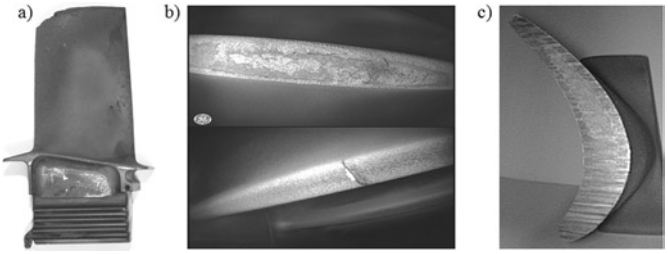

Fig. 2. The example forms of damage of the cooled turbines' blades made of the ŻS 32 type cast super alloy: a) the material overheated at the tip [2]; b) complete burning of the coating on the leading edge to expose the super alloy, and a crack on the leading edge [12]; c) blade leaf front chafing [12]

Despite using many endeavours in order to improve the efficiency of the gas turbine operation, its durability and reliability, over the long-term operation process, there are still all kinds of damages to the turbine elements, especially their blades (Fig. 1, Fig. 2). It is possible to differentiate defects being the results of material and technological faults, derogations from the quality of production and repairs. The important reasons can also include improper fuel atomization in the combustion chamber, as well as its diminished physical-chemical properties [5, 15].

The most frequent cases of damage include the overheating of the blades' leaves (Fig. 1a, 2a). It sometimes results in the blade leaf end fracture (Fig. 1a). The destruction process of the gas turbine blade usually begins with the destruction of its heat-resistant coating (Fig. 1b c, 2b).

As a result of it, the blade material is exposed to the direct heat and chemical effect of exhaust gases. This situation mainly causes the material overheating and the formation of the blade leaf cracks (Fig. 1c, 2b). The factors affecting that phenomenon are supercritical temperature, its impact time and chemical aggression of exhaust gases. As an effect of high temperature, and high tensile stresses derived from centrifugation and time, the phenomenon of the blade material thermal expansion occurs. It significantly affects the turbine rotor tip clearance reduction. Consequently, it results in rubbing the blade front against the turbine body (Fig. 2c), which causes additional heating of the blade leaf material and adverse changes in the super alloy microstructure. The changes typical for the high-temperature creeping process with the uniaxial stress state are usually observed in the blades with a plate.

2. Increased temperature impact on degradation of uncooled blades of the EI-867 WD type super alloy

In the gas turbine operation, there are often cases of short-term heating of the material of blades above their normal operating temperature. Therefore, it is important to maintain the alloy heat and creep resistance to increased temperature at the required blade operation time. Creep resistance of super alloys for the gas turbine blades relates to the *γ'* reinforcing phase. Under the influence of a work factor with high temperature, it is subject to coagulation and dissolution in the matrix. In order to determine the increased temperature impact on the super alloy degradation of forged blades, the experimental research was carried out. In case of the research, new gas turbine rotor blades made of the EI-867 WD (HN62MWKJu) alloy – uncooled blades – were adopted. The blades' leaves were divided into four equal samples, which were chosen at random for testing and heated (three of them) at five temperature values every 100 K starting from the temperature of 1023 K. The heating and cooling of samples took place in the vacuum oven (individually) – no interference of the core on the surface of blades.

Table 1. The list of the EI-867 WD alloy basic chemical composition (% of weight)

C	Mo	Si	Cr	Ni	Co	Mo	W	Al	B	Fe
max	max	max		other					max	
0.1	0.3	0.6	9.0		14	10.3	5.0	4.5	0.02	4.0

The EI-867 WD alloy belongs to a small group of nickel super alloys that do not contain titanium. It is a super alloy of a lower chromium content, and therefore, it is sensitive to corrosion [4, 16, 20]. Accordingly, protective coatings – aluminium coatings – are applied. The TU 14-1-232-72 standard includes the requirements for the super

alloy chemical composition (Table 1), heat treatment and mechanical properties.

The alloy structure is typical for nickel super alloys and is composed of: γ, phase, γ' phase, carbides and borides. The γ' phase is aluminium solid solution, titanium tubes in nickel. The γ' phase particles (Ni_3Al, Ni_3Ti) are cubical in shape [13, 16, 18]. The γ' phase relative volume after the alloy standard heat treatment is 31÷34%. The heat treatment includes solubilisation quenching and ageing. The cooling in air during solubilisation quenching results in precipitation of the γ' phase small particles, the relative volume of which is about 20%. The ageing results in further precipitation of the γ' phase particles and the growth of previously separated ones. Among the carbides, the relative volume of which does not exceed 2% in the alloy, $M_{23}C_6$ solid predominates. It is formed during heat treatment or it is released during operation, usually on the boarders of grains in the temperature range of 933K÷1253K. Inside the grains, there is a carbide M_6C [4, 16]. The temperature values of heating the samples cut out of the blades are associated with the temperature range, which occurs during normal and emergency operation of the exploited rotor blades. The stream temperature of the work factor at the inlet to the gas turbine, due to restrictions resulting from thermal and chemical characteristics of the materials used in the uncooled turbine blades should be within the range of 1173÷1223K [17, 20].

The initial stage of metallographic tests was to assess the structure in order to determine the duration of the heating process of the blades' parts. The time and temperature affect the kinetics of growth and coagulation of the γ' phase particles. The experiment involving the heating of samples in the temperature above T_{max} (maximum temperature behind the turbine, i.e. 1223 K for 0.5h, 1h, 2h and 3h) was conducted. Therefore, the information on structural changes both of the coating and the blades' material, depending on the heating time – modification of the size of the γ' dispersion phase (Fig. 3) was obtained. The changes of sizes (surface) of precipitation of the γ' reinforcing phase in the heating time function were determined (Fig. 4).

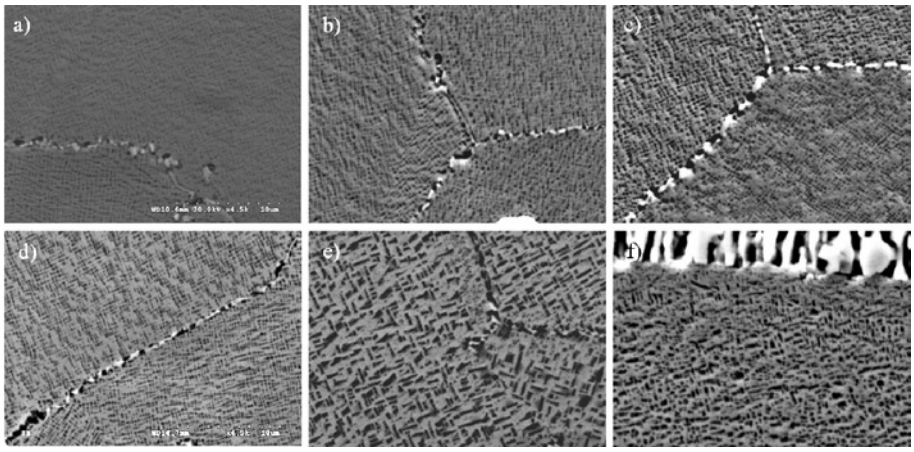

Fig. 5. EI - 867 WD super alloy subsurface microstructure: a) super alloy without heating and super alloy heated for 1 hour at: b) 1023K; c) 1123K; d) 1223K; e) 1323K; f) 1423K (surface x4500)

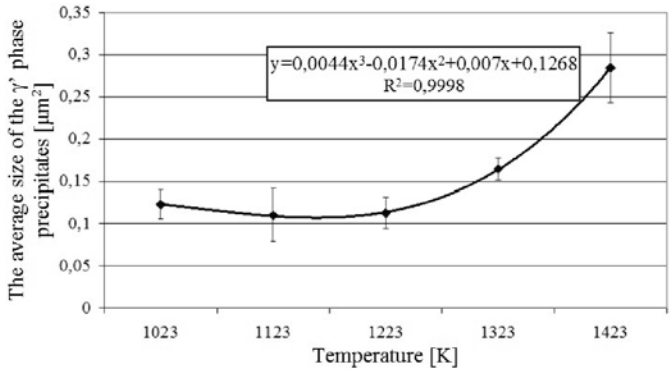

Fig. 6. Changes in the average size of the γ' phase particles in the temperature function

On the basis of Figure 4, the heating time, which was 1h in the research of the impact of high temperatures on the blade material, for a constant temperature, i.e. 1223K, was adopted. At that time, a sudden increase in the size of the γ' phase particles (an additional argument for such a choice is the aircraft task time in the operation conditions for the adopted jet engine type, which is also 1h) occurs.

The microstructure analysis of the super alloy subject to the high temperature impact was carried out, thanks to which detailed information on changes was obtained. The microstructure changes, mainly modification of sizes and distribution of the γ' dispersion phase, significantly affect strength properties. In Figure 5a÷f, the results of the super alloy metallographic test without heating and after heating for a period of 1h were presented taking into account five different temperature values.

The change in sizes of the γ' phase particles depending on the heating temperature was calculated (Fig. 6). It was found that the initial coagulation stage of precipitates of the γ' reinforcing phase, which is characterised by relatively high regularity and a large number of precipitates per are unit, occurs even at the temperature of 1123 K (Fig. 5b, c). As the temperature rises, the γ' phase structure becomes less regular while increasing the grain size (Fig. 6).

The initial stage of combining the γ' phase cubic precipitates in plates occurs at the temperature of 1223 K (Fig. 5d). At the temperature of 1323 K, a significant increase and coagulation of precipitates of the γ' reinforcing phase, which takes on the shape of plates, was found (Fig. 5e). The number of precipitates is much smaller, however,

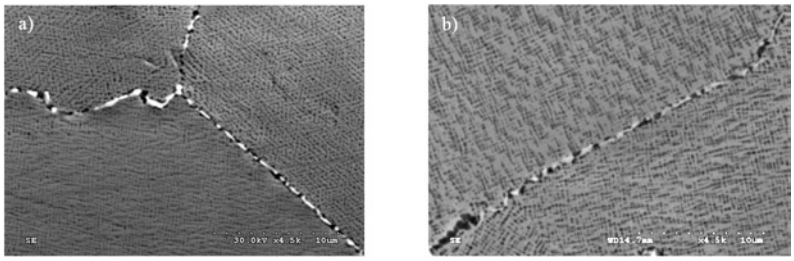

Fig. 3. Morphology of the γ' phase precipitates – heating in the temperature of 1223K for: a) 0.5h; b) 1h (surface x4500)

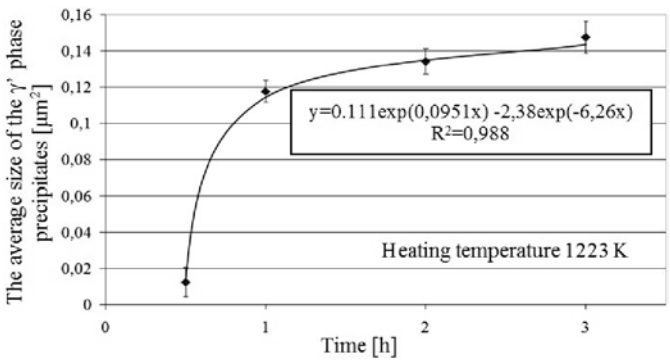

Fig. 4. Changes in the average size of the γ' phase particles depending on the heating time of samples of the blades at the temperature of 1223K

they are much larger than those created at 1223 K. The morphology of the γ' phase shows that after exceeding the temperature of 1223 K, the EI – 867 WD alloy is overheated.

3. Increased operating temperature impact on degradation of cooled blades of the ŻS 32 type super alloy

The research covered the blades cast from the ŻS 32 type cobalt and nickel super alloy. The content of basic alloy elements was presented in Table 2.

In case of the research, the new turbine rotor blades and those after increasingly long time of operation were adopted. The blades were prematurely removed from the turbine due to their overheating. In order to determine the increased temperature impact during operation on degradation of the ŻS 32 super alloy microstructure, metallographic tests were carried out.

Table 2. List of the ŻS 32 type super alloy basic chemical composition (% of weight)

Ni	Al	Cr	Co	Nb	Mo	Ta	W	Re
62.4	6.1	5.1	10.8	1.3	1.2	1.2	8.4	3.0

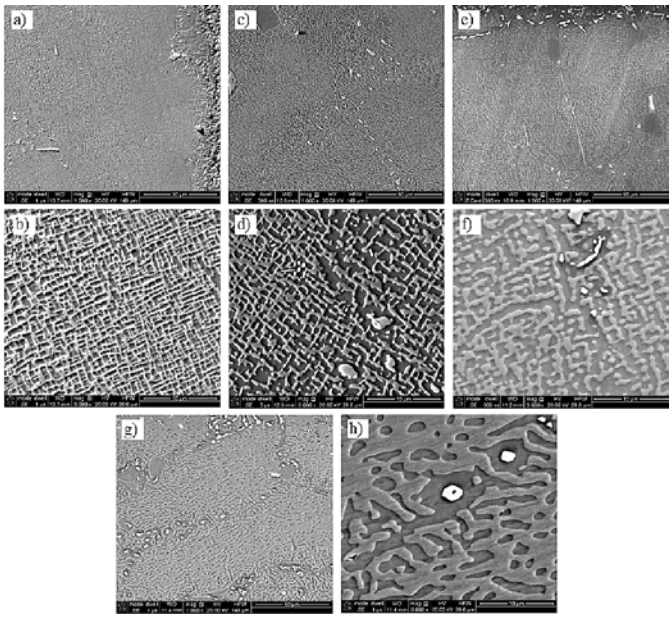

Fig. 7. The increased temperature impact on morphological changes in the cross-section of the leading edge: a, b) new blade No. 1; c; d) blade after the shortest time of operation No. 2; e, f) blade after the average time of operation No. 3; g, h) blade after the longest time of operation No. 4

On the basis of the structural observation conducted with the use of the Quanta 3D FEG scanning electron microscope, a very clear impact of the increased temperature on degradation of the microstructure of the analysed blades made of the ŻS 32 type super alloy was found. The microstructure of the tested blades consists mainly of γ and γ' phases and carbides. It was found that with the operating temperature increase and the time of operation, clear microstructural changes occur (Fig. 7). The significant changes in the morphology of the γ' reinforcing phase were observed. In the blade, the γ' phase new particles (Ni_3Al) have a cubic shape. As a result of the increased temperature impact, the change of their shape from cubic (Fig. 7a and b) to cuboidal one (Fig. 7c÷f) occurs, in order to reach an oval shape at the maximum temperature (Fig.7g and h).

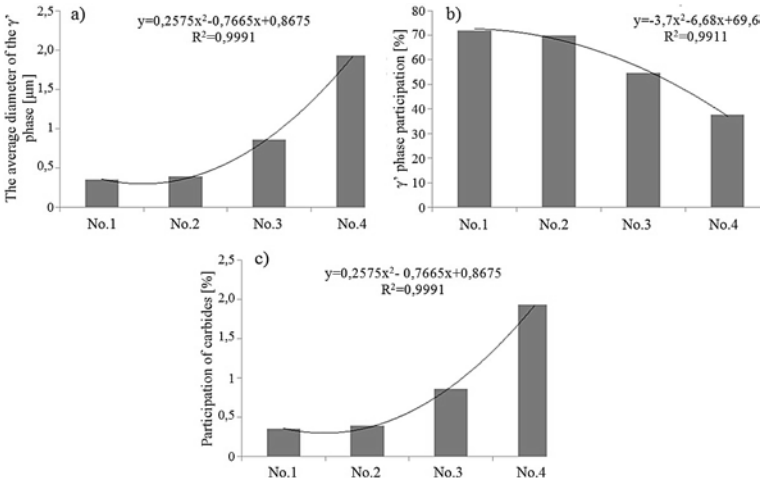

Fig. 8. The increased temperature impact on: a) the average diameter of the γ' phase, b) the γ' phase surface participation, c) surface participation of carbides

The observed changes are related to the expansion of the γ' reinforcing phase and a decrease in its participation (Fig. 8a). In case of a new blade, the average size of the γ' phase particles is approximately 0.3μm. As a result of the impact of increased temperature and operational factors, this value increases to the level of 2μm. The reported trend is also significantly reflected in the surface participation changes of the specified γ' reinforcing phase. It was observed that the surface participation of the γ' phase decreases from 70% for the new blade to 35% for the blade operated at the highest temperature (Fig. 8b). As a result of the increased temperature impact, the observed morphological changes of the γ' reinforcing phase are small, however, its impact on the surface participation of carbides takes place (Fig. 8c).

The surface participation of carbides in all the observed blades is at the level of 2-2.5%. Additionally, there were no significant changes in morphology of the observed carbides. However, a clear impact of the increased temperature and operating time of the tested blades on the γ' phase surface participation in particular zones within the cross-section of the tested blades was stated (Fig. 9). In case of the blade exposed to the highest temperature impact and the longest operation time No. 4, while measuring the surface participation of the described phase from the leading edge into the blade, it was found that the surface participation is the lowest (30%). In the distance of this blade, the participation of the described phase rises to the level of about 50%. However, no impact of the observed trend on the size changes of the γ' phase particles was observed in similar areas seen on the cross sections of other blades (Fig. 10).

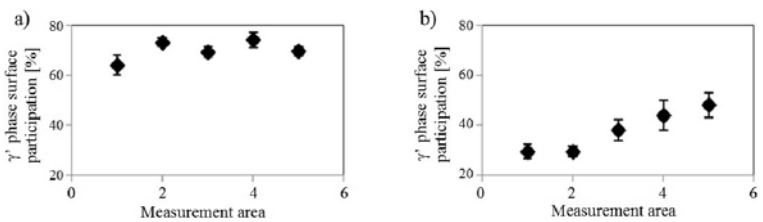

Fig. 9. Surface participation of the γ' reinforcing phase into the leading edge: a) blade No. 2, b) blade No. 4

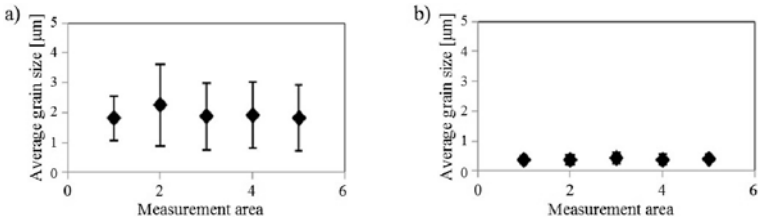

Fig. 10. The average diameter of the γ' reinforcing phase into the leading edge: a) blade No. 2, b) blade No. 4

4. Conclusion

Based on the research results, it can be concluded that both in case of new blades and the operated ones, which are subject to the increased temperature impact, there are microstructural changes in the material of blades. In case of the experiment with the EI-867 WD new blades, a high temperature and time of their impact are decisive factors. The heating time, which in testing of the increased temperature impact on the blade material was 1h, for a constant temperature, i.e. 1223 K; in that time, a sudden increase in the sizes of the γ' phase particles occurred. An additional argument for such a choice is the aircraft task time in the operation conditions for the adopted jet engine type, which is also 1h. However, the selected temperature values of heating the blades are also associated with the temperature range, which occurs during normal and emergency operation of the exploited rotor blades. The stream temperature of the work factor (exhaust gases) at the outlet from the aircraft jet engine combustion chamber, due to restrictions resulting from thermal and chemical characteristics of the materials used in the complete, uncooled turbine blades should be within the range of 1173÷1223K, as confirmed in the literature [17]. The *γ'* phase morphology shows that after exceeding the temperature of 1223 K, the EI – 867 WD alloy is overheated, and the tested blade cannot be considered useful for further operation. The obtained images of a microstructure of the EI - 867 WD alloy subject to the impact of increasingly higher temperature may be a basis for assessing the degree of overheating of the gas turbine blades.

In case of the operated blades (with different technical condition), in addition to the high temperature unstable at that time and the time of operation, there is also an important factor, i.e. aggressiveness of exhaust gases. As a result of the conducted tests of the operated blades, it is concluded that under the increased temperature influence, the chemical composition, morphology and distribution in the structure of the blade material of the *γ'* reinforcing phase adversely change. The morphology of the *γ'* phase particles depends on the mechanical stress. The tensile stress, occurring along the blade axis during the turbine rotor rotation, promotes expansion of the *γ'* phase on a plane perpendicular to the stress direction. As a result, the original cuboid shape changes into plates, whose wider walls are positioned perpendicularly to the stress direction and the narrow walls perpendicularly to other cube directions [9, 19]. These adverse changes in the super alloy microstructure exert a decisive influence on its strength properties. The *γ'* phase growth results in coagulation of precipitates, and therefore, an adverse change of its shape. Moreover, this phase percentage in the structure decreases. As a result, the heat and creep resistance of the blades' super alloy decrease. This condition significantly affects the durability of blades and has a major impact on the gas turbine premature major repair. In case of aircraft, it relates to the aircraft transition from the state of airworthiness, removal of the engine and its passing for the major repair. Although the end result are tremendous costs related to the repair due to e.g. one overheated turbine blade. However, the flight safety is an overarching principle of aircraft operation.

References

1. Bojar Z., et al. Changes of microstructure of blades made of ŁK-4 alloy during long-term operation of aircraft turbine engine. Military University of Technology Bulletin 1988; 12: 51-64.
2. Błachnio J, Bogdan M, Kułaszka A. New non-destructive methods of diagnosing health of gas turbine blades. Advances in Gas Turbine Technology 2011: 465-498, .http://dx.doi.org/10.5772/29548
3. Błachnio J, Pawlak W. Damageability of gas turbine blades - evaluation of exhaust gas temperature in front of the turbine using a non-linear observer. Advances in gas turbine technology2011: 435-464.
4. Błachnio J, Bogdan M. Ocena stanu łopatek turbiny gazowej na podstawie barwy ich powierzchni. Problemy badań i eksploatacji techniki lotniczej. [Evaluation of the condition of gas turbine blades based on their surface colour. Problems of research and aircraft technology operation]. Wydawnictwo Instytutu Technicznego Wojsk Lotniczych 2012 [Publishing and Printing House of the Air Force Institute of Technology 2012]; (8): 11-33.
5. Błachnio J, Spychała J, Pawlak W, Zasada D. The attempt to assess the technical condition of a gas turbine blade when information on its operating condition is limited. Journal of KONBIN 2014; 2(30): 75-86, http://dx.doi.org/10.2478/jok-2014-0016.
6. Błachnio J, Kułaszka A, Zasada D. Degradation of the gas turbine blade coating and its influence on the microstructure state of the superalloy. Journal of KONES 2015; 22(2): 17-24, http://dx.doi.org/10.5604/12314005.1165385.
7. Ciszewski A, Chodorowski J. Aviation materials science. Warsaw Technical University, Warsaw, 2003.
8. Dubiel B. Microstruktural changes during creep of single-crystalline nikel-base superalloys. Kraków: University of Science and Technology Press, 2011.
9. Góral M, Swadźba L, Moskal G, Jarczyk G, Aguilard J. Diffusion aluminide coatings for TiAl intermetallic turbine blades. Intermetallics 2011; 19(5): 744-747, http://dx.doi.org/10.1016/j.intermet.2010.12.015.
10. Hernas A. Creep resistance of steel and alloys. Gliwice: Silesian Technical University, 1999.
11. Hodor K. Gradient structure of surface layer of Ni- and Fe+Ni-based alloys. Doctor's thesis. Kraków: Academy of Mining and Metallurgy, 2002.
12. Kułaszka A, Giewoń J. Report No 28 and No 73. Warsaw: Air Force Institute of Technology, 2014.
13. Majka H, Sieniawski J. Research of kinetics and coagulation of γ' phase in nickel superalloy EI-867. Archive of Materials Science 1998;4(4): 237-254.
14. Mikułowski B. Heat and creep resistant alloys - superalloys. Kraków: Editions Academy of Mining and Metallurgy, 1997.
15. Pawlak W, Błachnio J. On the need to maintain homogenous temperature field within the working agent at the intake of a jet engine turbine. Journal of KONES 2014; 21(1): 205-213, http://dx.doi.org/10.5604/12314005.1134099.
16. Paton B. Creep resistance of cast nickel alloys and protection thereof against oxidation. Kiev: Naukowa Dumka, 1997.
17. Poznańska A. Lifetime of aircraft engine blades made of EI-867 alloy upon aspect of non-uniform distortion and structural changes. Doctor's

thesis. Rzeszów Technical University, 2000.
18. Reed R. C. The Superalloys. Fundamentals and applications. Cambridge: Cambridge University Press, 2006, http://dx.doi.org/10.1017/CBO9780511541285.
19. Scheibel J, White C, Yoo M. Met. Trans. 1985; 16A: 651, http://dx.doi.org/10.1007/BF02814239.
20. Sieniawski J. Criteria and methods of evaluation of materials for elements of aircraft turbine engines. Technical University Rzeszów, 1995.
21. Swadźba L, Formanek B, Maciejny A. Corrosion damage and regeneration of aluminide coatings on aircraft turbine blades. Materials Science and Engineering. 1989; A121:407-412, http://dx.doi.org/10.1016/0921-5093(89)90794-6.
22. Tajra S, Otani R. The theory of high-temperature strength of materials. Mietałurgija, Moscow,1986.

Józef BŁACHNIO
Air Force Institute of Technology
6 Księcia Bolesława str., 01-494 Warsaw, Poland

Mariusz BOGDAN
Department of Mechanical Engineering
Bialystok Technical University
45 Wiejska str., 15-333 Białystok, Poland

Dariusz ZASADA
Military University of Technology
2 Kaliskiego str., 00-908 Warsaw, Poland

E-mails: jozef.blachnio@itwl.pl, m.bogdan@pb.edu.pl, dzasada@wat.edu.pl

Article citation info:
RUSEK J. Application of Support Vector Machine in the analysis of the technical state of development in the LGOM mining area. Eksploatacja i Niezawodnosc – Maintenance and Reliability 2017; 19 (1): 54–61, http://dx.doi.org/10.17531/ein.2017.1.8.

Janusz RUSEK

APPLICATION OF SUPPORT VECTOR MACHINE IN THE ANALYSIS OF THE TECHNICAL STATE OF DEVELOPMENT IN THE LGOM MINING AREA

ZASTOSOWANIE METODY SUPPORT VECTOR MACHINE W ANALIZIE STANU TECHNICZNEGO ZABUDOWY TERENU GÓRNICZEGO LGOM*

The paper presents the results of the analysis of technical wear of buildings located within impact of mining plant in the Legnica - Głogów Copper District (LGOM). The study used method related to neural networks, support vector (Support Vector Machine) in regression approach ε-SVR (Support Vector Regression). The aim of the study was to assess the impact of variables describing the structural protection and renovations on the course modeled phenomenon. The basis for the analysis was created model of technical wear of buildings in the form of a network ε-SVR. In addition to the variables determining the level of structural protection and renovations in the model included variables describing: terrain deformation, mining intensity tremors and the age of the buildings. The choice of model parameters were performed using, as gradientlessness optimization method, genetic algorithm. Based on the established model ε-SVR two types of sensitivity analysis were applied. Assessing the impact of the structural protections have been studying by the analysis of variability of the gradient vector for the modeled hypersurface. The analysis of the impact of renovations on the course modeled process was carried out based on the comparator simulation results of ε-SVR model. The results confirmed the usefulness of the methodology of research and allowed to draw important conclusions on the impact of analyzed factors on the technical wear traditional buildings LGOM.

***Keywords**: Support Vector Machine, influence of mining, structure resistance, technical wear, technical condition.*

W pracy przedstawiono wyniki analizy zużycia technicznego budynków zlokalizowanych w zasięgu wpływów eksploatacji górniczej na terenie Legnicko-Głogowskiego Okręgu Miedziowego (LGOM). W badaniach zastosowano pokrewną sieciom neuronowym metodę wektorów podpierających (Support Vector Machine) w podejściu regresyjnym ε-SVR (Support Vector Regression). Celem badań było uzyskanie oceny wpływu zmiennych opisujących zabezpieczenia konstrukcyjne i remonty na przebieg modelowanego zjawiska. Podstawą do analiz był utworzony model zużycia technicznego budynków w postaci sieci ε-SVR. Oprócz zmiennych określających poziom zabezpieczeń konstrukcyjnych i remontów, w modelu uwzględniono zmienne opisujące: deformacje terenu pochodzenia górniczego, intensywność wstrząsów oraz wiek budynków. Dobór parametrów modelu przeprowadzono z wykorzystaniem, jako bezgradientowej metody optymalizacyjnej, algorytmu genetycznego. Bazując na utworzonym modelu ε-SVR przeprowadzono dwurodzajową analizę wrażliwości. Oceny wpływu zabezpieczeń konstrukcyjnych dokonano badając zmienność wektora gradientu modelowanej hiperpowierzchni. Natomiast analiza wpływu remontów na przebieg modelowanego procesu została przeprowadzona na bazie komparacji wyników symulacji modeluε-SVR. Wyniki badań potwierdziły przydatność przyjętej metodyki badań oraz pozwoliły na sformułowanie istotnych wniosków dotyczących wpływu analizowanych czynników na zużycie techniczne tradycyjnej zabudowy LGOM.

***Słowa kluczowe**: Support Vector Machine, wpływy górnicze, odporność budynków, zużycie techniczne, stan techniczny.*

1. Introduction

Resistance of building structures to the impacts of mining depends on their technical condition, defined in terms of technical wear. In recent years, the results of the research studies [6, 7] confirmed the significant influence of mining exploitation on the technical wear of building structures, both in the form of ground deformations and mining tremors. They also demonstrated the importance of structural preventive measures and of current repairs. These relationships, however, remained implicit in the context of mathematical functional form. Therefore, the use of more complex analytical methods, taking into account the multidimensionality and non-linearity of the modeled process, was justified in the further studies. Such a model should allow for a more effective assessment of the technical condition of building structures and for the analysis of the influence of individual variables included in the description of the modeled phenomenon. Taking this into consideration, a model of the course of technical wear as the *SVM* (*Support Vector Machine*) network in the *ε-SVR* regression approach (*Support Vector Regression*) was used in the studies which were presented in the article.

The *SVM* method [8, 25], as well as its regression approach *ε-SVR* [4, 21], comprise a subgroup of the methods belonging to *Machine Learning*. The structure of these systems is very similar to *Artificial Neural Networks* (*ANN*) [17]. The choice of the *SVM* method to carry out the research studies presented in this paper was dictated the fact that:

– in the *ε-SVR* method, it is not necessary to predetermine the mapping function, which allows to create a model for the multidimensional process in which the relationship between the variables are non-linear [6, 7] but without explicit strictly functional form,

(*) Tekst artykułu w polskiej wersji językowej dostępny w elektronicznym wydaniu kwartalnika na stronie ***www.ein.org.pl***

– in contrast to the artificial neural networks, the procedure of building the *ε-SVR* network allows for the optimal, in the generalizing sense, expansion of its structure, which takes place during the calibration process of the parameters *C*, *ε* and *γ*. These parameters, described in Chapter 3 of this article, are contained in the raw formulation of the objective function for the *ε-SVR* method [21.25]
– the final mathematical form of the *ε-SVR* network allows for a relatively simple determination of the values of the partial derivatives, which form the basis for the sensitivity analysis of the model with respect to the specified continuous input variables.

The model of technical wear presented in this paper was created by the optimal choice of the parameters *C*, *ε* and *γ* using the *LIBSVM* package [6] and the *genetic algorithm GA* [19]. In order to identify the effect of the variable describing the level of structural preventive measures, ($\boldsymbol{w_{ZAB}}$), the sensitivity analysis of the model was carried out, involving the study of the course of the gradient component for such a defined index. On the other hand, in order to determine the influence of the categorical variable $\boldsymbol{w_{REM}}$ describing the extent of the repair works, the values of the model prediction obtained by means of its simulation were compared.

2. Description of the database of building structures

A group of 930 masonry residential buildings located within the impacts of the Mining Plant of *KGHM* "*Polska Miedź*" *S.A.*, comprised the database for the analysis. The database of buildings was created as part of the examination of their technical condition. At the stage of detailed inspection, each building was cataloged using 93 variables. These variables describe the location of the structure, geometric data, type of development, the data on the structural components and finishing elements, the age of the buildings, technical wear determined by the *method of weighted average* [23], the scope of the repair works, the level of preventive measures against the impacts of mining and the current, at the time of the inspection, mining impacts in the form of deformation indices and characteristics of mining tremors.

This development has been subjected to mining impacts for more than 40 years. Initially, they resulted from the formation of the subsidence trough over the mining excavations and a large trough associated with rock mass drainage [23]. In the mining area of *LGOM*, also mining tremors have been occurring for 30 years [24].

The building structures located in *LGOM*, and erected after 1970, are protected against the effects of ground deformation caused by mining activities already during the construction stage. Older buildings are also regularly subjected to preventive measures (anchoring, reinforced concrete ties, etc.). Since the late 80's of the twentieth century, structural protection against paraseismic effects has also been introduced in newly constructed objects.

In order to assess the degree of wear of the studied buildings, the so-called *method of weighted average* was used [e.g. 23]. It involves an individual assessment of the degree of wear of individual elements, and then – by assigning appropriate weights to them – determining the weighted average degree of technical wear of the whole building structure.

To specify and describe quantitatively the indices affecting the technical condition of the development, two additional indices $\boldsymbol{w_{REM}}$ and $\boldsymbol{w_{ZAB}}$ were defined.

Protection index $\boldsymbol{w_{ZAB}}$ was defined using the *category of structure resistance* (*KO*), which is the structural characteristics of the building, and the *category of hazards to area from mining impacts* (*KT*).

Mining area categories (*KT*) describe the intensity of continuous surface deformation, expressed by assigning the characteristic values of the slopes (*T*), curves (*R*), and horizontal deformation (ε) to the specific ranges of these indices (from 0 to V). On the other hand, the *category of structure resistance* (*KO*) is understood as the resistance of a building structure to the horizontal strains and curvatures of the land, adapted to the ranges of the values of these indices in the *mining area categories* (*KT*) – (from 0 to 4) [e.g. 9]. A building structure is considered to be resistant to the effects of mining when the category of its resistance *KO* is not smaller than the mining area category *KT*. In practice, it is assumed that the implementation of protective measures in a building structure aims at increasing the category of structure resistance (*KO*), at least to the level of the hazard category occurring in a given area (*KT*).

Depending on the scope of these protective measures, the total number of points (p) was established for each building structure according to the *empirical point method for assessing the resistance of building structures* [9], in the range from *p*=0 (*a building protected at the level of foundations and all floor structures*) to *p*=15 (*no protection*). As a result, for each building structure, the value of the index $\boldsymbol{w_{ZAB}}$ was determined in accordance with the dependence (1):

$$w_{ZAB} = \begin{cases} \dfrac{(15-p)}{15} \cdot \left(\left|KT - KO\right|\right) + KO & dla \quad KO < KT \\ \dfrac{(15-p)}{15} + KO & dla \quad KO \geq KT \end{cases} \tag{1}$$

where: *KT* – mining area category, for which additional protective measures were implemented,
KO – category of structure resistance, predetermined during the design stage,
p – number of points from the point method for evaluating the resistance of building
structures for a given scope of protection.

On the other hand, the index $\boldsymbol{w_{REM}}$ reflects the extent of repair works for each building. This is a categorical variable, described by the following values: 1 - for building structures with no repairs implemented, and 2 - for building structures undergoing comprehensive repairs.

3. Research Methodology

This part of the study presents:
– mathematical interlude in the scope of basic formulations of the *SVM* method in regression approach,
– method of calibration of the parameters *C*, *ε* and *γ* determining the final form of the *SVM* network structure, which was used in the study,
– procedure of determining the gradient components in the sensitivity analysis.

3.1. Description of the SVM method in regression approach

In the regression approach in the SVM method, the sought approximating function is as follows [16]:

$$y(\mathbf{x}) = \mathbf{w}^T \phi(\mathbf{x}) + b \tag{2}$$

where: $\mathbf{x} \in R^n$ – is the input variable vector in *n*-dimensional space,

$\phi(\cdot): R^n \to R^{n_h}$ – is a certain transformation transforming the raw input variables into the so-called *feature space*,

$\mathbf{w}^T$ – is the vector of weights,
b – free component (*bias*)

Mapping $\phi(\cdot): R^n \to R^{n_h}$ is implicit, and it is the result of the use of the kernel function of a specific type (e.g. [25]).

The basis for the formulation of the problem of learning of the *SVM* system in regression approach is the definition of the error function, minimized in the adaptation process. With a certain set of reference data $\{\mathbf{x}_k, y_k\}_{k=1}^{N}$, the loss function for a single reference is expressed as (eg. [25]):

$$L_\varepsilon\left(y_k, y(\mathbf{x}_k)\right) = \left| \begin{array}{ll} \left|y_k - y(\mathbf{x}_k)\right| - \varepsilon & dla \left|y_k - y(\mathbf{x}_k)\right| \geq \varepsilon \\ 0 & dla \left|y_k - y(\mathbf{x}_k)\right| \leq \varepsilon \end{array} \right. \tag{3}$$

This formula is called *ε - insensitive loss function* [10]. As a result of using the above function, imposing a certain *tolerance margin ε*, the regression approach using *SVM* is usually called *ε-SVR* (*ε-Support Vector Regression* (e.g. [21]).

The introduction of such an error function is typical of the so-called robust methods resistant to interference in the data, or the outliers [14]. It also allows for the subsequent formulation of the problem of learning as the task of quadratic programming [2], which is one of the main advantages of the *ε-SVR* method.

With a predetermined error function, for a single reference (3), the objective function is written, the minimization of which will be followed by the learning process:

$$\min_{\mathbf{w}, b, \xi_k^*, \xi_k} J\left(\mathbf{w}, \xi_k^*, \xi_k\right) = \frac{1}{2}\mathbf{w}^T\mathbf{w} + C\sum_{k=1}^{N}\left(\xi_k^* + \xi_k\right), \; k = 1...N \tag{4}$$

With inequality constraints:

$$y_k - \mathbf{w}^T\phi(\mathbf{x}_k) - b \leq \varepsilon + \xi \tag{5}$$

$$\mathbf{w}^T\phi(\mathbf{x}_k) + b - y_k \leq \varepsilon + \xi \tag{6}$$

$$\xi_k, \xi_k^* \geq 0 \tag{7}$$

The above record is the so-called original minimization problem with inequality constraints (5), (6) and (7) (e.g. [2]). The problem presented in this way compromises between the generalization and the quality of fitting the approximator expressed as (2).

The component $\sum_{k=1}^{N}\left(\xi_k^* + \xi_k\right)$ in the equation (4), together with the constraints (5), (6) and (7) is responsible for the minimization of the global error function for all the learning references:

$$L_\varepsilon^N = \frac{1}{N}\sum_{k=1}^{N} L_\varepsilon\left(y_k, y(\mathbf{x}_k)\right) \tag{8}$$

The values ξ_k^*, ξ_k are the deviations of mapping each reference beyond the predetermined error tolerance *ε*. The learning process attempts to minimize them while complying with all the constraints of the function (5), (6) and (7). On the other hand, the component $\frac{1}{2}\mathbf{w}^T\mathbf{w}$ is responsible for the so-called maximizing the *margin of separation* [16]. In the regression approach, implemented in the feature space, minimization of that component leads to the optimal determination of the approximator hyperplane within the predetermined error tolerance *ε*.

All in all, both components of the equation (4) are opposing, and a compromise is determined by introducing a regularization constant *C*. The higher the value, the better fitting of the system, and the lower the generalization properties, and vice versa.

To solve the so defined problem of minimization, *Lagrange* functions are created (e.g. [2, 14]). Thus, the dependence (4) is obtained, extended by the set of all constraints (5), (6) and (7) controlled by *Lagrange multipliers*:

$$L\left(\mathbf{w}, b, \xi_k, \xi_k^*, \alpha_k, \alpha_k^*, \mu_k, \mu_k^*\right) = J\left(w, \xi_k^*, \xi_k\right) - \sum_{k=1}^{N}\alpha_k\left(w^T\phi(x_k) + b - y_k + \varepsilon + \xi_k\right) +$$
$$-\sum_{k=1}^{N}\alpha_k^*\left(y_k - w^T\phi(x_k) - b + \varepsilon + \xi_k^*\right) - \sum_{k=1}^{N}\left(\mu_k^*\xi_k^* + \mu_k\xi_k\right), \; k = 1...N \tag{9}$$

Then, using *Fermat's* theorem and *Karush-Kuhn-Tucker* conditions [25], dual formulation of the quadratic programming is obtained, expressed in the field of *Lagrange multipliers* in the following form [14]:

$$\max_{\alpha_k, \alpha_k^*} Q\left(\alpha_k, \alpha_k^*\right) = \sum_{k=1}^{N} y_k\left(\alpha_k - \alpha_k^*\right) - \varepsilon\sum_{k=1}^{N}\left(\alpha_k + \alpha_k^*\right) - \sum_{k=1}^{N}\sum_{j=1}^{N}\left(\alpha_k - \alpha_k^*\right)\left(\alpha_j - \alpha_j^*\right)K\left(\mathbf{x}_k, \mathbf{x}_j\right) \tag{10}$$

With inequality constraints:

$$0 \leq \alpha_k^* \leq C \tag{11}$$

$$0 \leq \alpha_k \leq C \tag{12}$$

$$\sum_{k=1}^{N}\left(\alpha_k - \alpha_k^*\right) \geq 0 \tag{13}$$

This formulation is subject to further maximization using *Lagrange multipliers*.

The factor $K\left(\mathbf{x}_k, \mathbf{x}_j\right)$ appearing in the equation (10) is the kernel of the system, which is given explicitly, and is the result of the equation of the implicit functions $\phi(\cdot)$ [14]:

$$K\left(\mathbf{x}_k, \mathbf{x}_j\right) = \phi(\mathbf{x}_k)\phi(\mathbf{x}_j) \tag{14}$$

The form of the kernel is selected arbitrarily from all the functions meeting the assumptions of *Mercer's Theorem* [14].

As a result of such a learning procedure, having determined the values of *Lagrange multipliers*, the weight vector is determined from the relationship:

$$\mathbf{w} = \sum_{k=1}^{N_{SV}}\left(\alpha_k - \alpha_k^*\right)\phi(\mathbf{x}_k) \tag{15}$$

Which, in turn, allows to write the final form of the approximator:

$$y(\mathbf{x}) = \sum_{k=1}^{N_{SV}}\left(\alpha_k - \alpha_k^*\right)K\left(\mathbf{x}, \mathbf{x}_k\right) + b \tag{16}$$

3.2. Calibration of the parameters C, ε and γ

An attempt to determine the sought parameters, hereinafter referred to as *hyperparameters*, was made in the paper [19], in which additionally, based on the concept of *Meta-SVM* [10], *FPE* (*Final Prediction Error*) was used [19]. In the course of further research, however, the author decided to use a more efficient method based on the concept described in [4]. The main stage in this method is the *n-fold cross-validation* carried out on preliminary sets: training set and testing set. For each iteration of the validation, a certain range of the discussed parameters C, ε and γ is examined, which are expressed in the logarithmic scale. Then, according to the proposed optimization algorithm *GS* (*Grid Search*, e.g. [4]), the minimization of the objective function is carried out, which was adopted as *MSE* (*Mean Squared Error*), averaged from all n testing sets used in the validation. As a result, an optimal set of the sought hyperparameters C, ε and γ is obtained. The *GS* algorithm is a gradientless global minimization method (e.g. [2]). It has one drawback, though. There is a necessity to define ranges for the searched area and a specific starting point. Therefore, instead of the *GS* algorithm, the optimization method was used, based on the *Genetic Algorithm* (*GA*). The applied *GA* method is also a gradientless algorithm, allowing to identify the global minimum, e.g. [2, 15].

3.3. Sensitivity analysis - study of the course of gradient components

The created *SVM* model, as in the case of artificial neural networks (*ANN*) is the so-called "*Black box*" and is primarily used to estimate the input variables. In recent years, more and more attempts have been made to analyze the internal structure of such models [26]. These activities aim to clarify the information about the interactions between the input variables and the output variable. The primary, and at the same time the simplest procedure, allowing to determine the quantitative influence of each of the dependent variables on the explanation of the raw variability contained in the output variables, is the so-*called variable elimination*. Basing on such a procedure, it is possible to make the selection of the most important variables in the model, the so-called *feature Selection* [3, 13]. Another approach, although rarely undertaken, is the analysis of the course of the gradient components relative to each of the input variables included in the model. Such an approach, used in the research studies presented in the paper, allows for the qualitative and quantitative assessment of the influence of each variable on the monotonicity of the estimated process [5].

This method was used here to study the influence of continuous variable such as the $\boldsymbol{w_{ZAB}}$ index. In order to carry out the analysis, the analogy of the structure of the *ε-SVR* model to the *Radial Basis Function Neural Networks* was used ([16]). Thus, the sensitivity analysis was performed in accordance with the procedures proposed in [5, 18, 22]. Considering the fact that the record of the *ε-SVR* approximator can be expressed in the form of a deterministic function in accordance with the equation (16), for any component of the vector of input variables i at a given point x_p, it is possible to determine the gradient component in the following form:

$$\frac{dy(\mathbf{x}_p)}{dx_{pi}} = 2\sigma \sum_{k=1}^{N_{SV}} \left(\alpha_k - \alpha_k^*\right) K\left(\mathbf{x}_p, \mathbf{x}_k\right)\left(x_{pi}, x_{ki}\right) \tag{17}$$

In the equation (17), the component $K\left(\mathbf{x}_k, \mathbf{x}_j\right)$ is the kernel of the system, and in the selection of radial basis functions, it takes the form:

$$K\left(\mathbf{x}_k, \mathbf{x}_j\right) = \exp\left(-\frac{\left(\mathbf{x}_k - \mathbf{x}_j\right)^2}{\gamma^2}\right) \overset{\sigma=\frac{1}{\gamma^2}}{=} \exp\left(-\sigma\left(\mathbf{x}_k - \mathbf{x}_j\right)^2\right) \tag{18}$$

4. Test results

4.1. The model approximating the course of technical wear of building structures

The basis for the inference on the influence of the indices $\boldsymbol{w_{REM}}$ and $\boldsymbol{w_{ZAB}}$ was the created predictive model in the form of the *ε-SVR* network structure. The general characteristics of the model were illustrated in Table 1 and Fig. 1. The average of the absolute values of the error between the model mapping and the actual variables V_{er}, and the so-called *Success Ratio SR* [%] as a function of the relative error *ep* [%], were used as measures specifying the assessment of the quality of the resulting model [11]. These results were presented in Tables 2, 3 and 4.

In addition to the examined indices, the set of the input variables included as well: the variable describing the age of the building, the index reflecting the impact of continuous deformation in the mining area ε (+), and the mining tremors intensity index a_{sg} [e.g. 24]. A detailed analysis confirming the necessity to include these variables in the model have been discussed in detail in [6, 7, 23].

All the analyses were performed in the *Matlab* environment using *LIBSVM* package [4] and *Genetic Algorithm Toolbox* [15].

Basing on the analysis of the results contained in Table 1, it is possible to conclude that the developed model is characterized by a high level of both fitting and generalization of the acquired knowledge, as evidenced by error values for training and testing sets, respectively. The confirmation of generalization features is also the number which has emerged, of 200 support vectors representing 33% of all references used for learning from the training set. An additional information on the "*smoothness*" of the resulting approximator is a relatively large width of the basis function $\gamma = 0.82$, which for the standardized variables $N(0.1)$ allows to continuously cover the ranges of all the analyzed variables.

Table 1. Basic parameters summarizing the ε-SVR model

Training set *MSE*	Testing set *MSE*	Number of support vectors *nSV*	Regularization parameter C	Width of radial basis functions γ	Tolerance margin ε
0,0026	0,0027	200	0,790	0,820	0,036

Table 2. Values of the V_{er} error for the training set and the testing set, expressed in units of technical wear s_z [%]

Training set	Testing set
6,05 [%]	6,28 [%]

Analysis of the value of the V_{er} error (cf. Tab. 2) allows to evaluate the model for fitting and generalization. Values of the V_{er} error, expressed in units of the degree of technical wear, both for the training and testing sets, oscillate around ± 6%. This is a good result in terms of fitting the model prediction to the reference data. Moreover, the values of the V_{er} error for the training and testing sets are very similar, which confirms good generalization properties.

Similar conclusions are drawn from the analysis of the distribution of the *Success Ratio* measure with respect to the relative error *ep*. In Table 3, for the accepted limit of the relative error *ep* of 30%, the

Table 3. Summary of the SR values [%] in the domain of the relative error ep [%] for the training and testing sets

Training set		Testing set	
ep [%]	*SR [%]- cumulated for ep<ep$_i$*	*ep [%]*	*SR [%]- cumulated for ep<ep$_i$*
0,0	10,2	0	14,4
5,0	34,0	5	40,4
10,0	52,6	10	51,4
15,0	65,0	15	68,5
20,0	74,8	20	76,7
25,0	80,2	25	82,2
30,0	83,4	30	86,3
35,0	87,3	35	93,2
40,0	89,5	40	95,2
45,0	91,7	45	95,2
50,0	92,6	50	96,6
55,0	93,7	55	97,3
60,0	95,3	60	97,3
65,0	95,4	65	97,3
70,0	95,8	70	97,9
75,0	95,9	75	97,9
80,0	96,4	80	97,9
85,0	96,6	85	97,9
90,0	97,0	90	98,6
95,0	97,5	95	99,3
100,0	100,0	100	100,0

accuracy of prediction, expressed by the *SR* measure, is 83.4% for the training set and 86.3% for the testing set, respectively. The level of accuracy proves good fitting of the model to the reference data. On the other hand, the approximate value of the course of the *SR* measure (cf. Tab. 4) for the training and testing sets demonstrates that the generalizing properties of the model are retained.

The comparison of the approximated values relative to the source data (Fig. 1) demonstrates that the correlation coefficient between them is close to 1.

Table 4. The graphs of the SR course [%] in the domain of the relative error ep [%] for the training and testing sets

The graph of the *SR* course *[%]* as a function of the relative error *ep [%]* for the training set	The graph of the *SR* course *[%]* as a function of the relative error *ep [%]* for the testing set
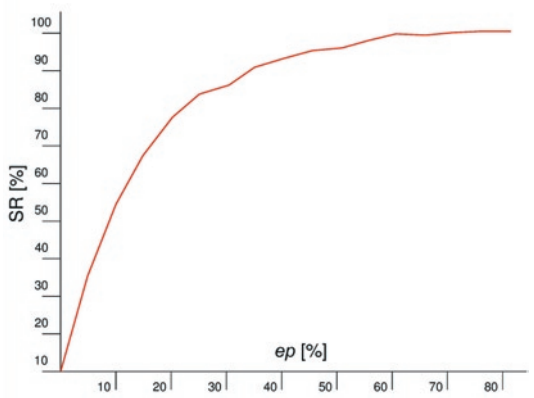	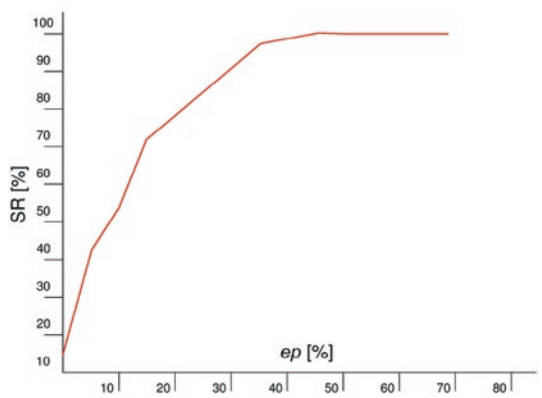

4.2. Studying the effect of the protection index w_{ZAB} on the technical wear of building structures

In this paper, according to the description of the adopted methodology contained in Section 3.3, the problem of analyzing the influence of the protection index w_{ZAB} was solved by the simulation of the model for uniformly distributed grid of points in the space of input variables. The scale of each of the standardized variables was divided into 20 equal parts. Given that the repair index w_{REM} adopted only two categorical values, simulation space equal to 388,962 points was obtained. At each point, according to the dependence (17), the values of the partial derivatives with respect to each continuous variable contained in the model was determined. The obtained values of the derivatives, calculated relative to the protection index w_{ZAB} were illustrated in Fig. 2 and 3. In Fig. 2, the value of the derivative calculated relative to the variable w_{ZAB} demonstrates that the modeled value of the technical wear of buildings increases in $w_{ZAB} = 0 \div 0.64$. Beyond this range, the degree of technical wear gradually starts to decrease.

On the other hand, Fig. 3 illustrates the course of the derivative calculated relative to the protection index w_{ZAB} in the domain of

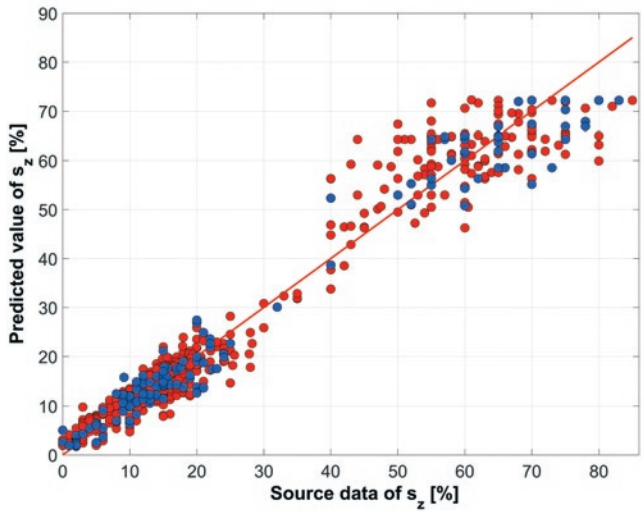

Fig. 1. Spread of the model prediction values relative to the reference data – the training set (red), the testing set (blue)

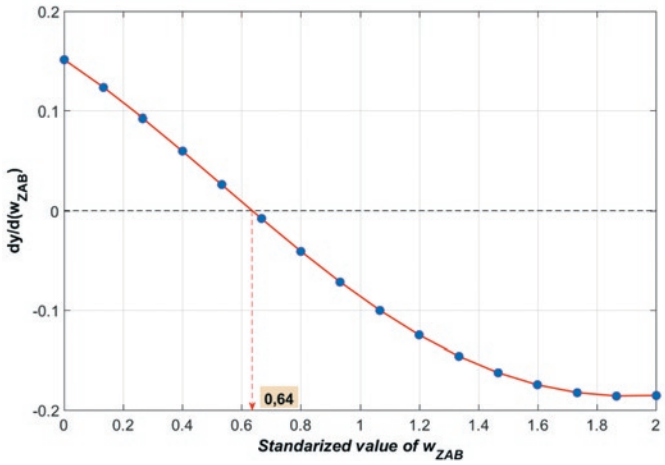

Fig. 2. Distribution of the gradient component for the variable wZAB

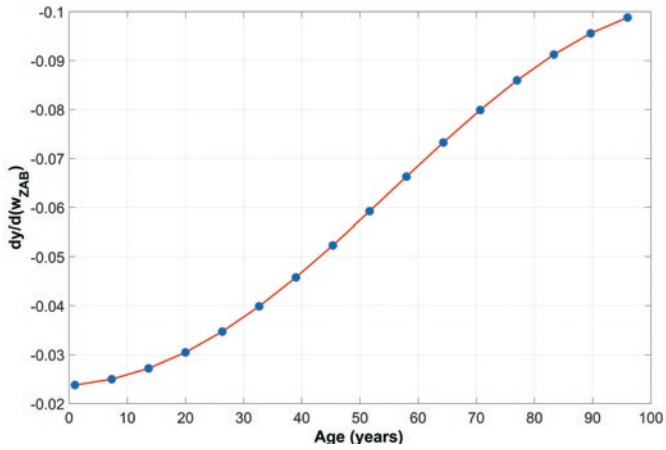

Fig. 3. Distribution of the gradient component of the model for the variable wZAB, illustrated relative to the variable describing the age of building structures

the variable describing the age of building structures. Apparently, the significance of the influence of protection increases with the age of buildings, causing a decrease in the modeled value of the degree of wear.

The analysis of the results leads to the following conclusions:

– noticeable reduction in the approximated values of the technical wear of buildings takes place at the time when the scope of the applied protective measures raises the category of structure resistance (*KO*) above the given mining area category (*KT*) by the relative value $w_{ZAB} = 0.64$ (cf. Fig. 2).
– the influence of protective measures on reducing the approximated value of technical wear becomes clearer with time, that is, with an increase in its natural wear (cf. Fig. 3).

4.3. Studying the effect of the repair index w_{REM}

The repair index w_{REM} used in this study is a categorical variable. To evaluate the influence of this index, the developed model was subjected to a simulation using two sets of variables. One included non-renovated building structures, the second one – renovated ones. The remaining values of the variables in both cases were the same, which allowed for a comparison of the course of the technical wear and for drawing conclusions. The measure of the influence was adopted as the value of the difference between the obtained prediction for the first set of variables (non-renovated building structures) and the prediction for the second set. The results of the differences were summarized in the domain of the variable describing the age of the buildings, and they were illustrated in Fig. 4.

The analysis of the results presented in Fig. 4 shows that repair works clearly contribute to the decrease in the approximated value of the degree of technical wear. It is also noticeable that this influence is associated with the age of the building. The change in the values of the differences between the prediction of the model for non-renovated and renovated building structures reaches up to 8% for the buildings aged more than 90 years (cf. Fig. 4).

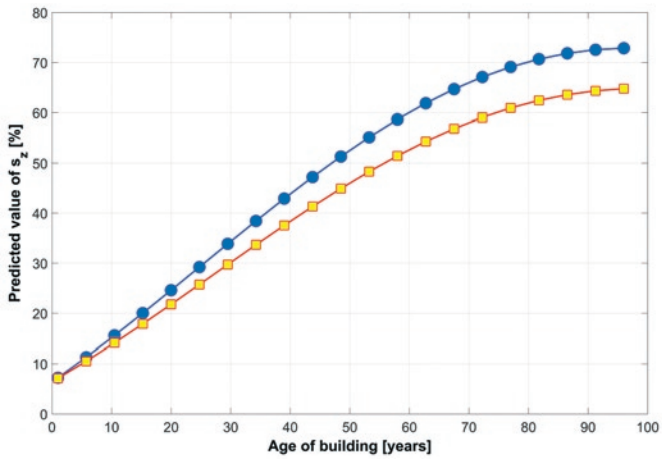

Fig. 4. Approximated values of the technical wear determined for a set of reference variables, separately for the renovated (yellow) and non-renovated (blue) building structures

5. Summary and conclusions

The results of the conducted research studies presented in this paper allow to draw conclusions both regarding the applicability of the *SVM* method for modeling technical wear of building structures, as well as the influence of different variables on the course of the modeled phenomenon.

In the case of the applicability of the *SVM* method, it was found that it allows to develop a model implementing nonlinear mapping of the multidimensional domain of input variables to the approximated value of technical wear. This model maintains the required level of accuracy and generalization. In addition, despite the lack of raw approximating function, the mathematical form, which is representative

for the model, allows to carry out the sensitivity analysis with respect to continuous variables.

As a result of the analysis of the influence of structural protective measures on the technical wear of the study group of building structures, the limit of significant influence of protective measures was established equal to $\mathbf{w_{ZAB}}$ = 0.64. The obtained value, according to the equation (1), demonstrates that the protection level becomes significant when, having applied the protective measures, the resistance category of a given building structure reaches the value of *KO* higher than the value of *KT* by 0.64. Generally speaking, it can be stated that protective measures contribute to the improvement of the technical condition of a building structure when they result in the resistance category *KO* exceeding hazard to mining area category *KT* by at least 1 category. This information can be very useful in evaluating the so-called *mining damage*.

The use of the SVM model simulation also showed the influence level of the repair index $\mathbf{w_{REM}}$ on the technical wear of the study group of buildings. The repair works, depending on the age of the buildings, have resulted in an improved technical condition ranging from 0 to 8%.

The analysis of the subject literature demonstrates that the *SVM* method may also be used in the case of approximating the response surface of a structure in the reliability analysis [1]. Therefore, it is planned to use this methodology for the risk assessment of building structures in mining areas subject to the reliability theory.

The article was prepared as part of the AGH statutory research No. 11.11.150.005.

References

1. Alibrandi, U., Alani, A. M., & Ricciardi, G. - A new sampling strategy for SVM-based response surface for structural reliability analysis. Probabilistic Engineering Mechanics 2015; 41: 1-12, http://dx.doi.org/10.1016/j.probengmech.2015.04.001.
2. Bierlaire M. - Optimization: principles and algorithms. EPFL Press 2015.
3. Chandrashekar, G., & Sahin, F. - A survey on feature selection methods.Computers & Electrical Engineering 2014; 40(1): 16-28, http://dx.doi.org/10.1016/j.compeleceng.2013.11.024.
4. Chang C-C., Lin C-J. - LIBSVM: a library for support vector machines. ACM Transactions on Intelligent Systems and Technology 2011; 2(3): 1–27. Software available at http://www.csie.ntu.edu.tw/~cjlin/libsvm.
5. Cortez, P., & Embrechts, M. J. - Using sensitivity analysis and visualization techniques to open black box data mining models. Information Sciences 2013; 225: 1-17, http://dx.doi.org/10.1016/j.ins.2012.10.039.
6. Firek K., Wodyński A. - Wpływ zabezpieczeń profilaktycznych oraz remontów na zużycie tradycyjnej zabudowy terenów górniczych (The influence of preventive security measures and renovation works on the wear of traditional buildings in mining areas). The scientific research problems of building. Pt. 3, pracazbiorowa pod red. M. Broniewicza, J. Prusiel. Wydawnictwo Politechniki Białostockiej 2007, ISBN 978-83-60200-33-9.
7. Firek K., Rusek J., Wodyński A. - Assessing the influence of mining impacts on technical wear of masonry buildings using multiple regression analysis. International Multidisciplinary Scientific GeoConference SGEM. Albena, Bulgaria, 2015.
8. Guo Y-M., Wang X-T., Chong L., Zheng Y-F.,Cai X-B. - Diagnoza uszkodzeń układu elektronicznego z wykorzystaniem Wielojądrowej Maszyny Wektorów Nośnych (SVM) zoptymalizowanej przy pomocy poprawionego algorytmu CPSO. Electronic System Fault Diagnosis with Optimized Multi-kernel SVM by Improved CPSO. Eksploatacja i Niezawodnosc – Maintenance and Reliability 2014; 16(1): 85–91
9. Instrukcja GIG nr 12 2000: Zasady oceny możliwości prowadzenia podziemnej eksploatacji górniczej z uwagi na ochronę obiektów budowlanych (Guidline GIG 12 2000: Principles for Evaluating opportunities for underground mining for the protection of buildings. Katowice 2000.
10. Jankowski N., Grabczewski K. - Toward optimal SVM. The third IASTED International Conference on Artificial Intelligence and Applications, Anheim, Calgary, Zurich. The International Association of Science and Technology for Development, ACTA Press, 2003.
11. Kuźniar, K. - Analiza drgań budynków ścianowych o średniej wysokości podlegających wstrząsom górniczym z wykorzystaniem sieci neuronowych, 2004.
12. Liao, P., Zhang, X., Li, K., Fu, Y., Wang, M., & Wang, S. - Parameter Optimization for Support Vector Machine Based on Nested Genetic Algorithms.Journal of Automation and Control Engineering 2015; 3(6): 78-83, http://dx.doi.org/10.12720/joace.4.1.78-83.
13. Lin, X., Yang, F., Zhou, L., Yin, P., Kong, H., Xing, W., ... & Xu, G. - A support vector machine-recursive feature elimination feature selection method based on artificial contrast variables and mutual information. Journal of Chromatography B, 2012; 910: 149-155, http://dx.doi.org/10.1016/j.jchromb.2012.05.020.
14. Łęski J. - Systemy neuronowo-rozmyte. WNT, Warszawa 2008.
15. MATLAB and Genetic Toolbox 2015b, The MathWorks, Inc., Natick, Massachusetts, United States
16. Osowski S. - Metody i narzędzia eksploracji danych. BTC. Legionowo, 2015.
17. Rojek I., Studziński J. - Porównanie różnych typów sieci neuronowych do lokalizacji awarii w sieciach wodociągowych. Comparison of different types of neuronal nets for failures location within water-supply networks. Eksploatacja i Niezawodnosc – Maintenance and Reliability 2014; 16(1): 42–47
18. Rueda I.E.A, Arciniegas F.A. - SVM Sensitivity Analysis: An Application to currency Crises Aftermarks. IEEE trans. Systems, Man and Cybernetic, 2004; 34: 3.
19. Rusek J. - Developing a model of the course of technical wear of building structures in mining areas using the method of Support Vector Machine in regression approach. X Days of Mining Metrology and Protection of Mining Areas. Cracow, 28–29.05.2009. Academic Scientific Publishing House of AGH University of Science and Technology in Cracow. Cracow, 2009.
20. Russell S., Norvig P. - Artificial Intelligence: A Modern Approach (3rd ed.). Upper Saddle River: Prentice Hall 2010. ISBN 9780136042594.
21. Schölkopf B., Smola A.J. - Learning with Kernels. MIT Press. Cambridge, Massachusetts 2002.
22. Tikka J., Hollmen J. - Selection of important input variables for RBF network using partial derivatives - ESANN'2008 proceedings, European Symposium on Artificial Neural Networks-Advances In Computational Intelligence and Learning. Bruges (Belgium), 2008.

23. Wodyński A. - Zużycie techniczne budynków na terenach górniczych (The process of technical wear of buildings in mining areas). Uczelniane Wydawnictwa Naukowo-Dydaktyczne, Akademia Górniczo-Hutnicza im. Stanisława Staszica w Krakowie, Kraków 2007.
24. Wodyński A., Lasocki S. - Conception Of Assessment Of Mining Tremor Effects On Technical Wear Of Buildings. Acta Montana, series A, 2002; 21.
25. Vapnik V. - Statistical learning theory. John Wiley & Sons, New York, 1998.
26. Yeh, I. C., & Cheng, W. L. - First and second order sensitivity analysis of MLP. Neurocomputing 2010; 73(10): 2225-2233, http://dx.doi.org/10.1016/j.neucom.2010.01.011.

Janusz RUSEK
AGH University of Science and Technology
Al. A. Mickiewicza 30, 30-059 Kraków, Poland
E-mail: rusek@agh.edu.pl

Article citation info:
DOMBEK G, NADOLNY Z. Thermal properties of a mixture of synthetic and natural esters in terms of their application in high voltage power transformers. Eksploatacja i Niezawodnosc – Maintenance and Reliability 2017; 19 (1): 62–67, http://dx.doi.org/10.17531/ein.2017.1.9.

Grzegorz DOMBEK
Zbigniew NADOLNY

THERMAL PROPERTIES OF A MIXTURE OF SYNTHETIC AND NATURAL ESTERS IN TERMS OF THEIR APPLICATION IN HIGH VOLTAGE POWER TRANSFORMERS

WŁAŚCIWOŚCI CIEPLNE MIESZANINY ESTRÓW SYNTETYCZNYCH I ESTRÓW NATURALNYCH W ASPEKCIE ZASTOSOWANIA W TRANSFORMATORACH DUŻEJ MOCY*

The article presents research results of thermal properties of mixtures of synthetic and natural esters in terms of their application in the cooling system of a high-voltage power transformer during its operation. The investigated properties of an analysed mixture were: thermal conductivity coefficient λ, kinematic viscosity υ, density ρ, specific heat c_p, and thermal expansion β. On the basis of presented research results, the authors determined the heat transfer factor α of a mixture of synthetic and natural esters. This factor defines the ability of an insulating liquid to transport heat in the transformer, thus determining its reliability. For the research the authors used the following percentage proportions of the mixture of both the esters: 100/0, 95/5, 80/20, 50/50, 20/80, 5/95, 0/100. The measurements were taken for the temperatures: 25ºC, 40ºC, 60ºC, and 80ºC.

***Keywords**: power transformers, natural esters, synthetic esters, heat transfer factor.*

W artykule przedstawiono wyniki badań właściwości cieplnych mieszaniny estrów syntetycznych i estrów naturalnych, w aspekcie ich zastosowania w układzie chłodzenia transformatora wysokiego napięcia w trakcie jego eksploatacji. Badanymi właściwościami analizowanej mieszaniny były przewodność cieplna właściwa λ, lepkość kinematyczna υ, gęstość ρ, ciepło właściwe c_p oraz rozszerzalność cieplna β. W oparciu o przedstawione wyniki badań określono współczynnik przejmowania ciepła α mieszaniny estrów syntetycznych i estrów naturalnych. Współczynnik ten określa zdolność cieczy elektroizolacyjnej do transportu ciepła w transformatorze, warunkując tym samym jego niezawodność. Do badań wykorzystano następujące procentowe proporcje mieszaniny obu estrów: 100/0, 95/5, 80/20, 50/50. 20/80, 5/95, 0/100. Pomiary przeprowadzono dla temperatury: 25ºC, 40ºC, 60ºC i 80ºC.

***Słowa kluczowe**: transformatory energetyczne, estry naturalne, estry syntetyczne, współczynnik przejmowania ciepła.*

1. Introduction

The power transformer is one of the most important electric power devices. Its key element is the insulating system; transformer reliability and its long operation depends on it. A substantial majority of used transformers is filled with insulating liquids. Due to their good dielectric properties, these liquids function as electric insulation. Moreover, they also have advantageous thermal properties (thermal conductivity, viscosity, specific heat, density, and thermal expansion), so that they also play the role of a cooling agent [13, 26]. Taking into consideration the fact that heat transfer proceeds along the following way: heat source → paper impregnated with liquid → insulating liquid → tank → air, thermal properties of the liquid filling the inside of the transformer are of high importance in the process of this transfer [4, 14-16].

The most frequently used insulating liquid in the transformer, because of a low price and very well investigated properties, is mineral oil [10, 20, 26, 32]. However, more and more restrictive regulations and requirements concerning reliability of electric power devices filled with liquids influence reduction of its domination [2, 6, 7, 17, 18, 23]. Therefore, research centres all over the world conduct numerous investigations on liquids alternative to mineral oil. These include mainly synthetic esters and natural esters [3, 4, 12, 21]. These liquids are characteristic of many properties, which in reference to mineral oil, are considered as their advantages. They are, first of all, ecological values such as biodegradability and non-toxicity, and also operation safety connected with their high flash point and fire point [12, 21].

Lately, the process of replacing the insulating liquid filling the transformer with another (*retrofilling*) has been more and more popular. This happens when the transformer up to now has been filled with one liquid (usually mineral oil) and now it is filled during a repair with another liquid (most often with synthetic or natural esters) [8, 18]. Retrofilling does not guarantee full removing of the original liquid because its small amount remains in the saturated paper insulation, windings, core, and other hardly-accessible crevices of the transformer. Then, unintentionally, a mixture is created which consists of remains of the original liquid (its amount does not exceed 8%) and the new liquid that the modernized unit is filled with, as described by Fofana et al in [8]. There are also investigations concerning intentional use of two or more insulating liquids in order to obtain a mixture characteristic of better properties in reference to the base liquids. This research concerns most often mixtures of mineral oil with synthetic or natural esters [6, 7, 10, 11, 17, 22, 23, 27, 30].

The research on the mixtures which are currently conducted in many research centres all over the world, concern mainly their electric properties, not thermal ones, which is not a proper approach. We

(*) Tekst artykułu w polskiej wersji językowej dostępny w elektronicznym wydaniu kwartalnika na stronie ***www.ein.org.pl***

should take into consideration that the application of insulating liquid mixtures, which in reference to the base liquids are characteristic of better electric properties and worse thermal properties, will result in accelerating the ageing process of the transformer's insulating liquid as a consequence of higher work temperature. As a result, this will reduce the time of its operation. Therefore, the research on the mixtures should tend to combine their electric, physicochemical, and thermal properties as described Nadolny et al in [19]. Dua et al undertook such an attempt in [5], in which they analysed a possibility to apply mixtures of insulating liquids while paying attention to their most important properties. However, with a lack of full information concerning thermal properties of the mixtures, such an approach can be difficult or impossible to do.

As it was mentioned before, a considerable number of articles referring to mixtures of insulating liquids present research results of their electric properties. In [6, 27, 29, 30] the authors present research results concerning the influence of proportions of oil and esters and the level of ageing on such electric properties as the dielectric loss factor tg(δ), electric permeability, and breakdown voltage. In turn, Suwarno in [28] presented the influence of thermal ageing of a mixture of mineral oil and natural ester on such electric properties as breakdown voltage, resistivity, the dielectric loss factor, and electric permittivity. Moreover, Trnka et al in [31] show research results concerning biodegradability of mixtures of mineral oil and natural ester. McShane et al in [18] also present information concerning the influence of proportions of mineral oil and natural ester on the flash point and fire point as well as pour point.

The literature does not provide complete information concerning thermal properties of insulating liquid mixtures. The only available data are those concerning selected thermal properties of mixtures of mineral oil with synthetic esters and mixtures of mineral oil with natural esters. In [23, 30] we can find information concerning viscosity of a mixture of mineral oil and synthetic esters depending on their proportions. The authors also provide information concerning the influence of temperature on mixture viscosity whose mineral oil content is 20% and 80%. In turn, McShane et al in [18] present information concerning viscosity of a mixture of mineral oil and natural esters depending on their proportions. However, these data were presented only for the mixtures whose temperatures were 40ºC and 100ºC. In [27, 29] we can find data concerning the influence of temperature and the proportions on the density of mixtures based on mineral oil and natural esters.

There is no investigations according thermal properties of insulating liquids mixtures. As it can be seen on the basis of references, only partial information about viscosity and density of mineral oil and the esters are available. There is no information according the influence of temperature and mixture proportion on rest thermal properties, such as thermal conductivity, specific heat and thermal expansion. There is no information about mixtures of natural esters and synthetic esters, either.

Independently of the way the mixture is created, the purpose of its application is the improvement of insulating liquid properties. Thus the research on properties of mixtures of different insulating liquids are primary in terms of their influence on the period of the transformer's life and adapting it to existing standards and regulations. Moreover, another important issue is compatibility of the newly created mixture with the remaining materials which make the insulating system of the transformer, because only such a mixture will enable prolonging its operation period and reliable work. Therefore, complete information about thermal properties of insulating liquid mixtures are desirable and they will also allow completing missing knowledge in the field of properties of new insulating liquids, which is the focus of this article.

2. Research goal and range

The goal of the undertaken investigations was to determine the influence of proportions of synthetic esters with natural esters on thermal properties of the created mixture. The research range covered measurements of thermal properties of the created mixture such as: thermal conductivity coefficient λ, kinematic viscosity υ, specific heat c_p, density ρ, and thermal expansion coefficient β. These properties determine the ability of the liquid to heat transfer: the heat transfer factor α. The heat transfer factor α was determined on the basis of the equation presented by Dombek and Nadolny in [4]:

$$\alpha = \sqrt[n+1]{c \cdot \lambda^{1-n} \cdot g^n \cdot \delta^{3n-1} \cdot \beta^n \cdot \rho^n \cdot c_p{}^n \cdot \upsilon^{-n} \cdot q^n} \qquad (1)$$

where: α – heat transfer factor [$W \cdot m^{-2} \cdot K^{-1}$], *c, n* – constants dependent on the flow character, temperature and geometry, λ – thermal conductivity [$W \cdot m^{-1} \cdot K^{-1}$], *g* – acceleration of gravity [$m \cdot s^{-2}$], δ – characteristic dimension [m], β – thermal expansion [K^{-1}], ρ – density [$g \cdot l^{-1}$], c_p – specific heat [$J \cdot kg^{-1} \cdot K^{-1}$], υ – kinematic viscosity [$mm^2 \cdot s^{-1}$], *q* – surface thermal load [$W \cdot m^{-2}$].

For the measurements of the mentioned above properties the authors used synthetic esters named Midel 7131 manufactured by the company M&I Materials and natural esters named Envirotemp FR3 manufactured by the company Cargil. The measurements of the properties were done according to standards [1, 9, 24, 25] using measurement systems which had been tested before on insulating liquids of thermal properties known from the literature. In order to do the investigations, the authors prepared mixtures of synthetic and natural esters of the following percentage concentrations of both the esters: 100/0, 95/5, 80/20, 50/50, 20/80, 5/95, and 0/100. The measurements were taken for the temperatures of 25ºC, 40ºC, 60ºC, and 80ºC. The research results are presented in the subsequent section.

3. Measurement results

3.1. Thermal conductivity λ of a mixture of synthetic and natural esters

Table 1 and Figure 1 present measurement results of thermal conductivity λ of a mixture of synthetic and natural esters for different temperature values. With an increase of the natural ester content thermal conductivity of the mixture increases. Thermal conductivity λ increased by 15.2% (for 25°C), by 15.4% (for 40°C), by 16.3% (for 60°C), and by 15.9% (for 80°C). This increase was independent of temperature. The reason of thermal conductivity increase is higher λ of natural esters in comparison to synthetic esters [4]. In natural esters, because of stronger interaction of molecules, distances among them

Table 1. Measurement results of thermal conductivity λ of a mixture of synthetic and natural esters

Thermal conductivity λ [$W \cdot m^{-1} \cdot K^{-1}$]							
Temperature	Proportion of synthetic esters (SE) and natural esters (NE)						
	100% SE 0% NE	95% SE 5% NE	80% SE 20% NE	50% SE 50% NE	20% SE 80% NE	5% SE 95% NE	0% SE 100% NE
25°C	0.158	0.161	0.163	0.170	0.178	0.181	0.182
40°C	0.156	0.159	0.162	0.168	0.176	0.178	0.180
60°C	0.153	0.155	0.159	0.166	0.174	0.177	0.178
80°C	0.151	0.153	0.157	0.163	0.171	0.174	0.175

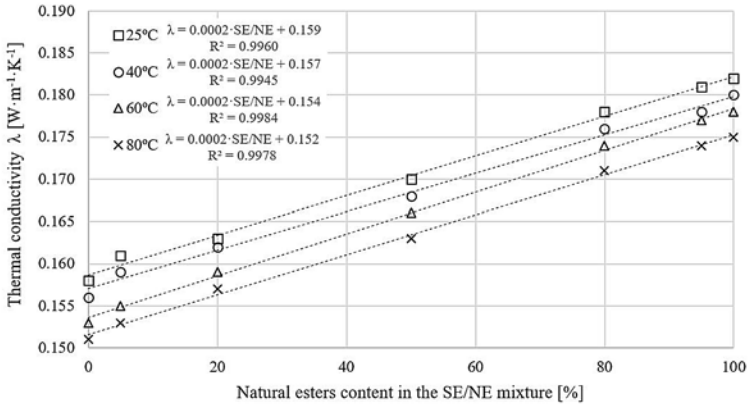

Fig. 1. Thermal conductivity λ of a mixture of synthetic and natural esters

are shorter than for the case of synthetic ester, thus kinetic energy transfer is easier. This means that the higher content of natural esters the better will be thermal conductivity of the mixture, which can advantageously affect the ability of the mixture to transfer heat in the transformer.

With temperature increase we can also notice a decrease of thermal conductivity of the analysed mixtures. This drop is caused by distance increase among the molecules of the liquid which, as a result, makes kinetic energy transfer more difficult. Eventually, this causes lowering thermal conductivity of the analysed liquids.

Figure 1 presents measurement results with the trend line, equation of the approximation model, and determination factor. The results were approximated with the linear equation:

$$\lambda = a \cdot SE / NE + b \qquad (2)$$

where: a, b – constants which are material parameters of the SE/NE mixture. Constant a is equal to tangent of inclination angle of the straight line to the axis of ordinates. This constant determines changes of thermal conductivity λ of an SE/NE mixture caused by the natural ester content. Constant b is equal to thermal conductivity λ for the natural ester content in the SE/NE mixture equal to 0%.

Results of the calculations of the remaining thermal properties (subsections 3.2-3.6) like for the case of thermal conductivity λ were also approximated with the linear function.

3.2. Kinematic viscosity υ of a mixture of synthetic and natural esters

Table 2 and Figure 2 present measurement results of kinematic viscosity υ of a mixture of synthetic and natural esters. As it is shown, viscosity of the mixture increases by respectively 2.1% (for 25°C), by 15.6% (for 40°C), by 30.5% (for 60°C), and by 41.8% (for 80°C) with an increase of the natural ester content. With temperature increase, the viscosity increase resulting from increasing the natural ester content is clearer and clearer. This is caused by higher viscosity of natural esters, as presented by Dombek and Nadolny in [4]. Kinematic viscosity of liquids results directly from their chemical structure. Higher viscosity of natural esters is connected with stronger intermolecular interactions. These interactions in natural esters make forces of internal friction greater than for synthetic esters. Thus, mixture viscosity increases with increase of natural ester content, which can negatively affect the ability of the mixture to transfer heat in the transformer.

We can notice that when the temperature rises the viscosity of the mixture decreases. This drop should be linked with decreasing of attraction forces acting among liquid molecules as a result of a decrease of their kinetic energy. Kinetic energy increase results from temperature increase. In turn, when the temperature is higher the molecules move at higher velocities, which weakens intermolecular forces and as a result causes decrease of internal friction forces and viscosity decrease.

3.3. Specific heat c_p of a mixture of synthetic esters and natural esters

Table 3 and Figure 3 present measurement results of specific heat c_p of a mixture of synthetic esters and natural esters.

Table 2. Results of kinematic viscosity υ measurements of a mixture of synthetic and natural esters

Kinematic viscosity υ [mm²·s⁻¹]							
Temperature	Proportion of synthetic esters (SE) and natural esters (NE)						
	100% SE 0% NE	95% SE 5% NE	80% SE 20% NE	50% SE 50% NE	20% SE 80% NE	5% SE 95% NE	0% SE 100% NE
25°C	55.14	55.18	55.32	55.62	56.02	56.25	56.29
40°C	28.25	28.34	28.69	29.91	31.84	32.58	32.66
60°C	14.02	14.16	14.59	15.78	17.32	18.16	18.29
80°C	8.11	8.23	8.59	9.57	10.71	11.32	11.50

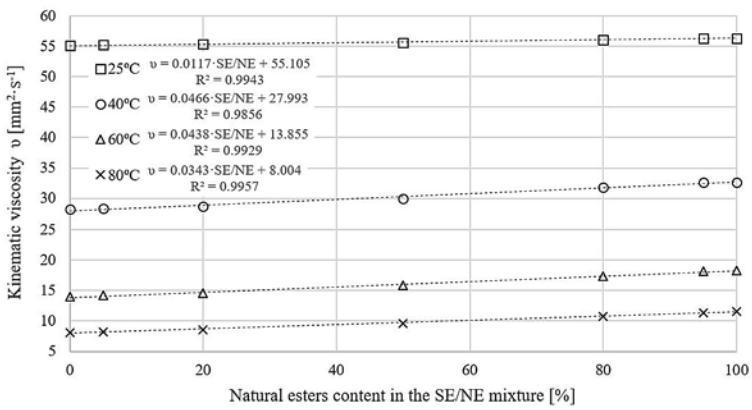

Fig. 2. Kinematic viscosity υ of a mixture of synthetic and natural esters

Table 3. Measurements results of specific heat c_p of a mixture of synthetic esters and natural esters

Specific heat c_p [J·kg⁻¹·K⁻¹]							
Temperature	Proportion of synthetic esters (SE) and natural esters (NE)						
	100% SE 0% NE	95% SE 5% NE	80% SE 20% NE	50% SE 50% NE	20% SE 80% NE	5% SE 95% NE	0% SE 100% NE
25°C	1905	1910	1923	1957	1977	2021	2028
40°C	1964	1969	1984	2014	2022	2069	2082
60°C	2052	2057	2078	2108	2117	2158	2166
80°C	2149	2154	2189	2218	2219	2246	2259

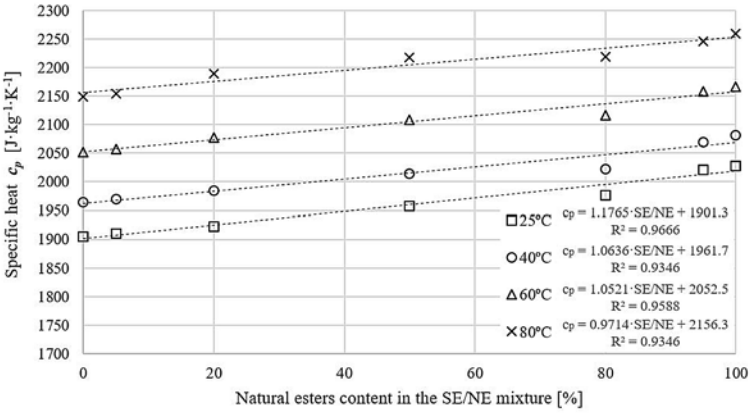

Fig. 3. Specific heat c_p of a mixture of synthetic esters and natural esters

With an increase of the natural ester content the specific heat of the mixture increased slightly. Specific heat increased by 6.5% (for 25°C), by 6.0% (for 40°C), by 5.6% (for 60°C), and by 5.1% (for 80°C). With temperature rise, the increase of specific heat of the mixture caused by increasing the natural ester content, slightly decreased. The increase of c_p of the mixture is caused by a higher value of specific heat of natural esters in comparison to the heat of synthetic esters. Specific heat is related to heat capacity, which determines the amount of energy that the molecules are able to absorb. Moreover, heat capacity is a function of molecule freedom degrees. It results from the above that the greater the particles the greater the number of freedom degrees they are characteristic of. Molecules of natural esters are larger than molecules of synthetic esters, therefore they can store more energy. The more energy a molecule can absorb the greater its heat capacity. In turn, the greater is heat capacity of a liquid, the greater its specific heat. As a result, an increase of the natural ester content caused an increase of specific heat of the mixture, which can result in improvement of the mixture's ability to heat transfer in the transformer.

With temperature increase, specific heat increase is noticeable. This is connected with kinetic energy increase and potential oscillation of ester molecule atoms, thus a larger number of freedom degrees is possible. Kinetic energy is the greater, the greater the velocity of the moving molecules.

3.4. Density ρ of a mixture of synthetic esters and natu ral esters

Table 4 and Figure 4 present measurement results of density ρ of a mixture of synthetic and natural esters. With an increase of the natural ester content, the density of the mixture decreased a little. Density ρ decreased by 4.9% (for 25°C), by 4.7% (for 40°C), by 5.1% (for 60°C), and by 5.0% (for 80°C). The density drop was practically independent of temperature. The drop of density ρ results from the fact that density of natural esters is a little lower than density of synthetic esters. Minor density differences of the analysed liquids result from differences of intermolecular interactions. Thus we can conclude that with an increase of the natural ester content in the mixture, the density of such a mixture will decrease, affecting negatively its ability to transfer heat in the transformer.

Mixture density decreases with temperature increase because the molecules of the liquid move at greater velocity. Higher molecule velocity affects decreasing intermolecular forces, which eventually results in increasing distances among them. The increase of the distance among the molecules causes increase of the liquid volume, which means decrease of its density.

Table 4. Measurement results of density ρ of a mixture of synthetic esters and natural esters

Density ρ [kg·m⁻³]							
Temperature	Proportion of synthetic esters (SE) and natural esters (NE)						
	100% SE 0% NE	95% SE 5% NE	80% SE 20% NE	50% SE 50% NE	20% SE 80% NE	5% SE 95% NE	0% SE 100% NE
25°C	964	962	955	941	926	919	917
40°C	953	951	944	931	917	910	908
60°C	940	938	930	916	902	894	892
80°C	926	924	917	903	889	882	880

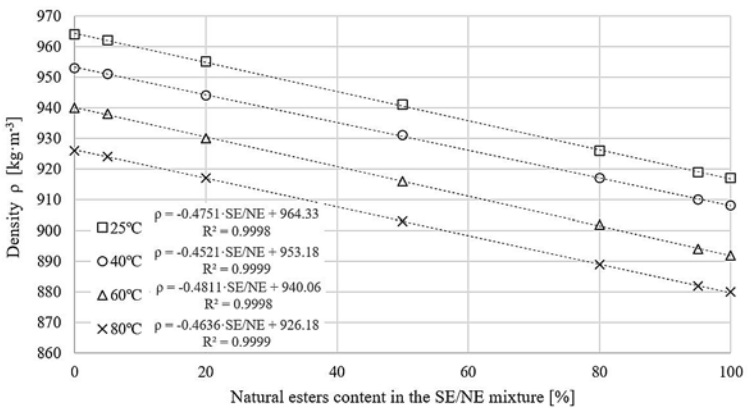

Fig. 4. Density ρ of a mixture of synthetic esters and natural esters

3.5. Thermal expansion β of a mixture of synthetic esters and natural esters

Table 5 and Figure 5 present measurement results of thermal expansion β of a mixture of synthetic and natural esters. As it is shown, an increase of natural ester content caused slight changes of thermal expansion of the mixture. Thermal expansion β decreased by 2.6% (for 25°C) and by 1.3% (for 40°C), it did not change its value for 60°C and increased by 1.3% (for 80°C). Minor changes of thermal expansion of the analysed liquids, like in the case of density, result from differences of intermolecular interactions. This means that with an increase of the natural ester content in the mixture, the thermal expansion of such a mixture changes slightly. This change should not significantly affect the ability of the mixture to heat transfer in the transformer.

With temperature increase, there is a noticeable increase of thermal expansion of the mixture. This increase results from the fact that liquid molecules vibrate at higher and higher frequency so their velocity increases. As a result of the velocity increase, the liquid molecules start moving apart, thus its spatial dimensions increase.

3.6. Heat transfer factor α of a mixture of synthetic esters and natural esters

Table 6 and Figure 6 present calculation results of the heat transfer factor α of a mixture of synthetic and natural esters. The calculations were done on the basis of measurement results of the thermal properties described in subsections 3.1-3.5.

The increase of the natural ester content in the SE/NE mixture basically caused increase of factor α. Its reason was an increase of thermal conductivity and specific heat resulting

Table 5. Measurement results of thermal expansion β of a mixture of synthetic esters and natural esters

Thermal expansion β [K^{-1}]							
Temperature	Proportion of synthetic esters (SE) and natural esters (NE)						
	100% SE 0% NE	95% SE 5% NE	80% SE 20% NE	50% SE 50% NE	20% SE 80% NE	5% SE 95% NE	0% SE 100% NE
25°C	0.00076	0.00076	0.00076	0.00075	0.00075	0.00074	0.00074
40°C	0.00077	0.00078	0.00077	0.00077	0.00077	0.00075	0.00076
60°C	0.00078	0.00078	0.00078	0.00078	0.00079	0.00078	0.00078
80°C	0.00079	0.00079	0.00080	0.00080	0.00081	0.00080	0.00080

Table 6. Calculation results of the heat transfer factor α of a mixture of synthetic esters and natural esters

Heat transfer factor α [$W \cdot m^{-2} \cdot K^{-1}$]							
Temperature	Proportion of synthetic esters (SE) and natural esters (NE)						
	100% SE 0% NE	95% SE 5% NE	80% SE 20% NE	50% SE 50% NE	20% SE 80% NE	5% SE 95% NE	0% SE 100% NE
25°C	78.43	79.17	79.60	80.98	82.58	83.21	83.46
40°C	92.85	93.97	94.27	95.04	95.50	95.22	96.12
60°C	110.72	111.18	111.81	112.00	112.09	111.64	111.80
80°C	127.51	127.88	128.83	127.70	127.10	126.19	126.17

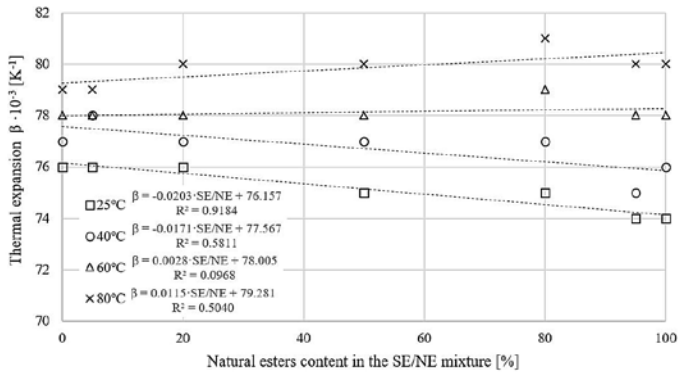

Fig. 5. Thermal expansion β of a mixture of synthetic esters and natural esters

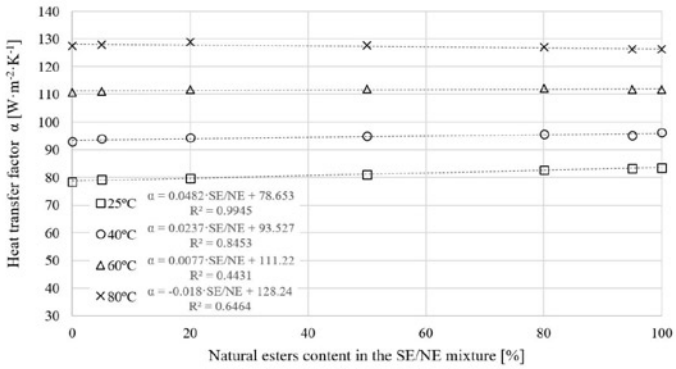

Fig. 6. Heat transfer factor α of a mixture of synthetic esters and natural esters

from adding natural esters, despite viscosity increase and decrease of density and thermal expansion. The authors also found that increases of factor α were getting smaller with temperature increase. The reason of this effect was a significant viscosity increase which resulted from adding natural esters for a higher and higher temperature values whereas changes of the remaining thermal properties remained at a constant level. The obtained results were predictable because the heat transfer factor of natural esters was greater than factor α of synthetic esters in the temperature range 25÷60ºC. At 80ºC factor α of natural esters was a little lower than of synthetic esters.

The analysis of Figure 6 does not show a clear maximum of factor α. This means that it is difficult to provide optimal proportions of both the esters. The only conclusions that come is the statement that in the case of the temperatures up to 60ºC, the application of natural esters is a more advantageous solution in terms of transformer cooling. At the temperature of 80ºC, factors α of both the esters are comparable.

4. Conclusions

An increase of the natural ester content in the SE/NE mixture caused changes of many thermal properties. Thermal conductivity increased by over 10 percent. Specific heat and density increased by a few percent. Viscosity, depending on temperature, increased by from a few to tens of percent. Thermal expansion practically did not change its value. The result of such changes was an increase of the heat transfer factor α, depending on temperature, by from a few to over 10 percent.

The SE/NE mixture did not have an optimal composition, in terms of the value of the heat transfer factor α. In fact, for 60ºC and 80ºC there are certain maxima but their values are only hardly by 1% higher for the value of factor α for 100% of synthetic ester (mixture 100/0) or 100% of natural ester (mixture 0/100). In such a situation we can state that from the practical point of view, the application of the SE/NE mixture is not justified.

Reference

1. ASTM D 1903-96. Standard test method for coefficient of thermal expansion of electrical insulating liquids of petroleum origin, and askarels.
2. Bertrand Y, Hoang L.C. Vegetable oils as substitute for mineral oils. Proceedings of the 7th International Conference on Properties and Applications of Dielectric Materials 2003: 491-494.
3. Cigre Brochure 436. Experiences in service with new insulating liquids. 2010.
4. Dombek G, Nadolny Z. Liquid kind, temperature, moisture, and ageing as an operating parameters conditioning reliability of transformer cooling system. Eksploatacja i Niezawodnosc – Maintenance and Reliability 2016; 18(3): 413-417, http://dx.doi.org/10.17531/ein.2016.3.13.
5. Dua R, Bhandari N, Kumar V. Multi-criteria optimization for obtaining efficiently blended transformer oil. IEEE Transactions on Dielectrics and Electrical Insulation 2008; 15(3): 879-887, http://dx.doi.org/10.1109/TDEI.2008.4543126.

6. Fofana I, Wasserberg V, Borsi H, Gockenbach E. Challenge of mixed insulating liquids for use in high-voltage transformers, part 1: Investigation of mixed liquids. IEEE Electrical Insulation Magazine 2002; 18(3): 18-31, http://dx.doi.org/10.1109/MEI.2002.1014964.
7. Fofana I, Wasserberg V, Borsi H, Gockenbach E. Challenge of mixed insulating liquids for use in high-voltage transformers, part 2: Investigation of mixed liquid impregnated paper insulation. IEEE Electrical Insulation Magazine 2002; 18(4): 5-16, http://dx.doi.org/10.1109/MEI.2002.1019901.
8. Fofana I, Wasserberg V, Borsi H, Gockenbach E. Retrofilling conditions of high-voltage transformers. IEEE Electrical Insulation Magazine 2001; 17(2): 17-30, http://dx.doi.org/10.1109/57.917528.
9. ISO 649-1:1981. Laboratory glassware – Density hydrometers for general purposes – Part 1: Specification.
10. Liao R, Hao J, Yang L, Grzybowski S. Study on aging characteristics of mineral oil/natural ester mixtures – paper insulation. IEEE International Conference on Dielectric Liquids (ICDL) 2011: 1-4.
11. Liao R, Hao J, Yang L, Liang S, Yin J. Improvement on the anti-aging properties of power transformers by using mixed insulating oil. International Conference on High Voltage Engineering and Application (ICHVE) 2010: 588-591, http://dx.doi.org/10.1109/ichve.2010.5640772.
12. Longva K. Natural ester distribution transformers; improved reliability and environmental safety. Nordic Insulation Symposium 2005: 293-295.
13. Lopatkiewicz R, Nadolny Z. Temperature field on high voltage power transformer. Przeglad Elektrotechniczny 2008; 84(10): 50-52.
14. Lopatkiewicz R, Nadolny Z, Przybylek P. Influence of water content in paper on its thermal conductivity. Przeglad Elektrotechniczny 2010; 86(11B): 55-58.
15. Lopatkiewicz R, Nadolny Z, Przybylek P. The influence of water content on thermal conductivity of paper used as transformer windings insulation. 10th IEEE International Conference on the Properties and Applications of Dielectric Materials (ICPADM) 2012: 1-4, http://dx.doi.org/10.1109/icpadm.2012.6318991.
16. Lopatkiewicz R, Nadolny Z, Przybylek P, Sikorski W. The influence of chosen parameters on thermal conductivity of windings insulation describing temperature distribution in transformer. Przeglad Elektrotechniczny 2012; 88(11B): 126-129.
17. McShane C.P. Relative properties of the new combustion resistant vegetable oil based dielectric coolants for distribution and power transformers. IEEE-IAS/PCA Cement Industry Technical Conference 2001: 31-40.
18. McShane C.P, Luksich J, Rapp K.J. Retrofilling aging transformers with natural ester based dielectric coolant for safety and life extension. IEEE-IAS/PCA Cement Industry Technical Conference 2003: 141-147, http://dx.doi.org/10.1109/citcon.2003.1204715.
19. Nadolny Z, Dombek G, Przybylek P. Thermal properties of a mixture of mineral oil and synthetic ester in terms of its application in the transformer. IEEE Conference of Electrical Insulation and Dielectric Phenomena (CEIDP) 2016: 857-860.
20. Nadolny Z, Dombek G, Przybylek P, Przadka D. Thermal properties of mineral oil admixed with C_{60} and TiO_2 nanoparticles. IEEE Conference of Electrical Insulation and Dielectric Phenomena (CEIDP) 2016: 538-541.
21. Oommen T.V. Vegetable oils for liquid – filed transformers. IEEE Electrical Insulation Magazine 2002; 18, 6-11, http://dx.doi.org/10.1109/57.981322.
22. Perrier C, Beroual A, Bessede J.L. Experimental investigations on different insulating liquids and mixtures for power transformers. IEEE International Symposium on Electrical Insulation 2004: 237-240, http://dx.doi.org/10.1109/elinsl.2004.1380540.
23. Perrier C, Beroual A, Bessede J.L. Improvement of power transformers by using mixtures of mineral oil with synthetic esters. IEEE Transactions on Dielectrics and Electrical Insulation 2006; 13: 556-564, http://dx.doi.org/10.1109/TDEI.2006.1657968.
24. PN-EN ISO 3104. Przetwory naftowe – Ciecze przezroczyste i nieprzezroczyste – Oznaczanie lepkości kinematycznej i obliczanie lepkości dynamicznej.
25. PN-EN ISO 3675. Ropa naftowa i ciekłe przetwory naftowe – Laboratoryjne oznaczanie gęstości – Metoda z areometrem.
26. Rouse T.O. Mineral oil in transformer. IEEE Electrical Insulation Magazine 1998; 14: 6-16, http://dx.doi.org/10.1109/57.675572.
27. Suwarno, Darma I.S. Dielectric properties of mixtures between mineral oil and natural ester. International Symposium on Electrical Insulating Materials (ISEIM) 2008: 514-517, http://dx.doi.org/10.1109/iseim.2008.4664471.
28. Suwarno, Marbun J. Effect of thermal aging on the dielectric properties of mixture between mineral oil and natural ester. IEEE Region 10 Conference TENCON 2015: 1-5.
29. Toudja T, Chetibi F, Beldjilali A, Moulai H, Beroual A. Electrical and physicochemical properties of mineral and vegetable oils mixtures. IEEE International Comference on Liquid Dielectrics (ICDL) 2014: 1-4.
30. Trnka P, Mentlik V, Cerny J. Electroinsulating fluids – new insulating mixtures. Conference on Electrical Insulation and Dielectric Phenomena (CEIDP) 2011: 575-578, http://dx.doi.org/10.1109/ceidp.2011.6232722.
31. Trnka P, Mentlik V, Svoboda M. Ecologically acceptable insulating liquids for electrical appliances. IEEE 18th International Conference on Liquid Dielectric (ICDL) 2014: 1-4, http://dx.doi.org/10.1109/icdl.2014.6893121.
32. Wotzka D, Zmarzly D, Boczar T. Numerical simulation of acoustic wave propagating in a spherical object filled with insulating oil. Acta Physica Polonica A 2010; 118(6): 1272-1275, http://dx.doi.org/10.12693/APhysPolA.118.12

Grzegorz DOMBEK
Zbigniew NADOLNY
Institute of Electric Power Engineering
Poznan University of Technology
Piotrowo 3A, 60-965 Poznan, Poland
E-mail: grzegorz.dombek@put.poznan.pl, zbigniew.nadolny@put.poznan.pl

Article citation info:
NOWAKOWSKA M. Spatial and temporal aspects of prior and likelihood data choices for Bayesian models in road traffic safety analyses. Eksploatacja i Niezawodnosc – Maintenance and Reliability 2017; 19 (1): 68–75, http://dx.doi.org/10.17531/ein.2017.1.10.

Marzena NOWAKOWSKA

SPATIAL AND TEMPORAL ASPECTS OF PRIOR AND LIKELIHOOD DATA CHOICES FOR BAYESIAN MODELS IN ROAD TRAFFIC SAFETY ANALYSES

PRZESTRZENNY I CZASOWY ASPEKT WYBORU ROZKŁADÓW APRIORYCZNYCH I DANYCH DLA FUNKCJI WIARYGODNOŚCI DLA MODELI BAYESOWSKICH W ANALIZACH BEZPIECZEŃSTWA RUCHU DROGOWEGO*

In a Bayesian regression model, parameters are not constants, but random variables described by some posterior distributions. In order to define such a distribution, two pieces of information are combined: (1) a prior distribution that represents previous knowledge about a model parameter and (2) a likelihood function that updates prior knowledge. Both elements are analysed in terms of implementing the Bayesian approach in road safety analyses. A Bayesian multiple logistic regression model that classifies road accident severity is investigated. Three groups of input variables have been considered in the model: accident location characteristics, at fault driver's features and accident attributes. Since road accidents are scattered in space and time, two aspects of information source choices in the Bayesian modelling procedure are proposed and discussed: spatial and temporal ones. In both aspects, priors are based on selected data that generate background knowledge about model parameters – thus, prior knowledge has an informative property. Bayesian likelihoods which modify priors are data that deliver: (1) information specific to a road – in the spatial aspect or (2) the latest information – in the temporal aspect. The research experiments were conducted to illustrate the approach and some conclusions have been drawn.

Keywords: *Bayesian regression model, informative prior distributions for model parameters, likelihood data, statistical classifier, road accident severity, road accident features.*

Parametry bayesowskiego modelu regresji nie są wartościami stałymi tylko zmiennymi losowymi opisanymi przez pewne rozkłady aposterioryczne. W celu zdefiniowania takiego rozkładu łączy się dwa źródła informacji: (1) rozkład aprioryczny, który reprezentuje wcześniejszą wiedzę o parametrze modelu oraz (2) funkcję wiarygodności (wiarygodność bayesowską), która uaktualnia wiedzę a'priori. Oba te elementy są przedmiotem badań w kontekście wykorzystania podejścia bayesowskiego w analizach bezpieczeństwa ruchu drogowego. Badaniom podlega model wielokrotnej regresji logistycznej, który klasyfikuje status zdarzenia drogowego. W modelu uwzględniono trzy grupy zmiennych objaśniających: charakterystyki miejsca lokalizacji wypadku, cechy kierującego sprawcy oraz atrybuty wypadku. Ponieważ wypadki drogowe są rozproszone w czasie i przestrzeni, zaproponowano i poddano dyskusji dwa aspekty wyboru źródeł informacji w procedurze modelowania bayesowskiego: czasowy i przestrzenny. W obu podejściach rozkłady aprioryczne są definiowane na podstawie danych wybranych jako te, które generują uogólnioną wiedzę o parametrach modelu, tworząc tło podlegające modyfikacji – w ten sposób wiedza aprioryczna ma cechę informatywności. Wiarygodność bayesowska, modyfikująca rozkłady a'priori, jest definiowana za pomocą danych wprowadzających: (1) informację specyficzną dla wybranej drogi – w przypadku aspektu przestrzennego lub (2) informację najnowszą – w przypadku aspektu czasowego. Zaproponowane podejście zilustrowano w eksperymentach badawczych i przedstawiono wynikające z nich wnioski.

Słowa kluczowe: *model regresji bayesowskiej, informatywne rozkłady aprioryczne parametrów modelu, wiarygodność bayesowska, klasyfikator statystyczny, status wypadku drogowego, cechy wypadku drogowego.*

1. Introduction

Traffic road safety, as an element of a *human–vehicle–road* system, has been the subject of scientific and research works for many years. There are many researchers and specialists in a wide range of fields or disciplines who are involved in the process of recognizing and understanding mechanisms related to a road crash. Many theories and models have been elaborated in order to evaluate the level of road traffic threats, as well as to identify circumstances, and cause and effect relationships of road accidents. The research area is extensive and covers: simulation and behavioural research (e.g. [8, 9]), elaboration of entropy models (e.g. [1, 12]), investigations of road polygons including road surroundings, and traffic and weather conditions (speed in particular) (e.g. [3, 10]), as well as exploration and mining of real road accident data (e.g. [15, 19]).

Statistical methods belong to the most important research techniques utilised in analysing real data. There are two approaches in such an analysis. The first one is a frequentist (also known as classical) approach, in which a random event's probability is assumed to be represented by the frequency of the event occurrence in a very large number of identical samples. The other one is a Bayesian (also known as non-classical) approach, according to which a prior (unconditional) probability of a random event is a measure of a rational belief that the event will occur. Then, the belief is modified using data from experiments or from observations of circumstances connected with the event. Prior knowledge is transformed into posterior

(*) Tekst artykułu w polskiej wersji językowej dostępny w elektronicznym wydaniu kwartalnika na stronie ***www.ein.org.pl***

knowledge, which is a resultant probability and a measure of a rational expectation of the event occurrence after getting information from the data. Bayesian thinking, supported by the development of numerical sampling techniques, has created modern statistics fundamentals, which enables formulating and solving problems not available in classical statistics.

Bayesian regression modelling is a non-classical methodology which becomes widespread in road traffic safety analyses, mainly because it allows eliminating various weaknesses of classical models. Bayesian regression models are difficult from both conceptual and computational points of view. Nevertheless, they bring a new quality to the development of scientific research methods, and they enable a flexible, though non-standard, approach to modelling issues. The models are used in order to develop safety performance functions (e.g. [6, 7, 13, 16]), including a before-after analysis (e.g. [17]), and also to classify descriptive road accident features, such as driver's behaviour, accident type, or accident severity (e.g. [2, 5, 16]).

The non-classical method of statistical inference was used in the study in order to develop logistic regression models, in which road accident severity is a response variable and selected features describing accident circumstances are input variables. A certain methodology of defining two basic sources of information for the Bayesian model was elaborated. The research is directed towards establishing informative priors as a general background for the model, and then towards choosing likelihood data in order to obtain posterior knowledge. Both elements would reflect various aspects of road safety research interests.

2. A Bayesian road accident severity classifier

The subject of the analysis is a statistical classifier – a logistic regression model that classifies road accident severity *AcSrv* into one of two values (categories): *LA* – light accident (assumed to be a failure) and *FSA* – fatal or serious accident (assumed to be a success). Input variables represent the description of a road accident location, at-fault driver's characteristics and accident features.

Logit is a link function in a logistic regression model. Conditional probability $P(AcSrv = FSA \mid X_1, \ldots, X_k)$ that an accident which occurred under circumstances described by a set of input variables values is fatal or serious constitutes the argument of the link function:

$$\begin{aligned}&\operatorname{logit}\left(P\left(AcSvr = FSA|X_1,\ldots,X_k\right)\right)\\&= \ln\left(\frac{P\left(AcSvr = FSA|X_1,\ldots,X_k\right)}{1-P\left(AcSvr = FSA|X_1,\ldots,X_k\right)}\right) = \beta_0 + \beta_1 X_1 + \ldots + \beta_k X_k \quad (1)\end{aligned}$$

The assumed model is relatively simple since the main purpose of the research is not to analyse the influence of the chosen features on the response variable, but to discuss the methodology that helps in developing a Bayesian regression model.

Contrary to the classical approach, it is assumed that Bayesian regression model parameters are not constants, but random variables. Therefore, each parameter is described by a certain posterior distribution that results from previous (prior) knowledge about the parameter and from the knowledge update using empirical data (Bayesian likelihood data) [18]:

$$\begin{aligned}&P(\boldsymbol{\beta} \mid Y, \boldsymbol{X}) = P(\beta_0,\ldots,\beta_k \mid Y, \boldsymbol{X}) = P(\beta_0,\ldots,\beta_k)\cdot P(Y, \boldsymbol{X} \mid\\&\beta_0,\ldots,\beta_k) / P(Y, \boldsymbol{X}) \propto P(\beta_0,\ldots,\beta_k)\cdot L(Y, \boldsymbol{X} \mid \beta_0,\ldots,\beta_k)\\&= P(\boldsymbol{\beta})\cdot L(Y, \boldsymbol{X} \mid \boldsymbol{\beta})\end{aligned} \quad (2)$$

The posterior distribution mean of the parameter $\boldsymbol{\beta}_i$ accompanying the variable X_i is the measure used to assess the magnitude and the direction of the variable influence on the response.

According to Bayes' rule, posterior distributions $P(\boldsymbol{\beta} \mid Y, \boldsymbol{X})$ contain information from two sources: prior distributions $P(\boldsymbol{\beta})$ and likelihood functions $L(Y, \boldsymbol{X} \mid \boldsymbol{\beta})$. A variety of posterior distributions for a regression parameter β_i is possible (Fig. 1), which is the consequence of the assumptions made about previous knowledge and likelihood data choices. Whenever one of the sources changes, the posterior changes as well.

Marcov Chains Monte Carlo (MCMC) sampling methodology [4, 18] is used in order to obtain posterior distributions $P(\boldsymbol{\beta} \mid Y, \boldsymbol{X})$. Each distribution is calculated from the series of numbers meeting the Marcov chain criteria. The Mertopolis-Hastings algorithm belongs to the most popular generators of the series. The Gibbs sampler is also frequently used. The results of the MCMC method depend on: the number of iterations in the chain, the number of burn-in values and the thinning rate. Converging the Marcov chain to stationarity is a significant issue in the generation process. It gives rise to an output sample from the stationary posterior distribution. Diagnostic tests (e.g. Gelman-Rubic, Geweke, Heidelberger-Welch), as well as trace diagnostic and correlations plots are used in order to assess the Marcov chain quality.

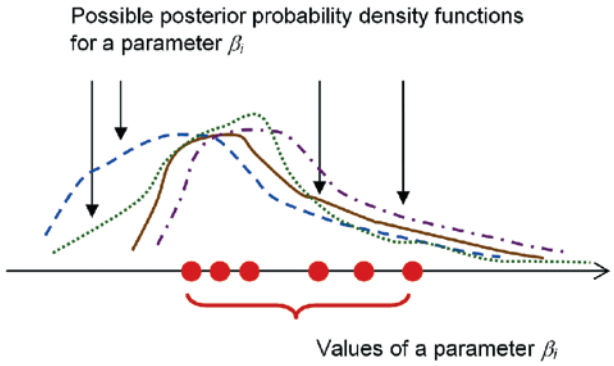

Fig. 1. A graphical interpretation of a Bayesian regression model parameter

3. Building a Bayesian road accident severity classifier

A Bayesian regression classifier (1) is created from a two-step Bayesian modelling procedure in which selected aspects of a road accident data investigation are adopted. The proposed approach and its results are strongly data-dependent: a several-year accident data registration period for a network of the same category roads in a given country region is needed (in particular roads supervised by a specific road administration unit). The data are selected in order to focus on either spatial or temporal aspect of the model estimation. The whole procedure extends and develops the concept presented in the investigation by Yu and Abdel-Aty [20] on the selection of informative priors for Bayesian models of a safety performance function.

The algorithm of building the Bayesian road accident severity classifier is presented hereafter.

Bayesian Modelling Step 1; defining the priors – the BM-S1 model

There are three general types of prior distributions used in Bayesian regression models: non-informative, semi-informative, and informative. The first one is utilized in road traffic safety analyses more often than the others, although it is dominated by likelihood data in the final output, and mean values of Bayesian model parameters are very close to parameter estimators of a classical regression model. Better results can be obtained when, instead of diffuse non-informative prior distributions, well-defined informative prior ones are used, because they reflect knowledge on an investigated subject. In order to generate such distributions, suitable data processing is proposed. It is

the first step of the above-mentioned procedure, thanks to which the Bayesian BM-S1 model is obtained.

There are the following sources of information for the BM-S1 model:

- priors – non-informative, normal distributions with zero mean and a very big standard deviation (1E+06),
- Bayesian likelihood (likelihood function) – road accident data selected according to the chosen aspect of the analysis: spatial or temporal one.

The Bayesian likelihood for the BM-S1 model is defined in the following way:

- for the spatial aspect: all accident data registered on the same category roads in a given country region for an assumed period of time,
- for the temporal aspect: all historical accident data registered on the same category roads in a given country region, excluding the data from the latest (most recent) registration period covering the whole season cycle (a calendar year).

Means and standard deviations of posterior distributions obtained for the BM-S1 model become means and standard deviations of prior normal distributions for the parameters of the Bayesian regression model created in the second step.

Bayesian Modelling Step 2; defining the likelihood – the final BM-S2 model

Since normal distributions derived in the first step are not diffuse, they generate informative prior knowledge constituting a basic background (a generalisation) for the final BM-S2 Bayesian model which follows the chosen aspect of the analysis. The likelihood data for the BM-S2 model define a training data set and they are treated as a factor emphasising and clarifying the research context:

- for the spatial aspect: accident data for a given road that are selected from the whole data set modify priors related to the road,
- for the temporal aspect: the latest (most recent) accident data update historical knowledge related to the whole area.

Fatal accident observations are extremely rare in road accident data, which usually results in a weak classification quality of the accident fatality. Therefore, in order to overcome such a negative phenomenon and to strengthen the rare values influence on final modelling results, balancing [1, 14, 15] is applied to the likelihood data in the BM-S2 model forcing smaller differences in the proportions of the values of the response variable *AcSrv*. Firstly, the primary data set is split into three subsets according to the accident severity *AcSrv*: light, serious, and fatal. Then, all fatal accident observations are taken to create a 20% stratum in a new training data set. Next, serious and light accident observations are selected at random from the remaining subsets in order to constitute, in the newly created data set, 30% and 50% strata respectively. Finally, the data modification is carried out so as to receive the binary-valued response variable *AcSrv* which defines a failure by the light accident severity category and a success by combining the serious and fatal accident severity categories. In such a balanced likelihood data set, the fatal accident observations grow considerably and, at the same time, the relatively rare success category does not exceed 50% of the data set size.

The research experiment has been carried out utilising the balancing scheme in each aspect of the data definition for the likelihood function in the BM-S2 model.

4. Data description

The road accident data used in the study, acquired from the SEWiK police database system, were provided by the Police Headquarters of the Świętokrzyskie province, Poland. The accidents registered during the time period from 2008 to 2014 on all of the nine national roads in the province are analysed in the study. The roads are supervised by a national road administration unit (a division of the General Directorate for National Roads and Motorways) because they serve interregional connections.

The observations which meet the following criteria were selected for the research:

- accidents were registered outside towns with civic rights on two-lane single carriageways (national roads have the highest technical parameters among all the roads with such a profile),
- only one adult driver caused the accident (in Poland, adult relates to a person who is at least 18 years old),
- only motor vehicles were involved in the accidents,
- no pedestrians participated in the accidents.

Prior to the analysis, the data were cleaned and the records with outliers, missing or extremely rare values that couldn't be aggregated (considering the physical meaning of the values) were removed. The resultant data set includes 1329 observations and it consists of the following variables chosen for the investigation:

- the group of accident location characteristics (input variables):
  - *ArTp* – area type with the following values: *Bt* – built-up area (39.2%), *NBt* – non-built-up area (60.8%),
  - *LgCnd* – road lighting conditions with the following values: *NgDrk* – night darkness, i.e. no lighting at night (16.6%), *PrLg* – poor lighting, e.g. dawn, dusk or artificial lighting (usually poor on non-urban roads) at night (14.7%), *Dlg* – daylight (68.6%),
  - *RdSrf* – roadway surface conditions with the following values: *NDr* – not dry, i.e. wet, snow-covered or ice-covered (38.5%), *Dr* – dry (61.5%),
- the group of at-fault driver's features (input variables):
  - *VhTp* – vehicle type with the following values: *HvVh* – heavy vehicle (15.6%), *Mtr* – motorcycle, scooter, moped, i.e. single-track motor vehicle (3.2%), *Cr* – car (81.3%),
  - *Gndr* – at-fault driver's gender with the following values: *F* – female (12,5%), *M* – male (87,5%),
  - *AgGrp* – at-fault driver's age group with the following values: 02 – <18; 25) (25.1%), 03 – <25; 35) (27.5%), 04 – <35; 50) (25.9%), 05 – <50; 65) (16.3%), 06 – at least 65 (5.1%),
  - *Alh* – at-fault driver under the influence of alcohol or other toxic substances with the following values: *N* – no (89.8%), *Y* – yes (10.2%),
- the group of road accident attributes (input variables):
  - *NrVhIn* – number of vehicles involved with the following values: *Sng* – single vehicle accident (31.2%), *Mlt* – multiple vehicle accident (68.8%),
  - *Bhv* – at-fault driver's behaviour with the following values: *DrWrSdRd* – driving wrong side of a roadway (5.2%), *InSpPrCn* – inappropriate speed for prevailing traffic and weather conditions (44.2%), *NGvWy* – not giving right of way (10.3%), *InTrUTr* – incorrect turning or U-turning (4.1%), *InPs* – incorrect passing by (1.6%), *InOvBp* – incorrect overtaking or bypassing (12.9%), *PrPsCn* – poor psychophysical condition (8.3%), *FlCl* – following too close (13.5%),
- *AcSvr* – the response variable; accident severity defined by the status of a road crash according to the highest level of injuries experienced by a human casualty as follows [14, 15, 21]: *LA* – light accident (57%), *SA* – serious accident (29.4%), *FA* – fatal accident (13.5%).

5. Results

The Bayesian regression models were obtained from the 10000-element Marcov chains generated using the Metropolis algorithm for the following settings: the number of burn-out samples = 50000, the number of final chain iterations = 300000, the thinning indicator = 30. All the

Marcov chains reached the stationarity, which was verified by the autocorrelation and trace plots, as well as by the Geweke and Heilderberger-Welch tests. The resultant posterior distributions were unimodal.

The research experiments were conducted using the SAS® software: the in-built MCMC procedure and the author's own SAS 4GL and SAS macro language computer programs.

The data were prepared taking into account:

- for the spatial (S) aspect:
  - BM-S1(S): all the national roads in the Świętokrzyskie province, for the time period 2008-2014 (the data set length is equal to 1329 records),
  - BM-S2(S): the DK74 and DK7 roads for two independent models, for the period 2008-2014 (after balancing, the data set length is equal to 220 and 196 for the DK74 and DK7 roads respectively); the main difference between the roads is that the DK7 road, being the part of the European road network, additionally serves international traffic,
- for the temporal (T) aspect:
  - BM-S1(T): all the national roads in the Świętokrzyskie province, for the time period 2008-2013 (the data set length is equal to 1221 records),
  - BM-S2(T): all the national roads in the Świętokrzyskie province, for the year 2014 (after balancing, the data set length is equal to 60 records).

The results of Bayesian modelling for the spatial aspect are presented in Table 1, and for the temporal aspect in Table 2. The BM-S1models obtained in the first step are called prior models since they deliver informative prior knowledge for the second step. The BM-S2 models obtained in the second step are called posterior models because they are the final classifiers of the whole modelling procedure. Both tables have a similar structure:

- mean, and standard deviation values (*Mean (S.D.)*) of parameter distributions for the prior models (*BM-S1 – prior*) and for the posterior models (*BM-S2 – posterior*),
- reference of each posterior model to its corresponding prior model by determining the index that, for any parameter, compares the posterior distribution mean with its corresponding prior distribution mean. The index is calculated by the expression $(mean_{posterior} - mean_{prior})/|mean_{prior}|$. The index values are given in the *Comparison* columns for: *DK74 vs. prior*, *DK7 vs. prior*, and *2014 vs. prior*,
- comparison of two posterior models for the spatial aspect (for the DK74 and DK7 roads) by showing the difference between the dis-

Table 1. Results of Bayesian accident severity classifiers for the spatial aspect

Model	BM-S1(S) – prior	BM-S2(S) – posterior for DK74		BM-S2(S) – posterior for DK7		Posteriors comparison
Specification	**Mean (S.D.)**	**Mean (S.D.)**	**Comparison: DK74 vs. prior**	**Mean (S.D.)**	**Comparison: DK7 vs. prior**	**DK74–DK7**
Constant	−1.396 (0.378)	−1.224 (0.235)	12.3%	−1.192 (0.249)	14.6%	−0.032
The group of accident location characteristics						
ArTp_Bt	0.311 (0.127)	0.381 (0.117)	22.5%	0.326 (0.119)	4.9%	0.055
LgCnd_NgDrk	0.341 (0.165)	0.434 (0.156)	27.1%	0.321 (0.153)	−5.8%	0.112
LgCnd_PrLg	−0.090 (0.174)	−0.103 (0.159)		0.020 (0.166)		
RdSrf_NDr	0.011 (0.126)	−0.070 (0.116)		0.009 (0.118)		
The group of at−fault driver's features						
VhTp_HvVh	−0.082 (0.172)	−0.039 (0.159)		−0.062 (0.159)		
VhTp_Mtr	1.217 (0.361)	1.101 (0.333)	−9.5%	1.203 (0.333)	−1.1%	−0.102
Gndr_F	−0.428 (0.191)	−0.386 (0.172)	9.8%	−0.422 (0.181)	1.5%	0.036
AgGrp_02	−0.043 (0.289)	0.202 (0.226)		0.023 (0.234)		
AgGrp_03	−0.156 (0.288)	0.003 (0.215)		−0.159 (0.229)		
AgGrp_04	−0.112 (0.288)	−0.026 (0.224)		−0.142 (0.224)		
AgGrp_05	−0.201 (0.300)	−0.509 (0.245)	153.2%	−0.078 (0.246)		0.432
Alh_N	0.008 (0.204)	0.062 (0.176)		−0.099 (0.184)		
The group of road accident attributes						
AcTp_Sng	−0.366 (0.158)	−0.339 (0.143)	7.3%	−0.440 (0.146)	−20.2%	0.101
Bhv_DrWrSdRd	2.342 (0.343)	2.390 (0.308)	2.0%	2.340 (0.304)	−0.1%	0.050
Bhv_InSpPrCn	1.175 (0.229)	1.161 (0.181)	−1.1%	1.149 (0.187)	−2.2%	0.013
Bhv_NGvWy	0.975 (0.263)	0.908 (0.225)	−6.8%	1.089 (0.237)	11.7%	−0.181
Bhv_InTrUTr	0.829 (0.345)	0.832 (0.307)	0.3%	0.753 (0.290)	−9.1%	0.079
Bhv_InPs	2.439 (0.569)	2.410 (0.511)	−1.2%	2.171 (0.500)	−11.0%	0.238
Bhv_InOvBp	1.354 (0.250)	1.450 (0.226)	7.1%	1.435 (0.222)	6.0%	0.016
Bhv_PrPsCn	1.336 (0.295)	1.405 (0.258)	5.2%	1.233 (0.262)	−7.7%	0.173
DIC	1168.6	249.5		231.5		
Sensitivity	38.9%	59.3%		57.9%		
Specificity	82.6%	67.8%		65.3%		
HMSS	52.9%	63.3%		61.4%		

tribution means of the corresponding model parameters calculated by the expression: ($mean_{posterior(DK74)} - mean_{posterior(DK7)}$). The difference values are given in the *Posterior comparison* column in Table 1,

- Deviance Information Criterion (*DIC*) measure calculated from the training data sets: the unbalanced one for the BM-S1 model and the balanced one for the BM-S2 model,
- classification quality assessment measures: sensitivity (the percentage of correctly classified *FSA* cases), specificity (the percentage of correctly classified *LA* cases), and the harmonic mean of sensitivity and specificity *HMSS* (which balances the two measures). All the indices were calculated from the primary likelihood data set for the BM-S1 model and from the primary (nor balanced) likelihood data set for the BM-S2 model.

For each parameter of a Bayesian model, the highest probability density HPD interval can be constructed unambiguously, provided that the parameter distribution is not uniform. To some extent, the HPD interval corresponds to a credible interval in classical statistics – if it contains zero, values of its parameter cannot be clearly interpreted. The uncertainty is also indicated when the absolute value of the parameter coefficient of variation exceeds 50%. Such statistically insignificant parameters are highlighted in red in Tables 1 and 2. The HPD intervals for the statistically significant parameters of the final models (the BM-S2 models obtained in the second step) are illustrated in Figures 2 and 3.

In Tables 1 and 2, and in Figures 2 and 3, all the input variables are grouped according to their substantial meaning, i.e. accident location characteristics, at-fault driver's features, and accident features.

Bayesian models for the spatial aspect

1. The sets of statistically significant input variables are roughly the same in the BM-S1(S), as well as in both BM-S2(S) models. The driver's age group proved significant in the BM-S2(S) model for the DK74 road only due to the significance of the coded variable *AgGrp_05* (50-65 years old).
2. The directions of the influence of the individual statistically significant variables on the accident severity are the same in the BM-S1(S) model and in both BM-S2(S) models.
3. The nature (magnitude and direction) of the change in the values of the statistically significant posterior parameters (the BM-S2(S) models) in relation to the values of the corresponding prior parameters (the BM-S1(S) model) is road-dependent:
   - the positive influence of the accident location characteristics on the accident severity is greater by more than 20% in the BM-S2(S) model for the DK74 road, whereas the change of the influence in the BM-S2(S) model for the DK7 road is different – there is a rise by 5% in the parameter mean for built-up area *ArTp_Bt* and a drop by 6% in the parameter mean for night darkness *LgCnd_NgDrk*,
   - the positive influence of single-track motor vehicle (motorcycle, scooter, and moped) *VhTp_Mtr* and the negative influence of female driver's gender *Gndr_F* on the accident severity identified in the prior parameter distributions become smaller by nearly 10% in the posterior distributions for the DK74 road, whereas they remain at almost the same level for the DK7 road,
   - the modification of the parameter prior distribution for the single vehicle accident variable *NrVhIn_Sng* by using the likelihood data taken from different roads caused different results in the posterior distributions: the parameter mean value rose by 7% for the DK74 road and dropped by 20% for the DK7 road,
   - the range of the change in the parameter posterior distributions for driver's behaviour is different for the DK74 and DK7 roads, which is particularly evident for not giving right of way *Bhv_NGvWy* (a drop in the mean value by 6.8% and a rise by 11.7% respectively), for incorrect turning or U-turning *Bhv_InTrUTr* (almost without a change and a drop by 9.1% respectively), and for poor psychophysical condition *Bhv_PrPsCn* (a rise by 5.2% and a drop by 7.7% respectively).

Bayesian models for the temporal aspect

Table 2. Results of Bayesian accident severity classifiers for the temporal aspect

Model	BM-S1(T) – prior	BM-S2(T) – posterior for 2014	
Specification	**Mean (S.D.)**	**Mean (S.D.)**	**Comparison: 2014 vs. prior**
Constant	−1.192 (0.393)	−1.169 (0.289)	1.9%
The group of accident location characteristics			
ArTp_Bt	0.383 (0.133)	0.351 (0.127)	−8.3%
LgCnd_NgDrk	0.319 (0.176)	0.353 (0.171)	10.6%
LgCnd_PrLg	−0.048 (0.178)	−0.040 (0.176)	
RdSrf_NDr	−0.042 (0.131)	0.008 (0.128)	
The group of at−fault driver's features			
VhTp_HvVh	−0.053 (0.177)	−0.077 (0.171)	
VhTp_Mtr	1.329 (0.387)	1.216 (0.362)	−8.6%
Gndr_F	−0.446 (0.202)	−0.448 (0.198)	−0.4%
AgGrp_02	−0.222 (0.304)	0.099 (0.272)	
AgGrp_03	−0.279 (0.300)	−0.388 (0.277)	
AgGrp_04	−0.258 (0.303)	−0.344 (0.280)	
AgGrp_05	−0.303 (0.314)	−0.283 (0.286)	
Alh_N	−0.051 (0.214)	−0.046 (0.198)	
The group of road accident attributes			
NrVhIn_Sng	−0.356 (0.166)	−0.377 (0.160)	−5.9%
Bhv_DrWrSdRd	2.423 (0.361)	2.389 (0.353)	−1.4%
Bhv_InSpPrCn	1.103 (0.239)	1.246 (0.220)	12.9%
Bhv_NGvWy	1.061 (0.272)	0.912 (0.263)	−14.0%
Bhv_InTrUTr	0.764 (0.357)	0.700 (0.352)	−8.3%
Bhv_InPs	2.211 (0.594)	2.344 (0.568)	6.1%
Bhv_InOvBp	1.240 (0.262)	1.395 (0.243)	12.5%
Bhv_PrPsCn	1.350 (0.306)	1.239 (0.295)	−8.2%
DIC	1092.4	74.8	
Sensitivity	36.9%	61.9%	
Specificity	82.8%	74.2%	
HMSS	51.0%	67.5%	

1. The sets of statistically significant input variables in the BM-S1(T) and BM-S2(T) models differ in two variables: (1) night lighting condition *LgCnd_NgDrk* is insignificant in the BM-S1(T) model,

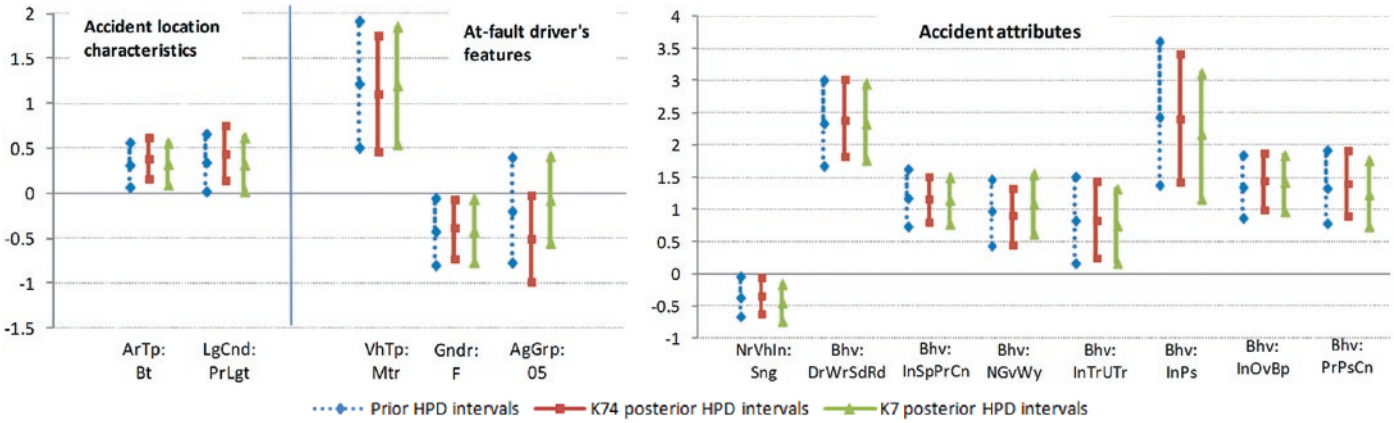

Fig. 2. HPD intervals for statistically significant parameters of Bayesian models for the spatial aspect

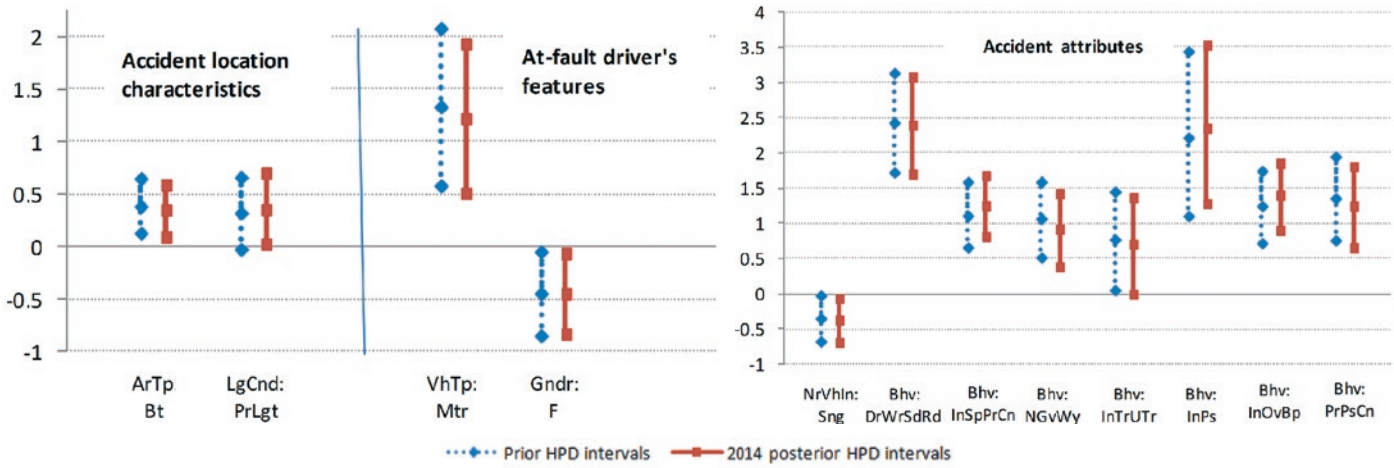

Fig. 3. HPD intervals for statistically significant parameters of Bayesian models for the temporal aspect

but significant in the BM-S2(T) model, (2) incorrect turning or U-turning *Bhv_InTrUTr* is significant in the BM-S1(T) model, but insignificant in the BM-S2(T) model.

2. Similarly to the spatial models, the influence directions of the corresponding statistically significant variables are the same in the BM-S1(T) model in the first modeling step and in the BM-S2(T) model in the second modeling step.
3. The latest information modified the up-till-now (prior) knowledge about the importance of the individual input variables in the posterior model, and in particular it caused strengthening the following:
   - the positive influence on the fatal or serious accident status of the factors: night lighting condition *LgCnd_NgDrk* (increase by 10.6%), inappropriate speed for the prevailing traffic and weather conditions *Bhv_InSpPrCn* (an increase by 12.9%), incorrect overtaking or bypassing *Bhv_InOvBp* (an increase by 12.5%),
   - the negative influence on the fatal or serious accident status of the single-vehicle accident variable *NrVhIn_Sng* (a decrease by 5.9%).

Balancing the likelihood data in the second modelling step, both in spatial and temporal aspects, improves the classification quality of all the final Bayesian models. The values of the quality assessment measures are satisfactory:

- sensitivity is greater than 57%,
- specificity is greater than 65%,
- the HMSS coefficient is greater than 61%.

A general picture of the coefficients of variation for the statistically significant parameters of the models is presented in Fig. 4 in the form of a bubble plot, where the centres represent mean values and the radii are standard deviations of the coefficients. The standard deviation values are similar, irrespective of the step (prior or posterior models) and the aspect (spatial or temporal) of modelling. A slightly greater difference can be noticed for the mean values – they are smaller for the parameters of the second step models, which indicates the better estimation precision of the final posterior models.

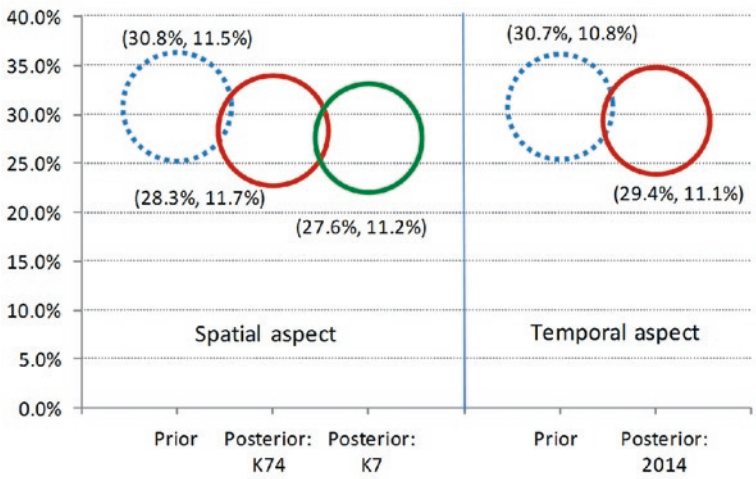

Fig. 4. Bubble plots of mean and standard deviation values of the coefficient of variation for statistically significant parameters of Bayesian models

6. Conclusions

Parameters are random variables in Bayesian regression models. Their so-called posterior distributions are obtained by combining systematic (prior) knowledge about the parameters with Bayesian likelihood – the knowledge derived from data. Some issues concerning the methodology of such models development for road traffic safety analyses is presented in the study. A logistic regression model that classifies road accident severity is analysed.

Road accident data are treated as a potential source of both information types for the Bayesian model: prior knowledge and Bayesian likelihood. Some researchers apply such an approach in their road safety investigations. In the study, however, a specific interpretation of both sources has been proposed and consequently their special application in the modelling process in which an additional task to obtain the best possible final classifiers was considered as well.

Prior knowledge about regression parameters can be obtained from data the range of which depends on the subject of a research. If the investigation focuses on the spatial aspect, all accident data recorded on the same technical class roads in a given country region are a possible source of informative priors, creating a reference background for being updated by Bayesian likelihood originating from accident data recorded on a chosen road. Thus, a model related to the road is obtained. If the investigation focuses on the temporal aspect, historical road accident data create informative prior background, and new accident data from the latest registration period update the priors, providing a new general picture of the region road network safety.

Balancing likelihood data, in both spatial and temporal aspects, positively affects the classification quality of the final Bayesian logistic regression models. The result is particularly important since the level of correct classification of rare success categories, i.e. serious or fatal road accident severity, is crucial.

Bayesian regression models work well when a quasi-complete or complete separation of data points appears [15] in a short data set with qualitative input variables. Classical regression models estimated on the basis of such data are not credible due to some constrains of the maximum likelihood method used in the estimation process. To solve the problem, enlarging the data set (not always efficient for some specific data structures) or a suitable aggregation of categories within chosen qualitative variables (which causes the reduction of information delivered to the model) is recommended. In the research, the quasi-complete separation was detected in the training data set for the time aspect. However, no interference into the data was necessary owing to the Bayesian approach to the modelling tasks.

Notwithstanding their complex nature, Bayesian models become more and more widely used in road traffic safety analyses. As it was shown in the study, they can provide great possibilities in interpreting and utilizing real data. Further studies are recommended to confirm the obtained findings and to widen possible implementations of the discussed technologies.

References

1. Bąk J., Bąk-Gajda D. Psychological factors in road safety. Eksploatacja i Niezawodnosc – Maintenance and Reliability 2007; 17(3): 22–29.
2. El-Basyouny K., Barua S., Islam M. T. Investigation of time and weather effects on crash types using full Bayesian multivariate Poisson lognormal models. Accident Analysis and Prevention 2014; 73: 91-99, http://dx.doi.org/10.1016/j.aap.2014.08.014.
3. Gaca S. Badania prędkości pojazdów i jej wpływu na bezpieczeństwo ruchu drogowego (The investigation of vehicle speed and its influence of road traffic safety). In Polish. Zeszyty Naukowe Politechniki Krakowskiej, Inżynieria Lądowa nr 75, Kraków, 2002.
4. Häggström O. Finite Markov Chains and Algorithmic Applications. Cambridge University Press (Virtual Publishing), 2003.
5. Helai H., Chor C.H., Haque M.M. Severity of driver injury and vehicle damage in traffic crashes at intersections: a Bayesian hierarchical analysis. Accident Analysis and Prevention 2008; 40: 45-54, http://dx.doi.org/10.1016/j.aap.2007.04.002.
6. Heydari S., Miranda-Moreno L.F., Lord D., Fu L. Bayesian methodology to estimate and update safety performance functions under limited data conditions: A sensitivity analysis. Accident Analysis and Prevention 2014; 64: 41-51, http://dx.doi.org/10.1016/j.aap.2013.11.001.
7. Huang H., Abdel-Aty M. Multilevel data and Bayesian analysis in traffic safety. Accident Analysis and Prevention 2010; 42: 1556-1565, http://dx.doi.org/10.1016/j.aap.2010.03.013.
8. Jurecki R., Jaśkiewicz M., Guzek Z., Lozia Z., Zdanowicz P. Driver's reaction time under emergency braking a car – Research in a driving simulator. Eksploatacja i Niezawodnosc – Maintenance and Reliability 2012; 14 (4): 295–301.
9. Jurecki R.S., Stańczyk T.L. Test methods and the reaction time of drivers. Eksploatacja i Niezawodnosc – Maintenance and Reliability 2011; 3 (51): 84–91.
10. Kieć M. Wpływ dostępności do dróg na warunki i bezpieczeństwo ruchu (The influence of road accessibility on road traffic conditionas and road traffic safety – PhD thesis). Rozprawa doktorska na Wydziale Inżynierii Lądowej Politechniki Krakowskiej, Kraków, 2009.
11. Larose D.T. Data Mining Methods and Models. John Wiley & Sons, Inc., 2006.
12. Mitas A.W., Czapla Z., Bugdol M., Ryguła A. Rejestracja i ocena parametrów biometrycznych kierowcy dla poprawy bezpieczeństwa ruchu drogowego. Zeszyty Naukowe Politechniki Śląskiej, seria Transport 2010; 6 (1825): 71-79.
13. Mitra S., Washington S. On the nature of over-dispersion in motor vehicle crash prediction models. Accident Analysis and Prevention 2007; 39: 459-468, http://dx.doi.org/10.1016/j.aap.2006.08.002.
14. Nowakowska M. Logistic models in the crash severity classification on the basis of chosen road characteristics. Transportation Research Record, Journal of the Transportation Research Board, Highway Safety Data, Analysis, and Evaluation, Volume 2, Washington D.C. 2010; 2148: 16-26.
15. Nowakowska M. Modelowanie związków między cechami drogi a zagrożeniami w ruchu na drogach zamiejskich (Modelling the relationship between road features and traffic threats on national roads). In Polish. Warszawa: Oficyna Wydawnicza Politechniki Warszawskiej, Warszawa, 2013.
16. Pei X. Wong S.C., Sze N.N. A joint probability approach to crash prediction models. Accident Analysis and Prevention 2011; 43: 1160-1166, http://dx.doi.org/10.1016/j.aap.2010.12.026.
17. Persaud B., Lan B., Lyon C., Bhim R. Comparison of empirical Bayes and full Bayes approach for before-after road safety evaluations. Accident Analysis and Prevention 2010; 42: 38-43, http://dx.doi.org/10.1016/j.aap.2009.06.028.
18. SAS/STAT® 9.2 User's Guide. Introduction to Bayesian Analysis Procedures. Second Edition, SAS Institute Inc., Cary, NC, USA, 2009.

19. Savolainen P.T., Mannering F.L., Lord D., Quddus M.A. The statistical analysis of highway crash-injury severities: a review and assessment of methodological alternatives. Accident Analysis and Prevention 2011; 43: 1666−1686, http://dx.doi.org/10.1016/j.aap.2011.03.025.
20. Yu R., Abdel-Aty M. Investigation different approaches to develop informative priors in hierarchical Bayesian safety performance functions. Accident Analysis and Prevention 2013; 56: 51-58, http://dx.doi.org/10.1016/j.aap.2013.03.023.
21. Zarządzenie nr 653 Komendanta Głównego Policji z dnia 30 czerwca 2006 r. w sprawie metod i form prowadzenie przez Policję statystyki zdarzeń drogowych (The regulation No 635 by the Main Commanding Officer of the Polish Police Headquarters from the 30-th of June 2006 regarding the methods and the forms of processing road crash statistics by the police). In Polish. Warszawa, 2006.

Marzena NOWAKOWSKA
Faculty of Management and Computer Modelling
Kielce University of Technology
Al. Tysiąclecia Państwa Polskiego 7, 25-314 Kielce, Poland
E-mail: spimn@tu.kielce.pl

Article citation info:
CHEN X, XU D, XIAO L. Joint optimization of replacement and spare ordering for critical rotary component based on condition signal to date. Eksploatacja i Niezawodnosc – Maintenance and Reliability 2017; 19 (1): 76–85, http://dx.doi.org/10.17531/ein.2017.1.11.

Xiaohui CHEN
Dawei XU
Lei XIAO

JOINT OPTIMIZATION OF REPLACEMENT AND SPARE ORDERING FOR CRITICAL ROTARY COMPONENT BASED ON CONDITION SIGNAL TO DATE

WSPÓLNA OPTYMALIZACJA WYMIANY I ZAMAWIANIA CZĘŚCI ZAMIENNYCH DLA KRYTYCZNEGO KOMPONENTU OBROTOWEGO NA PODSTAWIE DOTYCHCZASOWEGO SYGNAŁU STANU

It is widely accepted that condition-based replacement can not only make full use of components, but also decline inventory cost if the procurement of spare parts can be triggered upon accurate failure prediction. Most of the existing degradation or failure prediction models and approaches are population-based failures or suspensions, namely, to predict the failure time of a component, there are some failure or suspension histories of same type or similar components which can be used as reference. However, in practice, there exists the phenomenon in which no failure or suspension histories for some components can be used, what can be utilized is just the collected condition monitoring signals to date. In that case, failure time and probability are difficult to be estimated accurately. In this paper, a novel degradation prediction approach is introduced. Meantime, a new failure probability estimation function is developed based on component "service time" and "degradation extent" simultaneously. Then replacement and spare part ordering are jointly optimized according to the estimated failure probability. The optimization objective is to minimize long-run cost rate. Two bearing datasets are used to validate the proposed approach.

***Keywords**: degradation prediction, failure probability, condition-based replacement, spare part ordering.*

Powszechnie przyjmuje się, że wymiana w oparciu o stan techniczny pozwala nie tylko na pełne wykorzystanie elementów składowych, ale także na zmniejszenie kosztów magazynowych (związanych z przechowywaniem zapasów) jeśli zamawianie części zamiennych da się powiązać z trafnym prognozowaniem uszkodzeń. Większość istniejących modeli i teorii predykcji degradacji lub uszkodzeń opiera się na danych populacyjnych o uszkodzeniach lub zawieszeniu pracy co oznacza, że czas uszkodzenia komponentu przewiduje się w odniesieniu do historii uszkodzeń lub zawieszeń pracy tego samego typu lub podobnego typu elementów składowych. Jednak w praktyce zdarza się, że dla niektórych komponentów nie istnieją historie uszkodzeń lub zawieszenia pracy, do których można by się odnieść; jedyne co można wykorzystać to zgromadzone dotychczas sygnały z monitorowania stanu. W takim przypadku, trudno jest ocenić dokładnie czas i prawdopodobieństwo wystąpienia uszkodzenia. W niniejszej pracy, przedstawiono nowatorskie podejście do przewidywania degradacji. Opracowano nową funkcję szacowania prawdopodobieństwa uszkodzenia opartą na jednoczesnym wykorzystaniu "czasu pracy" oraz "stopnia degradacji" komponentu. Następnie wspólnie zoptymalizowano procesy wymiany i zamawiania części zamiennych zgodnie z szacowanym prawdopodobieństwem wystąpienia uszkodzenia. Celem optymalizacji była minimalizacja długoterminowego wskaźnika kosztów . Poprawność proponowanego podejścia zweryfikowano z wykorzystaniem dwóch zbiorów danych dotyczących łożysk.

***Słowa kluczowe**: prognozowanie degradacji, prawdopodobieństwo wystąpienia uszkodzenia, wymiana w oparciu o stan, zamawianie części zamiennych.*

1. Introduction

Unexpected system failures pose significant problems in power industry and most manufacturing companies. In some cases, a critical component failure can incur catastrophic events and huge economic loss. To maintain machines at high level of reliability, some companies perform time-based preventive maintenance or age-based preventive maintenance to avoid sudden failure of machines. Usually, preventive maintenance tasks includes lubrication, cleaning, inspection, adjustment, alignment and/or replacement [25]. Even though above maintenance schemes may decline the probability of sudden downtime to some extent, high maintenance cost may be generated due to frequent "over maintenance". Some companies hold lots of spare parts inventory in case the shortage of spare parts for maintenance actions. If the spares ordering is inappropriate, companies have to suffer high inventory quantity or high inventory holding cost.

A widely accepted view of decreasing unnecessary cost, including maintenance cost, inventory cost and equipment failure loss, is to perform condition-based maintenance on critical components. Recently, condition based maintenance has been studied extensively as one of the most important maintenance method. To guarantee the effectiveness and economy of maintenance, a new failure probability estimation function is established based on a novel remaining useful life prediction using condition monitoring signal to date. The estimated failure probability is the basis of replacement determination which is related to jointly optimize replacement time and spare ordering. In terms of spare ordering, spares should be ordered at right time to trade off spares shortage cost and inventory holding cost. Therefore, the reasonable decisions for replacement and spare ordering should include when to perform replacement and purchase spare parts. All the decisions are based on accurate failure prediction. The main con-

tribution is that this method focuses on the situation in which a critical component without failure or suspension histories of same type components.

Due to the importance of RUL prediction, many scholars proposed different methods or models for various applications. Lee et al. [6] reviewed the methodologies and applications of prognostics and health management design for rotary machinery systems. Li et al. [7] analyzed products reliability using unbalanced data, in which unbalanced data means the number and time of measurements are not identical for degradation units. Roughly, the existing work can be divided into two classes, one class is the prediction models and methods are population-based, which means there are failure or suspension histories of same type components can be used. The other class is individual-based, which uses the collected individual condition monitoring signal to date. Defined by Tian et al. [15], a failure history means that a component is replaced with a new one due to its failure. A suspension history refers that a component is replaced by a new component before its failure and never used again. Wu et al. [26] optimized condition-based maintenance using prognosis information with consideration of prediction uncertainty which is estimated by the artificial neural network (ANN) lifetime prediction errors during the ANN training and testing processes. Zhang et al. [28] made the maintenance decision based on the Bayesian belief network prediction results using failure data. Lu et al [9] predicted bearing remaining useful life only using truncated histories. All the works above are mainly population-based to predict RUL.

In practice, some components cannot obtain failure or suspension histories of same type or similar components, for example, high reliability requirement and unique designed work. In this case, failure prediction is difficult, especially for an individual. Because no failure or suspension histories can be used to reflect the degradation process during whole lifecycle of components. The prediction models or methods are hard to be developed because the parameters and network constructions cannot be estimated appropriately. Works on this area are few and limited. Di Maio et al [1] proposed a relevance vector machines and exponential regression method to estimate bearing remaining useful life. The results show that the prediction result can be more accurate if more data is collected. While, at the beginning of prediction, the difference between real values and predicted values is big. Xiao et al [27] proposed a novel bearing degradation approach based on shrunken time windows and back-propagation neural network (BPNN). The prediction method uses limited amount of collected condition monitoring data for a component to date.

Maintenance is not only related to component condition, it has a strong interconnection with the availability of spare parts. Van Horenbeek et al. [16] summarized the joint optimization of maintenance and inventory from the views of inventory policy, maintenance characteristics, delays, multi-echelon networks, single-unit versus multi-unit systems, objective function and optimization techniques. Wang [19] determined preventive maintenance interval, spare order interval and order quantity simultaneously. Spare parts are ordered periodically instead on demand. Nguyen et al. [12] studied the impact of the spare parts inventory level on maintenance and replacement decisions under technological change rather than determining optimal order level/order quantity for spare parts. Panagiotidou [13] performed periodically inspection and preventive maintenance to the detected items. Meanwhile, two types of silent failures are considered when optimizing spare parts ordering and maintenance policies. Gan and Shi [3] considered replacement part order and buffer inventory when optimizing the maintenance policy for the upstream machine. System and decision process are modeled by discrete Markov method with the minimal expected cost rate control-limit policy. Zhang et al. [29] utilized the semi-Markov decision process to propose a maintenance optimization. Wang et al. [17, 18] proposed condition-based replacement and spare provisioning policies for deterioration systems. Rausch and Liao [14] addressed a joint production and spare part inventory driven by condition based maintenance. However, these joint decision policies do not utilize the updated RUL prediction from observed information. Some other works focus on the joint optimization of periodic preventive maintenance/periodic replacement and spare inventory/ordering [5, 10, 20].

In recent decades, the sensor technology is developed and enables to conduct system health monitoring, the condition-based or sensor-based maintenance planning and spare ordering seems more reasonable. Elwany & Gebraeel [2] proposed a two-phase optimization for replacement and spare parts ordering. First, the replacement time is determined, then the spare ordering time is followed, accordingly. Most of the condition-based decision is using the population-based failure or suspension histories to approach the system failure. Wang et al. [22, 24] presented a prognostics-based spare part ordering and system replacement (PSOSR) policy. The spare part ordering time and the system replacement time is real-time determined according to the actual health condition. Recently, there is a few researches about the joint optimization of replacement and spare ordering that utilizing the online condition monitoring. Louit et al. [8] considered condition-based monitoring and optimized the spares ordering time. Wang et al. [23] proposed a prognostic-information-based joint order-replacement policy for a non-repairable critical system in service.

Even though there are some research on the joint optimization of replacement and spare ordering, the research is still deficient. This paper is an integrated view from RUL prediction to joint optimization of replacement and spare ordering. Mainly, this paper focuses on the situation in which no failure or suspension histories can be used for a single critical component. What can be used is only the collected condition monitoring data to date. A novel approach for degradation and RUL prediction from Xiao et al [27] is introduced. Then, a new failure probability function is defined based on "service time" and "degradation extent". According to the estimated failure probability, replacement and spare ordering are optimized simultaneously with the objective of minimizing the long-run expected cost per unit time. Different from the existing research, this paper focuses on the degradation properties of individual component. The introduced RUL prediction method can predict system degradation in the early phase of lifecycle with limited amount of data. Moreover, most of the existing failure probability estimation methods use population-based failure or suspension histories, the proposed failure probability estimation function connects system "service time" with "degradation extent". Owing to failure probability, the balance among preventive replacement, failure replacement, spare part shortage cost, and inventory holding cost are traded-off in the view of individual component lifecycle horizon.

This paper is organized as follows: Section 2 states the problem briefly and describes the procedure of joint optimization, assumptions and notations. Section 3 introduces the novel prediction approach, failure probability estimation and joint optimization model of replacement and spare ordering. Section 4 presents a case study using simulation bearing dataset and real dataset from PHM 2012 competition. Final conclusions are drawn in Section 5.

2. Procedure of joint optimization, assumptions and notations

Condition monitoring provides an opportunity to enhance component lifecycle management including component failure prediction, maintenance planning and spares inventory. Spares inventory can be declined and optimized via the implementation of condition-based maintenance with high accuracy of component failure prediction. Hence, accurate component failure prediction is the fundamental of condition-based maintenance and spare inventory ordering/control. Among the existing work, failure prediction for components using population-based failure or suspension histories is researched a lot.

While, the prediction work is difficult when no failure or suspension histories of same type or similar components can be used as reference. Because the whole degradation processes cannot be reflected by historical data. Moreover, the parameters of the prediction models are hard to be estimated with the limited amount of data to date. In this case, we introduced a novel method to predict an individual critical component degradation and RUL, then a new failure probability function is formulated and connected "service time" with "degradation extent". Based on the failure probability, the joint optimization of replacement and spare ordering is developed. The procedure of the proposed condition-based joint optimization of replacement and spares ordering is described in Fig. 1.

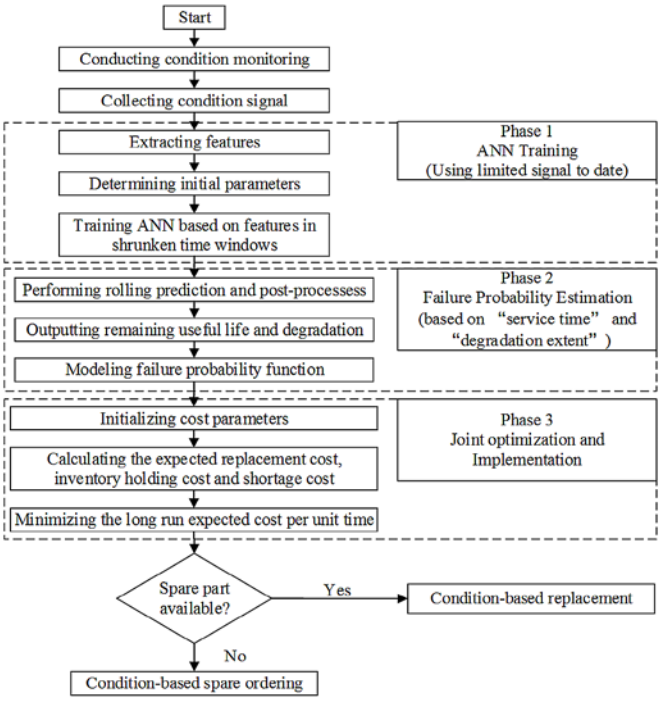

Fig. 1. Procedure of the proposed joint optimization of replacement and spares ordering

In the first phase, condition monitoring is conducted on an individual component. Condition monitoring signal is collected. Advanced feature extraction method is used to extract features which reflect degradation of the component and are prepared for training ANN. Some initial parameters are set before ANN training, such as, maximum training epoch, performance goal, initial time window, etc. Then the initial time windows are shrunken and the remained features in the shrunken time windows are used to train ANN.

In the second phase, the well trained ANN is used to perform lopfng-step ahead rolling prediction. After each prediction epoch, the predicted results are post-processed and compared with predetermined failure threshold, then the predicted RUL is outputted along with degradation.[27] According to the component "service time" and "degradation extent", failure probability is estimated.

In the third phase, the cost parameters are initialized, such as preventive replacement cost, failure replacement cost, inventory holding cost, spare shortage cost, and spare ordering cost. The failure probability function is used to estimate the expected costs. Finally, the best policy of replacement and spare ordering can be determined based on the minimizing long-run expected cost per unit time. According to the optimal policy, the availability of spare part is checked out, if the spare part is available, condition-based replacement is performed at the right time, alternatively, a spare ordering should be placed at the optimized ordering time.

In this paper, some basic assumptions and notations are listed as follows.

A1: During the condition monitoring process, sampling is periodic with equivalent sampling frequency.
A2: In general, the degradation signal shows an increasing tendency.
A3: No lead time for carrying out a preventive replacement or failure replacement, namely, replacement is performed immediately.
A4: Leading time of spare part is fixed elapsed from the moment of placing an order until order receipt.
A5: Inspection cost is not considered in this paper. We assumed the inspection cost can be neglected compared with other costs.

Notation	Description
f	Fluctuation factor
ST	Start time of prediction
ws_0	Initial time window size
$\mathbf{W}_{k1}$, $\mathbf{W}_{k2}$	Feature matrixes in the shrunken windows
ws_k	Shrunken time window size
m_{k1}, m_{k2}	Mean values of $\mathbf{W}_{k1}$ and $\mathbf{W}_{k2}$
r_k	Final increasing rate
inputn, hidden, outputn	Numbers of neurons in input layer, hidden layer and output layer
σ	A constant in interval (1,10)
$\mathbf{F}_p$	Predicted features matrix
$\mathbf{F}$	Features matrix of the whole life
f_{th}	Failure threshold
FN	Normalized feature matrix
cumsum	Accumulated summation
FNC	Cumulative feature matrix
FP	Cumulative failure probability
FP_t	Cumulative failure probability at time t
C_{pr}	Preventive replacement cost
C_{fr}	Failure replacement cost
C_o	Ordering cost
C_h	Holding cost per unit time
C_s	Shortage cost per unit time
c_e	System expected cost per unit time
SC	Expected shortage cost
HC	Expected holding cost
C_e	Total excepted cost
t_o	Spare part ordering time
t_r	Replacement time
L	Spare part transit time
T	Failure time
T_e	Expected time until replacement

3. Problem formulation

3.1. Degradation and RUL prediction for an individual component

The introduced individual component degradation and RUL prediction is proposed by Xiao et al. [27]. The method uses limited

amount of recorded condition monitoring data to date. According to the proposed prediction approach, the procedure of their method is summarized in Fig. 2 as follows.

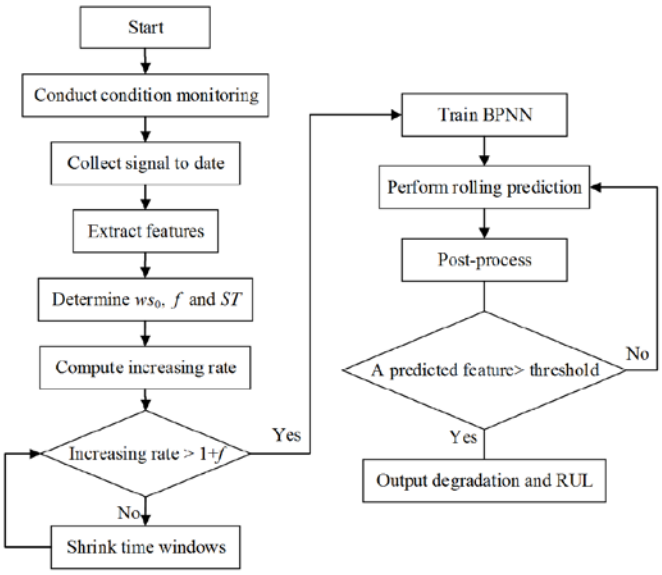

Fig. 2. Procedure of the proposed degradation and RUL prediction approach from Xiao et al.[27].

The extracted features from condition monitoring data to date are prepared for training BPNN. Before training BPNN, an initial time window size (ws_0) is given, mean values of the features in the initial time windows are calculated. The ratio of two mean values in two adjacent time windows is defined as increasing rate. Then increasing rate is compared with fluctuation factor which is set in the interval of (0, 0.1). If the increasing rate is greater than (1+f), features in the current time windows are used to train BPNN, otherwise, the time windows are shrunken step by step, then increasing rate is recalculated according to the features in the shrunken time windows. Shrinking is terminated until the increasing rate is greater than (1+f). Fig. 3 shows the comparison of time windows before and after the shrunken. The feature matrixes in the shrunken time windows, mean values and increasing rate are calculated by Eq. (1)-Eq. (3).

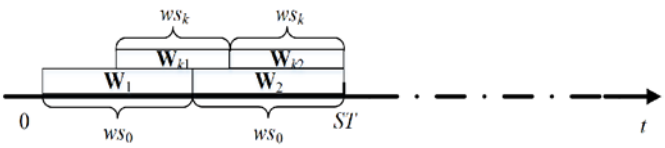

Fig. 3. Comparison of time window before and after shrunken

$$\begin{aligned}\mathbf{W}_{k1} &= [\mathbf{F}_{ST-2ws_k+1};\mathbf{F}_{ST-2ws_k+2};\cdots;\mathbf{F}_{ST-ws_k}]\\ \mathbf{W}_{k2} &= [\mathbf{F}_{ST-ws_k+1};\mathbf{F}_{ST-ws_k+2};\cdots;\mathbf{F}_{ST}]\end{aligned} \tag{1}$$

$$m_{k1} = \frac{\sum_{n=1}^{ws_k}\mathbf{F}_{ST-2ws_k+n}}{ws_k} \qquad m_{k2} = \frac{\sum_{n=1}^{ws_k}\mathbf{F}_{ST-ws_k+n}}{ws_k} \tag{2}$$

$$r_k = \frac{m_{k2}}{m_{k1}} \tag{3}$$

Where, ST is the start time of prediction, ws_0 is initial time window size, W_{k1} and W_{k2} are feature matrixes in the kth shrunken windows respectively, ws_k is the shrunken time window size. Mean values of W_{k1} and W_{k2} are m_{k1} and m_{k2} respectively, and r_k is the final increasing rate.

Features matrixes W_{k1} and W_{k2} in the final shrunken time windows are regarded as inputs and outputs for training BPNN respectively. The number of neurons in input layer and output layer depends on the features matrix dimension. The revised empirical formula for determining the number of neurons for hidden layer is as follows:

$$hidden = \left\lceil \sqrt{inputn + outputn} \right\rceil + \sigma \tag{4}$$

Where *hidden*, *inputn* and *outputn* are the numbers of neurons in hidden layer, input layer and output layer, respectively. σ is a constant in interval (1, 10).

After determining the training samples and BPNN construction, BPNN is trained. Multi-step ahead rolling prediction is performed. In each prediction epoch, there are ws_k tuples of feature predicted, the rolling prediction is performed as Eq. (5). The outputs in each prediction epoch should be post-processed using Eq. (6) and Eq. (7):

$$\begin{cases}[\mathbf{F}_{ST-2ws_k+1};\cdots;\mathbf{F}_{ST-ws_k}] \rightarrow [\mathbf{F}_{ST-ws_k+1};\cdots;\mathbf{F}_{ST}]\\ [\mathbf{F}_{ST-ws_k+1};\cdots;\mathbf{F}_{ST}] \rightarrow [\mathbf{F}_{ST+1};\cdots;\mathbf{F}_{ST+ws_k}]\\ \vdots\\ [\mathbf{F}_{m+1};\cdots;\mathbf{F}_{m+ws_k}] \rightarrow [\mathbf{F}_{m+ws_k+1};\cdots;\mathbf{F}_{m+2ws_k}]\end{cases} \tag{5}$$

$$\begin{aligned}&if\ \ \mathbf{NF}_t < \mathbf{NF}_{t\text{-}ws_k} \quad then\ \ \mathbf{NF}_t = \mathbf{NF}_{t\text{-}ws_k}\\ &if\ \ \mathbf{NF}_t > (1+f)\times\mathbf{NF}_{t\text{-}ws_k} \quad then\ \ \mathbf{NF}_t = (1+f)\times\mathbf{NF}_{t\text{-}ws_k}\end{aligned} \tag{6}$$

$$\begin{aligned}&if\ \ \mathbf{PF}_t \times r_k \geq ft \quad then\ \ RUL = t - ST\\ &if\ \ \mathbf{PF}_t \times r_k < ft \quad then\ \ rolling\ prediction\end{aligned} \tag{7}$$

3.2. Novel component failure probability estimation method

Component failure probability is the basis when balancing the joint optimization of replacement and spare ordering. Since no failure or suspension histories of same type or similar components can be used as population-based reference, a new failure probability estimation function is proposed using the predicted features based on "service time" and "degradation extent". The "degradation extent" of the features can be formulated as Eq. (8):

$$\mathbf{FN} = \frac{\mathbf{F}}{f_{th}} = \frac{[\mathbf{F}_1;\mathbf{F}_2;\cdots;\mathbf{F}_{ST};\mathbf{F}_p]}{f_{th}} \tag{8}$$

Where, F is features matrix of the whole life. F_p is predicted feature matrix. f_{th} is failure threshold. FN is normalized feature matrix.

Eq. (8) describes the relationship between features at current time and predetermined failure threshold. If a feature is closed to failure threshold, the failure probability is higher. In terms of "service time", it is based on a widely accepted assumption which is that the failure probability is higher if a component serves for longer time. Hence, the failure probability is formulated as follows:

$$\mathbf{FNC} = cumsum(\mathbf{FN}) \tag{9}$$

$$\mathbf{FP} = \frac{\mathbf{FNC}}{sum(\mathbf{FN})} \tag{10}$$

Where, *cumsum* represents accumulated summation. FNC is cumulative feature matrix. FP is cumulative failure probability which is a monotonic increasing function in interval of (0, 1]. A component is subject to random failure with the failure probability FP_t at time t.

3.3. Joint optimization of condition-based replacement and spare ordering

In this paper, the objective is to determine the optimal replacement and spare part ordering time along with the component being monitored. Two replacement policies are considered. One is preventive replacement which refers to performing replacement before the component failed. The other is failure replacement which refers to performing replacement after the component failed. The two replacement policies generate different maintenance costs which are C_{pr} and C_{fr}, respectively. In general, failure replacement can cause higher cost than preventive replacement, that is $C_{fr}>C_{pr}$. Before performing replacement, the availability of spares in stock should be checked out. If there are available spare parts before the required time, inventory holding cost is incurred with the cost per unit time C_h, alternatively, shortage cost with cost per unit time C_s is generated if the spare part is unavailable. If a spare part is needed while unavailable, an order is placed with ordering cost C_o.

Considering all the possible scenarios, the relationship among spare part ordering, replacement and component failure is shown in Fig.4. Where, t_o is spare part ordering time, t_r is replacement time, L is leading time of spare part. T is failure time of the component. Theoretically, it is possible for a component to be replaced at any time since ST until its failure. If a spare ordering is placed, a new spare can be available after a fixed leading time L. During the period, the system has to suffer a potential shortage of spare part with a shortage cost which is formulated as Eq. (11). However, if the spare is arrived before the required time, the system has to suffer the inventory holding cost which is as Eq. (12).

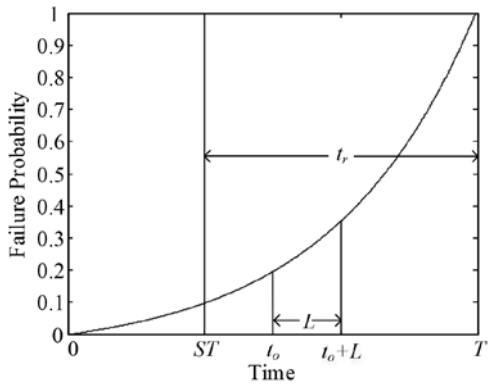

Fig. 4. The relationship among spare part ordering, replacement and component failure

$$SC = C_s \times \int_{t=0}^{L} FP_{t_0+t}dt \tag{11}$$

$$HC = C_h \times \int_{t=0}^{t_r-t_0-L} \left(1 - FP_{t_0+L+t}\right)dt \tag{12}$$

Where, SC and HC are the expected shortage cost and the expected holding cost, respectively. t is integration time step.

Therefore, the total excepted cost C_e is as Eq. (13). The expected long-run time until replacement is denoted as T_e can be deduced as Eq. (14). The expected long-run total cost rate, c_e, can be calculated by Eq. (15):

$$C_e = C_o + SH + HC + C_{pr} \times (1 - FP_t) + C_{fr} \times FP_t \tag{13}$$

$$T_e = \int_{t=0}^{L} FP_{t_0+t}dt + \int_{t=0}^{tr} \left(1 - FP_t\right)dt \tag{14}$$

$$c_e = \frac{C_e}{T_e} \tag{15}$$

The objective of this paper is to determine the best replacement time and spare ordering time by minimizing the expected long-run total cost per unit time. It can be formulated as follows:

$$\begin{aligned} \min \quad & c_e(\mathrm{t}) \\ s.t. \quad & ST \le t \le T \\ & FP_t \le 1 \end{aligned} \tag{16}$$

4. Case study

In this section, we validate the proposed model using two bearing datasets, one is simulated degradation dataset, and the other is a real-world condition monitoring dataset from PHM 2012 competition.

4.1. Simulated bearing dataset

The run-to-failure (RTF) simulation experiment is based on the work of McFadden and Smith [11] and Wang and Kootsookos [21], the more details can be found in Ref [28]. The simulated signal is extracted by wavelet packet analysis. The wavelet base is "db4", decomposition level is three. Energy of wavelet packet coefficients is the feature vector. The first dimension of the features is selected as the key element, if the feature at a time point in the first dimension exceeds 1400 Hz, the simulated bearing is regarded as failed. The degradation path of the key element of the simulated bearing is shown as Fig. 5.

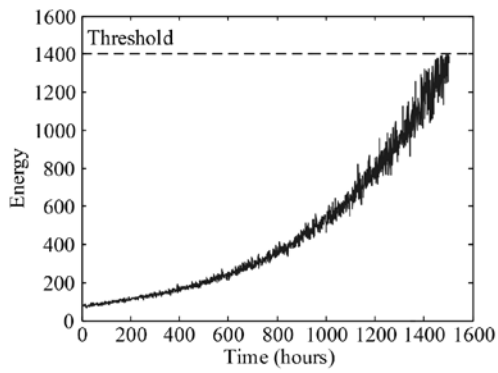

Fig. 5. Degradation path of the key element of the simulated bearing

Since 1400 Hz is set as failure threshold, the lifetime of simulated bearing is 1502 time units, here the time unit is hour. Due to feature extraction method, there are eight dimensions in the feature matrixes. Accordingly, there are eight neurons in input layer and output layer in BPNN, respectively. There is one hidden layer with ten neurons. The maximal iteration epoch for BPNN training is 1000, error goal is 1e-10. The initial time window size is 100, fluctuation factor is 0.02.

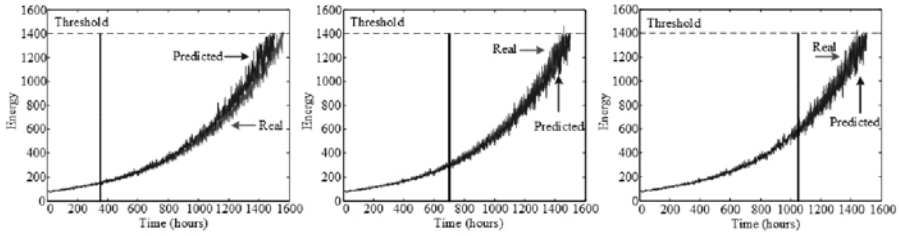

Fig. 6. Comparison of predicted and real degradation at different time points

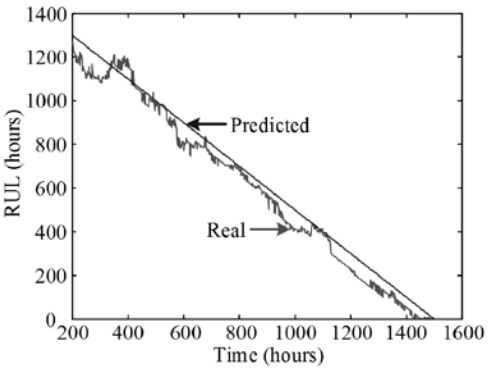

Fig. 7. Predicted RULs since ST=200

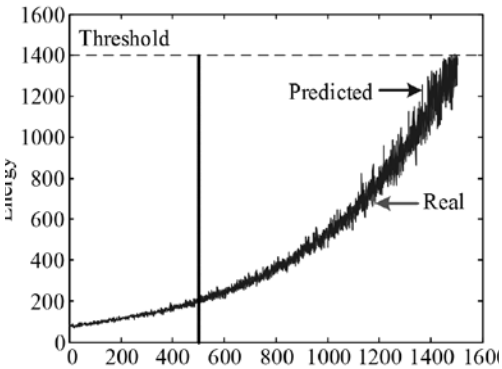

Fig. 8. Comparison of predicted degradation and real degradation at ST=500

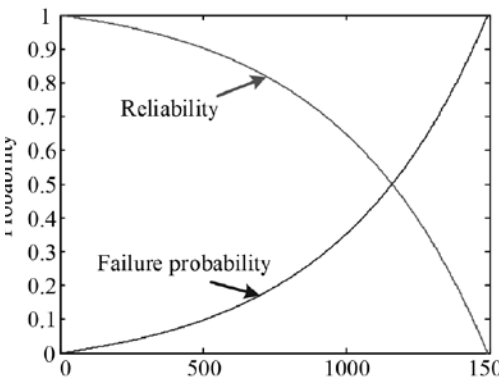

Fig. 9. Failure probability and reliability change over time

The predicted degradation and RULs at three different time points are illustrated in Fig. 6 and Table 1. Predicted RULs since *ST*=200 time units are shown in Fig. 7 compared with real values.

Taking *ST*=500 as an example, the comparison of predicted degradation and real values is descripted in Fig. 8, the corresponding failure probability and reliability change over time are shown in Fig. 9.

The following hypothetical data is used when optimizing replacement and spare ordering jointly, L=4 time units, C_{pr}=\$200, C_{fr}=\$1000, C_h=\$1/unit time, C_s=\$500/unit time, C_o=\$300. Using the above proposed method, the optimal spare ordering time is at 891 hours, the replacement time is at 900 hours, the long-run expected cost rate is 0.0066, and the expected total cost is \$1945, accordingly. The expected cost rate change over the predicted lifecycle is illustrated in Fig. 10.

Table 1. Comparison of predicted and real RULs at different time points

ST	Real RUL	Predicted RUL	Predicted error (%)
350	1152	1207	-3.66
700	802	758	2.93
1050	452	388	4.26

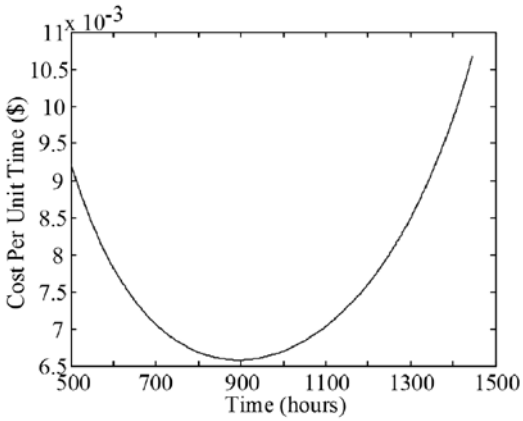

Fig. 10. Expected cost rate change over the predicted lifecycle

4.2. PHM Competition bearing dataset

PHM Competition bearing data is from IEEE Challenge 2012, it is real-field experimental data. Inspection was performed very 10 seconds and lasted for 0.1 second. Sampling frequency of vibration signal was 25.6 KHz, more detailed data information can be obtained from the website [4]. Shock Pulse Method (SPM) is used to extract degradation feature. The first bearing among PHM-2012 Competition

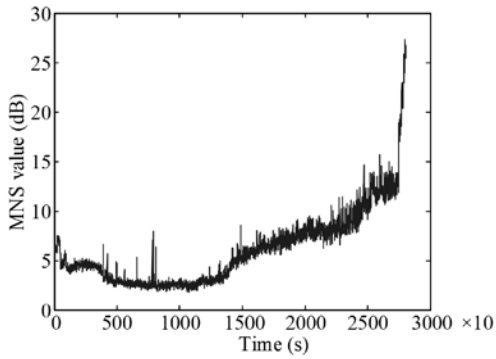

Fig. 11. MNS values of Bearing 1 from PHM-2012 Competition

bearings is used to validate the proposed method. The maximum normalized shock (MNS) value of Bearing 1 is depicted in Fig. 11.

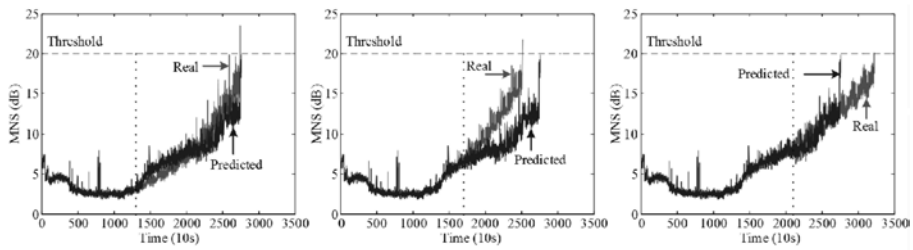

Fig. 12. Comparison of predicted and real degradation at different time points

Table 2. Comparison of predicted and real remaining useful life at different time points

ST	Real RUL	Predicted RUL	Predicted error (%)
1300	1465	1443	1.25
1700	1065	817	14.5
2100	665	1119	-25.72

From Fig. 11, MNS increases after 1000×10s, therefore, features before 1000×10s are not considered when training ANN and predicting RUL. The failure threshold of Bearing 1 is set 20dB. Hence, the bearing lifetime is 1765×10s. The essential parameters for degradation prediction and cost rate estimation are listed as followed. The number of neurons in input layer and output layer is one, there is one hidden layer with six neurons. The initial time window is 150, fluctuation factor is 0.05. The predicted degradation and RULs at three

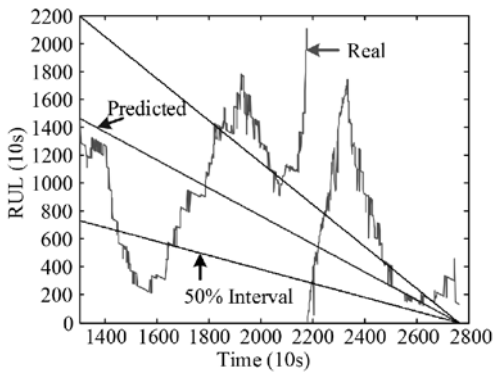

Fig. 13. RUL prediction results since ST=1300

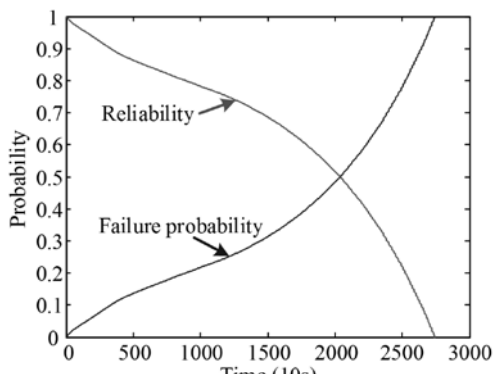

Fig. 14. Failure probability and reliability change over time

different time points are illustrated in Fig. 12 and the prediction performance is listed in Table 2. RUL prediction results since *ST*=1300 time units compared with real RULs are shown in Fig. 13.

Taking *ST*=1300 as an example, the estimated failure probability and reliability change over time is shown in Fig. 14. The hypothetical cost parameters are as followed, L=5 time units, C_{pr}=\$250, C_{fr}=\$1000, C_h=\$1/unit time, C_s=\$1200/unit time, C_o=\$500. The optimal spare ordering time is at 1894 time units, the best replacement time is at 1911 time units, the long-run expected cost rate is 0.0068, and the expected total cost is \$8512.9. The expected cost rate change over the predicted lifecycle is shown in Fig. 15.

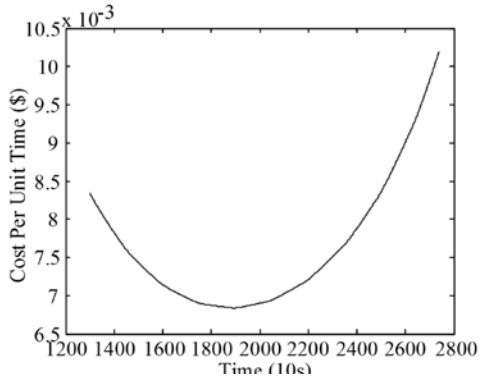

Fig. 15. Expected cost rate change over the predicted lifecycle

4.3. Comparative parameters tuning and discussion

For comparison, the method from Elwany & Gebraeel [2] is used to calculate the best replacement time and spare ordering time. For the simulated bearing, the optimal replacement time is at 1049 time units, the optimal spare ordering time is at 1037 time units along with the expected long-run cost rate is 0.0068. The total cost is \$ 2653.7. For the PHM-2012 competition bearing data, the best replacement time is 2189 time units, the best spare ordering time is 2164 time units, and the corresponding long-run cost rate is 0.0071.

(1) Comparison of cost rate and replacement time

In Elwany & Gebraeel [2] work, the best replacement time is determined according to the long-run average cost rate which is defined as followed:

$$C_r = \frac{c_p \overline{F}(t_r) + c_f F(t_r)}{\int_0^{tr} \overline{F}(t) dt} \tag{17}$$

Where, C_r is the expected long-run replacement cost, cp is the planned replacement cost, cf is the failure replacement cost. $F(t)$ is the cumulative density function of component's failure time. $\overline{F}(t) = 1 - F(t)$.

For more comparison, different inventory holding costs and shortage costs are tuned for comparative discussion. For the simulated bearing, inventory holding cost is varied from \$0.2/unit time to \$1/unit time, the interval is \$0.2/unit time, at the same time, shortage cost varies from \$50/unit time to \$250/unit time with the interval of \$50/unit time. For PHM 2012 Competition bearing, the inventory holding cost is changed from \$0.2/unit time to \$2/unit time with the interval of \$0.2/unit time, the shortage cost varies from \$50/unit time to \$1200/unit time with the interval of \$50/unit time. Comparing our proposed joint optimization method in this paper with the method in Elwany & Gebraeel [2], the respective cost rates and best replacement times are shown in Fig. 16 and Fig. 17.

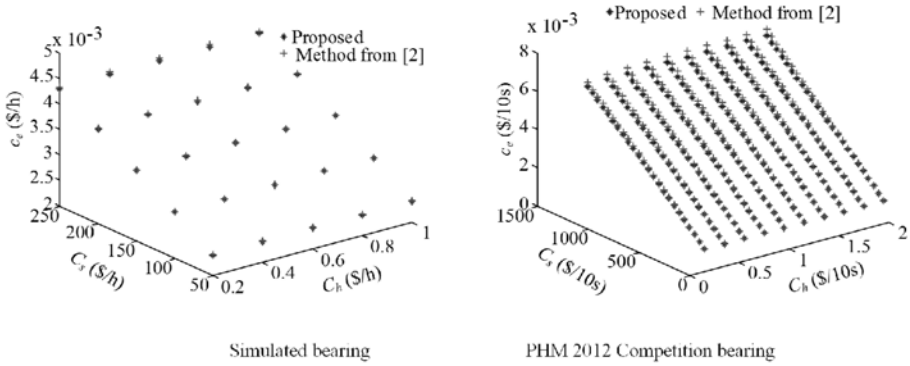

Fig. 16. Comparison of cost rates with different inventory holding costs and shortage costs

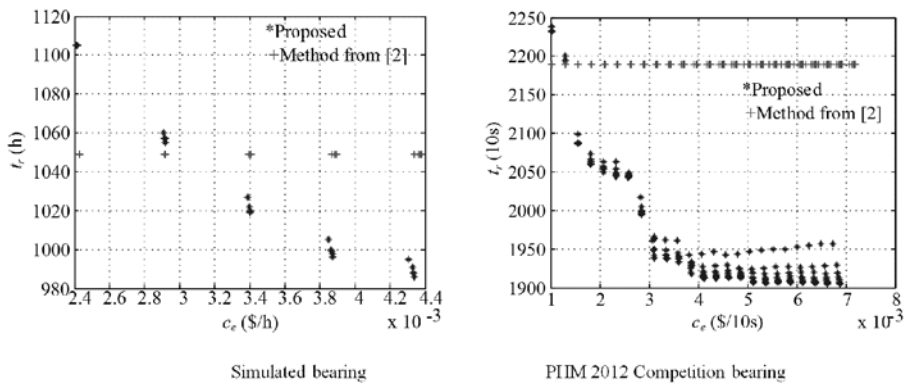

Fig. 17. Comparison of replacement times with different inventory holding and shortage costs

From Fig. 16, the comparison of cost rates, the cost rates from our proposed method are less than the ones from Elwany & Gebraeel's work [2]. Move to Fig. 17, the replacement time from Elwany & Gebraeel's work [2] is a constant. The replacement time from Elwany & Gebraeel's work [2] does not vary along with the spare holding cost and shortage cost. From Eq. (17), the replacement time is just impacted on the balance of planned replacement cost and failure replacement cost. After determining the best replacement time, the spare ordering time is calculated accordingly. Thus is different from our proposed method. In our proposed method, inventory holding cost and shortage cost can impact on the replacement time.

(2) Comparison of inventory time

Eq. (18) is defined to compare the inventory time for the two different methods. Where t_r^* and t_o^* are the optimal replacement time and spare ordering time from our proposed method, t_{r*} and t_{o*} are the optimal replacement time and spare ordering time from Elwany & Gebraeel's work:

$$x = t_r^* - t_o^* - L$$
$$y = t_{r*} - t_{o*} - L \tag{18}$$

Therefore, x is the inventory time for our proposed method, y is the inventory time for the method from [2]. Accordingly, the difference of x and y is the inventory time comparison. For the all sample data (which is same for the comparison of cost rates and replacement times. i.e., for PHM 2012 Competition bearing data, the inventory holding cost is changed from $0.2/unit time to $2/unit time with the interval of $0.2/unit time, the shortage cost varies from $50/unit time to $1200/unit time with the interval of $50/unit time.), the inventory time comparison is shown in Fig. 18.

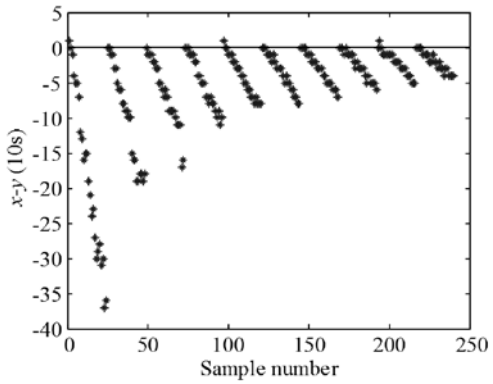

Fig. 18 Comparison of (x-y) with different inventory holding costs and shortage costs for PHM 2012 Competition bearing

From Fig. 18, in Elwany & Gebraeel's method [2], the inventory time is generally greater than our proposed method. In other words, their method scarifies inventory time to guarantee the component long service with higher cost rate.

Overall, their method can be regarded as two phases. The first phase is to determine the replacement which just concerns failure replacement cost and preventive replacement cost. The second phase is to determine the best spare order placing time according to the best replacement time. Their method may be less effective when inventory turnover ratio, inventory time and inventory quantity are critical concerns. While, in our proposed method, the replacement time and spare ordering are optimized jointly with lower cost rates.

5. Conclusions and prospects

This work focuses on the optimization of replacement and spare ordering for one individual critical rotary component. For the component, there are no failure or suspension histories of same type or similar components as references when predicting its failure time and degradation. To solve the prediction problem, a novel approach is introduced. Then a new failure probability estimation function is developed based on "service time" and "degradation extent". The difference between the developed method and the existing method, the failure probability is more focused on individual property, rather than the population-based character. Replacement and spare ordering time are determined simultaneously according to minimizing the expected long-run cost rate which is related to planned replacement cost, failure replacement cost, inventory holding cost, shortage cost and spare ordering cost. A simulated degradation bearing dataset and a real-world condition monitoring bearing dataset from PHM Competition 2012 are used to validate the proposed method. The degradation and RUL prediction performance is illustrated by comparing with the real values. The proposed approach is discussed by tuning the parameters of inventory holding cost and shortage cost. The results show that our method has lower long-run cost rate and less inventory time. It can be more effective when the inventory time, inventory turnover ratio and inventory quantity are critical concerns.

This proposed method can benefit to determining optimal replacement and spare ordering time for single component. Future research will focus on multi-component system optimization of replacement and spare ordering time with variable leading time.

Acknowledgment

The authors would like to thank great support from Key Project supported by National Science Foundation of China (51035008), as well as the National Science&Technology Major Project, China (No. 2016ZX04004-005).

References

1. Di Maio F, Tsui KL, Zio E. Combining Relevance Vector Machines and exponential regression for bearing residual life estimation. Mechanical Systems and Signal Processing 2012; 31: 405-427. http://dx.doi.org/10.1016/j.ymssp.2012.03.011.
2. Elwany AH, Gebraeel NZ. Sensor-driven prognostic models for equipment replacement and spare parts inventory. IIE Transactions 2008; 40(7): 629-639. http://dx.doi.org/10.1080/07408170701730818.
3. Gan S, Shi J. Maintenance optimization for a production system with intermediate buffer and replacement part order considered. Ekspolatacja i Niezawodnosc - Maintenance and Reliability 2014; 16(1): 140-149.
4. IEEE PHM 2012 Data Challenge. http://www.femto-st.fr/en/Research-departments/AS2M/Research-groups/PHM /IEEE-PHM-2012-Data-challenge.php.
5. Jiang Y, Chen M, Zhou D. Joint optimization of preventive maintenance and inventory policies for multi-unit systems subject to deteriorating spare part inventory. Journal of Manufacturing Systems 2015; 35: 191-205. http://dx.doi.org/10.1016/j.jmsy.2015.01.002.
6. Lee J, Wu F, Zhao W, Ghaffari M, Liao L, Siegel D. Prognostics and health management design for rotary machinery systems—Reviews, methodology and applications. Mechanical Systems and Signal Processing 2014; 42(1–2): 314-334. http://dx.doi.org/10.1016/j.ymssp.2013.06.004.
7. Li J, Zhang Y, Wang Z, Fu H, Xiao L. Reliability analysis of the products subject to competing failure processes with unbalanced data. Ekspolatacja i Niezawodnosc - Maintenance and Reliability 2016; 18(1): 98-109. http://dx.doi.org/10.17531/ein.2016.1.13.
8. Louit D, Pascual R, Banjevic D, Jardine AKS. Condition-based spares ordering for critical components. Mechanical Systems and Signal Processing 2011; 25(5): 1837-1848. http://dx.doi.org/10.1016/j.ymssp.2011.01.004.
9. Lu C, Tao L, Fan H. An intelligent approach to machine component health prognostics by utilizing only truncated histories. Mechanical Systems and Signal Processing 2014; 42(1–2): 300-313. http://dx.doi.org/10.1016/j.ymssp.2013.08.025.
10. Lynch P, Adendorff K, Yadavalli VSS, Adetunji O. Optimal spares and preventive maintenance frequencies for constrained industrial systems. Computers & Industrial Engineering 2013; 65(3): 378-387. http://dx.doi.org/10.1016/j.cie.2013.03.005.
11. McFadden PD, Smith JD. Model for the vibration produced by a single point defect in a rolling element bearing. Journal of Sound and Vibration 1984; 96(1): 69-82. http://dx.doi.org/10.1016/0022-460X(84)90595-9.
12. Nguyen TPK, Yeung TG, Castanier B. Optimal maintenance and replacement decisions under technological change with consideration of spare parts inventories. International Journal of Production Economics 2013; 143(2): 472-477. http://dx.doi.org/10.1016/j.ijpe.2012.12.003.
13. Panagiotidou S. Joint optimization of spare parts ordering and maintenance policies for multiple identical items subject to silent failures. European Journal of Operational Research 2014; 235(1): 300-314. http://dx.doi.org/10.1016/j.ejor.2013.10.065.
14. Rausch M, Liao H. Joint Production and Spare Part Inventory Control Strategy Driven by Condition Based Maintenance. IEEE Transactions on Reliability 2013; 59(3): 507-516. http://dx.doi.org/10.1109/TR.2010.2055917.
15. Tian Z, Wong L, Safaei N. A neural network approach for remaining useful life prediction utilizing both failure and suspension histories. Mechanical Systems and Signal Processing 2010; 24(5): 1542-1555. http://dx.doi.org/10.1016/j.ymssp.2009.11.005.
16. Van Horenbeek A, Buré J, Cattrysse D, Pintelon L, Vansteenwegen P. Joint maintenance and inventory optimization systems: A review. International Journal of Production Economics 2013; 143(2): 499-508. http://dx.doi.org/10.1016/j.ijpe.2012.04.001.
17. Wang L, Chu J, Mao W. A condition-based order-replacement policy for a single-unit system. Applied Mathematical Modelling 2008; 32 (11): 2274-2289. http://dx.doi.org/10.1016/j.apm.2007.07.016.
18. Wang L, Chu J, Mao W. A condition-based replacement and spare provisioning policy for deterioration systems with uncertain deterioration to failure. European Journal of Operational Research 2009; 194(1): 184-205. http://dx.doi.org/10.1016/j.ejor.2007.12.012.
19. Wang W. A stochastic model for joint spare parts inventory and planned maintenance optimisation. European Journal of Operational Research 2012; 216(1): 127-139. http://dx.doi.org/10.1016/j.ejor.2011.07.031.
20. Wang Y, Zhao J, Cheng Z, Yang Z. Integrated decision on spare parts ordering and equipment maintenance under condition based maintenance strategy. Ekspolatacja i Niezawodnosc - Maintenance and Reliability 2015; 17(4): 591-599. http://dx.doi.org/10.17531/ein.2015.4.15.
21. Wang YF, Kootsookos PJ. Modeling of low shaft speed bearing faults for condition monitoring. Mechanical Systems and Signal Processing 1998; 12(3): 415-426. http://dx.doi.org/10.1006/mssp.1997.0149.
22. Wang Z, Hu C, Wang W, Kong X, Zhang W. A prognostics-based spare part ordering and system replacement policy for a deteriorating system subjected to a random lead time. International Journal of Production Research 2014; 53(15): 4511-4527. http://dx.doi.org/10.1080/00207543.2014.988892.
23. Wang Z, Wang W, Hu C, Si X, Zhang Wei. A Prognostic-Information-Based Order-Replacement Policy for a Non-Repairable Critical System in Service. IEEE Transactions on Reliability 2015; 62(2): 721-735. http://dx.doi.org/10.1109/TR.2014.2371016.
24. Wang Z, Wang Z, Hu C, Liu X. An Integrated Decision Model for Critical Component Spare Parts Ordering and Condition-based Replacement with Prognostic Information. CHEMICAL ENGINEERING TRANSACTIONS 2013; 33: 1063-1068. http://dx.doi.org/10.3303/CET1333178.
25. Wong CS, Chan FTS, Chung SH. A joint production scheduling approach considering multiple resources and preventive maintenance tasks. International Journal of Production Research 2013; 51(3): 883-896. http://dx.doi.org/10.1080/00207543.2012.677070.
26. Wu B, Tian Z, Chen M. Condition-based Maintenance Optimization Using Neural Network-based Health Condition Prediction. Quality and Reliability Engineering International 2013; 29(8): 1151-1163. http://dx.doi.org/10.1002/qre.1466.
27. Xiao L, Chen X, Zhang X, Liu M. A novel approach for bearing remaining useful life estimation under neither failure nor suspension histories condition. Journal of Intelligent Manufacturing 2015. http://dx.doi.org/ 10.1007/s10845-015-1077-x.

28. Zhang X, Kang J, Jin T. Degradation Modeling and Maintenance Decisions Based on Bayesian Belief Networks. IEEE Transactions on Reliability 2014; 63(2): 620-633. http://dx.doi.org/10.1109/TR.2014.2315956.
29. Zhang Z, Zhou Y, Sun Y, Ma L. Condition-based mainteannce optimization without a predetermined strategy structure for a two-component series system. Ekspolatacja i Niezawodnosc – Maintenance and Reliability 2012; (2): 120-129. http://dx.doi.org/10.1007/978-1-4419-0820-9.

Xiaohui CHEN
Dawei XU
Lei XIAO
The State Key Lab of Mechanical Transmission
Chongqing University
Chongqing 400030, China
Emails: chenxiaohui@cqu.edu.cn, DavidXu1036@163.com, leixiao211@163.com

Article citation info:
SMOLINSKI M, PERKOWSKI T, MYSTKOWSKI A, DRAGAŠIUS E, JASTRZEBSKI RP. AMB flywheel integration with photovoltaic system for household purpose – modelling and analysis. Eksploatacja i Niezawodnosc – Maintenance and Reliability 2017; 19 (1): 86–94, http://dx.doi.org/10.17531/ein.2017.1.12.

Michal SMOLINSKI
Tomasz PERKOWSKI
Arkadiusz MYSTKOWSKI
Egidijus DRAGAŠIUS
Darius EIDUKYNAS
Rafal P. JASTRZEBSKI

AMB FLYWHEEL INTEGRATION WITH PHOTOVOLTAIC SYSTEM FOR HOUSEHOLD PURPOSE – MODELLING AND ANALYSIS

INTEGRACJA ŁOŻYSKOWANEGO MAGNETYCZNIE ZASOBNIKA ENERGII KINETYCZNEJ Z UKŁADEM PANELI FOTOWOLTAICZNYCH DLA ZASTOSOWAŃ W GOSPODARSTWACH DOMOWYCH – MODELOWANIE I ANALIZA

Abstract—This paper presents the design and investigation of a photovoltaic–flywheel system for household purposes. The main goal of this work is the electrical and mechanical integration of the electromechanical high speed kinetic energy storage as UPS (Uninterruptible Power Supply) with photovoltaic solar system. The paper contains calculation and division of photovoltaic panels system according to its integration with active magnetic bearing (AMB) flywheel and external electric grid. The photovoltaic solar installation costs as well as its size were considered. The composite shell AMB flywheel prototype configuration design (using CAD-software) and two different material variants are investigated and presented. In particularly, the structural composite shell stress calculations of two different materials vs rotational speed are performed using a direct coupling of SolidWorks and Matlab® software. The analytical calculations of PV–flywheel system are provided in order to choose optimal type of photovoltaic panels according to motor/generator flywheel and household energy system requirements. All elements of PV–flywheel system as transducers, bridges, wiring diagrams, etc., are optimized using Simscape tools. Finally, short- and long-time simulations results of PV–AMB–flywheel system and initial experimental results are presented and discussed.

***Keywords**: photovoltaic solar system, photovoltaic panels, AMB flywheel, kinetic energy storage, UPS device, motor/generator, composite materials.*

W artykule przedstawiono wstępne badania zintegrowanego układu paneli fotowoltaicznych z łożyskowanym magnetycznie zasobnikiem energii kinetycznej. Głównym celem pracy jest próba integracji elementów elektrycznych i mechanicznych wysokoobrotowego elektromechanicznego magazynu energii kinetycznej jako urządzenia UPS z układem paneli fotowoltaicznych. W szczególności przeprowadzono obliczenia najważniejszych parametrów elektrycznych łożyskowanego magnetycznie zasobnika energii połączonego z układem paneli fotowoltaicznych celem jego integracji z trakcją sieci elektrycznej niskiego napięcia. Wykorzystując pakiety oprogramowania: CAD, SolidWorks i Matlab, wykonano badania symulacyjne wskaźników wytrzymałości koła zamachowego zasobnika energii kinetycznej w szerokim zakresie prędkości obrotowej dla dwóch różnych typów materiałów kompozytowych. Następnie, wykorzystując między innymi narzędzia Simscape, przeprowadzono optymalizację elementów systemu celem dopasowania jego głównych parametrów do wymagań stawianym domowym instalacjom fotowoltaicznym z akumulatorami energii elektrycznej. Wyniki badań symulacyjnych, przeprowadzone w cyklach krótko– i długo– czasowych, układu paneli fotowoltaicznych zintegrowanych z elektromechanicznym akumulatorem energii potwierdziły wstępne obliczenia i założenia.

***Słowa kluczowe**: instalacja fotowoltaiczna, panele fotowoltaiczne, łożyskowany magnetycznie zasobnik energii kinetycznej, magazyn energii kinetycznej, urządzenie UPS, silnik/prądnica, materiały kompozytowe.*

1. Introduction

A UPS device is an uninterruptable power supply, the main objective of which is to maintain the operation of other devices in the event of a power supply failure. These devices belong to an important group and may be useful in many fields. Small-scale UPS devices are mostly used in hospitals to maintain the operation of medical equipment in case of a power blackout; many of these devices are also used to maintain power in server computers and home appliances. Energy storage devices support electric grids where uninterruptible power supply is needed. Main advantages of energy storage systems and applications in electrical power systems have been described in [19, 22].

Photovoltaic (PV) panels (solar cells) make it possible to convert solar energy into electric energy, which can supply electric devices. These panels are useful in many fields of science and applications of residential distribution grids as well as in PV–thermal domestic systems [21, 24]. Solar cells can be used to power many domestic

devices, for example in the field of home appliances, where charge accumulators and conventional UPS are suitable for further supply [3]. Due to the cycle of day and night, as well as changes in weather conditions, the panels are not able to fully supply devices designed to work continuously.

Nowadays, flywheels and batteries are viable energy storage technologies, which become practical solutions for applications where energy has to be saved for further use at any time. An overview of distributed energy storage systems for applications in future smart grids is presented in work [10]. Due to significant improvements in materials and mechatronics technology, the flywheels find the most promising applications for energy storage and become an alternative to batteries in UPS systems [4, 5]. In comparison to batteries, the flywheel has higher energy density (up to 100 Wh/kg), higher maximum peak power (over 10 kW/kg) and higher efficiency. A review of flywheel-based energy storage systems has been given in [17]. The active magnetic bearing (AMB) flywheel prototype design and control approach have been given by the author in [11, 12]. Major advantages of AMB flywheels result from modern technologies of composite materials with high tensile strength, which allow for high rotational speeds and high energy density [2, 7]. Also, flywheel design needs efficient solutions in electric motor/generator technologies using permanent magnet solutions and advanced control systems [8, 13, 23].

In a context where renewable energy from solar panels has low predictability and strong variability, integration into power systems may cause instabilities of these grids [14, 21]. Moreover, there are other, similar aspects that make integration of solar panels and electromechanical flywheel technology a challenge [9]. Therefore, this system always requires initial modelling and calculations according to the specific power system integration. In particular, the main advantage of UPS-flywheel integration with a photovoltaic solar system is that it provides efficient production control as well as good power management with energy saving and smooth power grids. Flywheels can address solar frequency variability and offer fast power response with high ramp rates and amplitude [1, 8].

If these renewable energy technologies are synthesized, it will be possible to charge accumulators and supply households by using both photovoltaic panels and solar panels' energy [6]. In the case of adverse weather conditions, accumulators should also be charged from the electric grid to provide continuous power supply. Integrated energy storages have huge potential because they reduce usage of the power grid by devices which require continuous power supply, and they are also irreplaceable for devices sensitive to voltage spikes.

2. Photovoltaic system

The application of photovoltaic solar panels as alternative sources of energy makes a device independent from the power grid. Solar cells can convert solar energy directly and supply devices with electric power or store it (e.g. in the accumulator as flywheel) for later use or for sale. Unfortunately, solar cells are very vulnerable to varying weather conditions. Nowadays, the market offers many standalone photovoltaic panels and whole photovoltaic systems. In this paper, the system design will concentrate on offered solutions that contain only photovoltaic panels without any additional components.

The selection of a photovoltaic installation should be made in a few steps. The first step is to determine the type of the installation. The most optimal solution is a hybrid installation, which is a combination of an in-grid installation (a photovoltaic solar system connected to power grid) and fixed installation (which is attached to the defined surface at a certain angle).

The second step involves determination of the quantity of solar panels. The chosen method uses nominal power of photovoltaic panels and includes losses accounted for by corresponding coefficients:

$$E_a = P_{PV} \cdot W_1 \cdot W_2 \cdot W_3 \cdot S \tag{1}$$

where: S – losses, W_1 – average daily number of hours of sunshine in STC (*Standard Test Conditions*), W_2 – deviation from the horizontal plane factor, W_3 – module temperature factor, P_{PV} – nominal module power, and E_a – the electrical efficiency of the photovoltaic solar system.

Losses of the system are given as:

$$S = S_1 \cdot S_2 \cdot S_3 \tag{2}$$

where: S_1 – coefficient including losses from the storage device and the voltage drops occurring on the lines (these losses should be assumed to be 6 %), S_2 – electric to kinetic energy conversion of the flywheel (since electromechanical storage is characterized by high efficiency, we can assume that the average loss is 10 %), S_3 – the losses generated by variable insolation and temperature differences (based on the datasheets, we may assume that this value is about 10 %).

Then, the calculated nominal module power is given as:

$$P_{PV} = \frac{U}{W_1 \cdot W_2 \cdot W_3 \cdot S} \tag{3}$$

where: U – daily energy consumption, usually ranging from 1.7 up to 3.5 kW/day for an average household.

These calculations should be carried out for different seasons. In summer higher nominal power should be selected. In winter season smaller W_1 factor should be applied. Solar PV systems generate large excess of energy in the summer season, and this excess energy can be discharged to the grid.

The *I-V* characteristics of PV are important properties during design of the photovoltaic energy system. In particular, the *I-V* model of the PV cell is described by:

$$V_{PV} = ln\left(\frac{I - I_{PV}}{I_{sat}} + 1\right)\frac{KT}{q} \tag{4}$$

where: V_{PV} and I_{PV} are photovoltaic operating voltage and current respectively, I and I_{sat} are the short-circuit and saturation currents, K – the Boltzmann constant, and T is absolute temperature. In the case of a PV array, the total voltage and current are $V_{array}=N_s V_{PV}$ and $I_{array}=N_P I_{PV}$, where N_s and N_P are the number of series and parallel PV cells respectively. In our case, the characteristics of PV power and current vs. voltage are given in Fig. 5 in the section containing PV simulation calculations.

2.1. Flywheel integration with pv array photovoltaic solar system

The proposed household photovoltaic solar system consists of 10 PV panels connected in series with a total electric power of 2.5 kW and output voltage of 240 V. The photovoltaic solar system and energy storage flywheel interconnection is given in Fig. 1.

Solar panels are connected in series configuration for easier installation, and in the absence of complicated wiring, with less components.

The PV–flywheel installation requires the use of energy converters. Commercial converters adjusted to PV systems (for e.g. Sunny Boy 1300TL) are used. The basic parameters of the converter are: 600 V maximum input voltage and 180–260 V rated voltage. The final

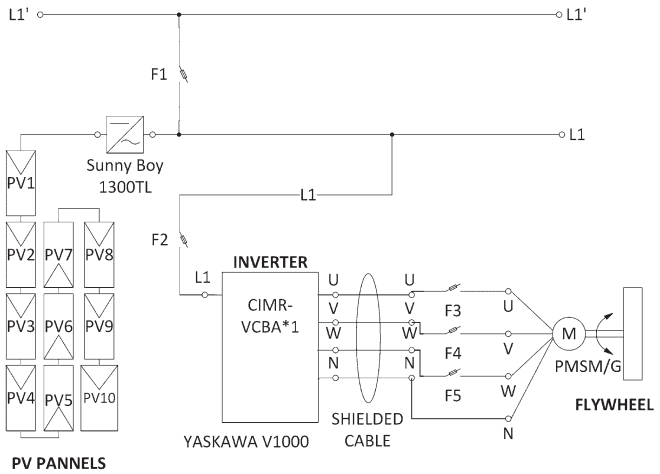

Fig. 1. Power system interconnection

element required for integration of the photovoltaic solar system with the flywheel is an inverter (for e.g. Yaskawa V1000 CIMR-VCBA*1). This inverter is fitted with a built–in control system that allows for motor control (to put it simply, the inverter controls the "charging" process of the flywheel).

3. AMB flywheel

Flywheel is the electromechanical energy storage device where storage energy is in the form of kinetic energy. This energy is stored using a flywheel coupled to the electrical machine. Stored energy depends on rotational speed. In order to provide flywheel high rotational speed operation the robustness of the control system is essential. The AMB system identification with disturbance observer–based control is one of common approach [15, 16]. In embodiments of the AMB flywheel the electric machine works alternately both as a generator and as a motor. The use of rotating mass requires precise control (loss of control of the moving object may cause a serious crash). Authorial AMB flywheel configuration is presented in Fig. 2.

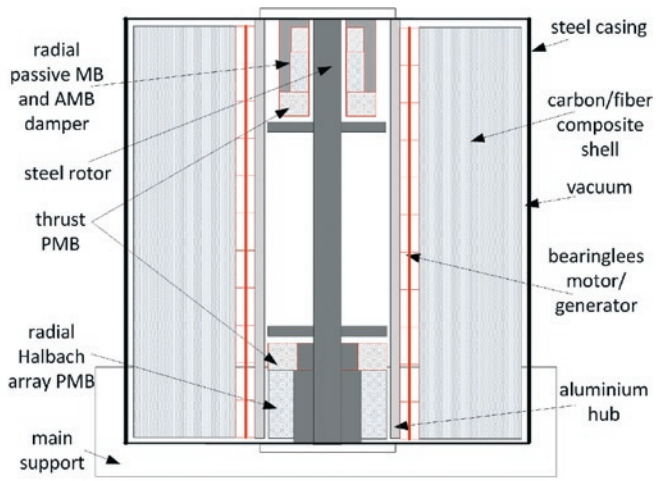

Fig. 2. AMB flywheel configuration as electromechanical energy storage device

The flywheel configuration (Fig. 2) consists of the coreless synchronous motor/generator attached to the high-strength aluminium cylinder rotor supported by hybrid magnetic bearings. Technologies of the Halbach arrays based solid-magnets supports combinations with the active magnetic dampers are used as the energy saving suspension rotor system. The main rotor with motor drive and generator are connected with the composite shell. The bearingless motor in the middle of the shaft provides efficient damping of first bending mode of the rotor. Flywheel's composite shell rotor along with the motor/generator unit are assumed to be placed into a sealed vacuum chamber, which provides serious problem with heat transfer, produced by rotor losses [20]. The main parameters of the flywheel prototype given for two different shell material variants (see Table 1) are collected and presented in Table 2.

3.1. Flywheel design

The flywheel shell composite material data are collected and presented in Table 1. The advanced composite materials were selected to reduce cost as much as possible and achieve desired performances. During performed simulations, two variants of proposed materials were considered. In both cases, the most important factor was resistance against to stress, deformation of the material, radial displacement, and the rotor strength for wide range of rotational speeds. Particularly, the composite material properties for the both considered variants A and B can be found in datasheets.

Table 1. Summary of different variants of materials for composite rotor

	variant A	**variant B**
carbon fibre	without impregnation	impregnated with resin (CFRP)
fiberglass	type ECR	type S
aluminium	6060-T6; 7020	6082-T6; 7075-T6
steel	E590K2; 1.4034	E590K2; 1.4122
POM	C	H
magnet	neodymium sintered	neodymium tied W4

Table 2. Summary of the results of calculations for various variants of composite rotor

	variant A		**variant B**	
mass [kg]	25.56		24.01	
volume [m^3]	0.01		0.01	
density [kg/m^3]	2496.20		2344.67	
outer radius [mm]	136		136	
inner radius [mm]	84		84	
height [mm]	256		256	
moment of inertia [$kg \cdot m^2$]	0.29		0.27	
rotation speed [r/min]	15 000	30 000	15 000	30 000
linear speed [m/s]	213.52	427.04	213.52	427.04
the angular velocity [rad/s]	1570	3140	1570	3140
angular acceleration [rad/s^2]	26.17	52.33	26.17	52.33
torque [Nm]	7.68	15.35	7.21	14.42
power [KW]	12.06	48.2	11.32	45.3
kinetic energy [MJ]	0.36	1.46	0.34	1.36

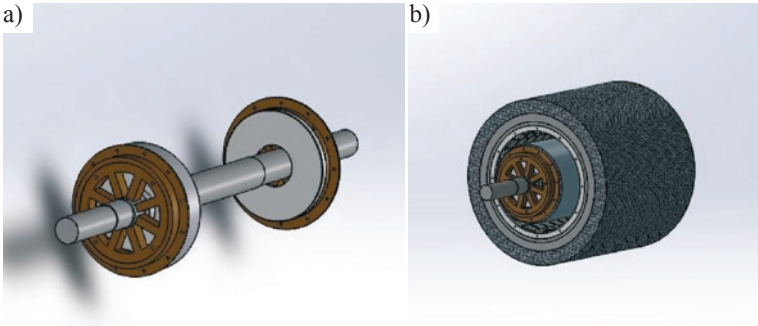

Fig. 3. SolidWorks models: a) AMB rotor, b) composite shell flywheel

In the meantime, preliminary studies were performed with associated with the power of the motor/generator, the stored kinetic energy and torque. The results are shown in Table 2.

As we can see mechanical properties of both variants of the materials are similar. Design and stress analysis of both material sets are needed to determine the maximum energy densities and shape factors of the flywheel rotor. In particularly, usage of the material will be undertaken after material stress calculations results for the desired rotational speed range.Ic Figure 3a presents the AMB rotor and Figure 3b shows the flywheel with composite shell designed in SolidWorks.

4. System modelling

In this section, the simulation models of photovoltaic (PV)-array and UPS flywheel are presented. The calculations and simulations results are given according to PV–array measured characteristics, long-cycle time response of charging and discharging of the PV–flywheel, and structural calculations of the composite rotor for desired rotational speed range. Modelling of the PV–flywheel system integration was realized using Matlab/Simulink® software. Simulink/Simscape tools and libraries are used to create a virtual model of the system dynamics. Modelling of composite rotor and structural calculations were made using SolidWorks.

4.1.1. Simulation model and calculation results

The photovoltaic panels model is created using tools from the Simscape library. The PV model presents photovoltaic array and allows determining connection method (series or parallel).

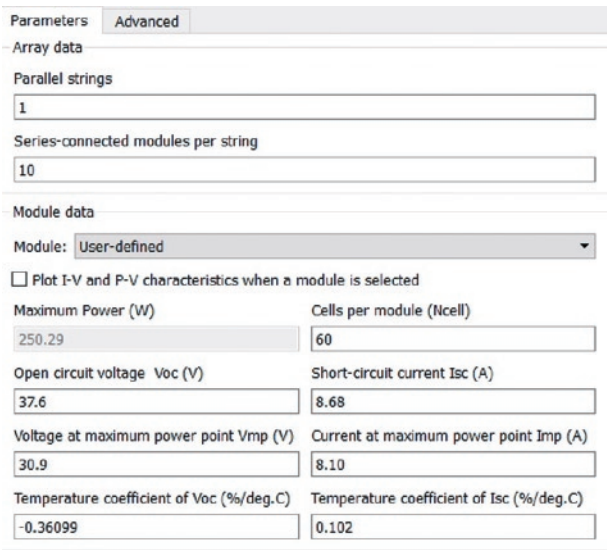

Fig. 4. PV–array model block settings

Moreover, this model also allows to determine the photovoltaic panel's parameters (Fig. 4). The main parameters were chosen based on the PV datasheets. The PV simulation model enables to change default parameter for more suitable by the user (user-define).

The PV model also allows conducting a preliminary study of the whole photovoltaic solar system. For example, this preliminary study includes current and power of PV system due to voltage and temperature change. These results are presented in Fig. 5, where given relations between voltage vs power, and voltage vs current provide useful information about PV system performances.

Another analysis according to PV parameter design is given

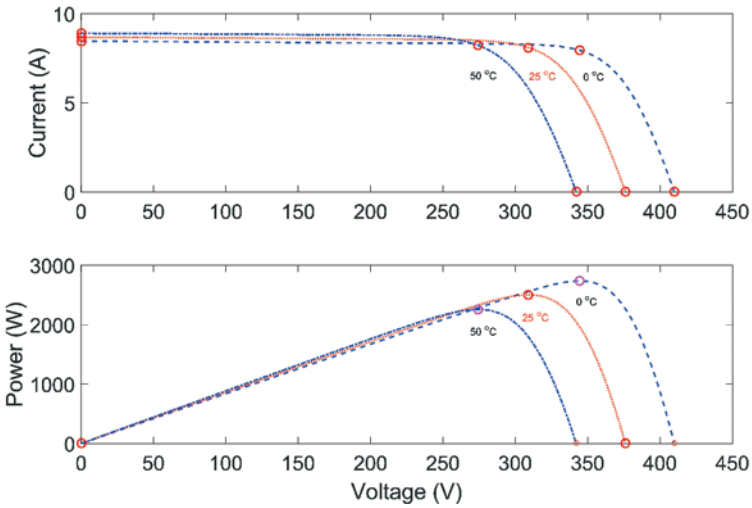

Fig. 5. Preliminary study of PV–array

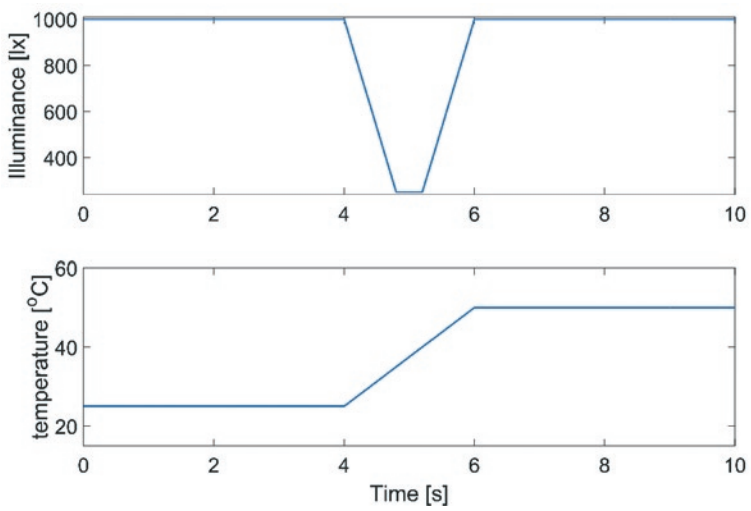

Fig. 6. Designed PV array input signals

for luminescence and temperature response in the time-domain. In particularly, the PV–array model block contains two inputs: I_r – light intensity, and T - temperature. The first parameter, light intensity, allows to simulate changes of the weather conditions and cycle of day and night. Second parameter represents temperature which allows increasing performance of the simulation. In our case, for the selected PV system, the designed reference of I_r and T are plotted in Fig. 6.

In case of the PV power system modelling, which consists of the AMB flywheel, the sufficient model of electric motor/generator is performed. We considered the motor/generator model and signals

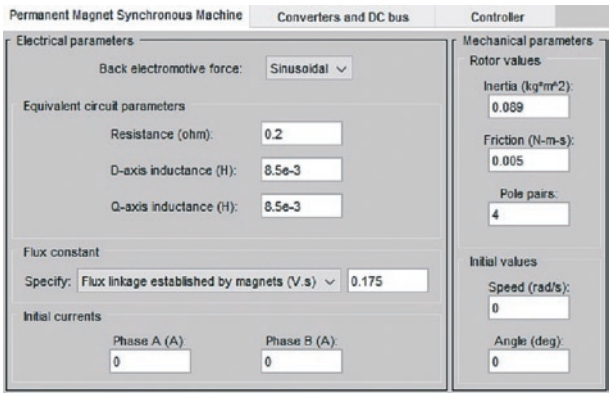

Fig. 7. Dialog window with motor configuration

connections with the flywheel core parameters (i.e. moment of inertia, angular speed, etc.). Simulink/Simscape library was used to design dynamic model of the electric motor/generator. However, this motor/generator model should be fully compatible with other system components. Particularly, the model contains control system which enables the bypass control logic inverter. The model block of PM synchronous motor drive (with major parametrization presented in Fig. 7) gives the ability to configure the motor parts as well as allows to configure the control system. PM synchronous motor drive includes the ability to work as generator.

The motor/generator dynamics are given as result of following governing equations:

$$\frac{d}{dt}i_d = \frac{1}{L_d}V_d - \frac{R}{L_d}i_d + \frac{L_q}{L_d}p\omega_m i_q \tag{5}$$

$$\frac{d}{dt}i_q = \frac{1}{L_q}V_q - \frac{R}{L_q}i_q - \frac{L_d}{L_q}p\omega_m i_d - \frac{\lambda p\omega_m}{L_q} \tag{6}$$

$$T_e = 1.5p\left[\lambda i_q + (L_d - L_q)i_d i_q\right] \tag{7}$$

where: – inductances in q and d axes respectively, – resistance of the stator windings, – currents in q and d axes, – voltages in q and d axes, – angular velocity of the rotor, – amplitude of the flux inducted by the permanent magnets of the rotor in the stator phases, – number of pole pairs, – electromagnetic torque.

The model of the entire system composed of the motor/generator dynamics Eqs. (5–7), all mentioned components and signal blocks al-

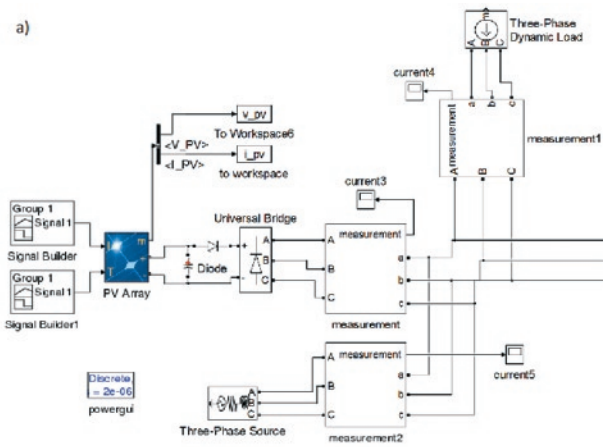

Fig. 8. Simscape model of PV– flywheel storage system: a) photovoltaic system

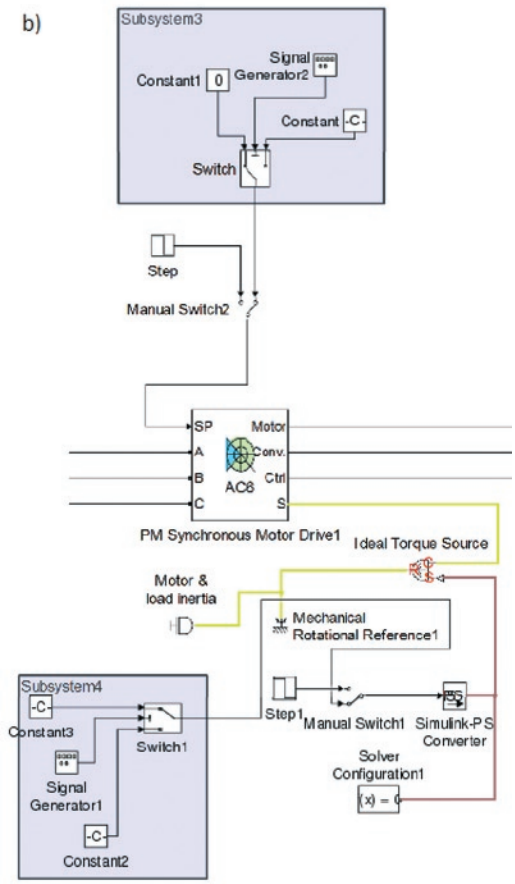

Fig. 8. Simscape model of PV– flywheel storage system: b) PM synchronous motor/generator

low to provide control system simulation. In this simulation the reference input values such as illumination and additional measurement blocks are used to analyse the correctness of operation of the system.

The whole simulation model is presented in Fig. 8, and total amount of elements is divided into two subsystems: photovoltaic model (Fig. 8a) and PM synchronous motor/generator (Fig. 8b). Main parts of the PV model are: PV array, system diodes and universal bridges, and as well as designed models of electric signals measurements. The outputs of the photovoltaic solar system (Fig. 8a) are connected to the inputs of the PM motor (Fig. 8b). The model of motor/generator includes both electric and mechanical signals measurements and control as torque, rotational speed, etc.

4.2. Simulation results

Simulation of the PV–flywheel system should be performed for two time different periods. The short period about 10 sec and long period representing a complete cycle of operation. Due to the long–time simulation and large amount of computer memory needed to analyse the data received during of the simulation is limited to 120 sec, where 5 sec for each represents a time unit (120/5=24 hours as a day/night cycle). During the simulation mode, the motor/generator is charged regularly every 10 sec, in order to investigate effects of charging and discharging of the system. The obtained results for long-time simulations as system outputs: torque, rotational speed and currents, are presented in Fig. 9.

As shown in Fig. 9, visible changes in the timing of positive to negative values indicate charging/discharging modes of the motor/generator operations. These modes provide significant drops in flywheel speed.

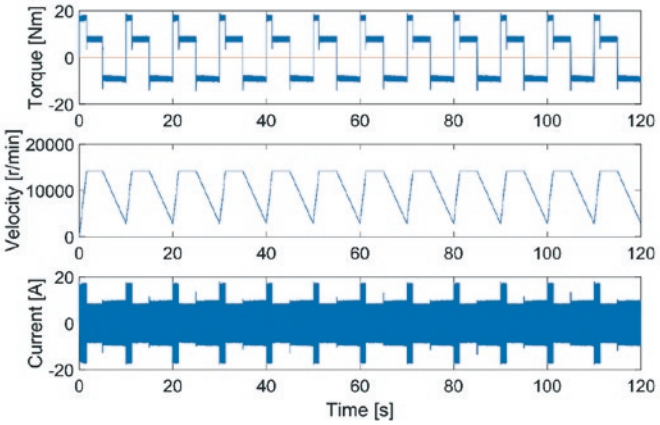

Fig. 9. Graph obtained by long-time simulation with charging and discharging of the PV–flywheel

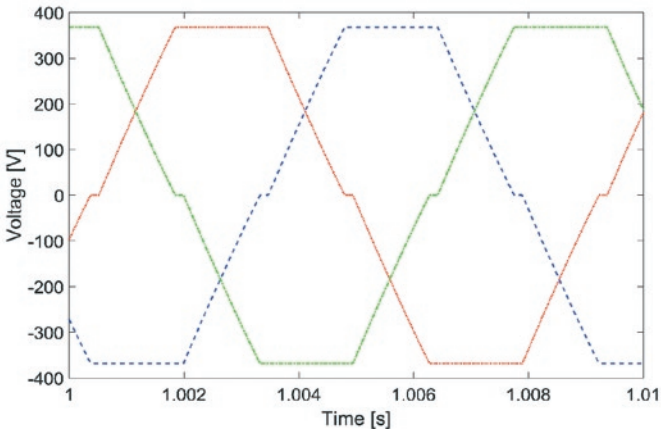

Fig. 10. Voltage waves generated by the photovoltaic panels at zoom

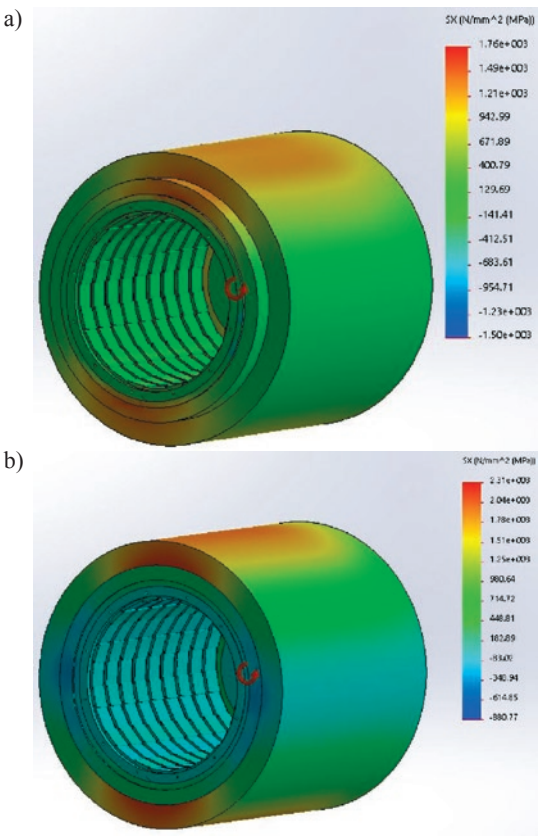

Fig. 11. SolidWorks results for normal stress in X axis: a) material A, b) material B

The current time responses (Fig. 9) prove that motor/generator operation is stable at the acceleration moments of the flywheel. In the simulation model the PV–flywheel is connected simultaneously to the power grid. Therefore, during the simulation of the photovoltaic panels operation is not possible to see any loses due to changes in light intensity. The PV-array generated output voltage waves for fixed time-window is presented in Fig. 10.

4.3. Structural calculations of flywheel shell

In this section, the shell structural calculations were carried out for the material variants A and B using SolidWorks. The radial stress results for maximum rotational speed 60 000 rpm are given in Fig. 11.

Figure 12 presents the SolidWorks cross section view of normal stress distribution in X axis. Based on obtained results given in Fig. 11 and Fig. 12, one can conclude, that in case of material A the maximum stress value is much less compared with material B. The maximum stress values are obtained for the flywheel rotational speed limit and equals 1 760 MPa and 2 310 MPa for shell material sets A and B respectively. Based on the stress distribution (Fig. 11 and 12) we can predict how much each shell of material set-ups A and B will expand in the radial direction.

The simulation calculations given in Fig. 11 show also that the variant A is a better option than B. The maximum value of stress for

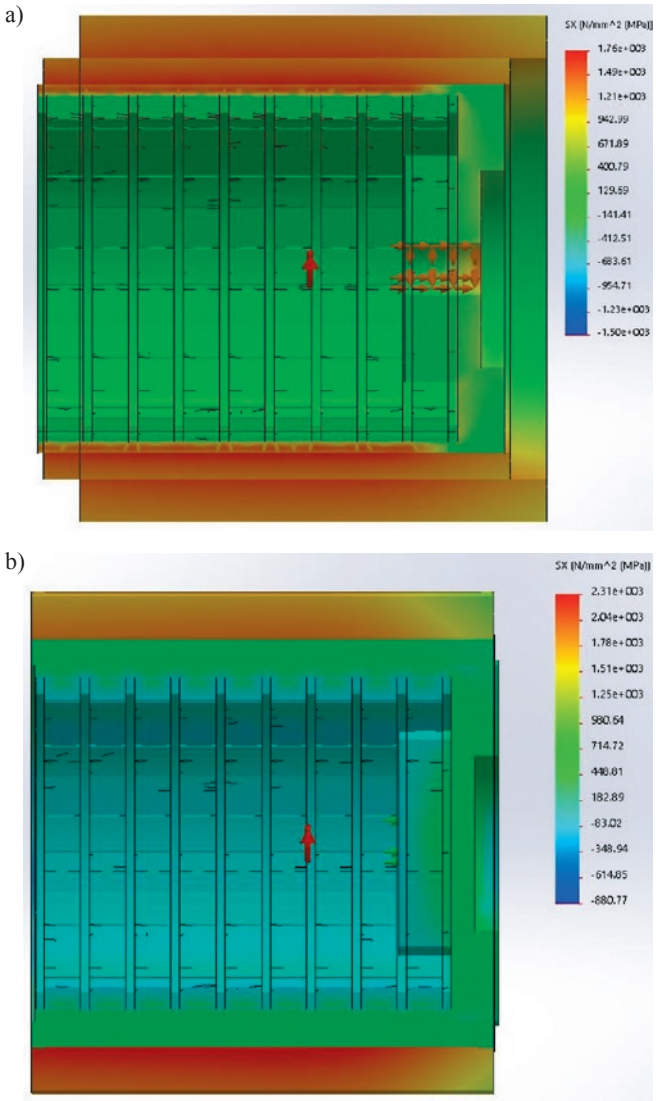

Fig. 12. SolidWorks cross section view of normal stress distribution in X axis: a) material A, b) material B

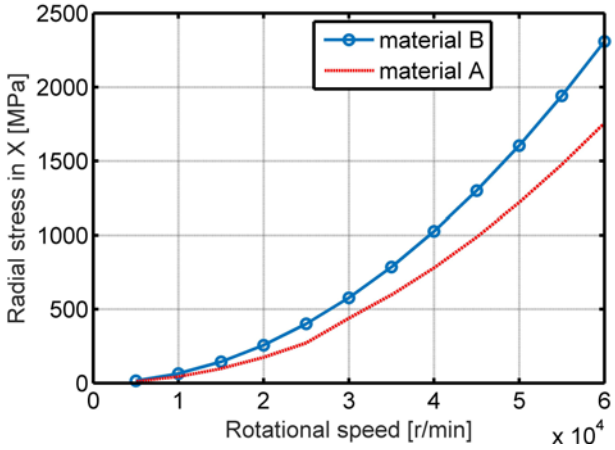

Fig. 13. Radial stress vs rotational speed in the X axis

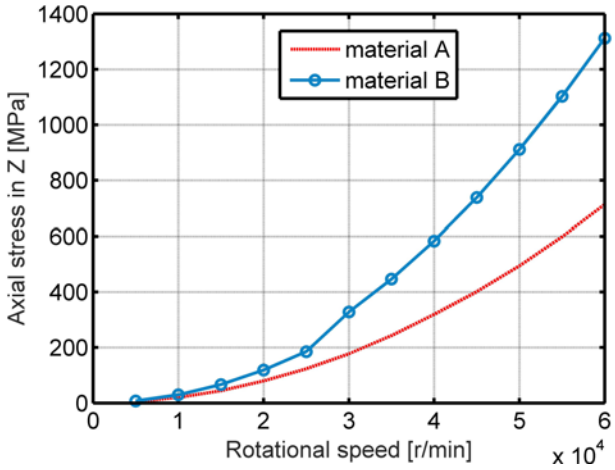

Fig. 14. Axial stress vs rotational speed in the Z axis

material B is higher, and their scope is larger compared with material A.

Next, simulation results are given according to radial stress versus rotational speed (Fig. 13 and Fig. 14).

In addition, after exceeding 25 000 r/min there is a sudden increase in the value of stress, and the flywheel variant A is deformed, while material set-up B remains the same, see Fig. 12a.. This is caused by lower ratio of tensile strength of the materials used in the embodiment A. The simulation show good cooperation between the photovoltaic system and electromechanical uninterruptable power supply.

5. Experimental investigations

In this section the AMB flywheel pre-prototype and its experimental results are given according to energy storage investigations. The proposed AMB flywheel is designed and fabricated during the research grant [18].

The flywheel energy storage system (FESS) is designed to run in vacuum and is supported on low-energy controlled active magnetic bearings (AMBs). The total storage energy capacity is approx. 5 MJ which is achieved at the maximum rotational speed equal to 20 000 rpm. Total mass of the rotor with the composite shell equal to 150 kg. Two integrated synchronous (3 pole pairs and 3 phases) motors/generators of total 100 kW power density are performed to operate the flywheel. These motor/generators' cores consists of lamination sheets and permanent magnets mounted on outer rotor. Motor/generators are controlled by electronic inverters using the FPGA controllers. The flywheel ratio of the moments of inertia I_z/I_x equal to 2.28/5.75 kgm^2.

Table 3. Parameters of the AMBs

parameter	radial AMBs	axial AMB
nominal width of air gap	0.4 mm	0.7 mm
bias current	5 A	5 A
maximum current	10 A	10 A
number of coils	8	2
displacement stiffness	2.6e6 N/m	9.1e6 N/m
current stiffness	208 N/A	1.2e3 N/A

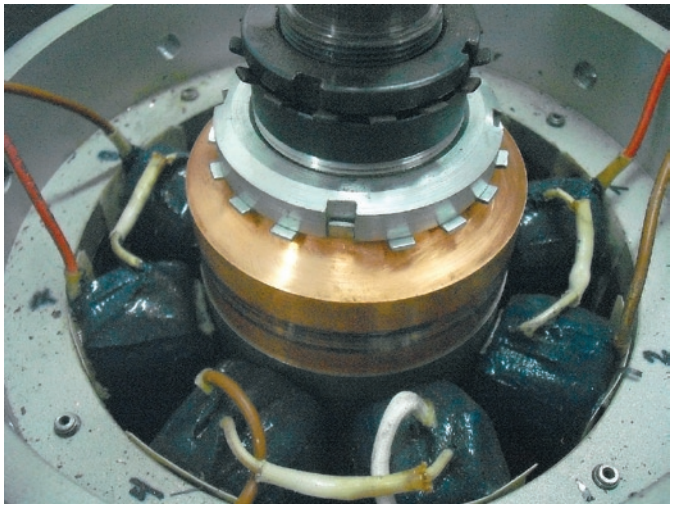

Fig. 15. Radial AMB of flywheel pre-prototype

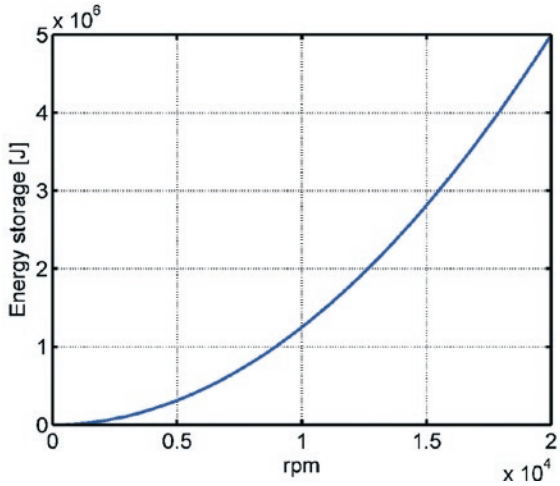

Fig. 16. Energy storage vs flywheel rotational speed range

The position control of the 5 DOF (degree of freedom) flywheel is realized by active magnetic bearings in the closed-loop configuration. The low bias-current PD control algorithm with anti-wind up filter is realized. Each of the radial magnetic bearing has 8 electromagnets which are connected to 4 pairs in serial configuration. The magnetic bearings parameters are presented in Table 3.

The radial AMB of pre-prototype flywheel is given in Fig. 15. The flywheel rotor radial and axial displacements are measured by using 5 eddy-current proximity sensors. The axial bearing (thrust bearing) carriers the weight of the rotor. The radial and axial AMBs are supplied by controlled 10-chanells current PWM amplifiers. The maximal current of the AMB is equal to 10 A. The flywheel-rotor position digital control system is realized in the real time. The control algorithm was

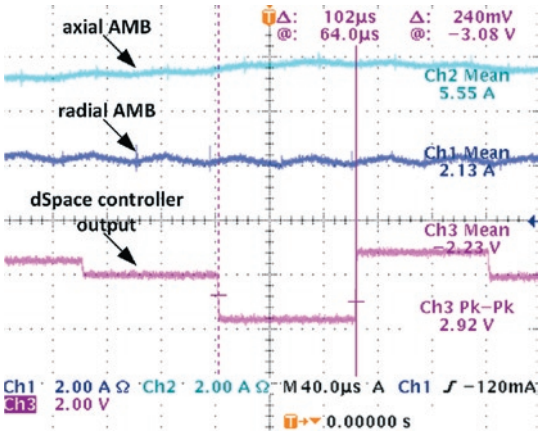

Fig. 17. AMB currents during the flywheel stand-alone

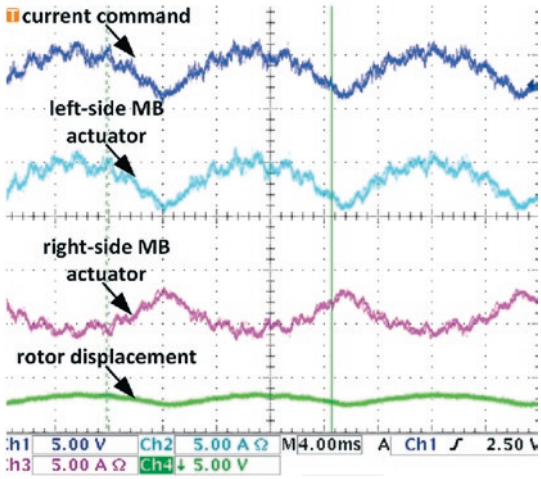

Fig. 18. AMB currents during the flywheel operation at 5 300 rpm

implemented in digital signal processor (DSP) dSpace. The sampling frequency of the AMBs controllers equal to 10 kHz. For more details of AMB flywheel configuration please refers to [11, 12, 18].

For given flywheel mass and moment of inertia, the calculated total energy storage characteristic is given in Fig. 16.

A stable levitation of the FESS rotor was achieved successfully. The measured results of total AMB currents and control command signal are shown in Fig. 17. The mean value of total current supplied to the radial AMBs is about 2 A, where thrust AMB operates at 5.55 A.

Next results are given for flywheel operation at angular speed of 5 300 rpm. The measured currents in one radial AMB bearing are given in Fig. 18. Also, Fig. 18 presents the current command and flywheel-rotor displacement signals. In this case, AMB output currents oscillate around the bias current with the absolute amplitude up to 2.5 A. The obtained currents waves are caused by the flywheel-rotor unbalance. However, in spite of rotor unbalance and disturbances caused by the flywheel energy charging and discharging, the stable flywheel operation is achieved successfully. Thus, measured total consumed power during the AMB flywheel operation is below 0.4 kW.

6. Conclusions

In this paper, a PV–flywheel integration system for household purposes has been designed and investigated. Photovoltaic systems suffer from the memory effect, which significantly increases the cost of exploitating such systems. This report has shown that the use of alternative magazines, such as an electromechanical flywheel, significantly reduces operating costs, proving that solutions of this kind are advantageous, and eliminates the memory effect occurring in the common energy reserve. Due to smooth cooperation of electromechanical flywheels and photovoltaic systems, integration of these devices is not a major problem. Integration of the photovoltaic system is possible for each type of uninterruptable power supply; however, in some cases it may be unprofitable. Surroundings of photovoltaic panels, such as tall buildings or trees, were not taken into account during designing of the installation, but they can affect the performance of the actual system.

In order to obtain an efficient system for household purposes with high energy densities and high energy power, the combination of a composite flywheel integrated with a photovoltaic system is required. Designing of this system includes: PV parameter calculations, design and strength computations of the flywheel, and integration.

Acknowledgment

This work is supported with University Work no S/WM/1/2016 of Department of Automatic Control and Robotics, Bialystok University of Technology also supported with Polish Ministry of Science and Higher Education (MNiSW) and by the Academy of Finland 270012 and 273489 and by Academy of Lithuania.

References

1. Abbezzot C., Tran T., Poggi P., Serre-Combe P., Perrin M. and Muselli M., Using a flywheel associated to PV power plant in order to increase the integration of PV into island electrical grid, International Conference on Renewable Energies and Power Quality (ICREPQ'13,) Bilbao (Spain), 20–22 March, 2013.
2. Abrahamsson J., Hedlund M., Kamf T. and Bernhoff H., High-speed kinetic energy buffer: optimization of composite shell and magnetic bearings, IEEE Trans. Ind. Electron., 2014; 61(6): 3012–3021, http://dx.doi.org/10.1109/TIE.2013.2259782.
3. Cavallaro C., Musumeci S., Santonocito C. and Pappalardo M., Smart photovoltaic UPS system for domestic appliances, Proc. of IEEE-ICCEP 09, 9–11 June 2009, Capri, 699–704, http://dx.doi.org/10.1109/iccep.2009.5211952.
4. Daryl R.B. and William D.C., Flywheel energy storage: an alternative for batteries in UPS systems, Energy Engineering: Journal of the association of Energy Engineering, 2005; 102(5): 7–26.
5. De Andrade R., Stephan R.M. and Sotelo G.G., Third generation of flywheels: a promising substitute to batteries, Eletronica de Potencia, 2008; 3, 171–176.
6. Giaconia G.C., Fiscelli G., et all., Integration of distributed on site control actions via combined photovoltaic and solar panels system, Clean Electrical Power, 2009 International Conference on, 9–11 June 2009, 171–177.
7. Kamf T., High speed flywheel design: using advanced composite materials, M.S. thesis, Div. Elect., Uppsala Univ., Uppsala, Sweden, 2012.
8. Kan H.P., Chau K.T. and Cheng M., Development of a doubly salient permanent magnet motor flywheel energy storage for building integrated photovoltaic systems, Proc. of the 16th Applied Power Electronics Conference, 4–8 March 2001, Anaheim, CA, 314–320, http://dx.doi.org/10.1109/apec.2001.911666.
9. Mohd A., Ortjohann E., Schmelter A., Hamsic N. and Morton D., Challenges in integrating distributed energy storage systems into future smart grid, Proc. IEEE Int. Symp. Ind. Electron., 2008; 1627–1632, http://dx.doi.org/10.1109/isie.2008.4676896.

10. Molina M.G., Distributed energy storage systems for applications in future smart grids, Transmission and Distribution: Latin America Conference and Exposition (T&D-LA), 2012 Sixth IEEE/PES, 3–5 Sept. 2012, 1–7.
11. Mystkowski A., Energy saving robust control of active magnetic bearings in flywheel, Acta Mechanica et Automatica, 2012; 6, no 3(21): 72–76.
12. Mystkowski A. and Rowinski R., Construction and control of AMBs high speed flywheel, Archive of Mechanical Engineering, 2011; 58(1): 79–89, http://dx.doi.org/10.2478/v10180-011-0005-7.
13. Nagorny A., Dravid N., Jansen R. and Kenny B., Design aspects of a high speed permanent magnet synchronous motor/generator for flywheel applications, in Proc. IEEE International Conference on Electric Machines and Drives, May 2005, 635–641, http://dx.doi.org/10.1109/iemdc.2005.195790.
14. Navarro G., Torres J., Moreno-Torres P. and Blanco M., Technology description and characterization of a low-cost flywheel for energy management in microgrids, Power Electronics and Applications (EPE'15 ECCE-Europe), 2015 17th European Conference on, 8–10 Sept. 2015, Geneva, 1–10.
15. Noshadi A., Shi J., Lee W.S., Shi P. and Kalam A., System identification and robust control of multi-input multi-output active magnetic bearing systems, IEEE Transactions on Control Systems Technology, 2016; 24 (4), 1227–1239, http://dx.doi.org/10.1109/TCST.2015.2480009.
16. Noshadi A., Shi J., Lee W.S., Shi P. and Kalam A., Robust control of an active magnetic bearing system using H∞ and disturbance observer-based control, Journal of Vibration and Control, 2015, http://dx.doi.org/10.1177/1077546315602421.
17. Pena-Alzola R., Sebastian R., Quesada J. and Colmenar A., Review of flywheel based energy storage systems, in Proc. POWERENG'11, May 2011, 1–6, http://dx.doi.org/10.1109/powereng.2011.6036455.
18. Pirog S. and Gosiewski Z., eds., Electromechanical, high-speed, stationary energy store, project no PBZ-KBN-109/T-10/2004, supported by Polish Ministry of Science and Higher Education, 2010; in Polish, 1–306.
19. Smith S., Sen P., and Kroposki B., Advancement of energy storage devices and applications in electrical power system, in Proc. IEEE Power and Energy Society General Meeting, July 2008, 1–8, http://dx.doi.org/10.1109/pes.2008.4596436.
20. Sokolov M.A, Jastrzebski R.P., Saarakkala S.E., Hinkkanen M., Mystkowski A., Pyrhönen J., Pyrhönen O., Analytical method for design and thermal evaluation of a long-term flywheel energy storage system, The 23rd International Symposium on Power Electronics, Electrical Drives, Automation and Motion, 22-24 June 2016, Anacapri, Capri Island, Italy, pp. 270–275. (DOI: 10.1109/SPEEDAM.2016.7525911)
21. Tant J., Geth F., Six D., Tant P. and Driesen J., Multiobjective battery storage to improve PV integration in residential distribution grids, IEEE Trans. Sustain. Energy, 2013; 4(1): 182–191, http://dx.doi.org/10.1109/TSTE.2012.2211387.
22. Vazquez S., Lukic S., Galvan E., Franquelo L., Carrasco J., Leon J., and Hilton J., Recent advances on energy storage systems, in Proc. IEEE 37th IECON, Nov. 2011, 4636–4640.
23. Yali Y., Yuanxi W. and Feng S., The latest development of the motor/generator for the flywheel energy storage system, in Proc. MEC'11, Aug 2011, 1228–1232, http://dx.doi.org/10.1109/mec.2011.6025689.
24. Zondag H.A., Van Helden W.G.J., PV-thermal domestic systems, Proc. of 3rd World Conference on Photovoltaic Energy Conversion, May 11–18, 2003 Osaka, Japan, 2000–2003.

Michal SMOLINSKI
Tomasz PERKOWSKI
Arkadiusz MYSTKOWSKI
Automatic Control and Robotics, Mechanical Engineering Department, Bialystok University of Technology
ul. Wiejska 45A, 15-351 Bialystok, Poland

Egidijus DRAGAŠIUS
Darius EIDUKYNAS
Faculty of Mechanical Engineering and Design
Kaunas University of Technology
Studentu str., 56-321 Kaunas, Lithuania

Rafal P. JASTRZEBSKI
LUT Energy, Lappeenranta University of Technology
Skinnarilankatu 34, 53850 Lappeenranta, Finland

E-mails: michal.smolinski@onet.eu, tomperk2@gmail.com, a.mystkowski@pb.edu.pl, egidijus.dragasius@ktu.lt, darius.eidukynas@ktu.lt, Rafal.Jastrzebski@lut.fi

Article citation info:
GRYGIER D. The impact of operation of elastomeric track chains on the selected properties of the steel cord wires. Eksploatacja i Niezawodnosc – Maintenance and Reliability 2017; 19 (1): 95–101, http://dx.doi.org/10.17531/ein.2017.1.13.

Dominika GRYGIER

THE IMPACT OF OPERATION OF ELASTOMERIC TRACK CHAINS ON THE SELECTED PROPERTIES OF THE STEEL CORD WIRES

WPŁYW EKSPLOATACJI GĄSIENIC ELASTOMEROWYCH NA WYBRANE WŁASNOŚCI DRUTÓW STALOWEGO KORDU*

The track running systems enable movement of heavy vehicles on unpaved and rough terrain, snow-covered, marshy or swampy surfaces, as well as overcoming natural or artificial barriers. The important structural component of the elastomeric tracks is a steel cord sunk in the elastomer creating the tread with the purpose of stiffening the structure, maintaining its proper deflection and giving the adequate resistance to tensile forces. The results of the studies presented in the work have shown that operation of the elastomeric track chains in conditions where they are continuously exposed to contact with foundation, frequent braking and bumping against roughness lead to damage of the steel cord material and a change in its mechanical properties.

***Keywords**: elastomeric track, cord, pearlitic steel.*

Gąsienicowe układy bieżne umożliwiają poruszanie się ciężkich pojazdów po powierzchniach nieutwardzonych oraz w trudnym terenie, zaśnieżonym, bagnistym lub grząskim, a także pokonywanie przeszkód naturalnych i sztucznych. Ważnym elementem konstrukcyjnym gąsienic elastomerowych jest stalowy kord, zatopiony w elastomerze tworzącym rzeźbę bieżnika, ma on na celu usztywnienie konstrukcji, zachowanie jej właściwego ugięcia oraz nadanie odpowiedniej odporności na siły rozciągające. Wyniki badań prezentowanych w pracy wykazały, że eksploatacja gąsienic elastometrowych w warunkach, w których narażone są na ciągłą styczność z podłożem, częste hamowanie oraz uderzenia w nierówności prowadzi do uszkadzania materiału stalowego kordu i zmiany jego własności mechanicznych.

***Słowa kluczowe**: gąsienica elastomerowa, kord, stal perlityczna.*

1. Introduction

The track running systems enable movement of heavy vehicles on unpaved and rough terrain, snow-covered, marshy or swampy surfaces, as well as overcoming natural or artificial barriers [5, 7, 28]. This is possible by distributing the vehicle mass on greater surface which causes significant drop in unit pressure, increase in adherence of a vehicle and achieving greater driving force. The systems also improve quality of operation and maneuvering a vehicle in the difficult terrain conditions by reducing the rolling resistance and the tendency of a vehicle to sink.

The track is a closed band girding wheels and rolls of the track running system on the circumference of which four zones can be distinguished: the upper one rolled over tension rollers, the retaining one cooperating with the ground, since it determines the size of the resulting driving force necessary for the motion of the vehicle, and the two inclined ones contained between one of the support wheels and the drive wheel, as well as the carrier wheel and the directional wheel [5, 28]. The track chain bears all forces, vertical, longitudinal and transverse, appearing in contact of a vehicle with foundation. Due to the construction the metal, rubber-metal and elastomer tracks can be distinguished.

The elastomeric tracks are designed on the principle of the inner chain created by links responsible for carrying the drive from the driving wheel and preventing sliding the track off [5, 7, 28]. Additionally, the track is reinforced with steel cord sunk in elastomer creating the tread pattern aimed at stiffening the structure, maintaining its proper deflection and giving the proper resistance to tensile forces.

The cord is a structure composed of strands created by several intertwined individual wires. The cord may also be the strand itself made of several wires [3, 11, 16, 19, 20]. Individual wires have diameters from 0,15 to 0,38 mm, are produced as brass or zinc plated wires and have the following properties [16, 18, 19, 20]:

- very high dynamic module,
- high stiffness,
- high strength,
- low creep capacity,
- high compressive modulus,
- dimensional stability,
- high resonance frequencies.

Wires designated for production of steel cord reinforcing tracks are manufactured from unalloyed pearlitic steel. The pearlitic steels containing from about 0,70 to 0,95% C belong to the group of unalloyed steels of the quality class designated for cold drawing or rolling [1-3, 8, 11, 18, 20]. Their chemical composition and mechanical properties are in compliance with the PN-EN 10323:2006 (U) standard [12]. As standard the steel wires for cord are characterised with tensile strength within the range of 2573 to even 4116 MPa [11, 16].

One of the problems widely discussed in the subject literature is cracking of the pearlitic steel subjected to plastic working and during its operating [4, 18, 10, 14, 16]. The problem is the more serious that it concerns many industrial branches where the steel cord is applied and therefore it has been the subject of years of research conducted in numerous scientific centres all over the world [14, 25, 26, 31].

(*) Tekst artykułu w polskiej wersji językowej dostępny w elektronicznym wydaniu kwartalnika na stronie ***www.ein.org.pl***

The fatigue strength of steel wires greatly depends on metallurgical purity of the material, and especially on content of oxygen, silicon and sulphur. Presence of non-metallic inclusions in steel strongly decreases the fatigue resistance as it is around the impurities that the strong accumulation of stresses appear leading in effect to component cracking [1, 4, 11, 16, 20].

According to Golis [16] the maximum permissible content of non-metallic inclusions in unalloyed pearlitic steel of the D75, D78, D80 and D83 grades designated for production of cord wires should not exceed the size of the standard No. 2 according to EN 10247:2007 standard. The non-metallic inclusions, especially including those of minimum plasticity such as oxides or brittle silicates, cause lowering of the wire ductility hindering the technological processes. Presence of the inclusions constitutes the main reason for lowering the degree of the material deformation.

The research performed by Zelin [30] have shown that as a result of elastic deformations preceding the permanent plastic deformation of the material, the horizontal micro delamination of the single lamellae of cementite takes place. The changes were observed both, at tension and twisting of the wires. In the course of increasing the applied force the coalescence of the created micro delaminations follows and the cracking propagation resulting with decohesion of the whole component.

Sauvage and Ivanisenko [21, 22, 29] have shown that the cause of cracking of pearlitic steel subjected to plastic working is segregation of carbide precipitations at the phase boundaries. The studies have confirmed the theory earlier described by Gridnev and Gavriluk [15, 17, 20], according to which as a result of plastic deformation the carbon atoms occupy vacancies appearing in the cementite lattice, increasing by that the concentration of carbon atoms at the phase boundary ferrite-cementite and, as a consequence, resulting in brittleness of those structures. Both teams have shown the simple relation between the degree of plastic deformation and the susceptibility of the pearlitic steel to cracking. The deformation increase is accompanied by increase in the density of lattice defects and thus the intensity of carbide segregations at phase boundaries increases.

The structural analysis performed by Izotov et al. [23, 24] have unequivocally shown that cracking of the cementite lamellae follows as a result of dislocations pile-up at the phase boundary between ferrite and cementite precipitations. As a result of the applied force the movement of edge dislocations in the ferrite precipitation follows, as well as dislocation of crystal fragments over the slip planes and because the fact that each ferrite lamella has different crystallographic orientation the dislocations are crossing at the cementite lamellae initiating finally creation of microcracks. The studies have confirmed the earlier literature reports, the works of Langeford, Wilson, Embury and Fisher [12, 13, 31] indicating that in the course of plastic deformation of pearlitic steel it is just on the cementite lamellae that the strongest concentration of lattice defects appears which, in the consequence is the cause of cracking of these structural components.

The different theory explaining the mechanism of cementite lamellae cracking was presented by Languillaume et al. [27]. According to his research, as a result of plastic pearlite deformation the uncontrolled, very strong increase in energy at the contact of both phases takes place, i.e. in the inter-lamellar spaces of pearlite. The observed increase in energy leads to thermodynamic destabilisation of cementite resulting in cracking of its lamellae. The results of this research have been confirmed many times by the other research teams including Danoix and Sauvage [9, 29, 31].

2. Purpose and object of the tests

The elastomeric track chains of mini excavators are exposed during operation to continuous contact with base, frequent breaking and numerous strokes against roughness. Such working conditions may lead to damaging the material of the steel cord constituting stiffening of the track structure and, as a consequence, to a change in its functional properties. The results of questionnaires conducted among Lower Silesian companies of general building have shown that the average life of the elastomeric tracks applied in mini excavators is about 825 moto-hours, and the most frequent cause of their damage is rupture of the steel cord resulting in breaking continuity of the tread (Fig. 1).

The fractographic tests of wires from the defective steel cord performed using the scanning electron microscope have shown the presence of surfaces indicating for fatigue character of the damage (Fig.2). The fatigue part of the fracture was smooth with the characteristic fatigue striae arranged almost parallel to the direction of crack development. The fracture origin was localised at the external edge of the wire, i.e. in the area of the highest accumulation of the complex operating stresses. At the external circumference of the wire fractures the immediate zone of the plastic character and the expanded surface topography were visible. Thus, the results of those analyses have shown that damages were not created as a result of the operating overload of the tracks, but as a result of another factors causing decrease in the fatigue strength in the cord wires.

The research results presented in the work aimed to determining the impact of the elastomeric track operation in general purpose mini excavators on structure and selected mechanical and technological properties of the pearlitic steel applied to the wires of their cord.

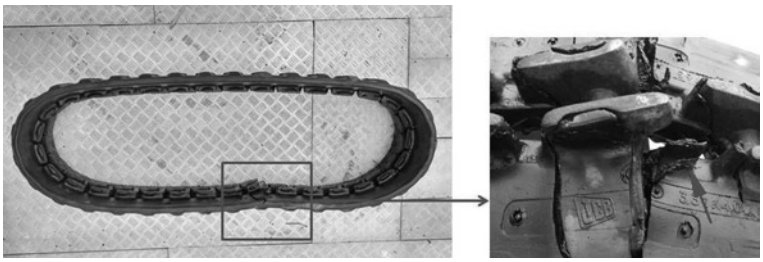

Fig. 1. Defective elastomeric track coming from mini excavator model 8018 CTS from JCB. Visible fragment of the steel cordu, which punched the layer of rubber and led to damaging the tread (see arrow)

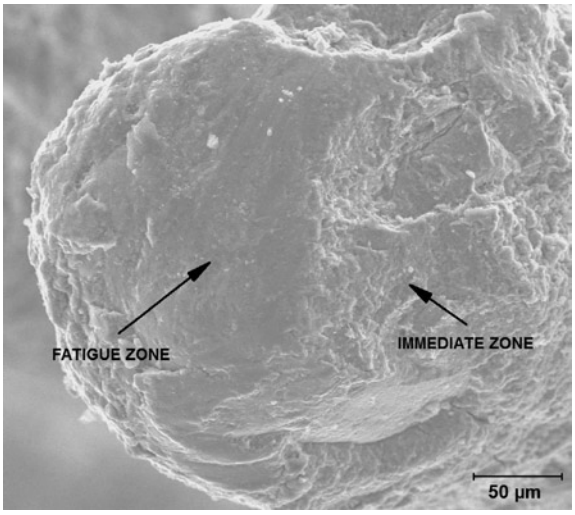

Fig. 2. Microscopic image of fatigue fracture of the wire coming from the track shown in Fig. 1. Visible smooth fatigue zone and the IMMEDIATE ZONE of the expanded surface topography. SEM

Fig. 3. Mini excavator model 8018 CTS from JCB, from which the tested elastomeric tracks came

Fig. 4. Schematic diagram of the steel cord shown in Fig. 3, visible seven strands of 0,9 mm in diameter

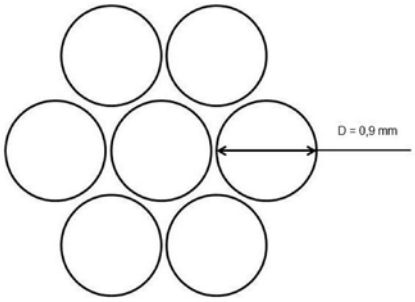

Fig. 5. Schematic diagram of the steel cord shown in Fig. 3, visible seven strands of 0,9 mm in diameter.

The object of the research were two elastomeric track chains of the 332/L5153 type coming from mini excavators from JCB, model 8018 CTS (Fig. 3). The tested tracks were differing with the degree of wear, the track No. 1 was the new sample, without operation, and the track No 2 was the sample in the after-operation state used for the general building for the period of 1228 moto hours.

For evaluating the impact of elastomeric track operating on structure and the selected mechanical properties of pearlitic steel the wire samples of d = 0,3 mm diameter were collected from the steel cord. Macroscopic tests of the type of the applied reinforcement have shown that in all tracks 36 lines of the steel cord appear arranged in two parallel layers of 18 lines each (Fig. 4). Each of the cord lines is built of 7 identical strands of 0,9 mm diameter. One of them is a core on which the remaining strands are wrapped in the form of one layer (Fig. 5). A line of the cord is wrapped in the right direction. All strands are built of 12 wires of 0,3 mm in diameter and consist of one convolution wire and two layers wrapped. The strand is made with wrapping in the left direction.

For microscopic tests in the etched and non etched states the NIKON ECLIPSE MA200 light microscope with the NIS Elements BR software was used, and the observations were conducted at magnification from 100x to 1000x. The observations of microstructures of the tested steel were performed also with application of the JEOL JSM 6610A scanning electron microscope at magnifications from 1000× to 10 000×. In course of the studies the accelerating voltage of 15 and 25 kVW was used. The observations were conducted in the material contrast using the SE detectors.

Hardness measurements of the specimens were performed with the Vickers method with the use of the MMT-X3 micro hardness meter in conditions complying with the PN-EN ISO 6507-2:1999 standard. The measurement time was 15 s and the load was 500 g.

The static tensile test was performed in conditions compliant with the PN-EN ISO 6892-1:2010 standard. The tests were performed at the MTS 858 Mini Bionix type testing machine. The specimens were made of wire of the initial measurement length L_0 = 100 mm. The tensile tests were performed with constant stretching rate controlled by the rate of straining (method A according to the standard) and amounting to e_{Lc} = 0,0067 1/s until the rupture. The basic strength properties of the material were determined: the tensile strength R_m and necking Z.

Analysis of technological properties involved the test of unidirectional turning and the test of bidirectional contraflexure of wires taken from the cord. The test of unidirectional turning was performed in conditions compliant with the PN-ISO 7800:1996 standard, which is the trial aimed at determining suitability of the material to the production processes. It involves turning the loaded wire around its own axis in one direction until rupture of the specimen. The tested specimens had length in accordance with the PN-ISO 7800:1996 standard and the applied load did not exceed 2% of the nominal load breaking the wire.

The trial of bidirectional contraflexure according to PN-ISO 7801: 1996 is applied to determining the resistance of wires to plastic deformations. It involves multiple bidirectional contraflexure of a specimen by the angle of 90° around rolls of diameters defined in the PN-ISO 7801: 1996 standard. Both tests were performed with constant rate until fracture, the measurements were performed in the ambient temperature.

3. The test results

The macroscopic tests of the track No. 1 have shown that the contact surface of the track with foundation was ideally flat and the remnants of the production process were observed at surface of the trade in the form of linear shoulders (Fig. 6). Edges of the tread of the tested track were ended sharply and walls of the segments were uniform. Material of which the tested component was made was uniform and did not show symptoms of ageing and thickness of the tread was about 47 mm.

The macroscopic tests of the track No. 2, in the after-operating condition have shown that it bears significant traces of wear resulting from utilizing of the machine. At its working surface many changes and damages resulting from direct contact with hard basement have been observed (Fig. 7). Edges of the tread were significantly rounded, which influences the decreased traction of the machine during maneuvering in the slushy terrain. Another trace of operating were losses in the form of ripped pieces of rubber as well as cuts and undercuts

Fig. 6. The elastomeric track No. 1, the non-operated specimen. There are no cracks and damages at its surface, the tread edges are sharp and the segment walls are uniform, Visible remnants ot the production process in the form of linear shoulders

Fig. 7. The elastomeric track No. 2, the specimen in the after-operating state through the period of 1228 working hours. Numerous cracks and damages visible at the surface, the tread edges are significantly rounded and the tread is porous

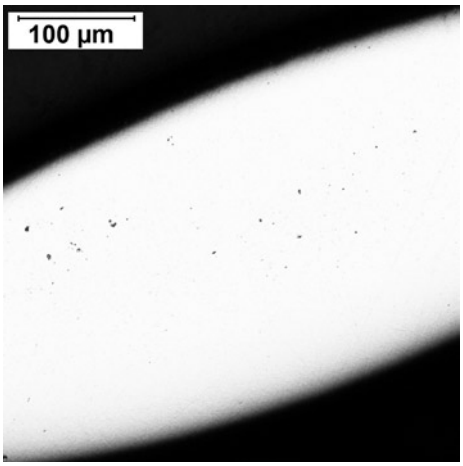

Fig. 8. Material of the cord wire from track No. 1, visible oxide non-metallic inclusions in the quantity equal to the standard 3 according to the PN-64/H-04510 standard. Non-etched state. Longitudinal section. LM

of the tread. The most important, and at the same time the most dangerous, symptom of the track wear were visible transverse cracks created as a result of maneuvering the vehicle around its own axis at the hard, e.g. concrete or asphalt surface. The surface of the tested track was porous and borne the traces of rubber ageing, its thickness amounted to about 40 mm.

Microscopic observations of the material of the tested wires performed in the non-etched state have shown presence of large amount of non-metallic inclusions, mainly in the form of oxides. The impurities were distributed punctually and appeared in the number from the standard 3 to 4 according to the EN 10247:2007 standard, which, according to the subject literature data [11, 16, 20] exceeds the maximum permissible content of non-metallic inclusions in the pearlitic steel designated for production of cord wires (Fig. 8 and 9). Fatigue strength of steel wires is greatly dependent on metallurgical purity of the material. Presence of that large number of non-metallic inclusions, especially in the form of brittle oxides, may cause lowering of material ductility making the technological processes difficult, and in particular cases leading even to cracking of the wires during operation.

The microscopic tests have shown that all the tested wires, according to recommendations of the PN-EN 10323:2005 (U) standard, were made of the unalloyed pearlitic steel and the applied cold drawing process disabled achieving the high degree of plastic deformation of the 80–90% row (Fig. 10 and 11). The initial microscopic tests have not shown significant differences in the structure of the tested samples but further observations with application of the scanning electron microscopy have shown the clear influence of operating on structure of the tested material (Fig. 12 and 13). Results of the microstructure analysis have shown that during operation of the track chain the material of steel cord is destroyed. Presence of numerous structure discontinuities oriented in line with the plastic working of the material was observed caused by presence of non-metallic inclusions in the tested materials (Fig. 13).

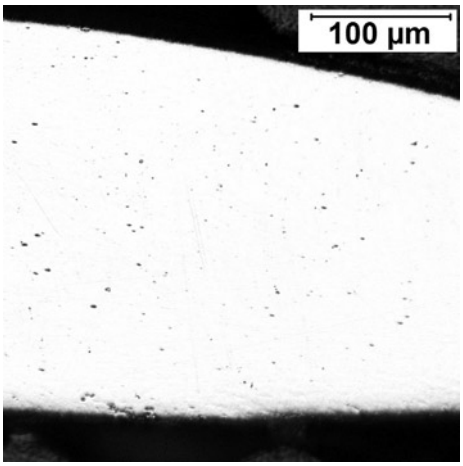

Fig. 9. Material of the cord wire from track No. 2, visible oxide non-metallic inclusions in the quantity equal to the standard 4 according to the PN-64/H-04510 standard. Non-etched state. Longitudinal section. LM

Results of these studies have confirmed the Golis theories [16] on negative impact of non-metallic inclusions on strength of the cord wires, as well as the theory of Zelin [30] indicating that the main cause of cracking of the pearlitic steel subjected to operating are micro delaminations created between the cementite lamellae. The obtained results

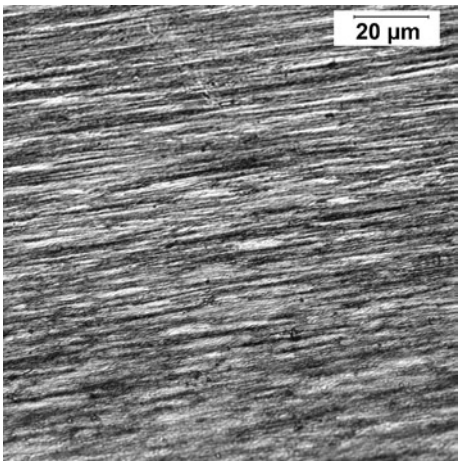

Fig. 10. Microstructure of the wire sample coming from cord of the new track No. 1. Visible strong material deformation texture amounting to about 90%. Longitudinal section. LM

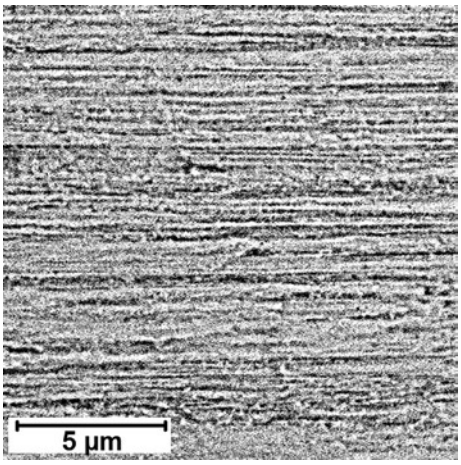

Fig. 11. Microstructure of the wire sample coming from cord of the new track No. 2 Visible strong material deformation texture amounting to about 80%. Longitudinal section. LM

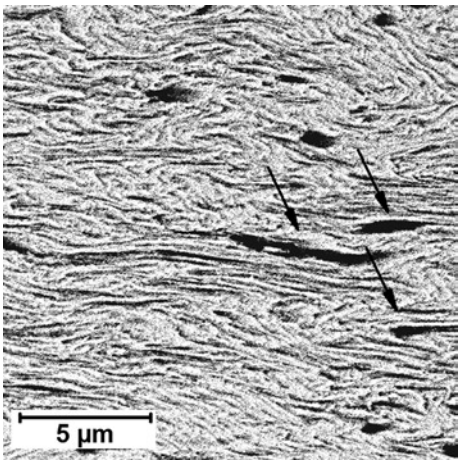

Fig. 12. Microstructure of the wire sample coming from cord of the track No. 1, not operated. Visible strong material deformation texture created as a result of cold drawing. Longitudinal section. SEM

have shown that around impurities the material discontinuities are created capable of exceeding the critical size of the defect and causing the wire cracking. The process can have the following course:

- micropores are created at plastic deformation around non-metallic inclusions,
- at proceeding the plastic deformation the micro pores grow and approach each other,
- when the bridges between pores become narrow they are breaking in sequence,
- as a result of micro bridges breaking the coalescence of discontinuities follows in the direction perpendicular to the acting load,
- as a result of discontinuities coalescence the pores created around the non-metallic inclusions reach the size of the critical defect at which the cracking develops unstably and leads to the fatigue damage of a component.

The results of strength tests have shown that the structure discontinuities observed in the microscopic tests significantly influence the mechanical and technological properties of wires (Table 1). The effect of operating the elastomeric track, the specimen No. 2, is clear drop in strength properties of the wires of its cord. The tensile strength for the wire sample coming from the cord of the non-operated track No. 1 amounted to about 3430 MPa, and for the wire sample coming from the track No. 2 – 2050 MPa. The material is less tough, which results from the fact, that during the static tensile test the discontinuities located around the non-metallic inclusions grow in the perpendicular direction to the acting load and accelerate destruction of the wire sample.

Table 1. Results of mechanical properties measurements for the tested wire samples.

SAMPLE	$Rm_{śr}$ [MPa]	$Z_{śr}$ [%]	$HV_{śr}$ 0,5
WIRE FROM THE TRACK NO. 1 CORD	3430 ± 100	15 ± 2	742 ± 20
WIRE FROM THE TRACK NO. 2 CORD	2050 ± 100	18 ± 2	621 ± 20

Table 2. Results of the technological trials on the tested wires.

SAMPLE	AVERAGE NUMBER OF ROTATIONS IN THE TORSION TEST	AVERAGE NUMBER OF CONTRAFLEXURES IN THE FLEXING TEST
WIRE FROM THE TRACK NO. 1 CORD	171 ± 10	103 ± 10
WIRE FROM THE TRACK NO. 2 CORD	84 ± 5	38 ± 5

At the same time, it has been observed in the results of the strength tests that the plasticity of the material increased. The narrowing from the value of 15% for the new specimen increased to 18% for the specimen in the after-operating state. The narrowing in the operated specimen is most probably related not to the increase in the material plasticity but with annihilation of material discontinuities observed in the microscopic tests.

The significant decrease in hardness of the material from after-operating specimens also seems interesting. The measurements have been performed for materials collected directly from the track cord. Hardness for the wire sample from the new track was equal to 742 HV0,5, and for the wire sample from the after-operating track it dropped to the value of about 621 HV0,5 (Table 1). The hardness drop can be explained by presence of discontinuities in the structure of the tested wires. Increase in the material porosity directly converts to decrease in hardness.

As a result of the performed technological trials of unidirectional torsion and bidirectional contraflexure of the tested wires it has been found that the increase in necking observed in the previous tests on the operated specimens definitely is not related to increase in plasticity of the material (Table 2). The plasticity of the material clearly drops, the number of turns in the torsion test falls from 171 to 84, and the number of contraflexures in the test decreases from 103 to the value of 38. Thus, this confirms the assumption that the increase of necking in the operated specimen is not related to the improvement in plasticity, but is a result of annihilation of the created material delaminations.

4. Conclusions

In the recent years the ever growing demand is observed for the fast and reliable transport means additionally characterised with large loading capacity. Pneumatic tires for cars, delivery trucks lorries, busses and agricultural or mining machines, or the specialist building equipment cannot be further reinforced with yarn, viscose or nylon. For strengthening tyres, track chains, conveyor belts, as well as the pressure hoses the high resistance wires made of unalloyed pearlitic steels

are currently applied. Unfortunately, one of the problems widely discussed in the subject literature is cracking of the pearlitic steels during the operating.

Results of the fractographic tests of the defective track chain have shown that frequent breakage of the steel cord wires continuity in the general building practice is not the result of its improper operation. The fatigue character of the fracture should not be attributed to the way and time of operation but directly from the metallurgical quality of the cord wire material.

There is plenty of theories describing causes of pearlitic steel cracking during operation. According to Golis [16], the fatigue strength of the cord wires is greatly dependant on the degree of contamination of the material with non-metallic inclusions, and particularly on the content of oxides, silicates and sulfides. The Author clearly indicates that the maximum permissible content of non-metallic inclusions in the unalloyed pearlitic steel of the D75, D78, D80 and D83 grades designated for production of cord wires must not exceed the size of the standard No. 2, according to the EN 10247:2007 standard.

Microscopic observations of the cord wire material coming from the tested track chains performed in the non-etched state have shown the presence of large number of non-metallic inclusions, mainly in the form of oxides. The impurities were distributed punctually and appeared in quantities from the standard 3 to 4 according to the EN 10247:2007 standard. At the same time, results of further microscopic analysis have shown that during operation of the tracks the material of the steel cord is clearly eroding. The presence of numerous structure discontinuities was observed and the detailed microscopic analysis has shown that around the brittle oxides precipitations the micro pores are created, which with the progress in plastic deformation are growing and approach to each other reaching the ever growing sizes.

In the work of Zelin [30] it can be read that as a result of the elastic deformations the horizontal micro delaminations of the individual cementite lamellae are created. During operation the cord wires are subjected to the complex state of stresses in the elastic range, which explains the fact, that the observed structure discontinuities were oriented in parallel to the cementite lamellae arranged in bands.

The consequence of the observed structural changes in the material of the tested cord wires was the significant decrease in the strength and technological properties. The drop in the tensile strength resulted from the fact, that during the static tensile test the discontinuities located around the non-metallic inclusions are growing in the perpendicular direction to the acting load and after reaching the size of the critical defect accelerate damage of the wire sample. The same relationship explains the results of the technological tests of unidirectional torsion as well as bidirectional contraflexure. Results of both trials indicate for a decrease in the material plasticity as a result of its operating, which is the consequence of annihilations of the described material discontinuities. The decrease in hardness can also be explained by presence of discontinuities in the structure of the tested wires. The longer the material was subjected to operation the porosity of the material was growing, translating directly to the decrease in its hardness.

References

1. Adamczyk J. Inżynieria materiałów metalowych. Gliwice: Wydawnictwo Politechniki Śląskiej, 2004.
2. Ashby MF, Jones DRH. Engineering Materials: An Introduction to Microstructures Processing and Design. Oxford: Elsevier, 2005.
3. Ashby MF, Jones DRH. Engineering Materials: An Introduction to Microstructures Application and Design. Oxford: Elsevier, 2005.
4. Berisha B, Raemy C, Becker C, Hora P. Multiscale modeling of failure initiation in a ferritic–pearlitic steel, Acta Materialia, 2015; 100: 11-18, https:/doi.org/10.1016/j.actamat.2015.08.035.
5. Burdziński Z. Teoria ruchu pojazdu gąsienicowego. Warszawa: Wydawnictwa Komunikacji i Łączności, 1972.
6. Cieśla M, Herian J, Junak G. Influence of pearlite morphology on creeping characteristic curves of R260 steel, Key Engineering Materials, 2014; 598: 39-44, https:/doi.org/10.4028/www.scientific.net/KEM.598.39.
7. Czabanowski R. Numeryczna analiza obciążeń wybranych elementów podwozia z gąsienicami elastomerowymi, Przegląd Mechaniczny, 2010; 7(8): 30-36
8. Czarski A, Skowronek T, Matusiewicz P. Stability of a Lamellar Structure – Effect of the True Interlamellar Spacing on the Durability of a Pearlite Colony, Archives of Metallurgy and Materials, 2015; 60(4): 2499-2503, https:/doi.org/10.1515/amm-2015-0405.
9. Danoix F, Julien D, Sauvage X, Copreaux J. Direct evidence of cementite dissolution in drawn pearlitic steels observed by tomographic atom probe, Materials Science and Engineering: A, 1998; 250(1): 8-13, https:/doi.org/10.1016/S0921-5093(98)00529-2.
10. De Knijf D. Optimization and characterization of a quenching and partitioning heat treatment on a low carbon steel, Book of Abstracts Modern Steels MS2014 Poland, 2014: 21-22
11. Dobrzański LA. Materiały inżynierskie i projektowanie materiałowe. Warszawa: WNT, 2006.
12. Embury JD, Fisher RM, The structure and properties of drawn pearlite, Acta Metallurgica, 1966; 14: 147-159, https:/doi.org/10.1016/0001-6160(66)90296-3.
13. Fedorko G, Molnar V, Ferková Ž, Tomašková M. Possibilities of failure analysis for steel cord conveyor belts using knowledge obtained from non-destructive testing of steel ropes, Engineering Failure Analysis, 2016; 67: 33-45, https:/doi.org/10.1016/j.engfailanal.2016.05.026.
14. Feng F. Texture inheritance of cold drawn pearlite steel wires after austenitisation, Materials Science&Engineering, 2014; 618(A): 14-21.
15. Gavriljuk VG. Decomposition of cementite in pearlitic steel due to plastic deformation, Materials Science and Engineering, 2003; 345(A): 81-89.
16. Golis B, Błażejowski Z, Pilarczyk JW. Druty stalowe do zbrojenia opon. Częstochowa: Wydawnictwo Wydziału Metalurgii i Inżynierii Materiałowej, 1998.
17. Gridnev VN, Gavriljuk VG, Meshkov YY. Strength and plasticity of cold-worked steel. Kiev: Naukova Dumka, 1974.
18. Grygier D, Rutkowska-Gorczyca M, Jasiński M, Dudziński W. The structural and strength changes resulting from modification of heat treatment of high carbon steel, Archives of Metallurgy and Materials, 2016; 61(2B): 971-976, https:/doi.org/10.1515/amm-2016-0165.
19. Grygier D, Rutkowska-Gorczyca M. Influence of operating conditions of the steel cord on the structure and selected mechanical and technological properties of high carbon steel, International Journal of Engineering Research & Science, 2015; 2(4): 1-6.
20. Grygier D. Analysis of the causes of damage to the wires of the steel belt of car tires, Interdisciplinary Journal of Engineering Sciences, 2016; 4(1): 45-49.
21. Ivanisenko Y, Lojkowski W, Valiev RZ, Fecht HJ. The mechanism of formation of nanostructure and dissolution of cementite in a pearlitic steel during high pressure torsion, Acta Materialia 2003; 51(18): 5555-5570, https:/doi.org/10.1016/S1359-6454(03)00419-1.

22. Ivanisenko Y, Sauvage X. The role of carbon segregation on nanocrystallization of pearlitic steels processed by severe plastic deformation, Journal of Material Science 2007; 42: 1615-1621, https:/doi.org/10.1007/s10853-006-0750-z.
23. Izotov V.I., at. all, Influence of a pearlite fineness on the mechanical properties, deformation behavior and fracture charcteristic of carbon steel, The Physics of Metals and Metallography 2007; 106, 5.
24. Izotov VI, Pozdnyakov VA, Luk'yanenko EV, Usanova OYu, Filippov GA. Study of slightly etched fracture surface of a perlitic-ferritic steel by scanning electrom microscopy, The Physics of Metals and Metallography 2007; 103(5): 519-529, https:/doi.org/10.1134/S0031918X07050122.
25. Knut A M, Ekh M, Brouzoulis J, Ahlström J. Modeling evolution of anisotropy in pearlitic steel during cold working, 28th Nordic Seminar on Computational Mechanics NSCM-28 Tallin 2015: 111-114.
26. Kulikowski K, Szpica D. Determination of directional stiffnesses of vehicles' tires under a static load operation, Eksploatacja i Niezawodnosc – Maintenance and Reliability 2014; 16(1): 66-72.
27. Languillaume J, Kapelski G, Baudelet B. Cementite dissolution in heavily cold drawn pearlitic steel wires Acta Materialia 1997; 45(3): 241-245, https:/doi.org/10.1016/S1359-6454(96)00216-9.
28. Mendygrał Z. Encyklopedia Techniki Wojskowej. Warszawa: Wydawnictwo Ministerstwa Obrony Narodowej, 1978.
29. Sauvage X, Thily L, Blavette D. Microstructure evolution during drawing of a pearlitic steel containing 0.7 st.% copper Scripta Materialia 2002; 46: 459-464, https:/doi.org/10.1016/S1359-6462(02)00002-7.
30. Zelin M. Microstructure evolution in pearlitic steels during wire drawing Acta Materialia 2002; 50: 4431–4447, https:/doi.org/10.1016/S1359-6454(02)00281-1.
31. Zhang M-X, Kelly PM. The morphology and formation mechanism of pearlite in steel Material Characterization 2009; 60: 545-554.

Dominika GRYGIER
Wrocław University of Science and Technology
Department of Materials Science, Strength and Welding Technology
ul. Smoluchowskiego 25, 50-3720 Wrocław, Poland
E-mail: dominika.grygier@pwr.wroc.pl

Article citation info:
ZALESKI K. The effect of vibratory and rotational shot peening and wear on fatigue life of steel. Eksploatacja i Niezawodnosc – Maintenance and Reliability 2017; 19 (1): 102–107, http://dx.doi.org/10.17531/ein.2017.1.14.

Kazimierz ZALESKI

THE EFFECT OF VIBRATORY AND ROTATIONAL SHOT PEENING AND WEAR ON FATIGUE LIFE OF STEEL

WPŁYW KULKOWANIA WIBRACYJNO – ROTACYJNEGO I ZUŻYWANIA STALI NA TRWAŁOŚĆ ZMĘCZENIOWĄ*

The paper reports the experimental results of investigation of the effect of tribological wear of C45 steel specimens subjected to grinding and vibratory and rotational shot peening on their fatigue life. The study also investigated the effect of wear on surface roughness and the distribution of residual stresses in the surface layer of the tested specimens. Counterspecimen pressure on the specimen was variable during the wear process. Fatigue life was investigated on a specially constructed test stand enabling cyclic bending of the tested specimen. It was found that increasing the counterspecimen pressure leads to an increase in surface roughness and fatigue life as well as generates undesired residual stresses. The negative effects of tribological wear were more visible for the specimens subjected to grinding than for those which were exposed to vibratory and rotational shot peening.

***Keywords**: vibratory and rotational shot peening, wear, surface roughness, residual stresses, fatigue life.*

W pracy przedstawiono wyniki badań doświadczalnych wpływu zużywania tribologicznego próbek ze stali C45, szlifowanych oraz kulkowanych wibracyjno – rotacyjnie, na trwałość zmęczeniową. Badano też wpływ zużywania na chropowatość powierzchni oraz rozkład naprężeń własnych w warstwie wierzchniej badanych próbek. Parametrem zmiennym w procesie zużywania był nacisk przeciwpróbki na próbkę. Trwałość zmęczeniową badano na specjalnym stanowisku, umożliwiającym cykliczne zginanie badanej próbki. Stwierdzono, że ze wzrostem nacisku przeciwpróbki następuje pogorszenie chropowatości powierzchni, ukształtowanie mniej korzystnych naprężeń własnych oraz zmniejszenie trwałości zmęczeniowej. Negatywne skutki zużycia tribologicznego bardziej widoczne są dla próbek szlifowanych niż dla kulkowanych wibracyjno – rotacyjnie.

***Słowa kluczowe**: kulkowanie wibracyjno – rotacyjne, zużycie, chropowatość powierzchni, naprężenia własne, trwałość zmęczeniowa.*

1. Introduction

During their operation machine parts can be exposed to varying loads and, at the same time, to sliding or rolling contact with mating components. This leads to the fatigue of material of these parts and their surface wear.

One of the methods for improving operational properties of machine parts is the use of shot peening**.** A variant of dynamic burnishing, this process consists in impacting a surface with shot in the form of round steel, glass or ceramic particles. This impact leads to the hardening of the surface layer and the production of compressive residual stresses. The results of numerous studies demonstrate that the application of shot peening significantly increases the fatigue life of shot peened parts [2, 4, 16, 19]. This increase mainly results from the presence of compressive residual stresses in the surface layer of the workpiece. The findings of tests conducted by the positron annihilation method demonstrate that the distribution of residual stresses is connected with evolution of crystalline structure defects concentration [20]. As in the case of static burnishing, the effect of shot peening greatly depends on the properties of material subjected to shot peening, workpiece shape, geometrical structure of the surface prior to shot peening, tool design and technological parameters [5, 9, 18].

The geometrical structure of surface and physical properties of the surface layer affect the wear of interacting parts exposed to sliding or rolling [7, 10]. Wear, described as a process of changes in the surface layer of interacting solids, leading to mass decrement or permanent strain of the surface of these solids, can be caused by different factors, and thus can have different characteristics [6, 8, 11].

A more wear-resistant surface can be produced by subjecting it to static or dynamic burnishing. The application of some burnishing methods enables forming lubricant-accumulating cavities on the surfaces of frictionally interacting components. The results of studies on wear resistance of slide bearings demonstrate that the forming of a helical groove on the pin surface results in decreased wear [15]. Higher wear resistance, a lower friction factor and higher seizure resistance can be obtained by the application of oscillating burnishing that enables formation of a suitable system of lubricating microgrooves [13]. The presence of oil-accumulating cavities on the interacting surfaces has a positive effect on lubrication but, on the other hand, leads to an increase in unit pressure. It was found that seizure resistance depends on the distribution of lubricant-accumulating cavities and their shape [3]. In shot peening, the impact of shot impacting a surface leads to formation of microcavities which can serve as ”lubricant reservoirs.” The geometrical structure of surface formed during shot peening can also lead to the occurrence of adhesive ”attachments” [14].

Wear leads to changes in properties of the surface layer of interacting components, which can affect their fatigue life. Examples of kinematic nodes in which interacting components are exposed to tribological wear and fatigue of material due to varying loads are given in the work [17]. There are few studies which examine wear and fatigue life at the same time. The study [1] reports the results of wear and fatigue life of titanium alloys used for biomedical implants, while the work [12] investigates the effect of various methods of thermal

(*) Tekst artykułu w polskiej wersji językowej dostępny w elektronicznym wydaniu kwartalnika na stronie ***www.ein.org.pl***

and thermochemical treatment on the fatigue life and friction factor of Ti-6Al-4V alloy.

A survey of the literature reveals that previous research on the effect of vibratory and rotational shot peening on fatigue life did not take account of changes in surface layer properties caused by tribological wear during operation of the tested parts. The aim of this study is to determine the combined effect of vibratory and rotational shot peening and wear during sliding friction on the fatigue life of tested specimens.

2. Methodology

The experiments were performed on ring-shaped specimens made of annealed C45 steel and described by the dimensions given in Fig.1a. The chemical composition of the examined steel was as follows: carbon – 0.44%, manganese – 0.57%, silicon – 0.23%, phosphorus – 0.02%, sulfur – 0.03%, chromium – 0.18%, nickel – 0.25%, copper – 0.10%, iron – other. To ensure required surface accuracy, the specimens were subjected to grinding.

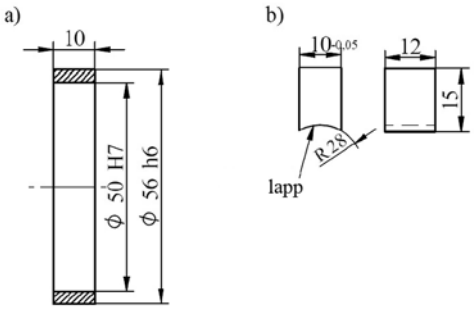

Fig. 1. Shape and dimensions of specimen (a) and counterspecimen (b)

The external surface of prepared specimens was subjected to vibratory and rotational shot peening on a test stand which is schematically illustrated in Fig. 2. The specimens 6 are fixed on a rotating mandrel 3, its bearings mounted in the walls of a working chamber 2. The working chamber is set into vibration by a vibrator 1 driven by an electric motor 10. The working chamber 2 contains shot (loose steel balls) 5 which is fed into it after removing a lid 4. Due to vibration of the working chamber, the shot 5 collides with the external surface of the specimens 6. The uniformity of treatment of the entire external surface of the specimens 6 is ensured by rotation of the mandrel 3,

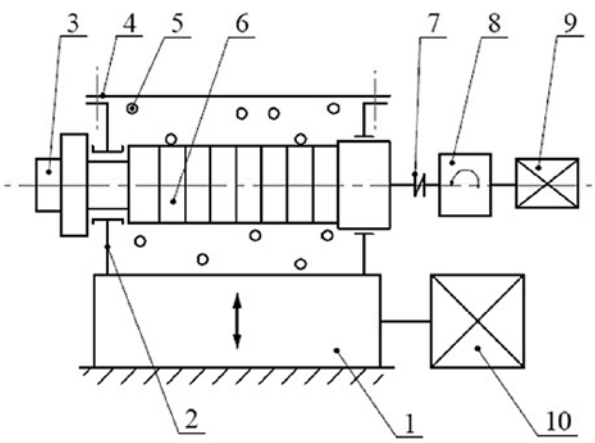

Fig. 2. Schematic design of the stand for vibratory and rotational shot peening tests: 1 – vibrator, 2 – working chamber, 3 – rotating mandrel, 4- lid, 5 – shot, 6 – specimen, 7 – elastic coupling, 8 – reducer, 9 – electric motor supplying power to mandrel, 10 – electric motor supplying power to vibrator

wherein the specimens are fixed. The mandrel 3 receives power from an electric motor 9 via a reducer 8 and an elastic coupling 7.

The technological parameters of the vibratory and rotational shot peening process were maintained constant at:

- vibration frequency of the vibrator, $\nu = 7$ Hz,
- vibration amplitude of the vibrator, $a = 60$ mm,
- time of shot peening, $t = 20$ min,
- shot diameter, $d_k = 6$ mm,
- rotational velocity of the workpiece, $n_k = 1.5$ rev/min.

Specimens subjected to grinding with vibratory and rotational shot peening were exposed to tribological wear on a test stand, the schematic design of which is shown in Fig. 3. A specimen 1 was fixed to a spindle 2 rotated with a velocity n. The external surface of the rotating specimen 1 was put under load of a counterspecimen 5 mounted in a chuck 6. Counterspecimens, the shape and dimensions of which are given in Fig. 1b, are made of cast iron EN-GJL-HB195. The pressure on the counterspecimen was applied by means of a lever 4 loaded using weights 3. The force F was changed by changing the weight of the weights 3.

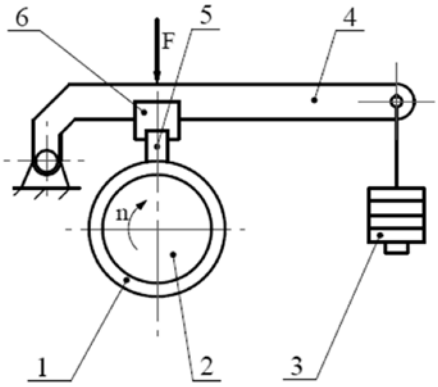

Fig. 3. Schematic design of a device for testing tribological wear: 1 – specimen, 2 – spindle, 3 – weights, 4 – lever, 5 – counterspecimen, 6 – chuck

The results of preliminary experiments helped determine the conditions for performing tribological tests. The constant parameters were the tangential velocity of the specimen, $v = 0.586$ m/s, and the friction path, $s = 10584$ m. The counterspecimen pressure on the specimen was variable and set to $p_1 = 1.92$ MPa and $p_2 = 3.73$ MPa. Lubrication was done using the HIPOL GL4 oil. Prior to the principal research, the specimen and counterspecimen were subjected to lapping. Following the wear, mass decrement in the specimens was measured (by comparing the difference in specimen mass prior to and after wear).

Worn and unworn specimens were divided into two batches. One was used for examining surface layer properties, the other – for comparative analysis of fatigue life. The surface layer was examined with respect to surface roughness (*Ra* parameter) and the distribution of residual stresses. The surface roughness parameter *Ra* was measured using the Surtronic 3+ roughness measuring instrument manufactured by Taylor Hobson. A selection of specimens was also subjected to 3D topography examination made using the T8000RC 120-140 device manufactured by Hommel – Etamic. The distribution of residual stresses was determined by mechanical method (measurement of strains after removal of subsequent layers of specimen material) using nitric acid solution etching.

The next stage of the study involved determination of the fatigue life of worn and unworn specimens after both vibratory and rotational shot peening and grinding. Fatigue life tests were performed on the test stand illustrated in Fig. 4. Prior to the tests, the specimens

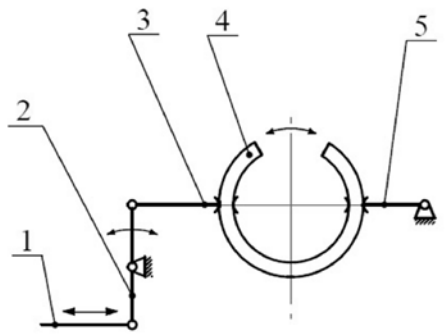

Fig. 4. Schematic design of a device for fatigue life tests: 1 – connecting rod, 2 – lever, 3 – left chuck, 4 – specimen, 5 – right chuck

were cut in order to remove a part of the ring in the specimen. Thereby prepared specimens were fixed in chucks 3 and 5. The motion of a connecting rod 1 generated by a lever 2 led to bending of the specimen 4. The testes were conducted at a constant amplitude of specimen strains. Fatigue life was measured as the number of contraflexures until specimen failure.

Each test was repeated seven times. Based on the results, mean and standard deviations were calculated.

3. Results

The investigation of surface roughness and residual stresses was conducted on specimens subjected to grinding and those subjected to grinding with wear as well as on specimens subjected to vibratory and rotational shot peening and those subjected to shot peening with wear.

The results of the surface roughness parameter *Ra* after grinding and after grinding with wear are illustrated in Fig. 5. The diagram gives mean values of the *Ra* parameter and the error columns show standard deviations. The wear of the ground specimens exposed to a pressure of 1.92 MPa led to a slight increase in *Ra* (by approx. 30%), while the wear at a pressure of 3.73 MPa led to a significant increase in surface roughness – the *Ra* parameter increased almost by three times (Fig. 5).

Fig. 6 shows the specimen surface topography after grinding while Fig. 7 shows the specimen surface topography following grinding with wear. One can notice visible marks of surface wear, particularly following wear under a pressure of 3.73 MPa.

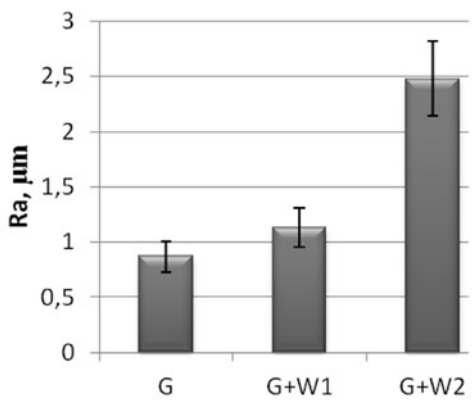

Fig. 5. Surface roughness parameter Ra after grinding (G), grinding with wear under pressures 1.92 MPa (G+W1) and 3.73 MPa (G+W2)

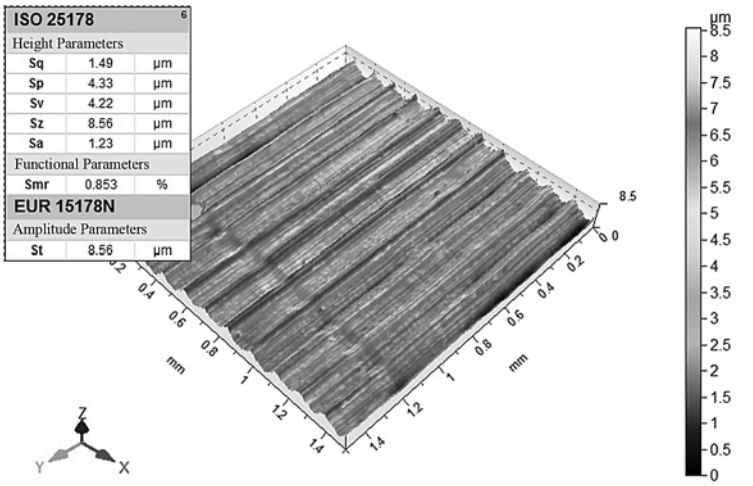

Fig. 6. Specimen surface topography after grinding

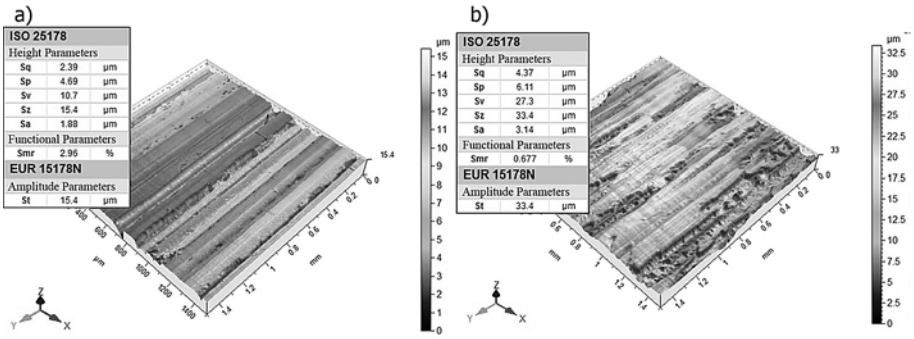

Fig. 7. Specimen surface topography after grinding with wear: a) pressure 1.92 MPa, b) pressure 3.73 MPa

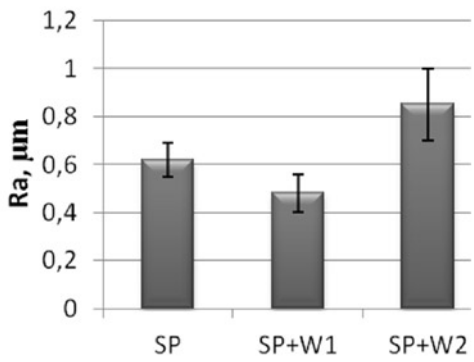

Fig. 8. Surface roughness parameter Ra shot peening after (SP), shot peening with wear under pressures 1.92 MPa (SP+W1) and 3.73 MPa (SP+W2)

The application of vibratory and rotational shot peening to the surface subjected to grinding led to decreasing surface roughness by approx. 30% (Fig. 8). The wear of shot peened surfaces had an insignificant effect on surface roughness. Wear at a pressure of 1.92 MPa resulted in a slight decrease in surface roughness, while wear under a pressure of 3.73 MPa led to a slight increase in surface roughness amounting to 37%.

Fig. 9 illustrates the specimen surface topography after shot peening whereas Fig. 10 shows the topography after shot peening and wear. The surface exposed to shot peening reveals the presence of microcavities produced due to the impact of shot (Fig. 9). As can be seen in Fig. 10a, the shot peening with wear at a pressure of 1.92 MPa

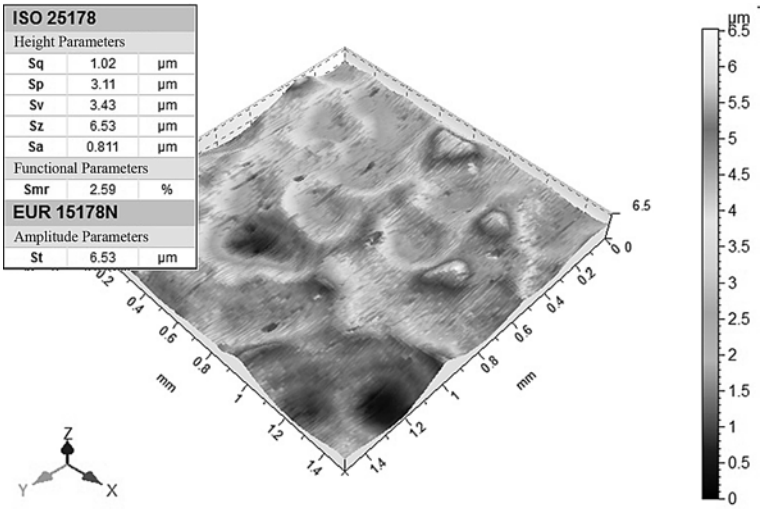

Fig. 9. Specimen surface topography after vibratory and rotational shot peening

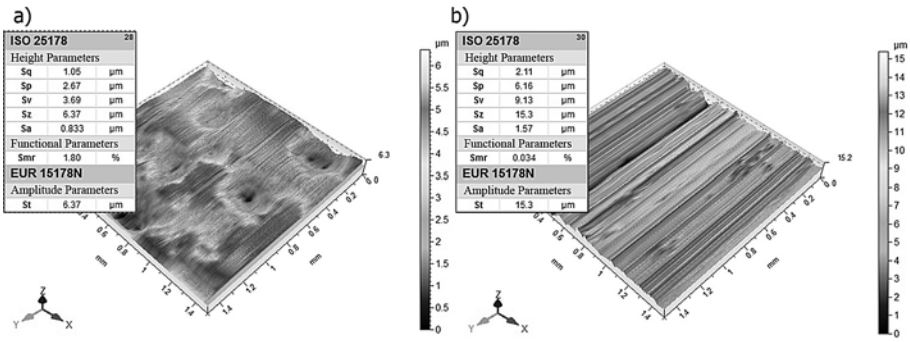

Fig. 10. Specimen surface topography after vibratory and rotational shot peening with wear: a) pressure 1.92 MPa, b) pressure 3.73 MPa

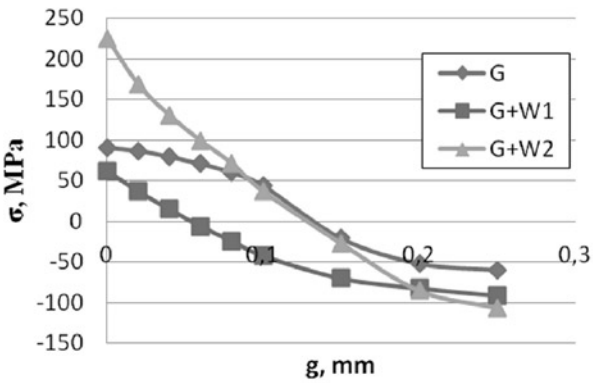

Fig. 11. Distribution of residual stresses σ at depth g in specimens exposed to grinding (G), grinding with wear at pressures 1.92 MPa (G+W1) and 3.73 MPa (G+W2)

did not cause total removal of the microcavities from the specimen surface. In contrast, the wear at a pressure of 3.73 MPa resulted in complete removal of microcavities while the traces of wear are more visible compared to the surface after wear under a smaller pressure (Fig. 10b).

The results demonstrate that balls impacting the specimen surface in vibratory and rotational shot peening form microcavities on the specimen surface where oil is accumulated during wear. The presence of oil reduces the direct impact of counterspecimen on the specimen, which has a positive effect on specimen surface roughness.

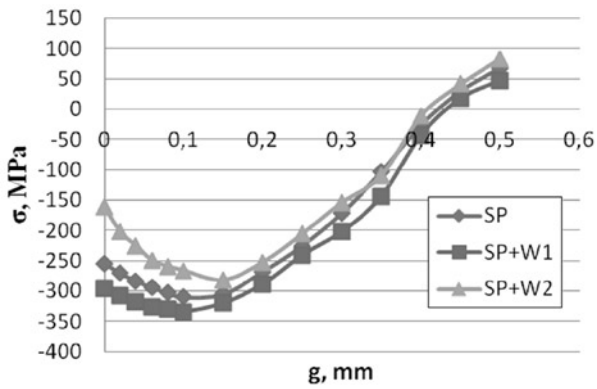

Fig. 12. Distribution of residual stresses σ at depth g in specimens exposed to shot peening (SP), shot peening with wear at pressures 1.92 MPa (SP+W1) and 3.73 MPa (SP+W2)

The distributions of residual stresses in the surface layer of the tested specimens are shown in Figs. 11 and 12. After grinding, the tensile residual stresses reach up to approx. 90 MPa and, at a depth of 0.13 mm, they change into compressive stresses. The wear of ground specimens at a pressure of 1.92 MPa resulted in a decrease in the tensile residual stresses, both their values and the depth of their location, while increasing the pressure to 3.73 MPa led to an over two-time increase in the tensile residual stresses (Fig. 11).

The application of vibratory and rotational shot peening led to formation of compressive residual stresses in the surface layer, with a maximum (absolute) value of about 300 MPa, at a depth of about 0.4 mm (Fig. 12). The wear of specimens subjected to shot peening at a pressure of 1.92 MPa did not cause any significant changes in the distribution of residual stresses, while in the specimens put under a pressure of 3.73 MPa, the compressive residual stresses decreased, particularly at the surface.

The increase in the tensile residual stresses in the specimens subjected to grinding and the decrease in the compressive residual stresses in the shot peened specimens due to wear at a pressure of 3.73 MPa can result from a larger amount of heat released during wear at higher pressures.

Fig. 13 illustrates the mass decrement due to wear of the specimens subjected to grinding and shot peening. One can observe a higher mass wear of the specimens subjected to grinding compared to shot peened specimens. This can be attributed to improved lubrication of the surface after grinding and, perhaps, to the hardening of the surface layer due to shot peening. The specimen wear also depends on the pressure exerted by the counterspecimen, which can particularly be observed in the case of specimens subjected to grinding (increase in pressure from 1.92 MPa to 3.73 MPa increases wear by three times).

Figs. 14 and 15 show the effect of wear on the fatigue life of specimens subjected to grinding and shot peening. The results reveal a positive effect of vibratory and rotational shot peening on fatigue life (over a three and a half increase compared to the ground specimens). The wear at a pressure of 1.92 MPa had little effect on fatigue life (it slightly decreases after the wear of specimens subjected to grinding), whereas increasing the counterspecimen pressure on the specimen to 3.73 MPa led to a significant decrease in its fatigue life – by 51% in the case of ground specimens, and by – 18% in the case of shot peened specimens. The decrease can be attributed to a

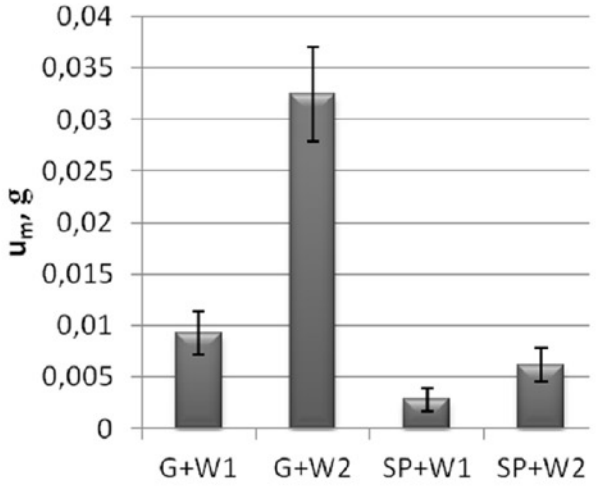

Fig. 13. Mass decrement u_m after grinding with wear at pressures 1.92 MPa (G+W1) and 3.73 MPa (G+W2) and after shot peening with wear at pressures 1.92 MPa (SP+W1) and 3.73 MPa (SP+W2)

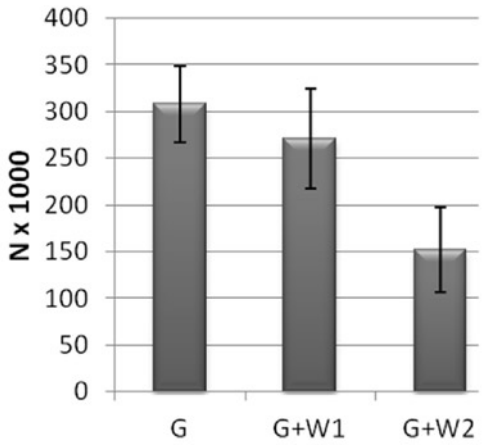

Fig. 14. Number of contraflexure cycles N until specimen failure after grinding (G), grinding with wear at pressure 1.92 MPa (G+W1) and at pressure 3.73 MPa (G+W2)

less desired distribution of residual stresses and increased surface roughness. These undesired changes in the surface layer properties occur to a lesser extent in the shot peened specimens, which leads to their longer fatigue life.

4. Conclusions

The experimental results led to formulation of the following conclusions:

1. The tribological wear of C45 steel specimens due to the effect of sliding on cast iron counterspecimens at a pressure of 3.73 MPa causes undesired changes in properties of the surface layer, which results in decreased fatigue life of these specimens.

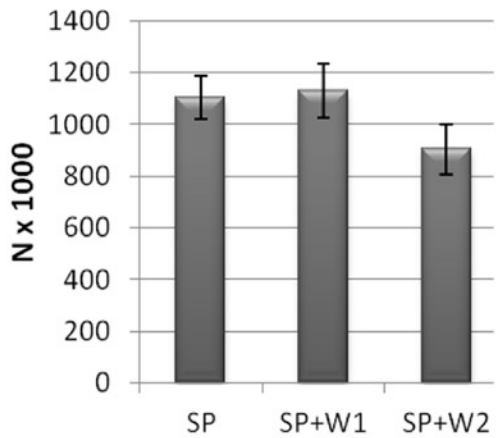

Fig. 15. Number of contraflexure cycles N until specimen failure after shot peening (SP), shot peening with wear at pressure 1.92 MPa (SP+W1), and at pressure 3.73 MPa (SP+W2)

2. The deterioration in the surface layer properties and the decrease in fatigue life are more visible for the specimens subjected to grinding with wear than for those subjected to shot peening.
3. As for the specimens exposed to wear at a counterspecimen pressure of 1.92 MPa, we can observe a slight decrease in the fatigue life of specimens subjected to grinding, while the wear of specimens subjected to shot peening does not significantly affect their fatigue life.
4. Vibratory and rotational shot peening leads to a higher fatigue life of both parts which are not exposed to tribological wear and, to a higher degree, parts which are exposed to the wear process.
5. Vibratory and rotational shot peening also increases tribological wear resistance of parts. The changes in geometrical structure of the specimen surface exposed to shot peening help accumulate oil between the surfaces of interacting components, which leads to a smaller mass decrement of these components.

The practical significance of the investigated problem stems from the fact that machines contain numerous components which are exposed to fatigue and tribological wear at the same time. The application of vibratory and rotational shot peening in the manufacturing of such components, a process which leads to formation of lubrication-improving microcavities on workpiece surface and generation of residual stresses, has a positive effect on operational life of such components.

References

1. Boehlert C.J, Cowen C.J, Quast J.P, Akahori T, Niinomi M. Fatigue and wear evaluation of Ti-Al-Nb alloys for biomedical applications. Material Science and Engineering C 2008; 28: 323-330, http://dx.doi.org/10.1016/j.msec.2007.04.003.
2. Carvalho A.L.M, Voorwald H.J.C. Influence of shot peening and hard chromium electroplating on the fatigue strength of 7050-T4751 aluminum alloy. International Journal of Fatigue 2007; 29: 1282-1291, http://dx.doi.org/10.1016/j.ijfatigue.2006.10.003.
3. Galda L, Dzierwa A, Sep J, Pawlus P. The effect of oil pockets shape and distribution on seizure resistance in lubricated sliding. Tribol Lett 2010; 37: 301-311, http://dx.doi.org/10.1007/s11249-009-9522-7.
4. Korzynski M, Dzierwa A, Pacana A, Cwanek J. Fatigue strength of chromium coated elements and possibility of its improvement with ball peening. Surface & Coatings Technology 2009 Dec; 204(5): 615-620, http://dx.doi.org/10.1016/j.surfcoat.2009.08.049.

5. Kulakowska A, Kukielka L, Kukielka K, Malag L, Patyk R, Bohdal L. Possibility of steering of products surface layer properties in burnishing rolling process. Applied Mechanics and Materials 2014; 474: 442-447, http://dx.doi.org/10.4028/www.scientific.net/AMM.474.442.
6. Lawrowski Z. Tribologia. Tarcie, zużywanie i smarowanie. Warszawa: PWN, 1993.
7. Leśniewski T, Krawiec S. Wpływ twardości stalowych materiałów ślizgowych na ich zużycie. Tribologia 2004; 3: 237-245.
8. Maruda R.W, Feldshtein E.E, Legutko S, Królczyk G.M. Improving the efficiency of running-in for a bronze-stainless steel friction pair. Journal of Friction and Wear 2015 Nov; 36(6): 548-553, http://dx.doi.org/10.3103/S1068366615060082.
9. Matuszak J, Zaleski K. Edge states after wire burnishing of magnesium alloys. Aircraft Engineering and Aerospace Technology: An International Journal 2014; 86(4): 328-335, http://dx.doi.org/10.1108/AEAT-09-2012-0155.
10. Matuszewski M, Styp-Rekowski M. Wpływ kierunkowości struktury geometrycznej powierzchni na intensywność zużywania par ciernych. Tribologia 2007; 2: 469-477.
11. Michalczewski R, Piekoszewski W, Szczerek M, Tuszynski W. The lubricant-coating interaction in rolling and sliding contacts. Tribology International 2009; 42: 554-560, http://dx.doi.org/10.1016/j.triboint.2008.05.001.
12. Morita T, Keita A, Chuji K. Effect of combination treatment on wear resistance and strength of Ti-6Al-4V alloy. Material Science & Engineering A 2014; 618: 438-446, http://dx.doi.org/10.1016/j.msea.2014.09.042.
13. Przybylski W, Hochschulz R. Technologia wytwarzania mikrorowków na powierzchni tarcia łożysk ślizgowych przez nagniatanie oscylacyjne. Tribologia 1999; 5: 625-638.
14. Rudawska A. Selected aspects of the effect of mechanical treatment on surface roughness and adhesive joint strength of steel sheets. International Journal of Adhesion and Adhesives 2014; 50: 235-243, http://dx.doi.org/10.1016/j.ijadhadh.2014.01.032.
15. Sep J, Pawlus P, Galda L. The effect of helical groove geometry on journal abrasive wear. Archives of Civil and Mechanical Engineering 2013; 13: 150-157, http://dx.doi.org/10.1016/j.acme.2013.01.001.
16. Sledz M, Bak L, Stachowicz F, Zielecki W. Analysis of the effect of shot peening on mechanical properties of steel sheets used as screener sieve materials. International Symposium on Dynamic Deformation and Fracture of Advanced Materials (D2FAM2013). Journal of Physics Conference Series; 2013 Sep (451) Loughborough Univ.
17. Sosnovskiy L.A, Bogdanovich A.V, Yelovoy O.M, Tyurin S.A, Komissarov V.V, Sherbakov S.S. Methods and main results of tribo-fatigue tests. International Journal of Fatigue 2014; 66:207-219, http://dx.doi.org/10.1016/j.ijfatigue.2014.04.006.
18. Zaleski K, Blawucki S. Evaluation of the effectiveness of the shot peening process for thin-walled parts based on the diameter of impressions produced by the impact of shot media. Advances in Science and Technology. Research Journal 2015; 9(26): 77-82.
19. Zaleski K. The effect of shot peening on the fatigue life of parts made of titanium alloy. Eksploatacja i Niezawodnosc Maintenance and Reliability 2009; 4(44): 65-71.
20. Zaleski R, Zaleski K, Gogol M, Wiertel M. Positron annihilation study of aluminum, titanium and iron alloys surface after shot peening. Applied Physics A 2015; 120: 551-559, http://dx.doi.org/10.1007/s00339-015-9214-0.

Kazimierz ZALESKI
Department of Production Engineering
Mechanical Engineering Faculty
Lublin University of Technology
ul. Nadbystrzycka 36, 20-618 Lublin, Poland
E-mail: k.zaleski@pollub.pl

Article citation info:
GNIŁKA J, MĘŻYK A. Experimental identification and selection of dynamic properties of a high-speed tracked vehicle suspension system. Eksploatacja i Niezawodnosc – Maintenance and Reliability 2017; 19 (1): 108–113, http://dx.doi.org/10.17531/ein.2017.1.15.

Jacek GNIŁKA
Arkadiusz MĘŻYK

EXPERIMENTAL IDENTIFICATION AND SELECTION OF DYNAMIC PROPERTIES OF A HIGH-SPEED TRACKED VEHICLE SUSPENSION SYSTEM

IDENTYFIKACJA DOŚWIADCZALNA ORAZ DOBÓR CECH DYNAMICZNYCH UKŁADU JEZDNEGO SZYBKOBIEŻNEGO POJAZDU GĄSIENICOWEGO*

The material diversity of subassemblies making up the tracked vehicle suspension system and the system wear level make it difficult to determine the value of forces acting in it. This paper presents a manner in which parameters of the model of a high-speed tracked vehicle suspension system can be adjusted using the genetic algorithm optimization method. The vehicle motion is tested experimentally to find reference characteristics of kinematic quantities of the system selected points. The simulation results obtained from numerical analyses are presented in charts and compared to the results of experimental testing. Finally, damping values in the vehicle shock-absorbers are determined based on an adopted criterion.

Keywords: *tracked vehicle suspension, identification of suspension properties, multibody dynamics, genetic algorithms.*

Zróżnicowanie materiałowe podzespołów wchodzących w skład gąsienicowego układu jezdnego oraz stopień jego zużycia wpływają na trudność określenia wartości sił działających w tym układzie. W artykule poprzez zastosowanie metody optymalizacji algorytmami genetycznymi, przedstawiono sposób dostosowania parametrów modelu układu zawieszenia szybkobieżnego pojazdu gąsienicowego. Przeprowadzono badania doświadczalne ruchu pojazdu, w celu wyznaczenia charakterystyk wielkości kinematycznych wybranych punktów układu, które zostały przyjęte jako referencyjne. W rezultacie przeprowadzonych analiz otrzymano wyniki symulacji numerycznych, które zestawiono na wykresach i porównano z wynikami badań doświadczalnych. W końcowym etapie na podstawie przyjętego kryterium określono wartości tłumienia w amortyzatorach pojazdu.

Słowa kluczowe: *zawieszenie pojazdu gąsienicowego, identyfikacja własności zawieszenia, metoda układów wieloczłonowych, algorytmy genetyczne.*

1. Introduction

The design and modification of the tracked vehicle suspension system is now supported with the vehicle motion numerical simulations based on the principles of multibody dynamics. Such analyses make it possible to reduce experimental testing costs and shorten the time of the new product commercialization. In terms of the vehicle motion nature simulation, it is essential to take account of the impact of the track on the suspension system as this enables precise selection of the suspension components.

A conventional tracked vehicle suspension system incorporates not only metal elements but also bushings made of rubber or other materials [17]. The material diversity of subassemblies and the vehicle operation time make it difficult to determine the forces acting in the track segments. A change in parameters describing the phenomena occurring in this area (cf. Fig. 1) has a direct effect on the performance of the vehicle entire suspension system.

The system properties are also affected by the track wear level, which is difficult to assess. Depending on the manufacturer, the track service life is estimated at the level of about 2000 km. The environment of the track system operation is another significant factor. For example, high air dustiness increases the intensity of wear [9].

According to [2], the forces occurring in the track system can be identified through testing carried out on a test stand. A method of the track tension determination in real time is presented in [14]. The method finds application in active suspension systems. Identification of the properties of damping elements of the tracked vehicle suspension with the use of neural networks is presented in [21, 22].

Sankar et al. [20] and Dhir & Sankar [7] developed a model for dynamic simulation of tracked vehicles with independent suspension, offering the possibility of using linear or nonlinear characteristics of spring and damping elements. A numerical simulation in the time domain makes it possible to improve the crew's comfort and safety by observing the suspension system performance. In [18], optimization of the suspension system spring elements is taken into consideration, adopting the criterion of minimization of the driver's seat vertical acceleration values during 8-hour exposure to vibrations. Gregory M. Hulbert et al. [10] developed a method of the rocker design optimization using characteristics of the forces acting on the suspension node which are obtained from the vehicle simulation. In [16], the methodology of modelling hybrid drive systems and elements of the tracked vehicle suspension is presented. Choi et al. [6] present the

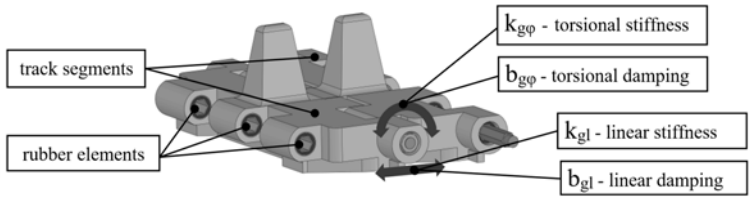

Fig. 1. Physical model and parameters describing forces in the track system

(*) Tekst artykułu w polskiej wersji językowej dostępny w elektronicznym wydaniu kwartalnika na stronie ***www.ein.org.pl***

method of modifying a four-wheeled armoured vehicle suspension to maximize the vehicle post-firing mobility, minimizing the driver's seat vertical acceleration at the same time. Issues related to the control of rotary shock-absorbers in the tracked vehicle suspension, aiming to improve the vehicle stabilization efficiency, are presented in [12]. The basic sources of dynamic loads acting on combat vehicles, resulting from off-road riding, firing the cannon, being hit by the enemy's projectile or the effect of explosives, are presented in [19]. The methodology of the tracked vehicle modelling using multibody dynamics simulations is applied in [13], where results of a numerical analysis performed in the LMS Virtual.Lab Motion environment are presented and compared to experimental testing results. The assessment of the conditions of comfort of persons carried in selected special vehicles is presented in [11]. A failure to meet the criteria concerning the human body exposure to vibrations caused by the vehicle motion may lead to serious perception disturbances and hinder the crew's performance. In [3] a model is presented of controlling an active suspension system using the Linear Quadratic Regulator (LQR) technique to improve the crew's comfort. Report [15] makes a survey of the functionality of the vehicle motion modelling software using multibody dynamics simulations, where functions of programs facilitating the tracked vehicle model construction, together with the possibility of conducting an analysis taking account of the ground deformability, are described.

The authors of this paper put forward a method of estimating parameters describing the track system operation based on genetic algorithms and taking account of the vehicle kinematic quantities recorded during experimental tests. The issues presented herein comprise an analysis of the impact of contact forces in kinematic pairs between the track segments and of the effect of the track tension degree realized by the setting of the tensioning wheel. The final part of the paper presents the criterion for selecting optimum damping values of shock-absorbers installed in the vehicle under consideration (cf. Fig. 2).

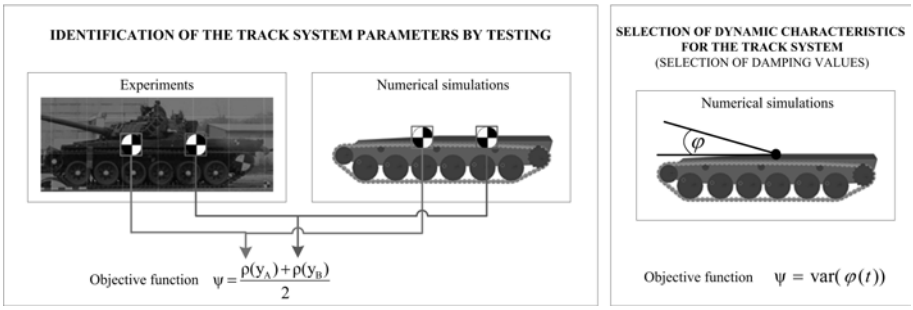

Fig. 2. Flowchart of works performed within the paper

2. Experimental testing

The aim of experimental tests of the vehicle passage over a field obstacle was to determine the trajectory of markers on the vehicle body (on the sprung mass). The tests resulted in characteristics of linear displacement, velocity and acceleration in points located on the body and marked as shown in Fig. 3.

The tests were carried out using a prototype of the PT-91 Twardy vehicle. The photogrammetric method of image recording was applied using a PHANTOM V9.1 high-speed wide-angle lens camera. The vehicle mass during the experimental tests totalled 42600 kg estimated based on the lack of any equipment elements.

The tests included instances of passage over an obstacle (cf. Fig. 4) attacked by the vehicle with both tracks at the same time. The proposed variant of passing over the obstacle is used to identify the track system parameters. The obstacle geometry is created based on existing elements of a track intended for long-distance testing that will be the subject of further analyses in this respect. The tests were conducted at the vehicle speed of 4, 8 and 13 km/h. For statistical purposes, each run was repeated three times. Example results of the testing are presented and compared to the results of numerical analyses in section 5.

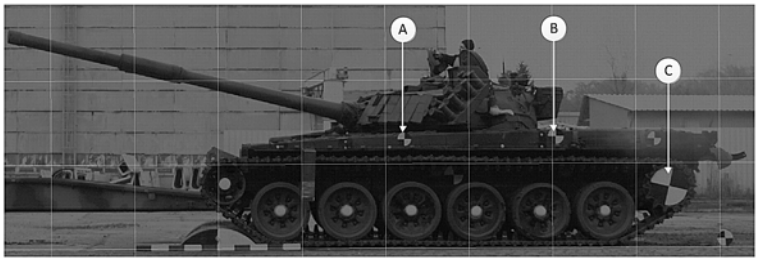

Fig. 3. On-vehicle marker location (X, Y); A (-3347, 587), B (-1445, 620), C (0, 0)

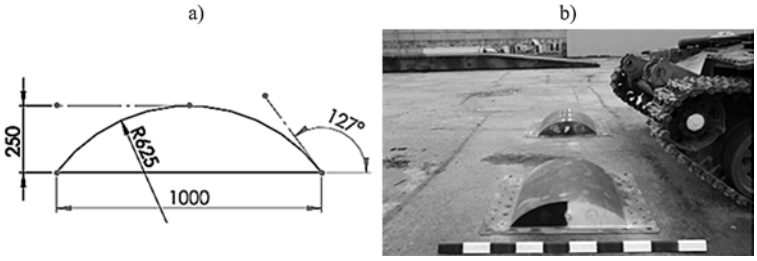

Fig. 4. Obstacle geometry (a) and location on the testing site (b)

3. Tracked vehicle mathematical model

Based on geometrical data and mass-inertia parameters, a tracked vehicle model was constructed using the multibody dynamics simulation method implemented in the ADAMS package. The model takes account of the track system, the suspension subassemblies connected by kinematic pairs, spring and damping elements as well as the vehicle deflection limiters (Fig. 5).

The dynamics of multibody systems in the MSC ADAMS environment is modelled by defining the coordinates of kinematic bodies and the type of kinematic constraints, as well as specifying mass-inertia parameters and parameters of contact between the system elements. Moreover, the computation process parameters are declared, such as: integration step, simulation time, initial velocity, etc.

The vehicle model is simplified by taking account of the longitudinal plane of symmetry. It is made of 118 non-deformable elements connected to each other by kinematic pairs into a kinematic chain.

The system theoretical mobility is determined using the Grübler-Artobolevsky formula for spatial systems:

$$W_T = 6k - \sum_{i=1}^{5} (6-i) p_i \tag{1}$$

where:

W_t – system theoretical mobility,
k – number of moving kinematic bodies,
p_i – number of i-th class kinematic bodies.

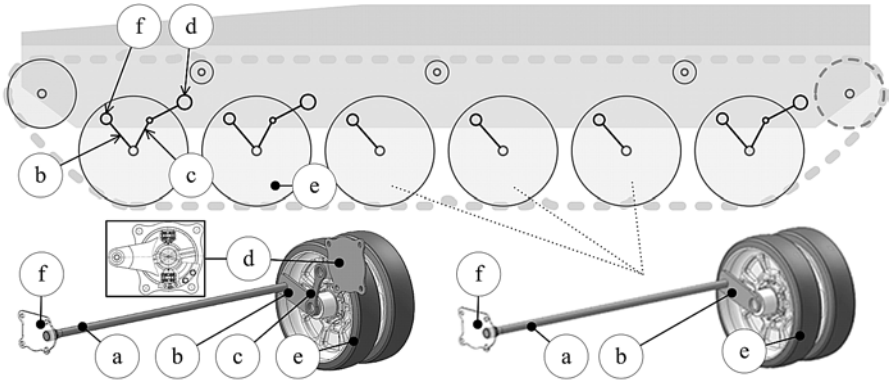

Fig. 5. Kinematic diagram of the PT-91 vehicle suspension: a) torsion bar; b) rocker; c) rocker – shock-absorber link; d) rotary vane damper; e) ground wheel; f) torsion bar socket

Substitution of respective values gives the following result:

$$W_T = 6*118 - 5*18 - 4*2 - 3*3 = 601 \tag{2}$$

The vehicle model created by means of the multibody dynamics simulation method requires a definition of generalized coordinates:

$$q = [q_1 + q_2 + ... + q_n] \tag{3}$$

Kinematic bodies are limited by constraint equations which can be written as follows:

$$(q,t) = [\Phi_1(q_1,t),\ldots,\Phi_n(q_n,t)]^T \tag{4}$$

The motion equation written in the first-order Lagrangian formalism can be expressed using the following vector notation:

$$M\ddot{q} + \Phi_q^T\lambda = Q \tag{5}$$

where:

q – location vector,
$\ddot{q}$ – acceleration vector,
M – mass matrix,
Φ_q – matrix of partial derivatives,
λ – column matrix of Lagrange multipliers,
Q – vector of generalized forces.

Considering the transformations resulting from the occurrence of velocity constraints expressed as local coordinates $(\gamma = \Phi_q\ddot{q})$ in the equations, the expressions making up a system of the first-order Lagrangian equations can be presented in the following form:

$$\begin{bmatrix} M & -\Phi_q^T \\ \Phi_q & 0 \end{bmatrix}\begin{bmatrix} \ddot{q} \\ \lambda \end{bmatrix} = \begin{bmatrix} Q \\ \lambda \end{bmatrix} \tag{6}$$

The presented equations of the system motion constitute a system of differential-algebraic equations composed of first-order differential equations with an independent variable in the form of time and algebraic constraint equations. The system of equations is determined through numerical integration, i.e. the solution is found with set accuracy at discrete time instants. The most popular numerical integration method in the MSC ADAMS software package is based on the backward difference formula (the Gear algorithm). A detailed description of the mathematical model and of the methods of computing the vehicle kinematics and dynamics mechanisms applied in the MSC ADAMS software can be found in [1].

4. Estimation of the model parameters

One of the factors that have an impact on dynamics and the suspension system efficiency is the force acting on the vehicle wheels, which results from the track tension. The track tension is adjusted by changing the tensioning wheel position. It is also important to take account of the track wear, which is mainly due to the wear of rubber elements affecting the system performance.

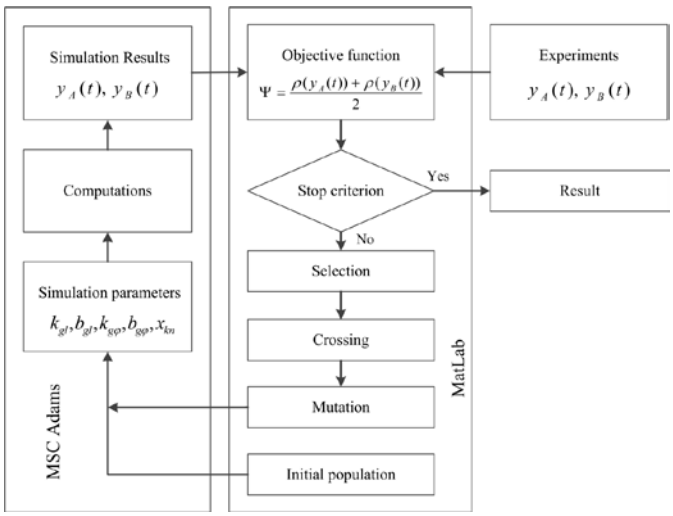

Fig. 6. Program flowchart

Apart from the tensioning wheel setting, the track system properties within the model are described by the following quantities: linear stiffness and linear damping as well as torsional stiffness and torsional damping of the track segment links (cf. Fig. 1).

The results obtained from experimental testing were used to adjust the tracked vehicle model parameters. For this purpose, an original in-house program was developed that couples simulations of the tested vehicle runs to the genetic algorithm included in the MatLab program optimization module. The program flowchart is presented in Fig. 6. The genetic algorithm efficiency is highly dependent on its objective function, being the index of the model behaviour similarity compared to the real object.

There are many statistical indices defining the degree of the model similarity to empirical data. In this paper, an analysis is applied of correlations needed to construct the objective function by specifying the correlation coefficients.

The correlation between two random variables X and Y is a measure of the force (level) of the linear relation between the variables [8]:

$$\rho = \frac{\mathrm{cov}(X,Y)}{\sigma_X\sigma_Y} \tag{7}$$

where covariance of variables X and Y occurs in the numerator:

$$\mathrm{cov}(X,Y) = E[(X-\mu_X)Y-\mu_Y)] \tag{8}$$

where:
μ_X and μ_Y – arithmetic means of X and Y within the population,
σ_X, σ_Y – standard deviations of variable X and Y.

Coefficient ρ is included in the interval $\langle -1;1 \rangle$. If ρ=0, the variables are non-correlated. If ρ=−1, regression lines exhibit a negative inclination, which means that negative correlation is found. If ρ=1, the reverse is the case, which means that correlation is positive [8].

The correlation coefficient described above was used to determine the index of similarity between the curves illustrating changes in linear displacement of the markers on the model body obtained from simulations and those obtained by means of video recording of the vehicle test run.

Markers A and B on the vehicle body (cf. Fig. 3) were used to compare the model to the experiment result.

Next, a column matrix was defined of design variables and intervals thereof which enable carrying out the simulation computation process and which are consistent with the design technological determinants:

$$x = \{x_1, x_2, x_3, x_4, x_5\} \tag{9}$$

where:

$$x_1 = k_{gl}, \quad k_{gl} \in [1.0e+5; 1.0e+9] \tag{10}$$

$$x_2 = k_{g\varphi}, \; k_{g\varphi} \in [10; 1.0e+5] \tag{11}$$

$$x_3 = b_{gl}, \quad b_{gl} \in [1; 1.0e+6] \tag{12}$$

$$x_4 = b_{g\varphi}, \; b_{g\varphi} \in [1; 1.0e+5] \tag{13}$$

$$x_5 = x_{kn}, \quad x_{kn} \in [-5590.0; -5550.0] \tag{14}$$

where:

k_{gl} – linear stiffness of the track segment link $\left[\frac{N}{m}\right]$

$k_{g\varphi}$ – torsional stiffness of the track segment link $\left[\frac{Nm}{rad}\right]$

b_{gl} – linear damping coefficient of the track segment link $\left[\frac{N*s}{m}\right]$

$b_{g\varphi}$ – torsional damping coefficient of the track segment link $\left[\frac{Nm*s}{rad}\right]$

x_{kn} – tensioning wheel setting [mm]

The estimation process using the optimization procedure was carried out based on the simulation of the vehicle run over the obstacle with the speed of 4 km/h. The objective function was defined in the form of the arithmetic mean of correlation coefficients of vertical displacement of markers A and B:

$$\Psi = \frac{\rho(y_A(t)) + \rho(y_B(t))}{2} \tag{15}$$

where:
$y_A(t)$ – marker A vertical displacement,
$y_B(t)$ – marker B vertical displacement,

The following optimization parameters were established:
- population size = 40,
- stop criterion: number of generations = 30.

The calculations gave the following values of the design variables:

$$k_{gl} = 2.676e+7 \left[\frac{N}{m}\right] \tag{16}$$

$$k_{g\varphi} = 6.257e+3 \left[\frac{Nm}{rad}\right] \tag{17}$$

$$b_{gl} = 1.0e+4 \left[\frac{N*s}{m}\right] \tag{18}$$

$$b_{g\varphi} = 7.74e+3 \left[\frac{Nm*s}{rad}\right] \tag{19}$$

$$x_{kn} = -5563[mm] \tag{20}$$

5. Testing results

The numerical and experimental results are shown and compared to each other in the charts below. The charts present curves illustrating time-dependent changes in the vehicle body displacement, velocity and acceleration in relation to the global system of coordinates.

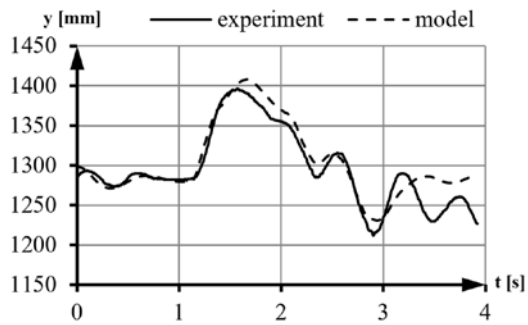

Fig. 7. Curves illustrating time-dependent changes in vertical displacement of marker A

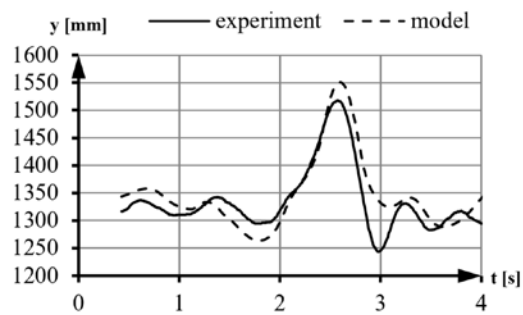

Fig. 8. Curves illustrating time-dependent changes in vertical displacement of marker B

The presented curves were plotted for the run speed of 13 km/h. The correlation coefficients of marker A and marker B vertical displacement – $\rho(y_A(t))$ and $\rho(y_B(t))$ – in the case of the model are 0.94 and 0.87, respectively.

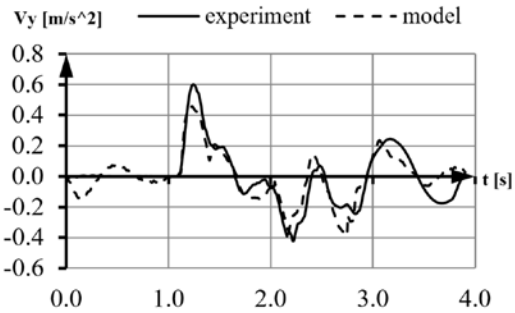

Fig. 9. Curves illustrating time-dependent changes in marker A velocity in the vertical direction

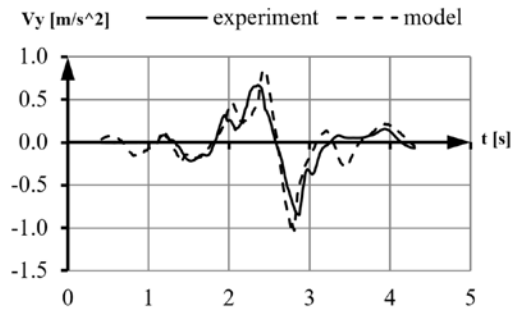

Fig. 10. Curves illustrating time-dependent changes in marker B velocity in the vertical direction

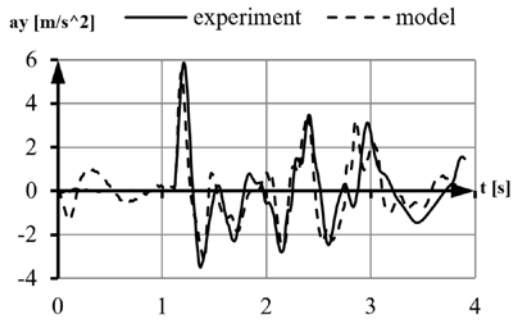

Fig. 11. Curves illustrating time-dependent changes in marker A acceleration in the vertical direction

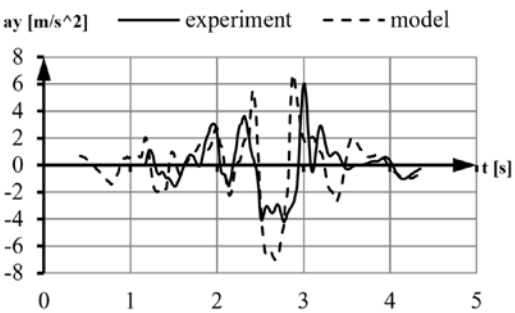

Fig. 12. Curves illustrating time-dependent changes in marker B acceleration in the vertical direction

The velocity characteristics obtained by means of numerical simulations demonstrate high convergence with the experiment, both qualitatively and quantitatively. The maximum velocity values for points A and B are found at the level of 0.6 and 0.8 m/s, respectively. In this case, instantaneous acceleration reaches the value of 6 m/s^2.

6. Selection of the shock-absorber damping values

The tracked vehicle model treated as a dynamic system enables an analysis of characteristics such as transfer function or frequency curves.

The two characteristics are dependent on the properties of the system itself, but they are independent of the kind of the input functions applied thereto. In practice, the suspension optimal parameters are selected using methods of the statistical theory of springing, which involves determination of numerical characteristics of the road and off-road bumps distribution, such as the mean value, variance or standard deviation. The measured terrain samples are then classified into groups. An example classification may be the effect of the division of the terrain irregularities (with respect to specific standard deviation for example) into groups such as roads with slight irregularities, dirt roads and very bumpy roads. Owing to that, it is possible to generate a random function describing the terrain profile. There are studies concerning determination of numerical characteristics of the irregularity distribution of terrains for which special vehicles are designed. However, their findings are not disclosed to the public. Therefore, a method was put forward [4] of the damping value selection through an analysis of the variance of the body longitudinal inclinations **Ψ=var[φ(t)]** at a specific input function acting on the vehicle depending on its velocity [4].

For this purpose, an input function model was used in the form of a field obstacle as presented in Fig. 3. Analyses were conducted of the developed vehicle model in variants taking account of the change in the speed of the vehicle attack on the obstacle and the change in the damping value in shock-absorbers. Each simulation lasted 15 s. In every case, velocity ranged from 5 to 55 km/h and the simulations were performed with the step of 5 km/h. The analyses were conducted for different values of the damping coefficient, according to the variants listed in Table 1.

Based on that, the velocity-dependent vehicle body variance of longitudinal inclinations **Ψ=var[φ(t)]** was determined (cf. Fig. 13).

Analysing the results, it can be observed that the variance of the body longitudinal inclinations illustrated by curve 4 is low for the entire range of the velocities under analysis. However, the damping value selection is also dependent on the vehicle purpose and determination of the velocity criterion for which the vehicle should exhibit smaller variance of the body longitudinal inclinations [5].

7. Conclusions

The photogrammetric method made it possible to obtain results in the form of curves illustrating changes in displacement, velocity and acceleration of selected points of the tracked vehicle suspension body, which constituted the basis for verification of the assumptions adopted in the modelling process. The data obtained in this way were used for

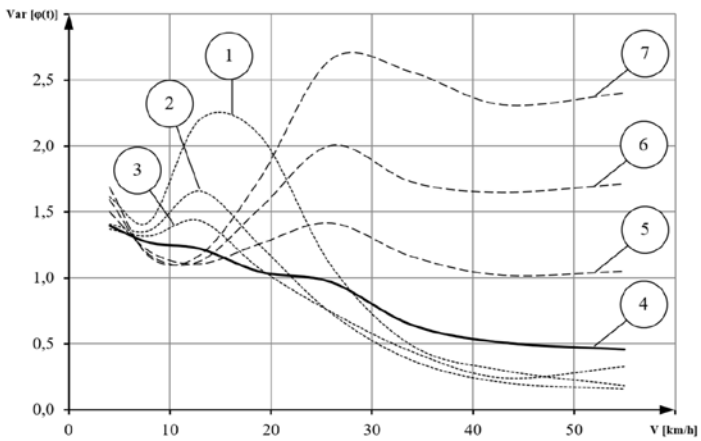

Fig. 13. Curves illustrating variance of the vehicle body longitudinal inclinations depending on the vehicle velocity for different damping values

Table 1. Variants of performed simulations

Curve number	1	2	3	4	5	6	7
Damping in shock-absorbers [Nm*s/rad]	0	11272	22545	45090	90180	135270	180360

the purposes of the objective function in the procedure of the model parameter estimation. The developed model of the tracked vehicle described herein was adjusted through estimation of the parameters describing the forces occurring in the track system. The vehicle body displacement, velocity and acceleration results obtained numerically and experimentally are highly convergent.

A universal method has thus been developed of selecting the track system parameters which are difficult to establish otherwise. The method can be applied in modelling dynamic phenomena in tracked vehicles and in the selection of operating parameters, such as the track tension degree or the damping value in shock-absorbers.

It also enables an analysis of phenomena occurring in wheeled vehicles, to identify the parameters of the tyre model for example.

Scientific work conducted under Contract 2828/B/T00/2010/40, financed from budgetary means for science in the years 2011–2014 as Research Project O N501 282840.

References

1. ADAMS Standard Documentation and Help, MSC Software Corporation, MD/ADAMS R3, 2007.
2. Automotive Research Center. Dynamic analysis and design of tracked vehicles http://arc.engin.umich.edu/events/archive/annual/conf98/case2.pdf, 16.05.2016.
3. Bello M M, Shafie A A, Khan R M. Off-Road Vehicle Suspension Performance Improvement Using Linear Quadratic Regulator, Techniques. International Conference on Mechanical and Industrial Engineering (ICMAIE'2015), Kuala Lumpur, Malaysia 2015.
4. Burdziński Z. Teoria ruchu pojazdu gąsienicowego [Theory of the tracked vehicle motion]. Warszawa: Wydawnictwa Komunikacji i Łączności, 1972.
5. Chodkowski A. W. Konstrukcja i obliczanie szybkobieżnych pojazdów gąsienicowych [Design and calculation of high-speed tracked vehicles]. Warszawa: Wydawnictwa Komunikacji i Łączności, 1990.
6. Choi E, Ryoo J, Cho J. et al. Optimum suspension unit design for enhancing the mobility of wheeled armoured vehicles. Journal of Mechanical Science and Technology 2010; 24: 323-330, http://dx.doi.org/10.1007/s12206-009-1102-0.
7. Dhir A, Sankar S. Assessment of tracked vehicle suspension system using a validated computer simulation model. Journal of Terramechanics 1995; 32(3): 127-149, http://dx.doi.org/10.1016/0022-4898(95)00012-7.
8. Dietrich C F. Uncertainty, Calibration and Probability: The statistics of scientific and industrial measurement 2nd edition. Boca Raton: Taylor & Francis Group, 1991.
9. Djurić R, Milisavljević V. Investigation of the relationship between reliability of track mechanism and mineral dust content in rocks of lignite open pits. Eksploatacja i Niezawodnosc – Maintenance and Reliability 2016; 18(1): 142-150, http://dx.doi.org/10.17531/ein.2016.1.19.
10. Hulbert G M. et al. Case Study for network-distributed collaborative design and simulation: extended life optimization for M1 Abrams tank road arm. Mechanics of Structures and Machines 1999; 27(4): 423-451, http://dx.doi.org/10.1080/08905459908915706.
11. Jamroziak K, Kosobudzki M, Ptak J. Assessment of the comfort of passenger transport in special purpose vehicles. Eksploatacja i Niezawodnosc – Maintenance and Reliability 2013; 15 (1): 25–30.
12. Kciuk S, Duda S, Mężyk A, Świtoński E, Klarecki K. Tuning the Dynamic Characteristics of Tracked Vehicles Suspension Using Controllable Fluid Dampers. Innovative Control Systems for Tracked Vehicle Platforms. Studies in Systems, Decision and Control 2. Springer 2014; 243-258.
13. Kciuk S, Mężyk A, Mura G. Modelling of tracked vehicle dynamics. Journal of KONES Powertrain and Transport 2010; 17(1): 223-232.
14. Kunsoo H, Jungtak K, Hong D. Estimation of dynamic track tension utilizing a simplified tracked vehicle model. American Control Conference, 2001. Proceedings of the 2001, Arlington, VA, 2001; 5: 3335-3340, http://dx.doi.org/10.1109/acc.2001.946143.
15. Madsen J, Heyn T, Negrut D. Methods for Tracked Vehicle System Modelling and Simulation. Technical Report 2010-01.
16. Mężyk A. et al. Modelling and investigation of dynamic parameters of tracked vehicles. Mechanics and Mechanical Engineering 2011; 15(4): 115-130.
17. Ogorkiewicz R M. Technology of Tanks: Volumes I and II. Surrey: Jane's Information Group, 1991.
18. Qigang S, Hongyan W, Li Y. Design of the refitted high mobility tracked vehicle suspension system. 2009 International Conference on Mechatronics and Automation, Changchun, 2009; 4638-4643, http://dx.doi.org/10.1109/ICMA.2009.5244787.
19. Rybak P. Operating loads of impulse nature acting on the special equipment of the combat vehicles. Eksploatacja i Niezawodnosc – Maintenance and Reliability 2014; 16 (3): 347–353.
20. Sankar S S, Dhir A A, Shankhla V S. Simulation and field testing of tracked vehicle suspension dynamics. ASME. J. Dyn. Sys., Meas., Control, 1994; 116(4): 764-773.
21. Shengii Y, Daolin X. An application of a progressive neural network technique in the identification of suspension properties of tracked vehicles. Proceedings of the 9th International Conference on Neural Information Processing ICONIP '02, 2002; 2: 542-546, http://dx.doi.org/10.1109/ICONIP.2002.1198115.
22. Xu D, Yap F F, Han X, Wen G L. Identification of spring-force factors of suspension systems using progressive neural network on a validated computer model. Inverse Problems in Engineering, 2003; 11(1): 55-74, http://dx.doi.org/10.1080/1068276021000020177.

Jacek GNIŁKA
Arkadiusz MĘŻYK
Institute of Theoretical and Applied Mechanics,
Silesian University of Technology
Faculty of Mechanical Engineering
ul. Konarskiego 18A, 44-100 Gliwice, Poland
E-mails: jacek.gnilka@polsl.pl, arkadiusz.mezyk@polsl.pl

Article citation info:
OZ MA, KAYMAKCI OT, KOYUN A. A safety related perspective for the power supply systems in railway industry. Eksploatacja i Niezawodnosc – Maintenance and Reliability 2017; 19 (1): 114–120, http://dx.doi.org/10.17531/ein.2017.1.16.

Muhammet Ali OZ
Ozgur Turay KAYMAKCI
Ayhan KOYUN

A SAFETY RELATED PERSPECTIVE FOR THE POWER SUPPLY SYSTEMS IN RAILWAY INDUSTRY

BEZPIECZEŃSTWO SYSTEMÓW ZASILANIA W PRZEMYŚLE KOLEJOWYM

Within its structure railway transportation systems contain very critical subsystems that can seriously harm the system itself, people or the environment if not properly controlled. Therefore, these critical subsystems are analysed according to the related standards and necessary safety functions are implemented, verified and operated. On the other hand, railway power supply system, which is a critical subsystems, is generally properly analysed from a reliability perspective whereas the corresponding safety related functions are roughly examined. This paper proposes that the railway power supply systems should be considered as safety critical systems and justifies this proposal using risk analysis as presented in the standard IEC 61508. The safety related functions of the system are examined and each function is modelled in detail using Markov modelling method. These models are implemented over a power supply system of Istanbul Transportation Co. and SIL values of the safety functions are calculated using these modular and easily adaptable Markov models. Furthermore the obtained results are compared with simplistic Fault Tree analysis (FTA) and the significance of accurate calculation is demonstrated.

***Keywords**: Markov models, reliability, formal modeling.*

W skład struktury kolejowych systemów transportowych wchodzą krytyczne podsystemy, które, nieodpowiednio monitorowane, mogą narażać sam system, a także ludzi oraz środowisko na poważne szkody. Dlatego też, podsystemy krytyczne analizuje się zgodnie z odpowiednimi normami oraz wdraża w nich, weryfikuje i realizuje niezbędne funkcje bezpieczeństwa. W przypadku systemów zasilania kolei, które należą do grupy podsystemów krytycznych, system na ogół analizuje się dokładnie z punktu widzenia niezawodności, natomiast funkcje bezpieczeństwa bada się jedynie pobieżnie. W prezentowanej pracy postuluje się że systemy zasilania kolei powinny być traktowane jako krytyczne dla bezpieczeństwa, co autorzy uzasadniają z wykorzystaniem analizy ryzyka przedstawionej w normie IEC 61508. W proponowanym rozwiązaniu, bada się funkcje bezpieczeństwa systemu, przy czym każda funkcja zostaje szczegółowo zamodelowana za pomocą metody modelowania Markowa. Modele tego typu wdrożono w systemie zasilania firmy Istanbul Transportation Co. Wartości poziomu nienaruszalności bezpieczeństwa (SIL) badanych funkcji bezpieczeństwa obliczano za pomocą wspomnianych modularnych modeli Markowa charakteryzujących się łatwością adaptacji. Ponadto, uzyskane wyniki porównano z symplistyczną analizą drzewa błędów (FTA), a także wykazano znaczenie prowadzenia dokładnych obliczeń.

***Słowa kluczowe**: modele Markowa, niezawodność, modelowanie formalne.*

1. Introduction

Railways and highways are the two main means of public transport over the land. When compared to highways, railways are much more advantageous due to the fact that railways can carry a large amount of cargo and larger number of passengers faster and more comfortable over long distances. These advantages result in more railways being built especially in urban areas and more passengers choosing railway transportation. This increasing demand has forced the local operators to decrease the headway times up to 90 seconds and the availability of the overall system has become more important than ever. So that an incident or major failure can cause catastrophic problems for operating companies and this is unacceptable in any situation. Therefore analyzing the risks and the verification of the SRFs that satisfy the corresponding safety level is mandatory according to CENELEC 50126 [2].

Most of the railway systems, such as rolling stocks [13], fire safety systems [11] and railway trackside equipment [14], are already considered as safety related system. Whereas railway safety, railway power supply system's availability is usually analysed from a reliability perspective using methods such as Bayesian networks [22], state-space partitioning [7] and an innovative method supported by state enumeration technique [5]. In a study by Rosinski A. and Dabrowski T. issues related to the reliability of power supply systems have been discussed and analysed [19]. On the other hand, if a safety related function does not operate properly on time, the system and the establishment can be seriously harmed. Therefore only calculating the reliability of the power system is not enough to guarantee system availability but also system's safety level must be greater than an expected value. In this context, all safety functions of the railway power supply system should be assessed according to IEC 65108 perspective and a detailed analysis containing failure modes should be made. This paper proposes that the railway power supply systems have to be analysed as a safety related system. For this purpose a risk analysis is made and the corresponding safety related functions are examined and each function is modelled in detail using Markov modelling method. The justification of the proposal and the developed easily adaptable Markov models can be considered as the original contributions of this study. Also this study points out the risks of inaccurate calculation of the SIL level by comparing applied detailed Markov model results to applied Fault Tree results.

For safety assessments a system modelling method is needed in order to determine safety integrity level (SIL) of the system. In general, Fault Tree method is used and this method is also recommended by the standard IEC 61025 [9]. Fault Tree analysis is a simple and a primitive method. This method is also insufficient to reflect the dynamics of the system when the system have too many failure modes. In spite of all the drawbacks of Fault Tree analysis, it is frequently used. Collong and Kouta evaluated probability of explosion and identified critical failure sequences of a fuel cell system using Fault Trees [3].To overcome the drawbacks of FTA modified versions of Fault Tree method such as conditional Fault Tree [20] or combination of methods such as fuzzy logic [16] and generic algorithm [12] with FTA can be used. Detailed modelling capabilities of Markov modelling makes it a better alternative and is used by many researchers when modelling safety related systems for instance systems with self-diagnostic components [23] and redundant standby safety systems [8] and is also used for different purposes such as SIL verification [21] and performance assessments [15]. In this paper Markov modelling technique, which is recommended by the standard IEC 61165, will be used for its detailed modelling capabilities and precise results. It is also be noted that the created models are modular and easily adaptable for all railway power supply systems.

The organization of paper is as follows, in section 2 parameters and techniques used in the paper will be explained. In section 3 the power supply system, which is analysed, will be introduced and the desired SIL level of the power supply system is obtained by examining the risk factors. Railway power supply system's safety related functions are examined and each function is modelled in detail using Markov modelling method in section 4. Finally results and discussions are given in section 5.

2. Safety relaed system

A safety-related system is a system which ensures or maintains safety therefore correct operation of this system is crucial for ensuring or maintaining safety. The purpose of a safety related system is to transit the system to a safe state when a dangerous state is detected. All safety related systems are composed of a combination of sensors, logic solvers and final elements. There are three stages of a properly realized of safety life cycle SRS called design, implementation and operation phases. Existing standards act a guide and explain the important steps of the safety life cycle. Major necessities of all phases are defined in the IEC 61508 standard [9]. EN 50128 describes the essential aspects of developing software for E/E/PE systems used in railway safety related applications (CENELEC 2011) [10].

Table 1. Risk factor parameter explanations

Parameters		Description
Consequence (C)	C_a	Minor injury
	C_b	Serious injury
	C_c	Death of a person
	C_d	Death of more than one person
Frequency and exposure time risk (F)	F_a	Rare exposure risk
	F_b	Frequent exposure risk
Possibility of avoidance of hazard (P)	P_a	Possible under certain conditions
	P_b	Risk prevention very low
Frequency of occurrence of hazard without protection system (W)	W_1	Very slight probability of hazardous incident
	W_2	Slight probability of hazardous incident
	W_3	High probability of hazardous incident

2.1. The safety lifecycle

The safety life cycle is a series of phases starting from initiation to specifications of safety requirements. It covers the design and development of safety features in a safety-critical system, and the termination of that system. In the analysis phase a risk and hazard analysis is made for the designed system. Frequencies, causes and aftereffects of possible threats are considered when the operation mode of the SRS is determined. IEC 61508 determines the operation mode of the SRS with the demand rate. Also at this phase a SIL (Safety integrity level) is assigned to the system which is a measurement of performance required for a safety instrumented function.

One of the methods, which is approved by IEC 61508, for determining the required safety integrity level of the system is the risk graph. Risk graph method requires the knowledge of the risk factors of the system. The risk factors associated with the system are represented as C, F, P and W parameters. The description of these parameters is as give in table 1.

There are six possible outcomes of the risk graph. Numbers 1 through 4 indicate the safety integrity level where integrity level increases from level 1 to 4 meaning 4 represents the highest and level 1 represents the lowest integrity level. The symbol "a" represents there is no safety requirement and the symbol "b" means a single E/E/PE safety system is not sufficient. The risk graph method, which is obtained from IEC 61508 Part 5 Annex B (IEC 2002), is given in figure 1.

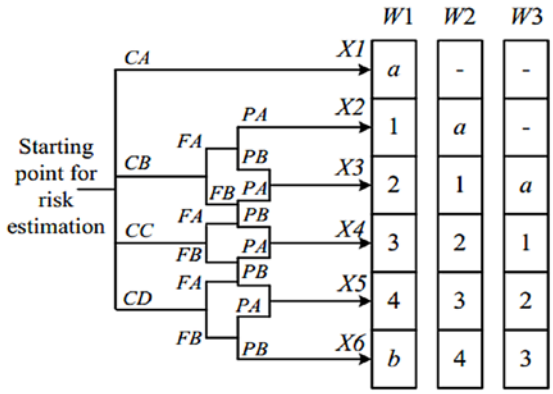

Fig. 1. The risk graph

2.2. Functional reliability parameters

Some reliability parameters for the safety related systems are introduced by the IEC 61508 standard. These parameters are used to classify hardware aspects of systems. Below are some of the major related parameters:

Failure rate: Failure rate is the frequency with which a system or component fails, expressed in failures per unit of time and is represented by λ. Failure rates can be categorized into safe failures (S) and dangerous failures (D). As shown in Equation (1) and Equation (2), dangerous failures can also be separated into two types called detectable dangerous failures (DD) and undetectable dangerous failures (DU) [1].

$$\lambda = \lambda_d + \lambda_s \tag{1}$$

$$\lambda_d = \lambda_{du} + \lambda_{dd} \tag{2}$$

Safe failure factor: the relation between λ_d and is λ_s described with safe failure factor S as given in equation (3):

$$S = 100(\lambda_d / \lambda) \tag{3}$$

Safe failure fraction (): Safe failure fraction is the ratio of the total safe failure rate of a subsystem plus the dangerous detected failure rate of the subsystem to the total failure rate of the subsystem. The calculation of SFF is shown in Equation (4) and is proposed in IEC 61508-6 Annex C:

$$SFF = \frac{\sum \lambda_s + \sum \lambda_{dd}}{\sum \lambda_s + \sum \lambda_d} \tag{4}$$

Proof test Interval (Ti): It is the interval of time between two proof tests. According to the IEC/EN 62061 proof test is a test to detect fault and degradation in SRCs in order to restore the system to brand new condition. All dangerous faults must be detected while proof testing.

Mean time to failure (MTTF): According to the standard IEC/EN 60050, it is the statistical average elapsed time until the first occurrence of failure of a system or a unit [17]. This time is depended on the architecture and the failure rate of the system.

Mean time to repair (MTTR): It represents the average time required to repair a failed component or device. IEC/EN 61508 defines MTTR as 8 hours.

Probability of failure on demand (PFD): A value that indicates the probability of a system failing to respond to a demand. Usually average probability of failure on demand is discussed in SRS [17]. PFD_{avg} value is defined in Equation (5):

$$PFD_{avg} = \frac{1}{T}\int_0^T P(t)dt \tag{5}$$

Hardware fault tolerance (HFT): HFT is the number of hardware faults that the system or the unit can tolerate until a dangerous failure [13]. The HFT is calculated as given in Equation (6):

$$HFT_{sys} = \min_{i=1}^{n} HFT_i \tag{6}$$

After the safety related system is designed its performance is calculated and a comparison is made in order to check if the required SIL level has been achieved or not. The SRS must be improved until the required SIL level is achieved. The performance of the SRS is measured using the PFD_{avg}, PFH, SFF and HFT measures. The standard takes into account PFD_{avg} for low demand system and PFH for high demand systems. Table 2 shows SIL levels and their corresponding probability intervals for PFD_{avg} and PFH. Table 3 shows the maximum allowable SIL when SFF and HFT is taken into account. Values of table 2 and table 3 are taken from the standard IEC 61508. IEC 61508 defines the safety level and safety conditions that must be ensured by all E/E/PE devices and all industrial standards are derived from this standard. Therefore these values are well suited for this study.

Table 2. PFD_{avg} and PFH values and their corresponding SIL levels

SIL	PFD_{avg}	PFH
4	$\geq 10^{-5}$ to $< 10^{-4}$	$\geq 10^{-9}$ to $< 10^{-8}$
3	$\geq 10^{-4}$ to $< 10^{-3}$	$\geq 10^{-8}$ to $< 10^{-7}$
2	$\geq 10^{-3}$ to $< 10^{-2}$	$\geq 10^{-7}$ to $< 10^{-6}$
1	$\geq 10^{-2}$ to $< 10^{-1}$	$\geq 10^{-6}$ to $< 10^{-5}$

Table 3. Maximum allowable SIL for a safety related function

SFF	HFT		
	0	1	2
≤ 60%	Not Allowed	SIL 1	SIL 2
60% – <90%	SIL 1	SIL 2	SIL 3
90% – <99%	SIL 2	SIL 3	SIL 4
≥ 99%	SIL 3	SIL 4	SIL 4

2.3. Markov Model Analysis

In safety related systems system availability is very important therefore these systems are usually repairable systems. Simple probabilistic methods cannot adequately model repairable systems when issues such as system configuration, entire or partial system repairs, repair time, diagnostic time, diagnostic coverage, etc. are taken into consideration. In order to introduce these parameters Markov model is a good alternative. Markov models have two components: states and the transitions. States are represented by circles while transition curves are represented by lines with direction arrows.

These transition rates and the states can be written as a matrix rows representing states and matrix entities representing transitions. System model can be expressed as equation (8) where P is the transition matrix and x is the probability vector of states at time t:

$$\dot{x}(t) = x(t) \cdot P \tag{8}$$

Probability of failure on demand is calculated as shown in equation (9) where the initial state condition vector is x_0 and c is a constant vector defining in which states the system is safe:

$$PFD(t) = 1 - x_0 \cdot x^{Pt} \cdot c^T \tag{9}$$

3. Description of railway power supply systems

Railway systems consist of many critical sub-systems that require clean power without drop-offs or variances which is why power supply systems are a crucial part of the railway systems. Power supply system generally converts the electrical energy from the national grid and feeds all components of the railway system. A malfunction in the power supply system can cause unacceptable situations resulting serious passenger grievances or accidents. In order to prevent these kinds of situations, the safety analysis of the system must be made and the required SIL level have to be accomplished. In this context, a railway power supply system of Istanbul Transportation Co. is analysed as an example system but introduced models in this paper can easily be extended and adopted to other railway power systems.

Railway power supply system consists of five main parts which are traction power transformers, the ring line which connects substations to each other, Medium Voltage Switchgear System, DC Switchgear System and the catenary line.

Power supply system is connected to the national grid via three main feeding points and the traction power needed on the catenary line is supplied through 11 substations. These substations are connected to each other because of high reliability and flexible management advantages. Electrical diagram of the power supply system is given in figure 2.

Inside the substation medium voltage busbar is connected to the traction power transformer via a medium voltage circuit breaker. Traction power transformers have one primary connected in delta and two secondary connected in delta and star. These power transform-

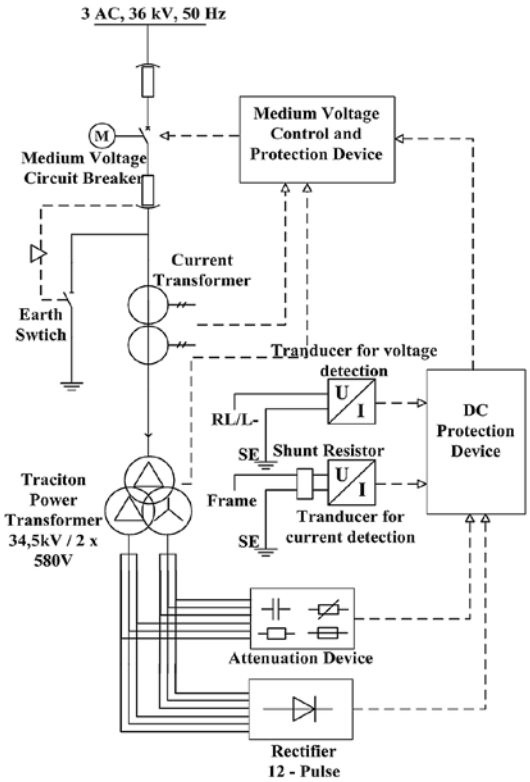

Fig. 2. Electrical diagram of the power supply system

ers transform incoming 34,5 kV to 580V. Afterwards a rectifier converts 580 V. AC into 750 V. DC. Positive pole of the rectifier is connected to DC busbar via manual disconnector. From the DC busbar using DC cables, four DC circuit breakers and a manual disconnector the catenary line is energized. Rolling stocks get the power they need from this catenary line using a pantograph and the circuit is completed when the rails are connected to the negative pole of the rectifier by means of disconnector. In this study only the safety system of the traction power transformer's medium voltage circuit breaker is analyzed by taking account the protection functions which protect the traction power transformer and rectifier from the AC and DC side. The safety system consists of four safety related functions which cause a tripping of the traction power transformer's medium voltage circuit breaker as listed below. In the system two control systems are used, one for the DC section and another for the medium voltage section of the system. Voltage detection and current detection which are called frame leakage faults are first received by the control system which is on the DC section then later transferred to the medium voltage control system. In this paper medium voltage control system is considered as the main control system and DC control system is considered as the secondary control system.

Current inside the traction transformers phases is tracked by a connected current transformer. Secondary winding of the current transformer is connected to the main control system and if the current exceeds a predetermined threshold value the main control system sends an open command to the medium voltage circuit breaker.

- The temperature of the traction power transformer's coils is tracked using a thermistor. The temperature readings of the thermistor is monitored by a temperature relay and if the temperature exceeds a predetermined value the main control system sends an open command to the medium voltage circuit breaker.
- This SRF is one of two types of frame leakage fault detections. In this case the voltage between DC switchgear frame (structure earth) and traction earth (negative potential) is measured. This voltage detection identifies dangerous touch voltages which may occur in the switchgear. The measuring value is determined by means of a voltage transducer. If the voltage exceeds a predetermined value four DC circuit breakers through secondary control system and medium voltage circuit breaker through main control system are switched off.
- The other frame leakage fault detection is the current detection between DC switchgear and structure earth. If a current is detected between DC switchgear frame and structure earth this means the isolation between +750 V positive circuits and the frame failed. The measuring value is determined by means of a shunt resistor and a current transducer. If the current exceeds a predetermined value four DC circuit breakers through secondary control system and medium voltage circuit breaker through main control system are switched off.

The block diagram of the system is given in figure 3.

Probability of someone getting harmed inside a power station is very unlikely but since the station feeds trams through the catenary line, high voltages or high currents or even the lack of power can indirectly harm many passengers, personnel and even people nearby tramlines. Based on figure 1, the risk parameters will be CD, FB, PA and W2 respectively. Based on these parameters the required SIL of the system have to be SIL 3 and from table 1 the of the system should be between.

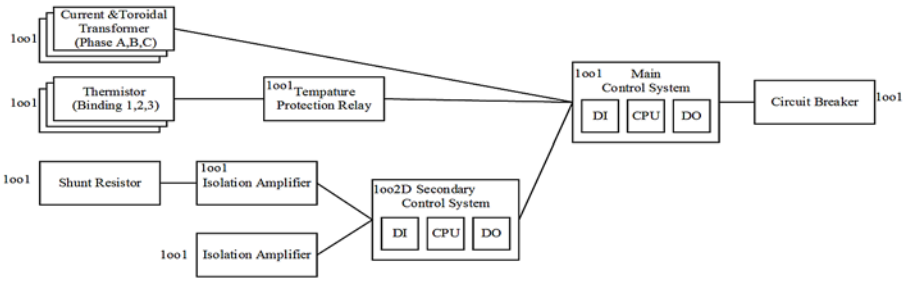

Fig. 3. The block diagram of the system

4. Reliability analysis of the power supply system

An SRS is made up of sensors, control units and actuators. For precise calculation the reliability parameters must be authentic, to ensure this data provided from the vendor and the OREDA (Offshore Reliability Data) has been used in this study and these failure rates of MV switchboard is given in table 5 [4]. There are 6 main SRFs in this safety system and they are described in table 4.

Table 4. The description of the SRFs

SRF Number	Description
SRF 1	Power transformers phase current is above limit detection function
SRF 2	Power transformers temperature is above limit detection function
SRF 3	Catenary voltage is above limit detection function
SRF 4	Catenary current is above limit detection function

Table 5. Failure rates of the MV switchboard

Parts and components	Failure Mode	Fault Type	Failure Rate	
Current & toroidal transformer	Burn out / loss of insulation	Dangerous undetected	λ_{Tdu}	0.28*10-6
Thermistor	Burn out / Faulty Measurement	Dangerous undetected	λ_{Thdu}	0.354*10-6
Main Control unit	Loss of function	Dangerous detected	λ_{Cdd}	0.322*10-6
Compartments of the Switchboard	Loss of insulation property & internal arc fault	Dangerous undetected	λ_{SBdu}	0.53*10-6
Apparatus Circuit Breaker	Spurious opening	Safe	λ_{Bs}	0.115*10-6
	Failure to close	Safe	λ_{Bs}	0.285*10-6
	Failure to open	Dangerous undetected	λ_{Bdu}	0.285*10-6
	Leakage of gas	Dangerous detected	λ_{Bdd}	0.148*10-6
Shunt Resistor	Faulty Measurement	Dangerous detected	λ_{SRdd}	2.0*10-9
	Loss of frame earthing	Dangerous detected	λ_{SRdd}	2.0*10-10
Isolation Amplifier	Faulty conversion	Dangerous detected	λ_{IAdd}	0.5930*10-6
	Failure of electrical isolation components	Dangerous detected	λ_{IAdd}	0.0053*10-6
Secondary Control Unit	Invalid info of switching status	Safe	λ_{DCPs}	0.3*10-6
	Faulty function of protection and control switchgear panel	Safe	λ_{DCPs}	1*10-6
	Faulty function of protection	Dangerous detected	λ_{DCPdd}	1.2*10-6
Temperature sensing element	Burn out / loss of insulation	Dangerous detected	λ_{Tsedd}	4.5*10-6
	Wire Short / Drift	Dangerous undetected	λ_{Tsedu}	0.25*10-6
Temperature transmitter	Loss of function	Dangerous detected	λ_{Ttdd}	0.193*10-6
	Loss of function	Dangerous undetected	λ_{Ttdu}	0.085*10-6

Calculations have been done with the following assumptions:

- For all SRF components proof test interval is assumed to be 1 year and testing is presumed to be ideal.
- All redundant components are assumed to have the same failure rate.
- Repair is presumed to be ideal and MTTR is presumed to be 8 hours.
- Cable and pipe installation failures are neglected.
- The beta factor is accepted as 2% which is recommended in IEC61508-6 Annex D.
- An exponential failure rate distribution is presumed for all components as suggested in the ABB Power Technologies handbook and OREDA.
- The detection time is assumed to be 1 hour.
- The probability of two or more components have state transitions at the same time is zero.

The Markov model developed for safety related function 3 is shown in figure 4, where μ_r, μ_{LT} and μ_d represents repair time, testing interval time and detection time respectively. Also μ_S is the addition of all safe failure rates. In the model, state 1 indicates that all components of the system are working flawlessly. State 6 shows the combined safe faults of all components and in this state the system is shut down until all detectable faults are fixed. Thus safe failures effects the reliability of the system negatively but does not affect the safety of the system. State 2 indicates that one of the two secondary control system have failed. Since the secondary control system is 1002D, SRS is still operational. From state 2 if the last secondary control system fails before fault is detected a transition is made to state 3 in which the SRS fails. States 9 and 5 represents when isolation amplifier and main control system fails respectively. If a failure is detected a transition is made to safe state immediately. Only exception being state 7 because it represents an error on the breaker, which is the component that transitions the system into safe state. Lastly states 4 and 5 represent where an undetectable dangerous fault happens on the switchboard and the breaker respectively. These faults are not repairable since they are not detected. Only in states 1, 2 and 6 our system is safe. From the Markov model in fig. 4 translation matrix and the constant matrix are obtained. Substituting probability vector of states, which is calculated from equation (8), into equation (9) PFD_{avg} values are calculated. Following a very similar path PFD_{avg} values for other SRFs can be calculated.

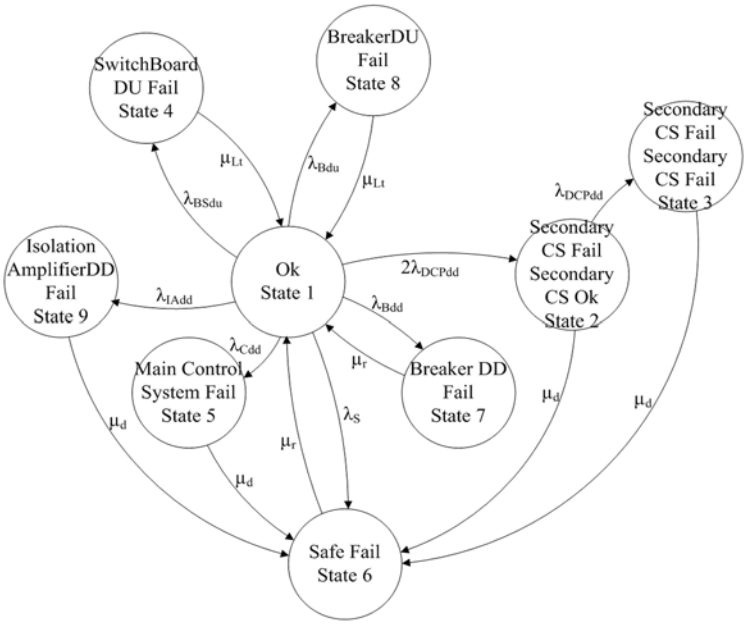

Fig. 4. Markov model for SRF4

Table 6. PFD_{avg} calculation results

SRF Number	PFD_{avg} calculation using Tree Analysis	PFD_{avg} calculation using Markov Analysis	SFF(%)	HFT	SIL
SRF 1	$9.3\ 10^{-3}$	$7.2\ 10^{-3}$	62.50%	1	2
SRF 2	$6.9\ 10^{-2}$	$7.2\ 10^{-3}$	62.50%	1	2
SRF 3	$8.2\ 10^{-3}$	$3.5\ 10^{-3}$	65.25%	1	2
SRF 4	$8.2\ 10^{-3}$	$3.5\ 10^{-3}$	65.25%	1	2

Table 6 shows the results of the analysis and the PFD_{avg} values calculated using Fault Tree analysis. The safety level of the overall system is the minimum SIL of all SRFs. Therefore desired SIL level, which has been decided on as level 3, is not accomplished meaning this railway system is not safe as required.

There is a huge gap between PFD_{avg} values calculated from Fault Tree analysis and Markov model analysis such that in SRF 2 this difference causes the SIL level to appear as level 1 when it should be level 2. It should be noted that if there is inadequate information or less information about the system components then the obtained values from FTA and Markov are nearly same. On the other hand if detailed information is obtained about the system components like detailed failure modes, its failure rates, repair times, diagnostic coverage, proof test interval time, proof test coverage factor, etc. than the calculated PFD_{avg} values are seriously different. This is actually an expected variation as the dynamics of the system can be further expressed by Markov models.

Then these results support our view which is that power supply subsystems of railway systems must be considered and analyzed as a SRS and furthermore while analysing SRSs Markov models should be used because of Markov models highly detailed modelling capabilities.

5. Conclusion

Railway power supply systems are generally not considered as a safety system and therefore they are also not analysed as one. This is a significant hazard for not only human life but also for the system itself. In this paper railway power supply system's safety related functions are examined and each function is modelled in detail using Markov modelling method. The introduced models are modular and can easily be applied to all railway power supply systems. Also the desired safety integrity level of the power supply system is calculated by examining the risk factors. In this context, a power supply system of Istanbul Transportation Co. is analysed to demonstrate how to apply our modelling method and the results strengthen the claim that all railway supply systems should be considered and analysed as safety related systems. Furthermore when Markov modelling and Fault Tree modelling is compared using data from the analysis, the superiority of Markov modelling is observed for this problem. The reason behind this superiority is that the introduced Markov models represent the system failure dynamics better when detailed information on the failure modes of the system components are known.

References

1. Börcsök J., "Functional Safety - Basic Principles of Safety - Related Systems. Huthig Gmbh & Co. KG Heidelberg, Germany, 2007.
2. CENELEC(European Committee for Electrotechnical Standardization). 2011. Railway Applications -Communication, Signaling and Processing Systems - Software for railway control and protection systems. EN 50126 London: British Standard Institution.
3. Collong S. and Kouta R. - Fault tree analysis of proton exchange membrane fuel cell system safety. Int. J. Hydrogen Energy 2015; 40 (25): 8248–8260, http://dx.doi.org/10.1016/j.ijhydene.2015.04.101.
4. DNV (Det Norske Veritas). 2002. OREDA, Offshore Reliability Data Handbook. 4th. ed. Norway: Det Norske Veritas AS (DNV).
5. Eliassi M., Dashtaki A. Khoshkholgh, Seifi H., Haghifam M.-R., and Singh C. - Application of Bayesian networks in composite power system reliability assessment and reliability-based analysis. IET Gener. Transm. Distrib. 2015; 9 (13): 1755–1764, http://dx.doi.org/10.1049/iet-gtd.2014.0660.
6. Eom B. G. and Lee H. S. - Assessment of running safety of railway vehicles using multibody dynamics. Int. J. Precis. Eng. Manuf. 2010: 11 (2): 315–320, http://dx.doi.org/10.1007/s12541-010-0036-x.
7. He J., Sun Y., Kirschen D. S., Singh C., and Cheng L. - State-space partitioning method for composite power system reliability assessment. IET Gener. Transm. Distrib. 2010; 4 (7): 780-785, http://dx.doi.org/10.1049/iet-gtd.2009.0281.
8. Hellmich M. and Berg H. P. - Markov analysis of redundant standby safety systems under periodic surveillance testing. Reliab. Eng. Syst. Saf. 2015; 133: 48–58, http://dx.doi.org/10.1016/j.ress.2014.08.007.
9. IEC (International Electrotechnical Commission). 2002. Electrical/Electronic/Programmable Electronic Safety-Related Systems. IEC 61508. New York: IEEE Standards Association.
10. International Electrotechnical Commission, "BS EN 50128:2011 "Railway applications. Communication, signalling and processing systems. Software for railway control and protection Systems", IEC Standards Online, 2011.
11. Kaymakci O. T., Ustoglu I., and Divriklioglu E. -Reliability assessment of fire safety systems in railway industry: a case study. Journal of the Chinese Institute of Engineers 2015; 38 (3): 286-296, http://dx.doi.org/10.1080/02533839.2014.981208.
12. Longhi A. E. B., A. A. Pessoa, and P. A. D. A. Garcia - Multiobjective optimization of strategies for operation and testing of low-demand safety instrumented systems using a genetic algorithm and fault trees. Reliab. Eng. Syst. Saf. 2015; 142: 525–538, http://dx.doi.org/10.1016/j.ress.2015.06.010.
13. Macii D., Dalpez S., Passerone R., Corrà M., Avancini M., and Benciolini L. - A safety instrumented system for rolling stocks: Methodology, design process and safety analysis. Measurement 2015; 67: 1–13, http://dx.doi.org/10.1016/j.measurement.2015.01.002.
14. Marquez F. P. G., Weston P., and Roberts C. - Failure analysis and diagnostics for railway trackside equipment. Eng. Fail. Anal. 2007; 14 (8): 1411–1426, http://dx.doi.org/10.1016/j.engfailanal.2007.03.005.
15. Mechri W., Simon C., Bicking F., and Othman K. Ben - Fuzzy multiphase Markov chains to handle uncertainties in safety systems performance assessment. J. Loss Prev. Process Ind. 2013; 26 (4): 594–604, http://dx.doi.org/10.1016/j.jlp.2012.12.002.
16. Purba J. H. - A fuzzy-based reliability approach to evaluate basic events of fault tree analysis for nuclear power plant probabilistic safety assessment. Ann. Nucl. Energy 2014; 70: 21–29, http://dx.doi.org/10.1016/j.anucene.2014.02.022.

17. Rausand M. and Høyland A. - System Reliability Theory: Models, Statistical Methods and Applications. Hoboken: John Wiley 2004.
18. Rocha J. M., Henriques A. a., Calçada R., and Rønnquist A. -Efficient methodology for the probabilistic safety assessment of high-speed railway bridges. Eng. Struct. 2015; 101: 138–149, http://dx.doi.org/10.1016/j.engstruct.2015.07.020.
19. Rosinski A, Dabrowski T. - Modelling reliability of uninterruptible power supply units. Eksploatacja i Niezawodnosc – Maintenance and Reliability 2013; 15 (4): 409–413.
20. Shalev D. M. and Tiran J. - Condition-based fault tree analysis (CBFTA): A new method for improved fault tree analysis (FTA), reliability and safety calculations. Reliab. Eng. Syst. Saf. 2007; 92 (9): 1231–1241, http://dx.doi.org/10.1016/j.ress.2006.05.015.
21. Shu Y. and Zhao J. - A simplified Markov-based approach for safety integrity level verification. J. Loss Prev. Process Ind. 2014; 29 (1): 262–266, http://dx.doi.org/10.1016/j.jlp.2014.03.013.
22. Villa-Jaén A. de la, Martínez-Laca-ina P. J., and Martínez-Ramos J. L. - Hybrid procedure including subtransmission systems and substations for reliability assessment. IET Gener. Transm. Distrib. 2013; 7 (12): 1461–1472, http://dx.doi.org/10.1049/iet-gtd.2012.0748.
23. Zhang T., Long W., and Sato Y. - Availability of systems with self-diagnostic components - Applying Markov model to IEC 61508-6. Reliab. Eng. Syst. Saf. 2003; 80 (2): 133–141, http://dx.doi.org/10.1016/S0951-8320(03)00004-8.

Muhammet Ali OZ
Ozgur Turay KAYMAKCI
Department of Control and Automation Engineering
Yildiz Technical University
Esenler/Istanbul, 34220 Turkey

Ayhan KOYUN
Department of Maintenance
Istanbul Transportation Co.
Esenler/Istanbul, 34200 Turkey

E-mails: maoz@yildiz.edu.tr, kaymakci@yildiz.edu.tr, ayhankyn@gmail.com

Article citation info:
MARCZUK A, CABAN J, SAVINYKH P, TURUBANOV N, ZYRYANOV D. Maintenance research of a horizontal ribbon mixer. Eksploatacja i Niezawodnosc – Maintenance and Reliability 2017; 19 (1): 121–125, http://dx.doi.org/10.17531/ein.2017.1.17.

Andrzej MARCZUK
Jacek CABAN
Petr SAVINYKH
Nikolay TURUBANOV
Dmitry ZYRYANOV

MAINTENANCE RESEARCH OF A HORIZONTAL RIBBON MIXER

BADANIA EKSPLOATACYJNE MIESZALNIKA WSTĘGOWEGO POZIOMEGO

During operation of the mixing device there are many technical problems affecting technological processes implemented with their involvement. In order to improve the efficiency of feeding with mixed feed, mixed feed should be prepared from quality mixes. Despite the widespread use of various types of mixers, their operation is not sufficiently understood, therefore the study of the effects of the design and technological parameters on mix quality is an urgent task. Experimental studies were carried out in the livestock farming mechanisation laboratory of the North-East Scientific Research Institute of Agriculture of the Federal State Budgetary Scientific Institution. The article presents the research of the feed mix composed of barley and rice as a base mix, and feed mix of peas used as a reference component.

***Keywords**: energy consumption, feed mixing, maintenance, mathematical modelling, mixing parameters.*

Podczas eksploatacji urządzenia mieszającego występuje wiele czynników technicznych wpływających na procesy technologiczne. W celu poprawienia przyswajalności mieszanek paszowych, powinny one być wytworzone na mieszalnikach zapewniających jednorodność i wysoką jakość mieszanek. Pomimo powszechnego stosowania różnych rodzajów mieszalników, procesy w nich zachodzące nie są do końca rozpoznane, a zatem badanie wpływu konstrukcji i parametrów technicznych na jakość mieszanki jest zagadnieniem stale aktualnym. Badania doświadczalne zostały przeprowadzone w Laboratorium Mechanizacji Produkcji Zwierzęcej w Strefowym Instytucie Naukowo-Badawczym Rolnictwa Północno-Wschodniego Rosyjskiej Akademii Nauk. W artykule przedstawiono badania mieszanki paszy złożonej z jęczmienia i ryżu jako mieszanki bazowej oraz mieszanki paszowej grochu wykorzystywanej jako komponent odniesienia.

***Słowa kluczowe**: zużycie energii, mieszanie pasz, konserwacja, modelowanie matematyczne, parametry mieszania.*

1. Introduction

Technological progress is the counterpart to the growing demand for novel machines and devices that should be characterised by high reliability, functionality, and an extended time of operation in extreme conditions [9], as well as the achievement of the assumed accuracy of machining [16]. Exploitation of structural elements of machines and technical devices usually significantly differs from the parameters in the above in standards [9] or technical data sheets machines. One of the contemporary challenges in the field of manufacturing systems design is to define the optimal level of their flexibility from the realized manufacturing tasks point of view [3]. The diversity of operating environments in which work feed mixers, created the demand for test and research apparatus and simulation methods enabling the reconstruction of the process in a way resembling real life operation conditions.

Experimental work published so far has focused on operating conditions such as rotation rate, mixer inclination angle, and flow rate [12]. The operation efficiency depended on friction conditions, collisions, cutting, and the machinery design features [1]. While several types of continuous mixers have been built, and many more can easily be conceived, only a few geometric designs have been examined in the literature [12]. Therefore the study of the effects of the design and technological parameters on mix quality is an urgent task.

The mixing process is essential for manufacturing animal feed, and due to the increased use of low-inclusion ingredients, its efficiency becomes even more important, as well as the methods to evaluate this efficiency [13]. When different ingredients are combined to supply a complete animal feed, manufacturers must be able to guarantee that each animal receives the same amount of nutrients and additives in adequate concentrations to meet growth, production, and health requirements [8]. With the increased use of low-inclusion ingredients, such as vitamins, micro-minerals, amino acids and other feed additives in animal nutrition, efficient mixing processes become even more necessary [5]. Feed cost accounts for up to 65% of the production cost of chicken meat and eggs, and therefore attracts attention as a major opportunity to lower the product cost and increase profits [15]. That is why the process costs of producing dry compound feedstuffs must be kept as low as possible, while complying with quality requirements [2]. The feeds are defined according to certain specifications with regard to nutritive composition based on specified descriptions for nutritional, hygienic and physical quality [17].

One way to increase the livestock production efficiency is to give high-quality complete feeds to livestock animals. When doing this, the best way an agricultural enterprise can provide itself with such feeds in accordance with its needs is if it manufactures its own mixed feed. Cereals are very common ingredients in the food and feed production chain [6].

The final operation in the preparation of mixed feed is the mixing of the components in a mixer. It is important in terms of the zootechnics not only to add the components into the feed mix in the correct proportions as provided by the diet, but also to achieve their uniform distribution throughout the mix. The homogeneity of the mix ensures the same nutritional value of the feed in all its portions [20].

2. Maintenance problems of a horizontal ribbon mixer

The operation of the horizontal ribbon mixer is based on the principle of mechanical fluidization of the mixed product. The special shape, position and rotation speed of the mixing tools generates centrifugal rotation, what allows the three-dimensional movement of material and its connection with the other components. Components of different particle size and bulk density will be well very finely homogenised and mixed in the shortest possible time.

Mixers of this type are used for mixing dry powders, granules or short fibers and for moistening, balling and granulation of the same materials or for mixing liquids and pastes with low viscosity. During operation they are exposed to a number of factors affecting their correct operation. These devices operate in varying load conditions and mixed delivery, particularly in animal production. Depending on the operating environment there can be identified the following operational problems:

- damage to the bearings on the shaft,
- damage to the drive unit,
- wear of working components of the mixer,
- wear of mixing tools,
- damage to shaft seals,
- abrasive wear of the operating chamber,
- maintenance for the unit to be clean,
- providing sanitary conditions.

The operation of the mixer in variable operating conditions is a difficult issue for the proper delivery of the material and the degree of difficulty depends on the nature of the variability of loads. This problem is particularly significant in the case of composition of compound feed and their delivery in good time for animals. To assess the value of the operating conditions is used a number of approaches, due to the fact that in practice there are different circumstances allowing (or not) the application of certain methods. The variable values of the loads and shock loads, and vibrations affect the shortening of the life of components of machines and equipment used in the production in the animal farms.

3. Study goals and objectives

A majority of the existing continuous mixing work examines the effect of the convective system and rotation rate on the mixing behaviour and residence time [12]. The goal and objective of the studies is to improve the process of preparing mixed feed in a horizontal ribbon mixer to make it comply with the zootechnical requirements, to improve the quality of the finished product, and to reduce the power consumption of the process.

3.1. Techniques

The experimental studies were carried out in the livestock farming mechanisation laboratory with the use of a PC, measuring and control devices and instruments as per GOST 15.101-98.

The novelty of the complete feed production process is covered by patent No. 2563689 of the Russian Federation, and the design and technological parameters of the mixer are covered by patent No. 2488434 of the Russian Federation [10, 11].

A mix of barley (80%) and rice (20%), specific gravity 0.742 t/m^3, was used as a base mix in the experiments, and peas of specific gravity 0.812 t/m^3 were used as a reference component.

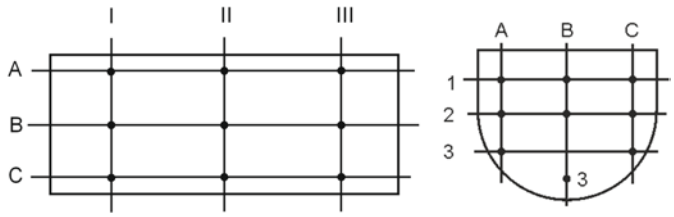

Fig. 1. Scheme of sampling from the mixer: a) horizontal plane; b) vertical plane

Figure 1 shows the scheme of sampling from a horizontal ribbon mixer. Sampling was performed in accordance with GOST R ISO 6497-2011 [4].

It has been experimentally established that if any component is distributed uniformly in the mix, the other components are distributed uniformly as well. We can estimate the homogeneity of a multi-component mix on the basis of the uniform distribution of the 1 or 2 main components in it.

The main qualitative criterion for the efficiency of any mixing device is the homogeneity of the final product. A mix is considered to be homogeneous if the content of components in any part of its volume corresponds to the mix composition prescribed.

The mixing efficiency is determined on the basis of the statistical characteristics of the mix. This characteristic is the uniformity coefficient of the distribution of the main components in the mix [14]:

$$V_c = \left(1 - \frac{\sqrt{\frac{\sum\left(x_i - \bar{x}\right)^2}{n-1}}}{\bar{x}}\right) \cdot 100\%, \tag{1}$$

where: x_i – is the current value of the observed quantity,
$\bar{x}$ – is the arithmetic mean of the observed quantity,
n – is the number of samples.

The mixer operating time is determined from the formula:

$$t_p = t_Z + t_{\mathrm{CM}} + t_{\mathrm{B}}, \tag{2}$$

where: t_Z – is the mixer loading time in min.,
t_{CM} – is the component mixing time in min.,
t_{B} – is the finished product discharge time in min.

Mixer capacity Q, in t/h, is determined from the formula:

$$Q = \frac{m_{\mathrm{o}} + m_{\mathrm{K}}}{t_p} \cdot 60, \tag{3}$$

where: m_{o} – is the mass of the base mix, t,
m_{K} – is the mass of the reference component, t.

The power W (in watts) supplied for the experiment is determined from the formula:

$$W = \frac{3 \cdot U_{\Phi} \cdot I \cdot \cos\varphi}{60} \cdot t_{\mathrm{CM}}, \tag{4}$$

where: U_{Φ} – is the phase voltage, V,
I – is the current measured with ammeter, in amperes,
$\cos\varphi$ – is the power coefficient = 0.85.

The specific energy consumption, in kWh/t is determined from the formula:

$$q = \frac{3 \cdot U_{\Phi} \cdot I \cdot \cos\varphi}{1000 \cdot Q} . \quad (5)$$

4. Research results and discussions

To determine the required mixing time for the components, single-factor experiments were carried out which showed the dependence of the uniformity coefficient on the mixing time (Figure 2).

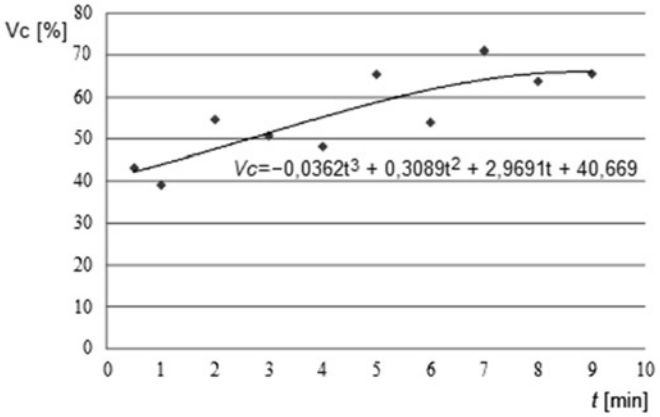

Fig. 2. Relationship between the mix uniformity coefficient and mixing time

An analysis of Figure 2 demonstrates that the best mix uniformity coefficient is achieved with a mixer operating time of 6-8 minutes. On this basis, the mixing time interval will be 4-8 minutes in future studies.

Following the single-factor experiments, research was carried out using multi-factor experiment planning techniques to establish the optimal design parameters and a more complete study of the working process. The factors indicated below were chosen as the factors to be studied, based on the single-factor experiments:

x_1 – quantity of the main component,
x_2 – quantity of the reference component,
x_3 – mixing time.

The indices indicated below were chosen as the optimisation criteria:

y_1 – mix uniformity coefficient V_c (%),
y_2 – power W supplied for experiment in watts,
y_3 – capacity Q in t/h,
y_4 – specific energy consumption in kWh/t.

The matrix of the Box-Behnken plan was used in the experiments (Table 1). The multi-factor experiment that was carried out let us obtain approximate mathematical models of the process which link together all the factors taken into account. From the experimental studies we can determine the numerical values of the coefficients of the equations of the mathematical models, the magnitude of which let us judge the extent of influence of the relevant factors.

The multi-factorial experiment carried out enabled approximate mathematical models for the process to be obtained which link together all the factors taken into account. From the experimental studies we can determine the numerical values of the coefficients in the equations in the mathematical models, the magnitude of which let us judge the significance of the relevant factors. The experimental results were processed on a computer and the following mathematical models were obtained (insignificant factors excluded):

Table 1. Matrix of Box-Behnken plan, intervals and variation in the levels of factors

Parameters	Factors		
	Quantity of base mix	Quantity of the reference component	Mixing time
	x_1	x_2	x_3
High level (+)	900 kg	150 kg	8 minutes
Basic level (0)	750 kg	100 kg	6 minutes
Low level (-)	600 kg	50 kg	4 minutes

$$y_1 = 79.76 - 11.87 \cdot x_1 - 2.42 \cdot x_3 - 8.08 \cdot x_1^2 + 2.12 \cdot x_1 \cdot x_3 - 2.14 \cdot x_3^2 \quad (6)$$

$$y_2 = 885.22 - 53.71 \cdot x_1 + 30.79 \cdot x_2 + 300.88 \cdot x_3 + 18.91 \cdot x_1^2 - 6.12 \cdot x_1 \cdot x_2 + 21.17 \cdot x_1 \cdot x_3 + 13.70 \cdot x_2 \cdot x_3 \quad (7)$$

$$y_3 = 5.1 + 0.91 \cdot x_1 + 0.30 \cdot x_2 - 1.06 \cdot x_3 - 0.18 \cdot x_1 \cdot x_3 - 0.06 \cdot x_2 \cdot x_3 + 0.2125 \cdot x_3^2 \quad (8)$$

$$y_4 = 1.732 - 0.213 \cdot x_1 - 0.045 \cdot x_2 + 0.358 \cdot x_3 + 0.078 \cdot x_1^2 - 0.037 \cdot x_1 \cdot x_3 + +0.005 \cdot x_2^2 \quad (9)$$

Analysis of the mathematical models (6-9) obtained on the basis of the significance of the coefficients in the regression equations leads to the conclusion that the amount of the reference component in the mix (x_2) has only a slight effect on the optimisation criteria considered. The main factor affecting the mix uniformity coefficient ν_c is the quantity of base mix in the mixer (x_1). The power supplied for experiment W, capacity Q, and specific energy consumption q are mostly affected by the product mixing time (x_3).

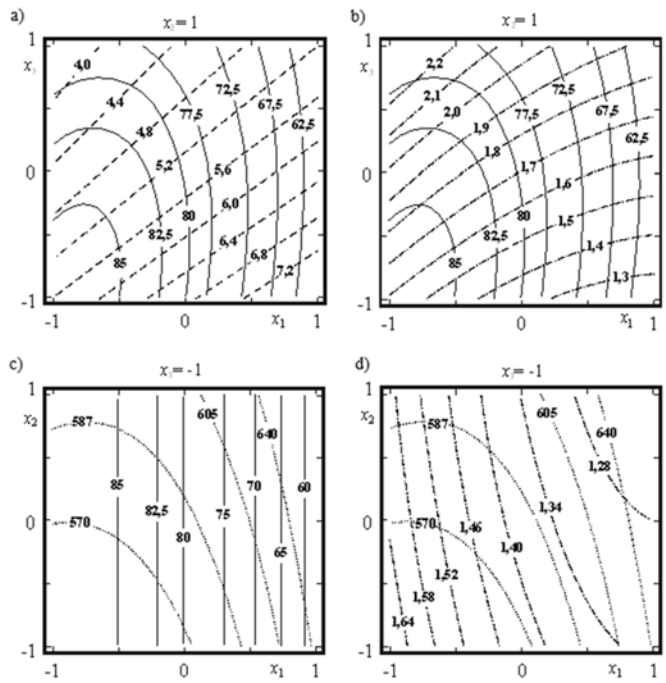

Fig. 3. Two-dimensional cross-sections of the response surface, characterising the influence of the weight of base mix (x_1), weight of reference component (x_2), and mixing time on the: a) finished product uniformity coefficient V_c (———— - y_1), mixer capacity Q (— — — — - y_3); b) finished product uniformity coefficient V_c (———— - y_1), specific energy consumption q (-·-·-·-·- y_4); c) finished product uniformity coefficient V_c (———— - y_1), power supplied for the experiment W (····· - y_3), d) power supplied for the experiment W (·····-y_3), specific energy consumption q (-·-·-·- y_4)

Based on the analysis of the mathematical models (6-9) and the two-dimensional cross-sections of the response surface (Fig. 3), the following may be concluded:

As illustrated in Figure 3a), if the amount of base mix (x_1) decreases from 900 to 650 kg, and mixing time (x_3) decreases from 8 to 4 minutes, with a quantity of reference component of 150 kg, the mix uniformity V_c increases from 62% to 86.1%, and the mixer capacity Q decreases from 7.2 t/h to 5.6 t/h. The maximum uniformity coefficient V_c = 86.1 of the finished product is achieved with a quantity of base mix x_1 = 620 kg, reference component in the mix x_2 = 146 kg, and mixing time x_3 = 4 minutes, in which case the capacity is Q = 5.6 t/h.

As illustrated in Figure 3b), if the amount of base mix (x_1) decreases from 900 to 650 kg, and mixing time (x_3) from 8 to 4 minutes, with the reference component content 150 kg, the mix uniformity V_c increases from 62 % to 86.1 %, and specific energy consumption q decreases from 1.9 to 1.6 kWh/t. With a maximum finished product uniformity coefficient ν_c = 86.1 %, the specific energy consumption q = 1.6 kWh/t.

Basing on the analysis of two-dimensional sections of the response surface (Figure 3c), the decrease in the amount of base mix (x_1) from 900 to 650 kg, and in the amount of reference component (x_2) from 150 to 50 kg with a mixing time 4 leads to a decrease in the power supplied to the experiment W from 640 kWh/t to 547.5 kWh/t, and an increase in the mix uniformity ν_c from 60% to 86.1%.

As illustrated in Figure 3 d), an increase in the weight of the base mix (x_1) from 650 to 900 kg, with a mixing time 4 minutes, and reference component weight 50 kg, leads to an increase in the power W supplied for the experiment from 547.5 kWh/t to 640 kWh/t, and a decrease in the specific energy consumption q from 1.64 kWh/t to 1.24 kWh/t. The increase in the content of the reference component in the mix (x_2) from 50 to 150 kg, with a weight of base mix of 600 kg and mixing time of 4 minutes, leads to a decrease in the specific energy consumption q from 1.64 kWh/t to 1.58 kWh/t. Even though the increase in the weight of base mix leads to an increase in the power supplied to the experiment, the specific energy consumption decreases due to the fact that the value of mixer capacity is greater than the variation value of the power supplied for the experiment.

5. Conclusion

Summarizing, it must be remembered that while identifying the mathematical model of the horizontal ribbon mixer the mathematical model describes the actual fodder mixer only in an approximate way. Furthermore, it must be added that the conditions in which the identification of the solution model is carried out may be materially different from the actual operation conditions of the blender [18]. The mixing process is highly complicated with a number of affecting parameters, such as the particle properties, the structure and performance of the mixer, the mixing process parameters and the particle feeding order [19].

Experimental studies have shown that mixing time have a clearly influence on the quantity of mixing component, mix uniformity coefficient, capacity and specific energy consumption. According to the experimental results, the maximum product uniformity coefficient V_c = 86.1% is achieved with 620 kg of the base mix, 146 kg of the reference component in the mix, mixing time 4 minutes, and a mixer capacity Q = 5.75 t/h, with a specific energy consumption q = 1.55 kW*h/t.

In the future work in continuous mixing will further increase the number of parameters examined in the analysis and determine the most significant parameters on its operational. The findings in this study can be the indications to the actual industrial production of feed. Above mentioned problems justify the need to develop new and improve existing solutions of lines for preparation and feeding, corresponding to the current criteria in terms of saving energy and resources, as well as fuller compliance of zootechnical requirements in the technological processes [7].

References

1. Flizikowski J, Sadkiewicz J, Tomporowski A. Functional characteristics of a six-roller mill for grainy or particle materials used in chemical and food industries. Przemysl Chemiczny 2015; 94(1): 69-75.
2. Fürll C, Hoffmann T. Flow properties of components for dry compound feed. Powder Technology 2013; 235: 838-841, http://dx.doi.org/10.1016/j.powtec.2012.11.019.
3. Gola A, Świć A. Computer-aided machine tool selection for focused flexibility manufacturing systems using economical criteria. Actual Problems of Economics 2011; 124: 383-389.
4. GOST R ISO 6497-2011 – Animal feeding stuffs. Sampling. Standard published on 1.1. 2013; 19.
5. Groesbeck C N, Goodband R D, Tokach M D, Dritz S S, Nelssen J L, DeRouchey J M. Diet mixing time affects nursery pig performance. Journal of Animal Science 2007; 85: 1793-1798, http://dx.doi.org/10.2527/jas.2007-0019.
6. Hernandez M, Esteve T, Pla M. Real-time polymerase chain reaction based assays for quantitative detection of barley, rice, sunflower, and wheat. Journal of Agricultural and Food Chemistry 2005; 53: 7003-7009, http://dx.doi.org/10.1021/jf050797j.
7. Marczuk A, Sysuev V A, Aleškin V A, Savinyh P A, Misztal W, Baran S. Podejście systemowe w badaniach maszyn do przygotowania pasz. Lublin: Uniwersytet Przyrodniczy w Lublinie, 2013.
8. McCoy R A, Behnke K C, Hancock J D, McEllhiney R R. Effect of mixing uniformity on broiler chick performance. Poultry Science 1994; 73: 443-451, http://dx.doi.org/10.3382/ps.0730443.
9. Mizak W, Mazurkiewicz A, Smolik J, Zbrowski A. Problems with abrasive dosing in erosive wear process modelling. Eksploatacja i Niezawodnosc – Maintenance and Reliability 2014; 16(4): 559-564.
10. Pat. 2488434 Russian Federation, MPK7 B 01 F 7/8. Mixer / Savinykh P A, Turubanov N V, Romanyuk V, Kiselev A S, Chernyatyev N A. Applicant and patentee – State Scientific Institution "N.V. Rudnitsky North-West Scientific Research Institute of Agriculture" (Russian Federation) and the Institute of Technology and Natural Sciences (Poland). No.2012104920/05, appl. 02/13/2012; publ. 07/27/2013, bull. No. 21.- 5 p: ill.
11. Pat. 2563689 Russian Federation, C1 MPK A 23N 17/00 (2006/01). Mixed feed preparation technique / Sysuev V A, Savinykh P A, Turubanov N V, Chernyatyev N A, Kazakov V A, Saitov V E. Applicant and patentee – State Scientific Institution "N.V, Rudnitsky North-West Scientific Research Institute of Agriculture" of the Russian Academy of Agricultural Sciences (RU); No. 2014113057/13; appl. 04/03/2014; publ. 09/20/2015, bull. No. 26. - 7 p.: ill.
12. Portillo P M, Ierapetritou M G, Muzzio F J. Effects of rotation rate, mixing angle, and cohesion in two continuous powder mixers – A statistical approach. Powder Technology 2009; 194: 217–227, http://dx.doi.org/10.1016/j.powtec.2009.04.010.

13. Rocha A G, Montanhini R N, Dilkin P, Tamiosso C D, Mallmann C A. Comparison of different indicators for the evaluation of feed mixing efficiency. Animal Feed Science and Technology 2015; 209: 249-256, http://dx.doi.org/10.1016/j.anifeedsci.2015.09.005.
14. Savinykh P A, Turubanov N V, Ustyugov S Y, Lodygin D G. Research results for mixing in the vertical screw mixer of a small-sized feed unit. Bulletin of the All-Russian Scientific Research Institute of Animal Husbandry Mechanisation 2005; 15(3): 75-79.
15. Singh Y, Amerah A M, Ravindran V. Whole grain feeding: Methodologies and effects on performance, digestive tract development and nutrient utilisation of poultry. Animal Feed Science and Technology 2014; 190: 1-18, http://dx.doi.org/10.1016/j.anifeedsci.2014.01.010.
16. Świć A, Wołos D, Litak G. Method of control of machining accuracy of low-rigidity elastic-deformable shafts. Latin American Journal of Solids and Structures 2014; 2(11): 260-278.
17. Thomas M, vun der Poe1 A F B. Physical quality of pelleted animal feed 1. Criteria for pellet quality. Animal Feed Science and Technology 1996; 61: 89-112, http://dx.doi.org/10.1016/0377-8401(96)00949-2.
18. Tomporowski A, Opielak M. Structural features versus multi-hole grinding efficiency. Eksploatacja i Niezawodnosc - Maintenance and Reliability 2012; 14(3): 222-227.
19. Xiao X, Tan Y, Zhang H, Jiang S, Wang J, Deng R, Cao G, Wu B. Numerical investigation on the effect of the particle feeding order on the degree of mixing using DEM. Procedia Engineering 2015; 102: 1850-1856, http://dx.doi.org/10.1016/j.proeng.2015.01.323.
20. http://seveks.ru/Smehivanie_kombikorma.htm.

Andrzej MARCZUK
Jacek CABAN
Department of Transporting and Agricultural Machinery
University of Life Sciences in Lublin
ul. Głęboka, 20-612 Lublin, Poland

Petr SAVINYKH
Nikolay TURUBANOV
Dmitry ZYRYANOV
Zone Scientific and Research Institute of North East Agriculture in Russia
The Russian Academy of Agricultural Sciences
164/43 Lenin Str., 610017 Kirov, Russia

E-mails: andrzej.marczuk@up.lublin.pl, jacek.caban@up.lublin.pl,
peter.savinyh@mail.ru, nikolaytu@mfil.ru, dimonzyryanov@vfil.ru

Article citation info:
SKAČKAUSKAS P, ŽURAULIS V, VADLUGA V, NAGURNAS S. Development and verification of a shock absorber and its shim valve model based on the force method principles. Eksploatacja i Niezawodnosc – Maintenance and Reliability 2017; 19 (1): 126–133, http://dx.doi.org/10.17531/ein.2017.1.18.

Paulius SKAČKAUSKAS
Vidas ŽURAULIS
Vaidas VADLUGA
Saulius NAGURNAS

DEVELOPMENT AND VERIFICATION OF A SHOCK ABSORBER AND ITS SHIM VALVE MODEL BASED ON THE FORCE METHOD PRINCIPLES

MODELOWANIE I OCENA AMORTYZATORA I JEGO ZAWORU TALERZOWEGO OPARTE NA ZASADACH METODY SIŁ

In this paper, a mathematical model of a monotube shock absorber's shim valve, which is developed by applying the force (flexibility) method, is described. This method expresses the relationship between displacements and the forces existing in the shock absorber structure. An application of the force method in the field of practical modification of vehicle shock absorbers enables to effectively analyse the influence of a wide range of parameters, including the number of shims in the valve, their disposition and the properties of the material on the level of the damping force. The damping of the shock absorber considerably impacts comfort and road holding characteristics of the vehicle. In addition, a whole model of a monotube shock absorber is designed in this paper. The validation and practical application of the mathematical model were evaluated by carrying out experimental measuring of the characteristics of the shock absorber using a special stand.

***Keywords**: damping characteristics, force method, mathematical model, monotube, shock absorber, shim valve.*

W danej publikacji został opisany model matematyczny zaworu talerzowego jednorurowego amortyzatora, wyprowadzenia którego zastosowano metodę sił. Metoda ta wyraża związki pomiędzy przemieszczeniami i siłami działającymi na elementy amortyzatora. Stosowanie metody sił w praktycznej sferze modyfikacji amortyzatorów samochodowych pozwala efektywnie analizować wpływ różnych parametrów, w tym ilość, wzajemne położenie i właściwości materiałów talerzy zaworu, na generowaną amortyzatorem wielkość siły tłumienia. Tłumienie, które generuje amortyzator, wywiera znaczący wpływ na komfort jazdy samochodem oraz jego dynamikę. W publikacji również został stworzony kompletny model jednorurowego amortyzatora. Walidacja modelu matematycznego oraz możliwość zastosowania jego w praktyce zostały ocenione na podstawie eksperymentalnych pomiarów charakterystyk amortyzatorów na specjalnym stanowisku.

***Słowa kluczowe**: charakterystyka tłumienia, metoda sił, model matematyczny, amortyzator jednorurowy, zawór talerzowy.*

1. Introduction

When a vehicle moves over road irregularities, the appearing oscillations of sprung and unsprung masses negatively affect the driving dynamics and safety [29]. Seeking to improve road holding and normal component of the tire/ground contact forces during various manoeuvres, acceleration and braking, it is necessary to determine precisely the damping characteristics of the modified shock absorber and to control them. It is practically impossible to experimentally evaluate the damping characteristics of shock absorbers, which are obtained upon applying various combinations of a modified shim valve and its shims, due to high costs and considerable time input [1]. It is an actual problem faced while designing shock absorbers for sports cars, so mathematical modelling is an alternative to experimental tests. Taking into account the above-described reasons, the aim of this paper is to develop a mathematical model of a monotube shock absorber with a shim valve, which can be applied in practical activities.

2. Background

Research works on the interaction between a shock absorber and a suspension [4, 5, 9, 12, 20, 24] prove it to be a relevant problem which has great influence on the dynamic stability of the vehicle. Nevertheless, the literature [7, 8, 25] point out that researches on the functional dependencies of damping characteristics on shock absorber and its shim valve properties are highly limited, i.e. the mentioned researches are focused on the impact of the absorber's properties on the suspension of the car and movement of the car and not on the influence of structural elements of the shock absorber on its damping properties.

The first mathematical model of a shock absorber based on experimental researches was presented by H. Lang in 1977 [14]. H. Lang used an 82-parameter analogue computer model that provided good realistic results; however, the designed model was insufficiently developed for investigation of functional dependences of various input parameters. In 1994, K. Reybrouck presented a simplified model of a shock absorber formed of 20 variables. The proposed model was based on the method of semi-empirical coefficients, so it did not consider the effect of internal modifications on shock absorber performance [1, 21]. In 1997, K. Lee presented a mathematical model of a monotube shock absorber. Accurate agreement between the model results and test data were achieved for shock absorber rod velocities up to ± 1 m/s. In the work presented by K. Lee, the impact of a disc valve on damping characteristics is discussed and the finite element method is applied to obtain solutions for the disk valve; however, a shim valve is not analysed [15]. M.S. Talbott designed a mathemati-

cal model of a monotube shock absorber for sports cars that includes a detailed model of a disk valve and a partial discussion of a shim valve [26]. The model proposed by M.S Talbott is used and improved in the literature [22]; however, a specific model of a shim valve is not provided. Nevertheless, in both above-mentioned works, it is proposed to apply Roark's formulas for stress and strain for calculation of deformation of a shim valve; in addition, an application of the superposition principle in the process of shim valve modelling is discussed. Linear and nonlinear models of a shim valve based on the principles of the finite element method, which evaluate the geometrical dimensions of the shims and the properties of the material, are presented in [6]. In this source, the results obtained on applying a linear model and a nonlinear model are compared between each other, their differences, complexity, variables of models are discussed; however, the results obtained on applying the mentioned models are not compared to the results obtained during experimental tests. It is indicated that the simulation time while applying the designed advanced model may take up to 16 hours. In [8], it is proposed to apply the principle of minimum potential energy and Rayleight-Ritz method for modelling a shim valve. Nevertheless, it is pointed out that a large amount of computation must be performed that is not necessary; however, there is no way to find the shim stack tip deflection without solving for all the unknown coefficients. This takes a long time and reduces the overall speed of the shock absorber model code. Y. Ping also designed mathematical models of monotube shock absorbers and examined the influence of the structures of absorbers on their damping characteristics. However, the problems dealt with by the author are not related to the structure of the valves [18, 19], and discrepancies, which were explained by the ignorance of physical properties of the oil (Oil Bulk modulus), were noticed during the model validation. The influence of the technical condition of structural elements of the shock absorber on its exploitation and damping characteristics is examined in literature [2, 3, 4, 11, 13, 28] as well. It can be seen from the provided examples that various research works, where the influence of the structure of a shock absorber on its damping characteristics is discussed, are published; however, in such works, including the reviewed ones, seeking to simplify the process of modelling, various simplifications are made and they predetermine inexact results of modelling or the models becomes too complicated and not ready for practical application. Because of these reasons, the designing of new more accurate mathematical models developed for practical application is a relevant task. The model presented in this paper distinguishes itself from other shim valve mathematical models by the principle of its developing upon applying the force method based on the examination of the interaction between shims and the appearing contact forces.

3. Mathematical model

3.1. Monotube shock absorber mathematical model

The scheme, based on which the general mathematical model of the monotube shock absorber is designed, is presented in Fig. 1.

In literature [8, 15, 18, 26], it has been shown that the chambers pressures depend on numerous parameters, including the shock absorber stroke and velocity. Under isothermal conditions, the pressure

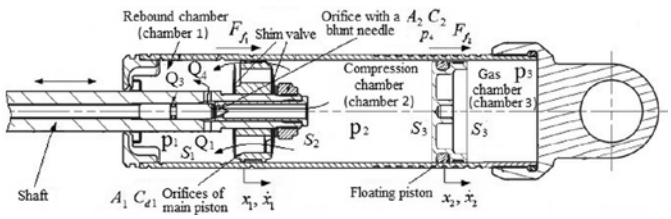

Fig. 1. The scheme of the modelled monotube shock absorber presenting its structure and main parameters

changes in the rebound chamber (the chamber 1 (Fig. 1)) and the compression chamber (the chamber 2 (Fig. 1)) are found from the continuity equations:

$$\frac{dp_1}{dt} = \frac{E}{V_{10} + S_1 x_1}\left(\left(Q_1 + Q_2 + Q_3 + Q_4\right) - \left(S_1 \dot{x}_1\right)\right), \tag{1}$$

$$\frac{dp_2}{dt} = \frac{E}{V_{20} + S_3 x_2 - S_2 x_1}\left(\left(-Q_1 - Q_2 - Q_3 - Q_4\right) - \left(S_3 \dot{x}_2 - S_2 \dot{x}_1\right)\right). \tag{2}$$

where E is Oil Bulk modulus, MPa; V_{10} and V_{20} are the initial volumes of the rebound and compression chambers, m^3; Q_i is the oil flow rate of corresponding orifices, m^3/s (the amount of orifices depends on the construction of the shock absorber, their indexes are explained further in this section (Fig. 1)); S_i is the cross-section area of the relevant chamber, m^2; $\dot{x}_1$ is the velocity of the main piston, m/s; $\dot{x}_2$ is the velocity of floating piston, m/s; x_1 is the displacement of the main piston, m; x_2 is the displacement of the floating piston, m.

Assuming the adiabatic process, the pressure change in the gas chamber (the chamber 3 (Fig. 1)) is expressed as follows:

$$\frac{dp_3}{dt} = -\frac{\gamma p_3 \cdot \left(-S_3 \dot{x}_2\right)}{V_{30} - S_3 x_2}, \tag{3}$$

where V_{30} is the initial volume of the gas chamber, m^3; x_2 is the displacement of the floating piston, m; S_3 is the cross-section area of the gas chamber, m^2; γ is the gas adiabatic constant; p_3 is the gas chamber pressure, Pa.

Eq. 1–3 are the first order coupled ordinary differential equations for p_1, p_2, p_3 and the Dormand-Prince integration method was used to solve these equations. The oil flow rate through the main orifices of the main piston (Q_1), the additional orifices of the piston (Q_2) and the variable orifices (Q_3), is determined by applying the following expression:

$$Q_i = C_{di} \cdot A_i \cdot \operatorname{sign}\left(p_2 - p_1\right) \cdot \sqrt{\frac{1}{\rho}\left(p_2 - p_1\right)}, \tag{4}$$

where C_{di} is the discharge coefficient; A_i is the cross-section areas of the orifices intended for compression or rebound strokes, respectively, m^2; ρ is the density of oil, kg/m^3.

Eq. 4 is not suitable for discharge calculation when the oil leaks between the piston Teflon band and the cylinder of the shock absorber. According to the literature [14, 26], the leakage between the piston Teflon band and the cylinder wall (Q_4) can be modelled as a flow between two parallel plates. The equation for the flow between two parallel plates is derived from the Navier-Stokes equations:

$$Q_4 = \left(\frac{\left(p_2 - p_1\right) b^3}{12 \eta l} + \frac{\dot{x}_1 b}{2}\right) \cdot \pi \cdot D_p, \tag{5}$$

where b is the width of the gap between the piston Teflon band and the cylinder of the shock absorber, m; l is the length of the gap between the piston Teflon band and the cylinder of the shock absorber, m; D_p is the diameter of the piston, m; η is the dynamic viscosity of oil, mPa·s.

The discharge coefficient is strictly a function of Reynolds number, piston acceleration and the geometry [7, 8, 15]. In this study, the dis-

charge coefficients are assumed to be geometry dependent only. In addition, it is assumed that the discharge coefficient is constant and was chosen such that the maximum agreement between the experimental tests' data and the mathematical model is achieved. However, different values were used for compression and rebound since the geometry around orifices is not symmetric. The optimum value of the discharge coefficient for variable diameter orifices during compression is 0.65, during rebound – 0.48. The tested shock absorbers are in excellent working condition, so the oil loss discharge is not modelled.

The dependence of the dynamic viscosity of oil on temperature is evaluated by applying Vogel-Tamman-Fulcher type equation [10]:

$$\eta = \eta_0 e^{\frac{E_0}{R\left(T-T_\eta\right)}}, \tag{6}$$

where η_0 is the constant dynamic viscosity of oil determined at certain temperature T_η, mPa·s; e is Euler's number; E_0 is the oil molecules activation energy, J/mol; T_η is the oil temperature at which the constant dynamic viscosity η_0 of oil was fixed, K; T is the oil temperature during the experiment, K; R is the ideal gas constant, J/mol·K.

The functional dependence of density on temperature is expressed as follows [7]:

$$\rho = \frac{\rho_0}{1+\alpha\left(T-T_t\right)}, \tag{7}$$

where ρ_0 is the constant density of oil determined at certain temperature T_t, kg/m^3; T_t is the oil temperature at which the constant density of oil ρ_0 was fixed, K; α is the coefficient of volumetric thermal expansion, K^{-1}. For the oils usable in shock absorbers, the approximate value of the said coefficient is 0.001 K^{-1} [7].

If a variable orifice with a blunt needle is provided in the shock absorber (Fig. 1), the opened area of the said orifice for oil flowing during the compression and rebound strokes at a certain position of the needle shall be calculated as follows [23]:

$$A_3 = \frac{\pi}{4} d_b^2 \left(1-\left(1-\frac{n_c}{2M_c}\right)^2\right), \tag{8}$$

where d_b is the diameter of the additional orifice, m; n_c is the click number of the variable diameter needle; M_c is the maximum possible number of the needle clicks.

Summing forces on the floating piston, the equation of motion for the floating piston can be written as (Fig. 1):

$$m_2\ddot{x}_2 = S_3 p_2 - S_3 p_3 - F_{f2}\mathrm{sign}\left(\dot{x}_2-\dot{x}_1\right) - m_2 g, \tag{9}$$

where m_2 is the mass of the floating piston, kg; $\ddot{x}_2$ is the acceleration of the floating piston, m/s2; S_3 is the cross-section area of the gas chamber, m^2; g is the standard acceleration due to gravity, m/s^2; F_{f2} is the friction force appearing between the floating piston and the body of the shock absorber, N.

Equation of motion for the main piston can be written as (Fig. 1):

$$m_1\ddot{x}_1 = S_1 p_1 - S_2 p_2 - F_{f1}\mathrm{sign}\left(\dot{x}_1\right) - m_1 g + F, \tag{10}$$

where m_1 is the mass of the main piston, kg; $\ddot{x}_1$ is the acceleration of the piston motion, m/s^2; S_1 is the area of the rebound chamber cross-section, m^2; S_2 is the area of the compression chamber cross-section, m^2; F_{f1} is the friction force appearing between the piston and the body of the shock absorber, N; F is the damping force created by the shock absorber, N.

Eq. 10 is used for expressing the damping force created by the shock absorber as a function of the shock absorber motion:

$$F = m_1\ddot{x}_1 - S_1 p_1 + S_2 p_2 + F_{f1}\mathrm{sign}\left(\dot{x}_1\right) + m_1 g \tag{11}$$

During the compression and rebound, the damping force formed by the shock absorber consists of resistance forces, affecting the main piston in a longitudinal direction. Due to this reason, in order to obtain the expression of the damping force, firstly the equation of motion of the main piston is formed (Eq. 10). The equation of the main piston's motion on the longitudinal axis is formed by projecting the forces in corresponding directions. The directions of the operating forces depend on whether the compression or the rebound process is occurring. The mass m_1 and the acceleration $\ddot{x}_1$ of the main piston are put on the left side of the equation, and on the right side – the sum of all the projections of the operating forces (Eq. 10). By putting all the projections of the forces operating in the corresponding directions in the equation, and reorganising Eq. 10, the sum of all the projections of the operating forces around the main piston is obtained, which is named as the damping force formed by the shock absorber (Eq. 11).

3.2. Shim valve mathematical model

The shim valve model is necessary to model the oil flow rate by the orifice, which allows estimating the theoretical area for oil flowing through the piston formed by the valve deformation. In this paper, while applying the force method for shim valve modelling, it is assumed that, because of deformation of the valve during operation of the shock absorber, gaps appear between shims and the shims contact in the external radii only (Fig. 2a).

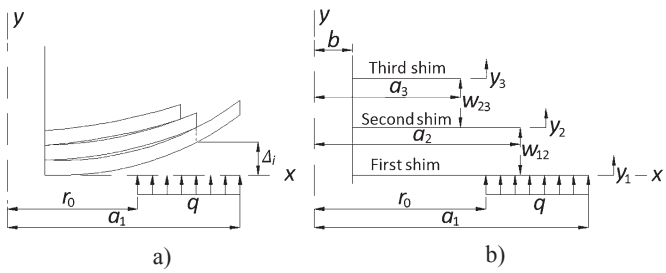

Fig. 2. The scheme of a shim valve when the shims contact in the external radii only: a) the forming gaps between the shims during deformation; b) the computational scheme of the shim valve

It may be seen from the scheme presented in (Fig. 2b) that two main cases of the operating loads may be singled out:

1. Deformation of a shim is caused by the pressure difference (uniform load) appearing between the compression chamber and the rebound chamber during the operation of the shock absorber. This type of load is valid only for the first shim of the valve situated on the piston;
2. The shims of the valve are deformed by contact forces in the contact radii of the shims.

On the basis of the above-mentioned assumption and upon applying the force method, the shim valve is analysed as a statically indeterminate beam system (structure). Also the modelling is based on determining the degree of static indeterminacy and the formation of the system of the principal compatibility equations that expresses the conditions of deformation of the beam structure:

$$\begin{cases} \delta_{11}w_{12} + \delta_{12}w_{23} + ... + \delta_{1i}w_i + \Delta_1 = d_2 w_{12} \\ \delta_{21}w_{12} + \delta_{22}w_{23} + ... + \delta_{1i}w_i = d_3 w_{23} \\ \dots \\ \delta_{n1}w_{12} + \delta_{n2}w_{23} + ... + \delta_{ni}w_i = 0 \end{cases}, \quad (12)$$

where δ_{ni} is the displacement of the beam structure in the direction of the released relationship in the shim contact radius caused by the additional unit force, m; Δ_i is the displacement of the beam structure in the direction of the released relationship in the shim contact radius caused by the pressure difference between the working chambers of the shock absorber, m; w_i is the support reaction (the contact force) acting in the shim contact radius, N; d_i is the deformability coefficient of the deformed basis (a relevant shim), m/N.

The solutions of the formed compatibility equations are the values of support reactions w_i of the released relationship, i.e. contact forces between shims of the valve that are considered unknown. Because only the first shim of the valve is deformed by the uniform load q and other shims do not directly interact with the said load, the value Δ_i is also evaluated only in the first equation of the system (Eq. 12) that describes deformations of the first shim in the direction of the axis y. In the case of the first shim deformation, the deformed basis is the second shim; in the case of the second shim deformation – the third shim is deformed basis and so on. The deformability coefficient of a shim that is a deformed basis is determined in the contact radius of the shims. If the last shim of the valve is rigid, in such case a presumption that displacements of the next-to-last shim in the directions of released relationships are impossible, i.e. equal to zero (the n-th equation of the system (Eq. 12)) is accepted. If the n-th shim of the valve is movable, its deformability coefficient is determined by applying a unit force in the contact radius of shims and evaluating the deflections of the shim caused by the said force. The deformability coefficients of other shims and their combinations are determined by evaluating the relative position of the shims and their number as well as formation and application of a subsidiary system of equations (the additional forces are shown in Fig. 3):

$$\begin{cases} \delta'_{22}w'_{23} + \Delta_p = dw'_{23} \\ \dots \\ \delta'_{ni}w'_i + \Delta_{p-1} = d_{n-1}w'_i \end{cases}, \quad (13)$$

where δ'_{ni} is the displacement of the beam structure in the direction of the released relationship in the contact radius of relevant shims caused by the additional unit force $\overline{w}'_i$, m; Δ_p, Δ_{p-1} is the displacement of a shim in shim contact radius caused by the additional unit force $\overline{w}'_{i-1}$ applied to the external radius of the relevant shim, m; d_{n-1} is the known (found) deformability coefficient of the shim, m/N; w'_i is the support reaction caused by the additional unit force w'_i, N.

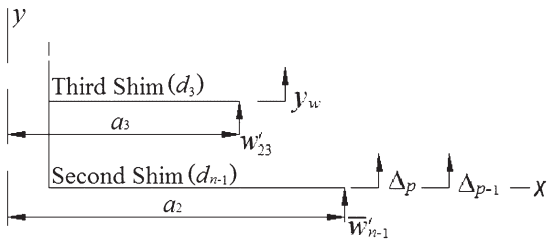

Fig. 3. The scheme for explanation of the system of equations (Eq. 13)

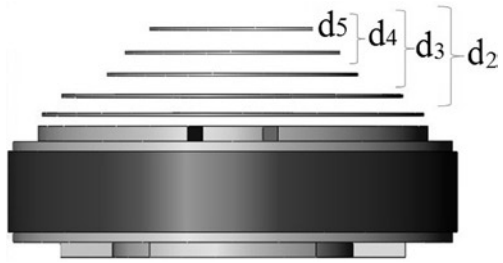

Fig. 4. The scheme for progressive determining of the deformability coefficients for each shim of the valve

Based on the system of equations (Eq. 13), the deformability coefficients for each part of the shim stack are determined progressively (Fig. 4). The deformability coefficients for each part of the shim stack are expressed by the following equation:

$$d_{n\pm1} = \frac{y_w + \Delta_{p-1}}{\overline{w}'_i}, \quad (14)$$

where y_w is the displacement of a relevant shim caused by the support reaction $\overline{w}'_i$, m.

The interdependence between the cross-section area of principal orifices of the shock absorber's piston and the radius r_0 of applying the uniform load to the first shim of the valve is expressed as follows:

$$r_0 = \frac{\sqrt{-\pi\left(A_s - \pi a_1^2\right)}}{\pi}, \quad (15)$$

where A_s is the total cross-section area of orifices of the piston intended for compression or rebound stroke, m^2; a_1 is the external radius of the first shim of the valve, m.

Eq. 15 is obtained by equating the cross-section area formed by all of the orifices of the main piston with the area $\pi\left(a_1^2 - r_0^2\right)$ of the shim of a certain size, and in this way expressing the value from the obtained expression.

During the shock absorber's operation, the shims of the valve at any moment are affected simultaneously by more than one load (Fig. 2b). Consequently, the superposition principle is applied to determine the deflections of the shims and the following system of equations is formed [26]:

$$\begin{cases} y_1 = (y_1)_q + (y_1)_{12} \\ y_2 = (y_2)_{12} + (y_2)_{23} = (z_1)_q + (z_1)_{12} \\ y_3 = (y_3)_{23} = (z_2)_{12} + (z_2)_{23} \end{cases}, \quad (16)$$

where y_1 is the deflection of the first shim of the valve in its external radius, m; y_2 is the deflection of the second shim of the valve in its external radius, m; y_3 is the deflection of the third shim of the valve in its external radius, m; z_1 is the deflection of the first shim of the valve in the radius of the contact of the shims, m; z_2 is the deflection of the second shim of the valve in the radius of the contact of the shims, m; z_3 is the deflection of the third shim of the valve in the radius of the contact of the shims, m.

If a shim valve consists of more than three shims, the system of equations (Eq. 16) is supplemented with equations analogous to the second equation of this system. Application of the system of equations (Eq. 16) is described in detail in literature [26]. The theoretical area

A_1 for oil flowing through the piston formed by the valve deformation is estimated as circumference $2\pi a_1$ multiplied by valve opening height y_1 [8]:

$$A_1 = 2\pi \cdot a_1 \cdot y_1 , \tag{17}$$

If the initial deflection of the shim stack occurs, then, according to literature [15]:

$$A_1 = 2\pi \cdot a_1 \cdot \left(y_1 - y_0\right) , \tag{18}$$

where y_0 is the initial deflection of the shim stack in the fully closed position, m.

It is accepted that thermal deformations of the shims do not exist. Based on the literature [6, 8, 28], deformations of the valve shims are solved by choosing relevant algorithms from Roark's formulas for stress and strain described in the literature [27].

The described mathematical model of monotube shock absorber and its shim valve was implemented in the environment of software package MATLAB/Simulink by dividing it into interrelated subsystems. During the modelling, the unknowns are the chamber pressures, oil flow rates, the deflection of the shim stack and the damping force, so, at each time step, the said parameters are solved by applying the Eq. 4, 5, 11 and 16. Based on the literature [16], the possible value of the friction force is 30 N.

4. Experimental procedure

The designed mathematical model was validated by comparison with the experimental tests results carried out on two different modified monotube shock absorbers. During the experimental tests, the damping characteristics of the shock absorbers were measured by a special electromechanical stand (Fig. 5a) that forms sinusoidal characteristics of the compression and rebound strokes of a shock absorber. Experimental tests of the modified shock absorbers were carried out at 0.03 m amplitude of compression/rebound strokes. The duration of a shock absorber's test was 80 s; the maximum frequency of compressions and rebounds of the shaft of a shock absorber was 4.25 Hz.

The nominal parameters of the tested shock absorbers and their modified shim valves used for the modelling are provided in Table 1 and Table 2, respectively. In Table 1 the symbol "*" points out that the shim is rigid in the valve and its thickness is 3.5 mm. The Poisson's ratio (0.28) and the elasticity modulus (210 GPa) of the shim material were determined by optical emission spectrometer PMI Master Pro; the material of the valve shims is C55E carbon steel.

During modification of the shock absorbers, only new parts of good technical condition and high quality engineering maintenance materials (sealants, oil rings, oil, valve shims and so on) were used. The experimental tests of the monotube shock absorber 1 by the electromechanical stand were repeated twice, when the orifice with the blunt needle is fully opened (to fully open the orifice, 30 clicks are needed) and when the orifice with the blunt needle is fully closed (0 clicks) (Fig. 1). Monotube shock absorber 2 was tested when the said orifice with the blunt needle was only fully opened. In the both abovementioned shock absorbers, a symmetric piston was used (Fig. 5b).

At the initial time moment, the value of pressure in chambers of the shock absorber is 1.5 MPa. The shim clamping radius of valve shims is 8.4 mm (shim clamping radius is marked by symbol *b* in Fig. 2b) in monotube shock absorber 1 and 7 mm – in monotube shock absorber 2. The diameter of the variable orifice with the blunt needle is 2 mm when it is fully opened. All experimental tests were carried out at the temperature of 293 K.

a)

b)

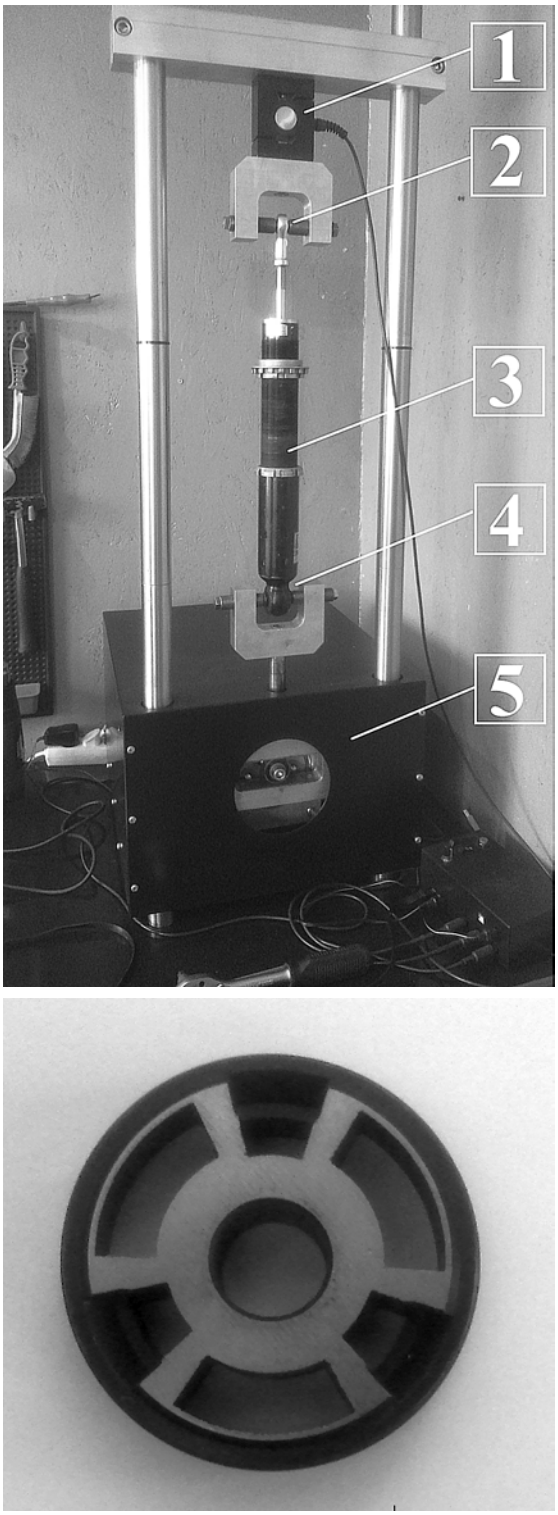

Fig. 5. The equipment used during tests: a) The shock absorber test stand used for experimental tests and the monotube shock absorber 1 mounted in it, 1 – Load cell; 2 – The upper mounting point; 3 – Monotube shock absorber 1; 4 – The lower mounting point; 5 – electromechanical test stand; b) The side of the piston of the monotube shock absorber 1 intended for the compression stroke

Table 1. The nominal parameters of shim valve structures in the researched shock absorbers

Monotube shock absorber 1	Position of the shim	1	2	3	4	5	6	7	8	9
	External radius of the shim, mm									
	Compression	19	19	19	19	19	15	13	8.5	8.5
	Rebound	17	17	17	15	12.5	8.5	8.5	8.5*	-
Monotube shock absorber 2	Position of the shim	1	2	3	4	5	6	7	8	9
	External radius of the shim, mm									
	Compression	17	15	12.5	11	9	7.5	7.5	-	-
	Rebound	15	15	13.75	11	9	8.5	8.5	-	-

Table 2. The nominal parameters of the tested shock absorbers

Shock absorber	A parameter			
	Shim thickness, mm	The orifice cross-section area during compression/ rebound stroke, mm^2	Oil	The piston diameter, mm
Monotube shock absorber 1	0.3	325.5/102.4	Castrol Fork Oil 10W	45
Monotube shock absorber 2		237.2/72.8		40
Shock absorber	The shaft diameter, mm	Heights of compression/ rebound/ gas chambers, mm	Adiabatic process constant for Nitrogen	Oil Bulk modulus, MPa
Monotube shock absorber 1	20	105/105/50	1.4	1500
Monotube shock absorber 2	12.4			

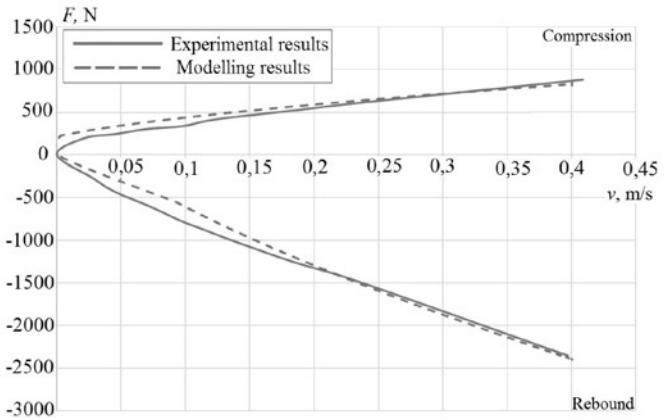

Fig. 6. The damping characteristics of the monotube shock absorber 2, when the variable orifice with the blunt needle is open

5. Results and discussion

The results of the damping force modelling were compared with the data of the damping force of the tested shock absorbers determined during the experimental tests and a good level of agreement was obtained. The value of the total relative error between the results of the mathematical modelling and the results of the experimental tests does not exceed 3 % both for compression and rebound strokes. The types of the characteristics obtained by mathematical modelling and experimental tests coincide: all the characteristics are of a linear type.

In this section, the impact of the structures of the variable orifice with a blunt needle and the shim valve on the value of the damping force is analysed. The diagrams, reflecting the dependence of the damping force vs. piston velocity (*F*-*v*), that were formed based on the experimental and the mathematical modelling results, are presented for monotube shock absorber 2 in Fig. 6 and for monotube shock absorber 1 – in Fig. 7.

5.1. Low velocity phase

The value of the damping force generated in the low velocity phase ($\dot{x}_1 \leq 0.05$) and the position of the knee point directly depend on the position of the needle in the variable orifice. When the variable orifice is closed, a resistance to oil flowing through the said orifice appears. Consequently, the generated damping force increases and the knee point, i.e. the moment when the shim valve opens is clearly visible (Fig. 7a). At higher values of the pressure difference between the compression chamber and the rebound chamber required for opening the shim valve, the knee point is more clearly visible. The value of the pressure difference required for opening the shim valve depends on the properties of the shims that are in the positions 1 and 2 (Table 1.). At higher values of stiffness of the shims that are in the positions 1 and 2, the value of the damping force generated in the low speed phase is higher and the knee point is more clearly visible. A higher stiffness of a shim causes an increased preload for the shim stack and a larger pressure difference is needed across the shim stack to deflect it. When the variable orifice is open, no additional resistance to oil flowing through the said orifice is formed; in such a case, the growing of the damping force generated in the low velocity phase is linear and the knee point is not visibly expressed (Fig. 6; Fig. 7b); however, the value of the generated damping force is lower as compared to the closed orifice. For example, when the variable orifice of the monotube shock absorber 1 is closed, the maximum value of its damping force generated in the low velocity phase that was found in the experiments equals to 369 N and when the orifice is open – the said force equals to 128 N (Fig. 7). Nevertheless, an evaluation of the values of the damping force generated in the low velocity phase discloses discrepancies between the experimental

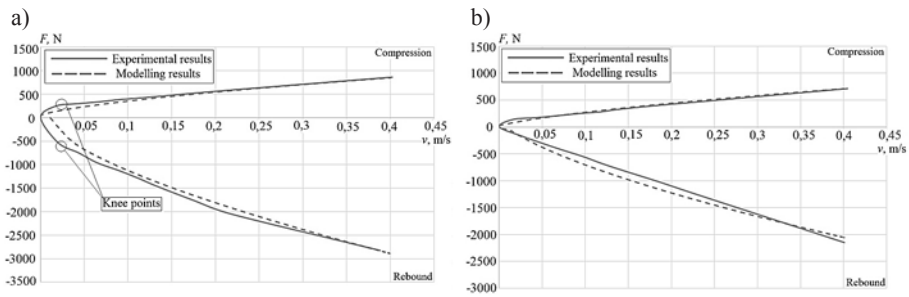

Fig. 7. The damping characteristics of the monotube shock absorber 1: a) when the variable orifice with blunt needle is closed; b) when the variable orifice with blunt needle is open

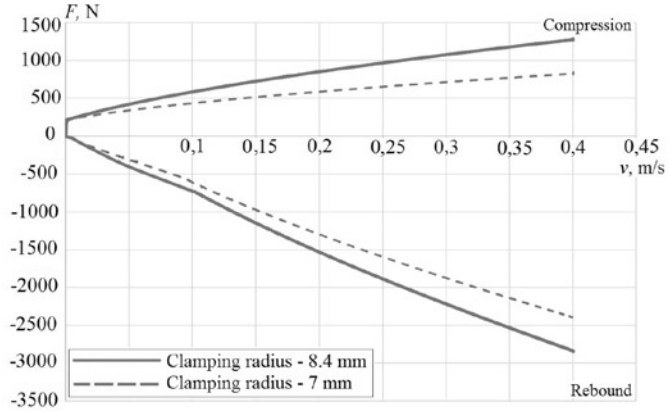

Fig. 8. The damping characteristics of the monotube shock absorber 2 at different values of the shim clamping radius

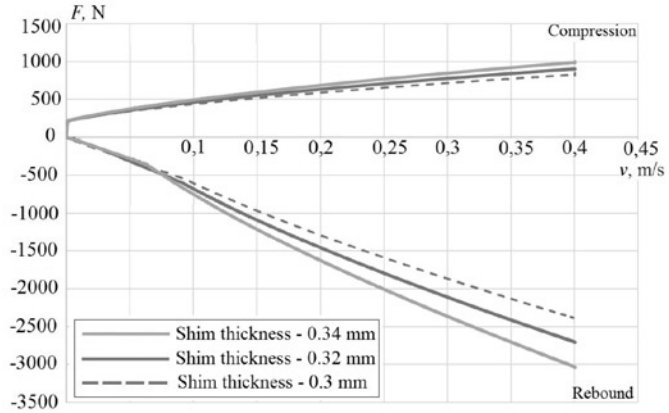

Fig. 9. The damping characteristics of the monotube shock absorber 2 at different values of the shim thicknesses

and modelling results that attain to 17.83 % in some time steps. The appeared errors may be explained by an observed formation of the damping force loop in the low velocity phase, the meaning of which is close to the phenomenon of formation of hysteresis loop. During mathematical modelling, the hysteresis loop is formed because of the accepted constant friction force between elements of the shock absorber.

5.2. Normal and high velocity phase

During the experiment, it was found that oil flowing through the variable orifice influences also the maximum value of the damping force generated in normal $(0.05 < \dot{x}_1 \leq 0.2\ \mathrm{m/s})$ and high velocity $(0.2 < \dot{x}_1 \leq 0.4\ \mathrm{m/s})$ phase. It can be seen from Fig. 7 that when the structure of the valve is the same and the variable orifice is closed, the value of the generated damping force is 860 N during the compression stroke and 2890 N during the rebound stroke. When the orifice is open, the value of the generated damping force is 710 N during the compression stroke and 2050 N during the rebound stroke. It may be explained as follows: during damping the vibrations in the high velocity phase, the variable orifice is not closed or blocked, so the oil flowing through it during the operation of the shock absorber is constant independently from the velocity of the piston's compression/rebound. It is clear based on the obtained results that the maximum value of the generated damping force is higher when the variable orifice is closed and is lower when the orifice is open. The extent of the increase/decrease of the damping force on changing the position of the needle of the orifice during compression or rebound stroke depends on the diameter of the orifice on operation of the shock absorber and the accepted values of the discharge coefficient. A value of the damping force generated in normal/high velocity phase is influenced by the shims of the positions 3-9 (Table 1.) and their stiffness. At higher shim clamping radius (Fig. 2b), the stiffness of the shim valve is higher, so the generated damping force increases as well (Fig. 8).

During the mathematical modelling, it was also found that the shim thickness affected the stiffness of the valve and the value of the generated damping force. At higher values of the shim thickness, the generated damping force increases as well (Fig. 9).

However, the source of literature [17] points out that the stiffness of a shim is not linear in relation to its thickness. To calculate how many thin shims it takes to equal one thicker shim, the formula is approximately the same as for comparing the stiffness of dissimilar constant section beams [17]:

$$N = \left(\frac{x_s}{x_p} \right)^3 \tag{19}$$

where x_s is the thickness of the thicker shim, m; x_p is the thickness of the thinner shim, m.

Taking into account the obtained results as well as the Eq. 4 and 17, it becomes clear that the valve y_1 and the oil flow rate Q_1 through the valve depend on the shim stack stiffness. For these reasons, it is obvious that the parameters of the shim valve and its stiffness impact considerably the damping force generated by the shock absorber.

6. Conclusion

This paper presents the variety of mathematical model types for monotube shock absorbers and the new method for modelling shim valves for shock absorbers is developed and proposed together with a discussion of this model performance.

Application of the force method (intended for analysing the statically indeterminate systems) allows determining the contact forces appearing between shims of the valve with a good adaptation to wide range of various parameters of shim valve. The algorithm for applying the suggested model has been clarified and detailed.

The effectiveness of the suggested model has been verified by experimental tests. The new model has demonstrated clear advantages, because the found values of the relative errors were ≤ 3 % both during the compression stroke and the rebound stroke. This fact attests the created mathematical model to be correct and applicable for seeking better vehicle road holding characteristics.

In addition, the influence of the shim valve construction and the variable orifice construction on the shock absorber damping characteristics has been discussed. The obtained results confirm the relationship between the properties of all shims of the valve and the damping force generated by the shock absorber.

Acknowledgement: *We wish to express our most sincere gratitude and appreciation to "We Are Dynamic" for sharing their experience in the activities related to shock absorbers modification and for the opportunity to carry out the experimental tests.*

References

1. Boggs C, Ahmadian M, Southward S. Efficient empirical modeling of a high-performance shock absorber for vehicle dynamics studies. Vehicle Systems Dynamics 2009, 48(4): 481-505, http://dx.doi.org/10.1080/00423110902906292.
2. Burdzik R, Konieczny L, Piwnik J, Baranowski P. The influence of oil leak in modern vehicle shock absorber on its damping characteristics. Transport Problems 2009; 4(4): 99-106.

3. Calvo J A, Diaz V, San Roman J l, Garcia-Pozuelo D. Influence of shock absorber wearing on vehicle brake performance. International Journal of Automotive Technology 2008, 9(4): 467-472, http://dx.doi.org/10.1007/s12239-008-0056-z.
4. Calvo J A, Lopez-Boada B, San Roman J L, Gauchia A. Influence of a shock absorber model on vehicle dynamic simulation. Proc. of the Institution of Mechanical Engineers Part D Journal of Automobile Engineering 2009, 223(2): 189-203, http://dx.doi.org/10.1243/09544070JAUTO990.
5. Cui Y, Kurfess T R, Messmen M. Testing and Modeling of Nonlinear Properties of Shock Absorbers for Vehicle Dynamics Studies. Proc. of the World Congress on Engineering and Computer Science 2010, 2: 949-954.
6. Czop P, Slawik D, Sliwa P, Wszolek G. Simplified and advanced models of a valve system used in shock absorbers. Journal of Achievements in Materials and Manufacturing Engineering 2009, 33(2): 173-180.
7. Dixon J C. The Shock Absorber Handbook. Great Britain: Professional Engineering Publishing Ltd and John Wiley and Sons Ltd, 2007.
8. Farjoud A, Ahmadian M, Craft M, Burke W. Nonlinear modeling and experimental characterization of hydraulic dampers: effects of shim stack and orifice parameters on damper performance. Nonlinear Dynamics 2011, 67(2): 1437-1456, http://dx.doi.org/10.1007/s11071-011-0079-2.
9. Fernandes C, Noguchi E, Castro R, Almeida U. Influence of Shock Absorber Non-Linearities Over the Vehicle Dynamics Behaviour. SAE Technical Paper 2014-36-0018 2014: 10 pp, http://dx.doi.org/ 10.4271/2014-36-0018.
10. Haj-Kacem R B, Ouerfelli N, Herraez J V, Guettari M, Hamda H, Dallel M. Contribution to modeling the viscosity Arrhenius-type equation for some solvents by statistical correlations analysis. Fluid Phase Equilibria 2014, 383: 11-20, http://dx.doi.org/ 10.1016/j.fluid.2014.09.023.
11. Kim Y H, Bae W B, Lim D J, Suh Y S. A Study on the Development of Engineering Plastic Piston Used in the Shock Absorber. Metals and Materials 1998, 4(4): 852-858, http://dx.doi.org/10.1007/BF03026412.
12. Koylu H, Cinar A. Dynamical investigation of effects of variable damper settings induced brake pressure oscillations on axle and wheel oscillations during ABS-braking based on experimental study. Meccanica 2013, 48(5): 1093-1115, http://dx.doi.org/10.1007%2Fs11012-012-9654-y.
13. Koylu H, Cinar A. The influences of worn shock absorber on ABS braking performance on rough road. International Journal of Vehicle Design 2011, 57(1): 84-101, http://dx.doi.org/10.1504/IJVD.2011.043598.
14. Lang H. Automotive dampers at high stroking frequency. Doctoral diss., University of Michigan, Ann Arbor, MI, 1977, 288 pp.
15. Lee K. Numerical Modelling for the Hydraulic Performance Prediction of Automotive Monotube Dampers. Vehicle Systems Dynamics 1997, 28(1): 25-39, http://dx.doi.org/10.1080/00423119708969347.
16. Lizarraga J, Sala J A, Biera J. Modelling of friction phenomena in sliding conditions in suspension shock absorber. Vehicle System Dynamics 2009, 46(1): 751-764, http://dx.doi.org/10.1080/00423119708969347.
17. Ohlins Racing AB, Inside Ohlins T44 manual. Part 1. Theory and Design [online] [accesed 10 March 2016] Available from Internet: http://www.motorsportsspares.com/files/inside_the_tt44_theory_and_design.pdf.
18. Ping Y. Experimental and mathematical evaluation of dynamic behaviour of an oil – air coupling shock absorber. Mechanical Systems and Signal Processing 2003, 17(8): 1367-1379, http://dx.doi.org/10.1006/mssp.2002.1528.
19. Ping Y. Mechanical characteristics of oil-damping shock absorber for protection of electronic-packaging components. Tsinghua Science and Technology 2005, 10(2): 216-220, http://dx.doi.org/10.1016/S1007-0214(05)70057-2.
20. Qian X, Qinghua L, Chao C. The influence of lateral shock absorber valve parameters on vehicle dynamic performance. Journal of Mechanical Science and Technology 2015, 29(5): 1907-1911. http://dx.doi.org/10.1007%2Fs12206-015-0412-7.
21. Reybrouck K. A nonlinear parametric model of an automotive shock absorber. SAE Technical Paper 940869 1994: 10 pp, http://dx.doi.org/10.4271/940869.
22. Rhoades K S. Development and experimental verification of a parametric model of an automotive damper. Master's thesis, Texas A&M University, Canyon, TX, 2006, 126 pp.
23. Shim ReStackor, Needle Geometry [online] [accesed 24 October 2015] Available from Internet:http://www.shimrestackor.com/Code/User_Manual/Sections/Input/Aux_Comp/Needle_Geom/needle-geom.htm.
24. Simms A, Crolla D. The Influence of Damper Properties on Vehicle Dynamic Behaviour. SAE Technical Paper 2002-01-0319 2002: 14 pp, http://dx.doi.org/10.4271/2002-01-0319.
25. Skačkauskas P, Žuraulis V. Research of characteristics of sports cars' shock absorbers. Proc. 19th International Conference Transport Means 2015: 231-235.
26. Talbott M S, Starkey J. An Experimentally Validated Physical Model of a High-Performance Mono-Tube Damper. SAE Technical Paper 2002-01-3337 2002: 20 pp, http://dx.doi.org/10.4271/2002-01-3337.
27. Young W C, Budynas R G. Roark's Formulas for Stress and Strain. New York: McGraw-Hill, 2001.
28. Yukimasa T, Motohashi H, Ohtaki M, Chikamori H. Comments on Oil Seals for Gas Pressurized Shock Absorbers of Automotive Suspensions. SAE Technical Paper 850333 1985: 12 pp, http://dx.doi.org/10.4271/850333.
29. Žuraulis V, Levulytė L. The Influence of Comfort and Sport Driving Modes of Modern Vehicles on the Vibration of Sprung and Unsprung Masses. Proc. 18th International Conference Transport Means 2014: 15-19.

Paulius SKAČKAUSKAS
Vidas ŽURAULIS
Vaidas VADLUGA
Saulius NAGURNAS
Department of Automobile Transport
Vilnius Gediminas Technical University
Basanavičiaus str., 28 LT-03224 Vilnius, Lithuania
E-mails: paulius.skackauskas@vgtu.lt, vidas.zuraulis@vgtu.lt, vaidas.vadluga@vgtu.lt, saulius.nagurnas@vgtu.lt

Article citation info:
LEGÁT V, MOŠNA F, ALEŠ Z, JURČA V. Preventive maintenance models – higher operational reliability. Eksploatacja i Niezawodnosc – Maintenance and Reliability 2017; 19 (1): 134–141, http://dx.doi.org/10.17531/ein.2017.1.19.

Václav LEGÁT
František MOŠNA
Zdeněk ALEŠ
Vladimír JURČA

PREVENTIVE MAINTENANCE MODELS – HIGHER OPERATIONAL RELIABILITY

MODELE KONSERWACJI ZAPOBIEGAWCZEJ A WYŻSZA NIEZAWODNOŚĆ EKSPLOATACYJNA

The authors present a method for determining the optimal interval for preventive periodical maintenance and an optimal diagnostic parameter for predictive maintenance/replacement. Additionally, the authors raise the question: how does preventive maintenance influence the probability of failure and the operational reliability of system elements that have undergone preventive periodical maintenance? They answer the question using analytical and simulation computing approaches. The results are in quantitative form, giving relationships between preventive maintenance intervals and reliability functions. Examples demonstrate suitability of the method for typical engineering objects using a three parameters Weibull distribution. Application of the method is of substantial benefit to both the manufacturer and the user of technical equipment.

***Keywords**: preventive maintenance, predictive maintenance, maintenance interval optimization, reliability improvement.*

Autorzy przedstawiają metodę określania optymalnego czasu przerwy na okresową konserwację zapobiegawczą oraz optymalnego parametru diagnostycznego dla konserwacji predykcyjnej/wymiany Dodatkowo, autorzy zadają pytanie, jaki jest wpływ konserwacji zapobiegawczej na prawdopodobieństwo wystąpienia uszkodzenia oraz na niezawodność eksploatacyjną elementów systemu, w stosunku do których zastosowano okresową konserwację zapobiegawczą. Odpowiedzi na te pytania, autorzy poszukują posługując się metodami analizy i symulacji komputerowej. Wyniki podane w formie ilościowej, informują o związkach między przerwami na konserwację predykcyjną a funkcjami niezawodnościowymi. Podane przykłady pokazują, z wykorzystaniem trójparametrowego rozkładu Weibulla, że proponowana metoda może być stosowana w przypadku typowych obiektów inżynieryjnych. Zastosowanie omawianej metody przynosi znaczące korzyści zarówno wytwórcom jak i użytkownikom sprzętu technicznego.

***Słowa kluczowe**: konserwacja zapobiegawcza, konserwacja predykcyjna, optymalizacja przerw konserwacyjnych, doskonalenie niezawodności.*

1. Introduction and literature survey

Many maintenance strategies, policies and methods have been developed, which are aimed at making maintenance cheaper and more effective. Such programs have the minimization of costs, downtime and losses due to failure of critical objects of the equipment as their main objective. Cost minimization improves the effectiveness and profitability of the organization [1, 2, 9, 12, 13, 20].

For creation of the maintenance policies, well described data mining input is very important. [4].

In recent years, useful models of preventive and predictive maintenance optimization with different complexity and applicability have been further developed.

In the paper, [5] the authors proposed a quasi-periodic imperfect preventive maintenance policy. Finally, a real case study of preventive maintenance on Chinese diesel locomotives is examined to illustrate the proposed maintenance policy.

The paper [6] proposes an approach in which preventive and failure replacement costs as well as inspection cost are taken into account to determine the optimal replacement policy and an age-based inspection scheme, such that the total average costs of replacements and inspections is minimized.

Determination of the preventive effect of optimal replacement policies in the paper [8] is based on aging intensity and the cost ratio of failure and preventive replacements. One of its conclusions is that not every preventive maintenance is fully effective and a policy of, "run to failure" can be more effective (note: in some cases).

The proposed model in the paper [10] takes into consideration the stochastic nature of equipment failures. The output from the model is a cost distribution against the time from which the minimum cost may be found for a particular period and this period is defined as the optimum lifespan of the machine part.

The paper [11] considers periodic preventive maintenance policies for a deteriorating repairable system. On each failure, the system is repaired and, at the planned times, it is periodically maintained to improve its performance reliability. Most periodic preventive maintenance (PM) models for repairable systems have been studied assuming that the failure process between two PMs follows the nonhomogeneous Poisson process (NHPP), implying the minimal repair on each failure.

The paper [14] regarding warranty policy considering three maintenance options for products with multiple failure modes also showed the broad usability of the Weibull distribution. This fact supports the decision of the authors to also use the Weibull function.

The paper [15] presents a new mathematical function to model an improvement based on the ratio of maintenance and repair costs, and demonstrate how it outperforms fixed improvement factor models by analyzing the effectiveness in terms of cost and reliability of a system.

It determines the optimal preventive maintenance and replacement schedule of the system.

The paper [16] takes into account degradation modeling and maintenance policy for a two-stage degradation system, which degradation process is nonlinear and degradation rate is change over time in both stages. Influence analysis of different model parameter and maintenance policy is studied in numerical examples with results that the proposed optimal maintenance policy can help to reduce the mean cost rate.

In the paper, [17] the authors proposed a hybrid imperfect maintenance model with random adjustment-reduction parameters and a maintenance policy. Furthermore, a numerical example and an example of the fuel injection pump of diesel engines are carried out and presented to illustrate the proposed method.

A mathematic model of optimization of maintenance intervals having regard to the risk is presented in the paper [18]. Precise calculations were made for steam turbines that operate in power units.

Maintenance can represent a significant portion of the cost in asset intensive organizations, as breakdowns have an impact on the capacity, quality and cost of operation [21]. However, the formulation of a maintenance strategy depends on a number of factors, including the cost of down time, reliability characteristics and redundancy of assets. Consequently, the balance between preventive maintenance (PM) and corrective maintenance (CM) for minimizing costs varies between organizations and assets. Nevertheless, there are some rules of thumb on the balance between PM and CM, such as the 80/20 rule.

In the paper [22], an approach is presented, which allows evaluation of various possible maintenance scenarios with respect to both reliability and economic criteria. Authors included three deterioration states ($D1 \div D3$) and three repairs: minor (index = 1), medium (2) and major (3), but in real machine operation it is difficult to define these general states and repairs exactly.

In the paper [23] a double-fold Weibull competing risk model using the real failure data from railway operation, was developed for the engine system of a diesel locomotive and its current maintenance. Results show that the maintenance period varies widely between winter and summer, and that optimized maintenance can increase the availability and decrease cost more than the existing policy.

The paper [7] is a very large review on machinery diagnostics and prognostics implementing condition-based maintenance using 271 references and other reviews in the paper [19] using 104 references which point to future perspectives on maintenance optimization. These two references [7, 19] fully support the authors method, from data collection through data processing to optimal maintenance decision making.

These references proposed interesting models regarding concrete application on particular technical systems with different structures and as well a general solution. The authors did not find in the review, a simple model of predictive maintenance optimization for industrial practice and no idea that preventive maintenance improves reliability including utilization of a three parameters Weibull distribution. According to authors' experiences from different fields of industry, maintenance managers need simple and general methods for design of maintenance programs and policies optimization. Therefore, the objective of this paper is to contribute to the optimization of predictive maintenance with a new simple semi-stochastic model. A further objective was to give maintenance staff evidence that preventive maintenance improves operational reliability based on a mathematical theory of reliability [1, 20] and authors works [9, 12, 13]. Finally, all models are demonstrated using numerical simulation with a three parameters Weibull distribution supported by table processor Excel.

2. Optimization of predictive maintenance

In discussing machine maintenance strategy, it is customary to distinguish between the following methods (policies) [3]:

a) **corrective maintenance** - maintenance carried out after fault recognition and intended to put an item into a state in which it can perform a required function,
b) **preventive maintenance -** maintenance carried out at predetermined intervals or according to prescribed criteria and intended to reduce the probability of failure or the degradation of the functioning of an item; following policies c), d) and e) are also preventive maintenance,
c) **predetermined maintenance**, preventive maintenance carried out in accordance with established intervals of time or number of units of use but without previous condition investigation,
d) **condition based maintenance** - preventive maintenance which includes a combination of condition monitoring and/or inspection and/or testing, analysis and the ensuing maintenance actions; the condition monitoring and/or inspection and/or testing may be scheduled, on request or continuous,
e) **predictive maintenance** - condition based maintenance carried out following a forecast derived from repeated analysis or known characteristics and evaluation of the significant parameters of the degradation of the item.

The proposed model of predictive maintenance optimization is based on minimization of unit maintenance, diagnostics and failure risk cost $c(S_p)$ of a component [1]:

$$c(S_p) = \frac{C_{pr} + L_f \cdot F(S_p)}{\bar{t}(S_p)} + c_d \tag{1}$$

where S_p is a diagnostic signal for predictive maintenance; diagnostic signal is allowed to be a random variable, C_{pr} is cost of preventive maintenance, L_f *is* loss due to failure risk ($L_f \cdot F(S_p)$); loss due to failure risk can be calculated as a difference between cost of corrective maintenance and cost of preventive maintenance, it means $L_f = C_{cm} - C_{pr}$, $F(S_p)$ is probability of failure depending on diagnostic signal S_p, c_d denotes unit costs of condition monitoring to obtain diagnostic signal S_p, $\bar{t}(S_p)$ is the mean time corresponding to diagnostic signal S_p, which can be determined from operational data using the formula:

$$\bar{t}(S_p) = \frac{1}{n}\left[\sum_{i=1}^{m(S_p)} t_i(S_p) + \sum_{j=1}^{n-m(S_p)} t_j(S_p)\right] \tag{2}$$

where $t_i(S_p)$ denotes the operating time of the *i*th object surviving at the level S_p, $t_j(S_p)$ denotes the time to failure of the *j*th object which failed before reaching the state S_p, $m(S_p)$ is the number of objects reaching state S_p without failure and n is the total number of objects in the investigated population. To obtain these data it is necessary to carry out an operational observation – life test of objects population including on-line diagnostic measurement till failure or at least diagnostic signals S_{pf} closely before failure occurs. In the first case, it is easy to apply equation (2) and probability of failure (distribution function) $F(S_p)$ can be obtained by means of diagnostic signals S_p shortly before failure. If there are only recognized diagnostic signals (technical states) closely before failures, it is necessary to calculate operating time related to selected diagnostic signal S_p which is used as an indicator for predictive maintenance of an object.

For calculation of mean operating time, versus diagnostic signal for predictive maintenance $\bar{t}(S_p)$, authors use a simplified model in which the technical state degradation (a change of diagnostic signal)

runs along a straight line from start state S_{pz} to limit value of technical state (to failure) S_{pfi} i-th object. The accuracy of this approximation from point of technical solution is sufficient. Calculation of the $t_i(S_p)$ is carried out in a case of the $S_{pi} < S_{pfi}$ according to equation (3):

$$t_i(S_p) = t_i(S_{pfi})\frac{S_{pi} - S_{pz}}{S_{pfi} - S_{pz}}, \tag{3}$$

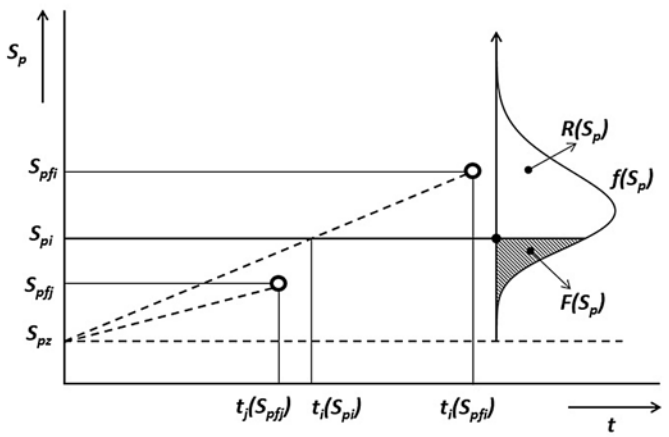

Fig. 1. Principle of input data determination for calculation of mean operating time versus diagnostic signal for predictive maintenance $\bar{t}(S_p)$

If $S_{pj} \geq S_{pfj}$, the operating time to failure of the *j*th object which failed before reaching the diagnostic signal S_p, we can read directly from the database of operating time to failure of the *j*th object which failed before reaching the diagnostic signal $t_j(S_p)$. Interpretation of these input data is clear from Fig. 1.

Unit costs of preventive maintenance and failure risk versus diagnostic signal for predictive maintenance and optimal diagnostic signal for predictive maintenance S_{po} (for $c(S_p)$ = minimum) we can calculate, using equation (4):

$$c(S_p) = \frac{C_{pr} + L_f \cdot F(S_p)}{\bar{t}(S_p)} + c_d = \frac{C_{pr} + L_f \cdot F(S_p)}{\frac{1}{n}\left[\sum_{i=1}^{m(S_p)} t_i(S_p) + \sum_{j=1}^{n-m(Sp)} t_j(S_p)\right]} + c_d \tag{4}$$

For a proposed model of predictive maintenance optimization (4) it is necessary to obtain or calculate input data as follows:

a) cost of preventive maintenance C_{pr}
b) losses due to failure risk L_f
c) probability of failure versus diagnostic signal for predictive maintenance $F(S_p)$
d) mean operating time versus diagnostic signal for predictive maintenance $\bar{t}(S_p)$
e) unit cost of diagnostics (condition monitoring) c_d
f) diagnostic signal for predictive maintenance S_p,

Optimal predictive dispositional operating time $t_d(S_{po})$ from actual operating time $t(S)$ in decision making state to optimal operating time $t(S_{po})$ for predictive maintenance (restoration, replacement) is calculated from equation

$$t_d(S_{po}) = t(S_{po}) - t(S) \tag{5}$$

3. Calculation of mean life and reliability functions of preventive predetermined maintained objects

If we should prove that preventive predetermined maintenance increases operational reliability, we must calculate reliability function of object predetermined maintained in operating time t_p and its mean life *ET* of preventively predetermined maintained objects in time t_p comparing with corrective maintenance of the same object.

Let us monitor a series of objects that underwent preventive predetermined maintenance (were replaced) after time interval t_p using a new object with the same reliability properties. Also, let us suppose that its durability is characterized by a random variable *X* with a continuous density function *f* and distribution function *F*.

Object reliability can be improved during operation by preventive predetermined replacement at time t_p. Durability of *k*-th component is also described by a random variable X_k with the same density function f and distribution function *F*. We suppose that random variables X_1, X_2,…are independent.

Let us denote by *T* a random variable which describes the life of preventively predetermined replaced objects. Further, we derive the formula of the density function f_T and the distribution function f_T for the random variable *T*. We are particularly interested in the mean value *ET*.

Let us denote $p = P[X_k < t_p]$, $q = P[X_k \geq t_p] = 1 - p$ and $I = \int_0^{t_p} xf(x)dx$. We express the random variable *T* using X_k in the following way:

$$T = \begin{cases} X_1 & \text{for } X_1 < t_p \\ t_p + X_1 & \text{for} X_1 \,{}^3 t_p, X_2 < t_p \\ 2t_p + X_1 & \text{for} X_1 \,{}^3 t_p, X_2 \,{}^3 t_p, X_3 < t_p \\ \ldots\ldots\ldots\ldots & \\ kt_p + X_{k+1} & \text{for } X_1 \,{}^3 t_p, X_2 \,{}^3 t_p, \ldots, X_k \,{}^3 t_p, X_{k+1} < t_p. \end{cases}$$

With respect to independence X_1, X_2, ..., from the total probability theorem it holds for arbitrary $x \in <0;\infty)$:

$$\begin{aligned} F_T(x) &= P[T < x] = \\ &= P[T < x / X_1 < t_p] \times P[X_1 < t_p] + \\ &+ P[T < x / X_1 \,{}^3 t_p, X_2 < t_p] \times P[X_1 \,{}^3 t_p, X_2 < t_p] + \ldots + \\ &+ P[T < x / X_1 \,{}^3 t_p, \ldots, X_k \,{}^3 t_p, X_{k+1} < t_p] \times \\ &\cdot P[X_1 \,{}^3 t_p, \ldots, X_k \,{}^3 t_p, X_{k+1} < t_p] + \ldots = \\ &= P[T < x / X_1 < t_p] \times p + P[T < x / X_1 \,{}^3 t_p, X_2 < t_p] \times pq + \ldots + \\ &+ P[T < x / X_1 \,{}^3 t_p, \ldots, X_k \,{}^3 t_p, X_{k+1} < t_p] \times pq^k + \ldots. \end{aligned} \tag{6}$$

Further, we calculate according to the definition of conditional probability with respect to the independence of X_1, X_2, …

$$\begin{aligned} &P[T < x / X_1 \,{}^3 t_p, \ldots, X_k \,{}^3 t_p, X_{k+1} < t_p] = \\ &= P[kt_p + X_{k+1} < x / X_1 \,{}^3 t_p, \ldots, X_k \,{}^3 t_p, X_{k+1} < t_p] = \\ &= \frac{P\left[X_{k+1} < x - kt_p, X_1 \geq t_p, \ldots, X_k \geq t_p, X_{k+1} < t_p\right]}{P\left[X_1 \geq t_p, \ldots, X_k \geq t_p, X_{k+1} < t_p\right]} = \\ &= \frac{P\left[X_{k+1} < \min(x - kt_p, t_p)\right] \cdot q^k}{q^k \cdot p}. \end{aligned} \tag{7}$$

After substitution (7) into equation (6) we obtain:

$$F_T(x) = P[T < x] = \sum_{k=0}^{\infty} P\left[X_{k+1} < \min(x - kt_p, t_p)\right] \cdot q^k = \sum_{k=0}^{\infty} F(\min(x - kt_p, t_p)) \cdot q^k$$

It is possible to itemize the distribution function F_T around the following intervals:

$$F_T(x) = \begin{cases} F(x) & \text{on } (0; t_p) \\ F(t_p) + qF(x - t_p) & \text{on } (t_p;\ 2t_p) \\ F(t_p) + qF(x - t_p) + q^2 F(x - 2t_p) & \text{on } (2t_p;\ 3t_p) \\ \ldots\ldots\ldots\ldots\ldots\ldots\ldots\ldots\ldots\ldots \end{cases} \quad (8)$$

Last, using a modified equation (8), we calculate the failure probability $F_T(t)$ and the reliability function $R_T(t)$ for the components that underwent preventive predetermined maintenance:

$$F_T(t) = F(t_{po}) + R(t_{po})F(t - t_{po}) + R^2(t_{po})F(t - 2t_{po}) + R^3(t_{po})F(t - 3t_{po}) + \ldots \quad (9)$$

and

$$R_T(t) = 1 - F_T(t) \quad (10)$$

We obtain density function f_T by differentiation of F_T:

$$f_T(x) = \begin{cases} f(x) & \text{on } (0; t_p) \\ qf(x - t_p) & \text{on } (t_p; 2t_p) \\ q^2 f(x - 2t_p) & \text{on } (2t_p; 3t_p) \\ \ldots\ldots\ldots\ldots\ldots\ldots\ldots\ldots \end{cases} \quad (11)$$

Finally, we calculate the mean value of life (sum of particular operating time) for objects that underwent preventive predetermined replacement:

$$ET = \int_0^{\infty} x f_T(x)dx = \sum_{k=0}^{\infty} \int_{kt_p}^{(k+1)t_p} q^k x f(x - kt_p)dx =$$

$$= \sum_{k=0}^{\infty} q^k \int_0^{t_p} (x + kt_p) f(x)dx = \left(\int_0^{t_p} xf(x)dx\right) \sum_{k=0}^{\infty} q^k + qt_p\left(\int_0^{t_p} f(x)dx\right) \sum_{k=0}^{\infty} kq^{k-1} =$$

$$= I\frac{1}{1-q} + pqt_p \frac{1}{(1-q)^2} =$$

$$= \frac{I + qt_p}{p}, \quad (12)$$

we have used the formula for the sum of the geometrical series $1 + q + q^2 + \ldots + q^k + \ldots = 1 / (1 - q)$ and from this formula through differentiation we have obtained the derived formula

$1 + 2q + 3q^2 + \ldots + kq^{k-1} + \ldots = 1 / (1-q)^2$.

Integral I can be modified using integration by parts:

$$I = \int_0^{t_p} xf(x)dx = t_p F(t_p) - \int_0^{t_p} F(x)dx =$$

$$= t_p p - t_p + \int_0^{t_p} R(x)dx = -qt_p + \int_0^{t_p} R(x)dx, \quad (13)$$

where $R(x) = 1 - F(x)$ is reliability function.

For mean value ET of the life of preventively predetermined maintained objects at time t_p we obtain the following equation:

$$ET = \frac{1}{F(t_p)} \int_0^{t_p} R(x)dx = \frac{\int_0^{t_p} R(x)dx}{1 - R(t_p)} \quad (14)$$

From equation (14) it is clear that mean life of preventive predetermined maintained objects $ET > \int_0^{\infty} R(x)dx$ (mean life of corrective maintained objects) for $t_p << \infty$. This fact proves that preventive predetermined maintenance increases operational reliability of objects comparing with corrective maintenance.

Optimal value of operating time to predetermined maintenance t_{po} [1] it is possible to calculate from equation (15) which is analogical to equation (1) and (4) and using three parameters Weibull distribution function, we obtain:

$$c(t_p) = \frac{C_{pr} + L_f \cdot F(t_p)}{\bar{t}(t_p)} = \frac{C_{pr} + L_f \cdot (1 - \exp(-(\frac{t_p - \gamma_t}{\beta_t})^{\alpha_t})}{\int_0^{t_p} \exp(-(\frac{t - \gamma_t}{\beta_t})^{\alpha_t} dt} \quad (15)$$

For solution of equation (14) and (15) it is possible to use a numerical method, e.g. to use MS Excel.

4. Numerical solution

We have simulated the life t_f of 44 objects to failure and their technical state (diagnostic signals) S_f shortly before failure, including costs and losses. Value of diagnostic signal may represent the ratio of a two values of variable, therefore, the value presented by diagnostic signal is a dimensionless number. There were obtained input data – see Table 1.

Using input reliability and economic data regarding life time t_f from Table 1 and software http://wessa.net/rwasp_fitdistrweibull.wasp we obtained mean operating time to failure (*MOTTF*), standard deviation (SD_t) and parameters α_t, β_t and γ_t of the Weibull distribution function – see Table 2.

Using input reliability data regarding technical state (diagnostic signal) S_f from Table 1 and software http://wessa.net/rwasp_fitdistrweibull.wasp, we obtained average diagnostic signal (technical state) $\bar{S}_f$, standard deviation (SD_S) and parameters α_S, β_S and γ_S of the Weibull distribution function – see Table 3.

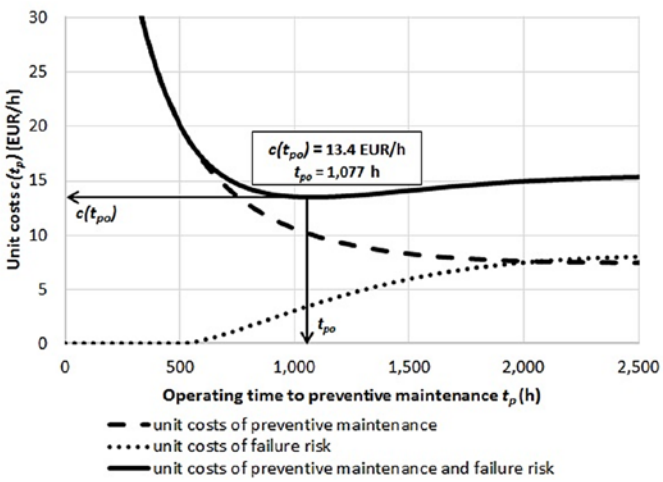

Fig. 2. Dependency of unit costs of preventive maintenance and unit costs of failure risk $c(t_p)$ versus operating time to preventive predetermined maintenance t_p

Table 1. Simulated input data – life t_f and diagnostic signal S_f closely before failure including costs

Object Nr.	1	2	3	4	5	6	7	8	9	10	11
t_f (h)	501	635	727	753	799	941	988	995	1012	1087	1111
S_f	3.01	3.07	3.09	3.10	3.13	3.16	3.18	3.19	3.20	3.21	3.22
Object Nr.	12	13	14	15	16	17	18	19	20	21	22
t_f (h)	1125	1163	1194	1199	1205	1210	1223	1238	1245	1256	1277
S_f	3.23	3.24	3.25	3.26	3.27	3.28	3.28	3.29	3.29	3.40	3.40
Object Nr.	23	24	25	26	27	28	29	30	31	32	33
t_f (h)	1298	1356	1375	1399	1410	1447	1492	1512	1544	1588	1625
S_f	3.41	3.43	3.46	3.47	3.48	3.49	3.49	3.50	3.52	3.53	3.55
Object Nr.	34	35	36	37	38	39	40	41	42	43	44
t_f (h)	1678	1739	1749	1763	1799	1832	1979	2030	2213	2375	2700
S_f	3.57	3.58	3.59	3.60	3.62	3.65	3.69	3.72	3.79	3.85	3.97
Costs of preventive maintenance C_{pr} (EUR)										10,000	
Costs of corrective maintenance C_{cm} (EUR)										21,000	
Production losses due to failure and following down time L_f (EUR)										11,000	
Unit costs of condition monitoring c_d (EUR/h)										1.2	

Table 2. Parameters of the Weibull distribution function – MOTTF, SD_t, α_t, β_t and γ_t

MOTTF (h)	Standard deviation SD_t (h)	Shape parameter α_t	Scale parameter β_t	Location parameter γ_t
$MTTF = \beta_t \cdot \Gamma(\frac{1}{\alpha_t}+1)+\gamma_t$ Γ is Gama function	$SD_t = \beta_t \sqrt{\Gamma(\frac{2}{\alpha_t}+1)-\Gamma(\frac{1}{\alpha_t}+1)^2}$ Γ is Gama function	1.823	971.465	500
1363.39	490.56			

Table 3. Parameters of the Weibull distribution function – $\bar{S}_f$, SD_S, α_S, β_S and γ_S

Mean value $\bar{S}_f$	Standard deviation SDS	Shape parameter α_S	Scale parameter β_S	Location parameter γ_S
$\bar{S}_f = \beta_S \cdot \Gamma(\frac{1}{\alpha_S}+1)+\gamma_S$ Γ is Gama function	$SD_S = \beta_S \sqrt{\Gamma(\frac{2}{\alpha_S}+1)-\Gamma(\frac{1}{\alpha_S}+1)^2}$ Γ is Gama function	1.825	0.450	3.00
3.4	0.227			

Table 4. Unit costs of preventive maintenance and failure risk versus operating time (period) of preventive predetermined maintenance (optimal data are formatted bold)

t_p (h)	1,000	1,020	1,040	1,060	**1,077**	1,100	1,120	3,500
$c(t_p)$ (EUR/h)	13.486	13.465	13.451	13.444	**13.442**	13.445	13.452	15.400

Table 5. Unit costs of predictive maintenance, diagnostics and failure risk versus diagnostic signal for predictive maintenance (optimal data are formatted bold)

S_p (-)	3.1	3.2	3.3	**3.4**	3.5	3.6	3.7	3.8
$\bar{t}(S_p)$ (h)	732.0	930.1	1,075.2	**1,186.3**	1,275.3	1,328.8	1,355.7	1,370.8
$c(S_p)$ (EUR/h)	15.182	12.753	11.861	**11.592**	11.613	11.937	12.445	12.999

Unit costs of preventive maintenance and failure risk $L_f \cdot (1-\exp(-(\frac{t_p-\gamma_t}{\beta_t})^{\alpha_t})$ versus operating time (period) of preventive predetermined maintenance we can calculate by means of equation (15) –see some results in Table 4 and on Fig. 2.

$$c(S_p) = \frac{C_{pr} + L_f \cdot (1-\exp(-(\frac{S_p-\gamma_S}{\beta_S})^{\alpha_S})}{\frac{1}{n}\left[\sum_{i=1}^{m(S_p)} t_i(S_p) + \sum_{j=1}^{n-m(S_p)} t_j(S_p)\right]} + c_d \qquad (16)$$

Now we can calculate optimal diagnostic signal (technical state) for restoration S_{po} using equation (4) substituting Weibull distribution function to equation (16) and by application MS Excel, we can calculate unit costs $c(S_p)$ of preventive maintenance, diagnostics and failure risk versus diagnostic signal for predictive maintenance, optimal diagnostic signal S_{po} (technical state) for restoration and mean operating time versus diagnostic signal for predictive maintenance $\overline{t}(S_p) = \frac{1}{n}\left[\sum_{i=1}^{m(S_p)} t_i(S_p) + \sum_{j=1}^{n-m(S_p)} t_j(S_p)\right]$ – see Table 5 and Fig. 3.

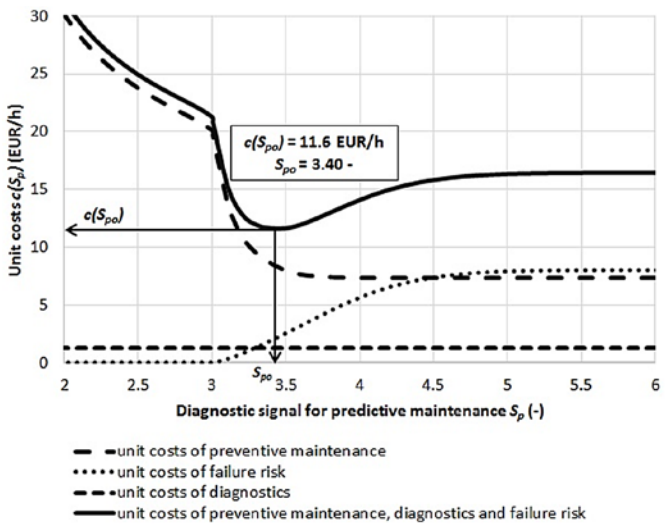

Fig. 3. Dependency of unit costs of preventive maintenance, diagnostics and failure risk versus diagnostic signal of predictive maintenance S_p

Knowledge of optimal diagnostic signal S_{po} (see Fig. 3) is very important for the design of predictive maintenance. We can very easily indicate dispositional operating time $t_d(S_p)$ according to equation (5) to be able to plan the maintenance of an object.

Now we use MS Excel to compute mean life *ET* of the objects that have undergone preventive maintenance after the optimal interval t_{po} = 1,076.7 hours (according to the equation (15)) by the Weibull distribution function with parameters α_t, β_t and γ_t using numerical method of *R(t)* integration.

$$ET = \frac{\int_0^{t_{po}} R(x)dx}{1-R(t_{po})} = \frac{\gamma_t + \int_{\gamma_t}^{t_{po}} exp(-(\frac{t_p-\gamma_t}{\beta_t})^{\alpha_t})dt}{1-\exp(-(\frac{t_{po}-\gamma_t}{\beta})^{\alpha})} = \frac{1{,}076.72}{1-0.6795} = 3{,}359.4 \text{ hours} \qquad (17)$$

Numerical calculation (for the Weibull distribution function with parameters α_t = 1.823, β_t = 971.466 and γ_t=*500*) of $R_T(t)$ is done according to equations (9) and (10) and of *R(t)* is done according to equation (18) – see Fig. 4.

$$R(t) = \exp(-(\frac{t-\gamma_t}{\beta_t})^{\alpha_t}) \qquad (18)$$

From this figure it is clear that the object with predetermined maintenance has a much better reliability function $R_T(t)$ than the same object maintained after failure (reliability function *R(t)*).

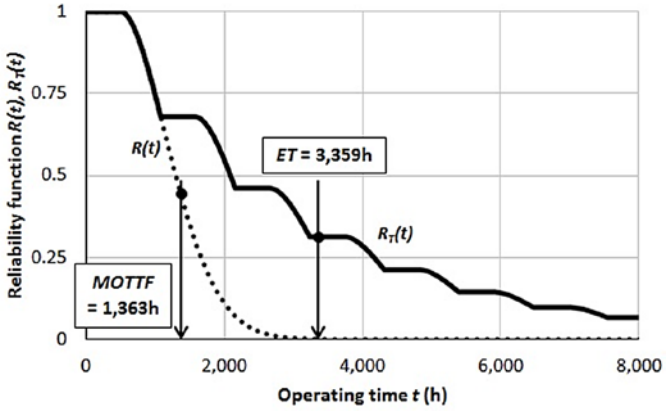

Fig. 4. Reliability functions R(t) (object is running to failure without preventive maintenance) and $R_T(t)$ (preventive predetermined maintained object) versus operating time

5. Conclusion

Authors offer a tool for maintenance managers which represents general methods of calculating the optimal interval for predetermined maintenance and the optimal diagnostic signal for predictive maintenance/replacement – equations (1) and (15). Further, the authors deduced equations for mean life and probability reliability function of predetermined maintained machine objects and equations for predictive maintenance optimization – equations (10), (12) and (14). Authors proof that preventive maintenance improves reliability. From equation (14) it is clear that mean life of preventive predetermined maintained objects $ET > \int_0^{\infty} R(x)dx$ (mean life of corrective maintained objects) for $t_p << \infty$. Numerical solution presented graphically on Fig. 4 also shows that reliability of preventive predetermined maintained objects decreases more slowly than the reliability of objects which are running to failure.

The example shows an application of the proposed mathematical model on a virtual machine object. When we replace the component after failure, the *MOTTF* = 1,363 hours and production losses due to the failure risk L_f= 11,000 EUR and unit costs of preventive maintenance and failure risk, then *c*(*MOTTF*) = 15.4 EUR/hour. When we introduce predetermined maintenance (for t_{po} = 1,077 hours) of the object, the *MOTTF* increases to *ET* = 3,360 hours and unit costs of preventive maintenance and failure risk decrease to 13.4 EUR/hour – see Fig. 2 and Fig. 4.

When we introduce predictive maintenance on the same object using the derived equation (16), we obtained optimal diagnostic signal S_{po} = 3.4 and unit costs $c(S_{po})$ = 11.6 EUR/hour. If we compare these unit costs with unit costs of periodic maintenance ($c(t_{po})$ = 13.4 EUR/hour), we see that this predictive maintenance strategy brings economical effect of 1.8 EUR/hour. We can see the comparison of all results of the example of chosen maintenance policies from Table 6.

Table 6. Comparison of all results of maintenance policies from the example

Maintenance policy	Diagnostic signal (h, -)	Unit costs (EUR/h)
Corrective maintenance	$t_p \to \infty$	$c(t_p \to \infty) = 15.4$
Predetermined maintenance	$t_{po} = 1.077$	$c(t_{po}) = 13.4$
Predictive maintenance	$S_{do} = 3.4$	$c(S_p) = 11.6$

The best maintenance policy from point of unit costs for this example is a predictive maintenance.

The benefit of the proposed mathematical models is not only the ability to compute the optimal interval of predetermined maintenance and optimal diagnostic signal for predictive maintenance, but also to provide quantitative proof that preventive predetermined maintenance increases operational reliability of machine objects. The decision lies with maintenance specialists, whether or not they adopt and apply these models and methods for improving maintenance effectiveness of industry production equipment.

Acknowledgement

The paper was prepared with support from project IGA CULS Prague 2016: 31190/1312/3117 Effect of mixtures of biofuels on production of nitrogen oxide and smoke of combustion engine during NRSC.

References

1. Barlow R E, Proschan F. Mathematical Theory of Reliability. John Wiley & Sons, New York 1965
2. Burduk A, Chlebus E. Evaluation of the risk in production systems with a parallel reliability structure. Eksploatacja i Niezawodność - Maintenance and Reliability 2009; 2(42): 84-95.
3. EN 13306:2010 Maintenance - Maintenance terminology.
4. Galar D, Gustafson A, Tormos B, Berges L. Maintenance Decision Making based on different types of data fusion. Eksploatacja i Niezawodnosc – Maintenance and Reliability 2012; 14 (2): 135–144.
5. Gao W, Zhang Z, Ji H, Zhou j, Liu Q. Optimal quasi-periodic preventive maintenance policies for a repairable system with stochastic maintenance interval. Eksploatacja i Niezawodnosc – Maintenance and Reliability 2015; 17 (3): 389–397, https://doi.org/10.17531/ein.2015.3.9.
6. Golmakani H R, Fattahipour F. Age-based inspection scheme for condition-based maintenance. Journal of Quality in Maintenance Engineering 2011; 17 (1): 93-110, https://doi.org/10.1108/13552511111116277.
7. Jardine A K S, Lin D, Banjevith D. A review on machinery diagnostics and prognostics implementing condition-based maintenance. Mechanical Systems and Signal Processing 2006; 20 (7): 1483-1510, https://doi.org/10.1016/j.ymssp.2005.09.012.
8. Jiang R, Ji P, Tsang A H C. Preventive effect of optimal replacement policies. Journal of Quality in Maintenance Engineering 2010; 12 (3): 267–274, https://doi.org/10.1108/13552510610685101.
9. Jurča V, Hladík T, Aleš Z. Optimization of preventive maintenance intervals. Eksploatacja i Niezawodnosc – Maintenance and Reliability 2008; 3: 41-44
10. Khalil J, Saad S M, Gindy N. An integrated cost optimisation maintenance model for industrial equipment. Journal of Quality in Maintenance Engineering 2009; 15 (1): 106–118, https://doi.org/10.1108/13552510910943912.
11. Lee H, Cha J H. New stochastic models for preventive maintenance and maintenance optimization. European Journal of Operational Research 2016; 255 (1): 80-90, https://doi.org/10.1016/j.ejor.2016.04.020.
12. Legát V, Mošna F, Červenka V, Jurča V. Optimization of preventive maintenance and information system. In: Eksploatacja i Niezawodność - Maintenance and Reliability 2002; 4: 24 -29.
13. Legat V, Zaludova A H, Cervenka V, Jurca V. Contribution to optimization of preventive replacement. Reliability Engineering and System Safety 1996; 51: 259 – 266, https://doi.org/10.1016/0951-8320(96)00124-X.
14. Li X, Jia Y, Wang P, Zhao J. Renewable warranty policy for multiple-failure-mode product considering different maintenance options. Eksploatacja i Niezawodnosc – Maintenance and Reliability 2015; 17 (4): 551–560, https://doi.org/10.17531/ein.2015.4.10.
15. Moghaddam K Z, Usher J S. Optimal preventive maintenance and replacement schedules with variable improvement factor. Journal of Quality in Maintenance Engineering 2010; 16 (3): 271–287, https://doi.org/10.1108/13552511011072916.
16. Ni X, Zhao J, Song W, Guo C, Li H. Nonlinear degradation modeling and maintenance policy for a two-stage degradation system based on cumulative damage model. Eksploatacja i Niezawodnosc – Maintenance and Reliability 2016; 18 (2): 171–180, https://doi.org/10.17531/ein.2016.2.3.
17. Peng W, Liu Y, Zhang X, Huang H Z. Sequential preventive maintenance policies with consideration of random adjustment-reduction features. Eksploatacja i Niezawodnosc – Maintenance and Reliability 2015; 17 (2): 306–313, https://doi.org/10.17531/ein.2015.2.19.
18. Rusin A, Wojaczek A. Optimization of power machines maintenance intervals taking the risk into consideration. Eksploatacja i Niezawodność - Maintenance and Reliability 2012; 14 (1): 72-76.
19. Sharma A, Yadava G S, Deshmukh S G. A literature review and future perspectives on maintenance optimization, Journal of Quality in Maintenance Engineering 2011; 17 (1): 5 – 25, https://doi.org/10.1108/13552511111116222.
20. Sherif Y S. Optimal Maintenance Schedules of Systems Subject to Stochastic Failure. Microelectronic Reliability 1982; 22: 15 29.
21. Stenstrom C, Norrbin P, Parida A, Kumar U. Preventive and corrective maintenance - cost comparison and cost-benefit analysis. Structure

and Infrastructure Engineering 2016; 12 (5): 603-617, https://doi.org/10.1080/15732479.2015.1032983.
22. Sugier J, Anders G J. Modelling and evaluation of deterioration process with maintenance activities. Eksploatacja i Niezawodnosc – Maintenance and Reliability 2013; 15 (4): 305–311.
23. Zhang Z, Gao W, Zhou Y, Zhang Z. Reliability modeling and maintenance optimization of the diesel system in locomotives. Eksploatacja i Niezawodnosc – Maintenance and Reliability 2012; 14 (4): 302–311.

Václav LEGÁT
Department for Quality and Dependability of Machines,
Faculty of Engineering, University of Life Sciences Prague
Kamycka 129, 16521 Prague 6 – Suchdol, Czech Republic

František MOŠNA
Department of Mathematics
Faculty of Engineering, University of Life Sciences Prague
Kamycka 129, 16521 Prague 6 – Suchdol, Czech Republic

Zdeněk ALEŠ
Vladimír JURČA
Department for Quality and Dependability of Machines,
Faculty of Engineering, University of Life Sciences Prague
Kamycka 129, 16521 Prague 6 – Suchdol, Czech Republic

E-mails: legat@tf.czu.cz, mosna@tf.czu.cz, ales@tf.czu.cz, jurca@tf.czu.cz

Article citation info:
KORNACKI A, WAWRZOSEK J, BOCHNIAK A, SZYMANEK A, PAWLAK H. Critical values of driver response time and its impact on reducing reliability and safety in road traffic. Eksploatacja i Niezawodnosc – Maintenance and Reliability 2017; 19 (1): 142–148, http://dx.doi.org/10.17531/ein.2017.1.20.

Andrzej KORNACKI
Jacek WAWRZOSEK
Andrzej BOCHNIAK
Andrzej SZYMANEK
Halina PAWLAK

CRITICAL VALUES OF DRIVER RESPONSE TIME AND ITS IMPACT ON REDUCING RELIABILITY AND SAFETY IN ROAD TRAFFIC

KRYTYCZNE WARTOŚCI CZASU REAKCJI KIEROWCY I ICH WPŁYW NA OBNIŻENIE NIEZAWODNOŚCI I BEZPIECZEŃSTWA RUCHU DROGOWEGO*

Road traffic is among the most dangerous types of human activity. The main causes of road accidents are driver fatigue, poor physical and mental condition of drivers and overestimating one's skills while driving. This study focuses on the estimation of driver response time, as the basis of a hypothetical system that uses short and long-range radars, which determines the physical and mental condition of a driver, based on the analysis of „acceleration noise" of the vehicle following its predecessor. This work highlights serious consequences of the fact that driver response time is described by means of a distribution with heavy tails, and thus may be a source of hazard in the driver-vehicle system. Extremes of driver response time were treated as outliers in this study. Their detection was attained by using the Akaike information criterion [1, 2], which is an alternative to conventional methods of testing hypotheses. Untypical, on account of their outlying nature, values are interpreted as critical driver response time values which potentially endanger the reliability of driving.

***Keywords**: driver response time, reliability of road traffic, outliers, Akaike information criterion, log-normal distribution.*

Ruch drogowy należy do najbardziej niebezpiecznych rodzajów działalności człowieka. Główne przyczyny wypadków drogowych to zmęczenie kierowców, zły stan psychofizyczny kierujących oraz przecenianie swoich umiejętności podczas prowadzenia pojazdu. W niniejszej pracy skupiono uwagę na estymacji czasu reakcji kierowców, jako podstawie hipotetycznego systemu wykorzystującego radary dalekiego i krótkiego zasięgu a określającego stan psychofizyczny kierowcy w oparciu o analizę „szumu przyspieszeń" pojazdu podążającego za poprzednikiem. Wskazuje się na groźne konsekwencje faktu, że czas reakcji kierowcy jest opisywany rozkładem z ciężkimi ogonami, gdyż z tego powodu może być źródłem zagrożenia w układzie kierowca-pojazd. Skrajne wartości czasu reakcji kierowców potraktowano w pracy, jako wartości odstające. Do ich wykrycia zastosowano kryterium informacyjne Akaike [1, 2] co stanowi alternatywę w stosunku do klasycznych metod testowania hipotez. Nietypowe, bo odstające wartości interpretuje się, jako krytyczne czasy reakcji kierowców potencjalnie zagrażające niezawodności jazdy.

***Słowa kluczowe**: czas reakcji kierowców, niezawodność ruchu drogowego, obserwacje odstające, kryterium informacyjne Akaike, rozkład logarytmiczno-normalny.*

1. Introduction

Road traffic is one of the most dangerous types of human activity. It is due to several factors, including the unreliability of the driver-vehicle system in the process of driving. According to WHO statistics, 1.2 million of people die in car accidents each year. In the past 10 years on EU roads ca 0.5 million people were killed with over 1.5 million seriously injured and many people remain disabled for the rest of their lives. The annual cost of road accidents in the EU amounts to € 160 billion, which constitutes 2% of EU GDP. The risk of being a fatality on Polish domestic roads is four times greater than on roads in Germany and the UK, and on highways it is even six times greater. In Poland, in 2005, as many as 57.3% of the accidents occurred on a straight stretch of road, and the most common cause of road accidents was excessive speed (28.8%), while failure to maintain a safe distance between vehicles causes 4.5% of accidents. In 2012, about 11% of accidents are the result of driving into the rear of another vehicle because of not maintaining a safe distance. The cause of up to one quarter of accidents on German highways is driver drowsiness. Most of these accidents have severe consequences. The main risk factors on roads are: human, as a participant of the traffic, the vehicle, and the road. As many as 90-95% of accidents are related to man and their behaviour. The vehicle contributes to causing 8-10% of road accidents, while the road and its surroundings contributes to 28-35% of road accident occurrence. These factors may impact the risk individually or several factors may combine (Fig. 1) [14, 20]. Archer [3] observed that at an average speed of 60 km/h average one risky situation for 120 km should be attributed to an average driver.

Human behaviour, ignorance of one's own body, response to stress or the level of fatigue or excessive confidence in one's own driving capability contribute to the occurrence of accidents. Other factors, such as weather conditions or the road surface condition, are much

(*) Tekst artykułu w polskiej wersji językowej dostępny w elektronicznym wydaniu kwartalnika na stronie ***www.ein.org.pl***

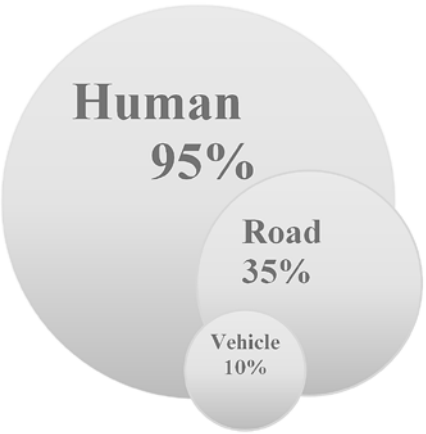

Fig. 1. The influence of the major risk factors on the incidence of road accidents.

less significant. Thus, in many centres there is ongoing development of integrated monitoring systems for the psycho-physical condition of drivers. An overview of some systems enhancing road safety, currently deployed and being in development, is included in works of Wicher [34], Mercedes-Benz [27], Cieślar and Karpińska [9]. They illustrate the extensive engineering work of, among others, SAAB, Mitsubishi, Toyota, Mercedes-Benz, Nissan, Lexus companies. Vehicle electronics is the fastest developing segment in consumer electronics. In 1980, the value of electronic vehicle equipment accounted for less than 1% of the vehicle price. In 1990, it was already close to 7%, and in 2007, this share increased to 22%. Current estimates exceed 40% of the vehicle value. The value of electronic vehicle control systems is currently growing at a rate of ten plus percent per annum.

Theoretical considerations presented in this article highlight the need and create the possibility to further develop the concept of yet another system, which this time monitors components of the psycho-physiological response time of the driver with regard to calculating accident risk in the process of dependent driving, which is the primary component of traffic flows.

2. System-based, on-going control of driver response time

Individual physiological characteristics define the limitations of the driver's organism. Engineering psychology involves checking the following psycho-physical parameters of drivers: response time and its consistency, assessing vehicle speed, spatial vision, sensitivity of proprioception, sensitivity to glare and the ability to distinguish shapes in the darkness, speed and accuracy of perception, speed and accuracy of decision making, divisibility and concentration of attention, technical knowledge, resistance to fatigue, neuroticism [23]. The following are among the most important characteristics of a driver: quality of vision, response time and age.

Response time constitutes part of the time needed to stop a car. The manoeuvre of stopping a car before an appearing obstacle can be divided into the following: perception time, actual driver response time, time required to activate the braking system of the car and the actual braking time. In some publications perception time, which is the time that elapses between the moment an obstacle can be noticed and the moment the central nervous system begins working, is included in the time slot called response time. Similarly, to this study, it stems from the conditions under which an experiment is conducted. The combined driver's perception and response times may change, ranging from 1 to even a few seconds depending on:

- driver's current health condition, mood, and physical characteristics (e.g. headache, being well-rested or tired),
- driver's degree of concentration (long and monotonous drive or prolonged noise in the driver's compartment can increase the response time by more than 10%),
- driver's circadian rhythm (decreased vigilance, fatigue, drowsiness), time of year, day and meteorological phenomena (changes in atmospheric pressure and temperature of the environment, precipitation),
- ergonomic conditions (e.g. inappropriate placement of the control system elements, poorly adjusted parameters of the auxiliary subsystems),
- complexity of the traffic situation (surprise as a result of an unusual road situation), the number of options considered by the driver and the actual manoeuvres undertaken,
- street lighting, type of road (street, suburban road, motorway),
- insobriety, influence of psychotropics, intoxicating substances.

If the driver anticipates danger, it is assumed that the response time is 0.5-0.8 *s*. If the driver is careful but does not anticipate danger, it is 0.7-0.9 *s*. When the driver steers carelessly, it is 1.4-1.9 *s*. Computer reconstructions of road collisions often assume that the total perception and driver response time is 1.75 *s*. During night time this duration is longer and amounts to 2.5 *s* [5].

Response times estimated on the basis of laboratory test simulations ought to be taken very carefully. Most of these tests consist in measuring driver response time to a simple signal, i.e. such as measuring the time that elapses between the appearance of red light and pressing the brake pedal. These tests do not reflect the real conditions encountered by a driver in traffic and the measured response times are much shorter [35].

The constituent elements of the currently installed optional equipment of the vehicle, i.e. a combination of a stereoscopic camera with long and short range radar sensors, after appropriate reprogramming, allow for direct measurements of the response time of a driver following another vehicle. Multiple measurements of the time elapsing between the moment the preceding vehicle brakes and the moment of the following vehicle driver's response can be a parameter that may be used in a variety of ways. It can, for example, be used to warn the driver about their poor psycho-physical condition, of the need to change their driving style or the parameters of auxiliary subsystems, it can also lead to reducing the speed of the vehicle, temporary exclusion from the traffic, signalling a problem to other users and even notifying the police about a threat.

3. Critical driver response time

In order to compare different traffic situations, Jones and Potts [21] proposed a probabilistic description of traffic flow, where a significant role was assigned to the parameter of σ_a – acceleration dispersion, commonly referred to as "acceleration noise" of a vehicle following its predecessor (the so-called dependent driving). Model testing has utilised this traffic quality indicator. Acceleration noise incorporates both the longitudinal and the transverse component. The latter is particularly visible on a winding road, but it has not yet been adequately examined [22]. Usually only the longitudinal component expressed by the following parameter is considered: σ_a – acceleration dispersion [4, 35]. The σ_a indicator was verified in simulation tests, and the results confirmed its correlation with statistical safety indicators. Effective research on real objects has not been yet conducted. The tragic death of the Polish precursor in real time traffic flow, Mieczysław Kaczor, D.Eng., discontinued the already initiated research [23].

Acceleration dispersion is a consequence of the time of the driver's response to the observed stimuli as well as their intensity, which are associated with the psycho-physical predispositions of the driver,

manifested in their driving style. Acceleration dispersion is also a performance function of the vehicles participating in road traffic.

"Acceleration noise" (sometimes referred to as "noise of accelerations") is the mean square deviation of the acceleration distribution of the vehicles participating in road traffic [13]. This indicator defines the inability to maintain a constant drive speed. If to determine the level of "acceleration noise" a measurement method called the "floating" vehicle is used, the "acceleration noise" of a traffic flow with a small error resulting from the limited time of T measurements can be determined by measuring changes in the tested vehicle acceleration. Then:

$$\sigma_a = \lim_{T\to\infty}\sqrt{\frac{1}{T}\int_0^T\left[a(t)-\bar{a}\right]^2 dt},$$

where $a(t)$ $\bar{a}$ – are respectively: realisations of the stochastic process $\boldsymbol{X}(t)$ (temporally random changes in the tested vehicle acceleration) and the average acceleration of the tested vehicle over the measuring distance $\langle 0;T\rangle$.

The examination of the critical response time of drivers should allow us to show the relationship between potentially dangerous road traffic situations and the following categories of driver response time: typical and untypical, permissible and impermissible, safe and endangering safety. The assignment of any of these categories may refer to a single measurement, as well as a group of measurements. In the latter case, we will refer to the current characteristics of the physiological features of the driver, e.g. fatigue, intoxication. When the exemplary, typical individual characteristics of driver response time are known, they can be easily compared with characteristics of the current data stream, and then prevent a potential threat. Just like in systems monitoring driver fatigue by analysing the movements and fixation of the eyeball; they also deploy the comparison of the digital "rested eye" pattern with actual camera observations of the driver's eye throughout the whole journey.

Each of these characteristics can be based on 1) the measurement of the percentage of stress exceeding a certain barrier or 2) filtering the data stream so that the highlighted group of multiple measurements will correspond to the actual probability of the response time distribution. By combining both methods, one can specify 3) the frequency parameter of the untypical driver response.

The system of managing the data stream coming from various sensors requires complex filtering and alarm activation in reaction to untypical observations [18]. In this study, the extreme values of driver reaction time are considered as the so-called "outlier measurements" values. While analysing the classical statistics of experimental results, it is important to determine whether the outliers are derived from a different population than the rest of the results. Then, in further analysis, untypical observations used to be customarily rejected. It is also possible, although unlikely to occur, that "strange" observations will emerge with the same distribution as for the remaining results. Then, it would be advisable to keep such observations for further statistical analysis, simultaneously increasing its effectiveness.

Methods of hypothesis testing are the most commonly used ones for the detection of outliers [6, 8, 15, 19, 30, 32]. However, conclusions in the hypothesis testing method are dependent on the assumed level of significance and may be different for its various values. Furthermore, there may appear the effect of outlier "masking". For the data on the strength of plastic materials, Grubbs [19] describes a situation where tests do not detect one smallest observation, while two smallest observations are readily identified as outliers (a certain contradiction).

In this study, it is suggested to use the Akaike criterion information to detect outliers. This criterion, derived from information theory, allows one to select it from among the models describing experimental data, which maximizes entropy [1, 2]. According to Sakamoto [31], the value of this criterion is equal:

$$AIC = -2\ln\left(\max\ likelihood\right) + 2K, \tag{1}$$

where max *likelihood* means likelihood calculated for the estimators of parameters obtained through the maximum likelihood method, and K the number of these parameters. We select the model for which the value of AIC is the lowest. This procedure is independent of the level of significance, the number of outliers and of whether the "suspicious" observations belong to the group of the smallest or largest observations.

4. Log-normal distribution

It appears that the log-normal distribution is well-suited for describing specific random positive values, which here take the form of the distribution of driver response time.

Definition: Random variable X has a log-normal distribution with parameters μ,σ^2 denoted $LN\left(\mu,\sigma^2\right)$ when its logarithm has normal distribution, i.e. $Y=\ln X \sim N\left(\mu,\sigma^2\right)$. Therefore, we have:

$$X \sim LN\left(\mu,\sigma^2\right) \Leftrightarrow Y = \ln X \sim N\left(\mu,\sigma^2\right). \tag{2}$$

Most probabilistic models have not considered the fact of the commonly occurring, so-called fat tails and asymmetry in the distributions of random variables describing extreme values [17 §3.2.1; 10; 16 §2]. It is estimated that the risk management methods based on the theory of extreme values do not have these disadvantages and allow one to effectively model rare but dangerous events. The log-normal distribution is often proposed for constructing models with extreme values for actual data [7 §3.3, §4.5.2]. Engineering applications of this distribution result from the fact that the description of measurement errors often must assume that the difference in the measurement result of the actual parameter value is a positive value. Examples include phenomena in which the nominal parameter values are equal to zero, e.g. reference levels for contaminants sedimentation in soil, water or air; or the distance between the centres (axes) of elements that should be concentric (coaxial). Kotulski and Szczepiński [25] give examples showing a good description of vanadium concentration in sediments and cadmium concentration in soil using the log-normal distribution. The study [28] shows that the log-normal distribution can be appropriate for describing the fragmentation test conducted for fibre-reinforced composites. An example of applying this distribution to describe a parameter in a model of fatigue crack growth can be found in Doliński [12]. Log-normal distribution applications associated with the problems of the reliability theory are offered in the works [23, 10, 28, 33], and for the extreme value theory applied to warning forecasts in hydrology they are found in the work [26]. Basic characteristics of the *LN* distribution are provided in Table 1 [29].

Table 1. Basic characteristics of the log-normal distribution

Parameters	$0 \le \mu < \infty, \quad \sigma > 0$
Support	$x \in (0,\infty)$
Expected value	$e^{\mu+\frac{\sigma^2}{2}}$
Variance	$(e^{\sigma^2}-1)e^{2\mu+\sigma^2}$

It is known that the maximum likelihood estimators of the log-normal distribution parameters are equal to [24]:

$$\hat{\mu} = \frac{\sum_{i=1}^{n} \ln x_i}{n}, \quad \hat{\sigma}^2 = \frac{\sum_{i=1}^{n} (\ln x_i - \hat{\mu})^2}{n}. \tag{3}$$

Let us consider a sample of n observations, which, after arranging in an ascending order, form a sequence: $x_{(1)} \le x_{(2)} \le \ldots \le x_{(n)}$. Therefore, x(i) denotes the value of the i-th positional statistics $X_{i:n}$ from an n-element simple sample $\boldsymbol{x}$. The following notation have been adopted in the further part of this article:

$\Psi(x,\mu,\sigma^2)$ denotes the probability density function of distribution $LN\left(\mu,\sigma^2\right)$,

$\Phi(x,\mu,\sigma^2)$ denotes the cumulative distribution function of $LN\left(\mu,\sigma^2\right)$,

$f_{i:n}(x,\mu,\sigma^2)$ denotes the probability density function of the i-th positional statistics $X_{i:n}$.

Therefore, we have [11]:

$$\Psi(x,\mu,\sigma^2) = \frac{1}{x\sigma\sqrt{2\pi}} \exp\left[-\frac{(\ln x - \mu)^2}{2\sigma^2}\right], \; x > 0, \tag{4}$$

$$\Phi(x,\mu,\sigma^2) = \frac{1}{2} + \frac{1}{2} erf\left[\frac{\ln x - \mu}{\sigma\sqrt{2}}\right], \; x > 0, \tag{5}$$

$$f_{i:n}(x,\mu,\sigma^2) = \left[B(i,n-i+1)\right]^{-1}\left[\Phi(x,\mu,\sigma^2)\right]^{i-1}\left[1-\Phi(x,\mu,\sigma^2)\right]^{n-i}\Psi(x,\mu,\sigma^2), \tag{6}$$

where *erf* is a special function (non-elementary) called the Gauss error function, $B(p,q)$ denotes the beta special function:

$$B(p,q) = \int_0^1 t^{p-1}(1-t)^{q-1}dt, \; p > 0, \; q > 0. \tag{7}$$

It is known that:

$$B(p,q) = \frac{\Gamma(p)\Gamma(q)}{\Gamma(p+q)} = \frac{(p-1)!(q-1)!}{(p+q-1)!} \tag{8}$$

for natural p and q, while $\Gamma(x)$ denotes the Euler's gamma special function.

Denoting $EX = \mu'$, $VAR(X) = \left(\sigma'\right)^2$ one can observe in the Table 1 that both μ' and $\left(\sigma'\right)^2$ depend on μ, σ^2 parameters and vice versa. Therefore, all the functions Φ, Ψ and $f_{i:n}$ are dependent on μ' and $\left(\sigma'\right)^2$.

5. Model of outliers

Consider the following situation: an ordered n-element sample is given:

$$\underbrace{x_{(1)} \le x_{(2)} \le \ldots \le x_{(n_1)}}_{n_1 \text{ of the lowest observations}} \le \overbrace{\underbrace{x_{(n_1+1)} \le \ldots \le x_{(n-n_2)}}_{n-n_1-n_2 \text{ observations}}}^{\text{Main part of the sample}} \le \underbrace{x_{(n-n_2+1)} \le \ldots \le x_{(n)}}_{n_2 \text{ of the highest ones}} \tag{9}$$

from the log-normal distribution. The 'main part' of the sample group is derived from a population with an average of μ', and the outliers may constitute the lowest observations group or the highest observations group. They originate from populations of different μ_1' and μ_2' average values. Detection of outliers is generally performed using the procedure of hypothesis testing at a certain level of significance. Then, relevant hypotheses have the following form:

H_0 – lack of outliers, that is $\mu_1' = \mu' = \mu_2'$,

H_{1a} – there exist lowest outliers, that is $\mu_1' < \mu'$,

H_{1b} – highest outliers, that is $\mu' < \mu_2'$,

H_{1c} – there exist lowest and highest outliers, that is $\mu_1' < \mu' < \mu_2'$,

Here outliers are determined using the Akaike information criterion. Thus, by setting the parameters accordingly: $\mu_1 < \mu < \mu_2$ and the same σ for all groups of observation, we obtain:

$$\mu_1' < \mu' < \mu_2' \quad \text{and} \quad \sigma_1' < \sigma' < \sigma_2'. \tag{10}$$

Therefore, the model with outliers can be described in the following way:

$$h(x_{(i)}) = \begin{cases} \Psi(x_{(i)},\mu_1,\sigma^2) & \text{for} \quad i = 1,\ldots,n_1 \\ f_{i-n_1:n-n_1-n_2}(x_{(i)},\mu,\sigma^2) & \text{for} \quad i = n_1+1,\ldots,n-n_2 \\ \Psi(x_{(i)},\mu_2,\sigma^2) & \text{for} \quad i = n-n_2+1,\ldots,n \end{cases}. \tag{11}$$

6. Akaike information criterion

In order to determine the value of the Akaike information criterion (1) for the model (11) we find its likelihood function:

$$L(n_1,n_2,\mu,\mu_1,\mu_2,\sigma^2 \mid \boldsymbol{x}) = \prod_{i}^{n_1}\Psi(x_{(i)},\mu_1,\sigma^2)\prod_{i=n_1+1}^{n-n_2} f_{i-n_1:n-n_1-n_2}(x_{(i)},\mu,\sigma^2)\prod_{i=n-n_2+1}^{n}\Psi(x_{(i)},\mu_2,\sigma^2)$$

Thus, in view of (4), (5) and (6) the logarithm of the likelihood function equals to:

$$\begin{cases} \ln L(n_1,n_2,\mu,\mu_1,\mu_2,\sigma^2 \mid \boldsymbol{x}) = l(n_1,n_2,\mu,\mu_1,\mu_2,\sigma^2 \mid \boldsymbol{x}) = \ln\prod_{i=1}^{n_1}\frac{1}{x_{(i)}\sigma\sqrt{2\pi}}\exp\left[-\frac{(\ln x_{(i)}-\mu_1)^2}{2\sigma^2}\right] + \\ +\ln\left[\prod_{i=n_1+1}^{n-n_2}\left[B(i-n_1,n-n_1-n_2-i+n_1+1)\right]^{-1}\left[\Phi(x_{(i)},\mu,\sigma^2)\right]^{i-n_1-1}\left[1-\Phi(x_{(i)},\mu,\sigma^2)\right]^{n-n_1-n_2-i+n_1}\times \right. \\ \left.\times\frac{1}{x_{(i)}\sigma\sqrt{2\pi}}\exp\left[-\frac{(\ln x_{(i)}-\mu)^2}{2\sigma^2}\right]\right] + \ln\prod_{i=n-n_2+1}^{n}\frac{1}{x_{(i)}\sigma\sqrt{2\pi}}\exp\left[-\frac{(\ln x_{(i)}-\mu_2)^2}{2\sigma^2}\right], \end{cases} \tag{12}$$

that is:

$$\begin{cases} l(n_1,n_2,\mu,\mu_1,\mu_2,\sigma^2 \mid \boldsymbol{x}) = -\frac{1}{2}\left\{n\ln(2\pi) + n\ln(\sigma^2) + \frac{1}{\sigma^2}\sum_{i=1}^{n}(\ln x_{(i)} - \mu^i)^2\right\} \\ -\sum_{i=1}^{n}\ln x_{(i)} - \sum_{i=n_1+1}^{n-n_2}\left\{\ln B(j,k-j+1) - (j-1)\ln\Phi(x_{(i)}) - (k-j)\ln[1-\Phi(x_{(i)})]\right\} \end{cases}, \tag{13}$$

where $j = i - n_1,\ k = n - n_1 - n_2$ and:

$$\mu^{i} = \begin{cases} \mu_1 & \text{if} \quad 1 \le i \le n_1 \\ \mu & \text{if} \quad n_1 < i \le n - n_2 \\ \mu_2 & \text{if} \quad n - n_2 < i \le n \end{cases}. \tag{14}$$

Finally, for the observed sample $\boldsymbol{x}$ the value of the Akaike information criterion function $AIC(n_1, n_2)$ dependent on n_1 and n_2 equals:

$$AIC(n_1, n_2) = \begin{cases} -2l(n_1, n_2; \hat{\mu}, \hat{\sigma}^2 \mid \boldsymbol{x}) + 2 \cdot 2 & \text{if} \quad n_1 = 0, n_2 = 0 \\ -2l(n_1, n_2; \hat{\mu}, \hat{\mu}_1, \hat{\sigma}^2 \mid \boldsymbol{x}) + 2 \cdot 3 & \text{if} \quad n_1 \ne 0, n_2 = 0 \\ -2l(n_1, n_2; \hat{\mu}, \hat{\mu}_2, \hat{\sigma}^2 \mid \boldsymbol{x}) + 2 \cdot 3 & \text{if} \quad n_1 = 0, n_2 \ne 0 \\ -2l(n_1, n_2; \hat{\mu}, \hat{\mu}_1, \hat{\mu}_2, \hat{\sigma}^2 \mid \boldsymbol{x}) + 2 \cdot 4 & \text{if} \quad n_1 \ne 0, n_2 \ne 0 \end{cases} \tag{15}$$

where $\hat{\mu}$, $\hat{\mu}_1$, $\hat{\mu}_2$ and $\hat{\sigma}^2$ denote estimators of model parameters obtained with the maximum likelihood method.

7. Experimental research

Experimental research was conducted at the Institute of Transportation Systems and Electrical Engineering of the University of Technology and Humanities in Radom. Driver response times were recorded at a fixed intensity level of real road traffic and fixed biometeorological conditions using a device allowing for measurements in both stationary and dynamic conditions. The device received a signal by radio from the preceding vehicle, in which a transmitter activated by pressing the brake pedal was installed. The voltage powering the brake lights switched on the signal in the measurement impulse transmitter. An impulse receiver and an electronic time measuring device were installed in the vehicle following with the test driver. This device measured the number of measurement impulses and converted this number into time, with the accuracy of $10^{-3}s$. Pressing the brake pedal by the test driver resulted in stopping the time measuring device and saving the driver response time with the above-mentioned accuracy. At the same time the situation on the road was filmed through the windscreen [23].

8. Results

An example of a representative measurement result stream of the response time obtained from one of the drivers is illustrated in the histogram (Fig. 2). It appears that the driver response time has a log-normal distribution. This is confirmed by the shape of the histogram, and the results of statistical tests (Table 2). The values of all the tests: Kolmogorov-Smirnov, Cramer-von Mises and Anderson-Darling, presented in the third column of Table 2, clearly indicate that there are no grounds to reject the hypothesis of the log-normal distribution of driver response time. The calculations of tests values and drawings were performed with the SAS version 9.3 program.

Using the theory developed in the previous chapters, the values of the Akaike information criterion *AIC* for various configurations of outliers (different numbers of the lowest and highest outliers) were found. The results are presented in Table 3.

As presented in Table 3, the lowest value of the Akaike information criterion *AIC*, marked with an asterisk, indicates that in the studied stream the outlying response times are the ones from the set containing two lowest and six highest values. Highlighted in Figure 3 are the times significantly deviating from a straight line which, using a logarithmic scale, corresponds to the regression line $y = 8.056 \cdot \exp(0.0306 \cdot i)$ for $n_1 < i \le n - n_2$ which provides characteristics of the psycho-physical condition of the analysed driver within the studied period. After rejecting extreme observations, the values in 2 out of 3 tests checking the fitting of data stream to the log-normal distribution in Table 2, reach the median value. Therefore, they unequivocally indicate that there are no grounds for rejecting the hypothesis of typical driver response time having a log-normal distribution. In addition, they confirm the validity of identifying those outliers as untypical of this driver. The validity of the chosen methodology is confirmed by the full compatibility of all applied statistical procedures.

Table 3. Values of the information criterion AIC for different configurations of outliers

Number of the lowest outlier values	Number of the highest outlier values: 0	1	2	3	4	5	6	7	8	9	10
0	−30.10	−41.77	−42.85	−44.95	−46.84	−47.75	−45.28	−40.82	−36.02	−30.40	−24.93
1	−23.35	−37.29	−39.57	−43.38	−47.37	−50.75	−50.22	−46.33	−42.26	−37.43	−31.70
2	−16.25	−31.55	−35.10	−40.71	−46.88	−52.49	**−53.43***	−50.10	−46.58	−41.80	−35.23
3	−12.11	−27.34	−30.78	−36.39	−42.69	−48.51	−49.48	−45.86	−42.01	−36.69	−29.35
4	−7.68	−22.82	−26.19	−31.86	−38.34	−44.44	−45.45	−41.52	−37.29	−31.24	−22.91
5	−3.64	−18.57	−21.80	−27.43	−33.96	−40.17	−41.02	−36.66	−31.86	−24.73	−15.16
6	−0.36	−14.98	−17.97	−23.44	−29.87	−35.98	−36.46	−31.55	−26.01	−17.49	−6.53
7	3.38	−10.84	−13.59	−18.87	−25.17	−31.04	−30.87	−25.19	−18.53	−7.72	5.40
8	4.07	−9.83	−12.22	−17.11	−23.00	−28.42	−27.62	−21.31	−13.80	−1.53	12.72
9	4.65	−9.00	−11.06	−15.59	−21.11	−26.13	−24.74	−17.82	−9.49	4.24	19.57
10	5.48	−7.98	−9.71	−13.92	−19.09	−23.74	−21.74	−14.17	−4.95	10.45	27.00

** optimal configuration of the sample*

Table 2. Tests of observation conformance to the log-normal distribution

	Data with outliers		Data after rejection of outliers	
Test	Statistics	p-value	Statistics	p-value
Kolmogorov-Smirnov	$D = 0.1244$	> 0.150	$D = 0.1003$	> 0.150
Cramer-von Mises	$W^2 = 0.1169$	0.067	$W^2 = 0.0412$	0.5
Anderson-Darling	$A^2 = 0.6769$	0.075	$A^2 = 0.3109$	0.5

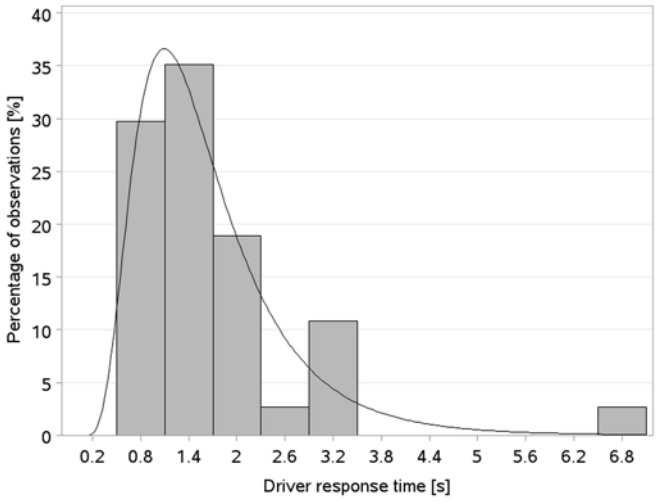

Fig. 2. The distribution histogram of the observed response time stream of one of the drivers, and conforming log-normal distribution.

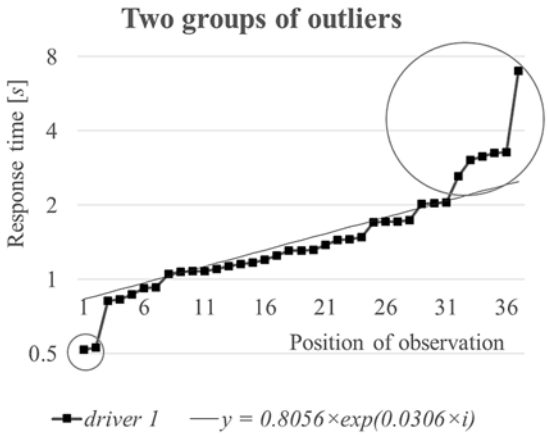

Fig. 3. The two observed groups of driver response time are critical to the reliability level of the driver-vehicle system in the process of driving

9. Conclusions

The probability function $R(t) = 1 - F(t) = P(T \geq t)$ conventionally known as the reliability function (*reliability function*) or survival function, on account of the pejorative nature of the long T time of the driver's response, should rather be termed as the "*risk function"* here. Due to the fact that for t = 0 value R (0) = 1 and $\lim_{t \to \infty} R(t) = 0$, the "risk function" is a non-growing function of t time and it expresses the probability of the right-hand *"tail"* distribution. That is to say, the "risk function" refers to the description of probability for the extreme values being the most adverse to the safety of road traffic. Therefore, attention should be paid to the rate of convergence of the right tail to 0. In systems described by normal distributions, the occurrence of extreme events (from tails) is so low that, in practice, such events are not observed. It is expressed by the three-sigma rule. While a single long driver response time constitutes a major threat to road safety. Hence, the statement that the driver response time in real traffic has a log-normal distribution means that the distribution of the driver response time has a heavy right-hand tail, i.e. the response times can reach relatively high values with significant probabilities. Therefore, the identification of driver response time in real traffic as a variable having a large right-hand tail of a log-normal distribution shows it to be a major risk source in road traffic. And then the observation made in the representative Fig. 3, whereby the six highest outliers from the right-hand tail significantly exceed the values of the already heavy right-hand tail, additionally compounds the horror of dangerous situations. Moreover, the downward deviation of the two shortest response times from the typical time distribution presented in Fig. 3, points to the driver's nervous reactions. These results may also indicate loss of (deterioration of) driving smoothness, and this is correlated with a risk increase, and consequently with the risk of traffic accident occurrence. Therefore, the additional identification of both groups of critical driver response times with a heavy right-hand tail of their distribution combines to indicate the existence of three potential threats to the reliability of the driver-vehicle system on the part of the driver, resulting in the deterioration of road safety. Thus, it is necessary to seek systems of driver support which are aimed at eliminating these threats.

References

1 Akaike H. Information theory and an extension of the maximum likelihood principle. 2nd International Symposium on Information Theory. Eds. B.N. Petrv and F. Csaki. Budapest: Akademia Kiado, 1973; 267-281.

2. Akaike H. On entropy maximization principle. Proc Symposium on Applications of Statistics. Ed. P.R. Krishnaiah. Amsterdam: North Holland, 1977; 27-47.

3. Archer J. Methods for the Assessment and Prediction of Traffic Safety at Urban Intersections and their Application in Micro-simulation Modelling Academic Thesis. Division of Transport and Logistics, Stockholm: Royal Institute of Technology, Kungliga Tekniska Högskolan (KTH) SE-100 44, 2004.

4. Ashton W D. The theory of road traffic flow. London: Methuen & Co. Ltd. 1966.

5. Badger J E. Human factors affecting perception. Law and Order Magazine, 1996.

6. Barnett V, Lewis T. Outliers in Statistical Data. John Wiley & Sons, 1994.

7. Benjamin J R, Cornell C A. Probability, Statistics, and Decision for Civil Engineers. New York: McGraw-Hill Book Company, 2014.

8. Breuning M, Kriegel H P, Sander J. LOF: Identifying Density-Based Local Outliers. In Proceedings of the ACM SIGMOND Conference, 2000; 93-104.

9. Cieślar K, Karpińska O. Przyszłość za kierownicą – czy samochód będzie myśleć za nas? Translogistics 2014; 95-108.

10. Cooke R M, Nieboer D. Heavy-tailed distributions: Data, diagnostics, and new developments. Resources for the Future Discussion Paper, Washington, 2011; (11-19), [online: http://www.rff.org/files/sharepoint/WorkImages/Download/RFF-DP-11-19.pdf, access: 2016-04-03].

11. David H A, Nagaraja H N. Orders Statistics. Wiley Series in Probability and Statistics, 2003, https://doi.org/10.1002/0471722162.

12. Doliński K. Comparison of stochastic model of fatigue crack growth with experiments. Fatigue Fract. Engng. Mater. Struct. 1993; 16 (10): 1021-1034, https://doi.org/10.1111/j.1460-2695.1993.tb00075.x.

13. Drew D R. Traffic flow theory and control. New York: McGraw-Hill Book Company, 1968; Chapter 12.

14. Euro RAP [online: http://www.eurorap.org/, access: 2016-04-03].

15. Ferguson T S. On the rejection of outliers. In Proc. Fourth Berkeley Symposium Math. Statist. Prob. 1961; 1: 253-287.

16. Foss S, Korshunov D, Zachary S. An Introduction to Heavy-Tailed and Sub exponential. Series in Operations Research and Financial Engineering Distributions. Springer, 2013, https://doi.org/10.1007/978-1-4614-7101-1.
17. Fronczak A, Fronczak P. Świat sieci złożonych. Od fizyki do Internetu. Warszawa: Wydawnictwo Naukowe PWN, 2009.
18. Golab L, Ozsu M T. Issues in data stream management. ACM Sigmod Record, 2003; 32 (2): 5-14, https://doi.org/10.1145/776985.776986.
19. Grubbs F E. Sample criteria for testing outlying observations. Ann. Math. Statist. 1960; 1: 27-58.
20. Guzewski P. Wypadki drogowe – statystyka i przyczyny. Szkolenie z zakresu ratownictwa technicznego dla Strażaków Ratownictwa OSP. Red. Surala Zb. CNBOP. 2008; 4-23.
21. Jones T R. and Potts R B. The measurement of acceleration noise – a traffic parameter. Operations Research, 1962; 10: 745-763, https://doi.org/10.1287/opre.10.6.745.
22. Jurecki R, Jaśkiewicz M, Guzek M, Lozia Z, Zdanowicz P. Driver's reaction time under emergency braking a car – Research in a driving simulator. Eksploatacja i Niezawodnosc – Maintenance and Reliability. 2012; 14 (4): 295–301.
23. Kaczor M, Marczak M. (red.) Badanie wpływu oznakowania tyłu pojazdu na jakość ruchu. – Praca naukowo badawcza. - Etap II. Zakład Modelowania Procesów Transportowych w Instytucie Systemów Transportowych i Eksploatacji Taboru Kolejowego, WSI Radom, 1983.
24. Krzyśko M. Mathematical Statistics. Poznań: Wydawnictwo Naukowe UAM, 2004 (in Polish).
25. Kotulski Z, Szczepiński W. Rachunek błędów dla inżynierów. Warszawa: WNT, 2004.
26. Kuźmiński Ł. The application of value extreme theory in warning forecast in hydrology for sequence of independent lognormal random variables. Studia Ekonomiczne, 2014; 207: 148-158 (in Polish).
27. Mercedes-Benz "Intelligent Drive". TecDay. Press Information. November,
28. Murzewski J. Niezawodność konstrukcji inżynierskich. Warszawa: Arkady, 1989.
29. Patel J, Kapadia C H, Owen D B. Handbook of statistical distribution. Marcel Dekker, 1976.
30. Rousseeuw P, Leroy A. Robust Regression and Outlier Detection. John Wiley & Sons, 2003.
31. Sakamoto Y, Ishiguro M, Kitagawa G. Akaike Information Criterion Statistics. Tokyo: Reidel Publishing Company, 1986.
32. Srivastava M S, Von Rosen D. Outliers in Multivariate Regression Models. J. Mult. Anal. 1998; 65: 195-208, https://doi.org/10.1006/jmva.1997.1729.
33. Suchodolski S. Probabilistyczna ocena wytrzymałości włókien szklanych oraz połączenia włókno-spoiwo epoksydowe na podstawie testu fragmentacji. Prace XVII Sympozjum Mechaniki Eksperymentalnej Ciała Stałego, Jachranka 1996, 550-557.
34. Wicher J. Bezpieczeństwo samochodów i ruchu drogowego. Warszawa: Wydawnictwa Komunikacji i Łączności, 2012.
35. Woch J. Teoria potoków ruchu. Katowice: Zakład Inżynierii Ruchu Instytutu Transportu, 2001 [online: http://dydaktyka.polsl.pl/kir/TPR_WWW/TPR.htm, access: 2016-04-03].

Andrzej KORNACKI
Jacek WAWRZOSEK
Andrzej BOCHNIAK
Department of Applied Mathematics and Computer Science
University of Life Sciences in Lublin
ul. Głęboka 28, 20-612 Lublin, Poland
E-mails: andrzej.kornacki@up.lublin.pl, jacek.wawrzosek@up.lublin.pl, andrzej.bochniak@up.lublin.pl

Andrzej SZYMANEK
Institute of Transportation Systems and Electrical Engineering
University of Technology and Humanities in Radom
ul. Malczewskiego 29, 26-600 Radom, Poland
E-mail: a.szymanek@uthrad.pl

Halina PAWLAK
Department of Technology, Ergonomics Unit
University of Life Sciences in Lublin
ul. Głęboka 28, 20-612 Lublin, Poland
E-mail: halina.pawlak@up.lublin.pl

INFORMATION FOR AUTHORS

Eksploatacja i Niezawodnosc – Maintenance and Reliability – the journal of the Polish Maintenance Society, under the scientific supervision of the Polish Academy of Sciences (Branch in Lublin), published four times a year.

The scope of the Quarterly

The quarterly *Eksploatacja i Niezawodnosc – Maintenance and Reliability* publishes articles containing original results of experimental research on the durability and reliability of technical objects. We also accept papers presenting theoretical analyses supported by physical interpretation of causes or ones that have been verified empirically. *Eksploatacja i Niezawodność – Maintenance and Reliability* also publishes articles on innovative modeling approaches and research methods regarding the durability and reliability of objects.

The following research areas are particularly relevant to the journal:

1. degradation processes of mechanical and biomechanical systems,
2. diagnosis and prognosis of operational malfunctions and failures.
3. analysis of failure risk/wear,
4. reliability-and-environmental-safety engineering in the design, manufacturing and maintenance of objects,
5. management and rationalization of object maintenance,
6. risk management in the processes of operation and maintenance,
7. the human factor and human reliability in operation and maintenance systems.

Terms and Conditions of Publication

The quarterly *Eksploatacja i Niezawodnosc – Maintenance and Reliability* publishes only original papers written in English or in Polish with an English translation. Translation into English is done by the Authors after they have received information from the Editorial Office about the outcome of the review process and have introduced the necessary modifications in accordance with the suggestions of the referees! Acceptance of papers for publication is based on two independent reviews commissioned by the Editor.

The quarterly *Eksploatacja i Niezawodnosc – Maintenance and Reliability* proceeds entirely online at submission.ein.org.pl

Technical requirements

- After receiving positive reviews and after acceptance of the paper for publication, the text must be submitted in a Microsoft Word document format.
- Drawings and photos should be additionally submitted in the form of high resolution separate graphical files in the TIFF, SVG, AI or JPG formats.
- A manuscript should include: names of authors, title, abstract, and key words that should complement the title and abstract (in Polish and in English), the text in Polish and in English with a clear division into sections (please, do not divide words in the text); tables, drawings, graphs, and photos included in the text should have descriptive two-language captions, if this can be avoided, no formulae and symbols should be inserted into text paragraphs by means of a formula editor; references (written in accordance with the required reference format); author data – first names and surnames along with scientific titles, affiliation, address, phone number, fax, and e-mail address.

The Editor reserves the right to abridge and adjust the manuscripts. All submissions should be accompanied by a submission form.

Detailed instructions to Authors, including evaluation criteria can be found on the journal's website: www.ein.org.pl

Editor contact info

Editorial Office of „Eksploatacja i Niezawodnosc - Maintenance and Reliability"
Nadbystrzycka 36, 20-618 Lublin, Poland
e-mail: office@ein.org.pl

INFORMATION FOR SUBSCRIBERS

Fees

Yearly subscription fee (four issues) is 100 zloty and includes delivery costs. Subscribers receive any additional special issues published during their year of subscription free of charge.

Orders

Subscription orders along with authorization to issue a VAT invoice without receiver's signature should be sent to the Editor's address.

Note

In accordance with the requirements of citation databases, proper citation of publications appearing in our Quarterly should include the full name of the journal in Polish and English without Polish diacritical marks, i.e.,

Eksploatacja i Niezawodnosc – Maintenance and Reliability.